From “Core” to “Periphery”:

Mapping enhancers in developmental gene regulatory networks

by

Renhe Luo

A Dissertation

Presented to the Faculty of the Louis V. Gerstner, Jr.

Graduate School of Biomedical Sciences,

Memorial Sloan Kettering Cancer Center

in Partial Fulfillment of the Requirements for the Degree of

Doctor of Philosophy

New York, NY

August, 2023

_____ _____

Danwei Huangfu/PhD Date
Dissertation Mentor

DEDICATION

I would like to dedicate this thesis to my family and all people that supported me. Without their supports, none of this work would have been possible.

ABSTRACT

Comprehensive enhancer discovery is challenging because most enhancers, especially those affected in complex diseases, have weak effects on gene expression. Focusing on mapping entire enhancer atlas of a gene regulatory network with improved enhancer discovery efficiency, we dissected the hierarchy in a network and divided the genes into two categories, the core transcription factors and the peripheral genes. Different strategies were designed based on their distinct regulation patterns. Our dynamic network modeling revealed that nonlinear enhancer-gene regulation during cell state transitions can be leveraged to improve the sensitivity of enhancer discovery. Guided by the modeling results, we conducted a mid-transition CRISPRi-based enhancer pool screen to map core enhancer of the core transcription factors, utilizing human embryonic stem cell to definitive endoderm differentiation as a dynamic transition system. The screen discovered a comprehensive set of enhancers (4 to 9 per locus) for each of the core endoderm lineage-specifying transcription factors, including many enhancers with strong effects during cell state transition but weak to moderate effects in post-transition. To map peripheral enhancers of peripheral genes in the endoderm gene regulatory network, we performed a genome-scale single-cell perturb-seq enhancer screen with multiple enhancer perturbations in each cell. In total, we identified more than 300 regions (including ~100 promoters and ~200 enhancers), perturbing which will significantly decrease target peripheral genes' expression. Together, our gene regulatory network hierarchy concept and dynamic network-guided enhancer screens provide generalizable strategies for sensitive and more comprehensive enhancer discovery, applicable in both normal and pathological cell state transitions.

ACKNOWLEDGMENTS

I would like to greatly appreciate my mentor, Dr. Danwei Huangfu, for generously supporting my ideas, training on my scientific thinking, and encouraging me to try different methods to achieve my project goals. I would also like to thank the future Dr. Jielin Yan for assisting with the optimization of ChIP-seq, ChIP-MS and 4C experiments, Drs. Bess P. Rosen, Julian Pulecio, Dapeng Yang, Tingxu Chen, Qing V. Li and Hyunwoo Cho for assisting with the experiments and computational analysis, and all lab members for creating great research environment in the lab.

I would like to thank my thesis committee members, Drs. Lorenz Studer and Andrea Ventura for their critically suggestions and supports throughout the years. In particular, I would like to thank Dr. Michael A. Beer for his great help with the bioinformatics and modeling in this project. I would also like to thank several members of his laboratory, including Jin Woo Oh, Dustin Shigaki and Dr, Wang Xi for computational supports. I would like to thank Drs. Effie Apostolou, Christina Leslie, Simone Sidoli and Thomas Vierbuchen for providing great technique support for this project, and several members of their laboratory, including Dylan Murphy, Wilfred Wong, Ronald Cutler and Rachel Glenn for assisting with the experiments and computational analysis.

Lastly, I would like to thank our graduate school, particularly Drs. Ken Marians, Michael Overholtzer, Joan Massagué, and our benefactor Louis V. Gerstner. If it wasn't with their initiative, generosity and supports, our graduate program would not exist.

TABLE OF CONTENTS

LIST OF TABLES

LIST OF FIGURES

LIST OF ABBREVIATIONS

3C: Chromatin conformation capture

AA: Activin A

Ab: Antibody

ABC model: Activity-by-contact model

ATAC-seq: Assay for transposase-accessible chromatin using sequencing

AUPRC: The area under precision-recall curve

Cas9n: Cas9 nickase

ChIA-PET: Chromatin interaction analysis by paired-end tag sequencing

ChIP-seq: Chromatin immuno-precipitation sequencing

CHIR: CHIR99021

CIA model: CTCF loop-constrained interaction activity model

CREs: *cis*-regulatory elements

CRISPR: Clustered Regularly Interspaced Short Palindromic Repeats

CRISPRa: CRISPR activation

CRISPRi: CRISPR interference

CROP-seq: CRISPR droplet sequencing

crRNA: CRISPR RNAs

dCas9: Dead Cas9

DE: Definitive endoderm

Del: Deletion

DHS: DNase I hypersensitive sites

DNA: Deoxyribonucleic acid

DNase-seq: Deoxyribonuclease I hypersensitive site sequencing

DSB: Double-strand break

ENCODE: The Encyclopedia of DNA Elements

ESCRO: Embryonic Stem Cell Research Oversight Committee

EZH2: Zeste homolog 2

FACS: Fluorescence-activated cell sorting

FC: Fold change

GFP: Green fluorescent protein

gkm-SVM: gapped k-mers-support vector machines

GRN: Gene regulatory network

gRNA: Guide RNA

GWAS: Genome-wide association studies

H3K27ac: H3K27 acetylation

H3K27me3: H3K27 tri-methylation

H3K4me1: H3K4 mono-methylation

H3K9me1: H3K9 mono-methylation

HATs: Histone acetyltransferases

HDR: Homology-directed repair

hESCs: Human embryonic stem cells

HiCAR: Hi-C on accessible regulatory DNA

IGH: Immunoglobulin heavy chain

KO: Knockout

KRAB: Kruppel-associated Box

LacZ: β-galactosidase

LE model: Loop competition and extrusion model

MM: Mismatch

MNase-seq: Micrococcal nuclease sequencing

MOI: Multiplicity of infection

MS: Mass spectrometry

MSKCC: Memorial Sloan Kettering Cancer Center

NHEJ: Nonhomologous end joining

NGS: Next generation sequencing

NIH: National Institutes of Health

NOMe-seq: Nucleosome occupancy and methylome sequencing

PAMs: Protospacer-adjacent motifs

PCA: Principal component analysis

PES: peripheral enhancer screen

PP1: Pancreatic progenitor stage 1

QTLs: Quantitative trait loci

RAREs: Retinoic acid response elements

RNA: Ribonucleic acid

RT-qPCR: Real-time quantitative polymerase chain reaction

SAM: synergistic activation mediator

SBE2: *SHH* Brain Enhancer 2

scRNA-seq: single-cell RNA sequencing

STARR-seq: Self-transcribing active regulatory region sequencing

TREE: three-component repurposed technology for enhanced expression

T-SSRs: Tyrosine site-specific recombinases

TADs: Topologically associating domains

TALEN: Transcription activator-like effector nuclease

TFBS: Transcription factor binding sites

TFs: Transcription factors

tracrRNA: *Trans*-activating crRNA

TSS: Transcription start site

UMI: Unique molecular identifier

VSV-G: Vesicular stomatitis virus G

WT: Wild-type

ZFNs: Zink finger nuclease

ZRS: ZPA regulatory sequence

INTRODUCTION

Gene regulation and gene regulatory network

Gene regulation is a highly intricate and dynamic process that controls the expression of genes in cells. It involves a complex crosstalk between proteins, *cis*-regulatory elements (CREs) of DNA, and other molecules to precisely tune gene expression[1,2]. The regulation of genes is essential for diverse biological processes such as development, tissue homeostasis, immune responses, and adaptation to environment changes.

Gene regulation can occur both at the transcriptional and post-transcriptional levels[3-7]. The transcriptional regulation is a level of regulation influences the initiation of transcription, the process of synthesizing RNA from DNA, and it involves mechanisms operating both on local chromatin and in 3D space. One of the key components of transcriptional regulation is transcription factors (TFs). TFs are proteins that bind to specific DNA sequences known as transcription factor binding sites (TFBS), which can be found in promoters, enhancers, and other CREs. TFs can activate or repress gene expression by recruiting or blocking the assembly of the transcriptional machinery at the gene's core promoter region through different cofactors[6,8]. Most of the TFs are thought to activate gene expression through recruiting coactivators like Mediators, histone acetyltransferases p300/CBP and other general transcription factors[9-12]. In addition to promoters, other CREs such as enhancers and insulators can also play important roles in transcriptional regulation. CREs can be located far from the gene they regulate but still be able to interact with the promoter through DNA looping[13-15]. They contain specific TFBS that allow lineage specific TFs to modulate gene expression in a spatiotemporal-specific

manner during development[16-18]. The packaging and the three-dimensional of DNA conformation will also influence on the gene expression. The compaction of chromatin structure can restrict or facilitate the accessibility of TFs to regulatory elements. For example, ATP-dependent chromatin remodeling complexes of the SWI/SNF family relocate nucleosomes to increase the accessibility of TFs to regulatory elements during the gene activation[19,20]. The three-dimensional of DNA conformation will affect the spatial proximity between the enhancers and promoters to affect gene expression[21-28]. Modifications to histone proteins like acetylation, methylation, ubiquitylation and otherwise chemically modification[29-32] as well as DNA methylation[33,34] can influence the gene expression. The interaction faces provided by these modifications provide different binding affinities for protein complexes (**Fig.1**). In contrast to acetylation by p300/CBP and other histone acetyltransferases (HATs), which can facilitate gene expression, Polycomb complex mediated H3K27 tri-methylation (H3K27me3) can silence gene expression at later development stages and differentiation as one of the repression mechanisms[32-37].

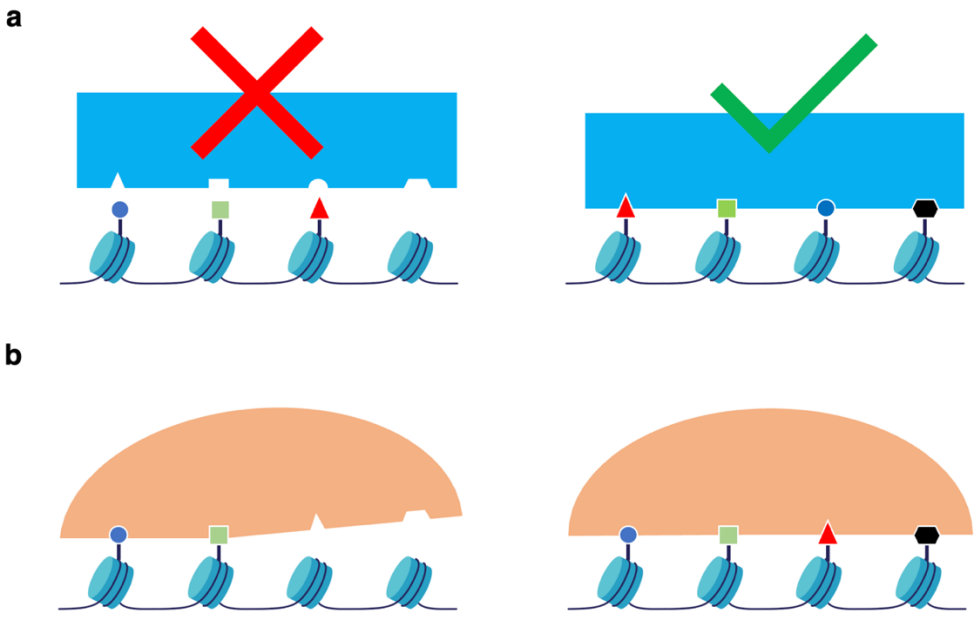

Figure 1. Histone modifications provide interaction face for protein binding. a, The schematic of correct combination of histone modifications provides interaction face necessary for corresponding protein recruitment. **b,** The schematic of different combinations of histone modifications that could affect the binding affinity between the protein and DNA (Plots are partially generated by using biorender).

The post-transcriptional regulation is a level of regulation that influences RNA maturation through several steps. Two important mechanisms of post-transcriptional regulation are alternative splicing and RNA stability. 1) Alternative splicing: Alternative splicing is a process in which different combinations of exons are included or excluded from the mRNA, resulting in the production of multiple mRNA isoforms from a single gene. This process substantially expands the diversity of protein isoforms that can be generated from a single gene. For example, the Dscam gene in fruit flies contains multiple clusters of alternative exons that can be selectively included or excluded during splicing[38]. *Dscam* potentially have 19,008 different extracellular domains linked to one of two alternative transmembrane segments, resulting in 38,016 isoforms[38,39]. 2) RNA stability: Post-transcriptional regulation also involves the modulation of RNA stability. Regulatory molecules such as microRNAs can bind to specific mRNA molecules and either inhibit their translation or promote their degradation[40-42]. This post-transcriptional regulation plays a crucial role in fine-tuning gene expression levels. An example is the *let-7* microRNA, a conserved microRNA family that plays important roles in developmental timing and cell fate determination. It is involved in regulating the transition from pluripotency to differentiation during embryonic development[43-45].

The gene regulation is not limited to the regulation of a single gene's expression. Due to the existence of interactions among proteins, CREs and other regulatory molecules that govern gene expression, they collectively form a complex network of regulatory relationships[7,46-48]. This intricate web of interactions controls the timing and dosage of gene activation or suppression within a cell or organism, commonly referred to as a gene

regulatory network (GRN). Like gene regulation, there are also two types of GRN: transcription regulatory networks and post-transcription regulatory networks[7]. In this thesis, I focus on GRNs involved in the gene regulation at the transcriptional level. Key components of GRNs at the transcriptional level usually include genes(proteins) and CREs. In a GRN, genes(proteins) act as nodes, while the regulatory interactions between genes are represented as edges[7,47]. These interactions can be hierarchical or form intricate feedback loops, creating a dynamic and interconnected system. The structure and dynamics of GRNs determine the overall gene expression patterns and cellular behaviors.

GRNs have a hierarchical organization, where core regulator genes (usually TFs) control the expression of downstream target genes (peripheral genes) (**Fig.2a**) and have a central role in cell fate determination and tissue development. In contrast, peripheral genes, which are the downstream of core TFs, usually perform the necessary functions of the cell once its fate is set[49]. GRNs often contain feedback loops, where the expression of one gene is influenced by another gene within the network, and vice versa. Feedback loops can be positive (amplifying the signal) or negative (dampening the signal), contributing to robustness, stability, and fine-tuning of gene expression[47]. These feedback loops can further form more complex modules. Examples include feed-forward loops, where one gene regulates another gene and both regulate a third gene, autoregulation loops, where one gene can self-regulate itself, and mutual inhibition loops, where two genes inhibit each other's expression[47] (**Fig.2b**). GRNs also integrate signals from various sources, such as external stimuli, signaling pathways, and cellular context, to orchestrate appropriate gene expression responses. Multiple regulatory inputs are integrated at different levels within the network to ensure precise control of gene expression.

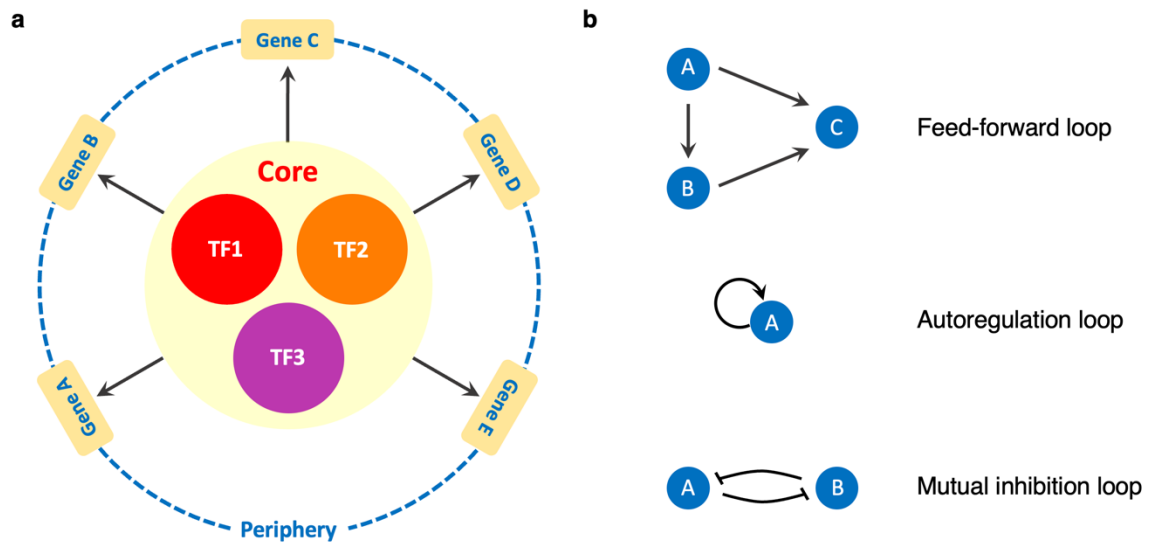

Figure 2. The hierarchy and feedback loops in the gene regulatory networks. a, The schematic of hierarchy in a GRN. Core TFs form the core circuit of a GRN and coregulate the expression of downstream peripheral genes. **b,** The schematic of feedback loops in a GRN. A, B and C represent three different genes in a GRN. In the feed-forward loop, A activates B and C, and B activates C. In the autoregulation loop, the gene can activate itself. In the mutual inhibition loop, A represses B and B represses A.

In summary, GRNs represent the intricate systems of interactions among genes and regulatory molecules that control gene expression. Studying GRNs has significant implications in understanding the complex regulatory mechanisms underlying biological systems such as developmental biology, systems biology, synthetic biology, and medicine. Disruptions or dysregulation of GRNs can lead to diseases, including cancer, developmental disorders, and neurodegenerative conditions. By unraveling the regulatory relationships within GRNs, researchers can identify key genes, signaling pathways, and potential therapeutic targets for intervention and treatment strategies.

Enhancer, the bridge between genes in gene regulatory networks

An enhancer is a specific type of DNA sequence or CREs that allow the binding of specific transcription factors and other regulatory molecules to create DNA-protein complexes to regulate the activity of gene expression. Therefore, enhancers are pivotal

components within GRNs, serving as vital bridges that connect different genes together. Enhancers have been further proved to associate with several histone markers, including but not limited to H3K4 mono-methylation (H3K4me1) and H3K27 acetylation (H3K27ac)[50-54]. Similar to the hierarchical organization in the gene level of a GRN, hierarchy also exists in the enhancer level. Enhancers can also be classified into two categories based on their endogenous activity and position of the genes they regulate in the network: Core enhancers, the enhancers of core TFs that have a global impact in cell fate determination and tissue development, and peripheral enhancers, the enhancers of peripheral genes that have little or no global impact in cell fate determination and tissue development[49] (**Fig.3**).

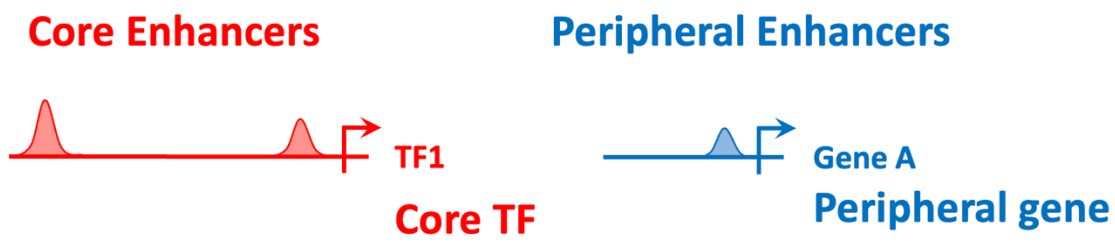

Figure 3. The relationship between core enhancer and core TF, peripheral enhancer and peripheral gene. Core enhancers are enhancers that regulate core TFs in a GRN. Peripheral enhancers are enhancers that regulate peripheral genes in a GRN.

While some enhancers are located with a few thousand base pairs (bps) of their target genes, others are located at a distance up to millions of bps away. Chromatin loops formed in 3D space enable these distal enhancers to interact with their cognate promoters. One of the prevalent looping models to explain the distal enhancer-promoter interaction is the cohesin-mediated loop extrusion model[21-28,55-58]. In this model, cohesin extrudes chromatin through its tripartite ring until reaching CTCF boundaries that impede its activity and form a DNA loop to bring distal enhancers into spatial proximity to promoters (**Fig.4**).

Despite their spatial separation, enhancers can exert powerful effects on gene expression by interacting with specific transcription factors and other regulatory proteins. When a transcription factor binds to an enhancer, it can enhance or increase the transcriptional activity of its target gene(s). This process involves the recruitment of additional proteins and the formation of a protein complex, like transcriptional machinary, which ultimately leads to the activation of gene transcription[59](**Fig.4**). Enhancers could exert their influence regardless of their orientation to the gene they regulate[60]. They can be upstream, downstream, within introns, or even within other nearby genes[61].

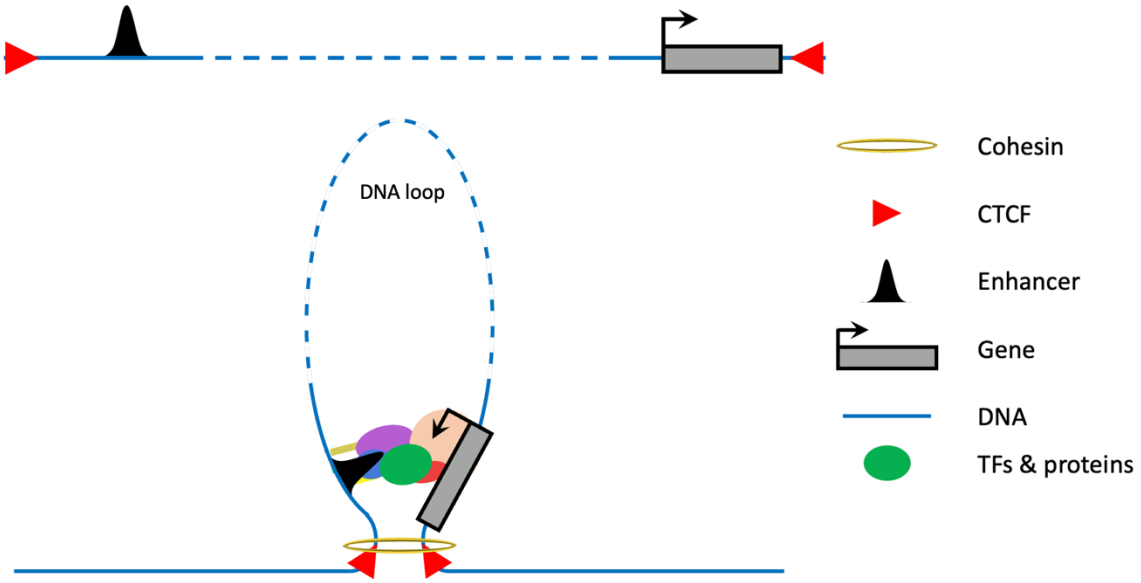

Figure 4. The cohesin-mediated loop extrusion model. Enhancer can be distal from the gene it regulates. Cohesin can bind to chromatin and extrudes DNA to relocate distal enhancer into spatial proximity to target gene for expression regulation.

Enhancers are highly modular and versatile in nature[62,63]. They can function across different cell types and developmental stages, controlling the precise spatial and temporal patterns of gene expression. These precise spatial and temporal patterns of gene expression are crucial for proper development and cellular differentiation and are precisely fine-tuned through the cooperation of enhancers and genes within the regulatory network[64,65]. These

enhancer-gene interactions are dynamic and adaptable, responding to various signals and environmental cues to ensure the appropriate gene expression patterns are achieved. By integrating multiple enhancers and their interactions, gene regulatory networks create a complex and interconnected web of regulatory relationships that coordinate the functioning of genes across various biological processes. The specificity and effectiveness of enhancers in regulating gene expression are determined by the presence of specific motifs, that are recognized by transcription factors[66,67]. The combination and arrangement of these binding sites within an enhancer dictate its ability to interact with transcription factors and modulate specific gene expression (**Fig.5**).

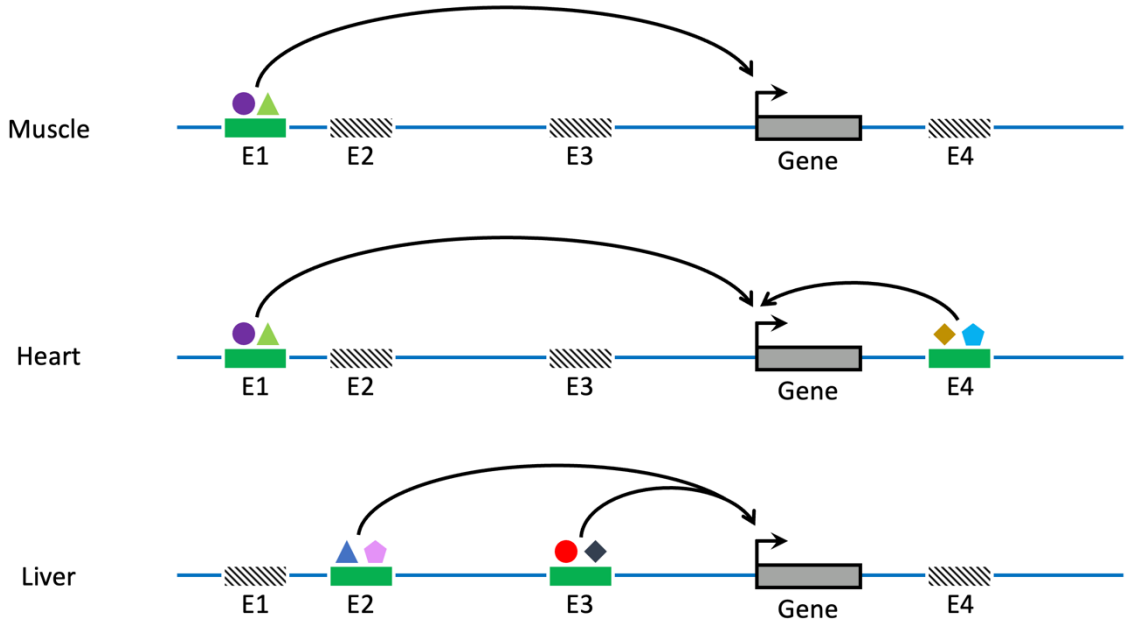

Figure 5. Enhancers and transcription factors together regulate the spatiotemporal-specific gene expression in different cell types. The schematic of the combination of different enhancers and TFs in different cell types to regulate the expression of the same gene in a spatiotemporal-specific manner.

Together, enhancers act as crucial intermediaries within gene regulatory networks, connecting genes and facilitating their precise regulation. Through their interactions with transcription factors and other regulatory molecules, enhancers contribute to the dynamic

control of gene expression, enabling the development, differentiation, and proper functioning of cells and organisms.

Enhancers and development

Enhancers play a fundamental role in the field of developmental biology through driving the intricate processes of cellular differentiation and organismal development. By exerting precise control on gene expression patterns, enhancers contribute to the formation of distinct cell types, tissues, and organs during embryonic development[64,65].

Enhancers contribute to the exquisite regulation of developmental processes by interacting with lineage-determining TFs and other regulatory proteins. These interactions help determine the cells' fate, as well as their subsequent differentiation and specialization[64,65]. Through the dynamic interplay between enhancers and genes, specific developmental pathways are activated, signaling cascades are initiated, and intricate morphological changes occur[64,65]. Furthermore, enhancers exhibit a remarkable degree of cell-type specificity. Different enhancers may be active in distinct cell populations or stages of development, allowing for the diversification of gene expression profiles and the emergence of specialized cell types (**Fig.5**). This specificity ensures the precise orchestration of developmental events and the establishment of intricate tissue architectures.

In early embryogenesis, enhancers are crucial for establishing the body plan of an organism. They control the precise spatial and temporal expression patterns of genes that guide the formation of the anterior-posterior axis, dorsal-ventral axis, and other body axes. Enhancers, like retinoic acid response elements (RAREs), regulate the expression of HOX

genes, which are responsible for specifying the identity and positioning of different body segments[68-73] .

During organogenesis, enhancers are instrumental in directing the development of specific organs and tissues. For example, in the vertebrate limb development, enhancers control the expression of genes involved in limb patterning, growth, and digit formation[74-77]. One of the most famous enhancers that regulate limb development is an enhancer of Sonic Hedgehog Signaling Molecule (*Shh*) named ZPA regulatory sequence (ZRS). *Shh* is the key of limb patterning[78]. ZRS locate in intron 5 of the *Lmbr1* gene and is 1 Mbp from the target gene *Shh*[13,75]. Single nucleotide mutation in ZRS can cause preaxial polydactyly[13,75]. There are more than 200 limb enhancers by computational prediction[76]. These enhancers ensure the precise spatial and temporal activation of genes that drive limb bud outgrowth and the establishment of limb polarity.

In neural development, enhancers also play a critical role in specifying different neuronal cell types and establishing neuronal connectivity in the brain[61,79,80]. Enhancers that regulate the expression of transcription factors *PAX1* govern the neuron specification and development populations[81,82]. Epigenetic state of enhancers regulated by the histone methyltransferase PRDM16 also affects gene expression and neuronal migration patterns through H3K9me1 and H3K4me1[83]. Activity of these enhancers controls the gene expression profiles and ensures the correct positioning and generation of accurate number of cortical neurons in the upper layer of the cortex[83].

Overall, enhancers occupy a central position in developmental biology, acting as critical regulators of the precise gene expression patterns that drive embryonic development, cellular differentiation, and the formation of complex tissues and organs.

Their involvement in establishing body axes, guiding organogenesis and specifying neuronal cell types highlights the crucial role of enhancers in the intricate processes of developmental biology. Studying enhancers in the context of developmental biology provides valuable insights into the molecular mechanisms that govern embryonic development, tissue morphogenesis and organogenesis. By understanding the roles of enhancers in regulating gene expression patterns during development, researchers can uncover the intricate regulatory networks that orchestrate cellular diversity, tissue patterning, and organ formation during development for the formation of complex organisms.

Enhancers and disease

Abnormal enhancer activities play a significant role in the context of disease by contributing to the dysregulation of gene expression patterns. Mutations or alterations in enhancer sequences or the proteins that interact with them can lead to abnormal gene expression, resulting in progress of diseases.

One important area of enhancers in disease is their involvement in cancer. Alterations in enhancer activity can lead to the abnormal activation or repression of genes involved in cell growth, proliferation and survival. These changes can contribute to the development and progression of cancer. Oncogenes, which are genes that promote cancer growth, can be activated by enhancer mutations or changes in the binding of transcription factors[84,85]. The first reported case of oncogene mis-regulation as a result of enhancer dysfunction is the overexpression of *c-MYC* caused by its relocation to the enhancer region of the immunoglobulin heavy chain (*IGH*) locus in Burkitt lymphoma cells[86-89]. Conversely,

tumor suppressor genes, which normally prevent uncontrolled cell growth, can be silenced or repressed due to disruptions in enhancer function[85]. For example, disruption of the super-enhancer of tumor suppressor gene *RCAN1.4* can promote the malignancy of breast carcinoma[90]. Deletion of *RCAN1.4-SE^{distal}*, which was enriched for consensus sequences of transcription factor RUNX3, decreased RCAN1.4 expression by over 90%[90].

Beyond cancer, enhancers have been involved in various other diseases. In neurodevelopmental disorders, enhancer dysregulation can have profound effects on brain development and function. For example, a point mutation of *SHH* Brain Enhancer 2 (SBE2) was identified as disease-causing mutation for Holoprosencephaly, a neurodevelopmental disorder characterized by craniofacial malformations[91]. SBE2 is located 460kb away from the *SHH*. The point mutation disrupts the SIX3 binding site, therefore resulting in the reduction of *SHH* expression at forebrain[91].

Genome-wide association studies (GWAS) have identified genetic variants that associate with various cardiovascular diseases[92-95]. Several variants associated with enhancers have been functionally validated. For example, rs12190287, a variant located within a *TCF21* enhancer, increases risks for coronary artery disease by altering histone modification and AP1 factor binding underlying normal *TCF21* expression [96]. rs6801957, located in a human-mouse conserved enhancer of *SCN5A,* reduces the enhancer activity in the cardiac conduct system through disrupting the binding of TBX/TBX5, core regulators of [insert cardiovascular cell type][97,98].

Additionally, enhancer dysfunction is relevant in autoimmune disorders, where aberrant immune responses occur. Studies have shown that more autoimmune disease-susceptible SNPs locate in immunocompetent cell-specific super enhancers than in protein-

coding regions[99,100]. Hyperactivity or failure of super enhancers in gene clusters encoding cytokine receptors and cytokines in T cells may lead to the pathogenesis of a set of autoimmune diseases like rheumatoid arthritis[99,101] and systemic lupus erythematosus[102-104].

Furthermore, metabolic disorders such as obesity and type 2 diabetes have been associated with enhancer dysregulation. Two enhancers of *Fto* gene have been discovered in mice that are correlated with transmission of obesity due to the exposure of pregnant mice to bisphenol A[105]. Sequence variants associated with type 2 diabetes and fasting glycemia have been discovered to be enriched in the clustered islet enhancers that form physical three-dimensional chromatin domains[106].

Overall, enhancers have a significant relationship with disease by influencing gene expression patterns. The examples provided highlight the diverse impact of enhancer dysregulation across various diseases, emphasizing the importance of understanding enhancer function in disease contexts. Alterations in enhancer activity or mutations within enhancer sequences can contribute to the development and progression of various diseases, including cancer, neurodevelopmental disorders, cardiovascular diseases, autoimmune disorders, and metabolic disorders. Unraveling the role of enhancers in disease pathology can shed light on underlying mechanisms and offer potential avenues for therapeutic interventions. Targeting disease-associated enhancers or the proteins that regulate them holds promise for restoring normal gene expression patterns and mitigating the impact of dysregulated gene networks, especially with gene editing tools like CRISPR[107].

The development of enhancer discovery methods

It has been over 40 years since the initial discovery of the enhancer element from the 72bp repeat of the SV40 viral sequence. This element plays a regulatory role in the β-globin gene expression in an orientation-independent and distance-independent manner[60]. The evolution of enhancer discovery methods has undergone several generations of development, progressing from transgenic reporter techniques to next generation sequencing-based methods, and most recently, the CRISPR-based system. Generally, the enhancer discovery methodology has followed four major developmental trends: from transgenic reporter to endogenous context, from low throughput to high throughput, from descriptive readout to functional readout and from pooled screen to single-cell resolution (**Fig.6**).

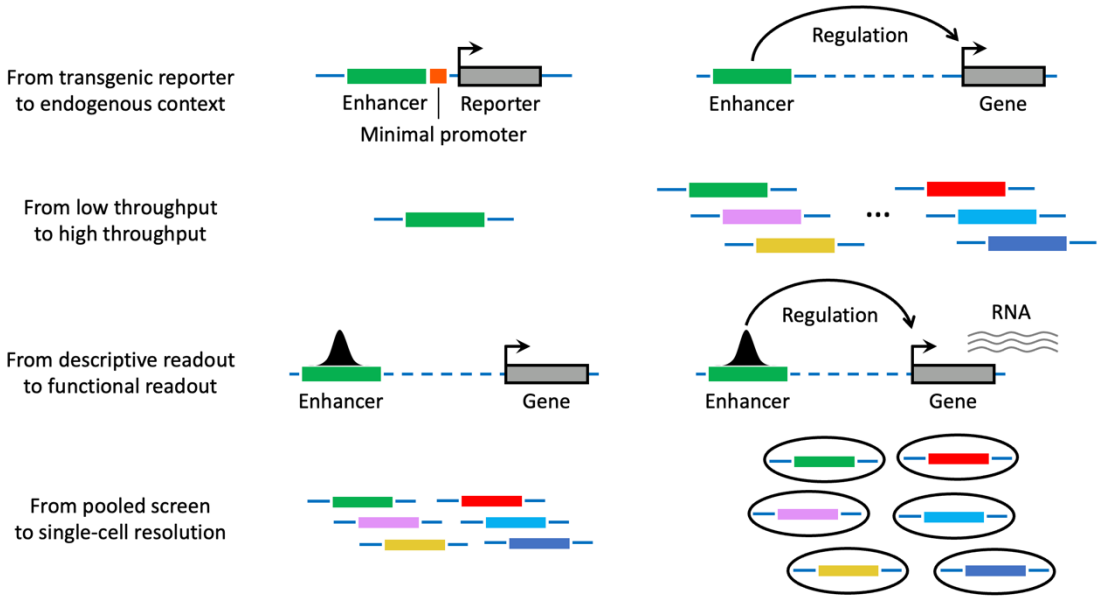

Figure 6. The development of enhancer discovery methods. The enhancer discovery methodology has four major developmental trends: from transgenic reporter to endogenous context, from low throughput to high throughput, from descriptive readout to functional readout and from pooled screen to single-cell resolution.

Transgenic reporter assay

A transgenic reporter assay is a widely recognized experimental technique in molecular biology and genetics used to evaluate enhancer activity and predictions[108]. The setup of an enhancer-reporter in a transgenic reporter assay usually involves linking an

enhancer DNA sequence to a minimal promoter, followed by a reporter gene (**Fig.6**). The reporter gene is carefully chosen for its easily measurable activity, which allows for simple detection and quantification. Commonly employed reporter genes include β-galactosidase (LacZ), green fluorescent protein (GFP), luciferase, and alkaline phosphatase[109]. The reporter can provide a direct readout of the enhancer activity in an *in vivo* based system, like mice, zebrafish, *C. elegans*. The reporter enables assessment of enhancer activity through either transient expression or constitutive expression after random integration into the genome . The spatiotemporal expression pattern of the reporter gene can be further evaluated using microscopy, staining, and other methods. However, it's important to note that this method lacks endogenous context and is mostly used for assessing the sufficiency of the enhancer function in a low throughput manner. To expand the usage of the transgenic reporter assay, other strategies have been developed, including enhancer-trap-based methods[110-112] and site-specific integration strategies[113,114]. These approaches aim to enhance the versatility and applications of the transgenic reporter assay.

Cre/loxP mediated enhancer knockout

Cre/loxP-mediated enhancer knockout is a robust genetic technique utilized to investigate the role of specific enhancer *in vivo*. This technique involves employing Cre recombinase and loxP sites to selectively remove enhancer regions in the genome. Cre recombinase is one of the tyrosine site-specific recombinases (T-SSRs) with a molecular weight of 38 kDa, produced from cre (cyclization recombinase) gene of bacteriophage P1[115-120]. It recognizes a 34 bp DNA fragment known as the loxP (locus of x-over, P1) site and facilitates the deletion of DNA sequences between two loxP sites[121] (**Fig.7**). The

Cre/loxP system allows specific deletion of enhancers in their endogenous context, enabling the assessment of the enhancer's necessity. However, establishing the Cre/loxP system in testing models like mice requires locus-specific targeting, making it challenging to perform enhancer deletions in high throughput manners *in vivo*. Despite this limitation, many optimizations have been developed to expand the usage of the Cre/loxP system. These include the inducible Cre/loxP system[115,120,122-126], tissue-specific promoters of Cre lines[127] and combining it with transgenic reporter assay[113,114].

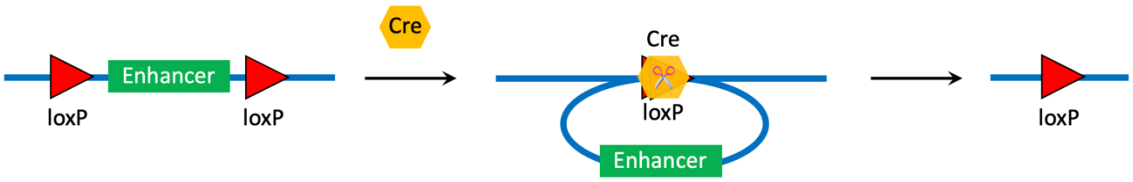

Figure 7. Cre/loxP-mediated enhancer deletion. Two loxP sites need to be inserted at both 5' and 3' of the target enhancer. When the Cre recombinase is expressed in the cell, it will delete the DNA sequences between the two loxP sites. One loxP site will remain in the genome as a scar.

Next generation sequencing-based chromatin features profiling

With the advancement of various next generation sequencing (NGS)-based techniques, high-throughput profiling of chromatin features has become more accessible and informative. Here, I will introduce three types of technologies frequently used for profiling enhancer chromatin features: DNase-seq/ATAC-seq for chromatin accessibility, ChIP-seq for protein-DNA interactions and chromatin conformation capture for DNA-DNA interactions.

1. DNase-seq/ATAC-seq for chromatin accessibility

Chromatin accessibility refers to the ability of chromatin to interact physically with macromolecules, such as proteins[128]. This interaction is influenced by the occupancy and topological arrangement of nucleosomes and other chromatin-binding factors[128]. Nucleosome organization varies significantly across the genome. In regions of

heterochromatin, nucleosomes are densely packed, limiting the binding of TFs to DNA. On the other hand, in active regulatory regions like enhancers, insulators, and transcribed gene bodies, histones are depleted, making the chromatin more accessible to TFs, RNA polymerase, and other DNA binding factors[129,130]. As a result, measuring chromatin accessibility has become a powerful approach for identifying enhancers and other types of CREs[131].

Taking advantage of the fact that open chromatin allows access to proteins, several technologies have been developed to measure genome-wide chromatin accessibility, including Deoxyribonuclease I hypersensitive site sequencing (DNase-seq)[132,133], Assay for transposase-accessible chromatin using sequencing (ATAC-seq)[134], Micrococcal nuclease sequencing (MNase-seq)[135] and Nucleosome occupancy and methylome sequencing (NOMe-seq)[136].

DNase I is an endonuclease that can selectively digest nucleosome-depleted DNA, whereas DNA wrapped in nucleosomes or tight compacted chromatin regions is not sensitive to DNase I. Therefore, the regions showing elevated DNase I cleavage are called DNase I hypersensitive sites (DHS). Utilizing this feature, the first genome-scale chromatin accessibility measured by DNase I has been reported with microarrays as readout[137]. Later, this workflow was adapted to the NGS platform for DNase-seq[132,133](**Fig.8a**). Cells were first treated with DNase I. Then cells were lysed and DNA of ideal size for sequencing was harvested using a second restriction enzyme cutting[132] or direct size selection[133]. The isolated DNA was then subjected to library preparation for Illumina sequencing.

ATAC-seq, similar to DNase-seq, employs a hyperactive Tn5 transposase to mark accessible chromatin regions and insert Illumina sequencing adaptors

simultaneously[134](**Fig.8b**). Due to Tn5's high efficiency in adaptor insertion and the combination of DNA fragmentation and adaptor insertion, highly complex ATAC-seq libraries can be generated using as few as 500 cells[134,138], but usually 10,000-20,000 cells in ~2h. In comparison, DNase-seq protocols need multiple days with thousands to millions of cells. Nonetheless, both DNase-seq and ATAC-seq methods yield similar regulatory information[138,139].

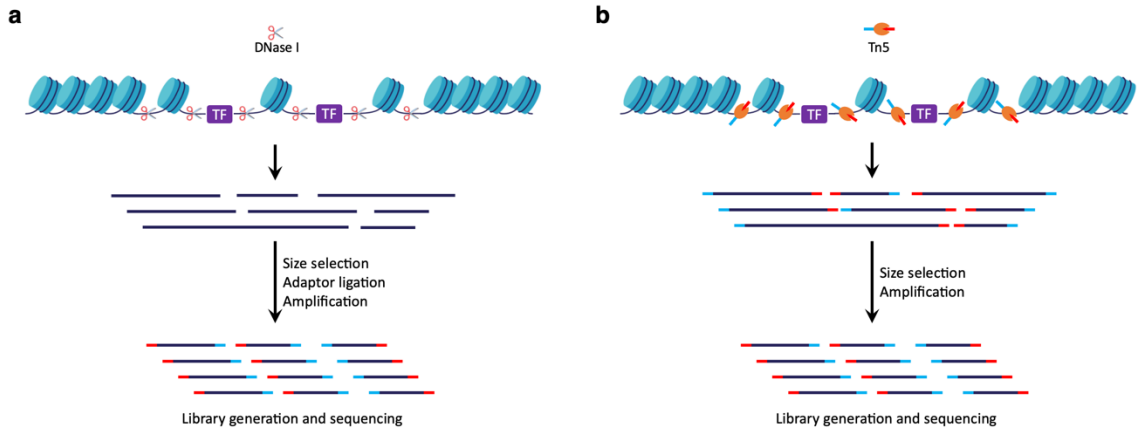

Figure 8. DNase-seq and ATAC-seq for measuring chromatin accessibility. a. The scheme of DNase-seq workflow. Chromatin were digested by DNase I based on the accessibility to the enzyme. Fragmented DNA went through size selection, adaptor ligation and amplification to generate library for Illumina sequencing. **b.** The scheme of ATAC-seq workflow. Chromatin were digested by Tn5 based on the accessibility to the enzyme. Tn5 can add the Illumina sequencing adaptors to the fragmented DNA at the same time. Fragmented DNA went through size selection and amplification to generate library for Illumina sequencing (Plots are partially generated by using biorender).

Other methods, such as Micrococcal nuclease sequencing (MNase-seq) and Nucleosome occupancy and methylome sequencing (NOMe-seq), are also adapted for chromatin accessibility measurement, providing additional information through different DNA fragmentation mechanisms. For example, MNase-seq is widely used to isolate fragments spanning single nucleosomes due to MNase's endonuclease and exonuclease activity[140-142], while NOMe-seq can capture both accessibility and methylation status of DNA[136].

In summary, due to the association between enhancers and open chromatin regions, where the DNA is more accessible to transcription factors and other regulatory proteins,

the accessibility of the chromatin has been widely used for enhancer prediction and description[49,143].

2. ChIP-seq for protein-DNA interaction

ChIP-seq, an abbreviation of Chromatin immuno-precipitation sequencing, is a well-developed method for genome-wide profiling of protein-DNA interactions and epigenetic marks[144]. The general workflow involves the initial fixation of cells to stabilize the DNA-protein/histone complexes. Subsequently, the cells are lysed, and DNA is fragmented using various methods. Specific antibodies, capable of recognizing the protein of interest or specific histone modifications, are added to immune-precipitate the complexes that contain the DNA fragments bound by the proteins or histones. Following this, proteins are digested using proteinases, leaving the naked DNA available for amplification and library preparation for sequencing (**Fig.9**).

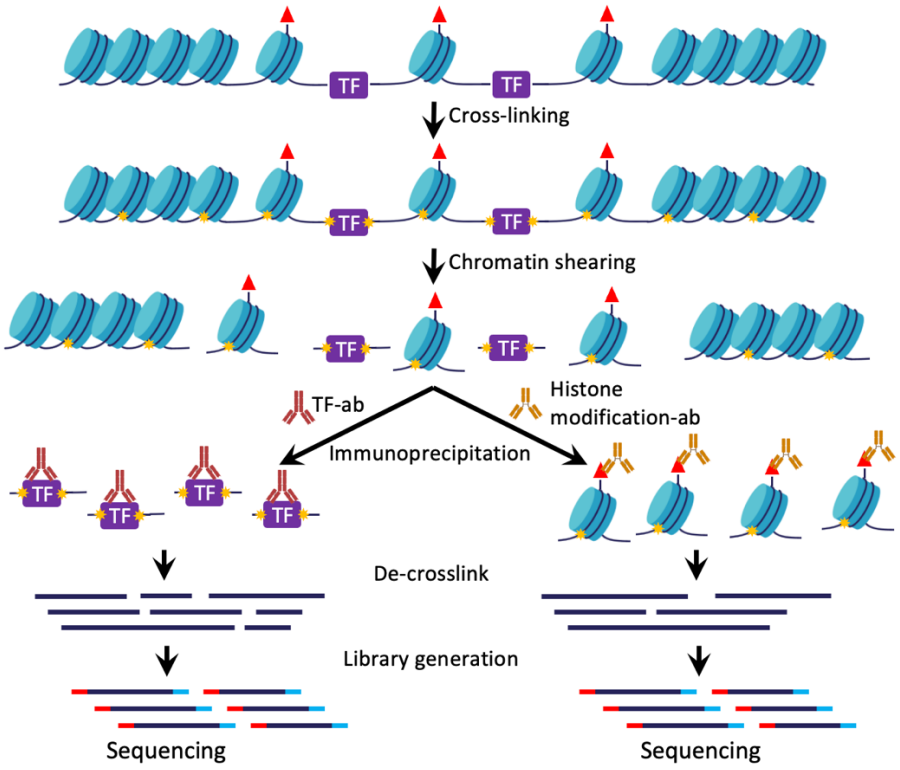

Figure 9. The scheme of ChIP-seq workflow. DNA-protein complexes were stabilized by cross-linking. After fixation, chromatin was sheared and incubated with antibody recognizing specific TFs or histone modifications. After immunoprecipitation, DNA-protein complexes were de-crosslinked, leaving the naked DNA alone for amplification and library preparation for sequencing. Ab: antibody. (Plots are partially generated by using biorender).

As the binding of TFs is essential for enhancers to carry out their regulatory function, precise mapping of TF binding sites across the genome is pivotal to predict enhancers and dissect the gene regulatory network[145]. With the help of ChIP-seq, certain histone modifications, like H3K4me1 and H3K27ac, have been discovered to be well associated with enhancer function[50-54]. The effective utilization of ChIP-seq enables genome-wide profiling and prediction of enhancers in different cell types and developmental stages. To generate high-quality ChIP-seq data, several factors require careful consideration: 1) Antibody quality. The quality of antibodies is a common concern in experiments that require their use. Antibodies with high sensitivity and specificity can increase the signal-to-noise ratio in ChIP-seq experiments, improve downstream peak calling, and avoid non-specific binding events[144]. Antibodies used in ChIP-seq experiments should be validated through techniques like western blotting or other protein detection experiments. 2) Sample quantity and quality. A typical ChIP-seq experiment requires approximately 10^7 cells to generate sufficient DNA for library preparation. While optimized protocols have reduced the cell number to ~10^3 cells in certain contexts[146], maintaining an adequate cell quantity as input material remains crucial for successful ChIP-seq experiments. Additionally, the quality of samples is as important as other protein-based experiments. The addition of protease inhibitors, phosphatase inhibitors, and the maintenance of low temperatures throughout the process are essential to prevent protein degradation and changes in phosphorylation status. 3) Experimental controls. Various factors, including antibody specificity, DNA fragmentation bias, and other procedural steps, can introduce systematic errors in ChIP-seq results[144]. Therefore, control experiments are necessary for accurate

peak calling and quantification in downstream analyses. “Input DNA control” and “non-specific control” are two commonly used experiment controls. The previous one utilizes DNA from the cell lysate directly without immunoprecipitation, while the later uses the IgG as a control antibody for immunoprecipitation. Both controls help reduce biases caused by uneven DNA sharing, PCR amplification, antibody specificity, and other procedural steps[147].

In summary, ChIP-seq has widespread applications in genomics and epigenetics research, enabling researchers to study transcriptional regulation, histone modifications, enhancer characterization, and the dynamics of protein-DNA interactions.

3. Chromatin conformation capture for investigating DNA-DNA interaction

Enhancer-promoter spatial proximity plays a crucial role in the regulation of target gene expression. Assessing this proximity is an important step in profiling and predicting enhancers, particularly in assigning enhancer-promoter pairs[148-152]. Chromatin conformation capture (3C)-based technologies[153] have made it feasible to measure genome-wide DNA-DNA interactions[154].

The fundamental principle underlying 3C-based technologies is the direct interaction between chromatin regions and proteins. By crosslinking the DNA-protein-DNA complexes through various methods, the interactions are fixed[153,155]. Subsequently, chromatins are digested with restriction enzymes to remove spatially distal DNA regions. The remaining spatially proximal regions, connected by proteins, are then ligated to form a single fusion DNA fragment. Through sequencing this newly generated fusion DNA and aligning it with the original genome positions, interactions between regions can be

assessed[156,157](**Fig.10a**). These 3C-based technologies can be categorized based on the scale of inspected regions: 3C for assessing the interaction between one region vs another region (one-vs-one), 4C for one-vs-all, 5C for many-vs-many and Hi-C for all-vs-all (**Fig.10b**). For individual enhancer-promoter interaction interrogation, 3C and 4C are the most frequently used methods, while Hi-C is required for genome-wide DNA-DNA interaction analysis.

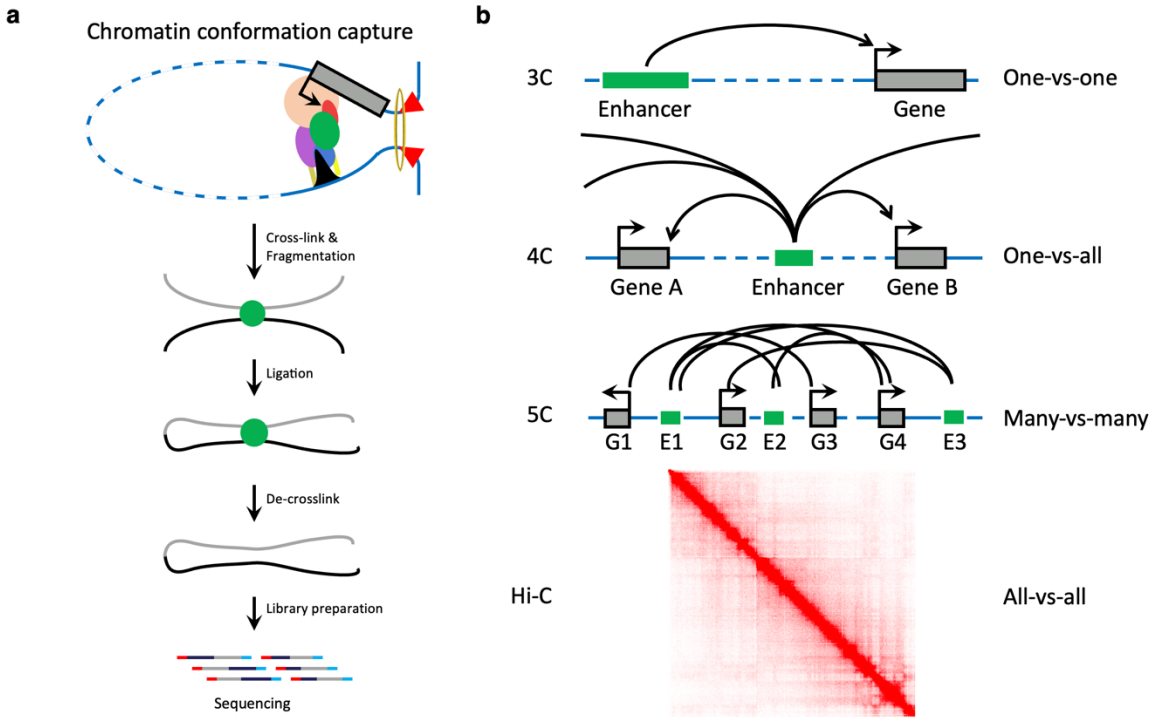

Figure 10. Chromatin conformation capture for DNA-DNA interaction. a. The scheme of 3C-based chromatin conformation capture technology workflow. DNA conformations, including DNA loop structures, were stabilized by cross-linking. After fixation, chromatin was fragmented using restriction enzymes. Fragmented DNA with interactions were ligated to form 3C library. DNA-protein-DNA complexes were de-crosslinked and naked DNA were used for library preparation and sequencing. **b.** categories of 3C-based chromatin conformation capture technologies. The 3C-based technologies can be divided into different categories based on the scale of inspected regions. 3C for one-vs-one, 4C for one-vs-all, 5C for many-vs-many and Hi-C for all-vs-all.

Analysis of DNA-DNA interactions generated by Hi-C has identified several features of chromatin conformation at different resolution: 1) At the megabase level, spatial compartmentalization of chromatin can be separated into two categories based on interaction activity, A-type domains with active and open chromatin and B-type domains

with inactive and more closed chromatin[158]. 2) At the 0.1-1 megabsae level, topologically associating domains (TADs) have been described as chromatin regions that more frequently interact within themselves than among other TADs[159-162]. CTCF sites usually serve as boundaries between different TADs[163]. The TADs structure has been shown to be consistent with the Cohesin-mediated loop extrusion model[21-28,55-58], which can be measured through other technologies, like Cohesin Chromatin interaction analysis by paired-end tag sequencing (ChIA-PET)[164] or CTCF ChIP-seq with computational modeling[165].

To improve the mapping resolution in Hi-C, the 6-base cutter HindIII[158] in earlier protocols has been replaced with DpnII or NlaIII, 4-base cutters that generate fragments in the hundred bases range, thus increasing the resolution to kilobases[24]. For even higher resolution, the newly optimized Micro-C leverages the endonuclease and exonuclease activity of MNase used in MNase-seq[140-142] to digest chromatin and reaches to single nucleosome resolution[166-168]. Besides the enzyme choice, cross-linking conditions and sequencing depth significantly affect the detection of interactions and looping structures [157]. One of the limitations of the conventional Hi-C technology is that it requires several billions of reads to reach 5-10kb resolution[24,158,169], a prohibiting expense despite the continuously decreasing sequencing cost. However, the recently developed chromatin conformation capture technology named Hi-C on accessible regulatory DNA (HiCAR) can achieve 5 kb resolution using less than 10% of the sequencing depth used in Hi-C[170]. HiCAR employs Tn5 for DNA fragmentation and adaptor insertion[170], similar to ATAC-seq[134].

In summary, chromatin conformation capture technologies, such as Hi-C, Micro-C and HiCAR have become valuable tools for studying the spatial organization of the genome and its influence on gene expression and other biological processes. The chromatin interactions measured by these technologies further enable the comprehensive profiling and precise prediction of enhancer-promoter pairs.

Functional enhancer screening

Next generation sequencing-based methods for profiling chromatin features can offer a comprehensive mapping of enhancers. These features include chromatin accessibility, TF binding, histone modifications, and DNA-DNA interactions, all with high accuracy, endogenous context, and genome-wide scale. However, it is important to note that these measurements primarily describe enhancer features rather than functionally validate their activity. To identify enhancers across the 3-billion-nucleotide human genome in different cell types, it becomes essential to perform functional screen using transcriptional readout. This process aids better enhancer identification and the construction of gene regulatory networks. Here, I focus on STARR-seq, CRISPR-based systems and perturb-seq as examples to illustrate how transcriptional readout is utilized for functional enhancer screens.

1. STARR-seq

STARR-seq, or Self-transcribing active regulatory region sequencing, was initially introduced in 2013 by the Stark lab to quantitatively measure enhancer activity throughout the genome in cells[171]. STARR-seq was developed based on the principle of a transgenic

reporter assay but incorporated NGS technology, enabling a high-throughput evaluation of enhancer activity[171,172]. Unlike the traditional transgenic reporter assay, where enhancers were typically cloned upstream of minimal promoters, the STARR-seq system placed the enhancers downstream of the GFP reporter but before the polyA signal (**Fig.6** and **Fig.11**). Consequently, the transcripts of the reporter gene contained the enhancer sequence, facilitating quantification using NGS platforms (**Fig.11**). This design allowed thousands of putative enhancers to be cloned and tested simultaneously. To refine the assessment of different enhancer strengths, fluorescence-activated cell sorting (FACS) can be utilized, enabling the segmentation of cells based on GFP intensity. However, similar to the traditional transgenic reporter assay, enhancers tested with this system lacked the endogenous context crucial for understanding development and disease progression *in vivo*[173].

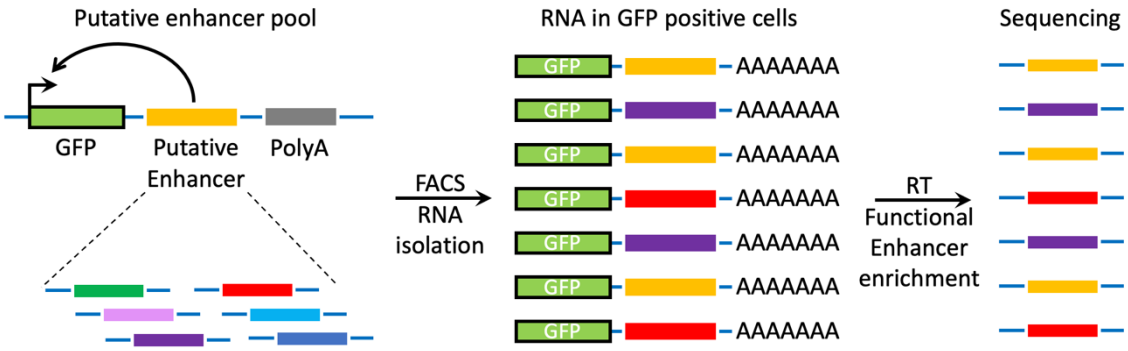

Figure 11. The scheme of STARR-seq workflow. Putative enhancers were cloned to the 5' of GFP but before the PolyA to generate putative enhancer plasmid library. Plasmid library then transfected to cells with various ways. GFP positive cells were harvested for RNA isolation. After reverse transcription (RT), enhancers that can functionally drive GFP expression were amplified from the cDNA to generate library for sequencing.

Despite being one of the first methods to enable quantitative, high-throughput functional testing of enhancers, STARR-seq still holds great potential for broader applications. Nevertheless, this potential was significantly impacted by the emergence of the CRISPR/Cas system in the same year[174,175].

2. CRISPR/Cas system

CRISPR, standing for Clustered Regularly Interspaced Short Palindromic Repeats, were initially observed in *E.coli*[176] and later identified in more than 40% of sequenced bacteria and 90% of archaea[177]. Before becoming widely used genome editing tools, the CRISPR system was first recognized as a defense mechanism in these microorganisms, enabling them to memorize and identify specific viral or foreign DNA sequences and mount an immune response upon subsequent encounters[178-181]. This immune response involves the utilization of CRISPR-associated (Cas) proteins and CRISPR RNAs (crRNA). The CRISPR repeat clusters were found to be separated by non-repeating DNA sequences called spacers[178]. In bacteria, these spacers can be transcribed into short crRNA to guide the activity of Cas enzymes, which are nucleases that can cleave and deactivate foreign DNA, thereby blocking horizontal DNA transfer from bacterial plasmids[182,183]. Following these discoveries, several critical findings about the mechanism of the CRISPR system led to the development of the CRISPR genome-editing technology: 1) The discovery of protospacer-adjacent motifs (PAMs). PAMs were first identified and characterized in the *S. thermophilus* during the early stages of CRISPR research[184]. Highly similar sequences were observed near the spacer sequences[184], which were named protospacer-adjacent motifs. The term "protospacer" refers to the specific DNA sequence guiding the cleavage by the CRISPR-Cas system, while "adjacent motif" refers to the short DNA sequence immediately neighboring the protospacer. Different CRISPR-Cas systems have distinct PAM sequences that they recognize. For example, the commonly used Cas9 from *S. thermophilus* (SpCas9) requires a PAM with the sequence "NGG" to function

effectively[174,175,185,186]. 2) The discovery of Cas9. Cas9 was the only one with DNA catalytic activity among many Cas proteins in *S. thermophilus*[187]. Biochemist Jennifer Doudna and her research team at the University of California, Berkeley, collaborated with microbiologist Emmanuelle Charpentier, who was then working at Umeå University in Sweden together demonstrated that the CRISPR-associated protein Cas9 was a dual-RNA-guided DNA endonuclease and could be programmed to target and cleave specific DNA sequences in prokaryotes[185,188]. 3) The fusion of tracrRNA and crRNA to generate sgRNA. In addition to understanding Cas9's working mechanism, Doudna and Charpentier's groups showed in their paper that Cas9 DNA endonuclease activity can be guided using a fused RNA called guide RNA (gRNA), which fuses the two short RNAs, the crRNA and a *trans*-activating crRNA (tracrRNA),[185] required by the endogenous CRISPR system. This optimization simplifies the process for programming and synthesis of the gRNA. 3) The adaptation of CRISPR/Cas from prokaryotes to eukaryotes. In 2013, one year after Doudna and Charpentier's groundbreaking work was published, several groups demonstrated that the CRISPR/Cas9 system could be adapted for *in vivo* genome editing in eukaryotic cells[174,175,186]. Compared to previous generations of genome-editing tools, like Zinc finger nuclease (ZFN)[189,190] and transcription activator-like effector nuclease (TALEN)[191-194], the CRISPR/Cas9 system provides a more flexible and easier genome-editing strategy with simple design for different gRNAs targeting nearly all genome regions[195].

With the evolution of prokaryotes, different CRISPR/Cas systems have been developed for various mechanisms of immune responses. The differences include PAM sequences, nuclease activities and target substrates. SpCas9 is the most widely used CRISPR/Cas system with NGG as PAM sequence and 3 bp 5′ of PAM as DNA cleavage

site[185,196] (**Fig.12**). Many other versions of Cas9 from different bacterial species have been identified with variable PAM sequences recognition: FnCas9 recognizes NGG[197], SaCas9 recognizes NNGRRT[198], NmCas9 recognizes NNNNGATT[199], St1Cas9 recognizes NNAGAAW[174,196], St3Cas9 recognizes NGGNG[174,196] and CjCas9 recognizes NNNNACAC[200]. They all cut DNA at 3 bp 5′ of PAM[174,196-200]. Another class of CRISPR/Cas system is Cas12a (formerly known as Cpf1). Two versions of Cas12a have been discoved from *Acidaminococcus sp* and *Lachnospiraceae bacterium*, respectivly, and are named AsCpf1 and LbCpf1 with TTTV as PAM sequence[201,202]. Besides the difference between the PAM sequences, there are several other differences between Cas9 and Cas12a (**Fig.12**): 1) Protospacer is at the 5' of Cas9 gRNA, while it is at the 3' of the Cas12a crRNA. 2) The DNA cleavage site of Cas12a is at the 19/24 bp 3′ of PAM. 3) Besides the ability to cleave DNA, Cas12a can also cut its premature crRNA tandem at the direct repeats between different protospacers[203]. This function gives Cas12a great potential for editing multiple genome regions in the same cells. So far, the substrate of all the Cas enzymes is DNA. However, there is a special type of Cas enzyme, Cas13, that has been reported to cut RNA instead of DNA[204]. In summary, these distinct PAM recognition sequences, nuclease activities, and target substrates expand the CRISPR toolbox with additional Cas enzymes for genome editing.

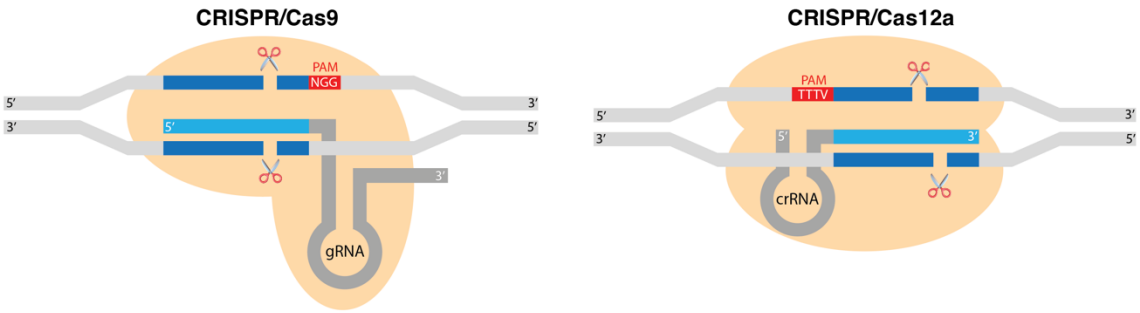

Figure 12. The comparison between CRISPR/Cas9 and CRISPR/Cas12a. Protospacer (Cyan bar) is at the 5' of Cas9 gRNA, while it is at the 3' of the Cas12a crRNA. For Cas9, the PAM sequence is "NGG" at the 3' of protospacer, while for Cas12a, the PAM sequence is "TTTV" at the 5' of protospacer. The DNA cleavage site of Cas9 is at 3 bp 5′ of PAM, while the DNA cleavage site of Cas12a is at the 19/24 bp 3′ of PAM.

Utilizing the nuclease activity of CRISPR/Cas9 and endogenous DNA repair mechanisms (nonhomologous end joining (NHEJ) or homology-directed repair (HDR)) in mammalian cells is becoming a highly efficient tool for genome editing[195]. The crystal structure of Cas9 further illustrates that its DNA cleavage activity is performed by two conserved nuclease catalytic domains: HNH and RuvC[205]. Each of these domains can cleave one DNA strand to generate a double-strand break (DSB) proximal to the PAM sequence at the target site. A single aspartate-to-alanine (D10A) or histidine-to-alanine (H840A) mutation in the RuvC or HNH catalytic domain of Cas9 leads to the loss of DNA cleavage activity of the domain[185,196]. Therefore, Cas9 with D10A or H840A mutation becomes a DNA nickase (Cas9n) to nick DNA with a single-strand break, resulting in a preference for HDR as the DNA repair mechanism to decrease the frequency of indel mutations from off-target DSBs by NHEJ[174]. Mutation of both domains by D10A and H840A results in the complete loss of DNA cleavage activity and generates catalytically inactive dead Cas9 (dCas9)[206]. The loss of DNA cleavage activity in Cas9 does not impact its binding to its target[206], providing the potential to expand the application of the CRISPR/Cas9 system. dCas9 can serve as a DNA binding protein. By connecting different functional domains ("X") to dCas9, the chimeric dCas-X molecules can be delivered to specific loci in the genome to perform assigned functions[207](**Fig.13**). Functional domains may include 1) base editing enzymes, like APOBEC1 deaminase and Uracyl Glycosylase inhibitor (UGI), for base editing[208]; 2) *trans*-effectors, like Kruppel-associated Box (KRAB) or $VP(16)_n$, for gene regulation[209-212]; 3) epigenome remodeling factors, like catalytic domain of DNA methyl transferase (DNMT3A) or histone demethylase LSD1, for

changing DNA methylation and histone modifications[213-216]; 4) protein dimers, like ABI1 and PYL1, for DNA loop formation[217,218]; 5) Fluorescent proteins, like GFP, for chromatin imaging[219]. Here, my focus is on the application of dCas9-X in gene regulation, which offers potential for functional enhancer studies. Generally, gene regulation using dCas9-X can be broadly categorized into two main approaches: CRISPR activation (CRISPRa) to promote active gene expression and CRISPR interference (CRISPRi) to repress gene expression.

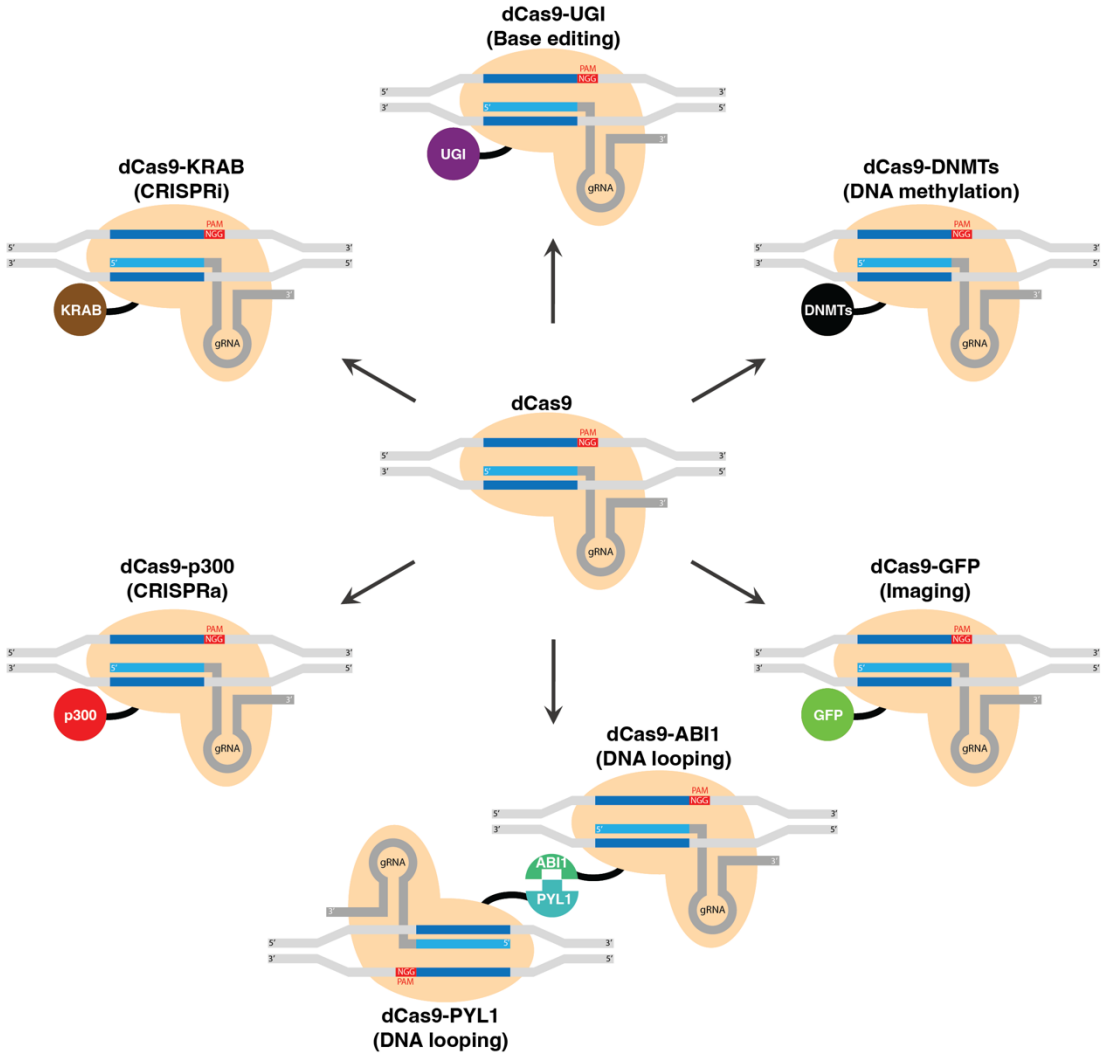

Figure 13. Application of dCas9-X. dCas9 can be fused to different functional domains for different applications. p300 for CRISPRa, KRAB for CRISPRi, UGI for base editing, DNMTs for DNA methylation, GFP for imaging and ABI1&PYL1 for DNA looping (adapted from Brezgin et al.[207]).

CRISPRa is built upon chimeric dCas-X proteins, where X is a domain that has transcriptional activation or can recruit endogenous transcriptional activation domains to regulatory genomic elements and induce target gene transcription[207,220]. In initial studies, dCas9 was fused with 4 tandem copies of a 16-amino-acid-long transactivation domain (VP16) from the Herpes simplex virus[221-223]. Other domains, such as p300[224], p65 or p65 with heatshock factor 1 (HSF1)[209,225] have also undergone testing. The gene activation efficiency of dCas9-VP64 was further enhanced by linking it with p65-Rta, where Rta represents an Epstein–Barr virus transcription factor[226,227]. Apart from linking transcriptional activation domains to dCas9, CRISPRa systems can also utilize affinity-binding assays to simultaneously recruit multiple domains to the target site, resulting in more robust gene activation[228]. Modifications can be introduced into the dCas9 protein, as seen in the SunTag system[229,230], gRNA scaffold, such as the addition of aptamer sequences MS2[231], or both, exemplified by the synergistic activation mediator (SAM)[225,231] and the three-component repurposed technology for enhanced expression (TREE)[232]. CRISPRa systems have been proven valuable in studying and identifying enhancers[224,233]. For instance, Hilton et al. employed dCas9-p300 and gRNA targeting enhancer regions and the promoter of the *MYOD* gene, leading to a significant increase in *MYOD* transcription[224]. However, dCas9-VP64 demonstrated limited ability to activate *MYOD* expression when targeted to enhancer regions[224]. Similar results were also observed at the *OCT4* locus[224]. The varying activation efficiencies of different CRISPRa systems on the same locus indicate that the mechanisms of enhancer activation may differ from those of promoter activation. Therefore, careful consideration and testing of the CRISPRa tool are essential when studying enhancers. One noteworthy aspect is that, like transgenic reporter assays,

CRISPRa can only evaluate the sufficiency of enhancer function. Besides the applications in research, CRISPRa also has therapeutic potential, as it could be used to upregulate the expression of beneficial genes to treat genetic disorders or other diseases caused by gene expression imbalances[234-236].

The CRISPRi system, instead of utilizing transcriptional activation domains, employs transcriptional suppressive domains, such as KRAB or enhancer of Zeste homolog 2 (EZH2), to link to dCas9[237]. When CRE of genes, such as promoters and enhancers, were bound to the dCas9-KRAB, KRAB will recruit histone deacetylases and methyltransferases to remove H3K27ac and add H3K9me3, leading to the formation of heterochromatin and suppressing CREs' function and mRNA transcription[210,238]. By additionally incorporating DNA methylation, like MECP2, into dCas9-KRAB, sustained transcriptional suppression can be achieved[239]. CRISPRi has widespread use in enhancer mapping and functional studies[150,233,240-242]. In comparison to CRISPRa, CRISPRi allows for the assessment of the necessity of enhancer function. Furthermore, when compared to STARR-seq, CRISPRi enables the evaluation of enhancer function in a high-throughput manner, but still within its endogenous context.

In summary, CRISPR technology has been widely employed in studying enhancers and their role in gene regulation. Utilizing WT CRISPR/Cas9-based approaches, researchers can delete, mutate or modify enhancer sequences in the genome, enabling investigation into their impact on gene expression and cellular function. By disrupting or altering enhancers using WT CRISPR/Cas9, scientists can identify the specific enhancers controlling the expression of particular genes, explore the effects of enhancer mutations on cellular phenotypes, and unveil regulatory networks governing complex biological

processes. Additionally, CRISPRa and CRISPRi techniques allow researchers to enhance or suppress the activity of specific enhancers, providing a high throughput way to investigate their functional roles and the consequences of gene expression modifications. Overall, the integration of CRISPR technology with enhancer studies has significantly advanced our comprehension of gene regulation and the intricate networks dictating cellular processes in development and disease.

Introduction to the thesis

Many consortia have made important progress in mapping putative enhancers based on chromatin accessibility and protein binding in a wide range of cell types and tissues [243]. Harnessing the atlas of enhancers predicted from chromatin features, functional interrogation with large-scale CRISPR screens has successfully identified some enhancers with relatively strong impacts on gene expression in various cell lines [150,233,240-242,244-252]. However, comprehensive enhancer discovery remains challenging. In some cases, enhancer perturbation only causes temporary phenotypes [246,247], while in other cases, the effect of enhancer perturbation is mitigated by the activity of "shadow" or redundant enhancers [252-258]. Furthermore, most genetic variants associated with common human diseases show relatively modest effects on expression in reporter assays [259,260]. A critical missing element is a quantitative model for how multiple enhancers work together at each locus to respond to physiological or experimental perturbations in a nonlinear way through altering GRN activity. GRNs control cell states through a handful of core TFs, which both self-regulate and cooperatively regulate each other through core enhancers [49]. Due to this self-regulation and cooperatively regulation, core TFs together form the core circuit of

GRNs and coregulate the downstream peripheral genes through peripheral enhancers. The different regulation patterns and the impact difference between core TFs and peripheral genes suggest different strategies are needed for mapping core enhancers and peripheral enhancers respectively.

First, we focused on deconstructing the core enhancers' activity in the GRN through determining the impact of their perturbation on the cell state. We developed a quantitative GRN model to simulate the dynamic process of core circuit establishment. The results predict that cell states are more susceptible to core enhancer perturbations during dynamic cell state transitions compared to post-transition when the GRN has been established. We utilized guided differentiation of human embryonic stem cells (hESCs) to definitive endoderm (DE) as a dynamic system for a dCas9-KRAB-based CRISPRi screen. The CRISPR library targeted 394 putative enhancers surrounding 10 core TF loci spanning 40 Mbp genomic regions. Using *SOX17* as the DE cell state readout [261], we identified multiple enhancers (4 to 9 per locus) for each of the core DE TFs (*EOMES*, *GATA6*, *MIXL1*, and *SOX17*). This affirms the feasibility of using a single core gene as the readout for discovering functional core enhancers during cell state transitions. The sensitive screening strategy also uncovered 12 enhancers >100 kbp away from the transcription start site (TSS) of the target gene, demonstrating the need for enhancer discovery beyond the immediate linear neighborhood. The relatively comprehensive discovery of functional enhancers allowed us to develop a CTCF loop-constrained Interaction Activity (CIA) model that outperformed previous Hi-C contact-based enhancer prediction methods [150,262-264].

Next, we focused on mapping the peripheral enhancers during ESC-DE cell state transition. Unlike the tight connection between core TFs, by definition, there are much less

crosstalk between different peripheral genes. Therefore, to map peripheral enhancers of multiple peripheral genes, each peripheral gene needs its own transcriptional readout. We selected 10614 putative peripheral enhancers flanking 860 DE peripheral genes with 3-4 gRNAs/region for the dCas9-KRAB perturbation. Utilizing the scRNA-seq-based perturb-seq with high multiplicity of infection (MOI) strategies, we harvested more than 200K cells and reached a representation of 200 cells/putative peripheral enhancer. In total, we identified more than 300 regions (including ~100 promoters and ~200 enhancers), perturbing which will significantly decrease target gene expression.

Our network-guided core enhancer mapping strategy, high MOI perturb-seq strategy for peripheral enhancer screen during cell state transitions and the CIA model provide a framework for systematic enhancer discovery in the GRNs applicable not only to normal development but also to pathological conditions such as diabetes and cancer.

MATERIALS AND METHODS

Cell lines and culture conditions

iCas9 *SOX17*$^{eGFP/+}$ HUES8 and idCas9-KRAB *SOX17*$^{eGFP/+}$ HUES8 hESCs were cultured on vitronectin-coated (Gibco; A14700) plates and maintained in E8 medium (Gibco; A1517001). Cells were dissociated by 3-5 mins treatment with 0.5 mM EDTA in 1X DPBS without calcium and magnesium at room temperature. 10 μM ROCK inhibitor Y-27632 (Selleck Chemicals; S1049) was added into E8 medium for the first 24h after passage. Medium was changed every day. hESCs were passaged every 3-4 days depending on the cell growth speed and confluency. All cell lines were routinely tested by Memorial Sloan Kettering Cancer Center (MSKCC) Antibody & Bioresource Core Facility to confirm there was no mycoplasma contamination and by MSKCC Molecular Cytogenetics Core to confirm there were no karyotyping abnormalities. Experiments with hESCs were conducted per NIH guidelines and approved by the Tri-SCI Embryonic Stem Cell Research Oversight (ESCRO) Committee.

hESC definitive endoderm differentiation

We found that DE differentiation is more robust when using hESCs during the logarithmic growth phase. To optimize the differentiation, cells were maintained in the logarithmic phase before seeding for DE differentiation with a recovery passage as follows. Please note that the cell numbers described below were optimized based on the growth of the HUES8 hESCs in our laboratory, and they may need to be adjusted for other hESC lines. hESCs were dissociated with 1X TrypLE Select (Gibco; 12563029) for 3 mins at room temperature. Then TrypLE was removed, and cells were washed and resuspended

into E8 medium with 10 μM ROCK inhibitor Y-27632. Cells were counted by using Vi-CELL XR Cell Viability Analyzer (Beckman Coulter), and 2-3 million cells were seeded per 10-cm plate with E8 medium containing 10 μM ROCK inhibitor Y-27632. The E8 medium was refreshed daily, and the cell number should reach 10-12 million per 10-cm plate 2 days after seeding. hESCs after the recovery passage were collected and counted again as described above and 1 million cells per well were seeded in a 6-well plate in E8 medium with 10 μM ROCK inhibitor Y-27632; and 18h later, hESCs were changed into fresh E8 medium. At 24h after seeding, hESCs should reach 2-2.4 million per well, and be ready for differentiation. For DE differentiation, hESCs were first washed with 1X DPBS once and then cultured in 2.5 ml S1/2 differentiation medium daily as previously described [261,265]: cells were treated with 50 ng/ml Activin A (Bon-Opus Biosciences; C687-1mg) for three days, and 5 μM CHIR99021 (TOCRIS; 4423) for the first day.

scRNA-seq and analysis

scRNA-seq was performed as previously described [266]. Cells were harvested every 12h during DE differentiation for scRNA-seq experiments with targeted collection ranging from 3000 to 6000 cells. Single-cell 3′ RNA-seq libraries were generated with 10x Genomics Chromium Single Cell 3′ Reagent Kit v.3 following the manufacturer's guidelines. The libraries were sequenced on NovaSeq 6000 platform following the manufacturer's guidelines.

Chromium v3 analysis software Cell Ranger (Version 3.1.0) was run using "cellranger count –expect-cells 1000". Genes with fewer than 10 reads summed over all cells were removed, yielding 21099 transcripts detected across 35988 cells, approximately

5000 cells per time point. The cells ranked in the bottom 10% of total transcript number per cell were removed from further analysis. For PCA we further restricted analysis to transcripts whose standard deviation across the 7 time points was greater than 0.2.

Per best practices of Seurat package [267], the quality control of cells included the number of features found in a cell and the percentage of tags mapped to the mitochondrial chromosome. Each sample was filtered according to the following criteria:

	ESC	DE-12h	DE-24h	DE-36h	DE-48h	DE-60h	DE-72h
Number of features (K)	1-4	1.5-5	1.8-5	2-5	1.5-4	1.8-5	2-6
Mitochondrial (%)	5-20	5-25	5-20	5-20	5-15	5-20	0-20

The data slot in the assay of the Seurat object, equivalent for the scaled expression of genes in cells, was used for gene-wise visualization by UMAP. For selecting the relevant expressed genes, each gene was applied a filter where the percentage of nonzero expression in cells was at least 55 percent at any time point. We focused on relevant expressed genes by removing mitochondrial, ribosomal, miRNAs, lincRNAs, antisense transcripts, and genes that were not yet named (e.g., those containing orf and starting with AC or AL). The matrix from the 2606 relevant expressed genes, after transposition for gene-centric embedding, was embedded in UMAP using the R package umap, using the Pearson correlation as the distance metric of umap.config. Each point was labeled with the color scale defined from the expression fold change from ES to DE-72 hr.

Dynamic Gene Regulatory Network Model

The network state in our GRN model is described by a vector of core TF concentrations $\psi = (\psi_1, \psi_2, \dots, \psi_n) = (\psi_{i=1..n})$. For example, a network with three genes

and $\psi = (A, B, C)$ is shown in Fig.1a. Each component TF gene i is described by an equation similar to Eq (1):

$$\frac{d\psi_i}{dt} = -r_i\psi_i + \frac{e_{i1}\left(c_i f_i(\psi_{i=1.n}) + \delta_i(t)\right)}{b_i + c_i f_i(\psi_{i=1.n}) + \delta_i(t)} + \frac{e_{i0} b_i}{b_i + c_i f_i(\psi_{i=1.n}) + \delta_i(t)} + \xi(t)\psi_i.$$

The activation probabilities for gene i are $p_{on} \sim c_i f(\psi_{i=1.n}) + \delta_i(t)$ and $p_{off} \sim b_i$, so together the probability that gene i is activated and transcribed at rate e_{i1} is $\frac{(c_i f_i(\psi_{i=1.n}) + \delta_i(t))}{b_i + c_i f(\psi_{i=1.n}) + \delta_i(t)}$, and the probability that gene i is transcribed at basal rate e_{i0} is $\frac{b_i}{b_i + c_i f(\psi_{i=1.n}) + \delta_i(t)}$, with parameters $b_i, c_i,$ and $\delta_i(t)$ specific to each core TF in the network. Each term $f_i(\psi_{i=1.n})$ will be a function of the activity of the core TFs binding gene i's enhancers. As a consequence of strong nonlinear cooperativity, we now make the simplifying assumption that the core TFs turn on synchronously ($\alpha_1\psi_1 \approx \alpha_2\psi_2 \approx \cdots \approx \alpha_n\psi_n$) where $\alpha_{i=1..n}$ are constants. This allows us to approximately represent the entire network activity with the scalar $\psi(t)$ and replace the gene specific enhancer activities with an average enhancer activity for each core TF gene, $f_i(\psi_{i=1.n}) \approx c\psi^n$, where n now represents an average degree of cooperativity, and could arise from either individual TF cooperativity at an enhancer or from multiple enhancers interacting non-additively. Because the probability that the gene is activated quickly saturates at large ψ, the precise form of this nonlinearity does not strongly affect the results, as long as $n \geq 3$. We similarly replace gene specific rates $b_i, c_i,$ and $\delta_i(t)$ with weighted averages, leading to Eq. (1). Eq.1 was solved by the Euler-Maruyama method using parameters $(b, c, e_0, e_1, r, n) = (.5,1,.1,3,1,3)$ unless stated otherwise, and with normally distributed noise $\xi(t)$ with amplitude $\xi_0 = 0.4$. For $e_1 \gg e_0$ the OFF fixed point is at $\psi \approx e_0/r$ and the ON fixed point is at $\psi \approx e_1/r$ and both are stable for $c \gtrsim br/e_1$ and $n \geq 3$. The stimulus $\delta(t)$ was

modeled as $\delta(t) = \delta_0(1 + \mathrm{erf}\big((t - t_0)/2\sqrt{2}\big))/2$, with $\delta_0 = 0.035$, which turns on smoothly at $t = t_0$, to model the sustained effect of Activin A in the experiments, which is known to act through WNT/Nodal signaling. The stimulus produces a weak increase in enhancer activity (p_{on}), that is independent of ψ, and is therefore independent of core TF network activity. Although the bifurcation and stability results are valid for any $e_1 \gg e_0$ and $c \gtrsim br/e_1$ and $n \geq 3$, the parameters δ_0, ξ_0, e_1, and e_0 were chosen to approximately match the distributions of SOX17 expression levels and population variation in the FACS data. A model with a similar mathematical form was previously derived to model cellular differentiation induced by MAPK signaling and was also shown to admit bistable solutions [268,269].

Stochastic Gillespie simulations

The stochastic Gillespie algorithm was used to simulate a strongly nonlinear cooperative autoregulatory gene circuit model [270,271], analogous to the rate equation Eq.1 but also valid for arbitrarily small numbers of molecules. In this model, up to three molecules of the TF A sequentially bind to an enhancer (E), and the differentially bound TF-enhancer complexes are denoted as EA, EAA, and $EAAA$. The eight possible reactions, their probabilities, a_i, and their impact on molecular species numbers are given as follows, where X_M indicates the number of molecules of species M:

Production of A: $X_A + 1$ $\quad a_1 = c_{bt} + c_{et_1} \cdot X_{EA} + c_{et_2} \cdot X_{EAA} + c_{et_3} \cdot X_{EAAA}$

Degradation of A: $X_A - 1$ $\quad a_2 = c_d \cdot X_A$

Binding of A to E: $\quad X_{EA} + 1, X_E - 1, X_A - 1 \quad a_3 = c_{f_1} \cdot X_A \cdot X_E$

Unbinding of A from EA: $\quad X_{EA} - 1, X_E + 1, X_A + 1 \quad a_4 = c_{r_1} \cdot X_{EA}$

Binding of A to EA: $X_{EAA}+1, X_{EA}-1\,, X_A-1 \quad a_5 = c_{f_2}\cdot X_A \cdot X_{EA}$

Unbinding of A from EAA: $X_{EAA}-1, X_{EA}+1\,, X_A+1 \quad a_6 = c_{r_2}\cdot X_{EAA}$

Binding of A to EAA: $X_{EAAA}+1, X_{EAA}-1\,, X_A-1 \quad a_7 = c_{f_3}\cdot X_A \cdot X_{EAA}$

Unbinding of A from $EAAA$: $X_{EAAA}-1, X_{EAA}+1\,, X_A+1 \quad a_8 = c_{r_3}\cdot X_{EAAA}$

Unless noted otherwise, the rates used are

$\left(c_{bt}, c_{et1}, c_{et2}, c_{et3}, c_{f1}, c_{r1}, c_{f2}, c_{r2}, c_{f3}, c_{r3}, c_d, \right) =$

$(.04, .04, .04, 2.4, .1, 15, .1, 15, .1, 15, .003)$.

The strong cooperativity of enhancer activity is reflected in the fact that we chose $c_{et3} \gg c_{bt}, c_{et1}, c_{et2}$. Fifty independent runs, each representing a single cell, were performed for each datapoint shown. The initial enhancer state at $t = 0$ is given by $(X_E, X_{EA}, X_{EAA}, X_{EAAA})$ = (1,0,0,0), and the initial number of TFs, X_A, was sampled from a uniform distribution. The stimulus is modeled by a transitory increase in the initial rate of A binding to E, c_{f1}.

Generation of the *idCas9-KRAB SOX17$^{eGFP/+}$* HUES8 hESC line

idCas9-KRAB *SOX17$^{eGFP/+}$* HUES8 hESC line was generated using a cassette switch strategy based on previously established iCas9 *SOX17$^{eGFP/+}$* HUES8 hESC line [261,272]. iCas9 *SOX17$^{eGFP/+}$* HUES8 hESCs were treated with 10 μM ROCK inhibitor Y-27632 and 2 μg/ml doxycycline one day before transfection. gRNAs that specifically targeted on *AAVS1-iCas9* allele were co-transfected with AAVS1-idCas9-KRAB donor vector into the cells by using Lipofectamine Stem Transfection Reagent (Thermo Fisher Scientific; STEM00001) following manufacturer's guidelines. Transfected cells were treated by Hygromycin selection for 7 days and single cell colonies were picked for

genotyping. Inducible dCas9-KRAB were validated by RT-qPCR and flow cytometry analysis. gRNAs and genotyping primer sequences are listed in **Supplementary table 1-2**.

ChIP-MS and analysis

ChIP-MS and analysis were performed as previously described[273] with minor modifications. Antibodies used for immunoprecipitation are listed in **Supplementary table 3**. Briefly, ChIP-MS was performed using the same ChIP protocol as in ChIP-seq. 30-40 million cells per sample were crosslinked with 1% formaldehyde and then lysed and sonicated. Clear supernatant was collected for chromatin immunoprecipitation. Total protein was eluted after immunoprecipitation by incubation with 5% SDS and 5mM DTT at 98°C for 5 min. Then protein samples were alkylated, trypsinized, and desalted for LC-MS/MS acquisition. For LC-MS/MS acquisition, samples were resuspended in 10 µl of 0.1% TFA and loaded onto a Dionex RSLC Ultimate 300 (Thermo Scientific), coupled with Orbitrap Fusion Lumos (Thermo Scientific). Chromatographic separation was performed with a two-column system, consisting of a C-18 trap cartridge (300 µm ID, 5 mm length) and a picofrit analytical column (75 µm ID, 25 cm length) packed in-house with reversed-phase Repro-Sil Pur C18-AQ 3 µm resin. Peptides were separated using a 60 min gradient from 4-30% buffer B (buffer A: 0.1% formic acid, buffer B: 80% acetonitrile + 0.1% formic acid) at a flow rate of 300 nl/min. The mass spectrometer was set to acquire spectra in a data-dependent acquisition (DDA) mode. Briefly, the full MS scan was set to 300-1200 m/z in the orbitrap with a resolution of 120,000 (at 200 m/z) and an AGC target of 5x10e5. MS/MS was performed in the ion trap using the top speed mode (2 secs), an AGC target of 10e4 and an HCD collision energy of 35.

Each experimental condition was performed with two biological replicates. Protein levels were log2 transformed, normalized by the average value of each sample and missing values were imputed using a normal distribution 2 standard deviations lower than the mean before statistics analysis. Statistical significance was calculated using a t-test. Specifically, we utilized the F-test to assess if the replicates for each protein are homoscedastic or heteroscedastic (equal or unequal variance). If the F-test resulted significant, i.e. p-value <0.05, we applied the heteroscedastic t-test; if not, the homoscedastic. Protein levels from EOMES, GATA6 and SOX17 ChIP-MS were further compared to IgG controls and the common interacting TFs with log2FC > 2 and -log10(p-value) > 2 were used to plot **Fig.20**.

RNA isolation, reverse transcription, and real-time quantitative PCR (RT-qPCR)

Total RNA was extracted using Quick-RNA MiniPrep kits (ZYMO research; R1055) following the manufacturer's guidelines. cDNA was produced by using High Capacity cDNA Reverse Transcription Kit (Applied Biosystems; 4368817) with 2 μg of total RNA per reaction. RT-qPCR reaction was performed with SYBR Green Master mix (Applied Biosystems; A25742) in the 7500 or QuantStudio 6 flex Real Time PCR system (Applied Biosystems). GAPDH was used as an internal control. Primers used in RT-qPCR are listed in **Supplementary table 2**.

RNA-seq and analysis

After RiboGreen quantification and quality control by Agilent BioAnalyzer, 500ng of total RNA with RIN values of 6.5-10 underwent polyA selection and TruSeq library preparation according to instructions provided by Illumina (TruSeq Stranded mRNA LT

Kit; RS-122-2102), with 8 cycles of PCR. Samples were barcoded and run on a HiSeq 4000 or NovaSeq 6000 platform in a PE50 run, using the HiSeq 3000/4000 SBS Kit or NovaSeq 6000 SP or S2 Reagent Kit (100 Cycles) (Illumina).

We followed the ENCODE RNA-seq processing pipeline, aligning reads to hg38 with STAR_2.5.1b and parameters "--outFilterMultimapNmax 20 --alignSJoverhangMin 8 --alignSJDBoverhangMin 1 --alignMatesGapMax 1000000 --outFilterMismatchNmax 999 --outFilterMismatchNoverReadLmax 0.04 --alignIntronMin 20 --alignIntronMax 1000000". Transcripts were quantified with RSEM v1.2.23.

Standard DESeq2 pipeline was used for downstream PCA map generation and differential expressed gene identification.

ATAC-seq and analysis

Profiling of chromatin was performed by ATAC-Seq as previously described [274]. Briefly, 50K cryopreserved cells were washed in cold PBS and lysed. The transposition reaction containing TDE1 Tagment DNA Enzyme (Illumina; 20034198) was incubated at 37°C for 30 minutes. The DNA was purified with the MinElute PCR Purification Kit (QIAGEN; 28004) and amplified for 5 cycles using NEBNext High-Fidelity 2X PCR Master Mix (New England Biolabs; M0541L). After evaluation by real-time PCR, 3-14 additional PCR cycles were done. The final product was cleaned by AMPure XP beads (Beckman Coulter; A63882) at a 1X ratio, and size selection was performed at a 0.5X ratio. Libraries were sequenced on a HiSeq 4000 or NovaSeq 6000 platform in a PE50 run, using the HiSeq 3000/4000 SBS Kit or NovaSeq 6000 S1 Reagent Kit (100 Cycles) (Illumina).

Paired-end reads were mapped to hg38 with bowtie2 using default parameters, duplicate reads were removed with picard, and peaks were called using macs2 using default parameters. gkm-SVM was run on top 10000 300bp distal peaks (>2 kb from TSS) and negative sequence following [49,275,276]. Motifs were extracted using gkm-PWM.

gRNA design of core enhancer perturbation screen

2 Mb up/down stream of the 10 core TFs were selected for further chromatin accessibility filtering. Only the regions showing accessibility in either ESC stage or DE-48h stage were kept. Regions that overlapped with promoters or exons were removed from the list, resulting in 394 putative enhancers being selected in total. gRNA design was performed by using CHOPCHOP [55] to achieve full-tiled coverage of the selected regions. We further added 3 gRNAs targeting *SOX17* promoter, and 1,100 gRNAs targeting safe harbor loci [277] as positive and negative controls, respectively. gRNA sequences of the library are listed in **Supplementary table 2**.

Oligo synthesis and library cloning

gRNA oligos were synthesized on-Chip (Agilent). Synthesized oligos were amplified and restriction cloned into lentiGuide-puro (Addgene; 52963) by the MSKCC Gene Editing & Screening Core Facility. Cloned plasmid library was PCR amplified to incorporate adapters for NGS. Samples were purified and sequenced using Illumina HiSeq 2500 platform. FASTQ files were clipped by position and reads were mapped back to the reference library file to show relative abundance of reads per gRNA. Reads within each sample were normalized to total number of mapped reads and library size. The Overall

Representation of Library was charted over a one-log fold change to evaluate if any gRNA was over- or under-represented in the final library. Primers used for PCR are listed in **Supplementary table 2**.

Lentiviral library generation

The core enhancer perturbation lentiviral library generation was performed as previously described [261] with minor modifications. Briefly, a total of 13.6 μg core enhancer perturbation library plasmids with 5.44 μg lentiviral packaging vector psPAX2 and 1.36 μg vesicular stomatitis virus G (VSV-G) envelope expressing plasmid pMD2.G (Addgene plasmid 12260 and 12259) were transfected with the JetPRIME (VMR; 89137972) reagent into 293T cells to produce the lentivirus. Fresh medium was changed 24h after transfection and viral supernatant was collected, filtered, and stored at −80°C 72h after transfection.

Core enhancer perturbation screen

We aimed for a ~1,000-fold coverage per gRNA to maximize sensitivity. 35 million idCas9-KRAB *SOX17*$^{eGFP/+}$ HUES8 hESCs were collected and infected with the lentiviral library at a low MOI of ~0.3 on Day 0 in 15-cm plates. A total of 6 μg/ml protamine sulfate per plate was added during the first 24h of infection to improve the infection efficiency. One day after infection (Day 1), cells were treated with 2 μg/ml doxycycline to induce dCas9-KRAB expression, which continues till the end of the screen at DE-36h. Infected cells were selected with 1 μg/ml puromycin from Day 2-Day 4 and harvested on Day 5 for recovery passage. 2 days after recovery passage, 60 million cells were collected and seeded into 15-cm plates for DE differentiation as described above. 36h after differentiation, cells

were dissociated using 1X TrypLE Select and sorted using FACS Aria according to GFP expression. Cells whose GFP expression levels were in the top or bottom 20% were pelleted individually, with each pellet containing 15 million cells.

gRNA enrichment sequencing and data analysis

The gRNA enrichment sequencing and data analysis were performed as previously described [261] with minor modifications, manipulated by MSKCC Gene Editing & Screening Core Facility. Briefly, genomic DNA from sorted cell pellets was extracted using the QIAGEN Blood & Cell Culture DNA Maxi Kit (QIAGEN; 13362) and quantified by Qubit (ThermoScientific; Q32850) following the manufacturer's guidelines. A quantity of gDNA covering 1000X representation of gRNAs was PCR amplified to add Illumina adapters and multiplexing barcodes. Primer sequences to amplify lentiGuide-puro are shown in **Supplementary table 2**. Amplicons were quantified by Qubit and Bioanalyzer (Agilent) and sequenced on the Illumina HiSeq 2500 platform. Sequencing reads were aligned to the gRNA library sequences and counts were obtained for each gRNA. The read counts were normalized to total reads of each sample to offset differences in read depth. To calculate the Z-score of each gRNA, we subtracted the mean log2FC of all negative control gRNAs targeting safe harbors from the log2FC of each gRNA, and then divided the result by the standard deviation of log2FC from the negative control gRNAs (**Supplementary table 4**). Off-targets of each gRNA were further assessed by CRISPOR [278]. gRNAs with 0 mismatch (MM)=1, 1MM<10, 2MM<30, 3MM<100 and total raw reads > 500 were kept for calculating average Z-score of each putative enhancer region. Putative enhancer region with less than 3 qualified gRNAs were filtered away (**Supplementary table 5**).

Core enhancer hits validation

The gRNA enrichment sequencing and data analysis were performed as previously described [261] with minor modifications. Briefly, selected gRNAs for each enhancer hit were cloned into lentiGuide-puro (for single perturbations) and lentiGuide-blast (when a second perturbation was used in combination). 1.36 μg lentiGuide-puro (or lentiGuide-blast), 0.1 μg pMD2.G and 0.4 μg psPAX2 plasmids were transfected with the JetPRIME (89137972; VMR) reagent into 293T cells to pack lentiviruses. Viral supernatant was made and collected as described above. idCas9-KRAB SOX17$^{eGFP/+}$ HUES8 hESCs were then infected with viruses containing different gRNAs individually following the same process as described above for the screen. One day after infection (Day 1), cells were treated with 2 μg/ml doxycycline to induce dCas9-KRAB expression, which continues till the end of the experiment (DE-36h or DE-72h). Infected cells were selected with 1 μg/ml puromycin from Day 2-Day 4 and harvested on Day 5 for recovery passage and followed by DE differentiation described above. For dual selection, cells were selected with 1 μg/ml puromycin and 10 μg/ml blasticidin together for 5 days. Cells were collected at both 36h and 72h for flow cytometry analysis. gRNA sequences selected from the core enhancer validation are listed in **Supplementary table 6**.

Flow cytometry

Flow cytometry analysis were performed as previously described [261]. Antibodies used for flow cytometry are listed in **Supplementary table 3**. Briefly, for live GFP and surface marker data collection, cells were dissociated and stained with DAPI and

corresponding antibodies. For TF data collection, cells were first stained with LIVE-DEAD Fixable Violet Dead Cell Stain (Invitrogen; L34955) and then fixed and stained with corresponding antibodies. Flow cytometry data were collected using BD LSRFortessa or BD LSRII. Flow cytometry analysis and figures were generated in FlowJo v10.

Generation of clonal enhancer KO hESC lines

Enhancer KO hESC lines were generated by using two paired crRNAs surrounding targeted enhancers to increase knockout efficiency. crRNAs and tracrRNA were ordered from IDT. iCas9 *SOX17*$^{eGFP/+}$ HUES8 hESCs were treated with 2 μg/ml doxycycline and 10 μM ROCK inhibitor Y-27632 for 24h, dissociated with 1X TrypLE Select, and transfected with 0.15 μM of each crRNA and 0.6 μM of tracrRNA by using Lipofectamine RNAiMAX Transfection Reagent (ThermoScientific; 13778100) following the manufacturer's guidelines. Transfected cells were further cultured in E8 with 10 μM ROCK inhibitor Y-27632 for 48h and ~2000 cells were seeded into 100-mm plate to raise colonies. Then, the genomic DNA of individual colony was extracted by using DNeasy Blood & Tissue DNA Kit (QIAGEN; 69506) for genotyping. crRNA and genotyping primer sequences are listed in **Supplementary table 1-2**.

ChIP-seq and analysis

ChIP-seq was performed as previously described [261] with minor modifications. Antibodies used for immunoprecipitation are listed in **Supplementary table 3**. Briefly, cells were crosslinked with 1% formaldehyde and then lysed and sonicated. Clear supernatant was collected for chromatin immunoprecipitation, decrosslinking and DNA

purification. Then the sequencing library was generated by using the NEBNext® Ultra II DNA Library Prep Kit (New England Biolabs; E7103S) and NEBNext® Multiplex Oligos for Illumina® (New England Biolabs Index Primers Set 1; NEB, E7335S). Samples were pooled and submitted to MSKCC Integrated Genomics Operation core for quality control and sequencing on Illumina HiSeq 4000 platform.

Paired-end reads were mapped to hg38 with bowtie2 using default parameters, and peaks were called using macs2 using default parameters. Processed ChIA-PET bedpe files for K562, GM12878 [279], H1, and HUVEC [280] were downloaded from encodeproject.org.

Hi-C and analysis

2 million cells were collected and fixed with 1% formaldehyde. The subsequent steps of Hi-C were then performed using the Arima-Hi-C kit (Arima; A510008) while libraries for sequencing were prepared with the KAPA Hyper Prep Kit (KAPA; KK8502) following the manufacturers' guidelines. Samples were pooled and submitted to MSKCC Integrated Genomics Operation core for quality control and sequencing on Illumina HiSeq 4000 platform.

Prior to alignment, Hi-C Pro 2.11.4 was used to fragment, with GATC and GANTC as the restriction sites, with all alternative haplotypes removed. Reads were aligned with default settings for Bowtie 2.4.1 in Hi-C Pro, for both the global and local alignment steps. After both alignment steps, reads with a MAPQ of at least 30 were retained for further analysis and duplicates were removed. Sample level Hi-C maps were converted to .hic file format with JuicerTools 1.22.01. Condition specific Hi-C maps were generated by combining all sample level .allValidPairs files, and then converting them to the .hic file

format with JuicerTools. Hi-C datafile ENCFF080DPJ.hic [24] for K562 was downloaded from encodeproject.org. Hi-C .hic datafiles for HUES64 and differentiated to (EC, MS, EN) were downloaded from NCBI GEO accession GSE130085 [281]. Contact frequency .bedpe files were generated from Juicer Tools version 1.22.01 or 2.13.05 (K562).

4C and analysis

For each primary digestion reaction, 10 million hESCs were transferred into 15 ml Falcon tubes and fixed with 12 ml of 1% formaldehyde (Thermo Scientific; 28908) in DPBS + 0.04%BSA for 10 min at room temperature (on a rotation device). After quenching with 1M glycine for 10 min at room temperature, tubes were centrifuged for 5 min 500g at 4°C. Cells were kept on ice, washed with DPBS, centrifuged for 5 min 500g at 4°C, and pellets were frozen in liquid nitrogen and stored at −80°C. Next, cells were vigorously resuspended in 1 ml of ice-cold lysis buffer (10 mM tris (pH 8), 10 mM NaCl, 0.2% NP-40, and 1 tablet of complete protease inhibitor (Roche; 04693159001)], transferred to 9 ml of prechilled lysis buffer, and incubated for 15 min on ice. Following centrifugation at 500g for 5 min at 4°C, the pellet was resuspended in 500uL 1.2x CutSmart buffer containing 0.5% SDS and incubated for 1 hr at 37°C while shaking at 750 rpm. After, SDS quenching was performed by adding 75uL 20% Triton X-100 and incubating for 1 hr at 37°C while shaking at 750 rpm. 10 uL of the sample were taken as an undigested control. The remaining samples were treated with DpnII enzyme (30ul) in CutSmart buffer (25ul) and samples were incubated ON at 37°C under agitation (750rpm). After first digestion, 5µl of the sample were taken as a digested control and the efficiency of the chromatin digestion was verified by electrophoresis, detecting a smear between 0.2 and 2 kb in a 1.5% agarose gel.

DpnII was deactivated by (65°C, 20 minutes, 750 rpm), and ligation of DNA ends between the cross-linked DNA fragments was performed in T4 ligation buffer (NEB; B0202), ATP (NEB; P0756S), 10% Triton X-100, 20mg/ml BSA and T4 DNA Ligase (NEB; M0202) ON at 16°C (gently rocking) followed by 30min at RT. Then, ligated samples were treated with proteinase K and reverse crosslinked overnight at 65C. Following RNase (Sigma-Aldrich; 10109142001) treatment, phenol/chloroform extraction and DNA precipitation, the pellets were dissolved in 10mM Tris pH 8. Then the efficiency of the DNA extraction was verified on a 1.5% agarose gel. For the second digestion 5uL NlaIII in CutSmart buffer was added to the DpnII-ligated 3C template and samples were incubated ON (37°C, 750rpm). NlaIII was inactivated at 65°C for 20 min, and a second ligation was performed by adding T4 ligation buffer, 10mM ATP, T4 DNA Ligase, and ddH2O, incubating ON at 16°C. Ligation product was extracted by phenol/chloroform. DNA concentration of each digested sample was calculated using the Qubit dsDNA BR assay kit (Invitrogen; Q32850). For library preparation, viewpoint primers were designed either around promoter of EOMES, GATA6, SOX17 and PDX1, depending on the availability of the nearest restriction enzyme sites. Library preparation was then performed using 200 ng of 4C-template DNA with the Expand Long Range PCR kit (Millipore; 4829042001) under specific PCR conditions (94 °C for 2 min, 16 cycles: 94 °C for 10 s; 59°C for 1 min; 68 °C for 3 min, final extension: 68 °C for 5 min). Amplified DNA was pooled, and primers were removed using AMPure beads (Beckman Coulter; A63881). A second round of PCR was performed using the amplified DNA as a template and overlapping primers to add the P5/P7 sequencing primers and indexes (94 °C for 2 min, 20 cycles: 94 °C for 10 s; 60 °C for 1 min; 68 °C for 3 min and 68 °C for 5 min). The samples quantity and purity were

determined using a Qubit fluorometer. 4C PCR library efficiencies were confirmed by Agilent Bioanalyzer and libraries were sequenced on a HiSeq4000 in PE150 mode by the MSKCC Genomics Core Facility. Three independent assays per viewpoint were performed.

A local model analogous to HiC-DC+ was used to identify local loop enrichments at an FDR of 0.1. For identifying differential loops between experimental conditions, DESeq2 was used. However, to further increase the ability to identify differential looping signatures Locally Adaptive Weighting and Screening (LAWS) was used to derive spatially informed FDR estimates. To score events observed within each replicate, we used a z-scoring procedure based on quantile residuals derived from the local model referenced above. After scoring, these quantile residuals should follow an approximately normal distribution, and so, $\bar{z}=1/\sqrt{n}\sum z \sim N(0,1)$ as well. These were then used to identify differences between the CCRs and non-CCRs. A kernel density estimator from the CRAN package sm 2.2-5.7.1 was used to estimate the KDE and its associated confidence band of equality.

Generation of enhancer deletion mouse lines

Enhancer deletion mouse lines were generated by the Mouse Genetics Core Facility in MSKCC. In general, Cas9 and gRNAs targeted on the enhancer regions were injected into zygotes followed by *in vitro* fertilization. Genomic DNA isolated from ear punch were used for genotyping. F1 mice carried enhancer deletion(s) were crossed with wild-type mice to isolate the enhancer deletion allele for the generation of stable enhancer deletion mouse lines. For details, please reach to the Mouse Genetics Core Facility in MSKCC.

Predictive modeling of core enhancer screen hits

Scores for ATAC, DHS, ChIP-seq, and H3K27ac signal features were mapped onto uniform 1000 bins centered on each target enhancer. For discriminative AUPRC analysis, positive hits were defined as log2FC > 0.15 for hESC-DE (24 positive hits out of 160 DE enhancers tested, **Supplementary table 7**). For K562 Reilly we downloaded all "Flow-Fish CRISPR Screen" "tsv" or "tsv guide quantification" files from https:// www.encodeproject.org which yielded experiments at 20 loci[241]. For analysis of the Reilly data, we mapped gRNAs to non-promoter (>2 kb from TSS) K562 DHS peaks and normalized high and low expression gRNA counts. 12 genes had an enhancer hit with log2FC>0.8 (36 positive hits out of 450 K562 regions, **Supplementary table 8**) and we included these loci in model evaluation (Supplementary Fig 8a). For the Nasser data we downloaded Supplemental Table 6 from Nasser 2021[282] and mapped all tested regions to non-promoter K562 DHS peaks within 1 Mb of a tested gene. Hits were defined by Regulated=TRUE in their Table 5 (69 positive hits out of 1931 K562 regions, **Supplementary table 9**), flanking 65 genes. For modeling, Hi-C contact frequency was calculated in 5kb bins from the .hic files normalized to one for the most promoter proximal bin using our data in ESC and DE, and in ENCFF080DPJ in K562. We also tried as a feature a distance corrected promoter Hi-C contact frequency, Hi-C * $|\text{dist}|^k$, but found no improvement in AUPRC over k=0 for k between 0 and 2. P(in loop) for each enhancer-promoter pair was calculated from ChIA-PET reads for all loops in a 2 Mb window spanning the promoter. Total P(in loop) for each distal enhancer-promoter pair is given by the ratio of total ChIA-PET read counts of all loops spanning both the enhancer and the promoter divided by the total counts of all loops containing the promoter (but not

necessarily also containing the enhancer). The minimum threshold for loop calls in the ChIA-PET data is either 3 or 4 reads, and we also used this threshold for loop counts. To reduce variability in the ChIA-PET data, we averaged counts for multiple datasets. For hESC-DE, H1, HUVEC, and GM12878 ChIA-PET was used, while for K562 Reilly and Nasser, K562 ChIA-PET was used, but different ChIA-PET datasets yield very similar P(in loop) and predictive performance. P(in loop) was normalized to one for the most promoter proximal bin. Logistic regression was used to combine features and predict performance. For these very low dimensional logistic regression models, test set performance is reduced by <2% compared to using the full dataset, which we used to reduce statistical variation when comparing all models. Spearman correlation was calculated between probability of being in the positive class and enhancer effect (log2FC). To compare all models in Fig 4f, log2FC in ESC-DE and K562 Reilly were scaled to "effect size" by dividing log2FC by 1.5 for ESC-DE and 8.0 for K562 Reilly so all datasets had a similar effect size threshold of 0.1 for hits. We took the top predictions from each model in each model to compare performance at constant recall (24 in ESC-DE, 36 in K562 Reilly, and 69 in K562 Nasser, 129 total).

gRNA design of peripheral enhancer perturbation screen

We selected 860 peripheral genes with expression 2-fold greater at DE48h compared to ESC (not including DE core TFs). 10614 ATAC peaks (including promoters) at DE48h flanking 250 kb up/down stream of the 860 peripheral genes' TSS were selected for further gRNA design. Maximum 4 specific gRNAs were selected for each ATAC peak by using GuideScan[283]. All gRNAs have 0MM=0, 1MM=0 and 2MM+3MM<50. We

further added 66 gRNAs targeting validated core enhancers and promoters of *EOMES, MIXL1, GATA6, SOX17*, as well as 1,100 gRNAs targeting safe harbor loci [277] as positive and negative controls, respectively. In total, 37929 gRNAs were selected as peripheral enhancer perturbation screen library. gRNA sequences of the library are listed in **Supplementary table 10**.

Lentiviral library concentration

1X peripheral enhancer lentiviral library were first generated as described above. 100ml of 1X lentiviral library were then transferred into Ultra-Clear Tubes (Beckman Coulter; NC9146666) for concentration under 25,000rcf at 4°C for 90min. Supernatant was gently removed after centrifugation. 2ml DPBS was used to resuspend virus to generate 50-fold concentrated peripheral enhancer lentiviral library.

Peripheral enhancer single cell perturb-seq screen

We aimed for a ~100-fold coverage per gRNA for peripheral enhancer single cell perturb-seq screen. 1.2 million idCas9-KRAB *SOX17*$^{eGFP/+}$ HUES8 hESCs were infected with 20μl of the 50-fold concentrated peripheral enhancer lentiviral library at an average MOI of 15 on Day 0 in 6-well plates (100K cells per well). A total of 6 μg/ml protamine sulfate per plate was added during the first 24h of infection to improve the infection efficiency. One day after infection (Day 1), cells were treated with 2 μg/ml doxycycline to induce dCas9-KRAB expression, which continues till the end of the screen at DE-48h. Infected cells were selected with 1 μg/ml puromycin from Day 2-Day 4 and harvested on Day 5 for recovery passage. 2 days after recovery passage, 6 million cells were collected

and seeded into 6-well plates for DE differentiation as described above. 48h after differentiation, cells were harvested for single cell perturb-seq experiments with targeted collection of 300K cells. Single-cell 3′ RNA-seq libraries and gRNA feature barcode libraries were generated with 10x Genomics Chromium Single Cell 3′ Reagent Kit v.3.1 (Dual Index) with Feature Barcode technology for CRISPR Screening following the manufacturer's guidelines. The libraries were sequenced on NovaSeq 6000 platform following the manufacturer's guidelines.

Peripheral enhancer single cell perturb-seq screen data analysis

Chromium v3 analysis software Cell Ranger (Version 7.0.1) was run using "cellranger count" with feature barcode libraries alignment. gRNAs with equal or greater than 10 UMI were determined as a qualified gRNA capture. Cells with $1 \leq$ types of gRNAs ≤ 40, $2000 \leq$ n_feature_RNA ≤ 9000 and MT-gene $\leq 10\%$ were kept for downstream Seurat analysis, resulting 186,399 cells with a representation of ~200 cells/putative peripheral enhancer. For two-sided Wilcoxon statistics test to determine the significance of a certain enhancer perturbation effect, the normalized gene expression in the cells with the gRNAs targeting on the enhancer was compared to it in all cells. Benjamini-Hochberg correction were further performed to adjust the p-value. Expression fold change were calculated using the mean normalized gene expression between the cells with the gRNAs targeting on the enhancer verses all cells.

RESULTS

Dynamic GRN model predicts temporal sensitivity to enhancer perturbation

We sought to develop a dynamic GRN model to study the temporal and threshold-dependent requirements for enhancers during cell state transitions. Our previous studies of cell state transitions [49,261,284,285] and sequence-based modeling [49,275,276] of a broad range of ENCODE epigenomic profiling data have identified key features of this model. Machine learning applied to chromatin accessible peaks identifies a small set of 5-10 lineage determining core TFs in each cell type whose binding sites can predict chromatin accessible peaks to a high degree of accuracy [49,275,276]. Each chromatin accessible peak contains combinations of multiple binding sites for these core TFs. Thus, the lineage determining core TFs cooperatively auto-regulate each other through multiple enhancers flanking each core TF gene and they co-regulate downstream peripheral genes (**Fig.14a and 14b**). This results in highly nonlinear regulation of gene expression. Since these core TFs determine the network state, we will describe the activity of the network with a time-dependent state variable, $\psi(t)$, whose amplitude reflects the activity of the core TFs. We use 'network state' and 'cell state' essentially interchangeably. The key features of this model are as follows: each gene is expressed at an activated (e_1) or basal level (e_0), depending on the activity of its flanking enhancers. Each gene will be in the activated state with probability $p_{on} \sim cf(\psi)$ and in the basal state with $p_{off} \sim b$, where $f(\psi)$ is a nonlinear function of the core TF activity and reflects cooperativity at the enhancers, and whose activity can be modulated through the parameter c, (e.g., via CRISPRi). In addition, we allow a time-dependent differentiation stimulus $\delta(t)$ that acts at the enhancers through a separate mechanism (e.g., differentiation signaling) to stimulate the transition, so $p_{on} \sim cf(\psi) +$

$\delta(t)$. Finally, we add degradation or export of the TFs $(-r\psi)$ and a stochastic noise term, $\xi(t)$, so the final network state equation is:

$$\frac{d\psi}{dt} = -r\psi + \frac{e_1(cf(\psi)+\delta(t))}{b+cf(\psi)+\delta(t)} + \frac{e_0 b}{b+cf(\psi)+\delta(t)} + \xi(t)\psi. \textbf{ (Fig.14c)}$$

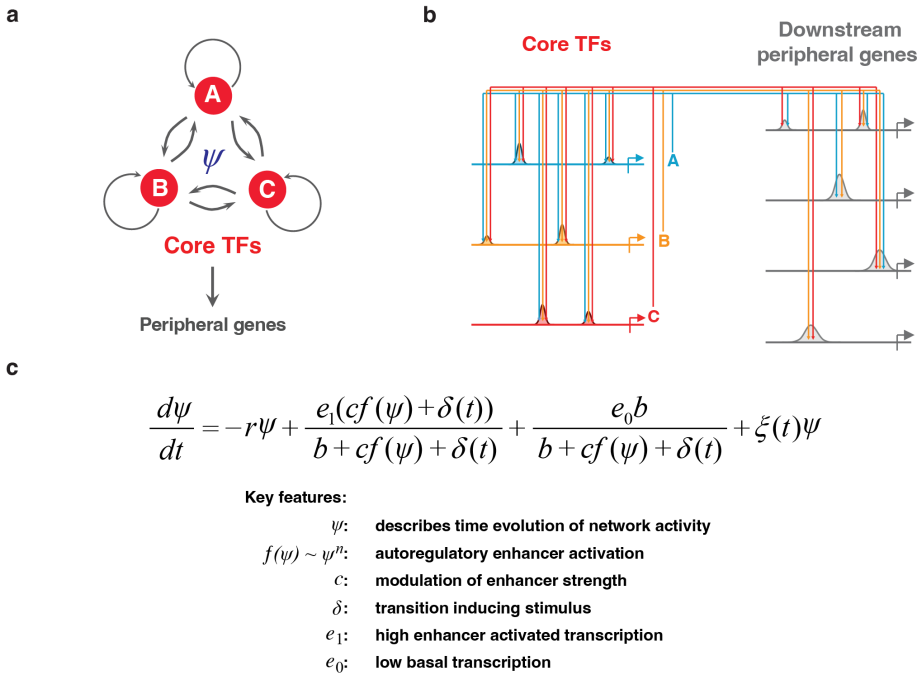

Figure 14. Dynamic Gene Regulatory Network model. a, The schematic of core circuit in the GRN. The core TFs cooperatively auto-regulate each other and co-regulate downstream peripheral genes. **b,** The detailed schematic of core circuit in the GRN. The core TFs cooperatively auto-regulate each other by binding to core enhancers and co-regulate downstream peripheral genes by binding to peripheral enhancers. **c**, The equation of the dynamic gene regulatory network model, created by Dr. Michael A. Beer.

The simplifications that lead to this one-dimensional network state equation, where $\psi(t)$ is a scalar representing the degree to which the network is activated, are described in **Materials and methods**. In the strongly cooperative limit, the enhancers together have an activity $f(\psi) \approx \psi^n$ where n is a typical number of TFs binding at each enhancer. For concreteness and simplicity, we will take $n = 3$, but our conclusions are robust for $n \geq 3$. Stochastic simulation of this model (**Materials and methods**) produces distributions of cells with either high or low network activity (**Fig.15a**). This can be understood from

stability analysis of this model, by plotting $d\psi/dt$ vs ψ (**Fig.15b**). Over a wide parameter range, the network has three fixed points where $d\psi/dt = 0$. Two of these are stable states: the OFF state, with low activity where basal activation balances degradation, and the ON state, with high activity where enhancer-driven transcriptional activation balances degradation. There is also an intermediate unstable fixed point (**Fig.15b**), above which the network activity will transition to the ON state, otherwise, it will fall to the OFF state.

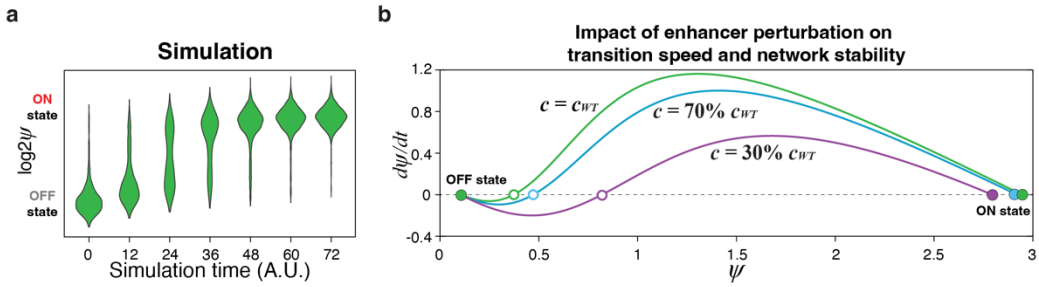

Figure 15. The simulation results of Dynamic Gene Regulatory Network model (generated by Dr. Michael A. Beer). **a**, The violin plots of core circuit establishment during cell state transition by simulation. **b**, Plot of $d\psi/dt$ vs ψ showing cell state transition with different enhancer strengths. The green line represents total enhancer strength without perturbation. The cyan line represents total enhancer strength reduced to 70% of full strength by perturbation. The purple line represents total enhancer strength reduced to 30% of full strength by perturbation.

The simulation results are in good agreement with single-cell RNA sequencing (scRNA-seq) experiments sampling every 12 hours (12h) during hESC-DE differentiation (**Fig.15a**, **Fig.16a and 16c**). To generalize the definition used in the equation, we used the projection of the expression of all TFs along principal component analysis (PCA) component 1 to measure the network state in each cell (**Fig.16b and 16c**). The scRNA-seq results show a bi-stable distribution of cell states during differentiation: a pre-transition steady state, from 0h to 24h, and a post-transition steady state 48h to 72h, when transcriptome profiles are relatively similar over time, and a transitional period, from 24h to 48h, when transcriptome profiles are changing more rapidly (**Fig.16a, 16c and 16d**). This transition behavior is also predicted in the simulation results (**Fig.15a and 15b**). The consistency between simulation and experimental results suggests that the simple dynamic

network model is nevertheless capturing the key features of the establishment of the core circuit in a GRN.

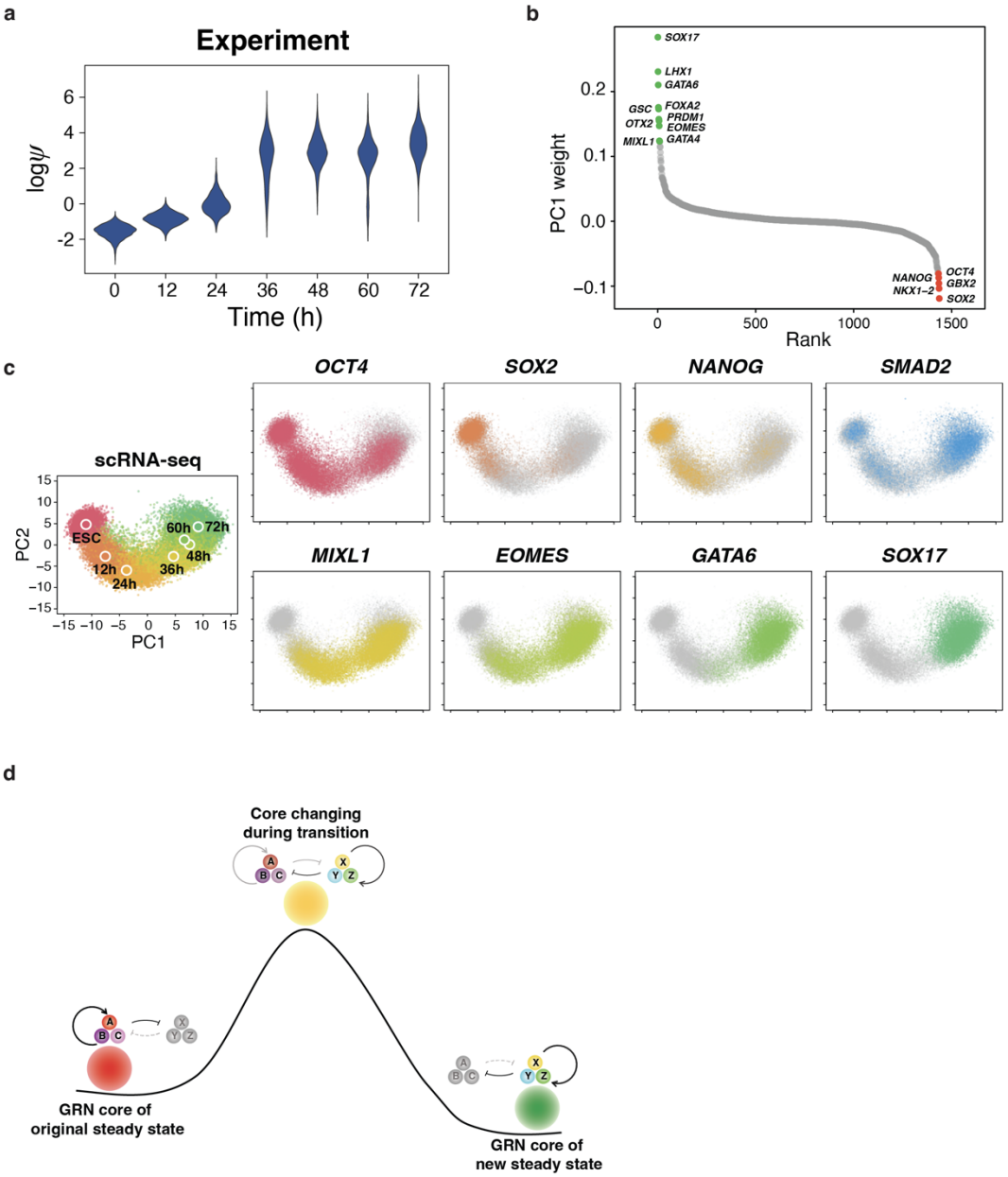

Figure 16. Validate the Dynamic Gene Regulatory Network model with scRNA-seq (a-c are generated by Dr. Michael A. Beer). **a**, The violin plots of core circuit establishment during hESC-DE transition by scRNA-seq experiments sampled every 12 hours during hESC-DE transition. **b**, The ranking plot of PC1 weight of all TFs in PCA analysis from scRNA-seq data during hESC-DE transition. **c**, PCA analysis of all TFs from scRNA-seq data during hESC-DE transition. Each dot represents a cell collected every 12h during hESC-DE transition. The large dots represent the average of all cells from the same time point (left). The PCA plots showing selective TFs from the PCA component 1 (Fig.2b) of scRNA-seq (right). **d**, The schematic of core circuit establishment during cell state transition, similar to *Moris et al* [286]. The transition of a cell from one steady state to another is accompanied by the deconstruction of the original core circuit (A, B, C) and the establishment of core circuit of the new state (X, Y, Z).

To quantitatively model enhancer perturbation during the cell state transition, we decreased the total enhancer strength (c) to varying degrees (with the same stimulus strength $\delta(t)$) and compared the simulation results. Mildly decreasing the total enhancer strength, which mimics perturbing one of the multiple core enhancers flanking a core TF, has a very weak effect on both the ON and OFF steady states, but has a much stronger effect on the network activity required to transition between states (the unstable fixed point where $d\psi/dt = 0$ in **Fig.15b**), indicating mild enhancer perturbation could delay the cell state transition without dramatically changing the final network state (**Fig.15b and Fig.17a left**). We also mimicked the enhancer perturbation in a steady state condition by decreasing the total enhancer strength (c) after cells have reached the steady state. Compared with the simulation during the forward cell state transition, the same enhancer perturbations show much weaker effects in steady state (**Fig.17a**). These results indicate that an optimal time window exists during cell state transitions, which could be utilized to increase the sensitivity of enhancer perturbation screens over screens conducted at a steady state [150,233,240,241,244-248]. We further validated the results of the simple GRN network model (Eq.1) with stochastic Gillespie simulations [270,271] (formally valid in the limit of small numbers of TFs) under the same nonlinear auto-regulatory assumptions. These simulations reproduce the main findings of the sensitivity to enhancer perturbation during the transition, temporal delay in the transition, and insensitivity to enhancer perturbation after the GRN is fully activated in the ON state (**Fig.17b; Materials and methods**).

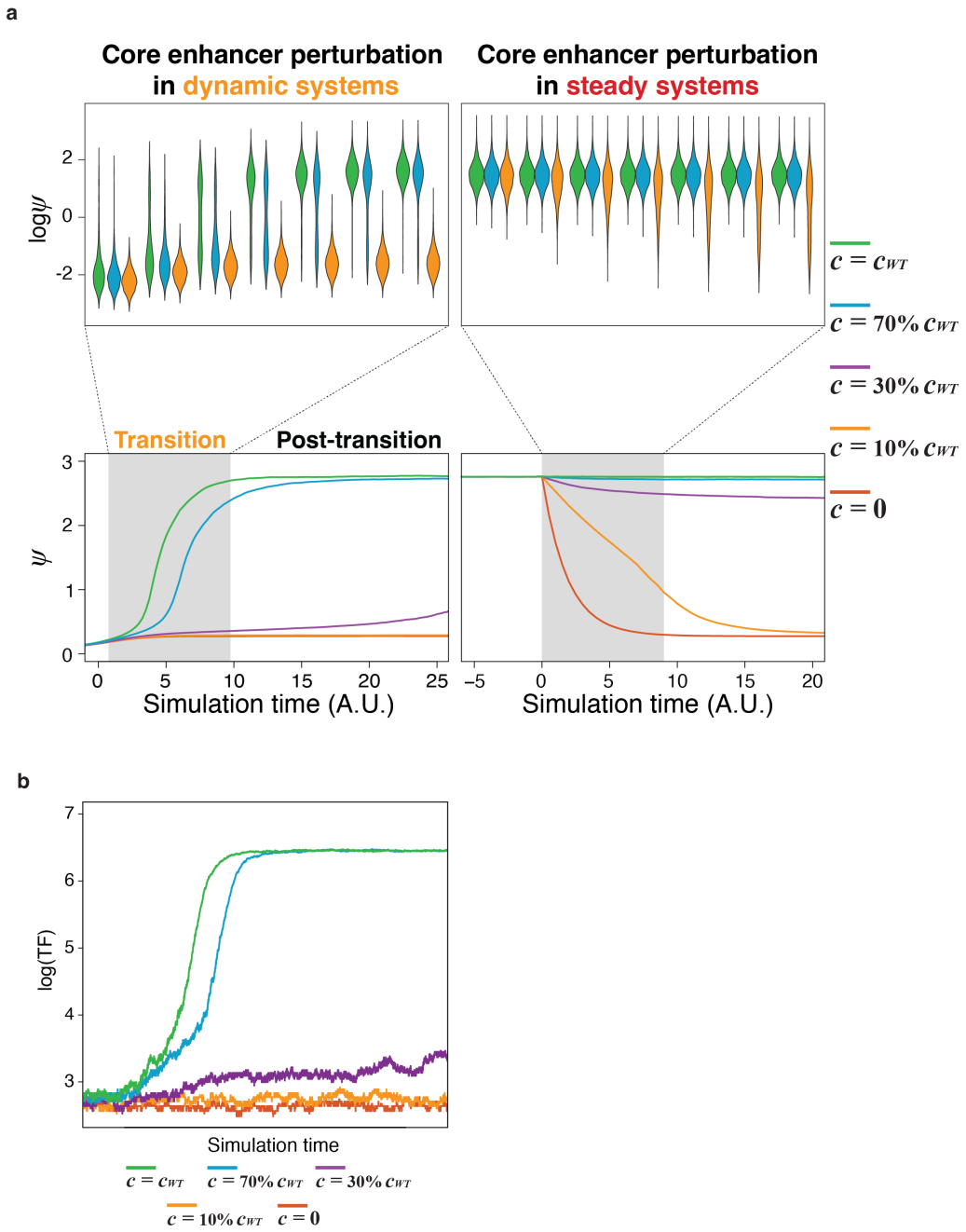

Figure 17. Dynamic Gene Regulatory Network model predicts temporal sensitivity to enhancer perturbation in the dynamic systems (generated by Dr. Michael A. Beer). a, The comparison between the same enhancer perturbation strength during cell state transition or at steady state. The line plots represent the median of simulation results. The violin plots correspond to a zoomed in time interval denoted by the grey box on the line plots. The green, cyan, purple, yellow and orange lines represent 100%, 70%, 30%, 10% and 0% of the original total enhancer strength respectively. **b**, Stochastic Gillespie simulations of the dynamic GRN network model. The green, cyan, purple, yellow and orange lines represent 100%, 70%, 30%, 10% and 0% of original total enhancer strength respectively.

Systematic identification of core TFs in hESC-DE transition

We applied our modeling results to discover core enhancers in cell state transitions using hESC-DE differentiation as a test case, for which core enhancers remain

incompletely defined [287]. Optimization of our existing differentiation protocol [261] allowed us to reproducibly generate >95% SOX17^{+}/CXCR4^{+} DE cells within 72 hours after the initiation of DE differentiation (DE-72h) (**Fig.18a; Materials and methods**). To identify core enhancers, we first took a systematic approach to define core TFs (**Fig.18b**). Since *OCT4* (*POU5F1*), *NANOG* and *SOX2* are well-known TFs essential for the ESC identity [288], we focused on identifying core TFs for the hESC-DE transition. We analyzed the genes required for hESC-DE transition identified from our unbiased genome-scale CRISPR-Cas9 screening data [261], and selected four core DE TFs (*EOMES*, *MIXL1*, *GATA6*, *SOX17*) and three signaling TFs (*SMAD2*, *SMAD4*, and *JUN*) (**Fig.18c and 18d**).

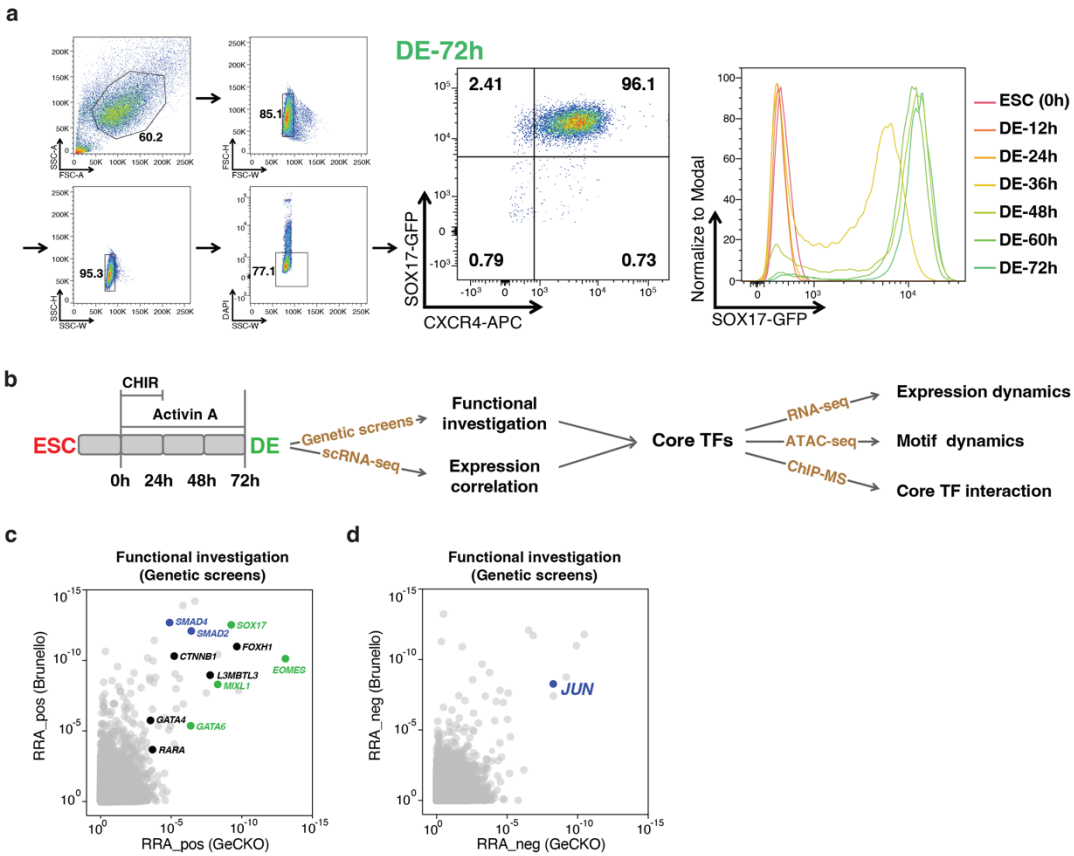

Figure 18. Systematically identify core TFs during ESC to DE cell state transition. a, Flow cytometry analysis showing the gating strategy (left), differentiation efficiency at DE-72h measured by DE markers SOX17 and CXCR4 (middle) or transition efficiency every 12h measured by SOX17 (right). **b**, The schematic of using a systematic approach to identify the core TFs during hESC-DE transition. **c**, MAGeCK robust ranking aggregation (RRA) scores for positive hits in two genome-scale DE screens from Li et al [261]. We overlapped the top 100 hits from each screen, there were 11 TFs (labeled). DE core TFs and signaling TFs identified for the network-guided core enhancer perturbation screen are

shown in green and blue, respectively. **d**, MAGeCK RRA scores for negative hits in two genome-scale DE screens from Li et al [261]. JUN is the only identified TF among the negative hits.

The DE and ESC TFs showed opposing changes in gene expression during hESC-DE transition with corresponding changes in their regulatory activities predicted by gkm-SVM [49,275] trained on the ATAC-seq data (**Fig.19a-d**). Analysis of gene expression from scRNA-seq data (collected every 12h during hESC-DE transition) using the Pearson correlation as the distance metric for UMAP visualization further demonstrated that the expression patterns of DE and ESC TFs clustered separately, and they each correlated amongst themselves (**Fig.19a; Materials and methods**). Compared to the ESC and DE TFs, the signaling TFs showed less dynamic changes in transcriptional and regulatory activities during differentiation (**Fig.19c**).

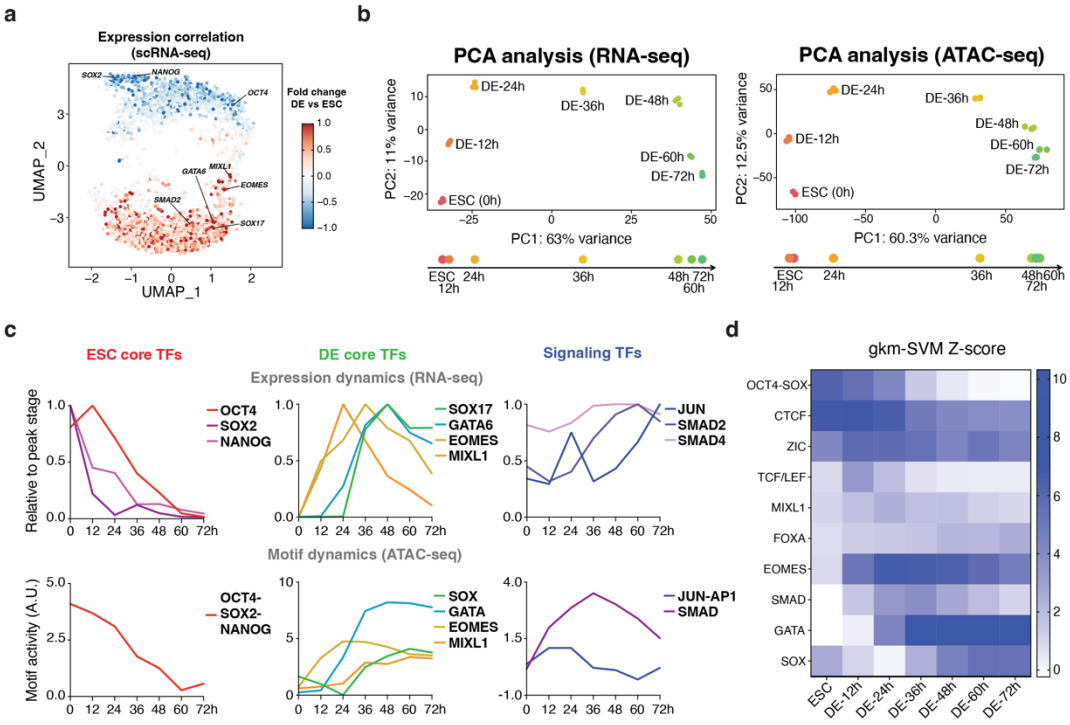

Figure 19. The dynamics of ESC to DE cell state transition. a, The expression correlation analysis from scRNA-seq of hESC-DE transition. Each dot represents a significant expressed gene during the hESC-DE transition (Methods). The distance between each pair of genes is defined by Pearson correlation. The color scale is defined from the expression fold change from ESC to DE-72h (generated by Dr. Hyein Cho). **b**, PCA analysis of bulk RNA-seq (top) and ATAC-seq (bottom) during hESC-DE transition. Data points are projected to PC1 (cell state) to determine the time window of cell state transition. **c**, The expression dynamics (top) and motif dynamics (predicted by gkm-SVM trained on the ATAC-seq data, bottom) of core TFs during hESC-DE transition. **d**, Motif Z-score of ATAC-seq by gkm-SVM at each time point during hESC-DE transition.

We further examined biochemical cooperation between the core DE TFs through chromatin immunoprecipitation followed by mass spectrometry (ChIP-MS) for EOMES, GATA6 and SOX17. Our analysis revealed that all three TFs interacted with each other, and they also interacted with many common partners including the DE TF MIXL1 and the signaling TF SMAD4 (**Fig.20a-d; Supplementary table 11**). In summary, we identified 10 core TFs for the study, starting with functional genomics data and corroborating with gene expression, chromatin accessibility and proteomics findings (**Fig.21a**).

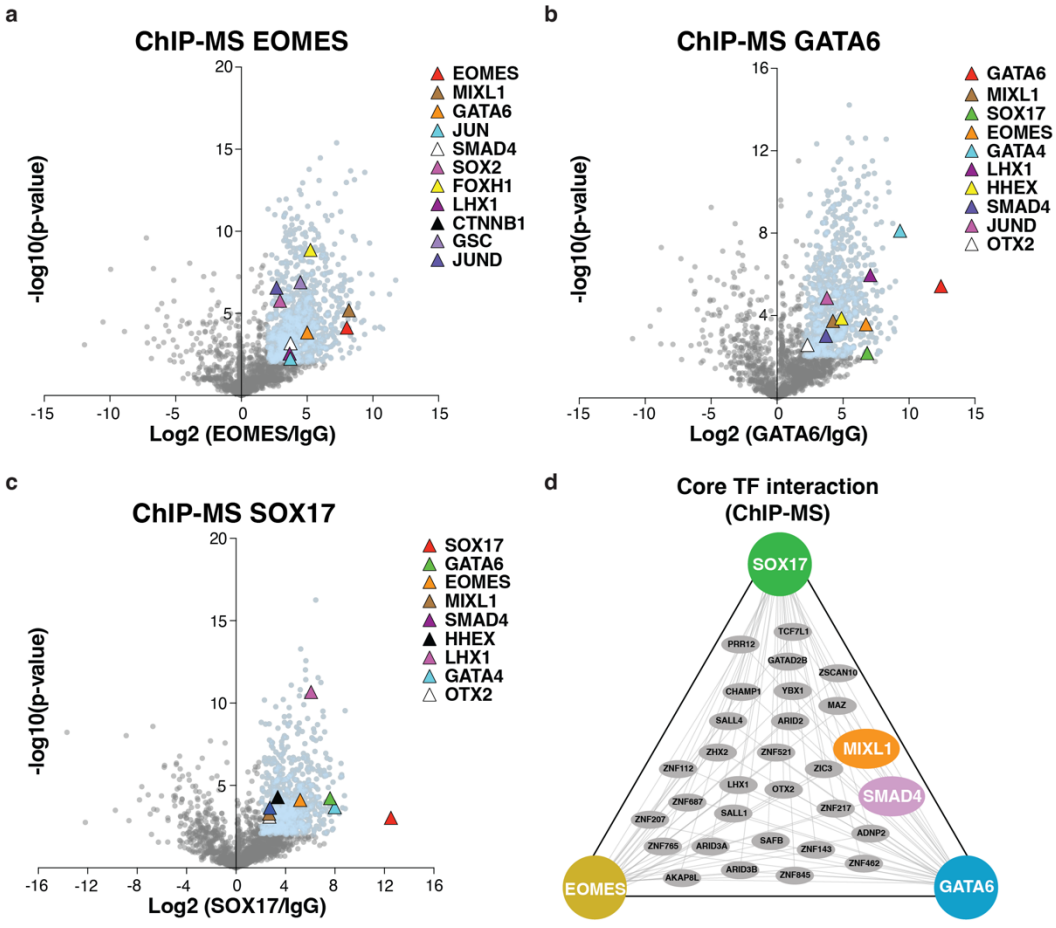

Figure 20. The protein-protein interactions between core TFs of ESC to DE cell state transition. a-c, Volcano plots showing protein-protein interactions identified by ChIP-MS using EOMES (**a**) as the bait at DE-24h, GATA6 (**b**) and SOX17 (**c**) as baits at DE-48h. Blue dots represent the significantly enriched proteins with log2FC > 2 and -log10(p-value) > 2. Selective TFs enriched in ESC and endoderm GO terms are labeled by triangles. **d**, The common protein interactive partners between core TFs identified by ChIP-MS using EOMES, GATA6 and SOX17 as baits during hESC-DE transition.

Discovery of core enhancers in hESC-DE transition

To discover core enhancers, we first examined 4 Mb genomic regions surrounding each of the 10 core TFs, and identified 394 regions that are accessible at either ESC or DE stage based on ATAC-seq (excluding the promoter regions). We then designed a tiling gRNA lentiviral library to target these regions with a total of 11,050 gRNAs (including 1,100 negative controls targeting safe harbor loci [277] and 3 positive controls targeting the *SOX17* promoter, **Fig.21a-e; Supplementary table 4**).

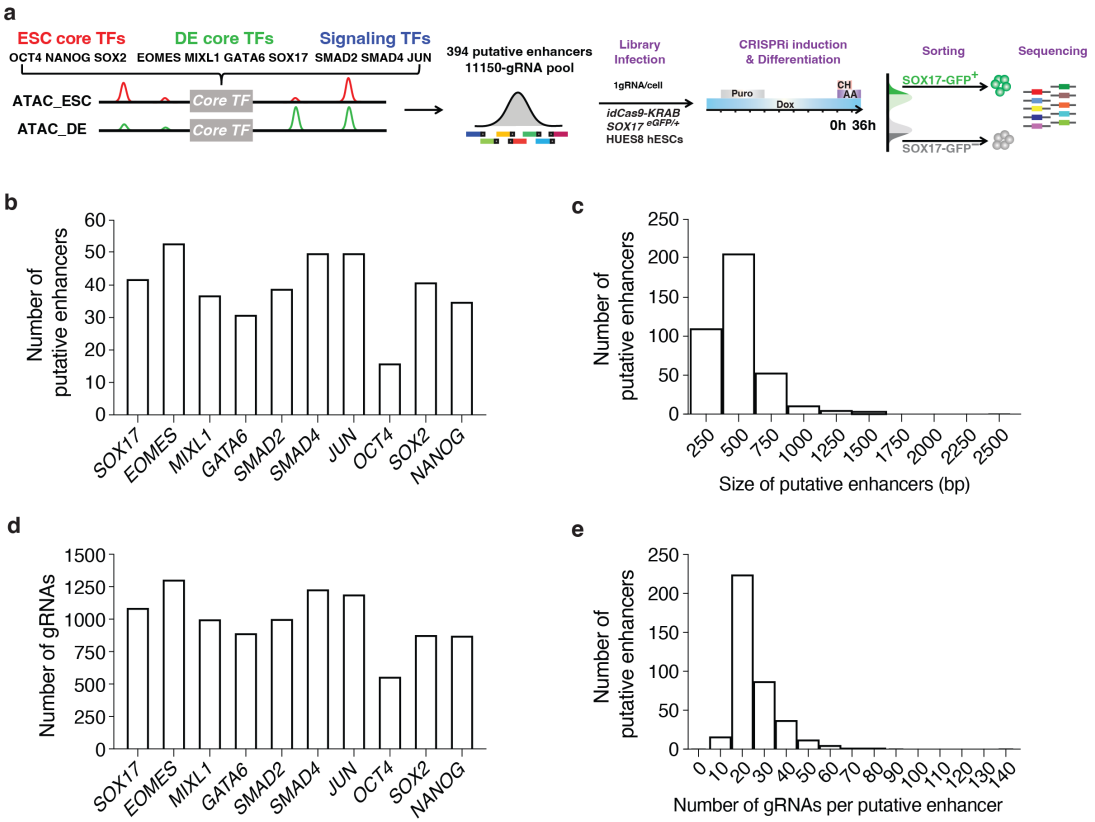

Figure 21. The design of dynamic network-guided core enhancer perturbation screen. a, The design of dynamic network-guided core enhancer perturbation screening. **b** to **e**, Statistics of putative enhancers selection and gRNAs design. The number of putative enhancers selected for each core TFs (**b**), the size of putative enhancers (**c**), the total number of gRNAs targeted on putative enhancers of each core TF (**d**), the number of gRNAs targeted on each putative enhancer (**e**).

We generated an hESC line with a doxycycline-inducible dCas9-KRAB cassette and a DE lineage reporter *SOX17*$^{eGFP/+}$ (**Fig.22a-d; Materials and methods**) and infected

the cells with the gRNA library at a multiplicity of infection (MOI) of ~0.3 to ensure that most infected cells received a single gRNA (**Fig.21a**).

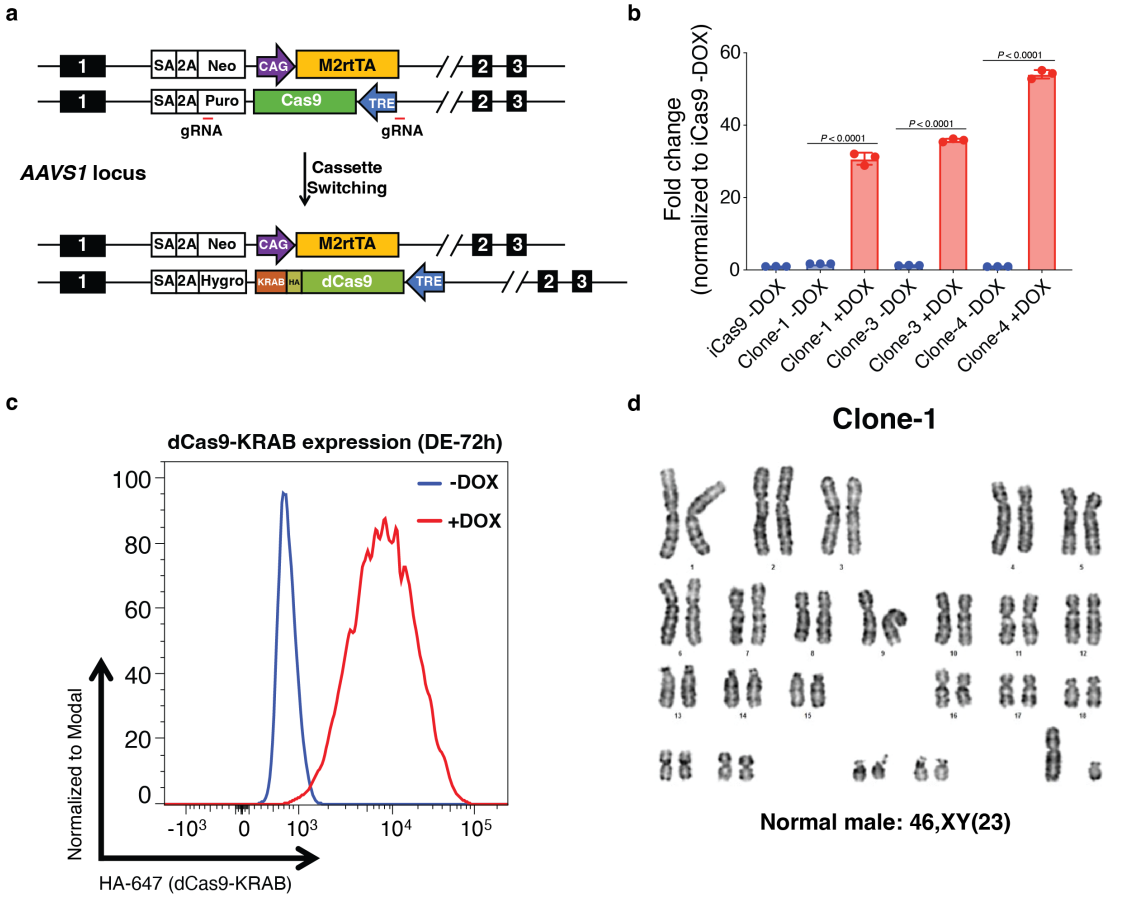

Figure 22. idCas9-KRAB *SOX17*$^{GFP/+}$ hESC line generation using cassette switching. a, The schematics of idCas9-KRAB *SOX17*$^{GFP/+}$ hESC line generation using cassette switching. gRNAs targeting the puromycin selection cassette and the 5' sequence outside TRE are designed for inducing double-strand break for homology repair. **b**, RT-qPCR results showing the inducible expression of dCas9-KRAB with doxycycline treatment. n=3 independent experiments. Error bars indicate mean ± SD. Statistical analysis was performed by two-tailed unpaired student t-test. **c**, Flow cytometry results showing the inducible expression of dCas9-KRAB with doxycycline treatment. **d**, Karyotyping results of the idCas9-KRAB *SOX17*$^{GFP/+}$ hESC line.

Based on flow cytometric analysis for SOX17-GFP expression during differentiation (**Fig.18a**), as well as PCA analysis of scRNA-seq, RNA-seq and ATAC-seq data, we identified DE-36h as an optimal mid-transition point for interrogation of enhancer perturbation effects (**Fig.19a-d**). SOX17-GFP^{+} (top 20%) and SOX17-GFP^{-} (bottom 20%) cells were isolated through FACS for gRNA enrichment analysis (**Fig.18a; Materials and methods**). We calculated the Z-score for each gRNA based on its logarithm of fold change

(log2FC) in the SOX17-GFP^{-} versus the SOX17-GFP^{+} cells (**Fig.23a**). Most gRNAs in the same hit regions had similar Z-scores (**Fig.24a-b**), supporting that the screen is both sensitive and robust.

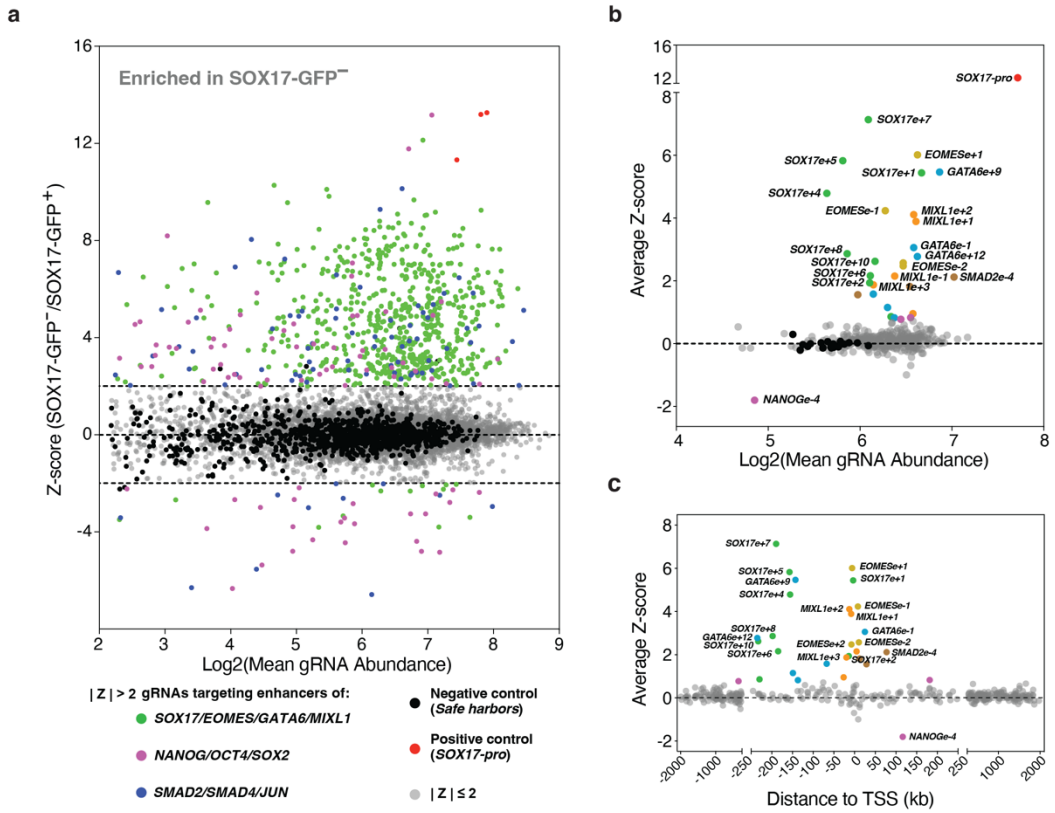

Figure 23. A dynamic network-guided enhancer screen identified core enhancers during hESC-DE cell state transition. a, The scatter plot of gRNA Z-score distribution from the screen. Each dot represents an individual gRNA. Dashed lines indicate the threshold of |Z-score| = 2. Gray dots represent gRNAs of |Z-score| ≤ 2. Black dots represent negative control gRNAs. Red dots represent positive control gRNAs. Green dots represent gRNAs of |Z-score| > 2 targeting on *SOX17*, *EOMES*, *GATA6* and *MIXL1* loci. Purple dots represent gRNAs of |Z-score| > 2 targeting on *NANOG*, *OCT4* and *SOX2* loci. Blue dots represent gRNAs of |Z-score| > 2 targeting on *SMAD2*, *SMAD4* and *JUN* loci. **b**, The scatter plot of average Z-score distribution of each putative enhancer region from the screening. Each dot represents an individual region. Black dots represent negative controls. 29 enhancer hits are labeled by different colors representing the core TFs they are surrounding. **c**, Scatter plots showing the distance of 29 enhancers to the TSS of their target genes.

Through calculating the average gRNA Z-score for each region, we discovered 29 enhancer hits with Z-scores ranging from 0.75 to 7.14 (**Fig.23b; Supplementary table 5**). Relatively few enhancers were found for the ESC and signaling TFs, likely reflecting that the ESC TFs mainly exert their regulatory effects at the ESC stages and that the signaling TFs are primarily regulated post-transcriptionally (e.g., through protein phosphorylation). In contrast, we discovered many enhancers for the core DE TFs, ranging from 4 to 9 for

each gene (**Fig.23b and Fig.24b; Supplementary table 5**). These findings demonstrate the high sensitivity of the screening strategy utilizing a dynamic transition and a single gene readout (e.g., *SOX17* for the DE identity) for discovery of core enhancers in multiple loci. Most of these enhancers were previously unknown, and their discovery expands the atlas of regulatory elements required for human development and provides a basis for understanding the complex gene regulatory networks that govern cell state transitions. Furthermore, 41% of the identified core enhancers are more than 100 kb away from the TSS of the cognate gene (**Fig.23c**), highlighting the need for examining putative enhancers in relatively broad genomic windows.

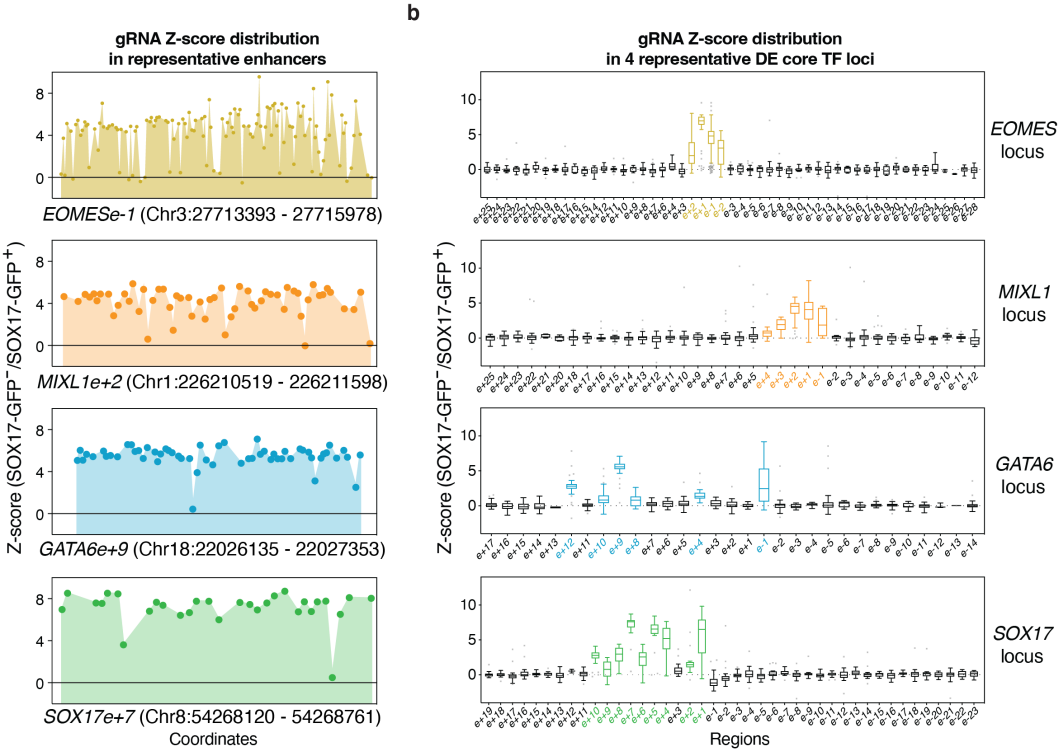

Figure 24. The statistics of gRNA enrichment analysis. a, The gRNA Z-score distribution at representative enhancers showing gRNAs targeting the same enhancer have similar perturbation effect. **b**. Box plots showing the gRNA Z-score distribution in all putative enhancers of *EOMES*, *MIXL1, GATA6* and *SOX17* loci. Center lines indicate median. Boxes limit upper and lower quartiles.

Core enhancers show temporal sensitivity to perturbation

We selected 20 top enhancer hits for validation. Individual CRISPRi perturbations of all 20 hits resulted in significantly reduced numbers of SOX17-GFP$^+$ cells at DE-36h based on flow cytometric analysis (**Fig.25a, b**). In addition to the cell state readout, we also confirmed the downregulation of the corresponding cognate gene expression after perturbation by RT-qPCR analyses (**Fig.25e**). In sharp contrast to the strong phenotypes observed at DE-36h, at DE-72h, the perturbations of most of the top 20 enhancers had little or no impact on the induction of SOX17-GFP$^+$/CXCR4$^+$ cells or their cognate gene expression (**Fig.25a-f**), which is reminiscent of the temporarily phenotypic enhancers previously described [246,247]. To investigate the enhancer perturbation effect on hESC-DE transition with a finer temporal resolution, we focused on two *GATA6* enhancers (*GATA6e+9* and *GATA6e+12*) and measured the differentiation efficiency based on SOX17 expression every 6 hours. Consistent with our dynamic GRN model (**Fig.17a**), the results show an exquisite temporal sensitivity to enhancer perturbations: a significant impact was observed only in a narrow time window (around DE-36h) during the transition (**Fig.25g and 25h**). In summary, these validation results show that the expression of core TF genes is frequently regulated by multiple enhancers, ensuring robustness in the regulatory network. Perturbing a single enhancer can significantly decrease target gene expression and delay cell-state transitions, but most perturbations do not substantially alter the post-transition state. The consistency of our experimental results with our dynamic GRN model suggests a cooperative autoregulatory mechanism underlying this effect. Together they support the utility of cell state transitions in perturbation screens as a generalizable approach for sensitized enhancer discovery.

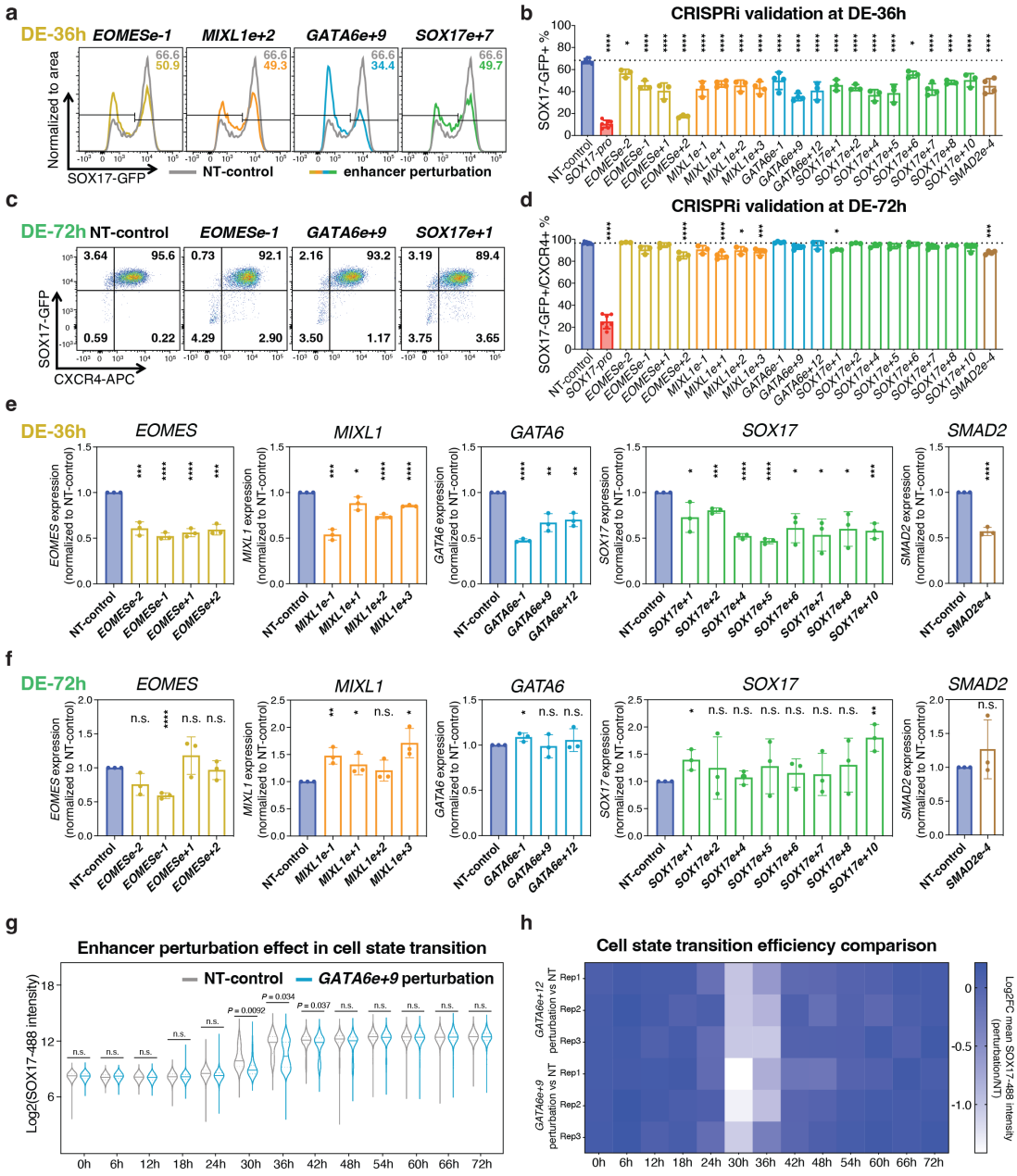

Figure 25. Validation of core enhancers using CRISPRi perturbation. a-d, Representative flow plots showing individual core enhancer perturbations decrease the hESC-DE transition efficiency measured by SOX17-GFP$^+$ at DE-36h (**a**) and SOX17-GFP$^+$/CXCR4-APC$^+$ at DE-72h (**c**). The bar graphs show the percentage of SOX17-GFP$^+$ cells at DE-36h (**b**) and SOX17-GFP$^+$/CXCR4-APC$^+$ at DE-72h (**d**). n≥3 independent experiments. Error bars indicate mean ± SD. Statistical analysis was performed by two-tailed unpaired multiple comparison test with Dunnett correction. Significance is indicated as: *P < 0.05, **P < 0.01, ***P < 0.001 and ****P < 0.0001. **e-f**, RT-qPCR showing the expression of the cognate genes decreases by enhancer perturbations at DE-36h (**e**) but mostly restored at DE-72h (**f**). n=3 independent experiments. Error bars indicate mean ± SD. Statistical analysis was performed by two-tailed unpaired student t-test. Significance is indicated as: *P < 0.05, **P < 0.01, ***P < 0.001 and ****P < 0.0001. n.s.: not significant. **g**, Violin plots showing the effect of *GATA6e+9* perturbation on hESC-DE transition efficiency (SOX17 intensity) measured every 6h through flow cytometry. n=3 independent experiments. Solid lines indicate median. Dashed lines indicate quartiles. Statistical analysis was performed by two-tailed paired student t-test with mean of each replicate. n.s.: not significant. **h**, Heatmap showing the comparison between the mean SOX17 expression intensity of cells with non-targeting control (NT) vs *GATA6e+9* or *GATA6e+12* perturbation measured every 6h through flow cytometry during

hESC-DE transition. A significant impact was observed only in a narrow time window (around DE-36h) during the transition.

Since functional enhancers will form enhancer-promoter contact to activate their cognate genes[63,289], we performed the 4C-seq experiments at the *SOX17* and *GATA6* loci to validate whether our screen identified DE core enhancers increase their interaction with the promoters during DE differentiation. We chose *SOX17* promoter and *GATA6* promoter as viewpoints (VPs) and collected cell at both ESC stage and DE48h. Compared to ESC stage, the upstream of both *SOX17* and *GATA6* showing significant increase of chromatin contact with the promoters at DE48h (**Fig.26a and Fig.26b**). The 4C signals have stronger increase at the regions overlapped with the identified DE core enhancers (**Fig.26a and Fig.26b**), further supporting the gain of chromatin contact between the DE core enhancers and promoters during DE differentiation. 4C-seq with enhancer as viewpoints in WT DE48h and enhancer perturbation conditions were also performed. The data analysis is still in processing.

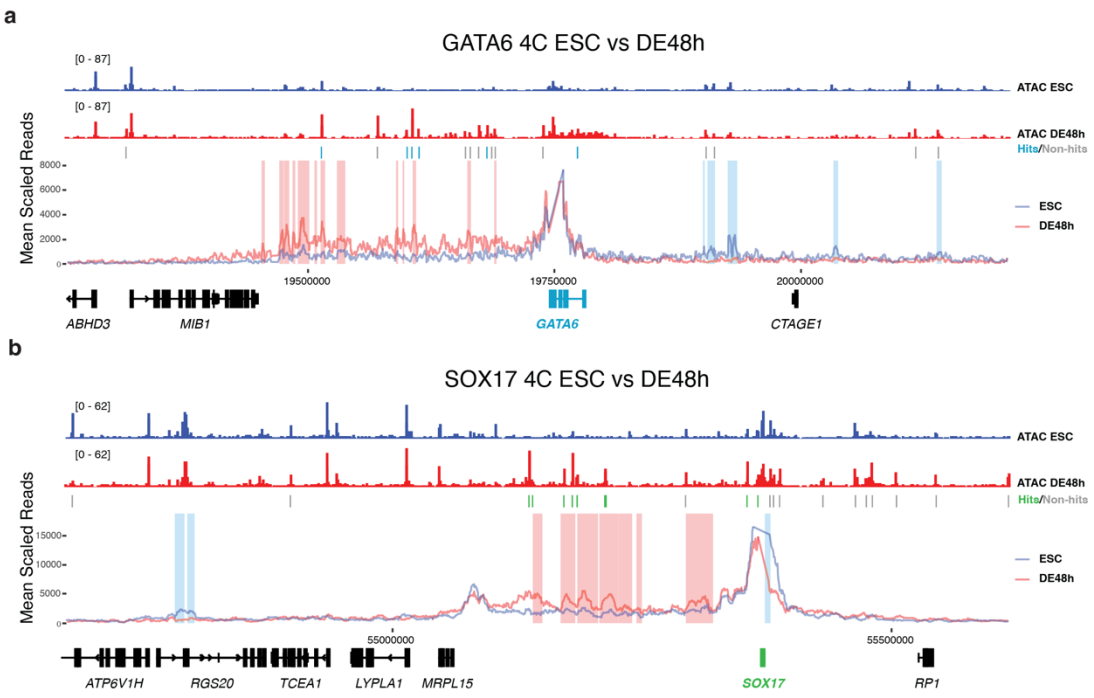

Figure 26. Evaluating the chromatin contact change between the identified DE core enhancers and promoters using 4C-seq during DE differentiation (generated by Wilfred Wong). a and **b**, 4C signals comparison between ESC stage (blue) and DE48h (red) at *GATA6* locus (**a**) and *SOX17* locus (**b**) using *GATA6* promoter and *SOX17* promoter as viewpoint respectively. Red boxes highlight the chromatin regions that have significant increase of contacts to the promoters. Blue boxes highlight the chromatin regions that have significant decrease of contacts to the promoters.

By definition, core enhancer perturbation should cause global effect on cell state transition. We performed bulk RNA-seq and bulk ATAC-seq with the cells that contain selective enhancer perturbations (*SOX17e+4*, *SOX17e+10*, *GATA6e+9* and *GATA6e+12*) at DE24h and DE48h to assess the global effects. Compared to the WT 12h time point RNA-seq results, core enhancer perturbation cells show a global delayed transcriptome using PCA mapping (**Fig.27**). More data analyses are still in progressing.

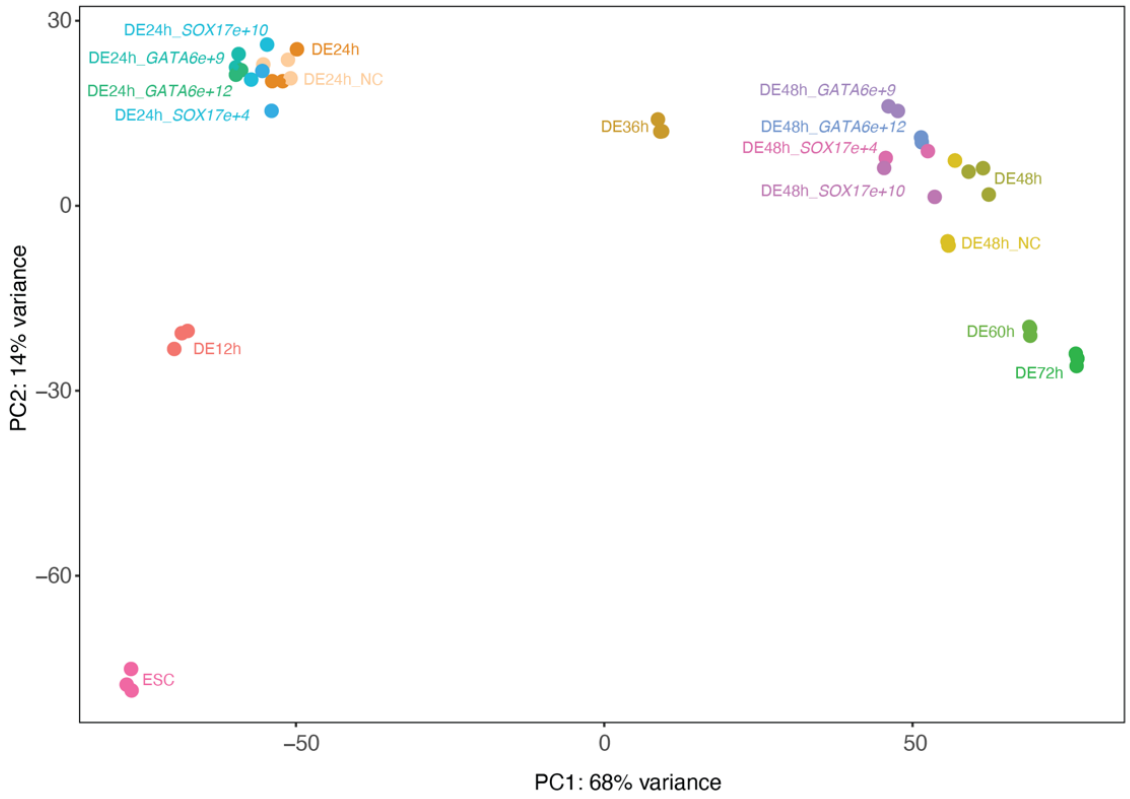

Figure 27. PC analysis of bulk RNA-seq with selective core enhancer perturbation at DE24h and DE48h. Cells with *SOX17e+4*, *SOX17e+10*, *GATA6e+9* and *GATA6e+12* perturbations were collected at DE24h and DE48h for RNA-seq and compared to WT cells.

Enhancer deletions exert stronger impacts than CRISPRi

We reasoned that the GRN is robust in part because multiple enhancers could interact additively or synergistically at a locus to regulate target gene expression. We applied CRISPR-Cas9 to generate single and double deletions of *GATA6e+9* and *GATA6e+12* (**Fig.28a**). The deletion of both *GATA6* enhancers showed a stronger impact on transition efficiencies compared to the expected additive effects of individual enhancer deletions at both DE36h and DE72h (**Fig.28b-d**). These results support synergistic interactions of these two core *GATA6* enhancers. Compared to single enhancer deletions, the double deletion produced a clearer separation of differentiated and undifferentiated cells at DE-72h. These experimental data closely match results from the dynamic GRN modeling (**Fig.28e**). We also compared the enhancer deletion results with single or double perturbations using CRISPRi and found that the latter had mild or no impact at DE72h (**Fig.28d**). Thus, although CRISPRi is more amenable for large-scale enhancer screens than CRISPR-Cas9 mediated deletion, it may miss *bona fide* enhancers especially when examining the perturbation effects in a steady state. The weaker effect of dCas9-KRAB could be due to competition with endogenous TFs and other technical differences between CRISPRi and deletion[290].

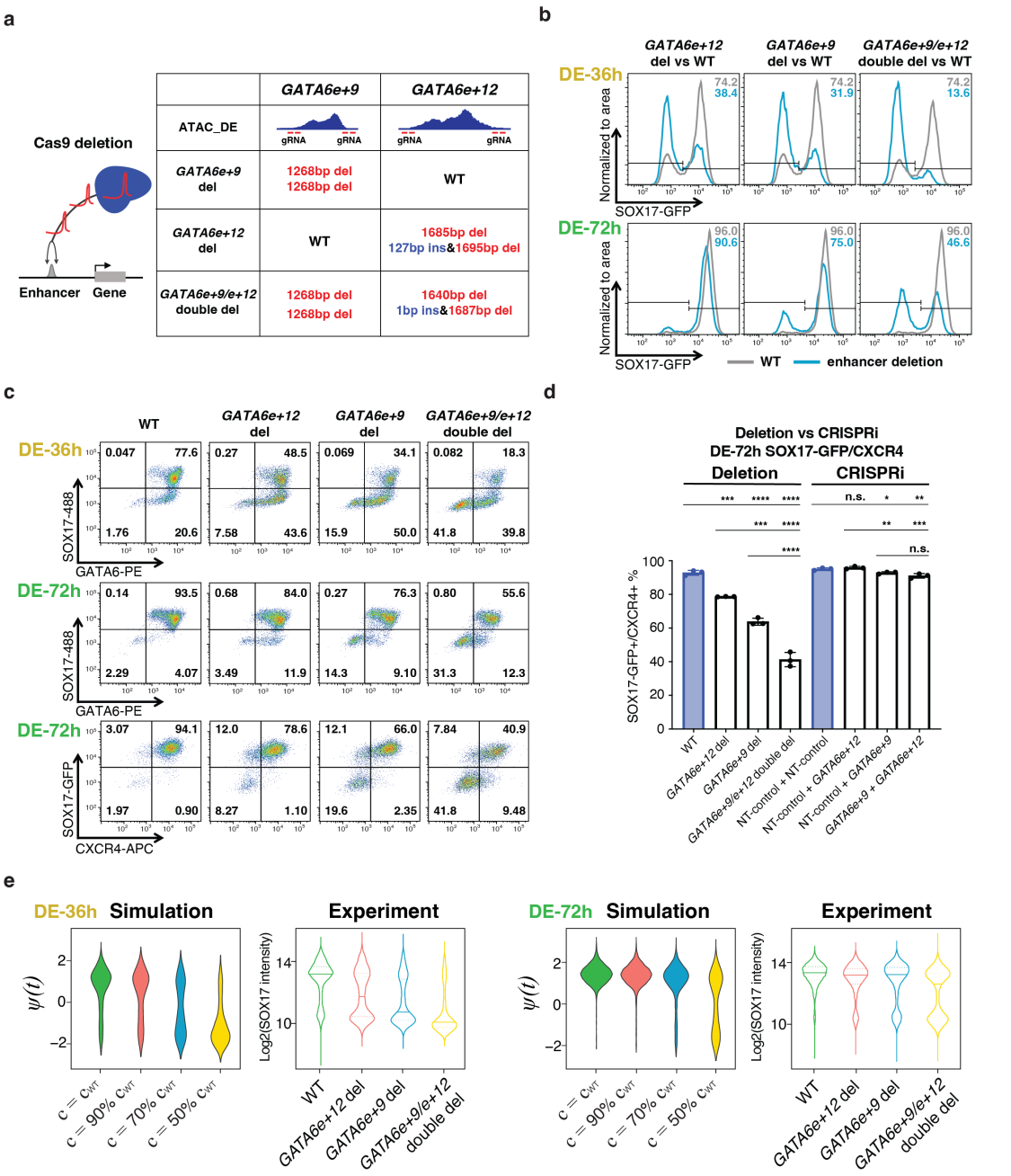

Figure 28. Validation of core enhancers using CRISPR-Cas9 mediated deletion. a, Illustration of *GATA6e+9* del, *GATA6e+12* del and *GATA6e+9/e+12* double del hESC lines generation using two pairs of gRNAs with Cas9. **b**, Flow plots showing *GATA6* core enhancer del reduced hESC-DE transition efficiency at DE-36h and DE-72h. **c**, Flow plots showing SOX17/GATA6 expression at DE-36h, DE-72h and SOX17-GFP/CXCR4 expression at DE-72h of WT, *GATA6e+9* del, *GATA6e+12* del, *GATA6e+9/e+12* double del. **d**, Statistics of SOX17-GFP/CXCR4 double positive cells at DE-72h in WT, *GATA6e+9* del, *GATA6e+12* del, *GATA6e+9/e+12* double del cells, as well as cells with non-targeting control, *GATA6e+9* perturbation, *GATA6e+12* perturbation and *GATA6e+9/GATA6e+12* dual-perturbation. n=3 biological replicates. Error bars indicate mean ± SD. Statistical analysis was performed by two-tailed unpaired multiple comparison test with Dunnett correction. Significance is indicated as: *P < 0.05, **P < 0.01, ***P < 0.001 and ****P < 0.0001. n.s. Not significant. **e**, The comparison between the simulation and experiment results of the impact of different levels of enhancer perturbation on cell state transition. Solid lines indicate median. Dashed lines indicate quartiles (partially generated by Dr. Michael A. Beer).

Despite the technical differences, the "differentiation delay" is observed with both CRISPRi and deletion (**Fig.29a and Fig.29b**). When we deleted two *SOX17* enhancers (labeled as *SOX17e+4/e+5* double del), the impact on differentiation was mostly recovered by DE-72h with only a small decrease in differentiation efficiency; and by DE-96h and DE-120h, there were no significant differences. A similar trend was observed for the deletion of *GATA6e+12* when we examined at DE-96h and DE-120h. However, for deletion of *GATA6e+9* or double deletion of *GATA6e+9/e+12*, the impact on differentiation remained strong even when examined at DE-120h (**Fig.29a and Fig.29b**). These findings are consistent with our conclusion that the network is robust post-transition but can still be disrupted with strong perturbations (which can be either CRISPRi perturbation of a strong enhancer, or deletion of one or multiple enhancers). Overall, our findings demonstrate that the GRN is robust post-transition but can still be disrupted with strong perturbations as achieved here through the double deletion of *GATA6* enhancers.

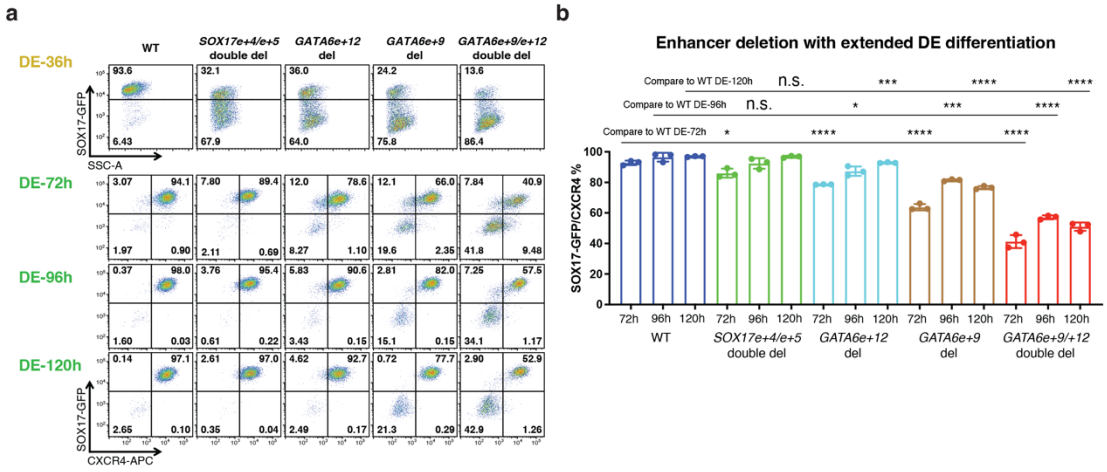

Figure 29. Differentiation delay by weak enhancer deletion(s) can be restored by extended differentiation. a, Flow plots showing SOX17-GFP expression at DE-36h and SOX17-GFP/CXCR4 expression at DE-72h, DE-96h and DE120h of WT, *SXO17e+4/e+5* double del, *GATA6e+12* del, *GATA6e+9* del, *GATA6e+9/e+12* double del. **b**, Statistics of SOX17-GFP/CXCR4 double positive cells at DE-72h, DE-96h and DE120h of WT, *SXO17e+4/e+5* double del, *GATA6e+12* del, *GATA6e+9* del, *GATA6e+9/e+12* double del. n=3 biological replicates. Error bars indicate mean ± SD. Statistical analysis was performed by two-tailed unpaired student t-test. Significance is indicated as: *P < 0.05, **P < 0.01, ***P < 0.001 and ****P < 0.0001. n.s. Not significant.

GATA6 plays a critical role in the development of various cell lineages, including but not limited to endoderm[291], precardiac mesoderm[292], pancreatic progenitor cells[293]. To further investigate the function of the two identified *GATA6* core enhancers during the development, we differentiated the *GATA6e+9* del, *GATA6e+12* del and *GATA6e+9/e+12* double del hESC lines to the pancreatic progenitor stage 1 (PP1). Compared to the WT, we observed a significant decrease in PDX1 expression in all enhancer deletion lines measured by flow cytometry, and the *GATA6e+9* del and *GATA6e+9/e+12* double del lines failed completely in PP1 differentiation (**Fig.30a and Fig.30b**).

Since *GATA6* function is conserved in mouse development and the corresponding conserved regions of *GATA6e+9* and *GATA6e+12* are present in the mouse genome (**Fig.30c**), we generated *Gata6e+9* del, *Gata6e+12* del and *Gata6e+9/e+12* double del mouse lines by injected gRNA and Cas9 into the zygotes to investigate their function during mouse development (**Materials and methods**). In sharp contrast to the strong phenotypes observed during PP1 differentiation in hESC lines, homozygous eletion of these enhancers did not cause any observable phenotypic abnormal (**Data not shown**). We further generated compound heterozygous mouse lines by crossing *Gata6* heterozygous knockout (KO) mice with each enhancer deletion mouse line, but again, no phenotypic abnormal was observed (**Data not shown**). Even though the enhancer deletion mice are in general phenotypically normal, subtle phenotype differences cannot be ruled out, as *Gata6* heterozygous KO mouse embryos showed a significantly lower number of primitive endoderm cells in previous studies[294]. Besides the potential subtle phenotype, previous studies have shown that GATA6 dosage requirement during pancreas development is lower

in mouse than in humans[293,295], which may explain the phenotypic differences observed in the hESC-derived PP1 differentiation and mouse development with enhancer deletion lines.

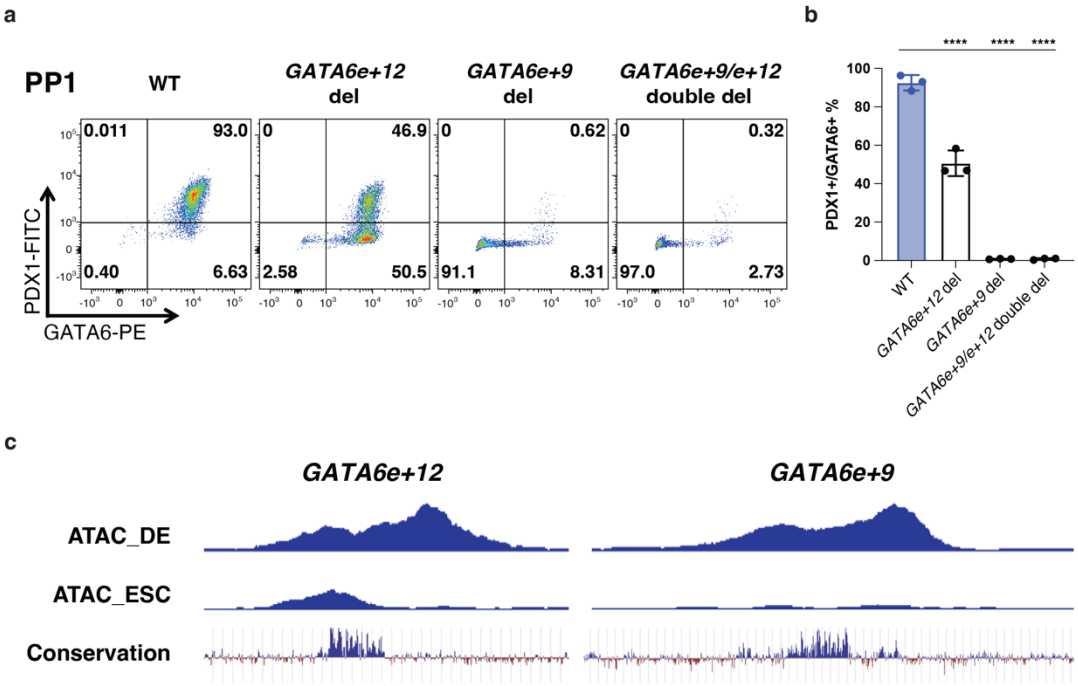

Figure 30. *GATA6* enhancers exhibit different phenotypes in human and mouse. a, Flow plots showing PDX1/GATA6 expression at PP1 of WT, *GATA6e+9* del, *GATA6e+12* del, *GATA6e+9/e+12* double del. **b**, Statistics of PDX1/GATA6 double positive cells at PP1 in WT, *GATA6e+9* del, *GATA6e+12* del, *GATA6e+9/e+12* double del cells. n=3 biological replicates. Error bars indicate mean ± SD. Statistical analysis was performed by two-tailed unpaired multiple comparison test with Dunnett correction. Significance is indicated as: *P < 0.05, **P < 0.01, ***P < 0.001 and ****P < 0.0001. n.s. Not significant. **c**, *GATA6e+9* and *GATA6e+12* are conserved among different species.

CIA model improves enhancer prediction

Our CRISPRi screen and validation studies identified multiple enhancers around the core DE regulators (GATA6, EOMES, SOX17, and MIXL1; **Supplementary table 7**). This high-quality dataset allowed us to explore genomic features that can distinguish the enhancers which were positive in the screen (hits) from those which were not (non-hits). As expected, all enhancer hits for the core DE TFs had elevated levels of H3K27ac and increased accessibility during hESC-DE transition, accompanied by the binding of DE core TFs EOMES, GATA6 and SOX17 (**Fig.31**).

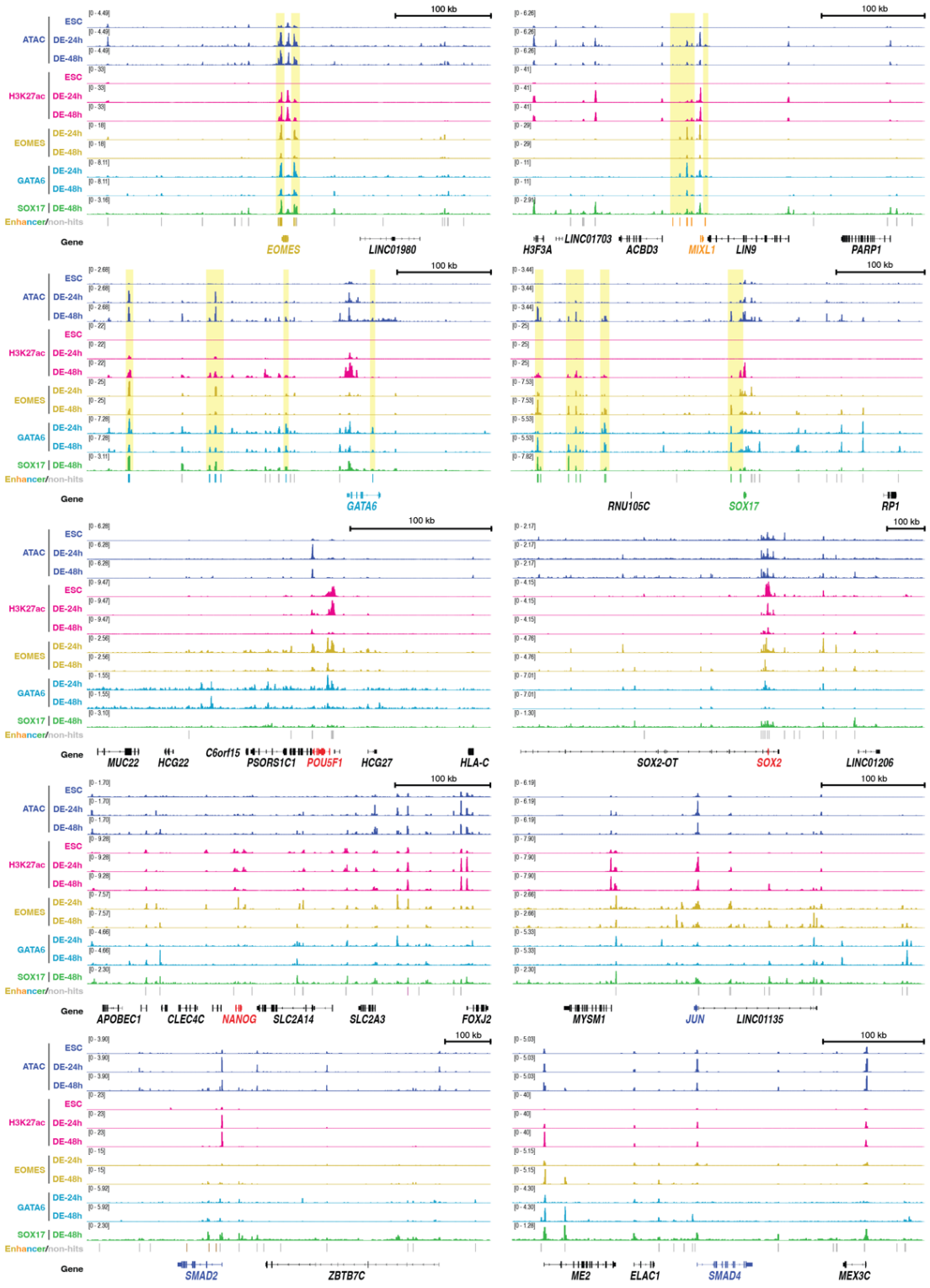

Figure 31. Epigenetic features of core enhancers. Relevant ATAC-seq and ChIP-seq tracks of all 10 selected loci. Yellow boxes highlight the DE core TFs (EOMES, GATA6 and SOX17) bind to DE core enhancers. Genomic coordinates from GRCh38 (human hg38) for each gene are labeled. kb, kilobase.

However, we also noticed that the hits were often located on one side of the TSS. We performed Hi-C and CTCF ChIP-seq experiments in ESC and DE, and observed strong concordance among bounded domains of increased Hi-C contact frequency (often referred to as TADs), CTCF loops measured by ChIA-PET in H1 hESCs [280], CTCF loops predicted by our loop competition and extrusion model (LE model) [165] and CTCF binding (**Fig.32**). While Hi-C does detect increased interactions between the promoter and distal enhancer hits (i.e., *SOX17e+10*) in DE, Hi-C contact frequency between the promoter and distal enhancers is only weakly correlated with the effect of enhancer perturbation (**Fig.33c**). In addition, enhancer hits are often distributed broadly around the target gene (**Fig.23c and Fig.24b**), while the Hi-C contact signals are primarily enriched near the promoter (**Fig.32**). In contrast, all the *SOX17* enhancer hits fall into a CTCF loop enclosing the promoter (**Fig.32**), both as measured by CTCF ChIA-PET [280] and as predicted by the LE model [165]. To quantify, we calculated the Hi-C contact frequency (with the promoter) for each enhancer along the locus. We also computed the probability (denoted as P(in loop)) that each distal enhancer is enclosed within the same CTCF loop as the promoter, using the ratio of the sum of counts for all loops enclosing both enhancer and promoter to the sum of all counts for all loops enclosing the promoter (**Materials and methods**). Comparing the genomic intervals with large P(in loop) against those intervals with large Hi-C contact frequency, the former is broader and encompasses more hits (**Fig.32**). Similar observations hold for the other loci (**Fig.32**). This suggests that we are less likely to miss impactful enhancers based on predictions by their enclosure within a CTCF loop than by enhancer-promoter Hi-C contact frequency.

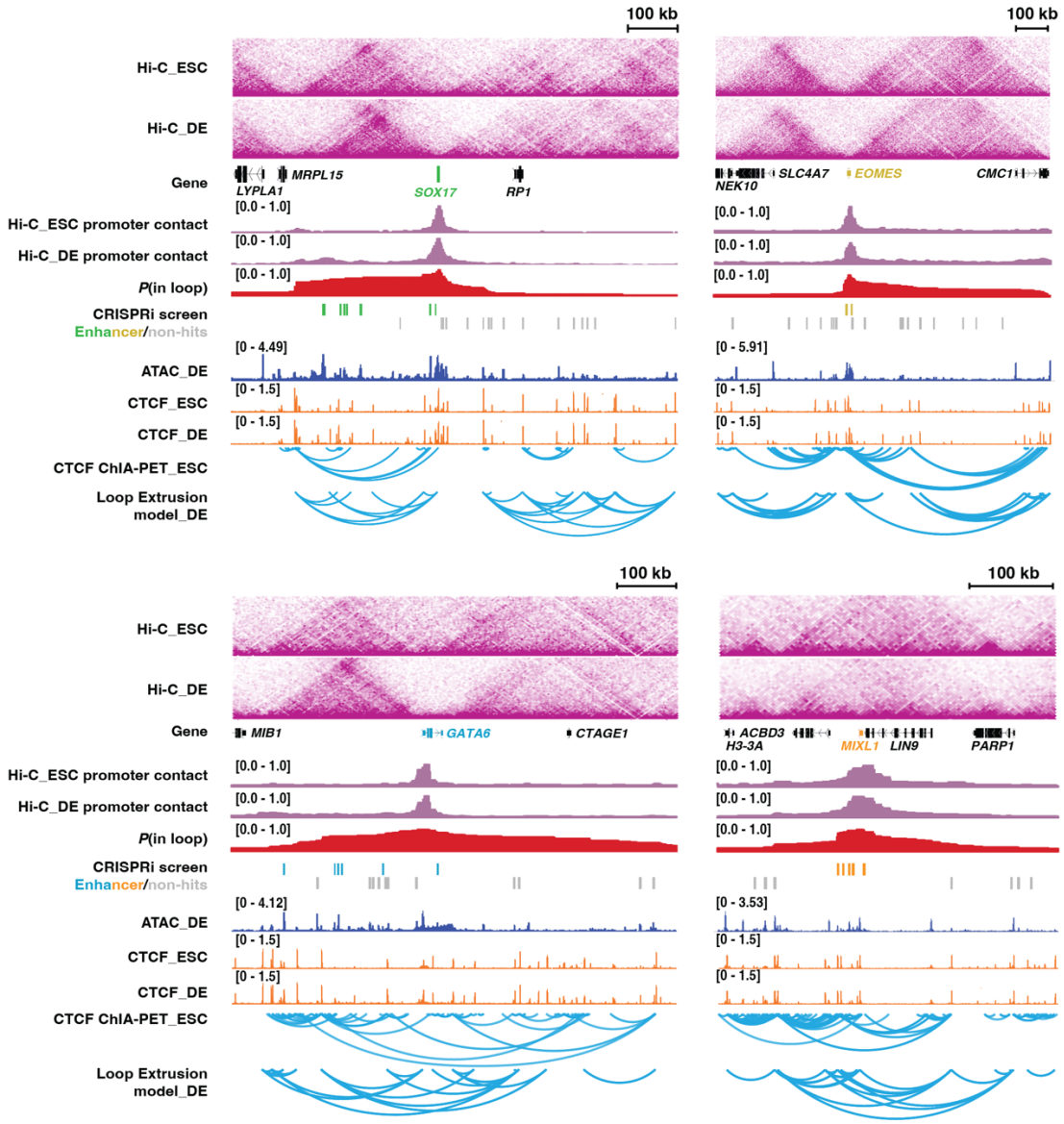

Figure 32. 3D conformation of DE core TF loci (generated by Dr. Michael A. Beer). Hi-C-based and CTCF loop-based chromatin conformation analysis at the *SOX17*, *EOMES*, *GATA6* and *MIXL1* loci.

To quantitatively compare the predictive power of these chromatin conformation features individually, we plot precision-recall curves for predicting hits (log2FC > 0.15) from non-hits for all DE gene enhancers (**Fig.33a and 33b; Supplementary table 7**). *P*(in loop) is more predictive (AUPRC=.818) than Hi-C contact frequency in DE (.692), Hi-C contact frequency in ESC (.598) or 1/|distance| from the promoter (.604). Many non-hit enhancers with a high *P*(in loop) have low chromatin accessibility, TF binding, and

H3K27ac (**Fig.31 and Fig.32**). Therefore, we tested all combinations of these features and the enhancer-promoter interaction information based on CTCF looping or Hi-C, using logistic regression, and assessed both AUPRC and correlation with log2FC (**Fig.33c and 33d**). Among the potential enhancers we tested, enclosure within a promoter-containing CTCF loop is more predictive than any other single feature. Combining interaction information with ATAC, H3K27ac and TF binding improves AUPRC, and in all cases CTCF loop-based models are more predictive than Hi-C contact frequency-based models. The combination of CTCF loop, ATAC, and H3K27ac achieves a very accurate prediction with AUPRC=.898. There is a further slight improvement by adding core TF binding data from EOMES, GATA6, SOX17 ChIP-seq (AUPRC=.925). Adding H3K4me1 to ATAC and H3K27ac can slightly improve the predictive power, but the prediction with H3K4me1 is not as good as H3K27ac when either is combined with ATAC alone or ATAC and core TF binding (**Fig.33e**). The ABC model [150] combines ATAC and H3K27ac into $Activity = \sqrt{ATAC * H3K27ac}$, and uses either Hi-C contact frequency or 1/|distance| as contact measurement. We found that CTCF loop-constrained models outperformed both (**Fig.33c and 33d**). Nevertheless, we found that combining the $Activity = \sqrt{ATAC * H3K27ac}$ with CTCF loop information is simpler and performs comparably to logistic regression using ATAC and H3K27ac independently (**Fig.33c**).

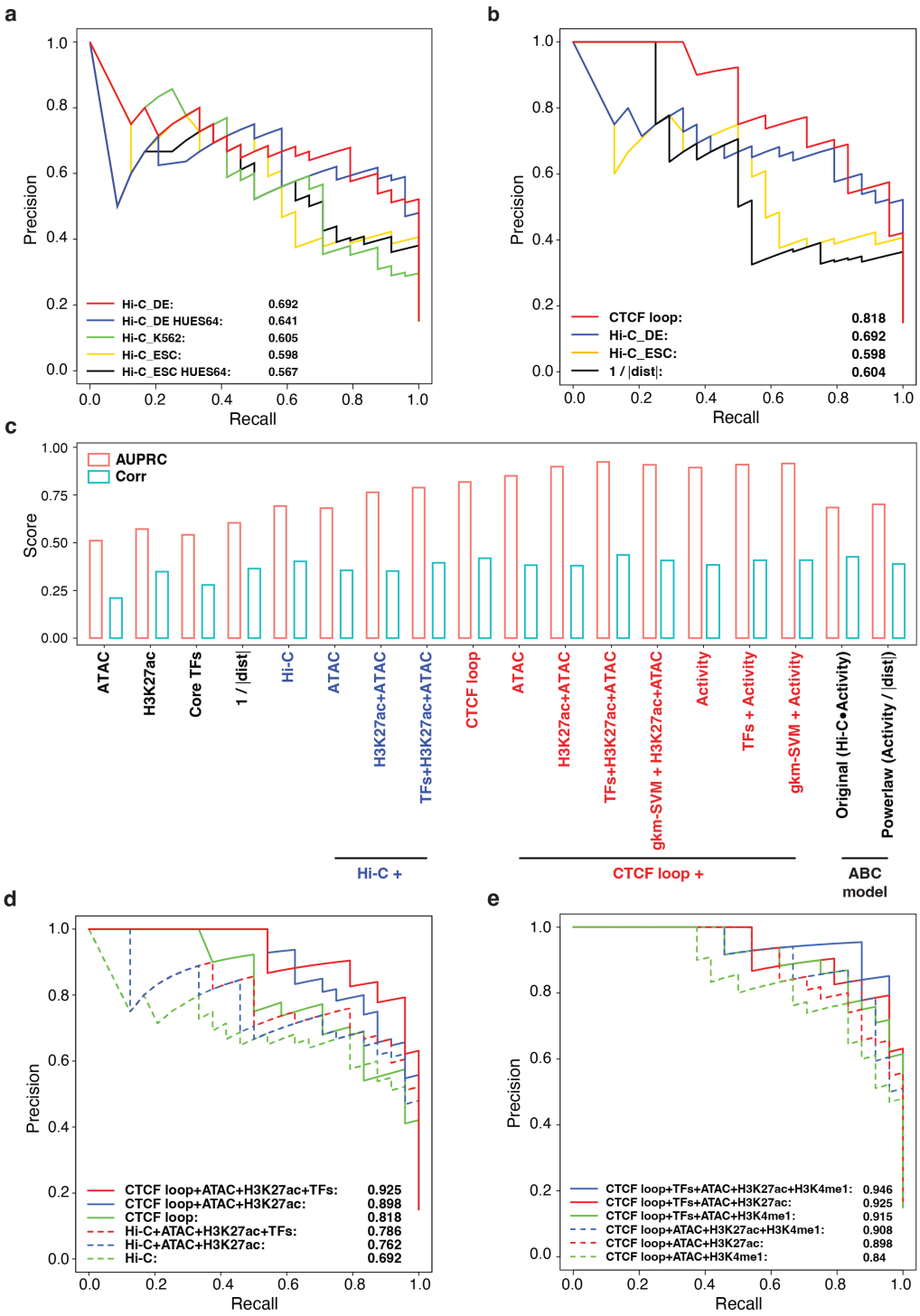

Figure 33. The CIA model provides improved enhancer prediction (generated by Dr. Michael A. Beer). **a**, Precision-recall plot comparing the performance for prediction of enhancer hits from the screen using different Hi-C datasets. **b**, A precision-recall plot comparing the performance for prediction of enhancer hits from the screen using *P*(in loop, red), DE Hi-C (blue), ESC Hi-C (yellow) and enhancer-promoter distance (black). **c**, Bar plots comparing the AUPRC and correlation scores between single chromatin feature-based, Hi-C-based, or CTCF loop-based enhancer prediction model with the ABC model. **d**, A precision-recall plot comparing the performance for prediction of enhancer hits from the screen using CTCF loop (solid line) and Hi-C (dash line) with or without additional chromatin feature combination. **e**, Precision-recall plot comparing the performance for prediction of enhancer hits from the screen using CIA model with additional H3K4me1 chromatin feature.

The combination of $P(\text{in loop}) > 0.5$ and $Activity$ can classify most hits more cleanly than $Activity$ in combination with Hi-C (**Fig.34a**). Our best classification result is with both $P(\text{in loop})$ above a threshold near 0.5 and $Activity = \sqrt{ATAC * H3K27ac}$ greater than a threshold value near 1; as shown in **Fig.34b**, almost all hits (green) are correctly classified, and non-hits are correctly classified either by being outside a CTCF loop (grey) or below the $Activity$ threshold curve (red). Since both $P(\text{in loop})$ and $Activity$ are required, we will refer to the combined rule $CIAscore = P(\text{in loop}) * Activity$ as the CTCF loop-constrained Interaction Activity (CIA) model.

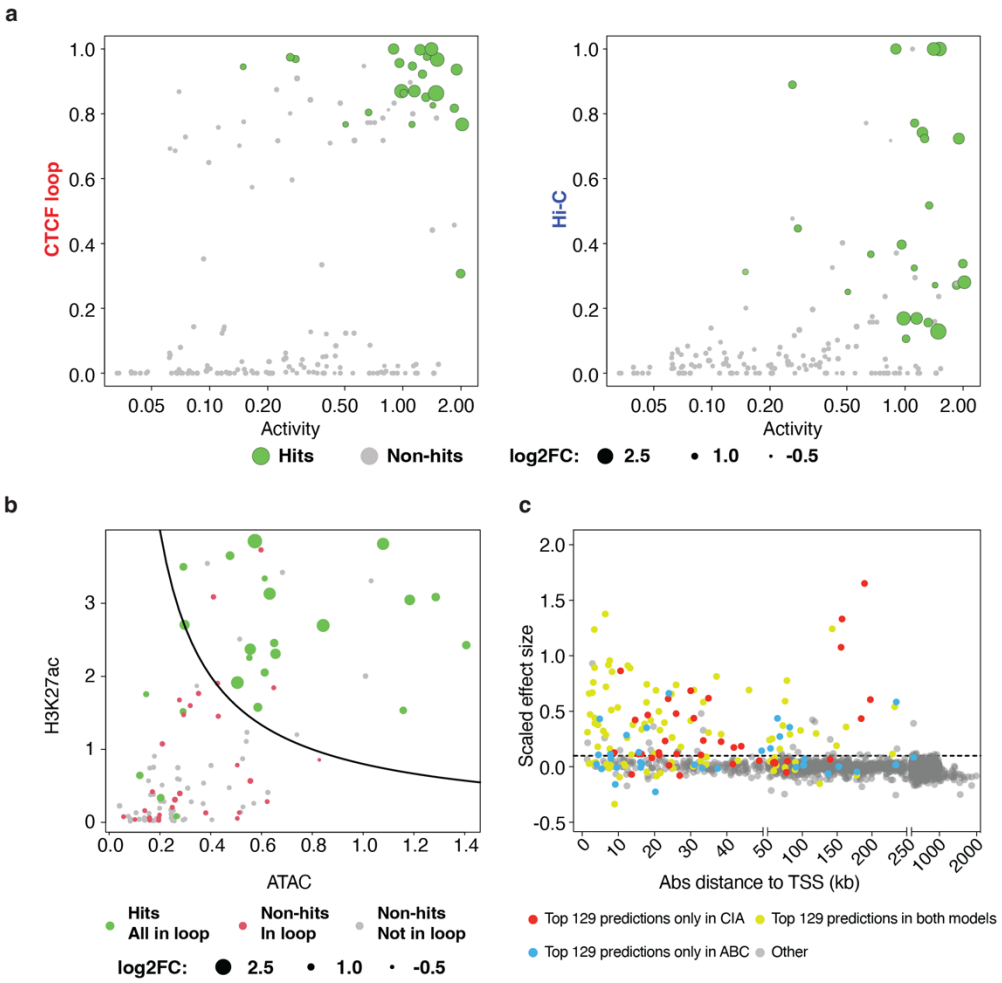

Figure 34. The CIA model provides clear separation of hits vs non-hits (a and b were generated by Dr. Michael A. Beer). a, A scatter plot showing the $P(\text{in loop})$ can classify hits (green) and non-hits (grey) more clearly than Hi-C-based enhancer-promoter contact frequency. The size of each dot represents the log2FC of each enhancer from the screen. **b**, A scatter plot showing the combinatory criteria of $P(\text{in loop})$, H3K27ac and ATAC can clearly separate the hits (green)

and non-hits (red and gray). P(in loop) > 0.5 is used to justify the enhancers and targeting promoters are in the same CTCF loop (green and red). The solid line represents the threshold value (criteria) of $Activity = \sqrt{ATAC * H3K27ac}$. The size of each dot represents the log2FC of each enhancer from the screen. **c**, A scatter plot showing the comparison between the CIA and ABC model with all 3 datasets (ESC-DE, K562 Reilly[241] and K562 Nasser[282]). The numbers of selected top predictions are based on the hits identified from each data set, including top 24 predictions from ESC-DE, top 36 predictions from K562 Reilly and top 69 predictions from K562 Nasser. Yellow dots represent top predictions in both models. Red dots represent top predictions only in the CIA model. Cyan dots represent top predictions only in the ABC model. Grey dots represent regions that do not belong to top predictions. The effect sizes from each data set are scaled to reach to the same threshold (~0.1 dashed line).

We further evaluated the generalizability of this model with additional CRISPRi datasets from K562 cells in Reilley *et al* [241] and Nasser *et al* [282]. The latter study summarized screening data from multiple sources [150,233,242,249-252]. After mapping gRNAs to distal accessible regions (DHS peaks) in K562 cells, we identified 36 hits and 414 non-hits around 12 genes from Reilley *et al* (**Fig.35a; Supplementary table 8**) and 69 hits and 1862 non-hits from Nasser *et al* (**Fig.36a; Supplementary table 9**). Using these data, we also found that CTCF loop information was more predictive than Hi-C contact frequency (**Fig.35b and Fig.36b**), and CTCF loop + $Activity$ was more predictive than the ABC model or Hi-C + $Activity$ (**Fig.35c, Fig.35d, Fig.36c and Fig.36d**). An $Activity$ threshold again clearly distinguished hits within loops (**Fig.35e and Fig.36e**). To better compare between the CIA and ABC models, we integrated all three datasets (ours, Reilley et al., and Nasser et al.). We scaled log2FC to "effect size" (**Materials and methods**) and show the effect size vs. distance from TSS for all enhancer-promoter pairs tested (**Fig.34c**). For an equal number of positive predictions by CIA and ABC in each dataset (24+36+69, fixed recall), many strong effect enhancers are predicted by both models (yellow). However, the predictions made by CIA alone (red) have larger effects than predictions made by ABC alone (blue). Adding TF binding to the CIA model more clearly distinguishes hits from non-hits and performs slightly better (**Fig.33c and Fig.33d**). In the absence of TF binding information, gkm-SVM scores can reproduce this small improvement in predictive accuracy (**Fig.33c, Fig.35c and Fig.36c**). In summary, using

three large functional enhancer screening datasets, we show that enhancer impact is more reliably predicted by enhancer location within a CTCF loop than by direct enhancer-promoter Hi-C contact frequency, and we constructed a simple predictive model of enhancer impact by combining CTCF loop-constrained interaction and enhancer activity.

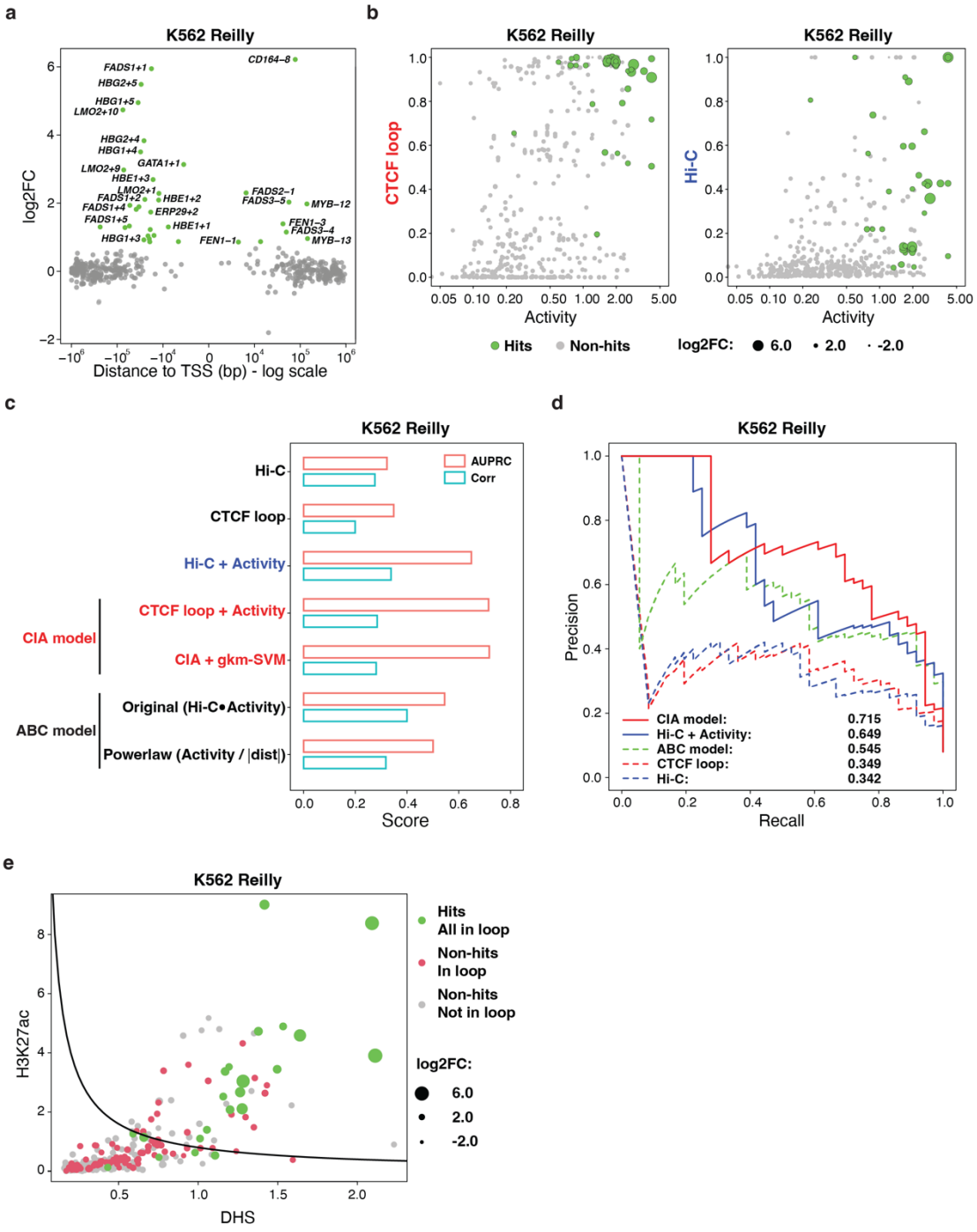

Figure 35. The CIA model predicts active enhancers in K562 Reilly (generated by Dr. Michael A. Beer). a, gRNA enrichment analysis identified 36 hits from the HCR-FF screen in K562 cells from *Reilly et al* [241] **b**, The scatter plot showing the *P*(in loop) can classify hits (green) and non-hits (grey) in K562 HCR-FF screen more clearly than Hi-C-based enhancer-promoter contact frequency. The size of each dot represents the log2FC of each enhancer from the screen. **c**, Bar plot comparing the AUPRC and correlation scores between Hi-C-based enhancer prediction with CIA model and ABC model using K562 HCR-FF screen results. **d**, Precision-recall plot comparing the performance for prediction of enhancer hits from the K562 HCR-FF screen using CTCF loop-based model and Hi-C-based model. **e**, The scatter plot showing the combinatory criteria of *P*(in loop), H3K27ac and ATAC can clearly separate the hits (green) and non-hits (red and gray) from the K562 HCR-FF screen. *P*(in loop) > 0.5 is used to highlight enhancers and targeting promoters in the same CTCF loop (green and red). The solid line represents the same threshold criterion of $Activity = \sqrt{ATAC * H3K27ac}$ in Fig.33b. The size of each dot represents the log2FC of each enhancer from the K562 HCR-FF screen.

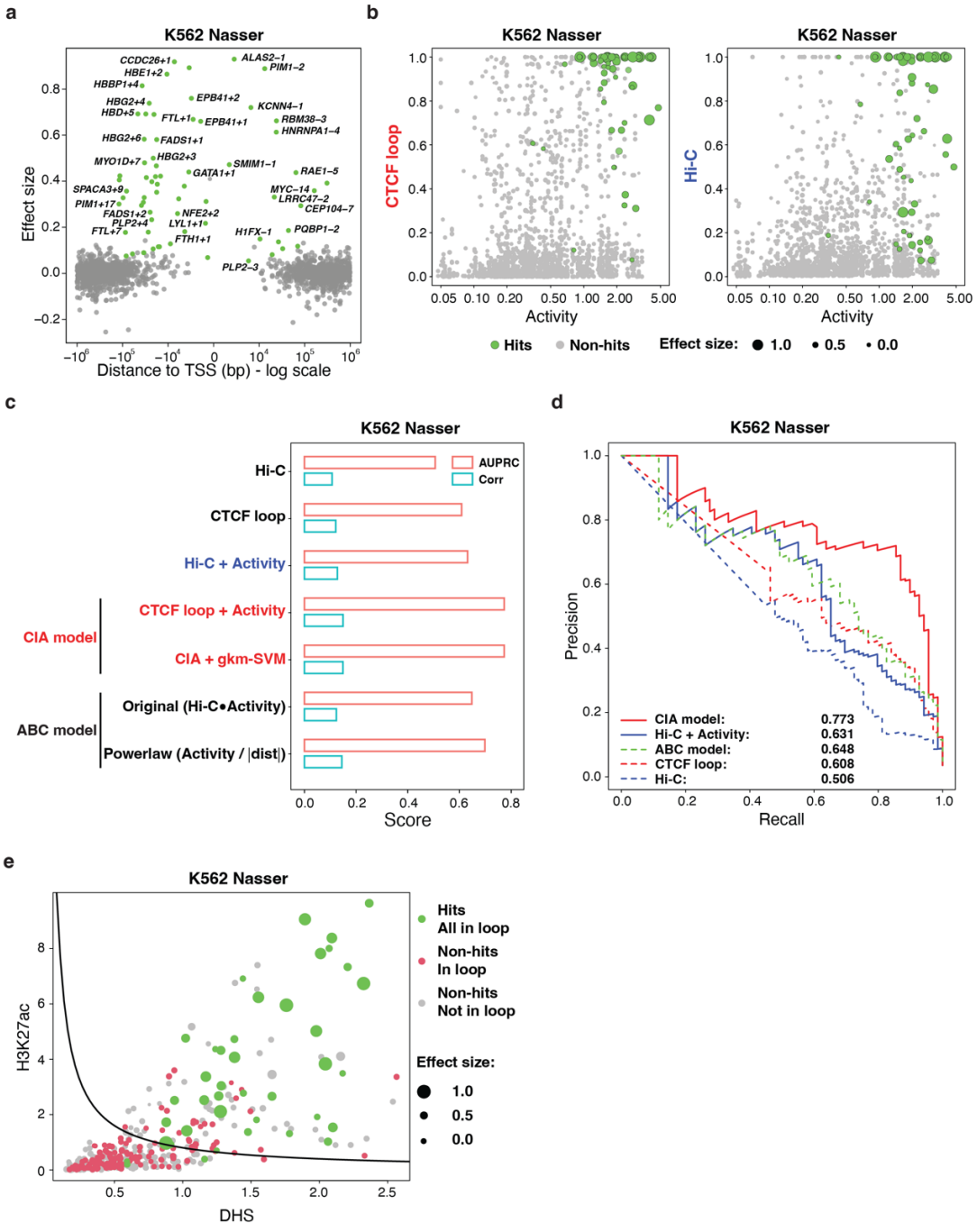

Figure 36. The CIA model predicts active enhancers in K562 Nasser (generated by Dr. Michael A. Beer). a, 69 identified hits in the K562 cells from *Nasser et al* are plotted[282]. **b**, The scatter plot showing the P(in loop) can classify hits (green) and non-hits (grey) in K562 Nasser more clearly than Hi-C-based enhancer-promoter contact frequency. The size of each dot represents the effect size of each enhancer from *Nasser et al*. **c**, Bar plot comparing the AUPRC and correlation scores between Hi-C-based enhancer prediction with CIA model and ABC model using K562 Nasser results. **d**, Precision-recall plot comparing the performance for prediction of enhancer hits from the K562 Nasser using CTCF loop-based model and Hi-C-based model. **e**, The scatter plot showing the combinatory criteria of P(in loop), H3K27ac and ATAC can clearly separate the hits (green) and non-hits (red and gray) from the K562 Nasser. P(in loop) > 0.5 is used to highlight enhancers and targeting promoters in the same CTCF loop (green and red). The solid line represents the same threshold criterion of $Activity = \sqrt{ATAC * H3K27ac}$ in Fig.33b. The size of each dot represents the effect size of each enhancer from the K562 Nasser.

Identified peripheral enhancers through genome-scale perturb-seq screen

Since the core DE enhancers have been identified, we further focused on mapping the peripheral DE enhancers to build the entire DE enhancer atlas. As previously described, peripheral genes are commonly not TFs. Therefore, they cannot direct regulate each other and are relative independent of each other (**Fig.2a, Fig.14a and Fig.14b**). Due to this intrinsic difference, we cannot use single reporter strategy to monitor the perturbation effect of peripheral enhancers like we used in the core enhancer screen. Instead, each peripheral gene needs its own expression readout. Besides the gene expression readout, identification of gRNA in each cell is also required to assess the function of a peripheral enhancer to regulate its cognate peripheral gene. Considering relative independency between peripheral genes, if multiple perturbation happened in the same cell, the perturbation effect will be less likely to have crosstalk. Perturb-seq, a method that combines the scRNA-seq as expression readout and gRNA capture as perturbation readout (**Fig.37**), have been used to study the gene and enhancer perturbation effect in multiple studies[252,296-299]. This method provides the technical feasibility for mapping the DE peripheral enhancers with large-scale CRISPRi screen.

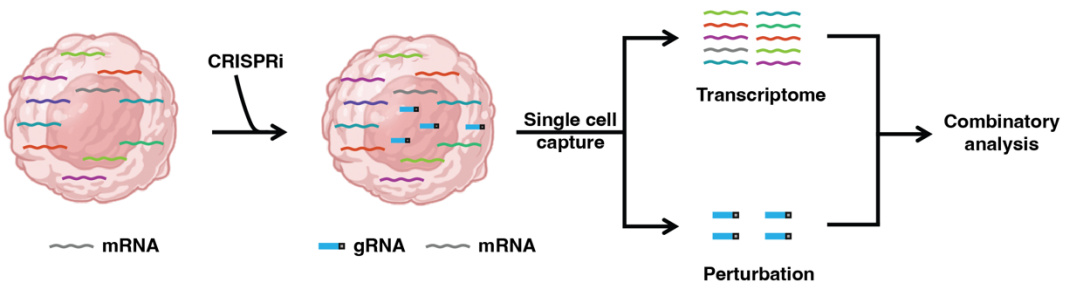

Figure 37. Perturb-seq. The schematic of perturb-seq experiment workflow (Plots are partially generated by using biorender).

To discover DE peripheral enhancers, we first selected 860 peripheral genes with expression 2-fold greater at DE48h compared to ESC (not including DE core TFs) and identified 10614 regions (including promoters) at DE48h flanking 250 kb up/down stream of the 860 peripheral genes. For each region, we then designed maximum 4 specific gRNAs to generate a 37929 gRNAs library (including 66 positive controls targeting validated core enhancers and promoters, as well as 1,100 negative controls targeting safe harbor loci [277], **Fig.38; Supplementary table 10**).

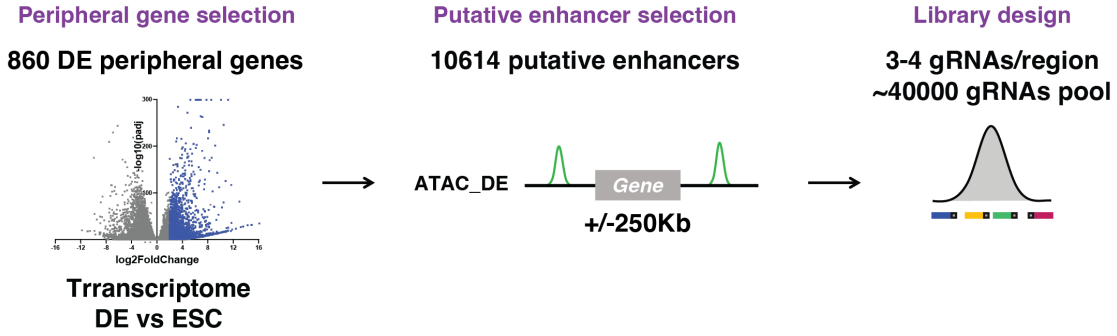

Figure 38. The gRNA library design of large-scale DE peripheral enhancer perturb-seq screen.

Since the peripheral enhancer gRNA library is very large for a perturb-seq experiment, therefore, a high gRNA capture efficiency is necessary to reduce experimental cost. The transcriptome capture of perturb-seq is same as normal scRNA-seq. But the gRNA capture technology has two major categories, poly-T capture and direct capture (**Fig.39**). gRNAs' expression is driven by RNA polymerase III, therefore, gRNAs don't have poly-A tail. Paul Datlinger *et al*. designed a CROP-seq backbone so that gRNA will

be transcribed into two version, the normal functional version without polyadenylated (poly-A) tail and a puromycin^{R}-gRNA fusion version RNA driven by polymerase II with poly-A tail[297]. This gRNA-contained fusion mRNA allows gRNA to be captured by the poly-T oligo that used for transcriptome capture in the 10x Genomics Chromium Single Cell 3′ Reagent Kits (**Fig.39**). However, unlike poly-T capture that needs to engineer gRNA to contain poly-A tail, direct capture uses a oligo that contain specific sequence within the gRNA scaffold (Capture Sequence 1 or 2, CS1 or CS2) to directly target the regular gRNA that driven by RNA polymerase III[296] (**Fig.39**).

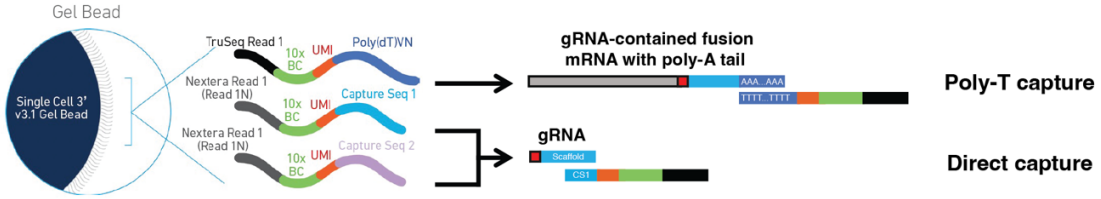

Figure 39. gRNA capture methods: Poly-T capture vs Direct capture. gRNA-contained fusion mRNA contains poly-A tail that can be captured by poly-T. gRNA contain Capture Sequence 1 can be directly capture (adapted from 10x Genomics).

We first assessed the poly-T capture efficiency with a 48-gRNA mini pool using CROP-seq backbone[297]. These 48-gRNA mini pool was designed and generated by Jielin Yan for her purpose. Here, I just used it for evaluating the CROP-seq gRNA capture efficiency. Each gRNA was cloned individually into the CROP-seq backbone and mixed equal amount to generate pooled lentiviral library (**Materials and methods**). We infected idCas9-KRAB *SOX17*$^{eGFP/+}$ HUES8 hESCs with the lentiviral gRNA library at a MOI of ~0.1 to ensure that most infected cells received a single gRNA. Cells were doxycycline treated and harvested at ESC stage and DE36h to perform perturb-seq experiments (**Fig.40a**). Sequencing results were aligned using 10x Cellranger with standard setup for custom feature barcode. Filtered_feature_bc_matrixs were used for downstream analysis. For two experiments, in total we identified 46856 cells with transcriptome captured. The

median of total gRNA unique molecular identifier (UMI) per cell is 18 (**Fig.40b**). We used 10 UMI and UMI of second-most abundant gRNA/most abundant gRNA is < 0.5 as threshold for gRNA assignment. Because we used a MOI of ~0.1 for infection, singlets should only contain one type of gRNA, whose UMI is ≥ 10. After gRNA assignment and live cell filters, only 38% of cells (17600 cells) have been classified as live singlets with successful capture of single type of gRNA for downstream analysis (**Fig.40c**). With this efficiency, we need to double the collected cells to reach the same gRNA representation, which is not feasible for a perturb-seq experiment with ~40K gRNAs library.

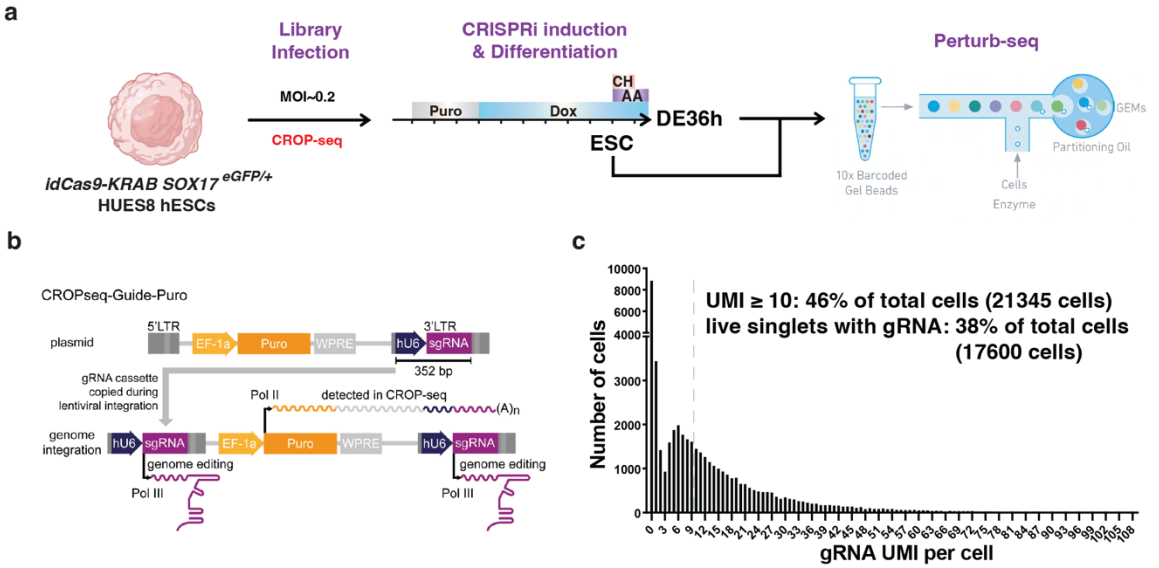

Figure 40. Assessing gRNA capture efficiency using CROP-seq backbone. a, The design of gRNA capture efficiency test using 10x poly-T capture with CROP-seq backbone (adapted from 10x Genomics). **b**, The CROP-seq backbone includes a gRNA cassette within the 3′ long terminal repeat (LTR), which is duplicated during viral integration. It expresses an RNA polymerase III transcript for genome editing and a polyadenylated RNA polymerase II transcript detected by single-cell RNA-seq[297]. **c**, The histogram of gRNA UMI counts per cell with CROP-seq backbone. (Plots are partially generated by using biorender).

Since gRNA and transcriptome use the same poly-T oligo for capture and transcriptome mRNA are much more abundant than the gRNA-contained fusion mRNA, there is competition for gRNA capture by poly-T oligo compared to transcriptome capture. However, direct capture uses a specific oligo for gRNA capture. This design in theory will provide a better gRNA capture efficiency. To assess the gRNA capture efficiency by direct

capture, we generated a direct capture capable gRNA vector (LentiGuide-puro-10x-CS1-3') and cloned our peripheral enhancer gRNA library into it (**Fig.41a**). Instead of using a MOI of ~0.1 for single gRNA delivery, we aim to have multiple gRNAs delivered into the same cells by using super concentrated lentiviral library. To generate super concentrated lentiviral library, 100ml of unconcentrated viral supernatant were collected for concentration under 25,000rcf at 4°C for 90min. Supernatant was gently removed after centrifugation. 2ml DPBS was used to resuspend virus to generate 50-fold concentrated peripheral enhancer lentiviral library (**Materials and methods**). We tested different volume of virus to achieve 15-20 gRNAs per cell. Cells infected with different amount of concentrated lentiviral library were harvested after selection for genomic DNA and RNA extraction. Copy number of genome-inserted gRNA was measure by qPCR with genomic DNA and gRNA expression was measured by RT-qPCR with cDNA as input. 1 gRNA/cell control was generated by using 0.5 µl of 1X lentiviral library to infected 1 million cells and selected with puromycin. Confirmed by both copy number qPCR and cDNA RT-qPCR, 15-20 gRNAs per cell can be achieved by using 20 µl of 50X concentrated lentiviral library to infect 100K cells in one well of a 6-well plate (**Fig.41b and Fig.41c; Materials and methods**). In this way, as described above, we can access multiple enhancer perturbation effects in the same cell without crosstalk between different peripheral genes. This high MOI strategy[248] can further decrease the cell numbers and experimental cost for the perturb-seq. We first performed a pilot experiment. 1.2 million idCas9-KRAB *SOX17*$^{eGFP/+}$ HUES8 hESCs were infected with 20µl of the 50-fold concentrated peripheral enhancer lentiviral library at an average MOI of 15 on Day 0 in 6-well plates (100K cells per well). Cells were puromycin selected, doxycycline treated and harvested at DE48h to perform

perturb-seq experiments with 10x Genomics Chromium Single Cell 3′ Reagent Kit v.3.1 (Dual Index) with Feature Barcode technology for CRISPR Screening following the manufacturer's guidelines (**Fig.41d**). We run 2 reactions of the kit aiming to harvest 20-30K cells per reaction. Sequencing results were aligned using 10x Cellranger with standard setup for custom feature barcode. Filtered_feature_bc_matrixs were used for downstream analysis. In total, we identified 39847 cells with transcriptome captured. The median of total gRNA UMI per cell is 2552 (**Fig.41e**). Because high MOI were used for gRNA library infection, we simply used 10 UMI as threshold for gRNA assignment without applying single type gRNA per cell filter. The average type of gRNA captured per cell is ~13 (**Fig.41f**), proving that the high MOI can be induced into cells with concentrated virus. The average UMI of qualified gRNA is 256, which is much higher than poly-T based gRNA capture. 89% of cells (35439 cells) are qualified as live singlets with 1-40 types of gRNA per cell, which is much higher than poly-T based gRNA capture.

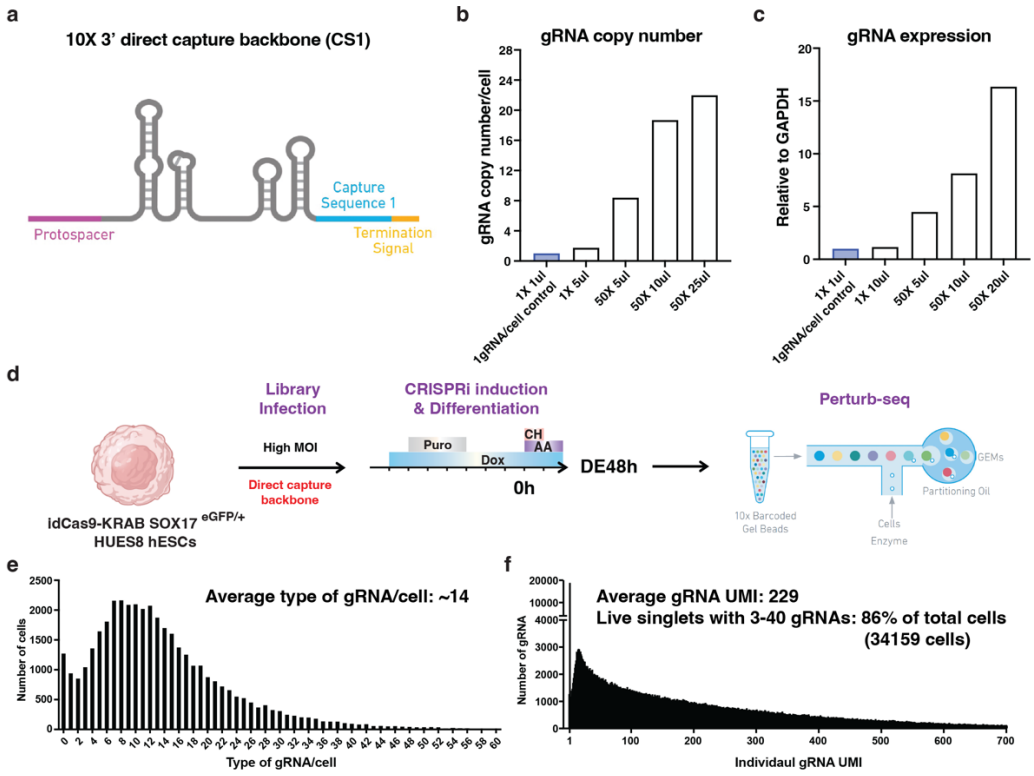

Figure 41. Assessing gRNA capture efficiency using 10x direct capture. a, The 10x 3' gRNA direct capture backbone with capture sequence 1 (CS1, adapted from 10x Genomics). **b** and **c**, Verify the high MOI with concentrated virus through genomic DNA PCR for copy number (**b**) and RT-qPCR for expression (**c**). **d**, The design of gRNA capture efficiency test using 10x 3' direct capture (adapted from 10x Genomics). **e**, The histogram of type of gRNA per cell with 10x 3' gRNA direct capture backbone. **f**, The histogram of gRNA UMI counts in each cell with 10x 3' gRNA direct capture backbone. (Plots are partially generated by using biorender).

We further analyzed this pilot test to assess the data quality for the enhancer identification. By comparing the cognate gene expression in the cells with corresponding putative enhancer perturbation and in all cells, we identified 183 regions showing significant decreased cognate gene expression when perturbing them (**Fig.42a and Fig.42b**). In summary, direct capture with high MOI strategy is the most ideal option for our genome-scale DE peripheral enhancer perturb-seq screen. Additionally, our pilot test with an average 42 representations of each regions shows promising data quality for peripheral enhancer identification.

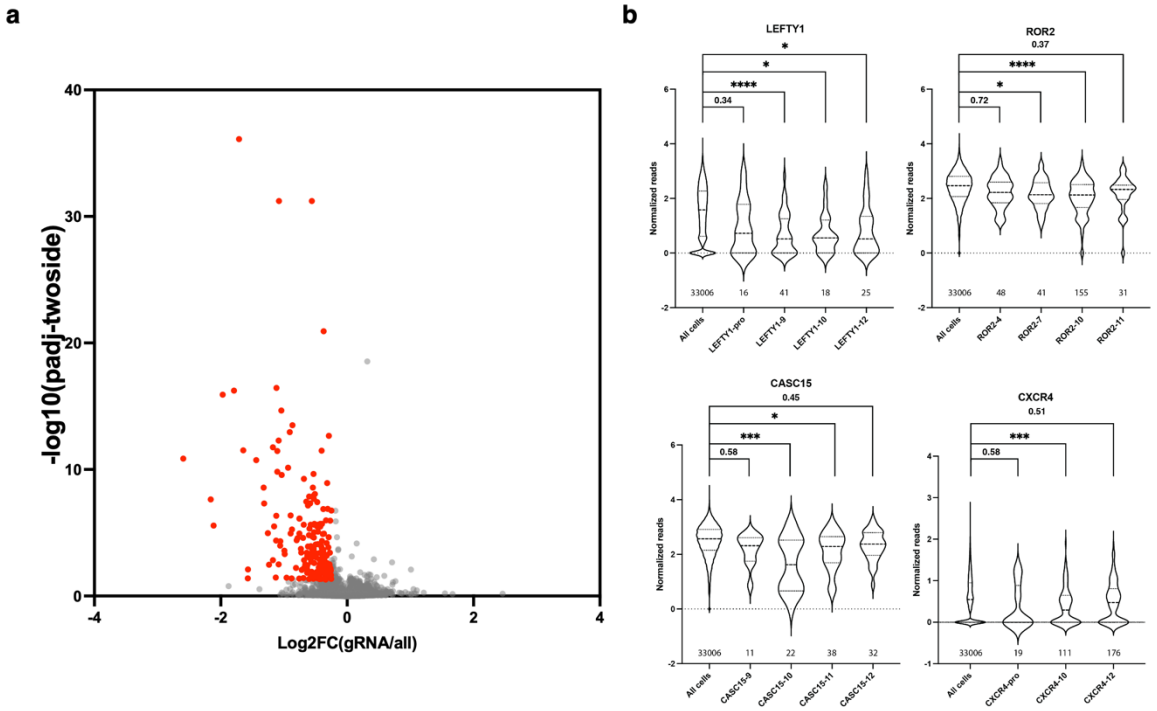

Figure 42. Perturbation effect analysis of pilot peripheral enhancer screen. a, The volcano plot showing the perturbation effect of the pilot test. Each dots represent a region identified in the test. Red dots represent hits with padj < 0.05 & Log2FC < -0.25. Two-sided Wilcoxon statistics test were performed using the normalized gene expression in the cells with the gRNAs targeting on the enhancer compared to it in all cells. Benjamini-Hochberg correction were further performed to adjust the p-value. **b.** Representative violin plots show the perturbation effect from selective regions. Statistics were perform as described in **a**.

After confirming the gRNA capture efficiency and perturbation effect from the pilot test, we further performed 8 more perturb-seq reactions to capture ~200K cells to complete peripheral enhancer screen with the same experimental setup as the pilot test, aiming a representation of at least 200 cells/region. 1.2 million idCas9-KRAB *SOX17*$^{eGFP/+}$ HUES8 hESCs were infected with 20μl of the 50-fold concentrated peripheral enhancer lentiviral library at an average MOI of 15 on Day 0 in 6-well plates (100K cells per well). Cells were puromycin selected, doxycycline treated and harvested at DE48h to perform perturb-seq experiments with 10x Genomics Chromium Single Cell 3′ Reagent Kit v.3.1 (Dual Index) with Feature Barcode technology for CRISPR Screening following the manufacturer's guidelines (**Fig.41d**). We run 8 reactions of the kit aiming to harvest 20-30K cells per reaction. Sequencing results were aligned using 10x Cellranger with standard setup for custom feature barcode. Filtered_feature_bc_matrixs were used for downstream analysis. gRNAs with equal or greater than 10 UMI were determined as a qualified gRNA capture. Cells with 1 ≤ types of gRNAs ≤ 40, 2000 ≤ n_feature_RNA ≤ 9000 and MT-gene ≤ 10% were kept for downstream Seurat analysis. In total of 10 reactions (including 2 pilot test reactions), 186,399 cells passed the filter resulting a representation of ~200 cells/putative peripheral enhancer. Standard Seurat pipeline analysis showing no batch effect between the two pilot test reactions versus the 8 reactions (**Fig.43**). More data analyses are still in progressing.

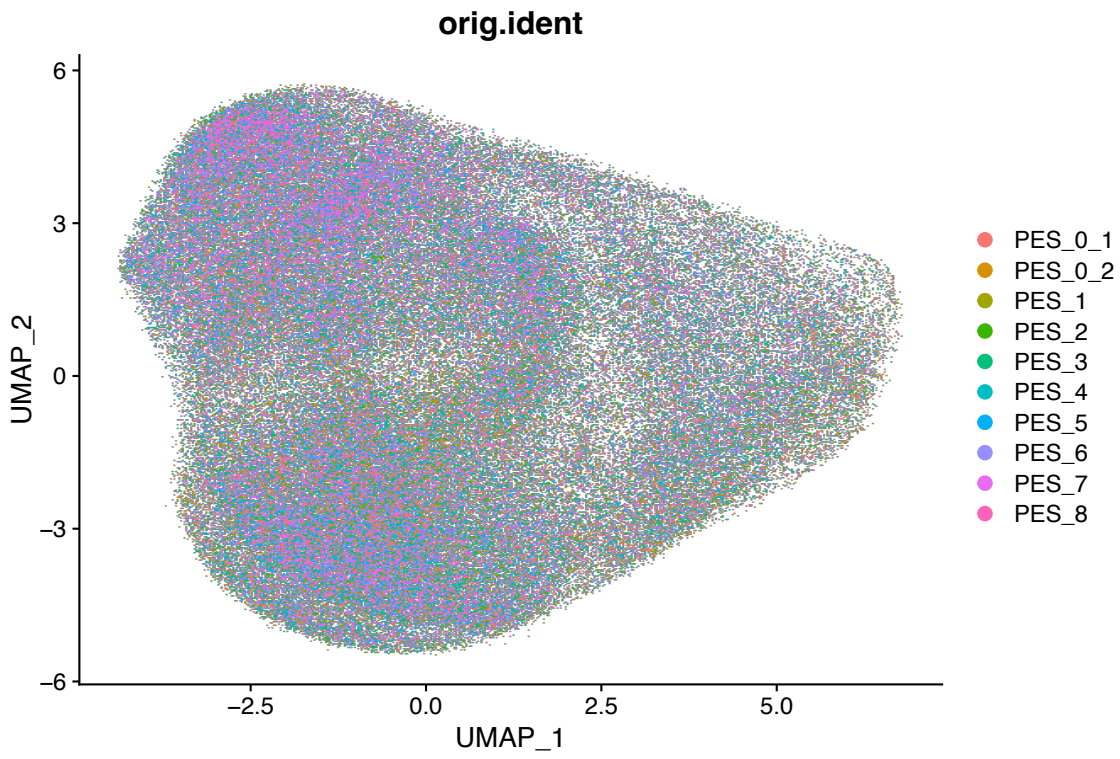

Figure 43. UMAP of peripheral enhancer screen. The UMAP of peripheral enhancer screen shows no batch effect between 10 reactions performed from two batches. PES: peripheral enhancer screen.

Discussion

We performed a CRISPRi screen for enhancers controlling the stimulated hESC-DE transition and discovered many novel enhancers flanking each core DE TF gene. ChIP-seq results show that each of these enhancers are bound by multiple core TFs, supporting that cooperative autoregulation through multiple TFs at enhancers is a prevalent feature of GRNs controlling cell state. All top enhancers were successfully validated individually. The results revealed that their perturbation delays the transition to DE, and the effect of enhancer perturbation is almost negligible after the transition to DE has been completed. A similar delayed phenotype in response to enhancer perturbation has been observed at the *Hox* cluster in flies [300] and mice [301,302]. Simulations of the hESC-DE transition using our dynamic GRN model agree with the observation of a delayed transcriptional response to enhancer perturbation, and show that nonlinear saturation of enhancer activity post-transition is responsible for this robustness once the GRN has fully activated the core TFs. In our simulations, the hysteresis of the GRN occurs via autoregulatory enhancer activity coupled to the translation of the TFs, and is at a longer time scale than simulations of nonlinearities which may also be present at the time scale of transcriptional activation [303]. Together, these observations provide a plausible explanation for why variants and putative enhancer regions from GWAS are often difficult to validate when tested individually in the steady state. These enhancers may contribute to cell state transitions and cell abundance while not strongly affecting transcript levels in the established state or when tested in isolation. This suggests a direct mechanism by which enhancers may contribute to human disease even in the absence of strong effects in post-transition cells, and recent reports have emphasized that cell type abundance quantitative trait loci (QTLs) can have profound

impact on human phenotypes [304-306]. Our results also predict that screens designed to target enhancers during a cell state transition will have greater sensitivity of detection. In addition, one may explore ways to weaken the GRN (e.g., through manipulating a core TF or enhancer) to increase its vulnerability to further enhancer perturbation, as suggested by the *GATA6* enhancer double deletion studies. Such strategies could mitigate the challenge of enhancer redundancies and support a more comprehensive discovery of enhancers. Beyond developmental cell fate changes, we envision that stimulating physiological or pathological cell state transitions can accelerate the discovery of disease-relevant enhancers or variants.

The sensitivity of our screen also revealed that most functional enhancers fell within CTCF loops, leading us to propose an interaction model whereby CTCF loops constrain enhancer interactions and activity (CIA model). Our large number of validated enhancers allowed comparisons between alternative hypotheses and showed that the CTCF constraint is significantly more predictive than Hi-C-based measurements of contact frequency between the enhancer and target promoter. Many distal enhancer hits within CTCF loops have large transcriptional impact but relatively low enhancer-promoter contact frequency as measured by Hi-C. Adjusting for the distance-dependency in Hi-C data through simple power law distance corrections did not significantly improve AUPRC (**Materials and methods**), but it may be possible to improve the predictions through developing newer methods based on Hi-C data or combining Hi-C with CTCF and other datasets. Mechanistically, while the prevailing model supports that transcriptional activity depends on enhancer-promoter contact, our observation at multiple enhancers implies a highly nonlinear relationship between contact frequency and transcription. This notion is supported by recent studies suggesting that the contact probability has a nonlinear impact

on transcription [58,303], and a contact-independent model has also been proposed [307]. Through simulations, multiple plausible mechanisms have been shown to generate this nonlinear relationship, including accumulation of promoter bound factors or post transcriptional modifications at the promoter [303]. Instead of relying on direct enhancer-promoter contact frequency measurements from Hi-C data, our CIA model utilizes CTCF loop information to constrain enhancer prediction. We combined the CTCF constraint with $Activity$ and showed that this CIA model outperforms the ABC model on results from our screen and screens conducted in K562 cells from other groups [241,282] This simple CIA model should be quite useful for prioritizing and understanding single nucleotide polymorphisms (SNPs) implicated in expression QTLs (eQTLs) or GWAS-associated loci.

Our CIA model is a quantitative improvement over the "insulated neighborhood" hypothesis [308] and is consistent with many studies showing that enhancer activity is largely restricted within CTCF loops and TADs [56-58], and that TAD disruption can lead to oncogenic misexpression and developmental diseases [309,310]. The CTCF loops are visually consistent with Hi-C TADs. However, TAD calling provides a binary result of whether a genomic region is within a TAD, which can be unstable and sensitive to parameters and methods. In comparison, *P*(in loop) calculates the probability that a genomic region is enclosed within a CTCF loop, thus providing a more reliable measurement. However, there are also seemingly conflicting findings that auxin degradation of CTCF can only have a modest effect on transcription on a short time scale [24]. We speculate that during cell state transitions, CTCF-mediated enhancer-promoter proximity is necessary for establishing *de novo* enhancer-protein-promoter complexes (specific to the succeeding cell state). While in post-transition steady states, the established complex can reinforce the proximity

together with the CTCF loop. Without the CTCF loop, the proximity can still be maintained, though it will likely become sub-stable, and the transcription efficiency may gradually decrease. Our dynamic GRN model shows a similar result that once the active transcriptional state is established, the transcriptional response to a perturbation of enhancer activity occurs at a much longer time scale (**Fig.17a**). The hysteresis in our model thus provides a plausible explanation for the long-standing paradox that CTCF is required to restrict enhancer activity, yet removing CTCF does not immediately affect transcription.

Perturb-seq is an innovative experimental technique that combines CRISPR-based gene/enhancer perturbation with scRNA-seq. It allows simultaneously perturb genes or enhancers and measure their transcriptional response at the single-cell level. This comprehensive approach provides valuable insights into how individual cells respond to specific genetic changes, revealing cell-to-cell heterogeneity and subtle alterations in gene expression that unnoticed in bulk analyses. By perturbing genes or enhancers and analyzing their impact on gene expression individually or globally, researchers can directly investigate the functional roles of genes, enhancers, and regulatory networks. The high throughput capability of perturb-seq enables the simultaneous analysis of multiple gene or enhancer perturbations in thousands of individual cells, expediting the discovery of gene functions, enhancers, and regulatory interactions on a large scale, which may unveil new therapeutic targets for various diseases.

However, perturb-seq also comes with its own set of disadvantages and limitations. First, the experimental design is highly complex, involving intricate procedures such as CRISPR perturbation design and delivery, cell/tissue dissociation, scRNA-seq library preparation, and bioinformatics analysis. Each step requires careful optimization and

multiple rounds of testing, making it challenging to execute and demanding specialized expertise. Second, the capture efficiency of the transcriptome and gRNA varies across different systems. Low mRNA capture efficiency, especially for low-expressed genes, poses a bottleneck in current scRNA-seq protocols[311,312] and this bottleneck becomes even more pronounced during enhancer perturbation screen experiments. Highly expressed genes, which are easier to capture, can result in higher UMI counts in scRNA-seq, leading to a larger threshold for enhancer perturbation effect detection. Consequently, detecting functional enhancers in highly expressed genes is more sensitive using perturb-seq compared to low-expressed genes, like TFs. Additionally, the variance in gRNA capture efficiency has a significant impact on perturb-seq experiments. Utilizing different backbones, such as CROP-seq and 10x direct capture backbone, yields very different gRNA capture efficiency. Low gRNA capture efficiency leads to difficulties in confidently assigning gRNA, and cells without such assignment must be discarded, resulting in wastage of both samples and money. Therefore, enhancing gRNA capture efficiency becomes a key necessity for successful perturb-seq experiments. Last but not least, the current commercialized 10x-based scRNA-seq kits are prohibitively expensive. With an average price of 5-16 cents per cell (excluding sequencing costs). Considering, for a genome-scale enhancer screen targeting 25,000 putative enhancer regions with 4 gRNAs/region and representation of 100 cells/gRNA would require collecting 10 million cells and using 1000 10x scRNA-seq reactions (10000 cells/reaction) amounting to $1600K (excluding sequencing costs). Such a high cost and labor-intensive design make it almost impossible to perform this kind of enhancer screen. However, a recent splitting-pool based scRNA-seq platforms, EasySci and PerturbSci, developed by the Cao Lab at Rockefeller

University, offer a new opportunity for genome-scale enhancer screens[313,314]. They claim that the cost for preparing a 1 million cells scRNA-seq library is only $700. Despite these challenges, perturb-seq remains a promising tool for genome-scale functional genomics and systems biology studies. As technology continues to develop and sequencing costs decrease, it will become more feasible to routinely harvest more than a million cells for genome-scale enhancer screens.

Supplementary Table

Supplementary Table 1. gRNA for cell line generation.

Name	Sequence
idCas9-KRAB cassette switch gRNA-1	GATGACCGAGTACAAGCCCA
idCas9-KRAB cassette switch gRNA-2	GACAGTACTAAGCTTTACTA
GATA6e+9 KO gRNA-1	TCCTTGGGTAGGTTACCCAT
GATA6e+9 KO gRNA-2	GTGCTGGTAGGTGTTAGCCA
GATA6e+9 KO gRNA-3	CCACTATGTCAAAGGACTAA
GATA6e+9 KO gRNA-4	CTAGATTTTACCTGACCCAG
GATA6e+12 KO gRNA-1	GCATCAAAACTGGGAGTGTA
GATA6e+12 KO gRNA-2	GTGGTTATGGTAAATCTGAG
GATA6e+12 KO gRNA-3	AGCACAACTTAGCCCCGACA
GATA6e+12 KO gRNA-4	TTCCATCCCTGAATGTGGGG
Gata6e+9 mouse KO gRNA-1	TGTAGTTAGTTTAGTTAACG
Gata6e+9 mouse KO gRNA-2	ACATCCAGATCCATACCAAT
Gata6e+12 mouse KO gRNA-1	GCAAAAAATACCCCAGGTGA
Gata6e+12 mouse KO gRNA-2	GACTCCACAAGGGTTGTCCA

Supplementary Table 2. Primer sequences for cell line genotyping, RT-qPCR and gRNA enrichment analysis.

Name	Sequence	Application
GT-AAVS1-R	TGGCCACGTAACCTGAGAAG	idCas9-KRAB genotyping
AttB2-F	TCCCCGGATCAACCACTTTG	idCas9-KRAB genotyping
TRE-pro-F	TTAGTGAACCGTCAGATCGCCT	idCas9-KRAB genotyping
dCas9-a	CAGCTGGTGCAGACCTACAA	idCas9-KRAB genotyping
dCas9-b	ACCAGAGCAAGAACGGCTAC	idCas9-KRAB genotyping
dCas9-c	AGAACCTGCCCAACGAGAAG	idCas9-KRAB genotyping
dCas9-d	AGTCCGGCAAGACAATCCTG	idCas9-KRAB genotyping
dCas9-e	AACGCCAAGCTGATTACCCA	idCas9-KRAB genotyping
dCas9-f	AGATGATCGCCAAGAGCGAG	idCas9-KRAB genotyping
dCas9-g	CATCGAGCAGATCAGCGAGT	idCas9-KRAB genotyping/RT-qPCR
HA-R	ATACCCTTATGATGTGCCAGA	idCas9-KRAB genotyping
KRAB-F	ACCATCGACCGGAAGAGGTA	idCas9-KRAB genotyping/RT-qPCR
KRAB-R	TACCTCTTCCGGTCGATGGT	idCas9-KRAB genotyping/RT-qPCR
HA-F	TCTGGCACATCATAAGGGTAT	idCas9-KRAB genotyping/RT-qPCR
GAPDH-F	GGAGCCAAACGGGTCATCATCTC	RT-qPCR
GAPDH-R	GAGGGGCCATCCACAGTCTTCT	RT-qPCR
SOX17-F	CGCACGGAATTTGAACAGTA	RT-qPCR
SOX17-R	GGATCAGGGACCTGTCACAC	RT-qPCR
GATA6-F	ATGCTTGTGGACTCTACATGAAACT	RT-qPCR
GATA6-R	TGCTATTACCAGAGCAAGTCTTTGA	RT-qPCR
SMAD2-F	ATGTCGTCCATCTTGCCATTC	RT-qPCR
SMAD2-R	CTCAAGCTCATCTAATCGTCCTG	RT-qPCR
EOMES-F	CAACATAAACGGACTCAATCCCA	RT-qPCR
EOMES-R	ACCACCTCTACGAACACATTGT	RT-qPCR

MIXL1-F	GGTACCCCGACATCCACTTG	RT-qPCR
MIXL1-R	TAATCTCCGGCCTAGCCAAA	RT-qPCR
GATA6e+9 GT-F	GCGTGGTCTCAGTTCACTCC	GATA6 enhancer KO genotyping
GATA6e+9 GT-R	CTGTGGCCTTGGTGGTTACA	GATA6 enhancer KO genotyping
GATA6e+12 GT-F	ATTTTCTTTGGACAGGGAGAGAG	GATA6 enhancer KO genotyping
GATA6e+12 GT-R	TTTGTCATGAGTCTTCACATAAGAG	GATA6 enhancer KO genotyping
CRISPRi-screen Hi-Seq primer F1	AATGGACTATCATATGCTTACCGTA ACTTGAAAGTATTTCG	gRNA amplification for CRISPRi screen
CRISPRi-screen Hi-Seq primer R1	CTTTAGTTTGTATGTCTGTTGCTAT TATGTCTACTATTCTTTC	gRNA amplification for CRISPRi screen
CRISPRi-screen Hi-Seq primer F2	AATGATACGGCGACCACCGAGATC TACACTCTTTCCCTACACGACGCTC TTCCGATCT (1-9bp variable length sequence) TCTTGTGGAAAGGACGAAACACCG	gRNA amplification for CRISPRi screen
CRISPRi-screen Hi-Seq primer R2	CAAGCAGAAGACGGCATACGAGAT (8bp barcode) GTGACTGGAGTTCAGACGTGTGCT CTTCCGATCTTCTACTATTCTTTCCC CTGCACTGT	gRNA amplification for CRISPRi screen
Gata6e+9 mouse KO GT-A	TGAGCTTCTGGGGGTCAAGTGG	*Gata6e+9* mouse KO genotyping
Gata6e+9 mouse KO GT-B	CAGGTGGCTCAGGAACTCAGC	*Gata6e+9* mouse KO genotyping
Gata6e+9 mouse KO GT-C	ACCATTGCAAGTCAGTGCCTTT	*Gata6e+9* mouse KO genotyping
Gata6e+9 mouse KO GT-D	CCCAGGCTGGCTTCAAACTTAC	*Gata6e+9* mouse KO genotyping
Gata6e+12 mouse KO GT-A	TTCAGGTCTTCGTGCTTGCAG	*Gata6e+12* mouse KO genotyping
Gata6e+12 mouse KO GT-B	GTGGCGCACGTCTTTAATCCC	*Gata6e+12* mouse KO genotyping
Gata6e+12 mouse KO GT-C	AAGGAGGTGACACGCAGATGGC	*Gata6e+12* mouse KO genotyping
Gata6e+12 mouse KO GT-D	AGCCATCTCTCTGACTCTCGC	*Gata6e+12* mouse KO genotyping
SOX17-pro-4C-F2	TACACGACGCTCTTCCGATCTGACT ATTAAACTTGTGTTTCGATC	4C
SOX17-pro-4C-R2	ACTGGAGTTCAGACGTGTGCTCTTC CGATCTACACATACGAGAAACAGT TTTGT	4C
GATA6-pro-4C-F1	TACACGACGCTCTTCCGATCTTGAA GAGGAGGAGGAGGGAT	4C
GATA6-pro-4C-R1	ACTGGAGTTCAGACGTGTGCTCTTC CGATCTCTGGGAGCACCCTCCG	4C
GATA6e+9-4C-F	TACACGACGCTCTTCCGATCTACAG AAATGGGCCCAAGATC	4C
GATA6e+9-4C-R	ACTGGAGTTCAGACGTGTGCTCTTC CGATCTTTGTAGAGATGGGGTTTCG C	4C
GATA6e+12-4C-F	TACACGACGCTCTTCCGATCTACTG GAGTGCAGTGGTGTGATC	4C

GATA6e+12-4C-R	ACTGGAGTTCAGACGTGTGCTCTTCCGATCTAGGCTCAGCTCACAAAGCC	4C

Supplementary Table 3. Antibody for flow cytometry, ChIP-seq and ChIP-MS.

Name	Catalog #	Company	Dilution/Quantity	Application
SOX17-488	562205	BD Biosciences	1:200	Flow cytometry
GATA6-PE	26452	Cell Signaling Technology	1:250	Flow cytometry
EOMES-660	50-112-8679	Fisher Scientific	1:200	Flow cytometry
CXCR4-APC	FAB170A-100	R&D System	1:50	Flow cytometry
HA-Tag	3724	Cell Signaling Technology	1:500	Flow cytometry
Donkey anti-Rabbit IgG-647	A-31573	Invitrogen	1:500	Flow cytometry
EOMES	66325	Cell Signaling Technology	10ug/30-40M cells	ChIP-seq
GATA6	5851	Cell Signaling Technology	10ug/30-40M cells	ChIP-seq
SOX17	81778	Cell Signaling Technology	10ug/30-40M cells	ChIP-seq
CTCF	07-729	EMD Millipore	3ul/30-40M cells	ChIP-seq
H3K27ac	39133	active motif	5ug/30-40M cells	ChIP-seq
IgG	2729	Cell Signaling Technology	10ug/30-40M cells	ChIP-MS
EOMES	66325	Cell Signaling Technology	10ug/30-40M cells	ChIP-MS
GATA6	5851	Cell Signaling Technology	10ug/30-40M cells	ChIP-MS
SOX17	81778	Cell Signaling Technology	10ug/30-40M cells	ChIP-MS

Supplementary Table 4. Core enhancer perturbation screen gRNA library sequences and gRNA enrichment analysis.

The table is too large to be included here. Please refer to Supplementary Table 2 of Luo et al[315].

Supplementary Table 5. Core enhancer perturbation screen gRNA enrichment analysis for regions.

Regions	Coordinates(hg38)	Average log2(FC)	Average Log2(Mean abundance)	Average Z-score
SOX17e+7	chr8:54268115-54268740	2.486	6.090	7.135
EOMESe+1	chr3:27728339-27729090	2.074	6.625	6.012
SOX17e+5	chr8:54300591-54300987	2.006	5.812	5.826
GATA6e+9	chr18:22026154-22027330	1.873	6.866	5.464
SOX17e+1	chr8:54454106-54455036	1.864	6.670	5.440
SOX17e+4	chr8:54301978-54302426	1.624	5.639	4.787
EOMESe-1	chr3:27713390-27715985	1.420	6.274	4.233
MIXL1e+2	chr1:226210507-226211585	1.375	6.584	4.108
MIXL1e+1	chr1:226215164-226215656	1.294	6.609	3.890
GATA6e-1	chr18:22194123-22194455	0.989	6.584	3.058

SOX17e+8	chr8:54259816-54260322	0.917	5.859	2.864
GATA6e+12	chr18:21933810-21935298	0.885	6.625	2.775
SOX17e+10	chr8:54224560-54225711	0.828	6.163	2.620
EOMESe-2	chr3:27712007-27712923	0.810	6.470	2.572
EOMESe+2	chr3:27730029-27730667	0.775	6.470	2.475
SOX17e+6	chr8:54273053-54273554	0.659	6.112	2.161
MIXL1e-1	chr1:226228164-226228831	0.655	6.377	2.150
SMAD2e-4	chr18:47853130-47853488	0.644	7.023	2.120
SOX17e+2	chr8:54443606-54444178	0.577	6.105	1.936
MIXL1e+3	chr1:226203745-226204150	0.553	6.145	1.872
SMAD2e-2	chr18:47918050-47918585	0.534	6.541	1.819
GATA6e+4	chr18:22101727-22102198	0.445	6.144	1.578
SMAD2e-3	chr18:47901736-47902193	0.437	5.975	1.557
GATA6e+10	chr18:22020271-22020802	0.288	6.300	1.151
MIXL1e+4	chr1:226197015-226197408	0.215	6.576	0.952
SOX17e+9	chr8:54228206-54228505	0.181	6.338	0.858
NANOGe-6	chr12:7970611-7971032	0.169	6.551	0.827
GATA6e+8	chr18:22032376-22032818	0.167	6.373	0.821
NANOGe+4	chr12:7439885-7440355	0.150	6.444	0.775
SOX17e+3	chr8:54381911-54382524	0.128	6.578	0.715
NANOGe-23	chr12:9450084-9450636	0.108	6.349	0.660
GATA6e-5	chr18:22559472-22560151	0.103	6.343	0.645
SMAD2e-1	chr18:47926317-47926674	0.083	5.673	0.592
JUNe+7	ch1:58903489-58904339	0.083	6.480	0.592
SMAD4e+16	chr18:50268276-50268776	0.077	6.651	0.576
SMAD2e-14	chr18:46419597-46419990	0.070	5.630	0.556
EOMESe+4	chr3:27770410-27770808	0.069	5.980	0.553
EOMESe-7	chr3:27589656-27590199	0.062	5.856	0.535
OCT4e+1	chr6:31171785-31173329	0.061	4.673	0.531
NANOGe+10	chr12:6764045-6764668	0.043	5.959	0.483
NANOGe+12	chr12:6205258-6205654	0.042	6.411	0.482
SMAD2e+2	chr18:48007513-48008816	0.039	6.616	0.473
NANOGe+8	chr12:6927503-6927934	0.038	6.487	0.470
SOX17e+16	chr8:53100828-53101127	0.037	6.772	0.468
SMAD2e-6	chr18:47749122-47749569	0.033	6.720	0.456
MIXL1e+5	chr1:226121438-226122305	0.029	6.781	0.446
SMAD4e+1	chr18:51028187-51028511	0.026	6.443	0.436
SMAD2e-13	chr18:46424977-46425269	0.025	6.763	0.435
SOX2e+7	chr3:180749408-180749770	0.020	6.049	0.422
MIXL1e+22	chr1:224819715-224820262	0.016	6.402	0.411
SOX2e-8	chr3:181892879-181893242	0.016	6.328	0.409
NANOGe-15	chr12:8692529-8692958	0.004	6.088	0.376
SOX2e-26	chr3:183548293-183548536	0.002	6.238	0.372
NANOGe-21	chr12:8911645-8912215	0.000	5.956	0.367
GATA6e+5	chr18:22093760-22095020	0.000	6.294	0.367
GATA6e+3	chr18:22106533-22106966	0.000	6.359	0.365
SMAD2e+14	chr18:48997881-48998680	-0.002	6.456	0.360
MIXL1e-4	chr1:226413945-226414598	-0.005	6.516	0.352
SMAD4e+19	chr18:50128814-50129196	-0.005	6.678	0.352
SMAD4e+9	chr18:50784586-50785153	-0.016	6.658	0.322

SOX2e+15	chr3:179865892-179866240	-0.017	5.175	0.319
SMAD2e+4	chr18:48059576-48060050	-0.018	5.859	0.318
OCT4e+2	chr6:31307900-31308766	-0.020	6.456	0.312
EOMESe-24	chr3:26308596-26308895	-0.021	6.519	0.310
SMAD2e-16	chr18:46344043-46344324	-0.021	6.753	0.308
SMAD4e+10	chr18:50748292-50748839	-0.024	6.637	0.300
NANOGe-9	chr12:8026481-8027296	-0.026	6.249	0.296
GATA6e+7	chr18:22079806-22080421	-0.030	6.277	0.285
SOX17e-19	chr8:55520864-55521248	-0.031	6.349	0.281
SOX17e-7	chr8:54568493-54568890	-0.031	5.821	0.281
MIXL1e+7	chr1:226109554-226110223	-0.033	6.479	0.275
OCT4e-9	chr6:30411513-30411827	-0.036	6.948	0.267
GATA6e+6	chr18:22084683-22085138	-0.038	6.286	0.264
MIXL1e+21	chr1:224880567-224880893	-0.038	6.614	0.263
EOMESe+22	chr3:28786478-28786777	-0.038	6.216	0.263
EOMESe-20	chr3:26712336-26712689	-0.039	6.676	0.260
JUNe+19	ch1:60052471-60053142	-0.039	6.327	0.260
GATA6e-6	chr18:22829813-22830148	-0.040	5.992	0.259
SOX2e-7	chr3:181859523-181859918	-0.041	6.220	0.256
SOX2e+1	chr3:181710468-181710925	-0.042	6.584	0.252
SOX17e-13	chr8:54763988-54764287	-0.042	6.074	0.251
SMAD4e-8	chr18:51417695-51418621	-0.043	6.243	0.250
SMAD4e+2	chr18:51025488-51025950	-0.043	5.883	0.249
SMAD4e-1	chr18:51110263-51110824	-0.043	6.791	0.249
MIXL1e-10	chr1:227356510-227356899	-0.043	6.442	0.249
MIXL1e-5	chr1:226429043-226429480	-0.045	6.315	0.245
SMAD4e-2	chr18:51164717-51165298	-0.045	6.494	0.242
GATA6e+2	chr18:22110463-22110896	-0.048	6.565	0.236
EOMESe+20	chr3:28716804-28717111	-0.048	6.149	0.236
JUNe-5	ch1:58432712-58433167	-0.048	6.549	0.235
NANOGe-11	chr12:8317324-8317960	-0.050	6.076	0.230
JUNe-23	ch1:57336761-57337238	-0.050	5.953	0.230
SMAD2e+1	chr18:47967963-47968432	-0.050	6.130	0.230
NANOGe-5	chr12:7933255-7933609	-0.051	6.301	0.227
SMAD4e-23	chr18:52101373-52101739	-0.051	6.054	0.227
MIXL1e+10	chr1:225948724-225949444	-0.052	6.451	0.226
SOX2e-6	chr3:181858929-181859318	-0.052	5.476	0.224
SMAD2e+9	chr18:48530947-48531279	-0.053	6.192	0.223
MIXL1e+6	chr1:226110623-226111183	-0.054	6.660	0.220
SOX17e-9	chr8:54632854-54633153	-0.054	6.698	0.220
JUNe+15	ch1:59184420-59185019	-0.054	6.410	0.218
GATA6e+17	chr18:21300746-21301299	-0.054	5.827	0.218
SOX17e-18	chr8:55425436-55425890	-0.055	5.864	0.216
SMAD4e-21	chr18:51988403-51988704	-0.056	6.032	0.213
SOX17e-6	chr8:54562988-54563510	-0.057	6.110	0.210
SMAD4e-13	chr18:51610457-51610852	-0.058	6.642	0.209
MIXL1e-2	chr1:226333379-226333738	-0.059	6.618	0.206
SMAD2e+7	chr18:48351430-48351989	-0.060	6.338	0.203
MIXL1e+23	chr1:224800643-224800942	-0.061	6.139	0.200
OCT4e-10	chr6:29759294-29759966	-0.061	6.343	0.199

NANOGe-14	chr12:8635705-8636461	-0.061	7.171	0.199
SMAD4e+13	chr18:50507126-50507490	-0.063	6.668	0.196
SOX2e-19	chr3:182715972-182716401	-0.063	5.990	0.195
JUNe+10	ch1:59013370-59013940	-0.064	6.538	0.193
OCT4e-5	chr6:30886145-30886763	-0.064	6.430	0.191
EOMESe+17	chr3:28606307-28606566	-0.066	6.216	0.185
JUNe-21	ch1:57409080-57409396	-0.067	6.112	0.184
OCT4e+4	chr6:31403237-31403935	-0.067	6.563	0.183
SMAD2e-5	chr18:47772660-47773051	-0.067	6.621	0.183
NANOGe-1	chr12:7806885-7807224	-0.068	5.704	0.181
SMAD4e-15	chr18:51651773-51652244	-0.070	6.056	0.177
OCT4e-6	chr6:30880554-30881232	-0.070	6.217	0.175
SOX2e-14	chr3:182238190-182238503	-0.072	6.507	0.171
JUNe+8	ch1:58982530-58982950	-0.072	6.531	0.170
SMAD4e-12	chr18:51573892-51574341	-0.072	6.897	0.170
SMAD4e+4	chr18:51007024-51007393	-0.073	6.052	0.168
GATA6e-2	chr18:22324077-22324907	-0.073	6.295	0.168
SMAD4e+12	chr18:50644812-50645270	-0.074	6.385	0.165
GATA6e-4	chr18:22536564-22537004	-0.074	6.736	0.165
GATA6e-14	chr18:23939039-23939461	-0.075	6.604	0.163
SOX2e+8	chr3:180713759-180714129	-0.076	5.982	0.161
EOMESe-8	chr3:27533646-27534382	-0.076	6.357	0.159
GATA6e-8	chr18:22871762-22872073	-0.077	6.566	0.156
SOX2e-13	chr3:182212483-182212793	-0.077	6.504	0.156
SOX17e-17	chr8:55372806-55373238	-0.077	6.427	0.156
EOMESe+12	chr3:27986232-27986646	-0.077	6.454	0.156
SMAD2e+5	chr18:48161487-48162215	-0.077	6.560	0.155
EOMESe-11	chr3:27213434-27213811	-0.079	6.171	0.151
SOX2e-20	chr3:183009735-183010374	-0.082	6.326	0.142
SOX17e+14	chr8:53286748-53287047	-0.083	7.063	0.141
JUNe-13	ch1:58003145-58003467	-0.083	5.636	0.141
SMAD4e-28	chr18:52682281-52682724	-0.083	5.973	0.140
SMAD4e-10	chr18:51563331-51564490	-0.083	6.530	0.140
SOX17e-4	chr8:54519925-54520457	-0.084	5.908	0.137
NANOGe-8	chr12:8018769-8019371	-0.084	6.501	0.137
SOX17e+15	chr8:53245389-53245688	-0.085	6.751	0.135
SMAD2e+6	chr18:48339546-48339965	-0.085	6.548	0.134
SMAD2e+3	chr18:48022567-48022957	-0.086	6.824	0.133
JUNe-29	ch1:56958548-56958959	-0.086	6.312	0.132
MIXL1e+11	chr1:225945524-225946059	-0.087	6.365	0.131
MIXL1e+16	chr1:225677297-225677730	-0.087	6.658	0.130
EOMESe-12	chr3:27072886-27073643	-0.087	6.075	0.130
JUNe-9	ch1:58123016-58123378	-0.087	5.931	0.129
JUNe-11	ch1:58031330-58032320	-0.088	6.104	0.128
MIXL1e+24	chr1:224701011-224701556	-0.088	6.698	0.126
SMAD4e-17	chr18:51656691-51657293	-0.088	5.929	0.126
SMAD4e-20	chr18:51984686-51985002	-0.088	6.009	0.126
EOMESe-4	chr3:27673634-27673933	-0.089	5.909	0.124
SOX2e-25	chr3:183544711-183545104	-0.089	6.588	0.123
SMAD4e+20	chr18:49988823-49989137	-0.090	6.349	0.122

SMAD4e-3	chr18:51167829-51168735	-0.090	6.214	0.122
SMAD2e+13	chr18:48841639-48842016	-0.090	6.193	0.121
SMAD2e-11	chr18:46469512-46469973	-0.090	6.583	0.121
MIXL1e+17	chr1:225627377-225627824	-0.090	6.423	0.120
JUNe-26	ch1:57088669-57089030	-0.091	6.474	0.118
SMAD2e-10	chr18:46536540-46536864	-0.091	6.319	0.117
OCT4e-4	chr6:30942575-30943019	-0.092	6.024	0.116
JUNe+5	ch1:58853383-58853865	-0.093	5.820	0.114
EOMESe+11	chr3:27943108-27943488	-0.093	6.468	0.112
SMAD4e-18	chr18:51658427-51659027	-0.094	6.138	0.110
SOX2e-24	chr3:183434362-183434759	-0.095	6.022	0.108
MIXL1e-8	chr1:226569911-226570224	-0.095	6.272	0.108
NANOGe-22	chr12:9364404-9365015	-0.095	6.363	0.107
SOX17e-22	chr8:55851759-55852058	-0.096	6.207	0.106
JUNe-16	ch1:57591865-57592261	-0.097	6.449	0.102
MIXL1e-3	chr1:226404829-226405733	-0.097	5.989	0.102
SMAD4e-26	chr18:52447109-52447501	-0.099	5.601	0.098
NANOGe-7	chr12:7982402-7982730	-0.100	5.485	0.095
SOX17e-23	chr8:56047909-56048208	-0.100	5.772	0.095
SMAD4e-9	chr18:51522341-51522679	-0.100	6.454	0.094
NANOGe-20	chr12:8819076-8819784	-0.101	6.316	0.092
MIXL1e-11	chr1:227357277-227357731	-0.101	6.730	0.092
SOX17e-14	chr8:54779575-54780390	-0.101	5.435	0.091
SOX2e+10	chr3:180135815-180136143	-0.101	5.931	0.090
SMAD4e-25	chr18:52439338-52439679	-0.102	5.923	0.088
JUNe-15	ch1:57596978-57597469	-0.102	6.202	0.088
EOMESe-3	chr3:27680704-27681662	-0.103	6.459	0.087
MIXL1e+13	chr1:225899094-225899920	-0.103	6.503	0.086
SMAD2e+17	chr18:49725910-49726582	-0.103	6.324	0.085
JUNe-6	ch1:58395382-58395769	-0.104	6.284	0.083
SOX2e+11	chr3:180135069-180135626	-0.104	6.005	0.083
SMAD2e+15	chr18:49487010-49487647	-0.105	6.606	0.080
SOX17e+11	chr8:53985497-53985816	-0.105	6.459	0.080
SMAD4e+14	chr18:50399050-50399433	-0.105	6.588	0.080
NANOGe-10	chr12:8145965-8146413	-0.106	6.550	0.078
GATA6e+11	chr18:21990845-21991662	-0.106	6.335	0.077
SMAD4e-24	chr18:52160616-52161063	-0.107	6.041	0.076
OCT4e+5	chr6:31683121-31683603	-0.107	6.402	0.074
NANOGe-3	chr12:7860012-7860815	-0.109	6.093	0.070
JUNe-19	ch1:57440110-57440477	-0.109	5.984	0.070
NANOGe+9	chr12:6924791-6925235	-0.109	6.502	0.070
SOX2e-22	chr3:183115987-183116501	-0.109	6.856	0.069
SMAD4e-6	chr18:51235255-51235554	-0.111	6.318	0.065
GATA6e-9	chr18:22913768-22914149	-0.111	6.081	0.064
SMAD2e-12	chr18:46433358-46433860	-0.111	6.347	0.064
SOX2e+2	chr3:181704479-181705316	-0.113	6.364	0.057
MIXL1e+15	chr1:225769103-225769432	-0.114	6.316	0.056
JUNe-3	ch1:58454445-58454791	-0.114	6.622	0.055
SOX17e+19	chr8:52467180-52467586	-0.114	6.600	0.055
JUNe+6	ch1:58896442-58896877	-0.115	6.602	0.054

EOMESe-5	chr3:27666309-27667145	-0.115	5.904	0.054
SOX2e+14	chr3:179868385-179868929	-0.115	6.174	0.052
SOX17e+17	chr8:53018805-53019483	-0.117	6.561	0.049
SMAD4e+17	chr18:50232555-50232840	-0.117	6.312	0.047
SMAD4e+21	chr18:49959231-49959693	-0.117	6.587	0.047
EOMESe-18	chr3:27021883-27022511	-0.118	6.341	0.046
EOMESe+25	chr3:29057465-29057844	-0.118	6.598	0.045
EOMESe+8	chr3:27888527-27888928	-0.118	6.038	0.045
SMAD4e+5	chr18:50992246-50992899	-0.119	6.607	0.043
JUNe+13	ch1:59100824-59101176	-0.119	6.294	0.042
SOX17e-15	chr8:54944007-54944459	-0.119	6.411	0.042
OCT4e-2	chr6:31143129-31143481	-0.119	6.419	0.041
SMAD2e-17	chr18:46293912-46294311	-0.119	6.228	0.041
SMAD2e-18	chr18:46283532-46284305	-0.120	6.337	0.039
EOMESe+24	chr3:28905919-28906218	-0.120	5.996	0.039
SMAD2e+18	chr18:49759690-49760460	-0.121	6.426	0.038
JUNe+14	ch1:59116880-59117309	-0.121	6.136	0.037
SOX17e-11	chr8:54736398-54736770	-0.121	6.505	0.036
JUNe+16	ch1:59186556-59186953	-0.122	6.416	0.034
JUNe-14	ch1:57600308-57600798	-0.122	6.100	0.034
SMAD4e+6	chr18:50899639-50900066	-0.123	6.025	0.032
SMAD4e-14	chr18:51622686-51623072	-0.123	6.802	0.031
MIXL1e+18	chr1:225424624-225425643	-0.123	6.090	0.030
SMAD2e+12	chr18:48813941-48814304	-0.124	6.919	0.029
EOMESe+18	chr3:28612117-28612616	-0.124	5.923	0.029
EOMESe-14	chr3:27043336-27044022	-0.124	6.372	0.027
SOX2e-23	chr3:183265242-183265557	-0.125	6.893	0.027
SMAD2e-19	chr18:46261777-46262021	-0.125	5.825	0.026
SMAD2e-9	chr18:46661019-46661371	-0.126	6.286	0.024
JUNe-28	ch1:57010553-57010883	-0.126	6.072	0.022
JUNe+17	ch1:59769380-59769711	-0.126	6.216	0.022
SMAD2e+10	chr18:48605316-48605872	-0.127	6.490	0.021
EOMESe-22	chr3:26406151-26406450	-0.127	6.389	0.020
EOMESe-15	chr3:27042582-27042975	-0.128	5.418	0.018
SMAD4e-4	chr18:51195492-51196012	-0.128	6.275	0.018
NANOGe+11	chr12:6214958-6215628	-0.129	6.252	0.016
NANOGe+3	chr12:7694596-7695016	-0.129	5.860	0.015
SMAD4e-16	chr18:51654477-51655784	-0.130	6.476	0.013
SOX17e+18	chr8:52589680-52589979	-0.130	6.545	0.012
SMAD4e+8	chr18:50806171-50806699	-0.131	6.582	0.009
SOX2e+12	chr3:179942223-179942654	-0.131	6.871	0.009
SOX2e+6	chr3:181383760-181384158	-0.131	6.097	0.009
EOMESe-27	chr3:26061662-26062214	-0.132	6.204	0.008
GATA6e+1	chr18:22159042-22159478	-0.132	6.638	0.008
MIXL1e+9	chr1:226002748-226003085	-0.133	6.394	0.004
JUNe-17	ch1:57553659-57554178	-0.133	6.204	0.003
SOX17e-20	chr8:55845004-55845458	-0.133	6.139	0.003
GATA6e-12	chr18:23285538-23285903	-0.134	6.740	0.000
GATA6e-10	chr18:23037629-23038000	-0.134	5.775	0.000
EOMESe+23	chr3:28791712-28792011	-0.135	6.274	-0.001

MIXL1e-7	chr1:226532594-226532893	-0.135	6.289	-0.001
EOMESe+6	chr3:27883317-27883616	-0.135	5.758	-0.002
SOX2e+4	chr3:181694876-181695751	-0.135	6.484	-0.002
SOX17e-12	chr8:54753877-54754176	-0.137	5.807	-0.006
GATA6e-11	chr18:23168967-23170035	-0.137	6.331	-0.006
JUNe-10	ch1:58033113-58033487	-0.137	6.284	-0.006
OCT4e+3	chr6:31366873-31367368	-0.137	6.453	-0.007
MIXL1e+25	chr1:224639378-224639762	-0.137	6.201	-0.008
SOX2e-21	chr3:183114025-183114400	-0.138	6.178	-0.009
EOMESe+9	chr3:27889367-27889855	-0.139	5.740	-0.012
EOMESe-23	chr3:26350873-26351172	-0.139	5.861	-0.013
SMAD2e-15	chr18:46408531-46408947	-0.140	6.243	-0.014
JUNe-4	ch1:58448047-58448480	-0.141	6.308	-0.018
EOMESe-21	chr3:26514425-26514958	-0.141	6.379	-0.018
EOMESe-6	chr3:27632594-27633388	-0.142	6.426	-0.021
SOX2e-4	chr3:181782417-181782835	-0.142	5.775	-0.022
SMAD4e-22	chr18:52060764-52061170	-0.143	6.524	-0.022
EOMESe-16	chr3:27036090-27036649	-0.143	6.086	-0.023
SOX2e-17	chr3:182450964-182451410	-0.143	6.191	-0.024
SOX2e-2	chr3:181756040-181756370	-0.144	5.902	-0.026
SMAD2e+11	chr18:48802807-48803161	-0.145	6.644	-0.029
SMAD4e-19	chr18:51659747-51660213	-0.145	6.299	-0.030
MIXL1e+14	chr1:225772247-225772639	-0.145	6.419	-0.030
MIXL1e-6	chr1:226520583-226520964	-0.147	6.599	-0.034
MIXL1e+20	chr1:225224397-225224756	-0.147	6.262	-0.035
SMAD2e-8	chr18:46899243-46899645	-0.147	5.754	-0.035
SOX2e-5	chr3:181796629-181797046	-0.148	5.628	-0.036
OCT4e-11	chr6:29661725-29662131	-0.148	5.994	-0.037
JUNe-2	ch1:58584632-58584988	-0.149	6.579	-0.039
SOX2e-18	chr3:182500240-182500696	-0.151	6.415	-0.044
SOX2e-10	chr3:182139969-182140348	-0.151	6.582	-0.045
GATA6e-3	chr18:22332665-22332945	-0.151	6.549	-0.045
MIXL1e+8	chr1:226097703-226098171	-0.152	5.841	-0.047
OCT4e-3	chr6:31070718-31071050	-0.152	6.760	-0.048
SMAD4e+3	chr18:51017016-51017779	-0.153	6.344	-0.049
SOX17e-10	chr8:54705309-54705765	-0.154	6.583	-0.054
OCT4e-8	chr6:30447291-30447652	-0.155	6.710	-0.055
EOMESe+19	chr3:28703783-28704174	-0.157	6.424	-0.061
SOX2e-3	chr3:181756560-181757155	-0.157	6.151	-0.062
SOX2e-12	chr3:182180587-182181075	-0.158	6.160	-0.063
SOX17e-3	chr8:54475793-54476540	-0.158	6.301	-0.064
NANOGe-13	chr12:8475523-8475886	-0.158	6.046	-0.065
JUNe+9	ch1:58987036-58987572	-0.159	6.040	-0.067
GATA6e+16	chr18:21305592-21305971	-0.160	6.083	-0.068
JUNe+20	ch1:60156837-60157185	-0.160	6.336	-0.070
EOMESe+7	chr3:27885601-27886032	-0.161	5.879	-0.071
SMAD4e+11	chr18:50737109-50737456	-0.161	6.537	-0.073
EOMESe-13	chr3:27045695-27046127	-0.162	5.852	-0.074
SOX17e-21	chr8:55847692-55848542	-0.162	6.360	-0.075
SOX17e+13	chr8:53492437-53493003	-0.162	6.153	-0.076

SMAD4e-27	chr18:52451811-52452165	-0.162	6.230	-0.076
GATA6e+14	chr18:21386694-21387267	-0.163	5.251	-0.079
JUNe-12	ch1:58006626-58007016	-0.164	5.987	-0.081
EOMESe+16	chr3:28200244-28200995	-0.165	6.277	-0.082
SMAD2e+19	chr18:49905119-49905642	-0.165	6.249	-0.082
SOX17e-8	chr8:54592753-54593211	-0.166	6.204	-0.085
GATA6e-7	chr18:22838659-22839062	-0.167	6.157	-0.089
EOMESe-28	chr3:26050676-26051162	-0.168	5.737	-0.092
NANOGe+2	chr12:7709907-7710386	-0.168	6.526	-0.092
SMAD4e+15	chr18:50396080-50396441	-0.169	6.297	-0.094
SOX2e+5	chr3:181384896-181385261	-0.170	6.527	-0.098
EOMESe+10	chr3:27905635-27906003	-0.171	6.562	-0.098
JUNe-8	ch1:58308211-58308576	-0.171	6.585	-0.099
GATA6e+15	chr18:21344847-21345238	-0.172	6.103	-0.103
SOX2e-9	chr3:181943190-181943753	-0.174	6.320	-0.107
SOX2e-15	chr3:182342298-182342701	-0.174	6.344	-0.107
SMAD4e+7	chr18:50875992-50876508	-0.174	5.760	-0.107
EOMESe-10	chr3:27228794-27229159	-0.175	6.595	-0.109
JUNe-27	ch1:57066997-57067651	-0.176	6.157	-0.112
JUNe+4	ch1:58848809-58849243	-0.177	6.575	-0.115
SOX17e-16	chr8:55119140-55119640	-0.177	6.049	-0.115
SMAD4e-29	chr18:52888004-52888429	-0.178	6.143	-0.119
JUNe+2	ch1:58815153-58815616	-0.179	6.467	-0.120
EOMESe+21	chr3:28765157-28765672	-0.181	5.301	-0.125
JUNe-18	ch1:57530966-57531319	-0.182	5.403	-0.129
JUNe-30	ch1:56811287-56811671	-0.182	5.830	-0.130
SMAD2e-20	chr18:46166565-46166893	-0.184	6.202	-0.135
EOMESe-19	chr3:26718139-26718438	-0.185	4.719	-0.138
SMAD4e+18	chr18:50231523-50232005	-0.185	6.592	-0.139
JUNe+18	ch1:59997540-59997850	-0.186	6.396	-0.141
SMAD4e-5	chr18:51227717-51228016	-0.186	5.551	-0.141
NANOGe+1	chr12:7787540-7788003	-0.186	4.808	-0.141
SMAD2e+8	chr18:48488443-48488918	-0.187	6.244	-0.144
MIXL1e-9	chr1:226679975-226680478	-0.188	6.618	-0.147
JUNe-20	ch1:57411366-57411748	-0.189	6.368	-0.149
SOX2e+13	chr3:179882334-179882737	-0.192	6.280	-0.157
JUNe-25	ch1:57262461-57262982	-0.198	6.670	-0.173
JUNe-22	ch1:57381840-57382261	-0.200	6.607	-0.179
SOX17e-5	chr8:54551669-54552099	-0.201	6.398	-0.180
JUNe+11	ch1:59063389-59063920	-0.201	6.640	-0.182
EOMESe+15	chr3:28118004-28118418	-0.204	6.266	-0.190
EOMESe-17	chr3:27025652-27026031	-0.210	6.532	-0.205
SMAD4e-7	chr18:51236239-51236589	-0.210	6.273	-0.206
SOX2e+9	chr3:180375778-180376217	-0.212	6.084	-0.212
SMAD2e+16	chr18:49663981-49664344	-0.214	6.489	-0.217
GATA6e+13	chr18:21735583-21736117	-0.216	6.586	-0.221
EOMESe-9	chr3:27357646-27358043	-0.219	5.661	-0.231
JUNe-1	ch1:58704566-58705086	-0.220	5.790	-0.234
EOMESe+14	chr3:28077591-28077942	-0.221	6.448	-0.237
EOMESe+3	chr3:27731291-27731666	-0.229	6.574	-0.258

JUNe+3	ch1:58816141-58816634	-0.231	6.518	-0.262
SOX2e-1	chr3:181715672-181716349	-0.231	5.925	-0.263
OCT4e-7	chr6:30763907-30764762	-0.237	6.184	-0.279
JUNe-24	ch1:57307375-57307935	-0.239	6.097	-0.285
SOX2e-11	chr3:182142927-182143340	-0.240	5.696	-0.286
MIXL1e+12	chr1:225903812-225904183	-0.244	5.823	-0.299
MIXL1e-12	chr1:228085318-228085713	-0.245	6.250	-0.301
SOX2e+3	chr3:181699613-181699902	-0.248	6.673	-0.309
SOX17e-2	chr8:54469946-54470715	-0.250	6.686	-0.314
NANOGe+7	chr12:6996020-6996398	-0.263	6.298	-0.349
NANOGe-2	chr12:7851725-7852073	-0.267	6.193	-0.360
OCT4e-1	chr6:31158069-31158722	-0.295	6.560	-0.436
JUNe+12	ch1:59077934-59078593	-0.323	6.361	-0.512
JUNe+1	ch1:58785059-58785725	-0.391	6.552	-0.699
SOX17e-1	chr8:54466172-54467633	-0.500	6.506	-0.995
NANOGe-4	chr12:7905637-7906132	-0.797	4.852	-1.804

Supplementary Table 6. gRNA sequences for hit validation.

Name	Sequence	Target
NT-control	ACGGAGGCTAAGCGTCGCAA	Non-target
Positive-control (SOX17-pro-8)	ATGTGGCCAATGGAGCGGCG	*SOX17 promoter*
EOMESe-2-33	GGGCAGCTGAATCCTTCCCT	*EOMESe-2*
EOMESe-1-112	TGGTCTCCAAGAGCCAGAAG	*EOMESe-1*
EOMESe+1-14	CATCTGGATCCACTCGCTGT	*EOMESe+1*
EOMESe+2-33	TCAGAGGAGGGAGAGACCAG	*EOMESe+2*
MIXL1e-1-11	AGACTGGTCTCAAACTCCTG	*MIXL1e-1*
MIXL1e+1-18	TATGGGCTTGGTGGAGAGGT	*MIXL1e+1*
MIXL1e+2-1	GTACTTGTGAAGCCCCCCAG	*MIXL1e+2*
MIXL1e+3-18	GGCTCAGGCCTGGAGAGGAT	*MIXL1e+3*
GATA6e-1-17	AGGCAGCACAGGCCAGGCGG	*GATA6e-1*
GATA6e+9-12	TCCTCTTAGGAGCTACAGGG	*GATA6e+9*
GATA6e+12-6	GGCTTATCTGCGACATCCCC	*GATA6e+12*
SOX17e+1-5	GCAGTGCTAACGCACCCGAA	*SOX17e+1*
SOX17e+2-19	ATGAGACCACAGCTATCACC	*SOX17e+2*
SOX17e+4-8	TCTGGAGAGCGCTCATGGGA	*SOX17e+4*
SOX17e+5-13	CTAAGGAAGTGACTTCCTCC	*SOX17e+5*
SOX17e+6-1	AGCCCACTCATTAGACCCCT	*SOX17e+6*
SOX17e+7-17	CTACATGAAAGGAGGCTGTT	*SOX17e+7*
SOX17e+8-11	AATTCAAGAGTTGCTAACAG	*SOX17e+8*
SOX17e+10-10	GGGGATGGGTCCCACGCTAC	*SOX17e+10*
SMAD2e-4-14	GGAAGGCTAAGGCAGAAGAA	*SMAD2e-4*

Supplementary Table 7. Data of core enhancer screening for regions surrounding core DE TFs.

Regions	Log2FC (GFP-/GFP+)	Dist_tss (bp)	ATAC DE	H3K27ac DE	Hi-C DE	Hi-C ESC	*P*(in loop)	*ABC score*	*CIA score*
SOX17e+7	2.4865	-189508	0.5738	3.8519	0.1286	0.079	0.8634	0.1912	1.2836
EOMESe+1	2.0740	-6391	0.8427	2.6965	1	1	0.9674	1.5074	1.4582
SOX17e+5	2.0056	-157146	0.5048	1.9144	0.1689	0.0862	0.87	0.166	0.8553
GATA6e+9	1.8726	-142847	1.0787	3.8144	0.2805	0.076	0.7673	0.569	1.5565
SOX17e+1	1.8639	-3364	0.632	3.1319	1	1	1	1.4069	1.4069
SOX17e+4	1.6240	-155733	0.5557	2.372	0.1689	0.0862	0.87	0.1939	0.9989
EOMESe-1	1.4204	7636	1.1837	3.0467	0.7236	0.7839	0.9365	1.3741	1.7785
MIXL1e+2	1.3746	-12618	0.655	2.3087	0.7423	0.7022	0.9976	0.9128	1.2268
MIXL1e+1	1.2943	-8254	0.2969	2.7055	1	0.8607	1	0.8963	0.8963
GATA6e-1	0.9888	24700	0.5855	1.5759	0.3967	0.2767	0.9567	0.381	0.9189
SOX17e+8	0.9174	-197866	0.4759	3.6528	0.1562	0.0683	0.8513	0.206	1.1224
GATA6e+12	0.8848	-235035	1.286	3.0856	0.3377	0.1573	0.307	0.6727	0.6116
SOX17e+10	0.8280	-232800	1.4063	2.4276	0.2713	0.0557	0.8172	0.5013	1.51
EOMESe-2	0.8101	9858	0.6499	2.4562	0.7236	0.7839	0.9225	0.9142	1.1655
EOMESe+2	0.7745	-8025	0.6124	2.0522	0.7714	0.6629	0.9474	0.8648	1.0621
SOX17e+6	0.6592	-184632	0.2923	3.4999	0.1061	0.0681	0.8634	0.1073	0.8732
MIXL1e-1	0.6554	4833	0.203	0.3362	0.8897	1	0.9745	0.2324	0.2546
SOX17e+2	0.5767	-14043	1.158	1.5343	0.5174	0.2773	0.9758	0.6897	1.3007
MIXL1e+3	0.5531	-19717	0.1208	0.6433	0.4464	0.3804	0.969	0.1244	0.2701
GATA6e+4	0.4451	-67627	0.2912	1.5178	0.3669	0.2031	0.8043	0.2439	0.5348
GATA6e+10	0.2882	-149053	0.552	2.2551	0.3246	0.1301	0.7673	0.3622	0.8561
MIXL1e+4	0.2152	-26453	0.2642	0.0842	0.3124	0.3096	0.9452	0.0466	0.141
SOX17e+9	0.1807	-229580	0.6126	3.3402	0.2713	0.0557	0.8261	0.3881	1.1817
GATA6e+8	0.1670	-136992	0.1457	1.7552	0.2507	0.0698	0.7673	0.1268	0.3881
SOX17e+3	0.1280	-75718	0.259	0.3103	0.1334	0.0807	0.9093	0.0378	0.2578
GATA6e-5	0.1026	390222	0.556	0.5672	0.1436	0.1754	0.7178	0.0806	0.4031
EOMESe+4	0.0686	-48286	0.2782	0.3965	0.1965	0.1267	0.8431	0.0653	0.28
SOX17e+12	0.0632	-691168	0.041	0.2261	0.0388	0.0258	0.0067	0.0037	0.0006
EOMESe-7	0.0620	132396	0.2016	0.3037	0.0359	0.0421	0.0467	0.0089	0.0115
SOX17e+16	0.0372	-1356958	1.0095	2.003	0.1588	0.2121	0.4414	0.2258	0.6277
MIXL1e+5	0.0292	-101793	0.7263	2.8863	0	0	0	0	0
MIXL1e+22	0.0163	-1403676	0.4107	3.088	0.2946	0.0999	0.7999	0.3318	0.9008
GATA6e+5	0.0003	-75199	0.2095	1.0748	0.402	0.1875	0.833	0.1908	0.3953
GATA6e+3	-0.0004	-62840	0.1006	0.0456	0	0	0	0	0
MIXL1e-4	-0.0051	190607	0.2705	0.749	0.0445	0.0569	0.0843	0.02	0.038
EOMESe-24	-0.0208	1413578	0.4178	0.0178	0.0224	0.0143	0	0.0019	0
GATA6e+7	-0.0298	-89476	0.598	3.7319	0.2365	0.1568	0.7869	0.3533	1.1755
SOX17e-19	-0.0313	1063121	0.3093	0.4689	0.071	0.025	0.3344	0.027	0.1274
SOX17e-7	-0.0315	110756	0.4011	0.1024	0	0	0	0	0
MIXL1e+7	-0.0335	-113776	0.625	0.4099	0.0813	0.0906	0.1233	0.0412	0.0624
GATA6e+6	-0.0375	-84679	0.0947	0.063	0	0	0	0	0
MIXL1e+21	-0.0379	-1342934	0.3519	1.7652	0.2365	0.1568	0.7869	0.1864	0.6202
EOMESe+22	-0.0381	-1064304	0.1183	0.0421	0.0212	0.034	0.0795	0.0015	0.0056
EOMESe-20	-0.0391	1009811	0.2938	0.0802	0.016	0.0135	0	0.0025	0
GATA6e-6	-0.0395	660391	0.1746	0.7544	0.0322	0.0291	0.0265	0.0117	0.0096
SOX17e-13	-0.0424	306202	0.2431	0.1704	0.0172	0.0196	0.0356	0.0035	0.0072
MIXL1e-10	-0.0432	1133040	0.1582	0.1021	0	0	0	0	0
MIXL1e-5	-0.0446	205597	0.4268	1.9031	0.3706	0.1443	0.833	0.334	0.7507

GATA6e+2	-0.0478	-58910	0.1885	0.07	0.0281	0.0146	0	0.0032	0
EOMESe+20	-0.0480	-994634	0.6824	3.4236	0.014	0.0155	0.0273	0.0214	0.0417
MIXL1e+10	-0.0515	-274580	0.4011	0.7792	0.0826	0.1036	0.1233	0.0462	0.0689
MIXL1e+6	-0.0537	-112761	0.2502	0.0273	0.0546	0.0278	0.1431	0.0045	0.0118
SOX17e-9	-0.0538	175068	0.3729	0.4115	0	0	0	0	0
GATA6e+17	-0.0545	-868567	0.4116	0.1085	0.0147	0.0138	0	0.0031	0
SOX17e-18	-0.0553	967728	0.1389	0.0623	0.0615	0.0262	0.3525	0.0057	0.0328
SOX17e-6	-0.0574	105314	0.1587	0.0618	0.1391	0.1961	0.6499	0.0138	0.0643
MIXL1e-2	-0.0588	109894	0.192	0.2211	0	0	0	0	0
MIXL1e+23	-0.0609	-1422872	0.083	0.0185	0.0182	0.0212	0.0042	0.0007	0.0002
EOMESe+17	-0.0664	-884113	0.3803	0.1297	0.0592	0.138	0.8747	0.0132	0.1943
GATA6e-2	-0.0730	154903	0.4297	1.4531	0.0432	0.0723	0.7178	0.0341	0.5671
GATA6e-4	-0.0740	367195	0.2024	0.2899	0.0516	0.0274	0.0422	0.0125	0.0102
GATA6e-14	-0.0745	1769661	0.174	0.3824	0.0264	0.0249	0.02	0.0068	0.0052
EOMESe-8	-0.0762	188309	0.2486	0.2044	0.0798	0.0594	0.7168	0.018	0.1616
GATA6e-8	-0.0771	702328	0.2439	0.112	0.0167	0.0306	0.0067	0.0028	0.0011
SOX17e-17	-0.0773	915087	0.0422	0.0368	0	0	0	0	0
EOMESe+12	-0.0773	-264116	0.0754	0.0816	0.0262	0.0488	0.0074	0.0021	0.0006
EOMESe-11	-0.0792	508701	0.2869	0.0563	0	0	0	0	0
SOX17e+14	-0.0827	-1171038	0.1703	0.4187	0.116	0.0505	0.5962	0.031	0.1592
SOX17e-4	-0.0841	62256	0.5961	0.7556	0	0	0	0	0
SOX17e+15	-0.0848	-1212397	0.2715	0.0842	0	0	0.0118	0	0.0018
MIXL1e+11	-0.0865	-277873	0.3867	3.5466	0.014	0.0155	0.0273	0.0164	0.032
MIXL1e+16	-0.0866	-546151	0.1793	0.0279	0	0.0369	0.003	0	0.0002
EOMESe-12	-0.0868	649059	0.3768	1.4563	0	0	0	0	0
MIXL1e+24	-0.0882	-1522381	0.5426	1.2335	0	0	0.0058	0	0.0048
EOMESe-4	-0.0889	48540	0.1952	0.0288	0.0836	0.0845	0.7286	0.0063	0.0546
MIXL1e+17	-0.0903	-596064	0.1728	0.0226	0.0275	0.0403	0.0566	0.0017	0.0035
EOMESe+11	-0.0934	-220975	0.1692	0.0709	0	0	0	0	0
MIXL1e-8	-0.0950	346403	0.1059	0.1318	0.0334	0.0381	0.1347	0.0039	0.0159
SOX17e-22	-0.0956	1393973	0.0799	0.024	0	0	0	0	0
MIXL1e-3	-0.0971	181617	0.1651	0.1879	0	0	0	0	0
SOX17e-23	-0.0997	1590123	0.2525	0.1622	0.0265	0.0136	0.0356	0.0054	0.0072
MIXL1e-11	-0.1009	1133840	0.5139	2.5101	0.0218	0.0323	0.0223	0.0248	0.0254
SOX17e-14	-0.1011	322047	0.5255	0.8711	0.1746	0.0636	0.0861	0.1181	0.0583
EOMESe-3	-0.1026	41140	0.0852	0.045	0.0474	0.0507	0.048	0.0029	0.003
MIXL1e+13	-0.1030	-324157	1.0317	3.3078	0.2761	0.1407	0.4568	0.51	0.8438
SOX17e+11	-0.1051	-472279	0.1571	0.1242	0.051	0.0258	0.0109	0.0071	0.0015
GATA6e+11	-0.1062	-178336	0.1836	0.0362	0.0199	0.0147	0	0.0016	0
GATA6e-9	-0.1110	744369	0.2405	0.0657	0	0	0	0	0
MIXL1e+15	-0.1139	-454397	0.2692	0.596	0.0908	0.0878	0.0517	0.0364	0.0207
SOX17e+19	-0.1144	-1990552	0.3717	0.5372	0.1019	0.0838	0.0531	0.0455	0.0237
EOMESe-5	-0.1146	55596	1.072	1.3209	0	0	0	0	0
SOX17e+17	-0.1167	-1438791	0.2441	0.0608	0.0227	0.0189	0.003	0.0028	0.0004
EOMESe-18	-0.1178	700126	0.3192	1.5992	0.1574	0.1149	0.773	0.1125	0.5522
EOMESe+25	-0.1180	-1335331	0.1401	0.0288	0.0151	0	0	0.001	0
EOMESe+8	-0.1181	-166404	0.37	0.2564	0.0112	0.0147	0.0175	0.0034	0.0054
SOX17e-15	-0.1191	486298	0.2913	0.0327	0.0388	0.0319	0.0178	0.0038	0.0017
EOMESe+24	-0.1203	-1183745	0.2983	0.0451	0.0628	0.0195	0.123	0.0073	0.0143
SOX17e-11	-0.1214	278649	0.5399	1.1085	0	0	0.0034	0	0.0026

MIXL1e+18	-0.1235	-798531	0.1632	0.3774	0.0256	0.0475	0.003	0.0064	0.0007
EOMESe+18	-0.1240	-890043	0.0828	0.0275	0.0183	0.0187	0.0042	0.0009	0.0002
EOMESe-14	-0.1244	678644	0.4536	1.9363	0	0	0	0	0
GATA6e-13	-0.1245	1120241	0.323	0.6976	0	0	0	0	0
EOMESe-22	-0.1271	1316023	0.4466	1.4258	0	0	0	0	0
EOMESe-15	-0.1278	679545	0.1599	0.744	0.0256	0.0475	0.003	0.0088	0.001
SOX17e+18	-0.1302	-1868106	0.0801	0.0137	0	0	0	0	0
EOMESe-27	-0.1316	1660385	0.6481	1.8436	1	1	0.8971	1.0931	0.9807
GATA6e+1	-0.1317	-10329	0.5176	1.5484	0	0	0	0	0
MIXL1e+9	-0.1330	-220748	0.3233	0.2817	0.0245	0.0347	0.042	0.0074	0.0127
SOX17e-20	-0.1333	1387296	0.1811	0.0858	0	0	0	0	0
GATA6e-12	-0.1343	1116131	0.4423	3.0591	0	0	0	0	0
GATA6e-10	-0.1345	868225	0.2159	0.2834	0.0279	0.025	0.0624	0.0069	0.0154
EOMESe+23	-0.1347	-1069538	0.0868	0.058	0	0	0	0	0
MIXL1e-7	-0.1351	309079	0.1199	0.0096	0	0.0143	0	0	0
EOMESe+6	-0.1352	-161143	0.5209	2.6537	0	0	0	0	0
SOX17e-12	-0.1365	296091	0.0922	0.057	0	0	0	0	0
GATA6e-11	-0.1366	999912	0.1402	0.1605	0.2007	0.1399	0.7753	0.0301	0.1163
MIXL1e+25	-0.1374	-1584094	0.2709	0.0795	0.0274	0.0101	0.0356	0.004	0.0052
EOMESe+9	-0.1389	-167288	0.0706	0.0239	0	0	0	0	0
EOMESe-23	-0.1392	1371301	0.2932	1.4742	0.1574	0.1149	0.773	0.1035	0.5081
EOMESe-21	-0.1411	1207632	0.113	0.0195	0	0	0	0	0
EOMESe-6	-0.1421	89332	0.5696	0.2603	0.0513	0.0409	0.0503	0.0198	0.0194
EOMESe-16	-0.1431	685954	0.1987	0.194	0.024	0.0425	0.003	0.0047	0.0006
MIXL1e+14	-0.1454	-451221	0.4728	0.4752	0	0.0136	0.0175	0	0.0083
MIXL1e-6	-0.1469	297109	0.2569	0.5953	0	0	0	0	0
MIXL1e+20	-0.1473	-999088	0.1412	0.0272	0.0139	0.0203	0.0624	0.0009	0.0039
GATA6e-3	-0.1512	163216	0.1598	0.0302	0.0571	0.1457	0.8683	0.004	0.0603
MIXL1e+8	-0.1519	-125727	0.1782	0.906	0.0754	0.0745	0.1209	0.0303	0.0486
SOX17e-10	-0.1543	247602	0.2766	1.6766	0.1574	0.1149	0.773	0.1072	0.5264
EOMESe+19	-0.1570	-981655	0.5268	0.2112	0.0417	0.0232	0.1274	0.0139	0.0425
SOX17e-3	-0.1580	18231	0.0693	0.0035	0.0148	0.0209	0	0.0002	0
GATA6e+16	-0.1596	-863808	0.5971	0.2181	0.0185	0.0139	0	0.0067	0
EOMESe+7	-0.1605	-163493	0.6223	0.284	0.3257	0.2336	0.7097	0.1369	0.2984
EOMESe-13	-0.1617	676412	0.3199	0.0884	0	0	0	0	0
SOX17e-21	-0.1620	1390182	0.2085	0.5096	0.0237	0	0.003	0.0077	0.001
SOX17e+13	-0.1623	-965215	0.4045	0.0351	0.0446	0.0225	0.1431	0.0053	0.017
GATA6e+14	-0.1634	-782609	0.5184	0.1395	0	0	0.0087	0	0.0023
EOMESe+16	-0.1646	-478296	0.0568	0.0774	0.0732	0.0616	0.686	0.0049	0.0455
SOX17e-8	-0.1658	135047	0.155	0.5691	0.0537	0.033	0.0265	0.016	0.0079
GATA6e-7	-0.1673	669271	0.2024	0.7331	0	0	0	0	0
EOMESe-28	-0.1682	1671404	0.4678	0.6487	0	0	0	0	0
EOMESe+10	-0.1706	-183496	0.1957	0.0628	0.0956	0.1071	0.7581	0.0106	0.0841
GATA6e+15	-0.1725	-824547	0.4164	1.1874	0	0	0	0	0
EOMESe-10	-0.1747	493347	0.2566	0.0188	0.0168	0.0203	0.0119	0.0012	0.0008
SOX17e-16	-0.1768	661455	0.1869	0.0545	0.022	0.0385	0.0133	0.0022	0.0013
EOMESe+21	-0.1805	-1043091	0.079	0.2295	0	0.0197	0	0	0
EOMESe-19	-0.1853	1004035	0.4214	0.1896	0.0158	0	0	0.0045	0
MIXL1e-9	-0.1884	456562	0.7393	1.2009	0.0155	0.0216	0.0222	0.0146	0.0209
SOX17e-5	-0.2005	93949	0.5046	0.0545	0.0732	0.0347	0.5737	0.0121	0.0951

EOMESe+15	-0.2043	-395888	0.499	2.1268	0	0	0	0	0
EOMESe-25	-0.2056	1544459	0.1015	0.0383	0.06	0.0401	0.6927	0.0037	0.0432
EOMESe-17	-0.2100	696482	0.1378	0.0325	0.0644	0.0165	0.003	0.0043	0.0002
GATA6e+13	-0.2158	-433739	0.2772	0.5861	0.0426	0.0431	0.0211	0.0172	0.0085
EOMESe-9	-0.2195	364479	0.2479	0.0381	0.0752	0.0674	0.0241	0.0073	0.0023
EOMESe+14	-0.2215	-355443	0.5045	0.7837	0.7714	0.6629	0.9474	0.4851	0.5957
EOMESe+3	-0.2292	-9155	0.1985	0.1024	0.061	0.0326	0.7018	0.0087	0.1001
MIXL1e+12	-0.2443	-319667	0.345	1.8689	0.0206	0.0229	0.0223	0.0165	0.0179
MIXL1e-12	-0.2451	1861851	0.5971	1.2847	0	0	0	0	0
SOX17e-2	-0.2500	12395	0.512	0.1332	0.4769	0.4364	0.8014	0.1246	0.2093
EOMESe-26	-0.3674	1557959	0.1793	1.0971	0	0	0	0	0
SOX17e-1	-0.5000	8967	0.8275	0.8561	0.7175	0.8848	0.8123	0.6039	0.6837

Supplementary Table 8. Data of K562 Reilly enhancer screen.

Regions	Log2FC	Dist_tss (bp)	DHS K562	H3K27ac K562	Hi-C K562	*P*(in loop)	*ABC score*	*CIA score*
CD164-8	6.217	77859	2.11167	3.9048	0.3585	0.9674	1.0294	2.7779
FADS1+1	5.946	-17854	2.09163	8.38249	1	0.9087	4.1873	3.8051
HBG2+5	5.487	-30014	1.28219	3.0405	0.1399	0.9794	0.2762	1.9339
HBG1+5	4.95	-34938	1.28219	3.0405	0.127	0.9736	0.2508	1.9223
LMO2+10	4.737	-75152	1.63902	4.58927	0.4267	0.9336	1.1703	2.5605
HBG2+4	3.832	-25980	1.27612	2.10912	0.1399	0.9794	0.2295	1.6068
HBG1+4	3.504	-30904	1.27612	2.10912	0.127	0.9736	0.2084	1.5973
GATA1-1	3.135	3522	1.26353	2.6694	0.8911	1	1.6365	1.8365
LMO2+9	2.974	-72033	1.41628	9.0087	0.4267	0.9374	1.5242	3.3483
HBE1+3	2.692	-16450	1.28219	3.0405	0.5958	0.995	1.1764	1.9647
FADS2+1	2.301	-6557	2.09163	8.38249	1	0.994	4.1873	4.1623
LMO2+1	2.286	-12249	0.659162	1.14331	0.7378	1	0.6405	0.8681
FADS1+2	2.109	-24891	1.37802	4.72765	0.6621	0.857	1.69	2.1874
HBE1+2	2.09	-12416	1.27612	2.10912	0.5958	0.995	0.9775	1.6324
FADS3-5	2.03	56688	2.09163	8.38249	0.427	0.5049	1.788	2.1141
MYB+12	1.977	-140180	1.20004	2.07832	0.0579	0.5676	0.0914	0.8964
FADS1+4	1.935	-52927	1.49605	3.44371	0.4638	0.7922	1.0527	1.7981
HBG2+6	1.894	-33498	1.16928	3.37118	0.1294	0.9661	0.2569	1.918
HBG1+6	1.818	-38422	1.16928	3.37118	0.1118	0.9603	0.222	1.9065
ERP29-2	1.737	18503	1.10617	0.532677	0.2187	0.9634	0.1679	0.7395
FEN1+3	1.392	-41946	2.09163	8.38249	0.0961	0.7175	0.4024	3.0044
FADS1+5	1.328	-54271	1.05484	1.39791	0.3901	0.7874	0.4737	0.9562
HBE1+1	1.301	-7642	1.15739	2.52275	0.9098	1	1.5546	1.7087
HBE1+15	1.3	-236133	0.75545	2.36111	0.0439	0.1956	0.0586	0.2612
LMO2+8	1.283	-67653	1.5333	4.8927	0.4159	0.9443	1.1391	2.5864
ERP29-3	1.225	18987	1.01165	1.10216	0.2187	0.9634	0.2309	1.0173
FADS3-4	1.15	49651	1.37802	4.72765	0.4258	0.5183	1.0868	1.3228
LMO2+2	1.051	-15700	0.980543	0.628533	0.5629	0.9939	0.4419	0.7803
HBG2+3	1.038	-21206	1.15739	2.52275	0.1426	0.9844	0.2437	1.6821
MYB+13	0.96	-144529	1.1939	3.5263	0.0469	0.5637	0.0962	1.1567
HBE1+4	0.951	-19934	1.16928	3.37118	0.4015	0.9818	0.7971	1.9493
HBG1+3	0.922	-26130	1.15739	2.52275	0.1114	0.9786	0.1904	1.6721
FADS2+2	0.87	-13594	1.37802	4.72765	0.2918	0.9382	0.7448	2.3947

FEN1-1	0.87	4599	0.432665	0.12759	0.8055	0.6553	0.1893	0.154
ERP29-4	0.865	19403	0.590762	1.25946	0.2187	0.9634	0.1886	0.831
FEN1+1	0.858	-4457	0.753767	0.470729	1	0.9785	0.5957	0.5828
LMO2-2	0.677	34191	0.331274	0.0759307	0.2561	0.4124	0.0406	0.0654
MYB+3	0.665	-10629	1.41964	2.63621	0.2171	0.7062	0.42	1.3661
MYB-11	0.588	82873	0.329624	0.130705	0.0653	0.195	0.0136	0.0405
ERP29-11	0.539	166522	0.774815	0.220113	0.0567	0.2673	0.0234	0.1104
CD164-8a	0.534	85379	0.76735	0.877265	0.325	0.9638	0.2667	0.7908
CD164-4	0.531	41898	0.748016	1.05782	0.338	0.9876	0.3007	0.8785
LMO2+44	0.53	-740204	0.697374	0.363426	0.0157	0	0.0079	0
ERP29-10	0.502	108603	0.394873	0.187581	0.0666	0.3072	0.0181	0.0836
LMO2+13	0.499	-101388	0.618629	0.367266	0.4642	0.9102	0.2213	0.4338
FEN1+2	0.491	-7853	0.931941	1.31329	0.3161	0.9668	0.3497	1.0695
HBG1+7	0.491	-41556	0.686834	0.82988	0.0869	0.9519	0.0656	0.7187
LMO2+22	0.482	-338910	0.408142	0.0809296	0.074	0.0485	0.0134	0.0088
LMO2+6	0.46	-49978	0.239885	0.203666	0.3641	0.9584	0.0805	0.2118
LMO2+11	0.453	-83173	0.556411	0.725475	0.4509	0.9295	0.2865	0.5906
FEN1+4	0.447	-48983	1.37802	4.72765	0.0839	0.6905	0.2141	1.7625
LMO2+5	0.444	-43038	1.06296	3.05297	0.3664	0.962	0.66	1.733
CD164-2	0.416	32769	0.782777	3.394	0.3481	0.9964	0.5674	1.6241
MYB-21	0.383	177769	0.30412	0.231706	0.0403	0.1272	0.0107	0.0338
FEN1+5	0.381	-67621	0.727777	0.931315	0.0998	0.6553	0.0822	0.5395
HBE1+5	0.381	-23068	0.686834	0.82988	0.2628	0.9735	0.1984	0.735
LMO2-7	0.373	153420	0.205921	0.202434	0.0922	0.0347	0.0188	0.0071
LMO2+47	0.367	-770623	0.251417	0.0468034	0.0257	0	0.0028	0
HBE1+6	0.361	-29559	0.486555	0.45834	0.2464	0.689	0.1164	0.3254
LMO2+50	0.348	-782529	0.53725	0.534778	0.0267	0	0.0143	0
HBG2+7	0.331	-36632	0.686834	0.82988	0.0895	0.9577	0.0676	0.723
MYB-16	0.329	96532	0.944045	1.14911	0.0625	0.1879	0.0651	0.1957
LMO2-15	0.325	539901	0.282822	0.057962	0.0346	0.0041	0.0044	0.0005
LMO2+17	0.323	-164413	0.460673	0.159397	0.1028	0.0898	0.0279	0.0243
MYB+11	0.314	-125621	1.01403	0.778729	0.0458	0.576	0.0407	0.5118
LMO2-9	0.312	181731	0.269218	0.093899	0.0403	0.0269	0.0064	0.0043
MYB-17	0.312	106136	0.482229	1.10636	0.0549	0.172	0.0401	0.1256
ERP29-19	0.301	271920	1.00772	1.6026	0.0208	0.0866	0.0264	0.1101
LMO2+12	0.3	-87866	0.384354	0.241704	0.4496	0.9295	0.137	0.2833
LMO2-1	0.295	11770	0.591615	0.113244	1	0.939	0.2588	0.243
LMO2+35	0.293	-623205	0.382466	0.133023	0.0394	0.0035	0.0089	0.0008
HBE1-6	0.287	96297	0.35967	0.241488	0.123	0.571	0.0362	0.1683
LMO2+40	0.282	-729880	0.860164	1.58839	0.0197	0	0.023	0
LMO2+41	0.282	-730675	1.49636	1.61513	0.0254	0	0.0395	0
LMO2+18	0.281	-167431	0.378312	0.155412	0.1235	0.0866	0.0299	0.021
LMO2+3	0.28	-29350	0.63903	0.621143	0.421	0.9731	0.2652	0.6131
ERP29+1	0.279	-70776	0.205026	0.256557	0.0734	0.6026	0.0168	0.1382
ERP29+11	0.276	-312448	0.208263	0.0704238	0.0184	0.3052	0.0022	0.037
MYB+9	0.276	-118154	0.514669	0.379944	0.0388	0.5779	0.0172	0.2556
ERP29+10	0.273	-281591	0.160211	0.101	0.0179	0.3181	0.0023	0.0405
MYB-18	0.269	107103	0.701831	1.04579	0.0509	0.172	0.0436	0.1474
ERP29-24	0.26	377679	0.905961	4.58209	0.0116	0.032	0.0236	0.0652
HBG1-8	0.259	125617	0.623451	0.401464	0.0464	0.5488	0.0232	0.2745

LMO2-4	0.256	61395	0.449852	0.0922328	0.1308	0.2586	0.0266	0.0527
LMO2-23	0.255	804042	0.356455	0.0623822	0.0174	0.0019	0.0026	0.0003
LMO2-10	0.254	211013	0.189943	0.115925	0.0136	0.019	0.002	0.0028
LMO2+49	0.253	-781966	0.601604	0.373569	0.0267	0	0.0127	0
ERP29-44	0.252	714410	0.270826	0.0182574	0.002	0	0.0001	0
LMO2-19	0.251	662201	0.544209	0.255254	0.0444	0.0019	0.0165	0.0007
LMO2+20	0.25	-292136	0.5263	0.135198	0.0861	0.058	0.023	0.0155
MYB+2	0.248	-2732	1.29733	1.82713	1	0.9876	1.5396	1.5205
ERP29+6	0.247	-103327	1.20898	1.9174	0.0585	0.5146	0.0891	0.7835
LMO2-16	0.246	548674	0.592175	0.144906	0.0385	0.0041	0.0113	0.0012
LMO2+25	0.242	-381478	0.306385	0.16186	0.042	0.0473	0.0094	0.0105
LMO2+43	0.235	-733947	1.54344	1.25844	0.0254	0	0.0354	0
HBE1+12	0.234	-112591	0.320529	0.0883925	0.0959	0.5439	0.0161	0.0915
MYB+1	0.234	-1898	1.34969	1.48377	1	1	1.4151	1.4151
CD164-18	0.23	279495	0.435265	1.03891	0.1754	0.1049	0.1179	0.0706
ERP29-6	0.227	37679	0.655634	1.34437	0.1662	0.9533	0.156	0.895
ERP29-30	0.226	483765	0.271387	0.0362982	0.0114	0.0192	0.0011	0.0019
LMO2-11	0.225	361603	0.185692	0.0377481	0.0165	0.015	0.0014	0.0013
LMO2-8	0.22	179250	0.427196	0.282205	0.0347	0.029	0.012	0.0101
ERP29-32	0.216	561559	0.353844	0.0965811	0.0099	0	0.0018	0
LMO2+51	0.216	-784398	0.38799	0.128025	0.0267	0	0.006	0
CD164-3	0.213	39739	0.444673	0.295391	0.338	0.9912	0.1225	0.3592
HBE1+13	0.21	-208057	0.369466	0.35647	0.0736	0.2194	0.0267	0.0796
ERP29-33	0.207	574797	0.352496	0.738517	0.0105	0	0.0054	0
LMO2+34	0.207	-598617	0.270977	0.0579628	0.0385	0.0035	0.0048	0.0004
GATA1+3	0.206	-55304	0.189384	0.122083	0.0486	0.8822	0.0074	0.1341
HBG1+1	0.205	-8900	0.930484	0.778946	0.2236	0.994	0.1904	0.8463
HBG2-1	0.203	11619	1.35564	3.14976	0.2123	0.9952	0.4387	2.0565
LMO2+24	0.201	-366958	0.651242	0.0466585	0.0551	0.0473	0.0096	0.0082
ERP29-38	0.199	613896	0.4746	0.537749	0.0108	0	0.0055	0
HBG2+1	0.199	-3976	0.930484	0.778946	1	1	0.8513	0.8513
GATA1+11	0.198	-155314	1.27945	4.32061	0.0475	0.5474	0.1117	1.2871
LMO2-17	0.198	596955	0.171494	0.010143	0.0481	0.0019	0.002	0.0001
HBG1-1	0.197	6695	1.35564	3.14976	1	1	2.0664	2.0664
LMO2+15	0.196	-127374	0.62672	0.0836848	0.161	0.1405	0.0369	0.0322
LMO2+7	0.193	-57506	0.743367	0.869295	0.3308	0.9562	0.2659	0.7687
LMO2+23	0.193	-364426	0.480977	0.189248	0.0561	0.0473	0.0169	0.0143
FADS2+4	0.191	-41630	1.49605	3.44371	0.1588	0.8522	0.3604	1.9343
LMO2-3	0.188	40099	0.470436	0.0815824	0.1825	0.3402	0.0358	0.0666
MYB+17	0.188	-257783	0.317961	0.191131	0.038	0.2002	0.0094	0.0494
ERP29-46	0.187	827934	0.45324	0.170337	0.0059	0	0.0016	0
ERP29-34	0.186	575433	0.451406	0.966962	0.0105	0	0.0069	0
MYB+4	0.184	-49810	0.742686	1.93921	0.0499	0.6319	0.0599	0.7583
LMO2+27	0.181	-489474	0.781537	0.226924	0.0731	0.0439	0.0308	0.0185
LMO2-14	0.17	526721	0.212309	0.565136	0.031	0.005	0.0107	0.0017
HBE1+24	0.167	-353011	0.30605	0.274743	0.0249	0.1708	0.0072	0.0495
ERP29-18	0.163	271447	0.836591	1.27692	0.0208	0.0866	0.0215	0.0895
LMO2-5	0.162	66995	0.298089	0.110056	0.116	0.1514	0.021	0.0274
MYB+7	0.162	-99625	0.468365	0.386104	0.0397	0.5817	0.0169	0.2474
CD164-9	0.161	86829	0.491658	0.244747	0.325	0.9599	0.1127	0.333

ERP29-21	0.16	325978	0.487731	0.339154	0.0243	0.0612	0.0099	0.0249
MYB-6	0.157	36141	0.790685	0.658166	0.1155	0.7567	0.0833	0.5459
CD164+4	0.156	-109404	0.475334	0.239458	0.1186	0.132	0.04	0.0445
LMO2+29	0.156	-501824	0.590697	0.903638	0.0555	0.0072	0.0405	0.0052
LMO2-6	0.155	145425	0.582239	1.67295	0.0909	0.0347	0.0897	0.0343
MYB+6	0.152	-81224	0.842179	0.589843	0.0417	0.6092	0.0294	0.4293
FADS3-3	0.151	31013	0.727777	0.931315	0.5504	0.5285	0.4531	0.4351
HBG2-8	0.151	130541	0.623451	0.401464	0.0523	0.5462	0.0262	0.2733
MYB-5	0.151	34950	0.705326	1.7533	0.1155	0.7567	0.1284	0.8415
HBE1-10	0.146	144105	0.623451	0.401464	0.1471	0.5401	0.0736	0.2702
FADS2+3	0.144	-32232	0.727777	0.931315	0.1926	0.8621	0.1586	0.7097
MYB-4	0.143	33431	0.751113	2.31974	0.1155	0.7586	0.1525	1.0013
ERP29-35	0.139	584447	0.285962	0.161933	0.0065	0	0.0014	0
ERP29+3	0.139	-97551	0.557651	0.406536	0.0556	0.5483	0.0265	0.261
ERP29-25	0.138	388696	0.448471	0.427475	0.0136	0.032	0.006	0.014
ERP29-8	0.136	68011	0.218933	0.0601363	0.182	0.9324	0.0209	0.107
HBE1+29	0.135	-578484	0.166996	0.192073	0.0203	0.0777	0.0036	0.0139
HBE1+30	0.135	-754809	0.17375	0.0859291	0.0204	0.0071	0.0025	0.0009
LMO2-12	0.131	498565	0.257113	0.0967235	0.0346	0.0094	0.0055	0.0015
LMO2+4	0.131	-29699	0.652203	0.613898	0.421	0.9731	0.2664	0.6158
LMO2+26	0.13	-396800	0.215038	0.0327474	0.0221	0.0473	0.0019	0.004
GATA1+16	0.129	-297042	0.325708	0.0869429	0.0166	0.1796	0.0028	0.0302
LMO2+21	0.129	-304683	0.555019	0.0689028	0.0648	0.0568	0.0127	0.0111
LMO2+45	0.128	-747146	0.482056	0.137082	0.0183	0	0.0047	0
HBE1-22	0.125	886277	0.256919	0.0578164	0.0223	0	0.0027	0
ERP29-9	0.124	100903	0.280924	0.137589	0.0863	0.3127	0.017	0.0615
HBE1+14	0.12	-218246	0.266586	0.171061	0.0376	0.1956	0.008	0.0418
HBE1-16	0.118	609304	0.830312	2.3977	0.0204	0.1311	0.0288	0.1849
ERP29-23	0.116	376728	1.35075	4.6602	0.0116	0.032	0.0291	0.0803
HBE1-5	0.114	72033	0.684514	0.682075	0.1833	0.5951	0.1252	0.4066
MYB-9	0.111	70952	0.616579	0.452978	0.0515	0.2008	0.0272	0.1061
CD164-1	0.108	30870	0.514616	0.4545	0.3504	1	0.1695	0.4836
ERP29-13	0.108	184695	0.213301	0.188378	0.0653	0.2601	0.0131	0.0521
ERP29-41	0.107	682072	0.358591	0.162948	0.0076	0	0.0018	0
LMO2+36	0.105	-623813	0.241481	0.186567	0.0394	0.0035	0.0084	0.0007
LMO2+33	0.103	-594999	0.330745	0.273438	0.0337	0.0035	0.0101	0.001
FADS2+5	0.101	-42974	1.05484	1.39791	0.1293	0.8467	0.157	1.0282
MYB-51	0.101	927409	0.410128	0.19671	0.0037	0	0.0011	0
CD164-14	0.1	152705	0.446043	0.27083	0.2435	0.9292	0.0846	0.323
LMO2+46	0.1	-749392	0.59321	0.0770177	0.0183	0	0.0039	0
MYB+5	0.097	-73405	0.496189	0.383786	0.0499	0.6175	0.0218	0.2695
ERP29-7	0.096	38153	0.613742	1.35662	0.1662	0.9533	0.1517	0.8699
MYB-22	0.095	200322	0.72016	0.786916	0.0282	0.0847	0.0212	0.0637
MYB-13	0.095	87499	0.434963	0.254745	0.069	0.1917	0.023	0.0638
HBE1+18	0.094	-263220	0.600633	1.10491	0.036	0.192	0.0293	0.1564
HBG1-16	0.094	623452	0.402663	0.160557	0.0095	0.0473	0.0024	0.012
GATA1-6	0.092	149600	0.172369	0.186132	0.0324	0.2842	0.0058	0.0509
GATA1+2	0.092	-7951	1.43163	2.90212	1	1	2.0383	2.0383
LMO2+42	0.092	-732644	0.653746	0.471599	0.0254	0	0.0141	0
GATA1-3	0.089	84420	1.09049	0.781917	0.0643	0.8394	0.0594	0.7751

LMO2+37	0.087	-695787	0.219008	0.0193441	0.0275	0	0.0018	0
ERP29-49	0.086	989042	0.296945	0.0833934	0.0054	0	0.0008	0
HBG1+13	0.081	-120193	0.261375	0.0909295	0.0562	0.6306	0.0087	0.0972
LMO2+31	0.079	-557720	0.595066	0.865672	0.0651	0.0035	0.0467	0.0025
CD164+6	0.078	-145727	0.201358	0.125489	0.0609	0.117	0.0097	0.0186
ERP29-48	0.077	956123	0.229668	0.400305	0.0051	0	0.0015	0
GATA1+17	0.077	-303117	0.34682	0.460804	0.0168	0.1796	0.0067	0.0718
ERP29-12	0.073	174848	0.787492	0.451456	0.0606	0.2673	0.0361	0.1594
HBE1+31	0.073	-981668	0.419784	0.179756	0.0081	0	0.0022	0
MYB+24	0.073	-494770	0.271603	0.01	0.0033	0.0156	0.0002	0.0008
LMO2+38	0.072	-716583	0.6694	0.384727	0.0123	0	0.0062	0
ERP29-17	0.07	237603	1.17665	2.27866	0.026	0.1003	0.0426	0.1642
LMO2+48	0.07	-780889	0.481624	0.347776	0.0267	0	0.0109	0
HBG2+28	0.069	-553845	0.276846	0.0383265	0.0129	0.1487	0.0013	0.0153
GATA1-4	0.068	105895	0.538513	0.487539	0.0447	0.7549	0.0229	0.3868
ERP29-14	0.065	187853	0.217855	0.0869444	0.0653	0.2601	0.009	0.0358
GATA1+32	0.065	-522459	0.419891	0.561369	0.0069	0	0.0033	0
HBE1+32	0.065	-982952	0.377871	0.161353	0.0081	0	0.002	0
LMO2+28	0.064	-496894	0.204768	0.043471	0.0579	0.0072	0.0055	0.0007
GATA1+19	0.062	-353402	0.405338	0.21591	0.0128	0.1375	0.0038	0.0407
ERP29+2	0.061	-83392	0.25925	0.847269	0.0741	0.5583	0.0347	0.2616
GATA1+13	0.056	-175157	1.09968	1.04021	0.0339	0.3172	0.0363	0.3392
LMO2+19	0.056	-175341	1.13266	4.80184	0.1505	0.0854	0.351	0.1992
CD164-6	0.054	58990	0.422709	0.303579	0.3275	0.9769	0.1173	0.35
HBG1+28	0.054	-558769	0.276846	0.0383265	0.0101	0.1485	0.001	0.0153
ERP29-40	0.053	653244	0.299663	0.144834	0.0078	0	0.0016	0
MYB+15	0.053	-238069	0.379974	0.354225	0.0672	0.4284	0.0247	0.1572
HBG2-2	0.052	29078	0.541857	0.281481	0.1292	0.9766	0.0505	0.3814
HBG2+9	0.051	-80566	0.517626	0.428634	0.0542	0.6521	0.0255	0.3071
LMO2-13	0.05	507276	0.214704	0.0541229	0.0444	0.0085	0.0048	0.0009
MYB+21	0.05	-342179	0.230596	0.29148	0.008	0.0445	0.0021	0.0115
HBE1-17	0.049	631274	0.404054	0.146211	0.0281	0.1311	0.0068	0.0319
MYB-49	0.048	887239	0.495983	0.550645	0.0035	0	0.0018	0
ERP29-39	0.047	619196	0.700967	0.254456	0.0085	0	0.0036	0
ERP29-29	0.045	443211	0.367287	0.721128	0.0079	0.0247	0.0041	0.0127
LMO2+39	0.044	-718406	0.558698	0.307854	0.0123	0	0.0051	0
MYB-43	0.044	807700	0.475	0.808507	0.0063	0.0019	0.0039	0.0012
GATA1-5	0.04	138129	0.236896	0.0434714	0.0377	0.724	0.0038	0.0735
ERP29-37	0.038	603399	1.66608	2.43052	0.0099	0	0.0199	0
CD164-15	0.037	194444	0.369422	0.200261	0.3933	0.9015	0.107	0.2452
LMO2-21	0.036	691216	0.237047	0.09774	0.0266	0.0019	0.004	0.0003
CD164-13	0.035	140246	0.434553	0.166063	0.3178	0.9475	0.0854	0.2545
ERP29+5	0.033	-102039	0.726321	0.543255	0.0585	0.5347	0.0367	0.3359
MYB+10	0.033	-123805	0.464384	0.334154	0.0458	0.5779	0.018	0.2276
HBE1-9	0.031	138719	0.938694	3.59803	0.122	0.5436	0.2242	0.9991
GATA1-2	0.03	71296	0.218264	0.133243	0.0622	0.8564	0.0106	0.146
MYB-29	0.03	595585	0.888322	0.334952	0.0088	0.0039	0.0048	0.0021
MYB+8	0.03	-110635	0.521369	0.444718	0.0427	0.5798	0.0206	0.2792
CD164-17	0.029	199158	0.25829	0.0930298	0.4486	0.8677	0.0695	0.1345
HBG2+13	0.029	-115269	0.261375	0.0909295	0.0485	0.6353	0.0075	0.0979

CD164-16	0.028	196232	0.312589	0.062744	0.3933	0.9015	0.0551	0.1262
HBE1+11	0.028	-101705	0.261375	0.0909295	0.1407	0.6431	0.0217	0.0991
ERP29-42	0.027	687988	0.184679	0.144906	0.0071	0	0.0012	0
ERP29+8	0.027	-169969	0.299535	0.0683948	0.0287	0.3727	0.0041	0.0533
CD164-19	0.026	300136	0.23518	0.134762	0.1346	0.0621	0.024	0.0111
HBG2+29	0.026	-555882	0.621014	1.52522	0.0103	0.1487	0.01	0.1447
HBE1-15	0.024	377908	0.166565	0.289885	0.0257	0.1487	0.0056	0.0327
LMO2+16	0.024	-128352	0.368787	0.0933925	0.161	0.1405	0.0299	0.0261
MYB-7	0.023	51940	0.236809	0.086944	0.0537	0.2265	0.0077	0.0325
LMO2+14	0.02	-118342	0.454156	0.144907	0.2496	0.4608	0.064	0.1182
MYB+16	0.02	-242543	0.465322	0.622084	0.0776	0.4265	0.0418	0.2295
HBG1-2	0.016	24154	0.541857	0.281481	0.1285	0.9815	0.0502	0.3833
HBE1-20	0.014	728548	0.208652	0.0305741	0.0096	0.0035	0.0008	0.0003
FADS2-1	0.011	27536	0.931941	1.31329	0.18	0.9208	0.1991	1.0186
HBE1+7	0.011	-67002	0.517626	0.428634	0.095	0.6595	0.0447	0.3107
HBE1+21	0.01	-296114	0.281248	0.333285	0.0417	0.1885	0.0128	0.0577
MYB+20	0.008	-325161	0.299448	0.100128	0.0076	0.0445	0.0013	0.0077
HBG2+35	0.005	-997429	0.530237	0.348501	0.0084	0	0.0036	0
MYB-20	0.005	174499	0.60196	0.554413	0.0429	0.1272	0.0248	0.0735
HBE1-21	0.002	774948	0.324704	0.057961	0.0151	0.0035	0.0021	0.0005
HBE1-4	0	42642	0.541857	0.281481	0.3009	0.9604	0.1175	0.3751
MYB-8	0	63000	0.468969	0.101144	0.0564	0.2149	0.0123	0.0468
ERP29-45	-0.003	744489	0.178389	0.0782498	0.004	0	0.0005	0
MYB-47	-0.003	865867	0.649095	0.637516	0.0047	0	0.003	0
MYB-1	-0.003	6577	0.344685	0.187002	0.1498	0.9506	0.038	0.2413
LMO2+30	-0.009	-552441	0.25706	0.0268065	0.0566	0.0035	0.0047	0.0003
MYB-50	-0.009	892222	0.317789	0.173887	0.0042	0	0.001	0
HBE1+27	-0.012	-542318	0.621014	1.52522	0.0477	0.1482	0.0464	0.1442
MYB-15	-0.012	93751	0.634661	0.593682	0.0677	0.1917	0.0416	0.1177
MYB-19	-0.017	118279	0.340164	0.0378209	0.0639	0.163	0.0072	0.0185
LMO2-18	-0.02	603134	0.211899	0.0936104	0.052	0.0019	0.0073	0.0003
CD164-10	-0.022	89849	0.482293	0.312057	0.3144	0.9599	0.122	0.3724
ERP29-20	-0.022	320392	0.308597	0.136574	0.0238	0.0612	0.0049	0.0126
FADS3-6	-0.023	90781	0.931941	1.31329	0.5356	0.4611	0.5925	0.5101
MYB+25	-0.023	-728649	0.269833	0.02898	0.0035	0.0039	0.0003	0.0003
CD164-24	-0.025	415247	0.281647	0.057962	0.0402	0.0349	0.0051	0.0045
HBE1+22	-0.026	-323541	0.650832	0.671353	0.0503	0.1779	0.0332	0.1176
FADS3-8	-0.028	103233	0.432665	0.12759	0.4253	0.1531	0.0999	0.036
HBG1+27	-0.028	-464029	0.166942	0.0642635	0.01	0.1592	0.001	0.0165
ERP29-36	-0.03	599637	0.701776	0.839009	0.0099	0	0.0076	0
GATA1+21	-0.03	-368849	1.33451	2.70881	0.0199	0.1036	0.0378	0.197
GATA1+30	-0.03	-496234	0.55764	0.21294	0.0038	0	0.0013	0
HBG1-14	-0.033	590816	0.830312	2.3977	0.0083	0.1316	0.0117	0.1857
MYB-28	-0.033	540164	0.463586	0.194538	0.0067	0.0197	0.002	0.0059
HBE1-13	-0.034	277084	0.286416	0.0991152	0.0304	0.1487	0.0051	0.0251
HBG1+25	-0.034	-350635	0.797072	0.45805	0.0131	0.1677	0.0079	0.1014
CD164-5	-0.035	49444	0.25433	0.147587	0.2627	0.9876	0.0509	0.1913
HBG1+9	-0.035	-85490	0.517626	0.428634	0.04	0.6472	0.0188	0.3049
ERP29-47	-0.039	946208	0.191854	0.0868692	0.0038	0	0.0005	0
ERP29-16	-0.039	225091	0.244675	0.210694	0.0276	0.1003	0.0063	0.0228

MYB-46	-0.04	865168	0.370426	0.677003	0.0047	0	0.0024	0
HBG2+34	-0.041	-996516	0.377871	0.161353	0.0084	0	0.0021	0
CD164-23	-0.042	410980	0.362033	0.043472	0.0494	0.0349	0.0062	0.0044
ERP29-43	-0.043	699492	0.305975	0.0724531	0.0046	0	0.0007	0
CD164-27	-0.044	488889	0.222072	0.02898	0.0384	0.0313	0.0031	0.0025
HBG1-5	-0.044	83794	0.295467	0.392698	0.0422	0.5728	0.0144	0.1951
FADS1-1	-0.046	16239	0.931941	1.31329	0.7247	1	0.8017	1.1063
HBE1-2	-0.047	9588	0.930484	0.778946	1	0.9918	0.8513	0.8443
CD164-11	-0.048	97555	0.568655	0.182365	0.2434	0.9599	0.0784	0.3091
HBG2-9	-0.048	167346	0.411757	0.387988	0.0228	0.1687	0.0091	0.0674
HBE1+33	-0.05	-983865	0.530237	0.348501	0.0081	0	0.0035	0
GATA1-17	-0.051	294078	0.529418	0.29916	0.0135	0.0663	0.0054	0.0264
GATA1-16	-0.051	292310	0.436171	0.0953495	0.0135	0.0889	0.0028	0.0181
HBE1+9	-0.051	-95547	0.352333	0.872556	0.122	0.6525	0.0676	0.3618
ERP29+4	-0.052	-101600	0.623019	0.25489	0.0585	0.5347	0.0233	0.2131
HBG1-7	-0.054	120231	0.938694	3.59803	0.0511	0.5523	0.0939	1.0151
HBE1+23	-0.057	-332147	0.797072	0.45805	0.0398	0.1779	0.024	0.1075
GATA1+33	-0.058	-529687	0.287678	0.305174	0.0186	0	0.0055	0
GATA1+31	-0.06	-505495	0.651707	0.172801	0.0126	0	0.0042	0
HBG2-6	-0.06	94472	0.352118	0.247283	0.0405	0.5704	0.012	0.1683
GATA1-13	-0.061	272694	0.367222	0.224389	0.0146	0.0889	0.0042	0.0255
MYB-23	-0.061	272233	0.287171	0.0983188	0.013	0.0385	0.0022	0.0065
GATA1+9	-0.062	-105142	1.59422	0.382047	0.0408	0.8822	0.0318	0.6885
ERP29-5	-0.063	34709	0.460759	0.919577	0.1662	0.9533	0.1082	0.6205
GATA1+14	-0.063	-243493	0.199956	0.021301	0.0177	0.2133	0.0012	0.0139
HBG2-14	-0.063	595740	0.830312	2.3977	0.0112	0.1319	0.0158	0.1862
HBG2-16	-0.065	628376	0.402663	0.160557	0.0104	0.0475	0.0026	0.0121
HBG1+29	-0.069	-560806	0.621014	1.52522	0.0099	0.1485	0.0096	0.1445
MYB-48	-0.07	885196	0.939632	1.13781	0.0055	0	0.0057	0
HBG1-19	-0.072	756460	0.324704	0.057961	0.0031	0.0036	0.0004	0.0005
LMO2-22	-0.073	710101	0.582616	0.724968	0.0278	0.0019	0.0181	0.0012
MYB-12	-0.076	83939	0.531575	0.207434	0.0653	0.195	0.0217	0.0647
MYB+26	-0.077	-757440	0.183535	0.116215	0.0024	0.0019	0.0004	0.0003
GATA1-18	-0.078	298929	0.68815	1.25076	0.0111	0.0663	0.0103	0.0615
GATA1+6	-0.08	-77789	0.309028	0.0824518	0.0515	0.8822	0.0082	0.1408
CD164+2	-0.082	-14806	0.230984	0.0927394	0.6555	0.591	0.0959	0.0865
CD164+3	-0.082	-63794	0.521595	0.737937	0.2402	0.2409	0.149	0.1495
HBE1-11	-0.083	180910	0.411757	0.387988	0.0583	0.1674	0.0233	0.0669
MYB-39	-0.084	758289	0.252323	0.213159	0.0095	0.0019	0.0022	0.0004
GATA1+18	-0.087	-320555	0.348289	0.260108	0.0177	0.1712	0.0053	0.0515
MYB+27	-0.088	-937701	0.146972	0.0689024	0.0025	0	0.0003	0
FADS2-2	-0.092	30932	0.753767	0.470729	0.1484	0.9197	0.0884	0.5478
HBG2+15	-0.094	-221621	0.369466	0.35647	0.0195	0.2134	0.0071	0.0775
HBG2-15	-0.098	617710	0.404054	0.146211	0.0117	0.1319	0.0028	0.0321
GATA1+27	-0.099	-404626	2.22935	0.900232	0.0189	0.0731	0.0268	0.1035
LMO2+32	-0.1	-576735	0.206893	0.126793	0.0721	0.0035	0.0117	0.0006
CD164-28	-0.101	519734	0.371009	0.132154	0.0509	0.0277	0.0113	0.0061
HBE1-3	-0.101	25183	1.35564	3.14976	0.3955	0.9741	0.8173	2.0129
GATA1+26	-0.102	-391088	0.592251	0.309521	0.0137	0.0814	0.0059	0.0349
HBG1+10	-0.103	-86656	0.39483	0.343284	0.04	0.6472	0.0147	0.2383

MYB-26	-0.103	358209	0.453843	0.0489037	0.008	0.0261	0.0012	0.0039
GATA1+22	-0.104	-369759	1.58651	2.2254	0.0199	0.1036	0.0374	0.1947
HBG2+25	-0.108	-345711	0.797072	0.45805	0.0164	0.1716	0.0099	0.1037
HBG1+26	-0.11	-371499	0.30605	0.274743	0.012	0.1677	0.0035	0.0486
FADS3-7	-0.111	94177	0.753767	0.470729	0.6356	0.4602	0.3786	0.2741
HBG2-3	-0.114	58469	0.684514	0.682075	0.0764	0.6019	0.0522	0.4113
GATA1+25	-0.116	-389047	0.773542	0.385017	0.0137	0.0814	0.0075	0.0444
HBE1+10	-0.116	-96010	0.360058	0.865165	0.122	0.6525	0.0681	0.3642
CD164+8	-0.119	-400981	0.185218	0.0675978	0.0319	0.0672	0.0036	0.0075
MYB-37	-0.119	744924	0.926201	0.893349	0.0052	0.0019	0.0047	0.0018
HBE1-12	-0.121	263713	0.235181	0.0598456	0.0326	0.1537	0.0039	0.0182
MYB-44	-0.121	822864	0.147167	0.0579625	0.0046	0	0.0004	0
CD164+7	-0.123	-322894	0.502618	0.125633	0.0285	0.0913	0.0072	0.0229
HBG1-13	-0.124	359420	0.166565	0.289885	0.0076	0.1494	0.0017	0.0328
CD164-26	-0.13	468053	0.263685	0.0579627	0.0843	0.0313	0.0104	0.0039
HBE1+26	-0.13	-540281	0.276846	0.0383265	0.056	0.1482	0.0058	0.0153
HBG2+27	-0.13	-459105	0.166942	0.0642635	0.0169	0.1595	0.0018	0.0165
GATA1+34	-0.133	-840585	0.322784	0.108246	0.0135	0	0.0025	0
HBG2+11	-0.133	-109111	0.352333	0.872556	0.0409	0.6449	0.0227	0.3576
HBG2+12	-0.134	-109574	0.360058	0.865165	0.0409	0.6449	0.0228	0.3599
GATA1-12	-0.135	254805	0.584892	1.3535	0.0179	0.0889	0.0159	0.0791
GATA1+24	-0.136	-388273	0.532762	0.441096	0.0152	0.0814	0.0074	0.0395
HBG1+15	-0.137	-226545	0.369466	0.35647	0.0115	0.2094	0.0042	0.076
ERP29-1	-0.142	5342	0.491172	0.790973	1	1	0.6233	0.6233
HBG1+8	-0.143	-48047	0.486555	0.45834	0.0724	0.677	0.0342	0.3197
CD164-25	-0.153	439469	0.226193	0.0833225	0.0563	0.0313	0.0077	0.0043
HBG2+20	-0.155	-276784	0.600633	1.10491	0.0189	0.186	0.0154	0.1516
HBG1-10	-0.157	245225	0.235181	0.0598456	0.0109	0.158	0.0013	0.0187
HBG1+20	-0.157	-281708	0.600633	1.10491	0.0146	0.182	0.0119	0.1483
HBG2-11	-0.157	263520	0.286416	0.0991152	0.0105	0.1499	0.0018	0.0253
CD164+5	-0.159	-144741	0.361558	0.121867	0.0609	0.117	0.0128	0.0246
HBG2+30	-0.16	-560942	0.180741	0.184321	0.0093	0.0932	0.0017	0.017
HBG2+14	-0.162	-126155	0.320529	0.0883925	0.0299	0.5356	0.005	0.0902
GATA1-9	-0.165	174717	0.177213	0.0579608	0.0217	0.1253	0.0022	0.0127
HBG2-7	-0.17	125155	0.938694	3.59803	0.0547	0.5498	0.1005	1.0105
ERP29+7	-0.173	-109584	0.709059	1.02239	0.0522	0.5092	0.0444	0.4335
HBG1+12	-0.173	-114498	0.360058	0.865165	0.0291	0.6401	0.0162	0.3573
HBG2-13	-0.173	364344	0.166565	0.289885	0.0099	0.1499	0.0022	0.0329
CD164-20	-0.176	308887	0.288045	0.0311542	0.1012	0.0621	0.0096	0.0059
GATA1-11	-0.176	239017	0.600094	0.134619	0.015	0.0972	0.0043	0.0276
HBG2-19	-0.176	761384	0.324704	0.057961	0.0035	0.0036	0.0005	0.0005
GATA1+23	-0.183	-380844	1.02138	4.76091	0.0219	0.0897	0.0483	0.1979
GATA1+8	-0.184	-97329	0.1721	0.01449	0.0495	0.8822	0.0025	0.0441
GATA1-15	-0.185	289713	0.33477	0.173886	0.0108	0.0889	0.0026	0.0214
MYB-24	-0.186	298665	0.245202	0.111505	0.0097	0.0366	0.0016	0.006
GATA1+10	-0.188	-130779	1.23891	0.673163	0.0564	0.765	0.0515	0.6986
HBG2+26	-0.188	-366575	0.30605	0.274743	0.016	0.168	0.0046	0.0487
HBG1+11	-0.189	-114035	0.352333	0.872556	0.0291	0.6401	0.0161	0.3549
GATA1-8	-0.19	168870	0.57924	0.644182	0.0246	0.1253	0.015	0.0765
HBE1+8	-0.19	-68168	0.39483	0.343284	0.095	0.6595	0.035	0.2428

GATA1+7	-0.192	-81517	0.386081	0.332343	0.0543	0.8822	0.0195	0.316
HBG2+8	-0.193	-43123	0.486555	0.45834	0.0628	0.682	0.0297	0.3221
HBG2-20	-0.194	872713	0.256919	0.0578164	0.0035	0	0.0004	0
HBG1-18	-0.196	710060	0.208652	0.0305741	0.0032	0.0036	0.0003	0.0003
GATA1+12	-0.197	-162238	0.392769	0.633604	0.0428	0.5305	0.0214	0.2646
HBG2-5	-0.198	88718	0.295467	0.392698	0.047	0.5704	0.016	0.1943
HBG2+10	-0.2	-81732	0.39483	0.343284	0.0542	0.6521	0.02	0.2401
FADS2-3	-0.201	39988	0.432665	0.12759	0.0808	0.2835	0.019	0.0666
GATA1+5	-0.202	-68465	0.206752	0.04347	0.0615	0.8822	0.0058	0.0836
GATA1+28	-0.204	-444435	1.08377	0.561006	0.0197	0.028	0.0154	0.0219
GATA1-14	-0.21	288099	0.284754	0.124547	0.0108	0.0889	0.002	0.0167
CD164-12	-0.211	117976	0.314606	0.119331	0.2308	0.9563	0.0447	0.1853
HBG1+14	-0.211	-131079	0.320529	0.0883925	0.0242	0.5311	0.0041	0.0894
HBG1-9	-0.212	162422	0.411757	0.387988	0.0231	0.1718	0.0092	0.0687
HBG1+30	-0.215	-565866	0.180741	0.184321	0.009	0.0931	0.0016	0.017
HBE1-14	-0.216	376158	0.244728	0.144616	0.0257	0.1487	0.0048	0.028
HBG1-3	-0.216	53545	0.684514	0.682075	0.0887	0.6042	0.0606	0.4128
CD164-21	-0.221	325632	0.272682	0.251196	0.0829	0.0384	0.0217	0.0101
HBG2-10	-0.231	250149	0.235181	0.0598456	0.0133	0.1549	0.0016	0.0184
MYB+23	-0.232	-387273	0.208339	0.057818	0.004	0.0294	0.0004	0.0032
HBE1+25	-0.234	-445541	0.166942	0.0642635	0.0275	0.1588	0.0028	0.0164
HBG1+16	-0.236	-236734	0.266586	0.171061	0.0258	0.1856	0.0055	0.0396
GATA1-19	-0.237	334689	0.199621	0.0925223	0.0094	0.0663	0.0013	0.009
HBG2-18	-0.238	714984	0.208652	0.0305741	0.0079	0.0036	0.0006	0.0003
CD164-22	-0.245	336825	0.415997	0.0724529	0.0687	0.0384	0.0119	0.0067
CD164+9	-0.245	-411427	0.268981	0.0753501	0.0326	0.0672	0.0046	0.0096
HBG1-15	-0.247	612786	0.404054	0.146211	0.0101	0.1316	0.0025	0.032
HBG1-11	-0.247	258596	0.286416	0.0991152	0.0113	0.1494	0.0019	0.0252
HBG2-12	-0.252	362594	0.244728	0.144616	0.0099	0.1499	0.0019	0.0282
HBE1-18	-0.254	641940	0.402663	0.160557	0.0231	0.0469	0.0059	0.0119
GATA1-10	-0.26	194943	0.49785	0.770179	0.021	0.1253	0.013	0.0776
HBG2+33	-0.262	-995232	0.419784	0.179756	0.0084	0	0.0023	0
HBG2+23	-0.272	-309678	0.281248	0.333285	0.0145	0.1824	0.0044	0.0559
HBG2+16	-0.274	-231810	0.266586	0.171061	0.0221	0.1896	0.0047	0.0405
HBG1+24	-0.276	-342029	0.650832	0.671353	0.0185	0.1677	0.0122	0.1109
HBG2+24	-0.28	-337105	0.650832	0.671353	0.0182	0.1716	0.012	0.1135
HBG1-6	-0.281	89548	0.352118	0.247283	0.0482	0.5728	0.0142	0.169
HBG1-20	-0.286	867789	0.256919	0.0578164	0.003	0	0.0004	0
GATA1+29	-0.291	-457797	0.859646	0.494421	0.0126	0.028	0.0082	0.0183
HBG2-4	-0.294	82733	0.35967	0.241488	0.0454	0.5776	0.0134	0.1702
ERP29+9	-0.296	-184896	0.401292	0.119331	0.0257	0.3672	0.0056	0.0803
GATA1+20	-0.306	-362299	1.06554	5.17599	0.02	0.1036	0.047	0.2433
HBG1-4	-0.314	77809	0.35967	0.241488	0.0382	0.5799	0.0113	0.1709
HBG2+32	-0.314	-768373	0.17375	0.0859291	0.0067	0.0072	0.0008	0.0009
GATA1-7	-0.324	154979	1.02761	0.251268	0.0323	0.2672	0.0164	0.1358
HBG1+23	-0.325	-314602	0.281248	0.333285	0.013	0.1785	0.004	0.0546
LMO2-20	-0.334	690185	0.213744	0.100203	0.0266	0.0019	0.0039	0.0003
HBE1-8	-0.344	108036	0.352118	0.247283	0.1322	0.5639	0.039	0.1664
HBG2+31	-0.346	-592048	0.166996	0.192073	0.0105	0.078	0.0019	0.014
HBG1-12	-0.354	357670	0.244728	0.144616	0.0076	0.1494	0.0014	0.0281

ERP29-31	-0.36	546186	0.174268	0.177293	0.0098	0.0055	0.0017	0.001
HBE1+28	-0.369	-547378	0.180741	0.184321	0.0266	0.0929	0.0049	0.017
ERP29-22	-0.376	375753	0.750304	1.45581	0.0116	0.032	0.0121	0.0334
HBG1+31	-0.384	-596972	0.166996	0.192073	0.013	0.0779	0.0023	0.0139
FEN1+6	-0.391	-77019	1.49605	3.44371	0.1044	0.652	0.237	1.4798
FEN1+7	-0.418	-78363	1.05484	1.39791	0.1124	0.6487	0.1365	0.7877
HBE1-7	-0.439	102282	0.295467	0.392698	0.1133	0.5639	0.0386	0.1921
FADS1+3	-0.446	-43529	0.727777	0.931315	0.44	0.8009	0.3622	0.6594
FADS3-2	-0.449	21615	1.49605	3.44371	0.795	0.9778	1.8045	2.2195
HBG1+32	-0.474	-773297	0.17375	0.0859291	0.0038	0.0071	0.0005	0.0009
CD164+1	-0.52	-9309	0.503893	0.114259	1	0.6421	0.2399	0.1541
FADS1-3	-0.613	28691	0.432665	0.12759	0.3048	0.2962	0.0716	0.0696
FADS1-2	-0.624	19635	0.753767	0.470729	0.5772	0.9989	0.3438	0.595
CD164-7	-0.647	74196	0.908712	0.52478	0.3606	0.9769	0.249	0.6746
HBG2+17	-0.888	-249697	0.75545	2.36111	0.0179	0.1896	0.0239	0.2533
HBG1+17	-0.921	-254621	0.75545	2.36111	0.0175	0.1856	0.0234	0.2479
FADS3-1	-1.803	20271	1.05484	1.39791	1	1	1.2143	1.2143

Supplementary Table 9. Data of K562 Nasser enhancer screen.

Regions	Effect	Dist tss (bp)	DHS K562	H3K27 ac K562	Hi-C K562	*P*(in loop)	*ABC score*	*CIA score*
ALAS2-1	0.930	2833	0.87798	0.97174	1.0000	1.0000	0.92367	0.92367
CCDC26+1	0.919	-7273	1.75898	5.95233	1.0000	1.0000	3.23574	3.23574
NFE2+1	0.893	-3438	2.04421	3.83242	1.0000	1.0000	2.79898	2.79898
PIM1-2	0.889	13251	2.32383	6.73700	1.0000	0.7879	3.95672	3.11763
HBE1+2	0.865	-10618	1.27612	2.10912	0.2932	0.9869	0.48102	1.61903
HBBP1+4	0.814	-37169	1.27612	2.10912	1.0000	1.0000	1.64058	1.64058
EPB41+2	0.760	-3076	1.89480	9.05899	0.6281	0.9995	2.60226	4.14113
HBG2+4	0.739	-25980	1.27612	2.10912	0.9814	0.9867	1.61006	1.61876
KCNN4-1	0.720	6588	1.97748	5.01826	1.0000	1.0000	3.15016	3.15016
HBD+5	0.692	-46133	1.27612	2.10912	1.0000	1.0000	1.64058	1.64058
HBG1+4	0.692	-30904	1.27612	2.10912	1.0000	1.0000	1.64058	1.64058
MYO1D+4	0.690	-20411	1.55404	6.23700	0.8540	1.0000	2.65875	3.11329
FTL+1	0.669	-2823	1.37940	4.06934	1.0000	1.0000	2.36923	2.36923
RBM38-3	0.662	23991	1.02998	1.41298	1.0000	1.0000	1.20638	1.20638
EPB41+1	0.660	-1925	2.00893	7.81996	1.0000	1.0000	3.96355	3.96355
HNRNPA1-4	0.613	23786	2.04421	3.83242	0.1659	0.8612	0.46435	2.41048
HBG2+6	0.583	-33498	1.16928	3.37118	0.9078	0.9729	1.80236	1.93161
FADS1+1	0.581	-17800	2.09163	8.38249	1.0000	1.0000	4.18725	4.18725
HBG2+3	0.500	-21206	1.15739	2.52275	1.0000	1.0000	1.70874	1.70874
MYO1D+7	0.480	-32915	0.87953	1.72222	0.5360	0.9722	0.65968	1.19657
SMIM1-1	0.472	2210	2.09886	1.53645	1.0000	1.0000	1.79577	1.79577
HBE1+4	0.467	-18136	1.16928	3.37118	0.1446	0.9736	0.28709	1.93306
GATA1+1	0.440	-3505	1.26353	2.66940	1.0000	0.9583	1.83654	1.76001
RAE1-5	0.437	64300	1.02998	1.41298	1.0000	1.0000	1.20638	1.20638
CCDC26+9	0.423	-114617	1.65375	3.44827	0.0740	0.5232	0.17671	1.24941
HBE1+3	0.422	-14652	1.28219	3.04050	0.2932	0.9869	0.57891	1.94853
HDAC6+3	0.420	-18947	1.26353	2.66940	0.6258	0.9474	1.1493	1.73993
HBG2+5	0.416	-30014	1.28219	3.04050	0.9814	0.9867	1.93774	1.9482

CCDC26+11	0.406	-117992	2.15568	4.10615	0.0753	0.4345	0.22403	1.2927
PIM2+1	0.398	-22768	1.27945	4.32061	1.0000	1.0000	2.35117	2.35117
MYC-35	0.392	309075	1.65347	2.65969	0.3313	0.5714	0.69476	1.19827
MYO1D+3	0.387	-17263	0.94022	2.51283	1.0000	1.0000	1.53708	1.53708
PLP2+1	0.379	-4402	1.02138	4.76091	0.7199	1.0000	1.58749	2.20515
MYC-14	0.359	162867	2.36495	9.63883	0.4992	0.7692	2.3834	3.67235
SPACA3+9	0.357	-81775	0.87953	1.72222	1.0000	1.0000	1.23075	1.23075
TMEM98+3	0.352	-17821	0.87953	1.72222	1.0000	1.0000	1.23075	1.23075
LRRC47-2	0.331	21534	2.09886	1.53645	1.0000	1.0000	1.79577	1.79577
TMEM98+7	0.329	-33473	0.94022	2.51283	0.4885	0.8940	0.75086	1.37409
SPACA3+13	0.328	-97427	0.94022	2.51283	0.8371	0.9273	1.28669	1.42533
HBE1+1	0.324	-5844	1.15739	2.52275	1.0000	1.0000	1.70874	1.70874
JUNB+1	0.312	-1464	2.06351	1.02080	1.0000	1.0000	1.45135	1.45135
HBG1+5	0.308	-34938	1.28219	3.04050	1.0000	1.0000	1.97446	1.97446
PIM1+17	0.301	-119759	2.20699	7.33438	0.5562	1.0000	2.23776	4.0233
HBG1+6	0.295	-38422	1.16928	3.37118	0.8803	0.9860	1.74776	1.95768
CEP104-7	0.293	82263	2.09886	1.53645	1.0000	1.0000	1.79577	1.79577
FADS1+2	0.265	-24837	1.37802	4.72765	0.6621	0.9409	1.68995	2.40165
NFE2+2	0.259	-6198	1.47777	1.36966	0.6041	0.9827	0.85945	1.39803
PLP2+4	0.233	-22947	1.06554	5.17599	0.1561	0.6581	0.36659	1.54552
LYL1+1	0.217	-1510	0.91245	0.91559	1.0000	1.0000	0.91402	0.91402
PQBP1-2	0.186	43993	1.27945	4.32061	0.1203	0.7036	0.28285	1.65428
FTH1+1	0.181	-4307	2.07190	8.00653	1.0000	1.0000	4.07293	4.07293
FUT1+3	0.179	-27296	1.44373	2.77330	0.6434	0.9783	1.28743	1.95749
FTL+7	0.178	-86548	1.78128	1.31155	0.1259	0.7386	0.19244	1.12893
H1FX-1	0.149	10448	1.16005	0.38929	0.7847	0.9672	0.52733	0.64999
PLP2+5	0.142	-31844	0.40534	0.21591	0.1116	0.6344	0.03301	0.18769
HNRNPA1-5	0.137	26546	1.47777	1.36966	0.1482	0.8465	0.21084	1.20435
JUNB-4	0.131	93756	2.17061	3.48841	0.0328	0.0959	0.09026	0.2638
JUNB+3	0.128	-8893	1.54032	1.80923	0.2059	0.9507	0.34372	1.58701
H1FX+27	0.122	-383157	0.49735	0.45240	0.0563	0.2653	0.02671	0.12586
H1FX-3	0.118	70355	0.59421	0.19910	0.1880	0.7130	0.06466	0.24523
GATA1-17	0.116	303134	0.34682	0.46080	0.0189	0.2733	0.00756	0.10926
PLP2+3	0.115	-16397	1.33451	2.70881	0.1871	0.8307	0.35573	1.57947
PLP2+2	0.115	-15487	1.58651	2.22540	0.1871	0.8307	0.35156	1.56094
HNRNPA1-2	0.114	7826	1.09507	0.92248	1.0000	1.0000	1.00508	1.00508
PQBP1+21	0.113	-366126	0.58489	1.35350	0.0206	0.0453	0.01833	0.04028
RAB7A-48	0.112	870838	0.59673	0.52688	0.1357	0.0078	0.07609	0.00437
PQBP1+11	0.110	-182617	0.21826	0.13324	0.0455	0.3967	0.00776	0.06766
RAB7A-56	0.109	932466	0.32472	0.58738	0.0859	0.0000	0.03751	0
PPP1R15A+20	0.108	-193989	0.49959	0.10136	0.1199	0.1337	0.02698	0.03008
FUT1-3	0.107	32856	1.98425	1.91436	0.4372	0.8965	0.8521	1.74727
NUCB1+3	0.106	-21289	1.78128	1.31155	0.5849	0.9287	0.89401	1.41955
PLP2+21	0.104	-329942	0.18938	0.12208	0.0135	0.2830	0.00205	0.04304
H1FX+40	0.100	-741422	0.24242	0.01449	0.0720	0.1111	0.00427	0.00658
H1FX-17	0.100	262672	0.49550	0.40639	0.0719	0.3232	0.03226	0.14505
PPP1R15A-7	0.099	70925	0.26023	0.15237	0.3709	0.8513	0.07386	0.16951
JUNB-53	0.095	791739	0.24931	0.01449	0.0015	0.0011	0.00009	0.00006
RAB7A-16	0.095	327470	0.49550	0.40639	0.2358	0.1308	0.10581	0.05871
HDAC6+27	0.093	-776181	0.32848	0.07267	0.0239	0.0000	0.00369	0

NFE2-5	0.093	80736	0.77095	0.63266	0.0351	0.4000	0.02451	0.27936
RAB7A-33	0.092	601533	0.47348	0.09100	0.1635	0.0110	0.03394	0.00228
PPP1R15A-20	0.092	263838	0.59661	0.55840	0.0831	0.1239	0.04796	0.07149
CNBP+50	0.091	-893898	0.21142	0.00065	0.0174	0.0164	0.0002	0.00019
PLP2-10	0.090	144441	0.28768	0.30517	0.0207	0.0401	0.00613	0.01187
FUT1+18	0.090	-189656	0.26023	0.15237	0.0901	0.1916	0.01794	0.03815
PRKAR2B+10	0.090	-34413	1.44046	6.91422	1.0000	1.0000	3.15589	3.15589
PRKAR2B+9	0.090	-34000	1.23876	4.36459	1.0000	1.0000	2.32523	2.32523
CNBP+5	0.089	-46902	0.49403	0.30640	0.6229	0.9542	0.24235	0.37125
FTL+3	0.088	-21992	0.26023	0.15237	0.1447	0.9294	0.02881	0.18507
RAB7A+26	0.087	-309952	1.54729	7.40038	0.2819	0.2508	0.95391	0.84867
RAB7A+25	0.087	-309124	1.38267	6.75808	0.2819	0.2508	0.86172	0.76665
HDAC6+12	0.086	-210368	0.49785	0.77018	0.0964	0.1782	0.05969	0.11037
RAB7A-54	0.084	900725	0.89953	0.52608	0.0700	0.0078	0.04815	0.00537
RAD23A+3	0.084	-60562	2.17061	3.48841	0.8741	0.8682	2.40528	2.38905
LYL1+33	0.083	-480074	0.24931	0.01449	0.0059	0.0811	0.00035	0.00487
WDR83OS+11	0.082	-215600	2.17061	3.48841	0.1691	0.2298	0.46532	0.63244
RPN1+31	0.082	-588250	0.63982	0.42190	0.1738	0.0337	0.0903	0.01751
PRDX2-3	0.081	19308	1.54032	1.80923	0.4528	0.9295	0.75589	1.55168
RAB7A-7	0.080	119855	0.92893	0.50102	1.0000	1.0000	0.68221	0.68221
NUCB1+1	0.077	-7970	1.08052	1.76018	1.0000	0.9861	1.3791	1.35993
RAB7A-34	0.077	602741	0.34007	0.01449	0.1635	0.0110	0.01148	0.00077
PPP1R15A+47	0.077	-517718	0.40442	0.52275	0.0185	0.0295	0.00851	0.01355
RAB7A+29	0.076	-315888	1.19535	2.40639	0.2872	0.2508	0.4871	0.42536
PPP1R15A-13	0.076	166461	0.27495	0.01449	0.1535	0.2005	0.00969	0.01266
PQBP1+3	0.076	-29804	0.38608	0.33234	0.1445	0.8026	0.05176	0.28748
HNRNPA1-13	0.076	102663	0.65085	0.82416	0.0705	0.2562	0.05163	0.18766
NUCB1+29	0.076	-247272	0.45173	0.24388	0.0840	0.0887	0.02788	0.02945
PRDX2+4	0.075	-83341	2.17061	3.48841	0.1768	0.1428	0.4865	0.39285
FUT1+33	0.075	-423554	0.55067	0.14107	0.0931	0.0382	0.02595	0.01065
PPP1R15A+41	0.074	-453596	1.03429	0.81604	0.0320	0.0497	0.0294	0.04569
PPP1R15A-10	0.074	103879	0.55502	0.71519	0.3633	0.6254	0.22889	0.39402
CALR+21	0.074	-736130	0.17898	0.00000	0.0370	0.0062	0	0
LYL1+17	0.074	-158092	0.42462	0.45928	0.0289	0.3440	0.01276	0.15191
HBE1+5	0.074	-21270	0.68683	0.82988	0.0912	0.9572	0.06885	0.72264
PPP1R15A-23	0.074	326660	0.44964	0.52333	0.1069	0.1034	0.05186	0.05014
WDR83OS+60	0.073	-913583	0.24931	0.01449	0.0278	0.0000	0.00167	0
CNBP+10	0.073	-143701	0.47348	0.09100	0.1104	0.1013	0.02292	0.02102
PPP1R15A+51	0.073	-538325	1.50949	2.18925	0.0310	0.0268	0.05635	0.04866
BAX+2	0.072	-11543	0.26023	0.15237	0.3443	0.9637	0.06856	0.19189
NFE2+4	0.072	-57285	0.89990	3.38190	0.0777	0.6583	0.13555	1.14836
RPN1-10	0.069	103277	1.56343	4.21809	0.6653	0.3642	1.7085	0.93518
NUCB1+16	0.069	-134039	0.47587	0.14020	0.0638	0.1577	0.01648	0.04073
BCAT2+1	0.068	-1351	1.24868	0.69823	1.0000	1.0000	0.93374	0.93374
RAB7A-50	0.068	873571	0.76283	0.66635	0.1357	0.0078	0.09675	0.00556
HDAC6-9	0.067	139889	1.27945	4.32061	0.2505	0.6095	0.58897	1.43312
PQBP1-33	0.067	971034	0.28903	0.73700	0.0081	0.0000	0.00374	0
JUNB-11	0.067	221972	0.58941	0.63013	0.0101	0.0395	0.00616	0.02405
RPN1-21	0.066	224387	0.75991	0.86901	0.3412	0.3038	0.27727	0.24685
HNRNPA1-24	0.066	315934	0.30507	0.06767	0.0066	0.0162	0.00095	0.00233

H1FX+31	0.065	-504465	0.25756	0.17360	0.0617	0.2480	0.01305	0.05244
PLP2-12	0.065	501817	0.18626	0.04347	0.0114	0.0245	0.00103	0.0022
PLP2-6	0.065	72551	0.85965	0.49442	0.0516	0.2022	0.03364	0.1318
LYL1-27	0.064	386064	0.48445	0.17635	0.0087	0.0473	0.00254	0.01383
FUT1-14	0.064	108687	1.03345	0.32495	0.3843	0.5144	0.2227	0.29812
PQBP1+33	0.063	-871048	0.46014	0.10730	0.0057	0.0000	0.00127	0
RNASEH2A+12	0.063	-284424	0.35832	0.07245	0.0730	0.0658	0.01176	0.0106
C19orf43-2	0.062	17679	0.48445	0.17635	1.0000	0.8201	0.29229	0.2397
FTL+5	0.062	-73229	1.08052	1.76018	0.1141	0.7847	0.15736	1.08218
PPP1R15A+19	0.061	-191169	0.44682	0.23323	0.1122	0.1337	0.03622	0.04315
H1FX+1	0.061	-11391	0.47348	0.09100	1.0000	0.9498	0.20757	0.19715
GATA1-5	0.060	68482	0.20675	0.04347	0.0690	0.8822	0.00654	0.08363
H1FX+24	0.060	-342324	0.32472	0.58738	0.0408	0.2730	0.01782	0.11924
HBE1-9	0.060	140517	0.93869	3.59803	0.0528	0.4518	0.09703	0.83025
RAB7A+34	0.060	-345135	0.30332	0.17201	0.2486	0.2508	0.05678	0.05729
NFE2-29	0.059	533146	0.27107	0.04347	0.0063	0.0166	0.00068	0.0018
PQBP1-26	0.058	775742	0.18626	0.04347	0.0144	0.0000	0.0013	0
BAX-2	0.058	21411	0.55502	0.71519	0.0860	0.6760	0.05418	0.42588
CNBP+33	0.057	-474634	0.32472	0.58738	0.0311	0.0440	0.01358	0.0192
PPP1R15A+27	0.057	-283255	1.19877	0.41581	0.0583	0.0701	0.04116	0.04949
FTL+63	0.057	-655789	0.73027	0.07992	0.0042	0.0120	0.00101	0.0029
RAB7A-27	0.057	503196	0.88456	2.13621	0.1241	0.0418	0.17059	0.05741
LYL1-32	0.057	580971	0.35832	0.07245	0.0042	0.0253	0.00068	0.00408
ITGA5-13	0.057	114791	2.04421	3.83242	0.0403	0.0780	0.1128	0.21823
CNBP-9	0.056	156773	1.05199	0.36777	0.1402	0.3588	0.08721	0.2232
DNASE2-10	0.056	164425	0.48445	0.17635	0.0418	0.1117	0.01222	0.03266
H1FX+28	0.056	-457876	0.34227	0.18679	0.0574	0.2538	0.01451	0.06416
ITGA5-39	0.056	474305	0.45323	0.05760	0.0170	0.0253	0.00275	0.00408
RAB7A-41	0.056	687815	1.21513	2.14621	0.2467	0.0110	0.3984	0.01776
HNRNPA1-17	0.055	142706	0.49272	0.33894	0.0299	0.0534	0.01222	0.02184
BCAT2+12	0.055	-132253	0.26023	0.15237	0.0415	0.2805	0.00826	0.05586
SEC61A1-28	0.055	374121	0.75991	0.86901	0.1126	0.1702	0.0915	0.13828
RAB7A+45	0.055	-580684	0.27883	0.39770	0.1934	0.0582	0.0644	0.01938
RPN1+45	0.054	-797560	1.02100	1.42074	0.0891	0.0056	0.10731	0.0067
SEC61A1-3	0.054	28100	0.46411	0.86306	0.7980	0.8595	0.50505	0.54395
PLP2-3	0.054	5842	0.59225	0.30952	1.0000	0.9163	0.42815	0.39232
BCAT2+30	0.054	-396952	0.72662	0.22555	0.0144	0.0299	0.00583	0.01209
BCAT2+31	0.054	-397424	0.63712	0.04753	0.0144	0.0299	0.00251	0.0052
H1FX+2	0.054	-12599	0.34007	0.01449	1.0000	0.9498	0.0702	0.06667
CALR-25	0.054	256111	0.36439	0.06376	0.1090	0.1307	0.01661	0.01992
LYL1+10	0.054	-88222	0.34326	0.07245	0.0420	0.4843	0.00662	0.07638
RAB7A+42	0.053	-499146	0.31187	0.13201	0.2921	0.1463	0.05927	0.02969
COPZ1-15	0.053	164990	0.19188	0.01449	0.0908	0.0252	0.00479	0.00133
RAB7A+40	0.053	-459456	0.14807	0.01891	0.1290	0.1568	0.00683	0.0083
CNBP-63	0.052	917288	0.14807	0.01891	0.0516	0.0000	0.00273	0
FUT1-9	0.052	75258	0.49959	0.10136	0.4196	0.7745	0.09442	0.1743
HDAC6+4	0.051	-86721	0.21826	0.13324	0.2292	0.6514	0.03909	0.11109
HDAC6+6	0.051	-121320	0.53851	0.48754	0.2135	0.5527	0.1094	0.28322
HNRNPA1-8	0.051	78665	2.56516	3.36227	0.1367	0.6411	0.40146	1.88288
CNBP-8	0.051	130362	0.49550	0.40639	0.1587	0.4759	0.07121	0.21354

RAB7A-40	0.051	673611	1.30077	3.00283	0.1404	0.0110	0.27748	0.02174
RAB7A-13	0.051	290706	1.10381	0.56499	0.3322	0.1386	0.26234	0.10948
BCAT2+28	0.051	-387988	0.44964	0.52333	0.0141	0.0362	0.00684	0.01758
PQBP1+22	0.051	-384015	0.36722	0.22439	0.0193	0.0453	0.00554	0.01299
CNBP-52	0.051	773720	1.19535	2.40639	0.0226	0.0010	0.03833	0.0017
PQBP1+27	0.051	-410250	0.68815	1.25076	0.0081	0.0094	0.00751	0.00875
H1FX+8	0.050	-83469	1.30077	3.00283	0.1492	0.3757	0.29487	0.74252
RAB7A+6	0.050	-141533	0.38827	0.19642	0.5916	0.3951	0.16338	0.1091
SEC61A1+9	0.050	-355895	0.30052	0.10970	0.2246	0.3565	0.04078	0.06473
CALR+3	0.050	-53348	2.17061	3.48841	1.0000	0.8693	2.75172	2.39198
HNRNPA1-12	0.050	96381	0.60701	0.44428	0.0680	0.2657	0.03531	0.138
RAB7A-39	0.049	659605	0.36108	0.13042	0.0665	0.0110	0.01443	0.00239
LYL1-33	0.049	607684	0.92663	1.05760	0.0058	0.0127	0.00574	0.01254
FUT1+24	0.049	-285192	0.27495	0.01449	0.1239	0.0951	0.00782	0.006
NUCB1+2	0.049	-9331	0.33922	0.34778	1.0000	0.9834	0.34347	0.33776
HDAC6+14	0.048	-270230	0.58489	1.35350	0.0932	0.1008	0.08292	0.08966
GATA1+4	0.048	-105878	0.53851	0.48754	0.0501	0.5570	0.02567	0.2854
PPP1R15A+45	0.048	-473503	1.76294	1.66049	0.0540	0.0497	0.09239	0.08509
H1FX+5	0.048	-45048	0.18631	0.00000	0.3033	0.5806	0	0
COPZ1+17	0.048	-149521	0.37139	0.10759	0.0880	0.0658	0.01759	0.01315
C19orf43+58	0.047	-848459	0.24931	0.01449	0.0125	0.0000	0.00075	0
CNBP-57	0.047	802967	0.30332	0.17201	0.0213	0.0010	0.00487	0.00023
RAB7A+37	0.047	-382369	0.70344	1.75844	0.2863	0.2107	0.31842	0.23437
BCAT2-15	0.047	132661	0.49959	0.10136	0.0328	0.1371	0.00738	0.03084
FUT1+34	0.047	-445391	0.44964	0.52333	0.0596	0.0322	0.02891	0.01562
FTL+2	0.047	-14019	0.55352	0.68700	0.1834	0.9662	0.1131	0.59582
PPP1R15A+37	0.046	-381075	1.13284	0.23772	0.0578	0.0547	0.02999	0.02839
RAB7A-38	0.046	657345	0.37017	0.05796	0.1478	0.0110	0.02165	0.00161
BAX-24	0.046	373231	0.30727	0.20287	0.0074	0.0460	0.00185	0.01148
PQBP1+23	0.046	-399420	0.28475	0.12455	0.0170	0.0220	0.0032	0.00414
WDR83OS+10	0.046	-166806	0.93136	0.41755	0.3913	0.3547	0.24402	0.22119
GATA1-37	0.046	967852	0.21738	0.07006	0.0133	0.0000	0.00164	0
BCAT2+15	0.045	-165207	0.55502	0.71519	0.0478	0.2320	0.03012	0.14617
RNASEH2A-4	0.045	78638	2.17061	3.48841	0.2754	0.2035	0.75782	0.55988
PLP2+35	0.045	-640051	0.58489	1.35350	0.0035	0.0891	0.00311	0.07931
PQBP1+15	0.045	-260921	0.17237	0.18613	0.0324	0.2453	0.0058	0.04394
CNBP+13	0.045	-160731	0.34765	0.03927	0.0878	0.0863	0.01026	0.01008
PLP2+34	0.045	-624263	0.60009	0.13462	0.0055	0.0925	0.00156	0.02629
ITGA5+2	0.044	-13314	1.21853	0.77576	0.3830	0.9544	0.37237	0.92792
CALR+2	0.044	-29857	0.52492	0.16440	0.9300	1.0000	0.2732	0.29376
BAX+39	0.044	-396353	0.33960	0.08173	0.0098	0.0356	0.00163	0.00593
DNASE2-7	0.044	120787	0.44079	0.07245	0.0515	0.1805	0.0092	0.03226
HNRNPA1+22	0.044	-331606	0.85567	0.40668	0.0148	0.0350	0.00873	0.02063
PPP1R15A-9	0.044	90094	1.37940	4.06934	0.6336	0.8250	1.50114	1.95469
LYL1-6	0.044	41599	0.66756	0.30894	0.0384	0.6861	0.01744	0.31159
RPN1+46	0.043	-818359	0.29207	0.21352	0.1375	0.0056	0.03434	0.00139
PPP1R15A+7	0.043	-84068	0.55020	0.04347	0.2991	0.4424	0.04626	0.06842
HBE1+7	0.043	-65204	0.51763	0.42863	0.0342	0.5474	0.01611	0.25786
LYL1+4	0.043	-59909	2.01447	4.08340	0.0590	0.5244	0.16922	1.50412
PPP1R15A+38	0.043	-409870	0.40601	0.07876	0.0438	0.0533	0.00783	0.00953

COPZ1-8	0.043	58263	0.65085	0.82416	0.2969	0.2508	0.21745	0.18366
C19orf43-8	0.043	239299	0.92663	1.05760	0.0634	0.0762	0.06276	0.07543
GATA1+5	0.043	-138112	0.23690	0.04347	0.0423	0.5261	0.00429	0.05339
SEC61A1-6	0.043	93083	0.27883	0.39770	0.5222	0.2983	0.17389	0.09932
HNRNPA1+6	0.043	-70584	0.42343	0.08644	0.0616	0.2087	0.01178	0.03993
HNRNPA1+24	0.043	-471458	0.36898	0.13411	0.0082	0.0288	0.00182	0.00641
PLP2+25	0.042	-456542	0.21826	0.13324	0.0116	0.1258	0.00198	0.02146
COPZ1+18	0.042	-163221	0.61744	1.26844	0.0885	0.0641	0.07832	0.05673
SEC61A1+5	0.042	-345232	0.58803	0.27496	0.3848	0.3565	0.15473	0.14335
RAD23A-2	0.042	32212	0.69199	0.18309	0.7940	0.4847	0.28262	0.17251
PPP1R15A+46	0.042	-487014	0.25824	0.20033	0.0333	0.0295	0.00757	0.0067
FUT1-2	0.042	16104	1.24833	0.99768	0.9260	1.0000	1.03341	1.11599
MYC-23	0.042	234847	0.43483	0.68896	0.3175	0.6628	0.17378	0.36278
H1FX-61	0.042	906030	1.19535	2.40639	0.0148	0.0000	0.0251	0
RAB7A+7	0.042	-148243	0.42979	0.09549	0.6578	0.3521	0.13326	0.07132
SEC61A1-2	0.042	24711	1.49586	2.11875	0.9742	0.9959	1.73434	1.77303
LYL1-18	0.041	266703	0.93136	0.41755	0.0096	0.0942	0.00599	0.05874
WDR83OS+7	0.041	-120380	2.06351	1.02080	0.4379	0.3924	0.63555	0.56951
DNASE2+1	0.041	-3730	2.17061	3.48841	1.0000	1.0000	2.75172	2.75172
H1FX-6	0.041	86946	0.88456	2.13621	0.1411	0.6602	0.19396	0.90753
GATA1+15	0.041	-289696	0.33477	0.17389	0.0121	0.0708	0.00292	0.01708
RAB7A+17	0.041	-228358	1.16700	1.31097	0.2727	0.2957	0.3373	0.36575
RPN1-44	0.040	517194	0.22384	0.00485	0.1814	0.0241	0.00598	0.00079
CNBP+3	0.040	-42644	0.48966	0.29923	0.5981	0.9666	0.22894	0.37
HNRNPA1-21	0.040	246593	0.28851	0.09796	0.0114	0.0302	0.00192	0.00507
RPN1-46	0.040	570408	0.46411	0.86306	0.1793	0.0000	0.11348	0
BCAT2-25	0.040	247447	0.60283	2.12491	0.0108	0.0363	0.01222	0.04112
NUCB1-5	0.040	76221	0.55502	0.71519	0.2991	0.6483	0.18844	0.40845
RAB7A-18	0.040	330813	0.47461	0.29155	0.3108	0.1308	0.11561	0.04867
NUCB1-15	0.040	236180	0.59661	0.55840	0.0515	0.1377	0.02973	0.0795
HNRNPA1-10	0.039	88671	1.67201	1.48776	0.0875	0.4358	0.138	0.68739
FUT1-40	0.039	419594	1.50949	2.18925	0.0418	0.0627	0.07599	0.11404
RAD23A-6	0.039	70975	0.54225	0.48008	0.3985	0.3825	0.20332	0.19517
DHPS+11	0.039	-203364	2.17061	3.48841	0.2202	0.1995	0.60593	0.54888
HDAC6-25	0.039	389201	2.22935	0.90023	0.0788	0.1110	0.11163	0.15725
GATA1-23	0.039	380861	1.02138	4.76091	0.0245	0.1210	0.05403	0.26682
C19orf43+8	0.038	-101682	0.93136	0.41755	0.2316	0.3235	0.14443	0.20174
H1FX-46	0.038	783096	0.57481	0.38487	0.0181	0.0000	0.00851	0
RAD23A+21	0.038	-743344	0.17898	0.00000	0.0905	0.0068	0	0
HNRNPA1-14	0.038	113732	0.70933	0.50978	0.0516	0.0910	0.03103	0.05472
RAB7A-25	0.038	485857	0.68357	0.47203	0.2421	0.0418	0.13752	0.02372
FTL-13	0.038	211906	0.55067	0.14107	0.0142	0.1445	0.00396	0.04027
BAX+61	0.038	-640295	0.30382	0.13339	0.0039	0.0117	0.00079	0.00236
PPP1R15A+48	0.038	-520922	0.50725	0.19186	0.0185	0.0268	0.00577	0.00835
COPZ1+12	0.038	-117111	0.52508	0.10462	0.1913	0.1026	0.04484	0.02405
BAX+19	0.037	-188849	0.47587	0.14020	0.0226	0.1251	0.00584	0.03232
HDAC6+19	0.037	-309503	0.52942	0.29916	0.0519	0.0477	0.02065	0.01897
COPZ1+29	0.037	-515858	0.36898	0.13411	0.0268	0.0159	0.00596	0.00353
NFE2+5	0.037	-58317	2.56516	3.36227	0.0777	0.6571	0.22819	1.92967
ITGA5+3	0.037	-20530	0.41126	0.48189	0.3117	0.7750	0.13876	0.345

HDAC6-19	0.037	353424	1.33451	2.70881	0.0818	0.1415	0.15553	0.2691
HDAC6-20	0.037	354334	1.58651	2.22540	0.0818	0.1415	0.1537	0.26594
PLP2-8	0.037	120249	0.65171	0.17280	0.0368	0.1170	0.01235	0.03926
PPP1R15A+13	0.036	-134835	1.24833	0.99768	0.1472	0.1795	0.16427	0.20028
GATA1+2	0.036	-71279	0.21826	0.13324	0.0698	0.6584	0.0119	0.11229
PQBP1+25	0.036	-403631	0.43617	0.09535	0.0120	0.0220	0.00245	0.00449
PLP2+13	0.036	-229932	1.27945	4.32061	0.0189	0.3019	0.04444	0.70982
PQBP1+2	0.036	-13992	0.17210	0.01449	0.2045	0.8328	0.01021	0.04159
PPP1R15A-16	0.036	225602	0.57710	0.32416	0.0931	0.1484	0.04027	0.0642
PPP1R15A-27	0.036	341628	0.32933	0.05796	0.0767	0.0864	0.0106	0.01193
HNRNPA1-6	0.036	71554	1.04793	1.04507	0.1329	0.6522	0.13908	0.68249
DNASE2+6	0.036	-102250	0.56166	0.19686	0.0403	0.2442	0.0134	0.08119
GATA1+29	0.035	-954595	0.26654	0.05796	0.0071	0.0000	0.00088	0
GATA1-9	0.035	105159	1.59422	0.38205	0.0458	0.8822	0.03574	0.68849
SEC61A1-63	0.035	964473	1.10381	0.56499	0.0671	0.0000	0.05299	0
HNRNPA1-25	0.035	322677	0.27330	0.07245	0.0087	0.0151	0.00122	0.00212
H1FX-11	0.035	209696	0.21230	0.09586	0.0671	0.3489	0.00957	0.04977
SEC61A1+1	0.035	-40991	0.35799	0.09847	1.0000	0.9950	0.18775	0.18682
H1FX-26	0.035	470287	0.92893	0.50102	0.0600	0.0256	0.04093	0.01744
FUT1+27	0.035	-344333	0.57710	0.32416	0.0715	0.0669	0.03093	0.02892
ITGA5-26	0.035	223262	0.96435	0.29576	0.0240	0.0443	0.01282	0.02368
HNRNPA1+17	0.035	-274560	0.65386	0.09129	0.0163	0.0647	0.00398	0.01581
H1FX+18	0.035	-283429	0.76283	0.66635	0.1160	0.2937	0.0827	0.20942
JUNB-46	0.035	637043	0.34986	0.07919	0.0015	0.0011	0.00025	0.00018
NFE2+21	0.034	-295586	0.30507	0.06767	0.0028	0.0117	0.0004	0.00168
HNRNPA1+12	0.034	-105121	0.37139	0.10759	0.0188	0.1133	0.00376	0.02265
RPN1+35	0.034	-676792	0.47348	0.09100	0.1949	0.0056	0.04046	0.00116
SEC61A1-62	0.034	963641	0.39553	0.45501	0.0671	0.0000	0.02847	0
WDR83OS+43	0.034	-578344	0.28100	0.04579	0.0314	0.0476	0.00356	0.0054
PQBP1-19	0.033	333114	1.08377	0.56101	0.0166	0.0436	0.01294	0.03402
H1FX-58	0.033	900094	1.54729	7.40038	0.0254	0.0000	0.08595	0
H1FX-57	0.033	899266	1.38267	6.75808	0.0254	0.0000	0.07764	0
BCAT2-2	0.033	22740	0.55020	0.04347	0.1148	0.6421	0.01775	0.09931
DNASE2-1	0.033	45064	0.93136	0.41755	0.1235	0.5054	0.07702	0.31519
ITGA5-16	0.033	131626	1.07689	1.68222	0.0439	0.0573	0.05909	0.07708
COPZ1+28	0.033	-380128	0.45323	0.05760	0.0649	0.0202	0.01049	0.00326
BCAT2-31	0.033	317997	2.34543	1.13042	0.0134	0.0301	0.02182	0.04901
CNBP+15	0.032	-199513	0.37017	0.05796	0.0568	0.0823	0.00832	0.01206
NUCB1+14	0.032	-119093	1.44373	2.77330	0.1362	0.1885	0.27253	0.37718
GATA1+8	0.032	-168853	0.57924	0.64418	0.0276	0.1801	0.01686	0.11001
PPP1R15A+5	0.032	-59977	1.24868	0.69823	0.3199	0.7089	0.2987	0.66193
C19orf43+15	0.032	-250666	1.06616	0.83749	0.0548	0.0692	0.05178	0.06539
FUT1+32	0.032	-398224	1.79277	1.48240	0.0687	0.0465	0.112	0.07581
RAB7A-15	0.032	301059	1.05199	0.36777	0.2780	0.1386	0.17292	0.08623
HNRNPA1+2	0.032	-60388	0.77095	0.63266	0.0844	0.5956	0.05894	0.41599
GATA1+6	0.032	-149583	0.17237	0.18613	0.0363	0.3702	0.0065	0.06632
FTL-23	0.032	362782	0.30727	0.20287	0.0097	0.0465	0.00242	0.01161
ITGA5+5	0.032	-108016	0.28851	0.09796	0.0388	0.0796	0.00652	0.01338
ITGA5-24	0.032	217761	0.62072	0.14759	0.0217	0.0449	0.00657	0.0136
PLP2+36	0.032	-657940	0.36722	0.22439	0.0093	0.0891	0.00267	0.02559

DNASE2+13	0.031	-198103	1.21784	1.64686	0.0401	0.1834	0.05679	0.25973
BCAT2+8	0.031	-67697	1.78128	1.31155	0.0468	0.3188	0.07153	0.48728
LYL1+5	0.031	-60719	1.64700	4.70519	0.0590	0.5244	0.16424	1.45991
LYL1+6	0.031	-61531	1.14509	1.78199	0.0590	0.5244	0.08428	0.74914
SEC61A1-27	0.031	372462	0.66256	1.43443	0.0997	0.1702	0.0972	0.16589
GATA1-7	0.031	81534	0.38608	0.33234	0.0609	0.8822	0.02181	0.31601
COPZ1+31	0.031	-557198	0.27107	0.04347	0.0447	0.0145	0.00485	0.00157
LYL1-11	0.031	117719	1.06616	0.83749	0.0414	0.5850	0.03912	0.55279
PQBP1+34	0.031	-872077	0.32848	0.07267	0.0057	0.0000	0.00088	0
MYC-21	0.031	231869	0.54653	1.14223	0.3670	0.6628	0.28997	0.52368
BAX+45	0.031	-463543	1.13284	0.23772	0.0038	0.0343	0.00197	0.0178
LYL1+22	0.031	-278990	0.94017	0.10774	0.0073	0.1379	0.00232	0.0439
LYL1+13	0.031	-109861	0.41749	0.12498	0.0344	0.4271	0.00786	0.09756
PPP1R15A+54	0.031	-562872	0.73027	0.07992	0.0381	0.0133	0.0092	0.0032
ITGA5-12	0.031	112031	1.47777	1.36966	0.0410	0.0780	0.05833	0.11092
PQBP1+1	0.031	-6179	1.59422	0.38205	1.0000	1.0000	0.78043	0.78043
JUNB-3	0.031	44962	0.93136	0.41755	0.0636	0.3846	0.03966	0.23984
NUCB1-28	0.031	431720	0.36270	0.18599	0.0272	0.0396	0.00706	0.01028
COPZ1+35	0.031	-628641	0.38804	0.11593	0.0432	0.0107	0.00916	0.00226
FTL-2	0.031	18355	0.33213	0.13027	0.2434	0.4118	0.05063	0.08566
GATA1+33	0.031	-983779	0.18742	0.06608	0.0064	0.0000	0.00071	0
FTL-8	0.031	141412	0.52055	0.18367	0.0251	0.1773	0.00776	0.05482
LYL1+11	0.030	-91550	0.36439	0.06376	0.0420	0.4818	0.0064	0.07344
C19orf43+2	0.030	-25959	0.44079	0.07245	0.5736	0.9655	0.10251	0.17254
MYC-31	0.030	278482	1.16036	1.66512	0.3121	0.5961	0.43382	0.82863
GATA1-8	0.030	97346	0.17210	0.01449	0.0556	0.8822	0.00278	0.04405
RAB7A+33	0.030	-342425	0.30134	0.14208	0.2486	0.2508	0.05144	0.05189
PQBP1+32	0.030	-814492	0.21991	0.04796	0.0120	0.0000	0.00123	0
CNBP+2	0.030	-28025	0.68357	0.47203	0.5192	0.9730	0.29492	0.5527
HNRNPA1+10	0.030	-84685	0.96435	0.29576	0.0212	0.1283	0.01132	0.06852
FTL+6	0.030	-74590	0.33922	0.34778	0.1141	0.7830	0.03919	0.26895
NUCB1+36	0.030	-341543	0.33960	0.08173	0.0308	0.0424	0.00513	0.00706
BAX+44	0.030	-461793	2.34543	1.13042	0.0038	0.0343	0.00619	0.05585
FUT1-6	0.030	55441	0.61356	0.33111	0.3413	0.8114	0.15383	0.36572
BCAT2-42	0.029	456390	0.40442	0.52275	0.0051	0.0140	0.00234	0.00644
LYL1-21	0.029	313129	2.06351	1.02080	0.0099	0.0692	0.01437	0.10048
FTL+58	0.029	-620215	0.27203	0.05796	0.0081	0.0235	0.00102	0.00295
MYC+2	0.029	-10176	0.31113	0.19831	1.0000	0.5698	0.24839	0.14153
PQBP1+36	0.029	-938765	0.31167	0.08448	0.0070	0.0000	0.00114	0
PPP1R15A+52	0.029	-539366	2.53815	2.46602	0.0310	0.0268	0.07756	0.06697
HNRNPA1-18	0.029	151891	1.21853	0.77576	0.0376	0.0505	0.03656	0.0491
COPZ1+10	0.029	-110211	1.07779	0.29604	0.3118	0.2656	0.17612	0.15005
H1FX-16	0.029	261428	0.85070	0.75996	0.0719	0.3232	0.05781	0.2599
C19orf43+17	0.029	-282013	0.54225	0.48008	0.0587	0.0642	0.02995	0.03276
MYC-30	0.029	271651	0.28710	0.34531	0.2759	0.6034	0.08687	0.19
BAX-7	0.029	120225	0.34101	0.06289	0.0181	0.2013	0.00265	0.02947
PPP1R15A-4	0.028	18327	0.33922	0.34778	1.0000	0.9629	0.34347	0.33073
LYL1-24	0.028	342426	0.44079	0.07245	0.0146	0.0473	0.00261	0.00845
FUT1-39	0.028	414107	0.44254	0.08694	0.0415	0.0627	0.00814	0.01231
NFE2-30	0.028	554259	0.62162	0.07419	0.0058	0.0158	0.00125	0.00339

DNASE2-18	0.028	679052	0.17898	0.00000	0.0057	0.0038	0	0
DHPS+20	0.028	-352356	0.47531	0.18715	0.0607	0.1214	0.0181	0.03621
FTL+51	0.028	-549711	0.97125	0.03456	0.0051	0.0302	0.00093	0.00553
ITGA5-11	0.028	67023	1.04793	1.04507	0.0659	0.0898	0.06896	0.09394
RAB7A+51	0.028	-714758	0.35799	0.09847	0.1304	0.0000	0.02448	0
FUT1+21	0.028	-222610	0.55502	0.71519	0.1617	0.1446	0.10188	0.09112
BAX-13	0.028	197025	1.79277	1.48240	0.0138	0.1388	0.0225	0.22622
CNBP+43	0.028	-648184	0.19653	0.05767	0.0310	0.0360	0.0033	0.00383
BCAT2+21	0.028	-286930	0.57710	0.32416	0.0145	0.0553	0.00627	0.02393
FUT1-43	0.028	444141	0.73027	0.07992	0.0490	0.0473	0.01184	0.01142
CNBP-10	0.028	161452	0.53604	0.08702	0.1520	0.3555	0.03283	0.07677
GATA1+18	0.028	-298912	0.68815	1.25076	0.0125	0.0169	0.0116	0.01571
GATA1+16	0.027	-292293	0.43617	0.09535	0.0151	0.0708	0.00308	0.01444
CNBP-11	0.027	167126	1.10381	0.56499	0.1543	0.3414	0.12185	0.26958
NFE2-22	0.027	311743	0.48203	0.19222	0.0226	0.0351	0.00688	0.01068
PPP1R15A+8	0.027	-87611	0.54594	0.41313	0.2320	0.4335	0.11018	0.20586
BCAT2-23	0.027	226675	0.94949	0.29989	0.0217	0.0401	0.01158	0.0214
COPZ1-16	0.027	202193	0.28851	0.09796	0.0495	0.0246	0.00832	0.00414
CALR-5	0.027	74868	0.58941	0.63013	0.2439	0.3459	0.14864	0.2108
HDAC6-7	0.027	89717	1.59422	0.38205	0.3880	0.9889	0.30281	0.77176
C19orf43+16	0.027	-278692	0.58941	0.63013	0.0556	0.0642	0.03388	0.03913
SEC61A1-65	0.027	974826	1.05199	0.36777	0.0707	0.0000	0.04398	0
LYL1-35	0.027	900691	0.17898	0.00000	0.0031	0.0000	0	0
MYC-48	0.027	431823	0.29021	0.11056	0.2925	0.4721	0.0524	0.08457
PRDX2+53	0.027	-781324	0.24931	0.01449	0.0129	0.0020	0.00078	0.00012
BCAT2-46	0.026	476997	1.50949	2.18925	0.0068	0.0123	0.01236	0.0223
NUCB1-3	0.026	51240	0.55352	0.68700	0.4744	0.9292	0.29254	0.57298
FTL-16	0.026	242707	0.72662	0.22555	0.0242	0.1166	0.0098	0.0472
FTL-17	0.026	243179	0.63712	0.04753	0.0242	0.1166	0.00421	0.02029
LYL1+3	0.026	-52545	1.57147	0.72808	0.0648	0.5889	0.06931	0.62996
COPZ1-5	0.026	44271	1.67201	1.48776	0.5545	0.4637	0.87456	0.73129
LYL1+8	0.026	-69354	0.46950	0.20896	0.0474	0.5062	0.01485	0.15855
PPP1R15A+28	0.026	-288003	0.94949	0.29989	0.0513	0.0647	0.02737	0.03452
RNASEH2A-24	0.026	356456	2.01447	4.08340	0.0574	0.0609	0.16463	0.17476
PPP1R15A+18	0.026	-186651	0.22362	0.04796	0.1235	0.1337	0.01279	0.01384
RPN1+32	0.026	-595046	0.59421	0.19910	0.1853	0.0337	0.06374	0.01159
H1FX-15	0.026	259329	0.47461	0.29155	0.1030	0.3232	0.03831	0.12024
PPP1R15A+36	0.026	-379325	2.34543	1.13042	0.0578	0.0547	0.09412	0.08907
ITGA5-22	0.026	209161	0.42343	0.08644	0.0400	0.0468	0.00765	0.00895
RNASEH2A+1	0.026	-16582	2.06351	1.02080	0.8941	0.9729	1.29766	1.41207
H1FX+12	0.026	-152958	0.29207	0.21352	0.1201	0.3400	0.02999	0.08491
HNRNPA1-26	0.026	378150	0.33027	0.06187	0.0070	0.0081	0.001	0.00116
BAX-21	0.026	270227	0.44413	0.06687	0.0098	0.0876	0.00169	0.01509
HNRNPA1+25	0.026	-488766	0.14834	0.02898	0.0065	0.0276	0.00043	0.00181
RAB7A+11	0.026	-177204	1.35814	2.53529	0.4572	0.2957	0.84838	0.5487
RAB7A+10	0.026	-176689	1.37151	2.25323	0.4572	0.2957	0.80373	0.51982
C19orf43+35	0.026	-456607	0.34326	0.07245	0.0302	0.0421	0.00476	0.00663
BCAT2+42	0.025	-580999	0.78564	0.32995	0.0085	0.0095	0.00433	0.00482
LYL1-14	0.025	128682	0.31007	0.13274	0.0600	0.5422	0.01217	0.11001
WDR83OS+12	0.025	-239091	0.52492	0.16440	0.1564	0.2298	0.04594	0.06752

FUT1-42	0.025	439096	0.30382	0.13339	0.0588	0.0473	0.01184	0.00952
NFE2-33	0.025	604589	0.38804	0.11593	0.0062	0.0120	0.00131	0.00255
FTL+50	0.025	-546513	1.03429	0.81604	0.0051	0.0302	0.00469	0.02774
PQBP1+37	0.025	-961201	1.15321	0.19613	0.0045	0.0000	0.00214	0
DNASE2-15	0.025	359332	0.35832	0.07245	0.0116	0.0528	0.00187	0.00851
SEC61A1-11	0.025	214311	0.14807	0.01891	0.1568	0.2684	0.0083	0.0142
BAX+28	0.025	-276457	0.49959	0.10136	0.0143	0.0875	0.00322	0.0197
HDAC6-10	0.025	146813	0.39277	0.63360	0.2107	0.5619	0.10511	0.28029
NUCB1+42	0.025	-408733	1.13284	0.23772	0.0468	0.0375	0.02429	0.01946
GATA1+34	0.025	-990005	0.40110	0.22881	0.0048	0.0000	0.00145	0
ITGA5-46	0.025	722818	0.38804	0.11593	0.0098	0.0154	0.00208	0.00327
LYL1-29	0.025	538913	0.44863	0.08694	0.0037	0.0253	0.00073	0.005
BAX+58	0.025	-615306	0.44254	0.08694	0.0043	0.0232	0.00084	0.00456
NFE2+3	0.025	-51206	1.04793	1.04507	0.0702	0.6711	0.07346	0.70234
PRDX2+1	0.025	-13420	0.37844	0.18113	1.0000	0.7629	0.26182	0.19973
CNBP+1	0.025	-11958	0.48299	0.84401	1.0000	1.0000	0.63848	0.63848
COPZ1-25	0.025	424289	0.18359	0.01761	0.0171	0.0022	0.00097	0.00013
DNASE2+37	0.025	-396641	0.40417	0.00739	0.0069	0.0449	0.00038	0.00245
DNASE2+50	0.025	-701713	0.24931	0.01449	0.0061	0.0147	0.00037	0.00088
CNBP+18	0.024	-229983	1.21513	2.14621	0.0253	0.0582	0.04086	0.09404
RNASEH2A-53	0.024	776621	0.24931	0.01449	0.0189	0.0020	0.00114	0.00012
ITGA5-43	0.024	672488	0.62162	0.07419	0.0081	0.0168	0.00174	0.0036
RAB7A-32	0.024	579694	1.16005	0.38929	0.1554	0.0110	0.10443	0.00739
CNBP+17	0.024	-215779	1.30077	3.00283	0.0495	0.0601	0.09783	0.11878
LYL1-19	0.024	270461	0.96819	0.11339	0.0124	0.0942	0.00411	0.03121
BAX-25	0.024	376910	0.36270	0.18599	0.0092	0.0460	0.00239	0.01195
CNBP-50	0.024	770892	1.37802	1.60042	0.0226	0.0010	0.03356	0.00149
SEC61A1-14	0.024	291398	0.70344	1.75844	0.1161	0.2684	0.12912	0.29855
RAB7A-22	0.024	380446	0.21230	0.09586	0.4327	0.1173	0.06173	0.01673
BAX+62	0.024	-645340	0.73027	0.07992	0.0033	0.0117	0.0008	0.00283
COPZ1-18	0.024	254819	0.41537	0.13629	0.0259	0.0138	0.00616	0.00328
BCAT2-7	0.024	62941	1.01167	3.18092	0.0369	0.1869	0.06619	0.33528
HDAC6-26	0.024	429010	1.08377	0.56101	0.0593	0.0588	0.04624	0.04582
PPP1R15A+49	0.024	-527298	0.27203	0.05796	0.0256	0.0268	0.00321	0.00336
LYL1-5	0.024	23536	1.21784	1.64686	0.0512	0.6905	0.07251	0.97784
FUT1-4	0.024	39392	2.33109	0.51217	0.3693	0.8721	0.40352	0.95291
HNRNPA1-19	0.024	159107	0.41126	0.48189	0.0409	0.0498	0.01821	0.02217
PPP1R15A+25	0.024	-227418	1.03345	0.32495	0.1554	0.1107	0.09005	0.06417
NUCB1-2	0.023	43267	0.26023	0.15237	0.5367	0.9325	0.10687	0.18568
HNRNPA1+5	0.023	-65811	1.07779	0.29604	0.0616	0.4134	0.0348	0.23353
DNASE2+32	0.023	-353249	0.59250	0.37270	0.0092	0.0640	0.00432	0.03009
RAD23A-18	0.023	217256	2.01447	4.08340	0.2339	0.1724	0.67084	0.49446
C19orf43+19	0.023	-317064	0.89935	0.11107	0.0604	0.0609	0.01909	0.01924
H1FX-10	0.023	195584	0.79677	0.96646	0.0828	0.3638	0.07266	0.31924
H1FX-65	0.023	932567	0.30134	0.14208	0.0176	0.0000	0.00364	0
ITGA5+8	0.023	-177357	0.30507	0.06767	0.0187	0.0298	0.00269	0.00428
WDR83OS-2	0.023	105404	0.44863	0.08694	1.0000	0.7905	0.1975	0.15613
KLF1-8	0.023	126469	0.44079	0.07245	0.1455	0.2158	0.026	0.03857
C19orf43+41	0.023	-513220	0.28100	0.04579	0.0225	0.0257	0.00255	0.00292
LYL1-25	0.023	345429	0.84767	0.13244	0.0117	0.0473	0.00392	0.01585

WDR83OS+23	0.023	-409973	1.21784	1.64686	0.0608	0.1303	0.0861	0.18458
MYC-22	0.023	232502	0.54861	1.01058	0.3670	0.6628	0.27326	0.49351
ITGA5-20	0.023	202937	0.84221	0.37169	0.0414	0.0492	0.02316	0.02755
ITGA5-19	0.023	202122	1.22745	0.89480	0.0414	0.0492	0.04339	0.0516
COPZ1+13	0.023	-123584	0.62072	0.14759	0.1529	0.0869	0.04628	0.02631
COPZ1+24	0.023	-335795	0.48203	0.19222	0.1084	0.0328	0.033	0.00997
LYL1+23	0.022	-293656	0.73862	0.42907	0.0108	0.1253	0.00608	0.07054
H1FX+42	0.022	-768497	0.29362	0.00246	0.0481	0.1111	0.00129	0.00299
FTL+36	0.022	-376172	1.19877	0.41581	0.0111	0.0396	0.00784	0.02798
NUCB1+35	0.022	-336433	0.60283	2.12491	0.0380	0.0424	0.04301	0.04795
KLF1+46	0.022	-650492	0.60170	0.25069	0.0152	0.0198	0.0059	0.00768
NUCB1+55	0.022	-560496	0.44254	0.08694	0.0287	0.0253	0.00563	0.00496
PPP1R15A+12	0.022	-124269	1.01167	3.18092	0.1226	0.1804	0.21993	0.32362
CNBP-17	0.022	337977	0.92893	0.50102	0.0483	0.0442	0.03295	0.03015
COPZ1+32	0.022	-578311	0.62162	0.07419	0.0343	0.0145	0.00737	0.00311
BCAT2-22	0.022	221927	1.19877	0.41581	0.0194	0.0434	0.0137	0.03064
GATA1-35	0.022	887080	0.18626	0.04347	0.0091	0.0000	0.00082	0
NFE2+8	0.022	-69395	1.03165	0.28873	0.0449	0.4188	0.02451	0.22857
RAD23A+10	0.022	-185079	0.44079	0.07245	0.2443	0.1515	0.04366	0.02707
KLF1+3	0.022	-87275	0.31007	0.13274	0.1761	0.3384	0.03573	0.06865
RPN1-36	0.022	311180	0.39863	0.29366	0.1901	0.2586	0.06504	0.08849
HDAC6+21	0.022	-350114	0.19962	0.09252	0.0391	0.0164	0.00531	0.00223
NUCB1+58	0.022	-585485	0.30382	0.13339	0.0234	0.0130	0.00471	0.00262
C19orf43+3	0.022	-47827	1.54032	1.80923	0.3727	0.4876	0.62217	0.81404
HNRNPA1+26	0.022	-512798	0.27107	0.04347	0.0055	0.0252	0.0006	0.00273
C19orf43+9	0.021	-150476	2.17061	3.48841	0.1519	0.1062	0.41799	0.29223
SEC61A1-25	0.021	363815	1.54729	7.40038	0.1039	0.1702	0.35158	0.57582
SEC61A1-26	0.021	364643	1.38267	6.75808	0.1039	0.1702	0.3176	0.52017
PLP2-20	0.021	712609	0.27617	0.10144	0.0070	0.0156	0.00117	0.00261
FTL+55	0.021	-579931	0.25824	0.20033	0.0073	0.0259	0.00166	0.00588
PLP2-16	0.021	669018	0.50896	0.12085	0.0106	0.0245	0.00263	0.00608
DHPS+47	0.021	-596275	0.40417	0.00739	0.0444	0.0450	0.00243	0.00246
BCAT2-45	0.021	471510	0.44254	0.08694	0.0066	0.0123	0.00129	0.00241
GATA1+14	0.021	-288082	0.28475	0.12455	0.0121	0.0708	0.00228	0.01333
H1FX-55	0.021	889788	0.75991	0.86901	0.0149	0.0000	0.01211	0
JUNB-25	0.021	372384	1.64700	4.70519	0.0054	0.0305	0.01503	0.085
JUNB-26	0.021	373196	1.14509	1.78199	0.0054	0.0305	0.00771	0.04362
H1FX-59	0.021	903202	1.37802	1.60042	0.0148	0.0000	0.02198	0
PQBP1+12	0.021	-195741	1.09049	0.78192	0.0455	0.3873	0.04201	0.35763
HDAC6+7	0.021	-153554	0.23690	0.04347	0.2079	0.5226	0.0211	0.05303
BCAT2+27	0.021	-366151	0.55067	0.14107	0.0148	0.0389	0.00412	0.01083
FTL+11	0.021	-122410	0.50052	0.18737	0.0987	0.6455	0.03023	0.19766
FTL-26	0.021	382684	0.47939	0.18584	0.0049	0.0465	0.00146	0.01388
SEC61A1-64	0.021	970147	0.53604	0.08702	0.0722	0.0000	0.01559	0
DNASE2+5	0.021	-96504	0.69199	0.18309	0.0449	0.2548	0.01598	0.09068
GATA1-31	0.021	505512	0.65171	0.17280	0.0141	0.0313	0.00473	0.01049
DNASE2-2	0.021	48822	0.96819	0.11339	0.1165	0.5054	0.0386	0.16747
HNRNPA1-28	0.021	421699	0.18028	0.01449	0.0056	0.0059	0.00029	0.0003
GATA1-19	0.021	353419	0.40534	0.21591	0.0144	0.1688	0.00426	0.04993
HBE1-20	0.021	730346	0.20865	0.03057	0.0039	0.0035	0.00031	0.00028

COPZ1-3	0.021	34265	2.56516	3.36227	0.8463	0.7314	2.48541	2.14807
RAD23A-47	0.021	637421	0.24931	0.01449	0.0759	0.0336	0.00456	0.00202
CNBP+47	0.020	-758423	0.24938	0.06897	0.0319	0.0196	0.00418	0.00257
GATA1-27	0.020	404643	2.22935	0.90023	0.0212	0.1043	0.03003	0.14781
DNASE2+25	0.020	-290993	0.46950	0.20896	0.0149	0.1130	0.00467	0.03539
NUCB1+13	0.020	-115269	0.54594	0.41313	0.1362	0.3678	0.06468	0.17466
HDAC6+18	0.020	-307735	0.43617	0.09535	0.0519	0.0695	0.01058	0.01418
RAD23A-34	0.020	332349	0.40417	0.00739	0.0930	0.0741	0.00508	0.00405
H1FX-44	0.020	768678	1.56343	4.21809	0.0119	0.0000	0.03056	0
DHPS-5	0.020	159698	0.35832	0.07245	0.3204	0.2564	0.05162	0.04132
PLP2+27	0.020	-491141	0.53851	0.48754	0.0161	0.1014	0.00825	0.05197
HDAC6-6	0.020	81904	0.17210	0.01449	0.3465	0.9889	0.0173	0.04938
RPN1-57	0.020	954403	0.30052	0.10970	0.0656	0.0000	0.01191	0
JUNB-12	0.020	225293	0.54225	0.48008	0.0100	0.0395	0.0051	0.02014
LYL1-12	0.020	119389	0.56166	0.19686	0.0528	0.5825	0.01756	0.19368
ITGA5-10	0.020	60944	0.89990	3.38190	0.0610	0.0918	0.10642	0.16021
NUCB1+19	0.020	-179245	1.98425	1.91436	0.0574	0.1216	0.11187	0.23706
BAX-8	0.020	143134	0.57710	0.32416	0.0113	0.1680	0.00489	0.07268
PQBP1+10	0.020	-114843	1.26353	2.66940	0.0687	0.5589	0.12617	1.0265
HDAC6-18	0.019	346874	1.06554	5.17599	0.0904	0.1415	0.2123	0.33238
GATA1+17	0.019	-294061	0.52942	0.29916	0.0151	0.0482	0.00601	0.01918
HDAC6+8	0.019	-165025	0.17237	0.18613	0.2314	0.3673	0.04145	0.06578
RPN1+19	0.019	-403973	0.85070	0.75996	0.4267	0.1143	0.34309	0.09188
COPZ1-13	0.019	107491	1.21853	0.77576	0.1938	0.0464	0.18842	0.04511
PQBP1+26	0.019	-405399	0.52942	0.29916	0.0120	0.0094	0.00478	0.00375
FUT1-36	0.019	398987	0.40442	0.52275	0.0459	0.0687	0.0211	0.0316
HNRNPA1+4	0.019	-64360	0.84221	0.37169	0.0841	0.5672	0.04705	0.31735
HNRNPA1+3	0.019	-63545	1.22745	0.89480	0.0841	0.5684	0.08814	0.59565
BAX+12	0.019	-135191	0.28128	0.05854	0.0382	0.5270	0.0049	0.06763
BAX+59	0.019	-620793	1.50949	2.18925	0.0047	0.0232	0.00854	0.04224
GATA1-24	0.019	388290	0.53276	0.44110	0.0170	0.1127	0.00824	0.05462
FUT1+14	0.019	-125100	1.78128	1.31155	0.1195	0.2493	0.18265	0.381
C19orf43+47	0.019	-647375	0.94017	0.10774	0.0241	0.0013	0.00767	0.00041
FTL+56	0.019	-610635	0.40442	0.52275	0.0051	0.0259	0.00234	0.01189
MYC-16	0.019	178426	0.61976	0.55876	0.4973	0.7475	0.29265	0.43988
H1FX-52	0.019	858999	0.37526	0.08151	0.0151	0.0000	0.00264	0
PLP2+19	0.019	-316781	0.20675	0.04347	0.0147	0.2830	0.00139	0.02683
SEC61A1-60	0.019	823388	0.35595	0.10144	0.0655	0.0000	0.01245	0
HBE1+23	0.019	-330349	0.79707	0.45805	0.0138	0.1463	0.00834	0.08838
DHPS+7	0.019	-108144	2.06351	1.02080	0.4706	0.5047	0.68301	0.73255
H1FX+4	0.019	-28421	0.34765	0.03927	0.5036	0.6589	0.05884	0.07699
BCAT2-13	0.018	125323	0.22362	0.04796	0.0325	0.1375	0.00337	0.01424
PRDX2+33	0.018	-411111	0.41749	0.12498	0.0262	0.0362	0.00598	0.00828
BAX+16	0.018	-170079	0.54594	0.41313	0.0349	0.3098	0.01657	0.14714
C19orf43+26	0.018	-369895	0.91245	0.91559	0.0590	0.0462	0.05393	0.04223
COPZ1-14	0.018	114707	0.41126	0.48189	0.2104	0.0434	0.09366	0.01932
NFE2-25	0.018	351954	0.85567	0.40668	0.0083	0.0224	0.0049	0.01321
C19orf43+7	0.018	-97924	0.96819	0.11339	0.2524	0.3235	0.08363	0.10719
RPN1-24	0.018	234693	1.54729	7.40038	0.4642	0.2996	1.57079	1.01381
RPN1-23	0.018	233865	1.38267	6.75808	0.4642	0.2996	1.41898	0.91583

CNBP-60	0.018	840201	0.70344	1.75844	0.0352	0.0010	0.03915	0.00111
BAX+26	0.018	-269119	0.22362	0.04796	0.0180	0.0875	0.00186	0.00907
CNBP+9	0.018	-121862	1.16005	0.38929	0.1016	0.1178	0.06828	0.07919
C19orf43-4	0.018	170528	0.44863	0.08694	0.1023	0.1013	0.0202	0.02001
GATA1-11	0.018	155331	1.27945	4.32061	0.0533	0.5536	0.12532	1.30161
GATA1-15	0.018	282025	0.24610	0.16490	0.0153	0.2733	0.00308	0.05506
PLP2-22	0.018	749463	0.51594	0.36567	0.0044	0.0156	0.00191	0.00676
FTL+14	0.018	-152894	1.24868	0.69823	0.0608	0.5149	0.05677	0.48078
FUT1-27	0.018	291139	0.40601	0.07876	0.0613	0.1053	0.01096	0.01883
H1FX+10	0.018	-108145	0.45029	0.60875	0.1309	0.3641	0.06853	0.19065
FTL-14	0.018	233743	0.44964	0.52333	0.0316	0.1372	0.01533	0.06655
GATA1-28	0.018	444452	1.08377	0.56101	0.0221	0.0593	0.01723	0.04624
NUCB1+32	0.017	-310913	1.19877	0.41581	0.0303	0.0464	0.02139	0.03278
RPN1-43	0.017	505425	0.27883	0.39770	0.2612	0.0671	0.08698	0.02234
MYC-20	0.017	213719	0.97430	1.33959	0.3070	0.6952	0.35073	0.79422
MYC+4	0.017	-168826	0.31963	0.78605	0.1767	0.3056	0.08857	0.15316
NUCB1+57	0.017	-567024	2.53815	2.46602	0.0164	0.0253	0.04103	0.06321
FUT1+9	0.017	-76618	0.37271	0.03840	0.2512	0.5245	0.03005	0.06274
LYL1+20	0.017	-175002	0.40417	0.00739	0.0147	0.2081	0.0008	0.01137
C19orf43+33	0.017	-437739	0.46950	0.20896	0.0386	0.0462	0.01209	0.01447
NUCB1-17	0.017	277165	0.55067	0.14107	0.0478	0.1229	0.01332	0.03424
KLF1+19	0.017	-268502	1.57147	0.72808	0.0573	0.1346	0.06129	0.14401
SEC61A1-52	0.017	711826	0.38004	0.05470	0.1375	0.0000	0.01983	0
FUT1-25	0.017	260594	2.34543	1.13042	0.0707	0.1236	0.11512	0.20126
KLF1-19	0.017	684734	0.17898	0.00000	0.0096	0.0055	0	0
NUCB1+41	0.017	-406983	2.34543	1.13042	0.0468	0.0375	0.0762	0.06106
GATA1+11	0.016	-239000	0.60009	0.13462	0.0168	0.1104	0.00477	0.03137
BAX+29	0.016	-279307	0.53744	0.06905	0.0143	0.0852	0.00275	0.01641
WDR83OS+30	0.016	-486054	1.57147	0.72808	0.0815	0.1086	0.08718	0.11616
COPZ1-20	0.016	278277	0.27330	0.07245	0.0125	0.0112	0.00176	0.00157
BAX+10	0.016	-111961	0.50052	0.18737	0.0485	0.6608	0.01485	0.20235
RAB7A+19	0.016	-242802	1.19538	2.19563	0.3371	0.2957	0.54612	0.47905
FTL+16	0.016	-176985	0.55020	0.04347	0.0966	0.3070	0.01494	0.04748
SEC61A1-33	0.016	443317	0.83051	0.91465	0.1612	0.1702	0.1405	0.14831
BCAT2+38	0.016	-520706	0.36270	0.18599	0.0107	0.0108	0.00278	0.00281
H1FX-50	0.016	820592	0.83051	0.91465	0.0235	0.0000	0.02048	0
NUCB1+50	0.016	-501161	1.76294	1.66049	0.0398	0.0326	0.0681	0.05578
RPN1-47	0.016	573797	1.49586	2.11875	0.1992	0.0000	0.35463	0
NUCB1+56	0.016	-565983	1.50949	2.18925	0.0164	0.0253	0.02981	0.04593
PPP1R15A+29	0.016	-303876	0.40867	0.28981	0.0533	0.0597	0.01834	0.02055
DNASE2-8	0.016	123790	0.84767	0.13244	0.0533	0.1727	0.01786	0.05785
BAX+53	0.016	-555971	1.76294	1.66049	0.0079	0.0299	0.01352	0.0511
FUT1+38	0.016	-460359	0.32933	0.05796	0.0829	0.0263	0.01145	0.00364
PQBP1-4	0.016	63836	1.09968	1.04021	0.0666	0.5145	0.07123	0.55031
FUT1+4	0.016	-31120	0.54594	0.41313	0.6434	0.9664	0.30556	0.45896
NUCB1+9	0.016	-80381	0.28128	0.05854	0.2045	0.6195	0.02624	0.0795
H1FX+7	0.016	-69463	0.36108	0.13042	0.2308	0.5430	0.05008	0.11783
NFE2-28	0.016	509114	0.14834	0.02898	0.0036	0.0174	0.00024	0.00114
ITGA5+12	0.016	-283122	0.18028	0.01449	0.0042	0.0055	0.00021	0.00028
FTL+12	0.016	-135030	0.37271	0.03840	0.0800	0.5250	0.00957	0.06281

DNASE2+20	0.016	-274184	1.57147	0.72808	0.0193	0.1148	0.02064	0.1228
NUCB1-12	0.015	206671	0.52055	0.18367	0.0718	0.1583	0.0222	0.04896
COPZ1-9	0.015	69332	0.70933	0.50978	0.2380	0.0911	0.14312	0.05476
HDAC6-14	0.015	281617	0.32571	0.08694	0.1413	0.2781	0.02378	0.0468
RAD23A+19	0.015	-450337	0.92663	1.05760	0.0745	0.0417	0.07375	0.04131
BAX+60	0.015	-621834	2.53815	2.46602	0.0047	0.0232	0.01176	0.05813
FTL-20	0.015	259778	0.44413	0.06687	0.0202	0.0983	0.00348	0.01694
DHPS+43	0.015	-566108	0.28100	0.04579	0.0389	0.0450	0.00441	0.00511
RNASEH2A+7	0.015	-89517	0.48445	0.17635	0.3383	0.2440	0.09888	0.07133
PLP2+12	0.015	-223008	0.39277	0.63360	0.0226	0.3182	0.01127	0.15872
FUT1+48	0.015	-638402	0.78564	0.32995	0.0235	0.0100	0.01196	0.00509
GATA1+12	0.015	-254788	0.58489	1.35350	0.0201	0.1020	0.01788	0.09078
PPP1R15A+21	0.015	-196839	0.53744	0.06905	0.1199	0.1310	0.0231	0.02523
WDR83OS+5	0.015	-112951	1.54032	1.80923	0.3609	0.3966	0.60248	0.66202
COPZ1+33	0.015	-581267	0.37514	0.12382	0.0364	0.0145	0.00785	0.00312
FUT1-10	0.015	78108	0.53744	0.06905	0.4196	0.7691	0.08083	0.14816
COPZ1+11	0.015	-114984	0.42343	0.08644	0.3118	0.1301	0.05965	0.0249
PRDX2+37	0.015	-459342	0.42462	0.45928	0.0196	0.0183	0.00866	0.00807
CALR+18	0.015	-416410	0.35832	0.07245	0.0293	0.0619	0.00472	0.00997
CNBP+37	0.015	-590186	0.34227	0.18679	0.0249	0.0378	0.0063	0.00957
HDAC6+26	0.015	-775152	0.46014	0.10730	0.0239	0.0000	0.00531	0
MYC-36	0.015	321052	0.44868	0.63114	0.3368	0.5404	0.17923	0.28759
CNBP+46	0.015	-753004	0.31324	0.09926	0.0439	0.0196	0.00774	0.00346
KLF1-2	0.015	50746	0.93136	0.41755	0.2940	0.5971	0.18334	0.37238
RPN1+12	0.015	-224880	0.35595	0.10144	0.9084	0.4822	0.17261	0.09163
RPN1-9	0.015	101945	1.35814	2.53529	0.6653	0.3642	1.23454	0.67575
RPN1-8	0.015	101430	1.37151	2.25323	0.6653	0.3642	1.16955	0.64018
PRDX2-13	0.015	306434	0.92663	1.05760	0.0415	0.0342	0.04108	0.03386
MYC-56	0.015	605598	0.23253	0.32872	0.2233	0.1478	0.06174	0.04087
BCAT2-43	0.015	459594	0.50725	0.19186	0.0051	0.0123	0.00159	0.00383
RPN1-42	0.014	479803	0.41950	0.12962	0.3129	0.1091	0.07296	0.02544
KLF1+29	0.014	-325818	0.41749	0.12498	0.0341	0.0949	0.00779	0.02168
BCAT2-40	0.014	412175	1.76294	1.66049	0.0066	0.0228	0.01129	0.03907
FUT1-23	0.014	242962	0.46228	0.08694	0.0631	0.1317	0.01265	0.02641
BAX+23	0.014	-240591	2.33109	0.51217	0.0172	0.0986	0.01879	0.10774
ITGA5-38	0.014	470183	0.85567	0.40668	0.0180	0.0253	0.01062	0.0149
BAX+37	0.014	-386344	0.40867	0.28981	0.0085	0.0356	0.00293	0.01224
RPN1+34	0.014	-654953	1.16005	0.38929	0.0953	0.0056	0.06404	0.00374
C19orf43+29	0.014	-428294	2.01447	4.08340	0.0412	0.0462	0.11816	0.13251
H1FX-19	0.014	293762	0.53604	0.08702	0.1089	0.2864	0.02352	0.06186
C19orf43+45	0.014	-543387	0.40417	0.00739	0.0194	0.0257	0.00106	0.0014
DHPS+12	0.014	-226855	0.52492	0.16440	0.1691	0.1995	0.04967	0.0586
LYL1+16	0.014	-144835	0.28100	0.04579	0.0242	0.3700	0.00275	0.04197
PRDX2+28	0.014	-370604	0.46950	0.20896	0.0209	0.0416	0.00655	0.01302
NUCB1+52	0.014	-545376	0.40442	0.52275	0.0286	0.0279	0.01315	0.01283
NUCB1+25	0.014	-221647	0.49959	0.10136	0.0561	0.1010	0.01262	0.02273
RAB7A+9	0.014	-171894	0.36679	0.43610	0.4260	0.2957	0.17038	0.11826
COPZ1-12	0.014	98306	0.49272	0.33894	0.1806	0.0559	0.0738	0.02284
DNASE2+34	0.014	-379731	0.42462	0.45928	0.0091	0.0449	0.00402	0.01981
BAX+49	0.014	-536064	1.03429	0.81604	0.0068	0.0299	0.00625	0.02744

DNASE2+4	0.013	-92957	0.31007	0.13274	0.0619	0.2566	0.01256	0.05205
CNBP-49	0.013	767784	1.54729	7.40038	0.0146	0.0010	0.0494	0.00338
CNBP-48	0.013	766956	1.38267	6.75808	0.0146	0.0010	0.04463	0.00306
H1FX+29	0.013	-477864	0.64832	0.14860	0.0724	0.2538	0.02247	0.07877
COPZ1+23	0.013	-320789	0.58339	0.17164	0.1346	0.0393	0.04259	0.01245
PPP1R15A+17	0.013	-174172	0.61356	0.33111	0.1148	0.1389	0.05174	0.06259
KLF1+41	0.013	-514390	0.68945	0.68099	0.0161	0.0221	0.01103	0.01517
CNBP-61	0.013	844271	0.39863	0.29366	0.0270	0.0010	0.00924	0.00034
RNASEH2A-23	0.013	349092	1.57147	0.72808	0.0598	0.0609	0.06397	0.06518
H1FX-21	0.013	300268	0.39553	0.45501	0.1321	0.2864	0.05604	0.12151
NUCB1+23	0.013	-214309	0.22362	0.04796	0.0696	0.1010	0.00721	0.01046
RNASEH2A+3	0.013	-24011	1.54032	1.80923	0.5086	0.8752	0.84904	1.46103
PRDX2-9	0.013	237663	0.44863	0.08694	0.0821	0.0463	0.01621	0.00915
NUCB1-4	0.013	62436	1.37940	4.06934	0.4705	0.9025	1.11472	2.13823
PQBP1+13	0.013	-217216	0.53851	0.48754	0.0361	0.3602	0.0185	0.18458
RNASEH2A-36	0.013	441382	0.28100	0.04579	0.0281	0.0253	0.00319	0.00287
FUT1-18	0.013	185145	0.40867	0.28981	0.1078	0.1472	0.0371	0.05066
HNRNPA1-23	0.013	299219	0.41537	0.13629	0.0028	0.0178	0.00067	0.00424
C19orf43+42	0.013	-526477	0.42462	0.45928	0.0284	0.0257	0.01254	0.01135
H1FX+32	0.013	-508874	0.15364	0.01449	0.0420	0.2480	0.00198	0.0117
SEC61A1-42	0.013	501873	0.36679	0.43610	0.1058	0.0658	0.04231	0.02632
RNASEH2A-25	0.013	357266	1.64700	4.70519	0.0574	0.0609	0.15979	0.16963
RNASEH2A-26	0.013	358078	1.14509	1.78199	0.0574	0.0609	0.08199	0.08704
MYC-34	0.013	303574	0.47194	0.44407	0.3375	0.5714	0.1545	0.26158
ITGA5-33	0.013	413137	0.65386	0.09129	0.0179	0.0271	0.00437	0.00662
C19orf43+5	0.013	-55256	2.06351	1.02080	0.4033	0.4864	0.58533	0.70589
RNASEH2A-42	0.013	575537	0.94017	0.10774	0.0145	0.0026	0.00461	0.00082
DNASE2+43	0.013	-547017	0.34986	0.07919	0.0068	0.0147	0.00113	0.00244
FUT1+42	0.013	-547771	0.46712	0.23185	0.0591	0.0203	0.01945	0.00668
KLF1+27	0.013	-307507	0.36439	0.06376	0.0362	0.1175	0.00552	0.01791
JUNB-43	0.013	605321	0.73862	0.42907	0.0042	0.0014	0.00236	0.00079
FUT1-35	0.013	368283	0.25824	0.20033	0.0495	0.0735	0.01126	0.01672
RAB7A+27	0.013	-313060	1.37802	1.60042	0.2872	0.2508	0.42651	0.37245
NUCB1-20	0.012	307966	0.72662	0.22555	0.0470	0.0935	0.01903	0.03784
NUCB1-21	0.012	308438	0.63712	0.04753	0.0470	0.0935	0.00818	0.01626
HDAC6+35	0.012	-999221	0.18742	0.06608	0.0155	0.0000	0.00172	0
WDR83OS+47	0.012	-608511	0.40417	0.00739	0.0368	0.0476	0.00201	0.0026
PLP2+6	0.012	-64691	0.34829	0.26011	0.0651	0.4127	0.01959	0.12422
NFE2+7	0.012	-68323	1.67201	1.48776	0.0496	0.4194	0.07823	0.66153
KLF1+20	0.012	-275866	2.01447	4.08340	0.0367	0.1346	0.10526	0.38614
COPZ1+16	0.012	-133367	0.81280	0.10404	0.1308	0.0747	0.03804	0.02172
H1FX-69	0.012	972511	0.70344	1.75844	0.0186	0.0000	0.02069	0
FUT1-33	0.012	353837	1.17217	2.28192	0.0678	0.0963	0.11089	0.1575
FUT1-32	0.012	353412	1.28275	1.87531	0.0537	0.0963	0.08329	0.14936
NUCB1-22	0.012	313970	0.32933	0.05796	0.0362	0.0921	0.005	0.01272
C19orf43-9	0.012	322768	0.39720	0.24446	0.0564	0.0762	0.01757	0.02374
H1FX+16	0.012	-280696	0.59673	0.52688	0.1160	0.3013	0.06504	0.16896
PPP1R15A+31	0.012	-313885	0.33960	0.08173	0.0606	0.0597	0.0101	0.00995
DHPS+14	0.012	-292591	0.31007	0.13274	0.0807	0.1487	0.01637	0.03017
PLP2-18	0.012	690417	0.32413	0.18338	0.0093	0.0245	0.00227	0.00597

H1FX+9	0.012	-97673	1.21513	2.14621	0.1285	0.3641	0.20752	0.58804
PLP2+15	0.012	-280104	1.59422	0.38205	0.0198	0.2864	0.01545	0.22349
DNASE2+7	0.012	-103920	1.06616	0.83749	0.0390	0.2442	0.03685	0.23072
COPZ1+20	0.012	-284772	0.36708	0.14831	0.0694	0.0509	0.01619	0.01187
NUCB1-32	0.012	492013	0.78564	0.32995	0.0240	0.0331	0.01222	0.01684
HDAC6-24	0.012	375663	0.59225	0.30952	0.0677	0.1193	0.02899	0.05109
FTL+57	0.012	-613839	0.50725	0.19186	0.0051	0.0235	0.00159	0.00732
HDAC6+31	0.012	-970037	0.26654	0.05796	0.0260	0.0000	0.00323	0
PPP1R15A-30	0.012	353814	0.52491	0.07332	0.0381	0.0720	0.00747	0.01413
CNBP+11	0.012	-144909	0.34007	0.01449	0.1104	0.1013	0.00775	0.00711
HDAC6+10	0.012	-184295	0.57924	0.64418	0.1417	0.1782	0.08656	0.10887
RNASEH2A-3	0.012	29844	0.93136	0.41755	0.7313	0.8775	0.45604	0.5472
HNRNPA1-16	0.011	136757	0.75465	2.92509	0.0321	0.0557	0.04769	0.08276
NUCB1-19	0.011	300402	0.74834	0.48732	0.0575	0.1150	0.03472	0.06943
LYL1-16	0.011	194418	0.52492	0.16440	0.0151	0.1036	0.00444	0.03042
CNBP-12	0.011	167958	0.39553	0.45501	0.1543	0.3406	0.06546	0.14449
COPZ1-7	0.011	51981	0.60701	0.44428	0.3526	0.2600	0.18311	0.135
RPN1+15	0.011	-365965	1.10381	0.56499	0.2880	0.1230	0.22744	0.09711
SEC61A1+6	0.011	-350013	0.43750	0.73091	0.2850	0.3565	0.16116	0.20159
NUCB1+39	0.011	-389351	0.46228	0.08694	0.0371	0.0389	0.00744	0.00779
BCAT2+14	0.011	-151422	1.37940	4.06934	0.0441	0.2732	0.10448	0.64719
FUT1-34	0.011	354772	1.76294	1.66049	0.0678	0.0963	0.116	0.16476
PQBP1-28	0.011	856514	0.21738	0.07006	0.0118	0.0000	0.00146	0
RAD23A+7	0.011	-155782	2.06351	1.02080	0.3254	0.2493	0.47227	0.36177
RPN1+23	0.011	-453812	0.31975	0.21990	0.2629	0.1004	0.06971	0.02661
HDAC6+29	0.011	-842869	0.31167	0.08448	0.0220	0.0000	0.00357	0
RPN1+16	0.011	-371639	0.53604	0.08702	0.2843	0.1230	0.0614	0.02656
PQBP1-21	0.011	384913	0.55764	0.21294	0.0148	0.0233	0.0051	0.00802
KLF1+35	0.011	-390139	0.53624	0.07245	0.0241	0.0523	0.00475	0.01032
PRDX2-1	0.011	11879	2.06351	1.02080	0.9375	1.0000	1.36065	1.45135
BCAT2-32	0.011	319747	1.13284	0.23772	0.0134	0.0301	0.00695	0.01562
GATA1+23	0.011	-703154	0.21991	0.04796	0.0056	0.0000	0.00058	0
PRDX2+36	0.011	-446085	0.28100	0.04579	0.0165	0.0183	0.00187	0.00207
KLF1+9	0.011	-147040	0.47531	0.18715	0.0671	0.2671	0.02001	0.07965
NUCB1+22	0.011	-201830	0.61356	0.33111	0.0724	0.1061	0.03263	0.04784
DHPS-8	0.010	479418	0.17898	0.00000	0.2181	0.1226	0	0
WDR83OS+16	0.010	-314120	0.56166	0.19686	0.0727	0.1696	0.02417	0.05638
BCAT2+26	0.010	-340821	1.79277	1.48240	0.0141	0.0419	0.02299	0.06825
BCAT2-26	0.010	252557	0.33960	0.08173	0.0150	0.0355	0.0025	0.00591
FUT1+40	0.010	-471426	0.44413	0.06687	0.0540	0.0233	0.00931	0.00402
ITGA5-35	0.010	429972	0.48203	0.19222	0.0233	0.0257	0.00709	0.00783
FUT1+15	0.010	-137058	0.33922	0.34778	0.1172	0.2269	0.04025	0.07794
RNASEH2A-37	0.010	454639	0.42462	0.45928	0.0264	0.0253	0.01166	0.01119
BCAT2-8	0.010	73507	1.24833	0.99768	0.0418	0.1801	0.04665	0.20103
CNBP+25	0.010	-413006	0.59673	0.52688	0.0469	0.0497	0.0263	0.02785
WDR83OS+1	0.010	-47445	0.48445	0.17635	0.6273	0.8556	0.18335	0.25007
DNASE2+11	0.010	-170318	0.89935	0.11107	0.0379	0.2032	0.01198	0.06422
CNBP+30	0.010	-431062	0.37721	0.23924	0.0511	0.0484	0.01535	0.01454
PRDX2+42	0.010	-580240	0.94017	0.10774	0.0183	0.0025	0.00582	0.00081
KLF1+11	0.010	-174358	0.66756	0.30894	0.0911	0.2407	0.04137	0.10931

BAX+11	0.010	-124581	0.37271	0.03840	0.0380	0.5396	0.00455	0.06455
HNRNPA1-7	0.010	77633	0.89990	3.38190	0.1367	0.6435	0.23848	1.12254
FUT1+29	0.010	-379590	0.80074	0.24431	0.0661	0.0533	0.02924	0.02357
FUT1+30	0.010	-380049	0.86882	0.22779	0.0661	0.0509	0.02941	0.02266
PLP2-14	0.010	582589	0.21738	0.07006	0.0069	0.0245	0.00085	0.00302
CNBP-22	0.010	419773	0.38004	0.05470	0.0244	0.0411	0.00352	0.00593
BAX-23	0.010	346572	0.46712	0.23185	0.0067	0.0544	0.0022	0.0179
NUCB1+46	0.009	-481254	1.03429	0.81604	0.0230	0.0326	0.02113	0.02995
HNRNPA1+7	0.009	-72711	0.52508	0.10462	0.0416	0.1667	0.00975	0.03907
ITGA5-27	0.009	227544	0.81280	0.10404	0.0246	0.0443	0.00715	0.01289
PQBP1+14	0.009	-249450	0.23690	0.04347	0.0310	0.3476	0.00315	0.03528
KLF1-3	0.009	54504	0.96819	0.11339	0.2858	0.5971	0.0947	0.19785
DHPS+23	0.009	-397737	1.21784	1.64686	0.0761	0.1214	0.10777	0.17193
CNBP+22	0.009	-306426	0.57086	0.25735	0.0549	0.0543	0.02104	0.02081
JUNB-36	0.009	456500	0.28100	0.04579	0.0057	0.0133	0.00065	0.0015
COPZ1+7	0.009	-104788	0.77095	0.63266	0.3442	0.3858	0.24039	0.26944
RNASEH2A-31	0.009	388097	0.36439	0.06376	0.0522	0.0563	0.00796	0.00858
FTL+23	0.009	-244504	1.98425	1.91436	0.0275	0.1072	0.0536	0.209
KLF1+5	0.009	-96568	0.56166	0.19686	0.1149	0.3085	0.03821	0.10257
NUCB1+26	0.009	-224497	0.53744	0.06905	0.0561	0.0984	0.01081	0.01895
MYC-43	0.009	370368	0.36231	0.10875	0.2539	0.5080	0.0504	0.10083
PQBP1+17	0.009	-280191	0.57924	0.64418	0.0427	0.1048	0.02608	0.06404
NUCB1-27	0.009	428041	0.30727	0.20287	0.0367	0.0396	0.00916	0.00988
PQBP1+4	0.009	-33532	0.30903	0.08245	0.1270	0.8026	0.02027	0.12811
NUCB1+10	0.009	-87635	1.24868	0.69823	0.1949	0.6188	0.18199	0.5778
GATA1+28	0.009	-849863	1.15321	0.19613	0.0068	0.0000	0.00323	0
HDAC6-4	0.009	62364	0.30903	0.08245	0.3950	0.9889	0.06305	0.15785
WDR83OS+32	0.008	-494228	1.64700	4.70519	0.0646	0.1086	0.17983	0.30232
WDR83OS+33	0.008	-495040	1.14509	1.78199	0.0646	0.1086	0.09228	0.15513
BCAT2+25	0.008	-325166	0.59661	0.55840	0.0182	0.0432	0.0105	0.02493
WDR83OS-6	0.008	174175	0.92663	1.05760	0.3976	0.4925	0.39361	0.48752
PQBP1-15	0.008	276952	0.53276	0.44110	0.0344	0.1445	0.01668	0.07005
FTL+22	0.008	-227752	1.24833	0.99768	0.0219	0.1119	0.02444	0.12484
DNASE2+27	0.008	-309861	0.34326	0.07245	0.0116	0.1025	0.00183	0.01616
BAX+35	0.008	-365723	1.19877	0.41581	0.0049	0.0392	0.00346	0.0277
PQBP1+19	0.008	-306264	0.49785	0.77018	0.0270	0.1048	0.01672	0.06491
DNASE2+28	0.008	-313189	0.36439	0.06376	0.0116	0.1025	0.00177	0.01562
RNASEH2A+15	0.008	-604144	0.17898	0.00000	0.0601	0.0144	0	0
PPP1R15A+15	0.008	-158123	2.33109	0.51217	0.1190	0.1488	0.13003	0.16259
BCAT2+35	0.008	-415142	0.52491	0.07332	0.0146	0.0235	0.00286	0.00461
NUCB1-16	0.008	251835	1.79277	1.48240	0.0521	0.1292	0.08493	0.21057
BAX+54	0.008	-569482	0.25824	0.20033	0.0050	0.0256	0.00114	0.00582
NUCB1+30	0.008	-255076	1.03345	0.32495	0.0950	0.0840	0.05505	0.04868
CNBP-37	0.008	650786	0.57481	0.38487	0.0197	0.0010	0.00927	0.00047
RPN1+17	0.008	-376318	1.05199	0.36777	0.2373	0.1230	0.1476	0.07649
CNBP-4	0.007	82030	0.26525	0.29445	0.1093	0.5114	0.03055	0.14291
DHPS+5	0.007	-100715	1.54032	1.80923	0.4295	0.5090	0.71699	0.84965
CNBP-34	0.007	635036	1.35814	2.53529	0.0326	0.0010	0.06049	0.00186
CNBP-33	0.007	634521	1.37151	2.25323	0.0326	0.0010	0.05731	0.00176
PPP1R15A-24	0.007	328060	0.74834	0.48732	0.0780	0.1034	0.0471	0.06242

CNBP+4	0.007	-45364	0.88456	2.13621	0.5981	0.9666	0.82216	1.32871
RNASEH2A-16	0.007	273011	1.21784	1.64686	0.1186	0.0775	0.16796	0.10976
PPP1R15A+34	0.007	-361693	0.46228	0.08694	0.0431	0.0561	0.00864	0.01125
SEC61A1-39	0.007	495231	1.56343	4.21809	0.0762	0.0807	0.19568	0.20732
H1FX+37	0.007	-620694	0.31324	0.09926	0.0310	0.1292	0.00547	0.02278
RPN1+42	0.007	-748870	1.30077	3.00283	0.1954	0.0056	0.38618	0.011
GATA1+9	0.007	-174700	0.17721	0.05796	0.0244	0.1801	0.00247	0.01825
FTL+45	0.007	-472242	2.34543	1.13042	0.0105	0.0347	0.0171	0.0565
HNRNPA1+8	0.007	-79184	0.62072	0.14759	0.0269	0.1430	0.00814	0.04327
BAX+5	0.007	-64141	0.33922	0.34778	0.0869	0.8016	0.02985	0.27531
KLF1-17	0.007	391727	0.92663	1.05760	0.0306	0.0399	0.03029	0.03947
KLF1+38	0.007	-494947	0.94017	0.10774	0.0245	0.0221	0.0078	0.00704
PQBP1-9	0.007	209234	0.34829	0.26011	0.0287	0.2729	0.00864	0.08213
BAX+18	0.007	-180250	0.21060	0.08354	0.0230	0.1326	0.00305	0.01758
DHPS-2	0.007	117640	0.44863	0.08694	0.4537	0.2908	0.08961	0.05743
FTL+21	0.007	-217186	1.01167	3.18092	0.0293	0.1127	0.05256	0.20217
FTL-7	0.007	132685	0.57710	0.32416	0.0246	0.1796	0.01064	0.07768
RNASEH2A-11	0.007	206854	0.58941	0.63013	0.0900	0.0826	0.05485	0.05036
MYC-39	0.007	329673	0.84509	2.24627	0.3368	0.5292	0.46404	0.72917
MYC+1	0.007	-7084	0.29455	0.05912	1.0000	0.5887	0.13196	0.07769
PPP1R15A-21	0.007	279493	1.79277	1.48240	0.0788	0.1178	0.12846	0.19204
KLF1-7	0.007	104601	1.54032	1.80923	0.1705	0.3091	0.28463	0.51606
KLF1+12	0.006	-192421	1.21784	1.64686	0.1140	0.2248	0.16145	0.31836
PPP1R15A-17	0.006	234329	0.52055	0.18367	0.0796	0.1459	0.02461	0.0451
ITGA5-34	0.006	414966	0.58339	0.17164	0.0184	0.0271	0.00582	0.00858
BAX-22	0.006	271346	0.52491	0.07332	0.0098	0.0876	0.00192	0.01718
DNASE2+30	0.006	-331500	0.41749	0.12498	0.0141	0.0832	0.00322	0.019
C19orf43+30	0.006	-429104	1.64700	4.70519	0.0412	0.0462	0.11469	0.12861
C19orf43+31	0.006	-429916	1.14509	1.78199	0.0412	0.0462	0.05885	0.066
PRDX2+31	0.006	-392800	0.36439	0.06376	0.0280	0.0389	0.00427	0.00593
BAX+27	0.006	-273637	0.44682	0.23323	0.0170	0.0875	0.00549	0.02826
BAX-12	0.006	181370	0.59661	0.55840	0.0129	0.1465	0.00745	0.08456
BAX-14	0.006	222355	0.55067	0.14107	0.0133	0.1331	0.00371	0.03709
ITGA5-45	0.006	717295	0.40247	0.17845	0.0112	0.0154	0.003	0.00413
PRDX2-4	0.006	41176	0.44079	0.07245	0.3831	0.5321	0.06846	0.09508
DNASE2+21	0.006	-281548	2.01447	4.08340	0.0162	0.1148	0.04646	0.32926
PLP2+31	0.006	-554116	0.57924	0.64418	0.0116	0.0925	0.00709	0.0565
DHPS+10	0.006	-154570	0.93136	0.41755	0.3992	0.4346	0.24894	0.27104
PPP1R15A-35	0.006	475601	0.47939	0.18584	0.0422	0.0363	0.0126	0.01082
PRDX2+12	0.006	-214878	0.54225	0.48008	0.0475	0.0557	0.02424	0.02844
NUCB1+34	0.006	-331534	0.40867	0.28981	0.0415	0.0424	0.01428	0.01458
CNBP+20	0.006	-264469	1.02100	1.42074	0.0441	0.0550	0.05311	0.06628
CNBP-66	0.006	988384	0.17428	0.21222	0.0138	0.0000	0.00265	0
NUCB1+33	0.006	-315661	0.94949	0.29989	0.0304	0.0438	0.01622	0.02335
BAX-16	0.006	245592	0.74834	0.48732	0.0153	0.1260	0.00924	0.07609
PRDX2-5	0.005	44179	0.84767	0.13244	0.3349	0.3996	0.11221	0.13388
NUCB1-11	0.005	197944	0.57710	0.32416	0.0782	0.1609	0.03382	0.06958
PLP2+39	0.005	-677556	0.43617	0.09535	0.0074	0.0122	0.00151	0.00249
H1FX+22	0.005	-310583	0.89953	0.52608	0.0646	0.2834	0.04444	0.19496
FTL+27	0.005	-279568	0.22362	0.04796	0.0206	0.0883	0.00213	0.00914

FUT1-41	0.005	420635	2.53815	2.46602	0.0418	0.0627	0.10458	0.15695
RAB7A-55	0.005	924323	0.32579	0.04347	0.1065	0.0000	0.01267	0
PLP2+26	0.005	-469666	1.09049	0.78192	0.0110	0.1136	0.01016	0.10493
H1FX+33	0.005	-513462	0.23687	0.03434	0.0420	0.2480	0.00379	0.02237
CNBP-30	0.005	606075	0.42979	0.09549	0.0455	0.0028	0.00922	0.00057
SEC61A1-18	0.005	331342	0.30134	0.14208	0.1173	0.2535	0.02427	0.05245
FTL+61	0.005	-632283	2.53815	2.46602	0.0096	0.0235	0.02402	0.05871
BCAT2-48	0.005	496499	0.30382	0.13339	0.0053	0.0065	0.00107	0.00131
HDAC6-28	0.005	480809	0.55764	0.21294	0.0467	0.0313	0.01609	0.01077
HDAC6+15	0.005	-288119	0.36722	0.22439	0.0509	0.1008	0.01461	0.02893
JUNB-16	0.005	288129	1.21784	1.64686	0.0094	0.0373	0.01331	0.05282
GATA1+27	0.005	-827427	0.31167	0.08448	0.0060	0.0000	0.00097	0
BAX+33	0.005	-309886	1.03345	0.32495	0.0234	0.0740	0.01356	0.0429
RPN1+54	0.005	-957918	0.67337	0.20649	0.1368	0.0000	0.05101	0
H1FX-23	0.004	440521	0.35595	0.10144	0.0509	0.1412	0.00967	0.02684
H1FX+38	0.004	-626113	0.24938	0.06897	0.0242	0.1292	0.00317	0.01694
HNRNPA1+29	0.004	-578718	0.40247	0.17845	0.0078	0.0188	0.00209	0.00504
NUCB1-25	0.004	326156	0.52491	0.07332	0.0340	0.0764	0.00667	0.01499
BAX+52	0.004	-555036	1.17217	2.28192	0.0079	0.0299	0.01292	0.04885
BAX+51	0.004	-554611	1.28275	1.87531	0.0055	0.0299	0.00853	0.04632
GATA1-10	0.004	130796	1.23891	0.67316	0.0633	0.7337	0.05781	0.67004
NFE2-7	0.004	84708	0.84221	0.37169	0.0351	0.3859	0.01964	0.21589
NFE2-6	0.004	83893	1.22745	0.89480	0.0351	0.3859	0.03679	0.40439
FUT1-24	0.004	251399	2.11845	0.89741	0.1023	0.1265	0.14105	0.17437
RAD23A-17	0.004	209892	1.57147	0.72808	0.2776	0.1724	0.29694	0.18441
MYC-41	0.004	342081	0.50216	0.62245	0.2762	0.5201	0.15442	0.29076
MYC-42	0.004	342366	0.46963	0.58390	0.2762	0.5201	0.14463	0.27234
FTL+38	0.004	-396793	0.40867	0.28981	0.0061	0.0360	0.0021	0.01238
MYC-63	0.004	820807	0.89798	3.11875	0.1476	0.0082	0.24701	0.01372
NUCB1+11	0.004	-104518	1.37925	0.61585	0.1702	0.5847	0.15686	0.53885
ITGA5-29	0.004	257398	0.61744	1.26844	0.0188	0.0414	0.01664	0.03661
COPZ1+3	0.004	-30720	1.39090	2.59115	1.0000	0.9168	1.89843	1.74042
RAD23A-30	0.004	302182	0.28100	0.04579	0.1613	0.0853	0.0183	0.00968
NFE2-13	0.004	105033	0.96435	0.29576	0.0123	0.0825	0.00657	0.04408
NUCB1+24	0.004	-218827	0.44682	0.23323	0.0572	0.1010	0.01847	0.0326
FUT1-38	0.004	408567	0.27203	0.05796	0.0414	0.0627	0.0052	0.00788
HDAC6+5	0.004	-99845	1.09049	0.78192	0.2859	0.6350	0.264	0.58636
NUCB1+37	0.004	-346060	0.78293	0.11593	0.0361	0.0389	0.01088	0.01171
HDAC6+11	0.004	-190142	0.17721	0.05796	0.1099	0.1782	0.01114	0.01806
NUCB1+18	0.004	-162493	1.24833	0.99768	0.0908	0.1424	0.10133	0.15888
KLF1+36	0.004	-390959	0.40417	0.00739	0.0241	0.0523	0.00132	0.00286
JUNB-24	0.004	371574	2.01447	4.08340	0.0054	0.0305	0.01549	0.08757
RAD23A-5	0.003	67654	0.58941	0.63013	0.4000	0.3825	0.24377	0.23313
DHPS+31	0.003	-481182	2.01447	4.08340	0.0673	0.0928	0.19302	0.26616
FUT1+35	0.003	-446791	0.74834	0.48732	0.0802	0.0322	0.04843	0.01945
KLF1-13	0.003	322956	0.44863	0.08694	0.0418	0.0662	0.00826	0.01307
NUCB1+17	0.003	-151927	1.01167	3.18092	0.1026	0.1433	0.18405	0.25706
GATA1+13	0.003	-272677	0.36722	0.22439	0.0164	0.1020	0.00471	0.02929
BAX+1	0.003	-3570	0.55352	0.68700	1.0000	1.0000	0.61666	0.61666
GATA1+19	0.003	-334672	0.19962	0.09252	0.0106	0.0169	0.00144	0.0023

MYC-27	0.003	256859	0.40909	0.22779	0.2746	0.6129	0.08383	0.18709
MYC-28	0.003	257233	0.42747	0.16896	0.2746	0.6129	0.0738	0.16471
COPZ1+34	0.003	-623118	0.40247	0.17845	0.0444	0.0107	0.0119	0.00286
GATA1+10	0.003	-194926	0.49785	0.77018	0.0236	0.1801	0.01461	0.11152
BAX+30	0.003	-293751	1.10066	1.72598	0.0234	0.0794	0.03225	0.10944
KLF1-5	0.003	97172	2.06351	1.02080	0.1883	0.3541	0.27329	0.51397
KLF1+33	0.003	-374049	0.42462	0.45928	0.0317	0.0523	0.014	0.02311
CNBP-46	0.003	757478	0.75991	0.86901	0.0196	0.0010	0.01593	0.00081
MYC-33	0.003	299241	0.60734	1.08238	0.3375	0.5736	0.27364	0.46504
BCAT2-4	0.003	30107	1.44373	2.77330	0.0813	0.2472	0.16268	0.49457
DHPS+18	0.003	-331580	0.58941	0.63013	0.0636	0.1323	0.03876	0.08063
FTL+60	0.003	-631242	1.50949	2.18925	0.0096	0.0235	0.01745	0.04266
COPZ1+19	0.002	-165731	0.58965	0.20859	0.0951	0.0641	0.03335	0.02248
NUCB1+12	0.002	-111726	0.55020	0.04347	0.1773	0.3766	0.02742	0.05824
CNBP-42	0.002	700634	1.19538	2.19563	0.0403	0.0010	0.06529	0.00162
HDAC6+25	0.002	-718596	0.21991	0.04796	0.0200	0.0000	0.00205	0
H1FX+6	0.002	-67203	0.37017	0.05796	0.1960	0.5594	0.02871	0.08194
MYC-62	0.002	819191	0.57899	1.43016	0.1476	0.0082	0.13431	0.00746
PLP2+11	0.002	-210089	1.09968	1.04021	0.0316	0.3215	0.0338	0.34389
ITGA5+1	0.002	-4129	0.49272	0.33894	1.0000	1.0000	0.40865	0.40865
PRDX2+8	0.002	-176115	0.69199	0.18309	0.0537	0.0605	0.01911	0.02155
LYL1+19	0.002	-174182	0.53624	0.07245	0.0147	0.2081	0.0029	0.04101
FUT1+10	0.002	-89238	0.50052	0.18737	0.1688	0.4179	0.05169	0.12796
BAX+13	0.002	-142445	1.24868	0.69823	0.0402	0.5264	0.03754	0.49149
NFE2-11	0.002	99532	0.62072	0.14759	0.0140	0.0926	0.00424	0.02804
FUT1-16	0.002	164524	1.19877	0.41581	0.1311	0.1750	0.09256	0.12358
BAX+56	0.002	-603390	0.50725	0.19186	0.0066	0.0232	0.00206	0.00725
H1FX-48	0.002	811129	0.71928	1.40733	0.0187	0.0000	0.01881	0
ITGA5-40	0.002	610035	0.36898	0.13411	0.0093	0.0174	0.00207	0.00386
FUT1+46	0.002	-594332	0.47939	0.18584	0.0353	0.0144	0.01054	0.00431
JUNB-40	0.002	486667	0.40417	0.00739	0.0015	0.0133	0.00008	0.00073
RPN1+27	0.002	-561116	0.68357	0.47203	0.1752	0.0424	0.09952	0.02408
DNASE2+12	0.002	-180040	0.66756	0.30894	0.0328	0.1982	0.0149	0.08999
BCAT2+2	0.002	-8605	0.28128	0.05854	0.7369	0.9289	0.09456	0.1192
GATA1+3	0.002	-84403	1.09049	0.78192	0.0721	0.6415	0.06658	0.59233
NFE2-16	0.002	139169	0.61744	1.26844	0.0134	0.0701	0.01186	0.06201
COPZ1+9	0.002	-108760	0.84221	0.37169	0.3812	0.3723	0.21328	0.20828
COPZ1+8	0.002	-107945	1.22745	0.89480	0.3812	0.3723	0.3995	0.39014
NUCB1+40	0.002	-397788	2.11845	0.89741	0.0474	0.0382	0.06536	0.05267
MYC-11	0.002	123921	1.06942	0.70758	0.4838	0.8226	0.42085	0.7156
RAD23A-10	0.002	133811	1.21784	1.64686	0.5576	0.3128	0.78967	0.44299
COPZ1+6	0.002	-97536	0.49767	0.19352	0.4001	0.4106	0.12417	0.12744
ITGA5-30	0.002	259908	0.58965	0.20859	0.0179	0.0414	0.00628	0.01451
RNASEH2A-28	0.002	365901	0.46950	0.20896	0.0385	0.0609	0.01206	0.01909
DNASE2-16	0.001	386045	0.92663	1.05760	0.0174	0.0348	0.01723	0.03442
ITGA5-23	0.001	211288	0.52508	0.10462	0.0269	0.0462	0.0063	0.01083
RAD23A-13	0.001	152228	2.01475	1.09289	0.7442	0.2886	1.1043	0.4283
RAD23A-14	0.001	152577	1.97102	1.45559	0.7442	0.2886	1.26053	0.48889
HNRNPA1+21	0.001	-330817	0.77052	0.31684	0.0148	0.0350	0.00731	0.01728
RPN1-16	0.001	155191	0.83051	0.91465	0.4546	0.3642	0.39621	0.31739

MYC-44	0.001	391945	0.34609	0.18186	0.2044	0.4888	0.05128	0.12263
CALR+7	0.001	-148568	2.06351	1.02080	0.2332	0.2588	0.33846	0.37566
MYC+5	0.001	-557379	0.16256	0.04347	0.0862	0.1294	0.00725	0.01088
ITGA5+15	0.001	-340672	0.17452	0.03927	0.0081	0.0036	0.00067	0.0003
BAX-26	0.001	384219	0.92898	0.30619	0.0097	0.0460	0.00517	0.02453
CNBP-43	0.001	726689	0.37526	0.08151	0.0119	0.0010	0.00208	0.00017
PQBP1-34	0.001	986534	0.27617	0.10144	0.0069	0.0000	0.00115	0
JUNB-19	0.001	306546	2.01475	1.09289	0.0072	0.0362	0.01068	0.05377
JUNB-20	0.001	306895	1.97102	1.45559	0.0072	0.0362	0.0122	0.06137
BAX+43	0.001	-452598	2.11845	0.89741	0.0082	0.0349	0.01131	0.04817
FTL+48	0.001	-540384	0.64064	2.21917	0.0053	0.0302	0.00632	0.03601
WDR83OS-5	0.001	147462	0.35832	0.07245	0.6808	0.5948	0.10969	0.09584
NFE2+28	0.001	-458901	0.17452	0.03927	0.0027	0.0022	0.00022	0.00018
HBE1-14	0.001	377956	0.24473	0.14462	0.0109	0.1401	0.00205	0.02635
RNASEH2A+13	0.001	-311137	0.92663	1.05760	0.0749	0.0511	0.07415	0.05059
SEC61A1-22	0.001	357879	1.19535	2.40639	0.1339	0.1702	0.2271	0.28861
RPN1-49	0.001	639499	0.35799	0.09847	0.1677	0.0000	0.03149	0
NUCB1+7	0.001	-57151	0.50052	0.18737	0.2748	0.7985	0.08415	0.24454
FUT1+45	0.001	-585418	0.92898	0.30619	0.0573	0.0144	0.03056	0.0077
CNBP-59	0.001	838582	0.34822	0.21396	0.0366	0.0010	0.00999	0.00027
FTL-1	0.001	10962	0.55502	0.71519	0.3505	0.7330	0.22083	0.46179
NUCB1-18	0.001	299002	0.44964	0.52333	0.0559	0.1150	0.02712	0.05577
KLF1+21	0.001	-276676	1.64700	4.70519	0.0367	0.1346	0.10216	0.37479
KLF1+22	0.001	-277488	1.14509	1.78199	0.0367	0.1346	0.05243	0.19232
RAB7A+23	0.001	-299646	0.75991	0.86901	0.1531	0.2532	0.12441	0.20576
RAB7A+36	0.001	-380750	0.34822	0.21396	0.2613	0.2107	0.07132	0.05752
C19orf43+14	0.001	-248996	0.56166	0.19686	0.0581	0.0692	0.01932	0.02301
RAD23A-31	0.001	315439	0.42462	0.45928	0.1277	0.0741	0.05639	0.03272
NUCB1+53	0.001	-548580	0.50725	0.19186	0.0286	0.0253	0.00892	0.00788
PPP1R15A+14	0.001	-151587	1.98425	1.91436	0.1050	0.1574	0.20464	0.30671
BAX-27	0.000	393133	0.47939	0.18584	0.0057	0.0460	0.0017	0.01373
GATA1-25	0.000	389064	0.77354	0.38502	0.0154	0.1127	0.0084	0.06149
PQBP1-14	0.000	269523	1.02138	4.76091	0.0322	0.1527	0.07101	0.33673
BAX+55	0.000	-600186	0.40442	0.52275	0.0066	0.0256	0.00303	0.01177
BCAT2-9	0.000	90259	1.98425	1.91436	0.0305	0.1637	0.05944	0.31905
SEC61A1-32	0.000	430965	1.19538	2.19563	0.1177	0.1702	0.19068	0.27568
RPN1-38	0.000	384197	0.14807	0.01891	0.3327	0.1903	0.0176	0.01007
DNASE2+33	0.000	-366474	0.28100	0.04579	0.0118	0.0510	0.00134	0.00579
HNRNPA1-30	0.000	468689	0.18359	0.01761	0.0054	0.0030	0.00031	0.00017
COPZ1-11	0.000	92357	0.75465	2.92509	0.1672	0.0592	0.24842	0.08796
PRDX2+5	0.000	-106832	0.52492	0.16440	0.1527	0.1147	0.04486	0.03369
RAD23A-7	0.000	88430	0.47531	0.18715	0.4021	0.3702	0.11993	0.1104
KLF1+24	0.000	-285311	0.46950	0.20896	0.0492	0.1322	0.01541	0.04142
BCAT2+18	0.000	-227789	0.27495	0.01449	0.0398	0.0763	0.00251	0.00482
DHPS+22	0.000	-379674	0.66756	0.30894	0.0882	0.1214	0.04005	0.05513
NUCB1+20	0.000	-185781	2.33109	0.51217	0.0863	0.1132	0.0943	0.12373
NUCB1+54	0.000	-554956	0.27203	0.05796	0.0222	0.0253	0.00279	0.00317
NUCB1+59	0.000	-590530	0.73027	0.07992	0.0219	0.0130	0.00529	0.00315
FTL+54	0.000	-566420	1.76294	1.66049	0.0078	0.0302	0.01335	0.05167
ITGA5-6	0.000	48834	1.03165	0.28873	0.1052	0.1475	0.05741	0.08052

SEC61A1-13	0.000	287328	0.39863	0.29366	0.1359	0.2684	0.0465	0.09184
BAX+21	0.000	-217303	1.24833	0.99768	0.0195	0.1108	0.02176	0.12369
ITGA5-15	-0.001	130751	1.09507	0.92248	0.0439	0.0581	0.04412	0.05836
HBE1+13	-0.001	-206259	0.36947	0.35647	0.0158	0.2006	0.00573	0.07279
MYC-32	-0.001	280590	0.46682	0.49797	0.3017	0.5932	0.14546	0.28602
SEC61A1-44	-0.001	525524	0.42979	0.09549	0.0983	0.0658	0.01991	0.01333
HNRNPA1-9	-0.001	80339	0.75194	0.48326	0.1103	0.6400	0.06649	0.38578
NUCB1-13	-0.001	233201	0.80074	0.24431	0.0635	0.1415	0.02809	0.0626
NUCB1-14	-0.001	233660	0.86882	0.22779	0.0635	0.1404	0.02825	0.06245
CNBP+42	-0.001	-645772	0.23687	0.03434	0.0330	0.0360	0.00298	0.00325
PPP1R15A-31	-0.001	429040	0.46712	0.23185	0.0463	0.0430	0.01524	0.01415
HBE1-2	-0.001	11386	0.93048	0.77895	0.2284	0.9821	0.19445	0.83611
H1FX-39	-0.001	738385	0.42979	0.09549	0.0211	0.0000	0.00427	0
RNASEH2A-9	-0.001	177158	0.56166	0.19686	0.0908	0.0910	0.03019	0.03027
BCAT2-3	-0.001	26283	0.54594	0.41313	0.0813	0.4708	0.03861	0.22359
FTL+24	-0.001	-251040	2.33109	0.51217	0.0206	0.0995	0.02251	0.10872
KLF1+4	-0.001	-90822	0.69199	0.18309	0.1185	0.3360	0.04218	0.1196
RPN1-31	-0.001	267166	0.30134	0.14208	0.3118	0.2996	0.06452	0.06199
BCAT2+19	-0.001	-262999	0.93844	0.49007	0.0268	0.0658	0.01817	0.04465
MYC-25	-0.001	244314	0.37531	0.44762	0.3069	0.6242	0.12579	0.25584
RAD23A+6	-0.001	-130483	0.37844	0.18113	0.4445	0.2785	0.11638	0.07292
PRDX2-15	-0.002	599441	0.17898	0.00000	0.0371	0.0097	0	0
PRDX2+16	-0.002	-277714	1.21784	1.64686	0.0640	0.0522	0.09064	0.07397
NFE2+18	-0.002	-226245	0.28851	0.09796	0.0058	0.0240	0.00098	0.00403
CNBP+40	-0.002	-636775	0.25756	0.17360	0.0205	0.0360	0.00433	0.00761
NUCB1-8	-0.002	138803	0.27495	0.01449	0.1142	0.2094	0.00721	0.01322
BAX+32	-0.002	-302082	0.45173	0.24388	0.0183	0.0764	0.00607	0.02536
RAD23A-33	-0.002	331529	0.53624	0.07245	0.0930	0.0741	0.01833	0.01461
NUCB1-30	-0.002	447943	0.47939	0.18584	0.0386	0.0396	0.01152	0.01181
PQBP1-11	-0.002	250978	1.06554	5.17599	0.0223	0.1664	0.05237	0.3907
CALR-47	-0.002	644635	0.24931	0.01449	0.0524	0.0306	0.00315	0.00184
KLF1+39	-0.002	-509613	0.73862	0.42907	0.0203	0.0221	0.01143	0.01246
RPN1+43	-0.002	-763074	1.21513	2.14621	0.1057	0.0056	0.1707	0.00899
HNRNPA1+19	-0.002	-291395	0.48203	0.19222	0.0337	0.0518	0.01026	0.01578
HNRNPA1+11	-0.002	-88967	0.81280	0.10404	0.0236	0.1252	0.00686	0.03641
SEC61A1-16	-0.002	301856	0.29986	0.29010	0.1474	0.2535	0.04347	0.07477
RPN1+25	-0.002	-469817	0.79677	0.96646	0.2014	0.0917	0.17673	0.08047
KLF1+31	-0.002	-347567	0.59250	0.37270	0.0322	0.0745	0.01513	0.03501
PRDX2-14	-0.003	389903	0.39720	0.24446	0.0328	0.0342	0.01022	0.01066
RPN1+36	-0.003	-678000	0.34007	0.01449	0.1949	0.0056	0.01368	0.00039
H1FX+23	-0.003	-334181	0.32579	0.04347	0.0550	0.2730	0.00655	0.03249
NFE2+15	-0.003	-131543	1.21853	0.77576	0.0177	0.0427	0.01721	0.04155
HDAC6+20	-0.003	-314354	0.68815	1.25076	0.0468	0.0164	0.04342	0.01522
NUCB1-9	-0.003	174013	0.93844	0.49007	0.0728	0.1855	0.04937	0.12582
KLF1+8	-0.003	-129585	0.54225	0.48008	0.1031	0.2768	0.0526	0.14121
RNASEH2A-43	-0.003	590203	0.73862	0.42907	0.0180	0.0026	0.01013	0.00144
COPZ1-21	-0.003	333750	0.33027	0.06187	0.0180	0.0061	0.00257	0.00087
COPZ1+22	-0.003	-318960	0.65386	0.09129	0.1466	0.0393	0.03582	0.00961
BAX-19	-0.003	259160	0.32933	0.05796	0.0118	0.1045	0.00163	0.01444
SEC61A1+7	-0.003	-350952	0.44721	0.55405	0.2850	0.3565	0.14186	0.17746

DHPS+21	-0.003	-369952	0.89935	0.11107	0.0878	0.1214	0.02775	0.03837
RNASEH2A-39	-0.003	470729	0.53624	0.07245	0.0213	0.0253	0.0042	0.00499
RNASEH2A-2	-0.003	26086	0.96819	0.11339	1.0000	0.9328	0.33133	0.30907
FUT1-17	-0.003	169272	0.94949	0.29989	0.0934	0.1643	0.04984	0.08765
DNASE2-12	-0.003	317274	0.44863	0.08694	0.0144	0.0566	0.00284	0.01117
NUCB1-26	-0.003	401382	0.46712	0.23185	0.0295	0.0463	0.00971	0.01523
H1FX-31	-0.003	552083	0.38004	0.05470	0.0445	0.0119	0.00642	0.00171
RPN1-55	-0.003	949460	0.44721	0.55405	0.0913	0.0000	0.04545	0
GATA1-21	-0.003	368866	1.33451	2.70881	0.0224	0.1349	0.04259	0.25642
GATA1-22	-0.003	369776	1.58651	2.22540	0.0224	0.1349	0.04209	0.25341
RNASEH2A-5	-0.003	102129	0.52492	0.16440	0.2106	0.1676	0.06187	0.04924
NUCB1+43	-0.003	-437528	0.40601	0.07876	0.0357	0.0361	0.00638	0.00646
DNASE2+9	-0.003	-135267	0.54225	0.48008	0.0369	0.2273	0.01883	0.11595
GATA1-26	-0.003	391105	0.59225	0.30952	0.0154	0.1127	0.00659	0.04824
ITGA5+9	-0.004	-184100	0.27330	0.07245	0.0150	0.0253	0.00211	0.00356
DNASE2+8	-0.004	-131946	0.58941	0.63013	0.0448	0.2273	0.0273	0.1385
BAX+34	-0.004	-345908	0.46485	0.11093	0.0101	0.0392	0.00229	0.00891
HNRNPA1+27	-0.004	-533911	0.62162	0.07419	0.0095	0.0236	0.00204	0.00508
BCAT2-39	-0.004	411240	1.17217	2.28192	0.0066	0.0228	0.01079	0.03734
BCAT2-38	-0.004	410815	1.28275	1.87531	0.0050	0.0228	0.00775	0.03541
RNASEH2A-12	-0.004	210175	0.54225	0.48008	0.0818	0.0826	0.04174	0.04216
NUCB1+51	-0.004	-514672	0.25824	0.20033	0.0198	0.0279	0.0045	0.00635
PLP2+28	-0.004	-523375	0.23690	0.04347	0.0151	0.1014	0.00153	0.01029
C19orf43+28	-0.004	-420930	1.57147	0.72808	0.0360	0.0462	0.03851	0.04942
CALR+13	-0.004	-221503	0.48445	0.17635	0.2345	0.1305	0.06854	0.03813
NFE2-20	-0.004	294908	0.65386	0.09129	0.0172	0.0416	0.0042	0.01016
PPP1R15A-32	-0.004	455699	0.30727	0.20287	0.0467	0.0363	0.01166	0.00905
MYC-51	-0.004	515886	0.18333	0.14382	0.2331	0.2278	0.03785	0.037
PRDX2+19	-0.004	-296131	2.01475	1.09289	0.0683	0.0506	0.10135	0.07513
PRDX2+20	-0.004	-296480	1.97102	1.45559	0.0683	0.0506	0.11569	0.08576
BCAT2-10	-0.004	96795	2.33109	0.51217	0.0305	0.1583	0.03333	0.17297
RPN1+47	-0.004	-839517	0.57086	0.25735	0.1850	0.0056	0.07091	0.00213
FTL+59	-0.004	-625755	0.44254	0.08694	0.0071	0.0235	0.00139	0.0046
DHPS+60	-0.004	-901347	0.24931	0.01449	0.0374	0.0000	0.00225	0
PRDX2+24	-0.004	-361159	2.01447	4.08340	0.0416	0.0416	0.11931	0.11922
FUT1+41	-0.004	-472545	0.52491	0.07332	0.0540	0.0233	0.01059	0.00458
BAX+46	-0.004	-492338	0.40601	0.07876	0.0061	0.0330	0.00109	0.00591
COPZ1-23	-0.004	377299	0.18028	0.01449	0.0212	0.0041	0.00108	0.00021
COPZ1+15	-0.004	-129085	0.96435	0.29576	0.1512	0.0768	0.08075	0.041
PQBP1-30	-0.004	942943	0.50896	0.12085	0.0070	0.0000	0.00174	0
RNASEH2A-13	-0.004	227630	0.47531	0.18715	0.0691	0.0783	0.02061	0.02335
C19orf43+36	-0.005	-459935	0.36439	0.06376	0.0302	0.0421	0.0046	0.00641
DHPS+46	-0.005	-595455	0.53624	0.07245	0.0444	0.0450	0.00875	0.00888
RAD23A-4	-0.005	39628	1.06616	0.83749	0.4866	0.4320	0.4598	0.40821
FUT1+8	-0.005	-66008	0.28128	0.05854	0.2342	0.5454	0.03005	0.06999
SEC61A1-46	-0.005	533125	0.57953	0.85278	0.0886	0.0360	0.06229	0.02528
MYC-17	-0.005	181596	1.04319	1.09535	0.4296	0.7417	0.45922	0.79284
ITGA5-21	-0.005	204388	1.07779	0.29604	0.0400	0.0488	0.02259	0.02755
SEC61A1-57	-0.005	793622	0.92893	0.50102	0.0554	0.0000	0.03779	0
PRDX2+35	-0.005	-432860	0.59250	0.37270	0.0260	0.0257	0.01222	0.01209

MYC-45	-0.005	394095	0.24649	0.07245	0.2084	0.4888	0.02785	0.06532
BAX-3	-0.005	28804	0.33213	0.13027	0.0644	0.3596	0.0134	0.0748
KLF1-11	-0.005	170107	0.48445	0.17635	0.0953	0.1344	0.02786	0.03927
RAD23A-8	-0.005	106026	0.89935	0.11107	0.3877	0.3449	0.12253	0.10901
H1FX+39	-0.005	-732674	0.31343	0.08694	0.0512	0.1111	0.00845	0.01834
RPN1+40	-0.005	-732604	0.37017	0.05796	0.1058	0.0056	0.0155	0.00082
KLF1+17	-0.005	-217467	0.91245	0.91559	0.0943	0.1511	0.08619	0.13814
MYC-29	-0.005	266606	0.42830	0.89205	0.2978	0.6085	0.18407	0.37612
MYC-18	-0.005	190252	0.86550	0.96704	0.4243	0.7283	0.38818	0.66632
BCAT2-44	-0.005	465970	0.27203	0.05796	0.0056	0.0123	0.0007	0.00154
CNBP+31	-0.005	-442893	0.89953	0.52608	0.0385	0.0466	0.02648	0.03203
H1FX-13	-0.005	214340	0.26525	0.29445	0.0714	0.3489	0.01995	0.09751
RAD23A-3	-0.006	37958	0.56166	0.19686	0.5955	0.4320	0.19801	0.14365
HDAC6-33	-0.006	871638	0.18626	0.04347	0.0555	0.0000	0.00499	0
H1FX-56	-0.006	891447	0.66256	1.43443	0.0202	0.0000	0.01969	0
ITGA5-37	-0.006	469394	0.77052	0.31684	0.0180	0.0253	0.00889	0.01248
JUNB-15	-0.006	270066	0.66756	0.30894	0.0083	0.0373	0.00377	0.01694
NUCB1+49	-0.006	-500226	1.17217	2.28192	0.0398	0.0326	0.06509	0.05332
NUCB1+48	-0.006	-499801	1.28275	1.87531	0.0360	0.0326	0.05584	0.05056
ITGA5-8	-0.006	58238	0.75194	0.48326	0.0736	0.0918	0.04437	0.05536
RPN1+28	-0.006	-575735	0.48966	0.29923	0.2584	0.0424	0.09891	0.01623
BAX+14	-0.006	-159328	1.37925	0.61585	0.0389	0.5022	0.03585	0.46282
RAD23A+15	-0.006	-381566	0.44863	0.08694	0.0782	0.0637	0.01544	0.01259
FTL+34	-0.006	-320335	1.03345	0.32495	0.0342	0.0746	0.01982	0.04321
PRDX2+10	-0.006	-183531	1.06616	0.83749	0.0706	0.0605	0.06671	0.0572
C19orf43-7	-0.006	212586	0.35832	0.07245	0.0704	0.0942	0.01134	0.01518
RPN1-15	-0.006	153099	1.16700	1.31097	0.4546	0.3642	0.56229	0.45043
PPP1R15A+4	-0.006	-52723	0.28128	0.05854	0.2538	0.7096	0.03257	0.09106
PLP2-19	-0.006	697109	0.28903	0.73700	0.0058	0.0245	0.00268	0.01131
BCAT2+9	-0.006	-79655	0.33922	0.34778	0.0395	0.3047	0.01357	0.10464
WDR83OS+19	-0.006	-347137	0.54225	0.48008	0.0704	0.1460	0.03592	0.07451
H1FX+20	-0.006	-292517	0.67337	0.20649	0.1134	0.2892	0.04229	0.10783
RPN1+14	-0.006	-365133	0.39553	0.45501	0.2880	0.1230	0.12218	0.05217
BCAT2+40	-0.006	-536929	0.47939	0.18584	0.0074	0.0108	0.00221	0.00322
C19orf43+21	-0.006	-344849	1.21784	1.64686	0.0507	0.0609	0.0718	0.0862
C19orf43+18	-0.006	-299468	0.47531	0.18715	0.0623	0.0609	0.01858	0.01815
KLF1+7	-0.006	-126264	0.58941	0.63013	0.1229	0.2768	0.0749	0.16867
ITGA5+7	-0.006	-160642	0.41537	0.13629	0.0194	0.0393	0.00462	0.00934
NUCB1+8	-0.006	-69771	0.37271	0.03840	0.1634	0.6366	0.01955	0.07616
MYC-5	-0.006	40772	0.21332	0.15940	0.5770	0.9800	0.1064	0.18071
RAB7A+49	-0.006	-649056	1.49586	2.11875	0.2437	0.0000	0.43385	0
FTL-18	-0.006	248711	0.32933	0.05796	0.0303	0.1154	0.00419	0.01594
RNASEH2A-33	-0.006	406408	0.41749	0.12498	0.0279	0.0516	0.00637	0.01179
GATA1-20	-0.006	362316	1.06554	5.17599	0.0224	0.1349	0.05261	0.31673
DNASE2+22	-0.006	-282358	1.64700	4.70519	0.0162	0.1148	0.0451	0.31958
DNASE2+23	-0.006	-283170	1.14509	1.78199	0.0162	0.1148	0.02314	0.16399
HDAC6-29	-0.007	490070	0.65171	0.17280	0.0626	0.0313	0.02101	0.01049
MYC-9	-0.007	115529	0.85088	1.43334	0.4883	0.8554	0.53926	0.9447
MYC-10	-0.007	116188	0.57862	1.55311	0.4883	0.8507	0.4629	0.80642
PLP2+37	-0.007	-673345	0.28475	0.12455	0.0082	0.0122	0.00154	0.0023

BCAT2-36	-0.007	392268	1.03429	0.81604	0.0053	0.0228	0.00487	0.02098
MYC-8	-0.007	95676	0.49430	0.34423	0.4402	0.8649	0.18158	0.35678
KLF1+15	-0.007	-210838	2.01475	1.09289	0.1366	0.2193	0.2027	0.32541
KLF1+16	-0.007	-211187	1.97102	1.45559	0.1366	0.2193	0.23137	0.37145
GATA1+24	-0.007	-759710	0.46014	0.10730	0.0086	0.0000	0.00191	0
NUCB1+44	-0.007	-475125	0.64064	2.21917	0.0304	0.0326	0.03625	0.03887
ITGA5+14	-0.007	-330112	0.18359	0.01761	0.0068	0.0036	0.00039	0.0002
RNASEH2A-19	-0.007	291428	2.01475	1.09289	0.0937	0.0747	0.13904	0.11085
RNASEH2A-20	-0.007	291777	1.97102	1.45559	0.0937	0.0747	0.15871	0.12653
RPN1-56	-0.007	953239	0.48294	0.40480	0.0656	0.0000	0.029	0
FTL+29	-0.007	-286906	0.49959	0.10136	0.0211	0.0883	0.00475	0.01986
HDAC6-22	-0.007	372848	0.53276	0.44110	0.0878	0.1193	0.04256	0.05785
C19orf43+44	-0.007	-542567	0.53624	0.07245	0.0194	0.0257	0.00382	0.00507
NFE2-15	-0.007	125469	0.37139	0.10759	0.0101	0.0717	0.00202	0.01433
BCAT2+37	-0.007	-517027	0.30727	0.20287	0.0081	0.0108	0.00202	0.0027
MYC-40	-0.007	341076	0.38172	0.40038	0.2762	0.5201	0.10798	0.20331
KLF1-18	-0.007	475196	0.39720	0.24446	0.0221	0.0399	0.00689	0.01242
BCAT2+3	-0.007	-19215	0.37271	0.03840	0.1848	0.9074	0.02211	0.10855
CNBP-35	-0.007	636368	1.56343	4.21809	0.0326	0.0010	0.08372	0.00257
KLF1-16	-0.007	365014	0.35832	0.07245	0.0403	0.0607	0.00649	0.00977
LYL1-10	-0.007	89693	0.58941	0.63013	0.0346	0.6025	0.02109	0.3672
PLP2+9	-0.007	-103238	0.24610	0.16490	0.0452	0.3816	0.00911	0.07688
H1FX-43	-0.007	767346	1.35814	2.53529	0.0119	0.0000	0.02208	0
H1FX-42	-0.007	766831	1.37151	2.25323	0.0119	0.0000	0.02092	0
MYC-7	-0.007	86643	0.25881	0.08521	0.5437	0.9062	0.08074	0.13457
FTL+40	-0.007	-406802	0.33960	0.08173	0.0141	0.0360	0.00235	0.00599
DNASE2-4	-0.008	91490	2.06351	1.02080	0.0673	0.3047	0.09768	0.44218
JUNB-35	-0.008	443275	0.59250	0.37270	0.0050	0.0190	0.00235	0.00891
COPZ1+4	-0.008	-36574	1.09507	0.92248	0.8771	0.7032	0.88155	0.70677
PLP2+8	-0.008	-88204	0.32571	0.08694	0.0485	0.3972	0.00816	0.06684
PLP2-5	-0.008	59189	1.08377	0.56101	0.0510	0.2022	0.03977	0.15764
MYC-54	-0.008	586866	0.29702	0.19388	0.1791	0.2131	0.04298	0.05114
BAX-29	-0.008	437203	0.78564	0.32995	0.0054	0.0400	0.00275	0.02038
KLF1-4	-0.008	71873	0.37844	0.18113	0.2020	0.3931	0.05289	0.10293
RNASEH2A-7	-0.008	167865	0.31007	0.13274	0.1058	0.0910	0.02146	0.01847
C19orf43+24	-0.008	-363266	2.01475	1.09289	0.0480	0.0584	0.07123	0.08661
C19orf43+25	-0.008	-363615	1.97102	1.45559	0.0480	0.0584	0.0813	0.09886
CNBP+32	-0.008	-466491	0.32579	0.04347	0.0198	0.0440	0.00236	0.00523
MYC-26	-0.008	251808	0.34049	0.26337	0.3125	0.6201	0.09358	0.18569
BAX+22	-0.008	-234055	1.98425	1.91436	0.0157	0.1062	0.0306	0.20692
H1FX-18	-0.008	289083	1.05199	0.36777	0.0790	0.2910	0.04914	0.181
KLF1-9	-0.008	129472	0.84767	0.13244	0.1608	0.2056	0.05388	0.06888
PLP2-17	-0.008	689345	0.35924	0.29170	0.0093	0.0245	0.00301	0.00793
PQBP1-20	-0.008	346476	0.85965	0.49442	0.0180	0.0436	0.01173	0.02845
GATA1+31	-0.008	-971545	0.30197	0.08694	0.0047	0.0000	0.00076	0
ITGA5-28	-0.008	243698	0.37139	0.10759	0.0295	0.0427	0.0059	0.00853
CALR-7	-0.008	95644	0.47531	0.18715	0.2102	0.3345	0.06269	0.09977
HDAC6-5	-0.008	66092	0.38608	0.33234	0.3687	0.9889	0.13207	0.35423
RAD23A-36	-0.008	436337	0.94017	0.10774	0.0652	0.0369	0.02075	0.01174
WDR83OS+46	-0.008	-607691	0.53624	0.07245	0.0368	0.0476	0.00725	0.00939

HBE1+12	-0.008	-110793	0.32053	0.08839	0.0311	0.3825	0.00523	0.06439
PLP2-7	-0.009	110988	0.55764	0.21294	0.0330	0.1447	0.01137	0.04986
FTL-25	-0.009	373770	0.92898	0.30619	0.0099	0.0465	0.00528	0.0248
PRDX2+9	-0.009	-181861	0.56166	0.19686	0.0579	0.0605	0.01925	0.02013
PRDX2+23	-0.009	-353795	1.57147	0.72808	0.0434	0.0416	0.04642	0.04446
MYC-64	-0.009	917497	0.18053	0.01449	0.2017	0.0060	0.01032	0.00031
RPN1-22	-0.009	226046	0.66256	1.43443	0.4531	0.2996	0.44172	0.29207
HNRNPA1+23	-0.009	-335728	0.45323	0.05760	0.0114	0.0350	0.00184	0.00565
SEC61A1-17	-0.009	328632	0.30332	0.17201	0.1173	0.2535	0.02679	0.0579
NUCB1+31	-0.009	-291098	0.46485	0.11093	0.0525	0.0464	0.01192	0.01054
RPN1+22	-0.009	-451061	0.26525	0.29445	0.2629	0.1004	0.07347	0.02805
BAX-5	-0.009	83993	0.27495	0.01449	0.0269	0.2291	0.0017	0.01446
FTL+10	-0.009	-111020	0.79073	0.12027	0.1085	0.6651	0.03346	0.20511
DNASE2+47	-0.009	-656174	0.60170	0.25069	0.0043	0.0147	0.00167	0.0057
BAX+36	-0.009	-370471	0.94949	0.29989	0.0028	0.0369	0.00149	0.01967
C19orf43+20	-0.009	-326786	0.66756	0.30894	0.0394	0.0609	0.01789	0.02764
DNASE2+18	-0.009	-223149	0.91245	0.91559	0.0370	0.1261	0.03382	0.11526
COPZ1+26	-0.009	-375217	0.77052	0.31684	0.0497	0.0202	0.02456	0.00998
H1FX-41	-0.009	762036	0.36679	0.43610	0.0156	0.0000	0.00624	0
HNRNPA1-31	-0.009	479249	0.17452	0.03927	0.0037	0.0030	0.00031	0.00025
MYC-61	-0.009	817269	0.38402	0.34995	0.1683	0.0082	0.0617	0.00301
PQBP1-32	-0.009	964342	0.32413	0.18338	0.0082	0.0000	0.002	0
FTL-28	-0.009	426754	0.78564	0.32995	0.0077	0.0405	0.00392	0.02062
PQBP1-1	-0.009	19458	1.23891	0.67316	0.1778	0.9296	0.16237	0.84897
ITGA5+4	-0.009	-70813	0.19188	0.01449	0.0651	0.0873	0.00343	0.0046
FTL-9	-0.009	167942	0.80074	0.24431	0.0236	0.1616	0.01044	0.07149
FTL-10	-0.009	168401	0.86882	0.22779	0.0236	0.1606	0.0105	0.07143
BAX+50	-0.009	-539262	0.97125	0.03456	0.0068	0.0299	0.00125	0.00547
BCAT2-12	-0.009	112844	0.61356	0.33111	0.0337	0.1424	0.01519	0.06417
RNASEH2A+9	-0.010	-242366	0.44863	0.08694	0.1181	0.0696	0.02332	0.01375
DNASE2-13	-0.010	336918	1.54310	6.53275	0.0168	0.0528	0.05334	0.16764
PLP2+33	-0.010	-580189	0.49785	0.77018	0.0117	0.0925	0.00724	0.05728
FUT1-26	-0.010	262344	1.13284	0.23772	0.0707	0.1236	0.03669	0.06414
BAX+25	-0.010	-256640	0.61356	0.33111	0.0160	0.0922	0.00721	0.04154
HDAC6-8	-0.010	115354	1.23891	0.67316	0.2452	0.7974	0.22392	0.72824
RPN1+52	-0.010	-948830	0.76283	0.66635	0.0829	0.0000	0.0591	0
HNRNPA1+30	-0.010	-584241	0.38804	0.11593	0.0064	0.0188	0.00136	0.00399
BCAT2-20	-0.010	166090	1.03345	0.32495	0.0465	0.1047	0.02695	0.06065
FUT1+31	-0.010	-382569	0.59661	0.55840	0.0742	0.0479	0.04283	0.02767
BCAT2+22	-0.010	-295657	0.52055	0.18367	0.0134	0.0537	0.00414	0.01659
RAD23A+13	-0.010	-228717	0.48445	0.17635	0.2442	0.1291	0.07138	0.03772
FUT1-37	-0.010	402191	0.50725	0.19186	0.0459	0.0627	0.01432	0.01957
KLF1+6	-0.010	-98238	1.06616	0.83749	0.1234	0.3085	0.1166	0.29148
RAB7A-52	-0.010	882659	0.67337	0.20649	0.1385	0.0078	0.05165	0.00291
RPN1-35	-0.010	307110	0.70344	1.75844	0.1977	0.2586	0.21988	0.28765
FUT1-8	-0.010	72438	0.44682	0.23323	0.4123	0.7745	0.1331	0.25003
PRDX2+11	-0.010	-211557	0.58941	0.63013	0.0613	0.0557	0.03736	0.03397
BCAT2-47	-0.010	478038	2.53815	2.46602	0.0068	0.0123	0.01701	0.03069
CNBP+6	-0.010	-55159	0.63982	0.42190	0.5695	0.8942	0.29589	0.4646
NUCB1-29	-0.010	439029	0.92898	0.30619	0.0334	0.0396	0.01781	0.0211

FUT1-30	-0.010	334865	1.03429	0.81604	0.0494	0.0963	0.04538	0.08847
RAB7A+14	-0.010	-192954	0.57481	0.38487	0.4052	0.2957	0.19058	0.13908
RPN1+56	-0.010	-975984	0.89953	0.52608	0.0822	0.0000	0.05655	0
C19orf43+38	-0.010	-478246	0.41749	0.12498	0.0299	0.0379	0.00683	0.00866
BAX+47	-0.010	-529935	0.64064	2.21917	0.0066	0.0299	0.00787	0.03561
RNASEH2A-15	-0.010	254948	0.66756	0.30894	0.0818	0.0775	0.03715	0.0352
KLF1+49	-0.011	-696031	0.24931	0.01449	0.0180	0.0198	0.00108	0.00119
C19orf43-10	-0.011	532306	0.17898	0.00000	0.0481	0.0328	0	0
DHPS+19	-0.011	-334901	0.54225	0.48008	0.0824	0.1323	0.04204	0.0675
BAX-9	-0.011	151861	0.52055	0.18367	0.0118	0.1657	0.00365	0.05124
HDAC6-11	-0.011	159732	1.09968	1.04021	0.1751	0.4544	0.18728	0.48603
FUT1+20	-0.011	-208825	1.37940	4.06934	0.1100	0.1886	0.26062	0.44684
BAX+20	-0.011	-206737	1.01167	3.18092	0.0201	0.1117	0.03606	0.20032
LYL1-23	-0.011	320558	1.54032	1.80923	0.0118	0.0473	0.0197	0.07896
PLP2-21	-0.011	743995	0.21564	0.05260	0.0061	0.0156	0.00065	0.00166
RPN1-25	-0.012	237801	1.37802	1.60042	0.3987	0.2996	0.59209	0.44492
ITGA5-9	-0.012	59912	2.56516	3.36227	0.0610	0.0918	0.17914	0.2697
BCAT2+39	-0.012	-528015	0.92898	0.30619	0.0094	0.0108	0.00501	0.00576
RAB7A-53	-0.012	888894	0.37721	0.23924	0.0801	0.0078	0.02406	0.00234
H1FX-12	-0.012	211589	0.31975	0.21990	0.0714	0.3489	0.01893	0.09252
JUNB+13	-0.012	-296019	0.92663	1.05760	0.0098	0.0257	0.0097	0.02544
MYC-37	-0.012	323022	0.43820	0.70135	0.3368	0.5318	0.18671	0.29482
WDR83OS+28	-0.012	-435019	0.91245	0.91559	0.0371	0.1086	0.03391	0.09926
FUT1-20	-0.012	195154	0.33960	0.08173	0.0903	0.1442	0.01504	0.02402
PLP2+32	-0.012	-559963	0.17721	0.05796	0.0110	0.0925	0.00111	0.00937
HDAC6-21	-0.012	365419	1.02138	4.76091	0.0925	0.1277	0.20398	0.28152
PRDX2-12	-0.012	279721	0.35832	0.07245	0.0660	0.0438	0.01063	0.00705
RPN1-59	-0.012	966958	0.18822	0.01449	0.0967	0.0000	0.00505	0
NFE2-9	-0.012	90932	0.42343	0.08644	0.0335	0.1367	0.00641	0.02615
PPP1R15A+35	-0.012	-370130	2.11845	0.89741	0.0607	0.0554	0.08369	0.07639
PRDX2+7	-0.012	-172568	0.31007	0.13274	0.0763	0.0605	0.01548	0.01228
RPN1-7	-0.012	96635	0.36679	0.43610	0.6543	0.3642	0.26168	0.14565
COPZ1-2	-0.012	33233	0.89990	3.38190	0.8463	0.7352	1.47639	1.28252
HDAC6+9	-0.012	-170404	1.02761	0.25127	0.2224	0.3509	0.11301	0.17829
PRDX2+13	-0.012	-232333	0.47531	0.18715	0.0544	0.0530	0.01622	0.01582
PRDX2+39	-0.012	-475432	0.53624	0.07245	0.0175	0.0183	0.00345	0.0036
FUT1+2	-0.013	-20949	0.21060	0.08354	1.0000	0.9843	0.13264	0.13055
SEC61A1+11	-0.013	-368450	0.18822	0.01449	0.3199	0.2603	0.01671	0.01359
RPN1+50	-0.013	-946097	0.59673	0.52688	0.0829	0.0000	0.04648	0
PLP2-24	-0.013	964560	0.38532	0.12179	0.0036	0.0000	0.00078	0
PLP2-25	-0.013	965084	0.45718	0.31481	0.0036	0.0000	0.00137	0
RAD23A-24	-0.013	245569	0.34326	0.07245	0.1795	0.1432	0.02831	0.02259
BCAT2-29	-0.013	300365	0.46228	0.08694	0.0106	0.0327	0.00213	0.00656
PQBP1-3	-0.013	50917	0.39277	0.63360	0.1087	0.6438	0.05423	0.32118
PRDX2+25	-0.013	-361969	1.64700	4.70519	0.0416	0.0416	0.11581	0.11571
PRDX2+26	-0.013	-362781	1.14509	1.78199	0.0416	0.0416	0.05942	0.05938
BCAT2-17	-0.013	149955	1.10066	1.72598	0.0350	0.1100	0.04824	0.15161
RNASEH2A-35	-0.013	428157	0.59250	0.37270	0.0371	0.0363	0.01743	0.01707
DNASE2+42	-0.013	-520072	0.68945	0.68099	0.0071	0.0165	0.00486	0.01128
PQBP1+16	-0.013	-266300	1.02761	0.25127	0.0454	0.2359	0.02307	0.11987

H1FX-9	-0.013	120352	0.48299	0.84401	0.0957	0.6448	0.0611	0.41167
FUT1+7	-0.013	-58754	1.24868	0.69823	0.2096	0.5807	0.19571	0.54225
BAX-15	-0.013	244192	0.44964	0.52333	0.0153	0.1260	0.00742	0.06112
DHPS+44	-0.013	-579365	0.42462	0.45928	0.0414	0.0450	0.01828	0.01989
BAX-6	-0.013	119203	0.93844	0.49007	0.0198	0.2036	0.01343	0.1381
HDAC6+1	-0.013	-7474	1.43163	2.90212	1.0000	0.9891	2.03832	2.01604
FTL-4	-0.013	73544	0.27495	0.01449	0.0463	0.2411	0.00292	0.01522
DHPS+35	-0.013	-490627	0.46950	0.20896	0.0502	0.0928	0.01572	0.02907
HDAC6-13	-0.013	266583	0.24610	0.16490	0.0908	0.2781	0.01829	0.05603
CNBP-1	-0.013	63274	0.79677	0.96646	0.1792	0.5810	0.15725	0.50981
RNASEH2A-14	-0.013	245226	0.89935	0.11107	0.0731	0.0775	0.0231	0.02449
SEC61A1-40	-0.013	496563	1.35814	2.53529	0.0762	0.0807	0.1414	0.14981
SEC61A1-41	-0.013	497078	1.37151	2.25323	0.0762	0.0807	0.13395	0.14192
FTL+35	-0.013	-356357	0.46485	0.11093	0.0164	0.0396	0.00372	0.009
BCAT2-33	-0.013	348542	0.40601	0.07876	0.0101	0.0240	0.00181	0.00429
BCAT2-14	-0.013	129841	0.44682	0.23323	0.0298	0.1371	0.00962	0.04425
PRDX2+21	-0.013	-302760	0.91245	0.91559	0.0620	0.0432	0.05667	0.03946
RAD23A-19	-0.013	218066	1.64700	4.70519	0.2339	0.1724	0.65113	0.47992
RAD23A-20	-0.013	218878	1.14509	1.78199	0.2339	0.1724	0.33412	0.24627
DHPS+9	-0.014	-150812	0.96819	0.11339	0.4314	0.4346	0.14294	0.14401
FTL+30	-0.014	-289756	0.53744	0.06905	0.0211	0.0858	0.00406	0.01653
RPN1+26	-0.014	-545049	0.48299	0.84401	0.1155	0.0424	0.07374	0.02707
WDR83OS+38	-0.014	-525059	0.36439	0.06376	0.0244	0.0890	0.00372	0.01357
PRDX2+15	-0.014	-259651	0.66756	0.30894	0.0444	0.0522	0.02016	0.02372
LYL1-17	-0.014	217909	2.17061	3.48841	0.0173	0.1010	0.0476	0.27802
COPZ1-6	-0.014	45343	1.03165	0.28873	0.4515	0.4594	0.24641	0.25073
PLP2+30	-0.014	-540225	1.02761	0.25127	0.0210	0.1014	0.01067	0.05154
DHPS+16	-0.014	-301884	0.56166	0.19686	0.0970	0.1487	0.03225	0.04944
PLP2+40	-0.014	-679324	0.52942	0.29916	0.0074	0.0122	0.00294	0.00486
RAB7A-36	-0.014	618563	0.34765	0.03927	0.1490	0.0110	0.01741	0.00129
JUNB-32	-0.014	404370	0.33126	0.09441	0.0054	0.0269	0.00095	0.00476
SEC61A1-54	-0.014	751965	0.37000	0.18012	0.0479	0.0000	0.01237	0
BCAT2-49	-0.014	501544	0.73027	0.07992	0.0059	0.0065	0.00143	0.00157
H1FX-4	-0.014	77151	0.63982	0.42190	0.1529	0.6602	0.07944	0.34301
DHPS-6	-0.014	186411	0.92663	1.05760	0.3025	0.2060	0.29946	0.20393
CNBP-56	-0.014	800257	0.30134	0.14208	0.0213	0.0010	0.00441	0.00021
NUCB1+15	-0.014	-125440	0.21060	0.08354	0.0789	0.1659	0.01047	0.02201
PQBP1-12	-0.014	257528	1.33451	2.70881	0.0105	0.1664	0.01996	0.31631
PQBP1-13	-0.014	258438	1.58651	2.22540	0.0105	0.1664	0.01973	0.3126
FTL+53	-0.014	-565485	1.17217	2.28192	0.0078	0.0302	0.01276	0.04939
FTL+52	-0.014	-565060	1.28275	1.87531	0.0086	0.0302	0.01334	0.04684
RPN1-54	-0.014	948521	0.43750	0.73091	0.0913	0.0000	0.05163	0
PLP2-4	-0.014	19380	2.22935	0.90023	0.0939	0.6893	0.13302	0.97655
MYC-55	-0.014	590969	0.37076	0.40226	0.1597	0.2131	0.06167	0.0823
CALR-15	-0.014	166071	0.91245	0.91559	0.3026	0.1762	0.27658	0.16102
BCAT2-21	-0.014	202112	0.46485	0.11093	0.0245	0.0434	0.00556	0.00986
FTL-22	-0.014	336123	0.46712	0.23185	0.0096	0.0648	0.00316	0.02134
ITGA5-44	-0.014	675444	0.37514	0.12382	0.0076	0.0168	0.00164	0.00361
FTL+47	-0.015	-502787	0.40601	0.07876	0.0109	0.0334	0.00195	0.00598
HDAC6-23	-0.015	373622	0.77354	0.38502	0.0677	0.1193	0.03695	0.06512

HBE1-21	-0.015	776746	0.32470	0.05796	0.0038	0.0035	0.00052	0.00048
FTL+31	-0.015	-304200	1.10066	1.72598	0.0292	0.0800	0.04025	0.11031
RAD23A-9	-0.015	115748	0.66756	0.30894	0.3631	0.3359	0.1649	0.15254
H1FX-20	-0.015	299436	1.10381	0.56499	0.1321	0.2864	0.10432	0.2262
KLF1+10	-0.015	-164636	0.89935	0.11107	0.0946	0.2480	0.0299	0.07839
RPN1-53	-0.015	943740	0.58803	0.27496	0.1087	0.0000	0.04371	0
RAD23A+18	-0.015	-423624	0.35832	0.07245	0.0869	0.0637	0.014	0.01027
WDR83OS+35	-0.015	-502863	0.46950	0.20896	0.0596	0.1086	0.01867	0.03402
PLP2+14	-0.015	-254467	1.23891	0.67316	0.0158	0.3019	0.01443	0.2757
H1FX-36	-0.015	725155	0.24689	0.15309	0.0260	0.0000	0.00505	0
LYL1-8	-0.015	68917	0.47531	0.18715	0.0320	0.6403	0.00954	0.19098
CNBP-27	-0.015	592845	0.24689	0.15309	0.0214	0.0028	0.00416	0.00055
RAD23A+2	-0.015	-37071	0.52492	0.16440	0.7990	1.0000	0.23471	0.29376
MYC-12	-0.015	130508	0.35862	0.30068	0.5017	0.8176	0.16475	0.26847
NUCB1+27	-0.015	-238941	1.10066	1.72598	0.0865	0.0921	0.11922	0.1269
CNBP-47	-0.015	759137	0.66256	1.43443	0.0213	0.0010	0.02076	0.00097
CALR-17	-0.015	217106	1.57147	0.72808	0.1737	0.1574	0.1858	0.16836
COPZ1+5	-0.015	-37449	1.07689	1.68222	0.8771	0.6461	1.18053	0.86957
HNRNPA1+28	-0.015	-536867	0.37514	0.12382	0.0084	0.0236	0.00181	0.00509
KLF1-14	-0.015	342600	1.54310	6.53275	0.0619	0.0607	0.19653	0.19262
JUNB+4	-0.015	-30761	0.44079	0.07245	0.1130	0.4969	0.02019	0.0888
BCAT2-24	-0.016	242548	0.40867	0.28981	0.0129	0.0363	0.00444	0.0125
RNASEH2A+4	-0.016	-45879	0.44079	0.07245	0.4718	0.6415	0.08431	0.11463
ITGA5-5	-0.016	42196	0.60701	0.44428	0.1098	0.2230	0.05702	0.11582
RPN1+44	-0.016	-773546	0.45029	0.60875	0.1126	0.0056	0.05895	0.00291
MYC-19	-0.016	192658	0.59595	0.56369	0.4243	0.7283	0.24592	0.42214
BAX+40	-0.016	-400870	0.78293	0.11593	0.0084	0.0356	0.00253	0.01072
BCAT2-16	-0.016	135511	0.53744	0.06905	0.0328	0.1362	0.00632	0.02624
BCAT2-41	-0.016	425686	0.25824	0.20033	0.0077	0.0145	0.00175	0.00329
LYL1-7	-0.016	51321	0.89935	0.11107	0.0421	0.6558	0.01331	0.20728
MYC-4	-0.016	24787	0.65532	0.47906	0.9716	1.0000	0.54439	0.5603
CALR-29	-0.016	296171	0.59250	0.37270	0.0785	0.0869	0.03689	0.04085
NFE2-27	-0.016	491806	0.36898	0.13411	0.0046	0.0180	0.00102	0.004
FTL+33	-0.016	-312531	0.45173	0.24388	0.0262	0.0770	0.0087	0.02556
SEC61A1+14	-0.016	-478217	0.21241	0.13904	0.2458	0.1376	0.04224	0.02365
DNASE2+16	-0.016	-216520	2.01475	1.09289	0.0391	0.1796	0.05802	0.2665
DNASE2+17	-0.016	-216869	1.97102	1.45559	0.0391	0.1796	0.06623	0.30421
LYL1-34	-0.016	691153	0.39720	0.24446	0.0047	0.0127	0.00146	0.00395
MYC-57	-0.016	607469	0.31852	0.99551	0.2233	0.1478	0.12574	0.08325
MYC-47	-0.016	409011	0.22500	0.02898	0.2425	0.4808	0.01958	0.03883
RAD23A-26	-0.016	250052	0.33126	0.09441	0.2097	0.1320	0.03708	0.02334
PPP1R15A+39	-0.016	-447467	0.64064	2.21917	0.0264	0.0497	0.03148	0.0593
ITGA5-14	-0.017	124897	1.39090	2.59115	0.0543	0.0759	0.10308	0.14403
MYC-38	-0.017	328299	0.58539	0.95392	0.3553	0.5292	0.26551	0.39548
NUCB1+47	-0.017	-484452	0.97125	0.03456	0.0230	0.0326	0.00421	0.00597
FUT1+43	-0.017	-574430	0.30727	0.20287	0.0293	0.0144	0.00732	0.0036
SEC61A1-7	-0.017	118705	0.41950	0.12962	0.2975	0.2684	0.06937	0.06259
PRDX2+40	-0.017	-476252	0.40417	0.00739	0.0175	0.0183	0.00096	0.001
RPN1+24	-0.017	-455705	0.21230	0.09586	0.2481	0.1004	0.03539	0.01432
C19orf43+37	-0.017	-461090	0.33126	0.09441	0.0204	0.0379	0.00361	0.0067

PPP1R15A-34	-0.017	466687	0.92898	0.30619	0.0367	0.0363	0.01957	0.01934
HDAC6+17	-0.017	-305138	0.33477	0.17389	0.0397	0.0695	0.00958	0.01678
NFE2-26	-0.017	356076	0.45323	0.05760	0.0116	0.0224	0.00187	0.00362
RAD23A-22	-0.017	226701	0.46950	0.20896	0.1282	0.1690	0.04015	0.05294
PRDX2+32	-0.017	-393955	0.33126	0.09441	0.0295	0.0362	0.00522	0.00641
C19orf43+40	-0.017	-499995	0.59250	0.37270	0.0300	0.0379	0.0141	0.01781
DHPS+30	-0.017	-473818	1.57147	0.72808	0.0699	0.0928	0.07477	0.09926
LYL1-13	-0.017	125135	0.69199	0.18309	0.0679	0.5472	0.02417	0.19476
PRDX2+50	-0.017	-735785	0.60170	0.25069	0.0156	0.0020	0.00606	0.00076
COPZ1-4	-0.017	35939	0.75194	0.48326	0.7013	0.7296	0.42276	0.43983
DNASE2-6	-0.017	98919	1.54032	1.80923	0.0693	0.2641	0.11569	0.44082
GATA1-6	-0.017	77806	0.30903	0.08245	0.0578	0.8822	0.00923	0.14082
CNBP+41	-0.017	-641184	0.15364	0.01449	0.0330	0.0360	0.00156	0.0017
MYC-15	-0.018	175788	1.13102	1.56564	0.4973	0.7594	0.66176	1.01058
FTL+44	-0.018	-463047	2.11845	0.89741	0.0113	0.0353	0.01558	0.04872
CNBP-7	-0.018	129118	0.85070	0.75996	0.1587	0.4759	0.1276	0.38262
RAB7A-21	-0.018	378553	0.31975	0.21990	0.1971	0.1173	0.05226	0.03109
RPN1-5	-0.018	72984	0.42979	0.09549	0.3969	0.4468	0.08041	0.09052
PLP2+41	-0.018	-684175	0.68815	1.25076	0.0047	0.0122	0.00436	0.01132
COPZ1-19	-0.018	271534	0.30507	0.06767	0.0191	0.0118	0.00274	0.0017
BAX+57	-0.018	-609766	0.27203	0.05796	0.0074	0.0232	0.00093	0.00292
WDR83OS+18	-0.018	-343816	0.58941	0.63013	0.0756	0.1460	0.04607	0.089
PRDX2+14	-0.018	-249929	0.89935	0.11107	0.0440	0.0522	0.01391	0.01651
DHPS+37	-0.018	-509495	0.34326	0.07245	0.0584	0.0791	0.00921	0.01248
KLF1+32	-0.018	-360792	0.28100	0.04579	0.0347	0.0610	0.00394	0.00692
NFE2-10	-0.018	93059	0.52508	0.10462	0.0249	0.1079	0.00584	0.0253
PRDX2+3	-0.018	-34547	0.93136	0.41755	0.4893	0.6491	0.30513	0.40476
CNBP-41	-0.018	688282	0.83051	0.91465	0.0312	0.0010	0.02719	0.00087
ITGA5-41	-0.019	627343	0.14834	0.02898	0.0137	0.0174	0.0009	0.00114
BAX+15	-0.019	-166536	0.55020	0.04347	0.0387	0.3146	0.00599	0.04865
SEC61A1-24	-0.019	360707	1.37802	1.60042	0.1339	0.1702	0.19885	0.25271
SEC61A1-34	-0.019	445409	1.16700	1.31097	0.1612	0.0868	0.19939	0.1074
RAD23A-15	-0.019	158857	0.91245	0.91559	0.5056	0.1994	0.46213	0.18229
H1FX+21	-0.019	-298752	0.37721	0.23924	0.0980	0.2892	0.02944	0.08687
DHPS+4	-0.019	-78847	0.44079	0.07245	0.4536	0.7928	0.08106	0.14168
BAX+42	-0.019	-444161	0.46228	0.08694	0.0049	0.0356	0.00098	0.00713
PLP2+17	-0.019	-303729	0.38608	0.33234	0.0143	0.2830	0.00512	0.10138
CNBP-6	-0.019	127019	0.47461	0.29155	0.1762	0.4802	0.06554	0.17862
RPN1-2	-0.019	59754	0.24689	0.15309	0.8693	0.5552	0.169	0.10794
RPN1-27	-0.019	240629	1.19535	2.40639	0.3987	0.2996	0.6762	0.50813
FUT1+5	-0.019	-34663	0.55020	0.04347	0.4491	0.9491	0.06946	0.14678
C19orf43+1	-0.019	-22956	0.84767	0.13244	0.7261	0.9919	0.24329	0.33234
BCAT2-34	-0.019	386139	0.64064	2.21917	0.0059	0.0228	0.00703	0.02723
BCAT2+36	-0.019	-490368	0.46712	0.23185	0.0063	0.0126	0.00207	0.00415
ITGA5-17	-0.019	191713	0.49767	0.19352	0.0530	0.0492	0.01645	0.01528
RPN1+9	-0.019	-195114	0.92893	0.50102	0.7247	0.7057	0.4944	0.48141
CALR-26	-0.019	257266	0.33126	0.09441	0.1018	0.1203	0.018	0.02127
PRDX2+45	-0.019	-599683	0.68945	0.68099	0.0209	0.0025	0.01432	0.00174
PRDX2-10	-0.019	257307	1.54310	6.53275	0.0631	0.0438	0.20034	0.13896
PQBP1-6	-0.019	170687	0.24610	0.16490	0.0408	0.3264	0.00822	0.06575

RPN1+29	-0.019	-578455	0.88456	2.13621	0.2584	0.0424	0.3552	0.05828
H1FX-49	-0.019	818500	1.16700	1.31097	0.0235	0.0000	0.02907	0
DNASE2+39	-0.019	-500629	0.94017	0.10774	0.0057	0.0165	0.00181	0.00524
ITGA5-31	-0.019	378949	0.36708	0.14831	0.0110	0.0301	0.00257	0.00703
DNASE2+10	-0.019	-152722	0.47531	0.18715	0.0270	0.2204	0.00805	0.06574
PRDX2-7	-0.020	84814	0.48445	0.17635	0.2694	0.1767	0.07874	0.05164
SEC61A1+8	-0.020	-354731	0.48294	0.40480	0.2246	0.3565	0.09931	0.15763
PPP1R15A-22	-0.020	304823	0.55067	0.14107	0.0662	0.1114	0.01845	0.03106
RAB7A-45	-0.020	764258	0.57086	0.25735	0.2101	0.0110	0.08053	0.00422
RAD23A+5	-0.020	-113114	0.96819	0.11339	0.4212	0.4026	0.13956	0.13339
FUT1-19	-0.020	190044	0.60283	2.12491	0.1156	0.1472	0.13084	0.1666
BAX-10	-0.020	178391	0.80074	0.24431	0.0150	0.1499	0.00663	0.06632
BAX-11	-0.020	178850	0.86882	0.22779	0.0150	0.1489	0.00667	0.06623
RPN1-33	-0.020	296652	0.29986	0.29010	0.2025	0.2909	0.05973	0.0858
FTL+17	-0.020	-180528	0.54594	0.41313	0.0647	0.3021	0.03073	0.14349
DHPS+40	-0.020	-531134	0.41749	0.12498	0.0298	0.0655	0.00681	0.01495
WDR83OS+17	-0.020	-315790	1.06616	0.83749	0.0761	0.1696	0.07191	0.16023
RNASEH2A-10	-0.021	178828	1.06616	0.83749	0.0944	0.0910	0.0892	0.08602
RPN1-34	-0.021	305491	0.34822	0.21396	0.2001	0.2586	0.05462	0.0706
PPP1R15A+30	-0.021	-308775	0.60283	2.12491	0.0441	0.0597	0.04991	0.06757
RAD23A+20	-0.021	-533806	0.39720	0.24446	0.0245	0.0417	0.00763	0.013
MYC-6	-0.021	64840	0.84616	0.35350	0.5533	0.9533	0.30261	0.52136
CNBP+29	-0.021	-424827	0.67337	0.20649	0.0397	0.0484	0.0148	0.01805
FTL+41	-0.021	-411319	0.78293	0.11593	0.0134	0.0360	0.00404	0.01084
H1FX-67	-0.021	962053	0.29986	0.29010	0.0130	0.0000	0.00383	0
RPN1+18	-0.021	-402729	0.49550	0.40639	0.4267	0.1143	0.19148	0.05128
NFE2+20	-0.021	-278871	0.41537	0.13629	0.0055	0.0131	0.00131	0.00312
CNBP-20	-0.021	379634	0.37000	0.18012	0.0344	0.0442	0.00888	0.01141
HNRNPA1+18	-0.021	-276389	0.58339	0.17164	0.0179	0.0635	0.00566	0.0201
RPN1-40	-0.021	423887	0.31187	0.13201	0.1720	0.1787	0.0349	0.03625
CNBP+51	-0.021	-900807	0.29362	0.00246	0.0170	0.0164	0.00046	0.00044
GATA1-13	-0.022	175174	1.09968	1.04021	0.0380	0.4526	0.04064	0.48403
PRDX2+43	-0.022	-594906	0.73862	0.42907	0.0120	0.0025	0.00676	0.00143
DNASE2+36	-0.022	-395821	0.53624	0.07245	0.0069	0.0449	0.00136	0.00884
CNBP-28	-0.022	598474	0.57953	0.85278	0.0253	0.0028	0.01779	0.00199
RPN1+6	-0.022	-153457	0.37000	0.18012	1.0000	0.7840	0.25816	0.20239
DHPS+8	-0.022	-133443	0.37844	0.18113	0.3493	0.4512	0.09145	0.11814
CALR+4	-0.022	-102142	0.93136	0.41755	0.4042	0.4130	0.25206	0.25755
RAD23A+16	-0.022	-401210	1.54310	6.53275	0.0926	0.0637	0.29401	0.20235
LYL1+25	-0.022	-298433	0.68945	0.68099	0.0100	0.1253	0.00685	0.08586
H1FX-66	-0.022	935277	0.30332	0.17201	0.0176	0.0000	0.00402	0
COPZ1-26	-0.022	434849	0.17452	0.03927	0.0214	0.0022	0.00177	0.00018
RPN1-14	-0.022	145728	0.71928	1.40733	0.6623	0.3642	0.66635	0.36639
PLP2+42	-0.022	-719935	0.19962	0.09252	0.0039	0.0122	0.00053	0.00166
GATA1+30	-0.022	-968985	0.54732	0.07245	0.0047	0.0000	0.00094	0
CALR+19	-0.022	-443123	0.92663	1.05760	0.0416	0.0405	0.04118	0.04013
RNASEH2A-40	-0.022	471549	0.40417	0.00739	0.0213	0.0253	0.00116	0.00138
ITGA5-18	-0.022	198965	0.77095	0.63266	0.0466	0.0492	0.03255	0.03438
RPN1-32	-0.023	269876	0.30332	0.17201	0.3118	0.2996	0.07122	0.06843
CNBP-32	-0.023	629726	0.36679	0.43610	0.0337	0.0010	0.01348	0.0004

BAX+17	-0.023	-173903	1.44373	2.77330	0.0349	0.1534	0.06983	0.30702
PPP1R15A+9	-0.024	-91435	1.44373	2.77330	0.2320	0.2323	0.46423	0.46483
H1FX+41	-0.024	-761588	0.21142	0.00065	0.0547	0.1111	0.00064	0.0013
FTL+28	-0.024	-284086	0.44682	0.23323	0.0221	0.0883	0.00713	0.02849
PPP1R15A+2	-0.024	-29493	0.50052	0.18737	0.5641	0.9657	0.17275	0.29574
WDR83OS-8	-0.024	467182	0.17898	0.00000	0.3564	0.3770	0	0
H1FX+11	-0.024	-132159	1.02100	1.42074	0.1314	0.3400	0.15826	0.4095
H1FX-37	-0.024	730784	0.57953	0.85278	0.0323	0.0000	0.02271	0
NFE2-32	-0.024	599066	0.40247	0.17845	0.0050	0.0120	0.00134	0.00322
CNBP-3	-0.024	79279	0.31975	0.21990	0.1093	0.5365	0.02898	0.14225
CNBP+21	-0.024	-285268	0.29207	0.21352	0.0377	0.0550	0.00941	0.01374
HDAC6+16	-0.024	-303524	0.28475	0.12455	0.0397	0.0695	0.00748	0.01309
SEC61A1-5	-0.024	81314	0.22384	0.00485	0.5096	0.6886	0.0168	0.0227
LYL1+15	-0.024	-131610	0.59250	0.37270	0.0355	0.3848	0.01668	0.18081
DHPS+42	-0.025	-552883	0.59250	0.37270	0.0444	0.0655	0.02086	0.03076
RPN1-3	-0.025	65383	0.57953	0.85278	0.9178	0.4898	0.64521	0.34433
NFE2+13	-0.025	-116409	0.75465	2.92509	0.0210	0.0544	0.0312	0.08087
RAB7A+20	-0.025	-268857	0.37526	0.08151	0.2101	0.2556	0.03674	0.0447
RPN1+55	-0.025	-964153	0.37721	0.23924	0.1411	0.0000	0.04239	0
DNASE2+2	-0.025	-27221	0.52492	0.16440	0.2303	0.7262	0.06765	0.21334
DHPS+39	-0.025	-513978	0.33126	0.09441	0.0385	0.0655	0.00681	0.01158
ITGA5-4	-0.025	35914	0.65085	0.82416	0.1359	0.2335	0.09953	0.17104
RNASEH2A-46	-0.025	621925	0.34986	0.07919	0.0440	0.0020	0.00732	0.00033
BCAT2-6	-0.025	45053	0.47587	0.14020	0.0495	0.2050	0.01279	0.05295
SEC61A1-45	-0.025	532234	0.38827	0.19642	0.0923	0.0360	0.02549	0.00993
PPP1R15A+44	-0.025	-472568	1.17217	2.28192	0.0540	0.0497	0.08832	0.08134
PPP1R15A+43	-0.025	-472143	1.28275	1.87531	0.0448	0.0497	0.06948	0.07714
DHPS+15	-0.025	-296138	0.69199	0.18309	0.1243	0.1487	0.04424	0.05293
FUT1-11	-0.025	92552	1.10066	1.72598	0.3155	0.5768	0.43485	0.79505
CNBP-29	-0.025	599365	0.38827	0.19642	0.0380	0.0028	0.01049	0.00078
FTL+46	-0.025	-473992	1.13284	0.23772	0.0105	0.0347	0.00545	0.01801
FTL+43	-0.025	-454610	0.46228	0.08694	0.0090	0.0360	0.0018	0.00721
NFE2-14	-0.025	109315	0.81280	0.10404	0.0140	0.0806	0.00407	0.02343
RAD23A-27	-0.026	267208	0.41749	0.12498	0.1358	0.1190	0.03102	0.02718
FTL+18	-0.026	-184352	1.44373	2.77330	0.0647	0.1514	0.12946	0.30301
DHPS+26	-0.026	-416154	2.01475	1.09289	0.1127	0.1132	0.16723	0.16798
DHPS+27	-0.026	-416503	1.97102	1.45559	0.1127	0.1132	0.19089	0.19174
NFE2-8	-0.026	86159	1.07779	0.29604	0.0335	0.2753	0.01892	0.15553
RPN1-17	-0.026	167543	1.19538	2.19563	0.4513	0.3572	0.73114	0.57874
JUNB-10	-0.026	193946	1.06616	0.83749	0.0087	0.0416	0.00822	0.03931
C19orf43+10	-0.026	-173967	0.52492	0.16440	0.1140	0.1045	0.03349	0.03069
RNASEH2A-21	-0.026	298057	0.91245	0.91559	0.0898	0.0637	0.08208	0.05825
H1FX-68	-0.026	970892	0.34822	0.21396	0.0179	0.0000	0.00489	0
ITGA5-42	-0.026	651375	0.27107	0.04347	0.0133	0.0168	0.00144	0.00182
MYC+3	-0.027	-117510	0.44822	0.44849	0.1548	0.3167	0.06941	0.14198
RPN1+41	-0.027	-734864	0.36108	0.13042	0.1327	0.0056	0.0288	0.00121
WDR83OS+44	-0.027	-591601	0.42462	0.45928	0.0331	0.0476	0.01462	0.02104
CALR-34	-0.027	339563	0.40417	0.00739	0.0674	0.0636	0.00368	0.00348
MYC-46	-0.027	404012	0.23932	0.28568	0.2726	0.4808	0.07128	0.12573
FTL-15	-0.027	235143	0.74834	0.48732	0.0268	0.1372	0.01618	0.08285

H1FX-7	-0.027	89666	0.48966	0.29923	0.1411	0.6602	0.05401	0.25271
LYL1+12	-0.027	-92705	0.33126	0.09441	0.0348	0.4776	0.00615	0.08445
GATA1-30	-0.027	496251	0.55764	0.21294	0.0043	0.0313	0.00148	0.01077
BCAT2+29	-0.028	-389388	0.74834	0.48732	0.0142	0.0362	0.00858	0.02188
LYL1-9	-0.028	86372	0.54225	0.48008	0.0327	0.6025	0.01668	0.30742
CNBP-2	-0.028	77386	0.21230	0.09586	0.1464	0.5365	0.02088	0.07653
DHPS+1	-0.028	-35209	0.48445	0.17635	1.0000	1.0000	0.29229	0.29229
PQBP1+18	-0.028	-286038	0.17721	0.05796	0.0376	0.1048	0.00381	0.01062
PPP1R15A+32	-0.028	-318402	0.78293	0.11593	0.0575	0.0561	0.01732	0.0169
LYL1+26	-0.028	-325378	0.34986	0.07919	0.0060	0.1235	0.001	0.02056
RAB7A-58	-0.028	964425	0.25861	0.12889	0.1702	0.0000	0.03107	0
RNASEH2A-32	-0.028	389252	0.33126	0.09441	0.0406	0.0516	0.00718	0.00913
CALR-31	-0.028	322653	0.42462	0.45928	0.0577	0.0636	0.02548	0.0281
C19orf43+12	-0.029	-239703	0.31007	0.13274	0.0631	0.0692	0.0128	0.01404
H1FX-38	-0.029	731675	0.38827	0.19642	0.0290	0.0000	0.00801	0
NUCB1-24	-0.029	325037	0.44413	0.06687	0.0340	0.0764	0.00586	0.01317
KLF1+26	-0.029	-304179	0.34326	0.07245	0.0362	0.1175	0.00571	0.01854
WDR83OS+39	-0.029	-526214	0.33126	0.09441	0.0424	0.0694	0.0075	0.01227
FTL-24	-0.029	366461	0.36270	0.18599	0.0121	0.0465	0.00314	0.01208
RPN1-18	-0.029	193598	0.37526	0.08151	0.4685	0.3079	0.08194	0.05386
KLF1+42	-0.029	-541335	0.34986	0.07919	0.0116	0.0198	0.00193	0.00329
MYC-24	-0.029	241805	0.76748	0.30459	0.2699	0.6264	0.1305	0.30285
PPP1R15A+22	-0.029	-211283	1.10066	1.72598	0.1657	0.1189	0.22838	0.16388
GATA1+7	-0.029	-154962	1.02761	0.25127	0.0363	0.3533	0.01845	0.17951
HDAC6-16	-0.029	305130	0.34829	0.26011	0.1101	0.2386	0.03314	0.07181
SEC61A1-15	-0.029	293017	0.34822	0.21396	0.0851	0.2684	0.02323	0.07327
LYL1+30	-0.029	-434535	0.60170	0.25069	0.0083	0.0852	0.00322	0.0331
NFE2-2	-0.029	12522	1.09507	0.92248	0.1503	0.7389	0.15106	0.74265
WDR83OS+4	-0.029	-91083	0.44079	0.07245	0.3573	0.6766	0.06385	0.12092
LYL1-30	-0.029	558557	1.54310	6.53275	0.0031	0.0253	0.00984	0.08033
WDR83OS+31	-0.030	-493418	2.01447	4.08340	0.0646	0.1086	0.18528	0.31147
RAB7A-10	-0.030	149621	0.35595	0.10144	0.7721	0.5954	0.14671	0.11313
FTL-12	-0.030	186576	1.79277	1.48240	0.0210	0.1502	0.03423	0.24491
FTL-21	-0.030	260897	0.52491	0.07332	0.0202	0.0983	0.00396	0.01928
BCAT2-27	-0.030	257074	0.78293	0.11593	0.0158	0.0327	0.00476	0.00985
DNASE2-3	-0.030	66191	0.37844	0.18113	0.0838	0.3341	0.02194	0.08746
RNASEH2A-45	-0.030	594980	0.68945	0.68099	0.0365	0.0026	0.02501	0.00176
CNBP-58	-0.030	829743	0.29986	0.29010	0.0197	0.0010	0.00581	0.00029
WDR83OS+50	-0.030	-727165	0.73862	0.42907	0.0420	0.0042	0.02364	0.00235
MYC-49	-0.030	440990	1.18766	4.55623	0.3451	0.4700	0.80278	1.09324
ITGA5+10	-0.030	-239573	0.33027	0.06187	0.0219	0.0151	0.00313	0.00216
HBE1+18	-0.030	-261422	0.60063	1.10491	0.0132	0.1788	0.01075	0.14566
C19orf43+48	-0.030	-662041	0.73862	0.42907	0.0278	0.0013	0.01565	0.00073
HNRNPA1+15	-0.030	-240372	0.36708	0.14831	0.0148	0.0855	0.00345	0.01996
RAB7A+18	-0.030	-230450	0.83051	0.91465	0.2727	0.2957	0.23768	0.25772
PQBP1+28	-0.031	-446010	0.19962	0.09252	0.0135	0.0094	0.00183	0.00128
RAB7A-14	-0.031	296380	0.53604	0.08702	0.3129	0.1386	0.06758	0.02994
PQBP1+20	-0.031	-350338	0.60009	0.13462	0.0216	0.0535	0.00614	0.0152
FTL+39	-0.031	-401692	0.60283	2.12491	0.0103	0.0360	0.01166	0.04071
WDR83OS+40	-0.031	-543370	0.41749	0.12498	0.0488	0.0694	0.01115	0.01585

CALR-40	-0.031	489939	0.34986	0.07919	0.0276	0.0306	0.00459	0.0051
CNBP+16	-0.031	-201773	0.36108	0.13042	0.0604	0.0823	0.01311	0.01786
NFE2+14	-0.031	-122358	0.49272	0.33894	0.0226	0.0519	0.00924	0.0212
FTL+15	-0.031	-169777	1.37925	0.61585	0.0840	0.4906	0.07742	0.45216
BCAT2+23	-0.031	-322187	0.80074	0.24431	0.0155	0.0448	0.00686	0.01983
BCAT2+24	-0.031	-322646	0.86882	0.22779	0.0155	0.0441	0.0069	0.0196
RAB7A-57	-0.032	961028	0.19264	0.04920	0.1702	0.0000	0.01657	0
BAX-17	-0.032	253156	0.72662	0.22555	0.0138	0.1058	0.00559	0.04282
BAX-18	-0.032	253628	0.63712	0.04753	0.0138	0.1058	0.0024	0.01841
FUT1-28	-0.032	328736	0.64064	2.21917	0.0470	0.0963	0.05604	0.11482
SEC61A1-35	-0.032	452780	0.71928	1.40733	0.1122	0.0868	0.11289	0.08736
JUNB-33	-0.032	421526	0.41749	0.12498	0.0044	0.0269	0.00101	0.00615
RNASEH2A+5	-0.032	-48882	0.84767	0.13244	0.4411	0.5041	0.1478	0.16891
DNASE2+40	-0.032	-515295	0.73862	0.42907	0.0086	0.0165	0.00484	0.00927
PQBP1-18	-0.032	293305	2.22935	0.90023	0.0231	0.1281	0.03272	0.18152
WDR83OS+22	-0.032	-391910	0.66756	0.30894	0.0855	0.1303	0.03883	0.05919
MYC-58	-0.032	608064	0.24520	0.41313	0.2233	0.1478	0.07107	0.04705
RPN1+4	-0.032	-113318	0.38004	0.05470	0.9007	1.0000	0.12987	0.14418
PQBP1-17	-0.032	279767	0.59225	0.30952	0.0299	0.1445	0.0128	0.06187
DHPS+17	-0.033	-303554	1.06616	0.83749	0.0662	0.1487	0.06255	0.14051
PPP1R15A+26	-0.033	-263440	0.46485	0.11093	0.0756	0.0701	0.01717	0.01592
HBE1-4	-0.033	44440	0.54186	0.28148	0.0955	0.9338	0.0373	0.36469
PQBP1-31	-0.033	963270	0.35924	0.29170	0.0082	0.0000	0.00265	0
H1FX-70	-0.033	976581	0.39863	0.29366	0.0114	0.0000	0.0039	0
PQBP1+9	-0.033	-108172	0.73199	1.50783	0.0681	0.5899	0.07154	0.61977
BCAT2+32	-0.033	-402956	0.32933	0.05796	0.0164	0.0289	0.00227	0.004
NFE2-31	-0.033	557215	0.37514	0.12382	0.0050	0.0158	0.00108	0.0034
PPP1R15A+6	-0.033	-76860	1.37925	0.61585	0.2720	0.6732	0.25069	0.62042
C19orf43+50	-0.033	-666818	0.68945	0.68099	0.0275	0.0013	0.01884	0.00089
RAB7A-12	-0.034	289874	0.39553	0.45501	0.3322	0.1386	0.14093	0.05881
HBE1+31	-0.034	-979870	0.41978	0.17976	0.0044	0.0000	0.00121	0
WDR83OS+21	-0.034	-382188	0.89935	0.11107	0.0658	0.1303	0.0208	0.04119
ITGA5-7	-0.034	49906	1.67201	1.48776	0.0981	0.1471	0.15472	0.23195
KLF1+28	-0.034	-308662	0.33126	0.09441	0.0319	0.1084	0.00564	0.01917
C19orf43+55	-0.034	-802920	0.60170	0.25069	0.0170	0.0000	0.0066	0
CALR-33	-0.034	338743	0.53624	0.07245	0.0674	0.0636	0.01329	0.01254
DHPS+49	-0.034	-700263	0.94017	0.10774	0.0285	0.0042	0.00907	0.00135
FTL+37	-0.034	-380920	0.94949	0.29989	0.0092	0.0372	0.00491	0.01985
FUT1+6	-0.034	-41871	1.37925	0.61585	0.2897	0.6749	0.267	0.62198
RNASEH2A+10	-0.034	-262010	1.54310	6.53275	0.0788	0.0658	0.25019	0.20892
BCAT2-30	-0.034	308802	2.11845	0.89741	0.0143	0.0310	0.01972	0.04274
NUCB1-6	-0.034	83614	0.33213	0.13027	0.2616	0.3307	0.05441	0.06878
SEC61A1-47	-0.034	538754	0.24689	0.15309	0.0939	0.0360	0.01826	0.00699
CALR+9	-0.034	-155997	1.54032	1.80923	0.2417	0.2244	0.40349	0.37461
CNBP-40	-0.034	686190	1.16700	1.31097	0.0312	0.0010	0.03859	0.00124
H1FX-29	-0.035	511944	0.37000	0.18012	0.0299	0.0256	0.00772	0.0066
C19orf43-5	-0.035	190172	1.54310	6.53275	0.1174	0.0942	0.37275	0.29909
CNBP-14	-0.035	308211	0.35595	0.10144	0.0670	0.0818	0.01273	0.01554
RAB7A-23	-0.035	394558	0.79677	0.96646	0.3852	0.1094	0.33802	0.09603
HBE1-15	-0.035	379706	0.16657	0.28989	0.0109	0.1401	0.0024	0.03078

RPN1-4	-0.035	66274	0.38827	0.19642	0.7059	0.4898	0.19494	0.13526
CALR-2	-0.035	39426	0.69199	0.18309	0.3425	0.4397	0.12191	0.15651
RPN1+57	-0.036	-999582	0.32579	0.04347	0.0934	0.0000	0.01112	0
WDR83OS+49	-0.036	-712499	0.94017	0.10774	0.0335	0.0042	0.01066	0.00133
RAB7A-24	-0.036	469790	0.48299	0.84401	0.2156	0.0418	0.13766	0.02667
BCAT2+16	-0.036	-172600	0.33213	0.13027	0.0507	0.1073	0.01055	0.02232
NFE2-21	-0.036	296737	0.58339	0.17164	0.0132	0.0416	0.00418	0.01316
PPP1R15A+3	-0.036	-42113	0.37271	0.03840	0.3382	0.7297	0.04046	0.0873
JUNB+10	-0.036	-246892	1.54310	6.53275	0.0122	0.0328	0.03874	0.10425
RAD23A-1	-0.037	28665	0.31007	0.13274	1.0000	0.4993	0.20287	0.1013
BCAT2+4	-0.037	-31835	0.50052	0.18737	0.1045	0.6656	0.032	0.20384
PQBP1-22	-0.037	394174	0.65171	0.17280	0.0150	0.0233	0.00503	0.00781
RAD23A-40	-0.037	482725	0.34986	0.07919	0.0760	0.0336	0.01265	0.00559
WDR83OS+15	-0.037	-308374	0.69199	0.18309	0.0835	0.1696	0.02972	0.06036
NFE2+16	-0.038	-138759	0.41126	0.48189	0.0191	0.0415	0.0085	0.01849
GATA1-18	-0.038	320572	0.34829	0.26011	0.0198	0.2337	0.00596	0.07035
SEC61A1-8	-0.038	143215	0.17428	0.21222	0.2180	0.2684	0.04192	0.05162
PLP2+22	-0.038	-377295	1.43163	2.90212	0.0125	0.1258	0.02548	0.25649
JUNB-21	-0.038	313175	0.91245	0.91559	0.0094	0.0305	0.00859	0.02791
HBE1-18	-0.038	643738	0.40266	0.16056	0.0091	0.0330	0.00231	0.00838
H1FX+35	-0.039	-610950	0.37016	0.22193	0.0427	0.1292	0.01224	0.03702
HBE1-13	-0.039	278882	0.28642	0.09912	0.0106	0.1462	0.00179	0.02463
RNASEH2A-30	-0.039	384769	0.34326	0.07245	0.0522	0.0563	0.00823	0.00887
RNASEH2A+14	-0.039	-394606	0.39720	0.24446	0.0684	0.0511	0.02131	0.01592
RPN1+20	-0.039	-406072	0.47461	0.29155	0.3167	0.1143	0.11781	0.04251
LYL1-20	-0.039	287830	0.37844	0.18113	0.0115	0.0717	0.00301	0.01878
BAX+6	-0.040	-76099	1.78128	1.31155	0.0824	0.7578	0.12595	1.15828
WDR83OS+14	-0.040	-304827	0.31007	0.13274	0.0809	0.1696	0.01641	0.0344
FUT1-15	-0.040	144709	0.46485	0.11093	0.1338	0.1810	0.03038	0.04111
FTL-11	-0.040	170921	0.59661	0.55840	0.0225	0.1581	0.01299	0.09127
CNBP+27	-0.040	-415739	0.76283	0.66635	0.0469	0.0484	0.03344	0.03451
PRDX2+46	-0.040	-626628	0.34986	0.07919	0.0150	0.0020	0.0025	0.00033
DHPS-7	-0.040	269880	0.39720	0.24446	0.1244	0.2060	0.03876	0.06419
FTL+62	-0.040	-650744	0.30382	0.13339	0.0049	0.0120	0.00099	0.00242
DHPS+50	-0.040	-714929	0.73862	0.42907	0.0201	0.0042	0.01132	0.00238
DHPS+3	-0.040	-75844	0.84767	0.13244	0.5120	0.8201	0.17155	0.2748
FUT1+11	-0.041	-100628	0.79073	0.12027	0.1733	0.2800	0.05344	0.08634
HNRNPA1-20	-0.041	209390	0.19188	0.01449	0.0104	0.0302	0.00055	0.00159
PPP1R15A+50	-0.041	-532838	0.44254	0.08694	0.0318	0.0268	0.00624	0.00525
PRDX2+30	-0.042	-389472	0.34326	0.07245	0.0280	0.0389	0.00442	0.00613
CALR-22	-0.042	233915	0.46950	0.20896	0.1489	0.1544	0.04664	0.04835
RAD23A+4	-0.042	-109356	0.93136	0.41755	0.4092	0.4026	0.25518	0.25106
KLF1+1	-0.042	-21539	0.52492	0.16440	1.0000	1.0000	0.29376	0.29376
HNRNPA1+13	-0.042	-118821	0.61744	1.26844	0.0185	0.1102	0.01637	0.09752
RPN1+38	-0.042	-693822	0.34765	0.03927	0.2291	0.0056	0.02677	0.00065
H1FX-5	-0.042	85408	0.49403	0.30640	0.1537	0.6602	0.0598	0.25686
WDR83OS+20	-0.042	-364592	0.47531	0.18715	0.0873	0.1303	0.02604	0.03887
CALR-30	-0.042	309396	0.28100	0.04579	0.0945	0.0739	0.01072	0.00839
HDAC6+33	-0.043	-986987	0.30197	0.08694	0.0324	0.0000	0.00525	0
NFE2-17	-0.043	141679	0.58965	0.20859	0.0122	0.0701	0.00428	0.02457

H1FX-8	-0.043	104285	0.68357	0.47203	0.1190	0.6448	0.0676	0.36625
WDR83OS+42	-0.043	-565119	0.59250	0.37270	0.0351	0.0694	0.01649	0.03261
BAX+9	-0.043	-100571	0.79073	0.12027	0.0606	0.6801	0.01869	0.20974
CALR-6	-0.043	78189	0.54225	0.48008	0.2480	0.3459	0.12653	0.17648
JUNB+5	-0.043	-33764	0.84767	0.13244	0.0929	0.4233	0.03113	0.14184
CNBP+19	-0.044	-240455	0.45029	0.60875	0.0509	0.0582	0.02665	0.03049
CALR-10	-0.044	141025	1.21784	1.64686	0.3316	0.2799	0.46961	0.39635
WDR83OS+26	-0.044	-428390	2.01475	1.09289	0.0603	0.1303	0.08948	0.1934
WDR83OS+27	-0.044	-428739	1.97102	1.45559	0.0603	0.1303	0.10214	0.22076
CALR-1	-0.044	35879	0.31007	0.13274	0.4536	0.4531	0.09202	0.09192
FUT1+44	-0.044	-578109	0.36270	0.18599	0.0506	0.0144	0.01314	0.00375
BCAT2+10	-0.044	-81016	1.08052	1.76018	0.0395	0.3022	0.05447	0.41672
RAD23A+11	-0.044	-188082	0.84767	0.13244	0.2753	0.1459	0.09224	0.04887
JUNB-5	-0.044	117247	0.52492	0.16440	0.0252	0.0785	0.0074	0.02307
RAB7A+12	-0.044	-178536	1.56343	4.21809	0.4572	0.2957	1.1741	0.75936
DHPS+32	-0.044	-481992	1.64700	4.70519	0.0673	0.0928	0.18735	0.25834
DHPS+33	-0.044	-482804	1.14509	1.78199	0.0673	0.0928	0.09614	0.13256
CNBP+44	-0.044	-743260	0.37016	0.22193	0.0325	0.0196	0.00931	0.00562
PQBP1-16	-0.045	277726	0.77354	0.38502	0.0299	0.1445	0.01632	0.07886
NFE2+25	-0.045	-401351	0.18028	0.01449	0.0000	0.0040	0	0.0002
FTL+19	-0.045	-190699	0.21060	0.08354	0.0353	0.1305	0.00468	0.01731
RNASEH2A-8	-0.045	171412	0.69199	0.18309	0.0838	0.0910	0.02983	0.0324
FUT1+19	-0.045	-197629	0.55352	0.68700	0.1140	0.1886	0.0703	0.1163
NUCB1+6	-0.045	-45761	0.79073	0.12027	0.2961	0.8296	0.09131	0.25583
SEC61A1-9	-0.045	174621	0.31187	0.13201	0.1186	0.2684	0.02406	0.05447
CALR-18	-0.045	224470	2.01447	4.08340	0.1515	0.1574	0.43451	0.45144
SEC61A1-31	-0.046	404910	0.37526	0.08151	0.0983	0.1702	0.01719	0.02976
RPN1+39	-0.046	-710449	0.18631	0.00000	0.2020	0.0056	0	0
NFE2+11	-0.046	-93384	0.70933	0.50978	0.0292	0.0824	0.01756	0.04953
RAD23A+9	-0.046	-163211	1.54032	1.80923	0.2994	0.2130	0.49981	0.35552
COPZ1+1	-0.046	-17854	1.47777	1.36966	0.8015	1.0000	1.14028	1.42269
CNBP+7	-0.046	-61955	0.59421	0.19910	0.3720	0.8692	0.12795	0.29898
WDR83OS+37	-0.047	-521731	0.34326	0.07245	0.0244	0.0890	0.00385	0.01404
GATA1-12	-0.047	162255	0.39277	0.63360	0.0480	0.5054	0.02395	0.25211
RAB7A-26	-0.047	500476	0.48966	0.29923	0.1241	0.0418	0.0475	0.01599
CALR-19	-0.047	225280	1.64700	4.70519	0.1515	0.1574	0.42174	0.43817
CALR-20	-0.047	226092	1.14509	1.78199	0.1515	0.1574	0.21641	0.22484
NFE2+6	-0.048	-59991	0.75194	0.48326	0.0658	0.6565	0.03967	0.39573
DHPS+57	-0.048	-855808	0.60170	0.25069	0.0305	0.0000	0.01185	0
H1FX+25	-0.048	-370886	0.19264	0.04920	0.0563	0.2653	0.00548	0.02583
WDR83OS+9	-0.048	-163048	0.96819	0.11339	0.3119	0.3547	0.10334	0.11752
C19orf43+13	-0.049	-243250	0.69199	0.18309	0.0416	0.0692	0.01481	0.02463
PLP2+29	-0.049	-534846	0.17237	0.18613	0.0182	0.1014	0.00326	0.01817
NFE2+22	-0.049	-302329	0.27330	0.07245	0.0034	0.0111	0.00048	0.00156
RAB7A+5	-0.049	-140642	0.57953	0.85278	0.5300	0.3951	0.37259	0.27773
PPP1R15A-33	-0.049	459378	0.36270	0.18599	0.0439	0.0363	0.0114	0.00942
GATA1-16	-0.049	297059	0.32571	0.08694	0.0186	0.2733	0.00313	0.04599
CNBP-65	-0.050	956978	0.31187	0.13201	0.0160	0.0000	0.00325	0
NFE2-24	-0.050	351165	0.77052	0.31684	0.0083	0.0224	0.0041	0.01107
BCAT2+5	-0.050	-43225	0.79073	0.12027	0.0784	0.3528	0.02418	0.1088

FTL-5	-0.050	108754	0.93844	0.49007	0.0321	0.2155	0.02177	0.14617
PRDX2+2	-0.050	-30789	0.96819	0.11339	0.5842	0.6819	0.19357	0.22593
HNRNPA1-11	-0.050	89743	1.03165	0.28873	0.0697	0.4347	0.03804	0.23723
RPN1-41	-0.051	455293	0.17428	0.21222	0.1736	0.1178	0.03339	0.02265
CNBP+35	-0.051	-506593	0.25861	0.12889	0.0419	0.0415	0.00765	0.00758
JUNB-42	-0.051	590655	0.94017	0.10774	0.0050	0.0014	0.00159	0.00045
JUNB-28	-0.051	381019	0.46950	0.20896	0.0054	0.0305	0.00169	0.00956
PPP1R15A-14	-0.051	201671	0.93844	0.49007	0.1346	0.1745	0.09128	0.11834
CNBP-39	-0.052	678819	0.71928	1.40733	0.0265	0.0010	0.02666	0.00101
PQBP1-10	-0.052	242081	0.40534	0.21591	0.0160	0.1852	0.00473	0.0548
RAD23A-37	-0.053	451003	0.73862	0.42907	0.0369	0.0369	0.02077	0.02077
H1FX+13	-0.053	-174116	0.57086	0.25735	0.1137	0.3354	0.04358	0.12857
JUNB-39	-0.054	485847	0.53624	0.07245	0.0015	0.0133	0.0003	0.00261
HBE1-17	-0.054	633072	0.40405	0.14621	0.0094	0.1163	0.00228	0.02826
COPZ1+30	-0.054	-533166	0.14834	0.02898	0.0415	0.0152	0.00272	0.001
FUT1-7	-0.055	67920	0.22362	0.04796	0.3579	0.7818	0.03707	0.08097
BCAT2-37	-0.056	395466	0.97125	0.03456	0.0053	0.0228	0.00097	0.00418
JUNB-2	-0.056	41204	0.96819	0.11339	0.0709	0.4058	0.02349	0.13447
JUNB+15	-0.056	-589026	0.17898	0.00000	0.0084	0.0071	0	0
CALR-39	-0.057	462994	0.68945	0.68099	0.0586	0.0336	0.04015	0.02305
WDR83OS+52	-0.057	-731942	0.68945	0.68099	0.0251	0.0042	0.0172	0.00286
CNBP+38	-0.057	-610174	0.64832	0.14860	0.0241	0.0378	0.00748	0.01174
DHPS+52	-0.059	-719706	0.68945	0.68099	0.0222	0.0042	0.01521	0.0029
CALR-3	-0.059	45172	0.56166	0.19686	0.2909	0.3915	0.09673	0.13019
C19orf43+51	-0.059	-693763	0.34986	0.07919	0.0159	0.0000	0.00265	0
NFE2-18	-0.059	260720	0.36708	0.14831	0.0120	0.0539	0.0028	0.01257
FTL+26	-0.059	-267089	0.61356	0.33111	0.0244	0.0930	0.011	0.0419
RAB7A+4	-0.060	-135013	0.24689	0.15309	0.5772	0.4454	0.11222	0.08659
RAB7A+43	-0.060	-530552	0.17428	0.21222	0.2604	0.1039	0.05008	0.01998
HDAC6+32	-0.060	-984427	0.54732	0.07245	0.0324	0.0000	0.00645	0
HBE1+22	-0.060	-321743	0.65083	0.67135	0.0141	0.1463	0.00932	0.09668
DHPS-3	-0.060	137284	1.54310	6.53275	0.3661	0.2564	1.16237	0.81418
WDR83OS+53	-0.060	-758887	0.34986	0.07919	0.0389	0.0000	0.00647	0
HBE1+27	-0.061	-540520	0.62101	1.52522	0.0143	0.1166	0.01392	0.11345
MYC-59	-0.061	617741	0.22235	0.22787	0.1946	0.1478	0.0438	0.03328
H1FX-51	-0.061	832944	1.19538	2.19563	0.0257	0.0000	0.04164	0
JUNB-30	-0.061	399887	0.34326	0.07245	0.0085	0.0287	0.00134	0.00453
FUT1+25	-0.061	-320402	0.93844	0.49007	0.1244	0.0727	0.08436	0.04932
DNASE2-17	-0.062	469514	0.39720	0.24446	0.0087	0.0348	0.00271	0.01083
RAB7A-44	-0.062	743100	0.29207	0.21352	0.2404	0.0110	0.06003	0.00275
CALR-13	-0.062	159442	2.01475	1.09289	0.3533	0.2566	0.52425	0.38076
CALR-14	-0.062	159791	1.97102	1.45559	0.3533	0.2566	0.59842	0.43463
RAB7A+16	-0.062	-220987	0.71928	1.40733	0.4390	0.2957	0.44168	0.29751
FUT1-31	-0.062	338063	0.97125	0.03456	0.0494	0.0963	0.00905	0.01764
COPZ1+27	-0.062	-376006	0.85567	0.40668	0.0497	0.0202	0.02932	0.01192
HBE1-10	-0.062	145903	0.62345	0.40146	0.0511	0.4400	0.02556	0.22015
PLP2+16	-0.063	-287917	0.17210	0.01449	0.0122	0.2830	0.00061	0.01413
HBE1+33	-0.063	-982067	0.53024	0.34850	0.0044	0.0000	0.00189	0
GATA1+25	-0.063	-760739	0.32848	0.07267	0.0086	0.0000	0.00133	0
NFE2-3	-0.064	13397	1.07689	1.68222	0.1503	0.6827	0.2023	0.91892

DHPS+38	-0.064	-512823	0.36439	0.06376	0.0584	0.0791	0.0089	0.01206
BCAT2+34	-0.064	-414023	0.44413	0.06687	0.0146	0.0235	0.00252	0.00405
BCAT2-5	-0.064	36454	0.21060	0.08354	0.0561	0.2191	0.00744	0.02906
DNASE2+29	-0.065	-314344	0.33126	0.09441	0.0113	0.0962	0.002	0.01701
DHPS+28	-0.065	-422783	0.91245	0.91559	0.0892	0.0928	0.08153	0.08482
RAD23A-29	-0.065	288957	0.59250	0.37270	0.1155	0.0983	0.05428	0.04621
BAX+38	-0.066	-391243	0.60283	2.12491	0.0107	0.0356	0.01211	0.04025
BAX+4	-0.066	-62780	1.08052	1.76018	0.0869	0.8033	0.11984	1.10778
JUNB-8	-0.066	186530	0.69199	0.18309	0.0116	0.0416	0.00413	0.01481
JUNB-23	-0.066	364210	1.57147	0.72808	0.0054	0.0305	0.00578	0.03266
CNBP+48	-0.067	-864984	0.31343	0.08694	0.0445	0.0164	0.00735	0.00271
FTL+20	-0.067	-199298	0.47587	0.14020	0.0322	0.1262	0.00832	0.0326
NFE2+9	-0.067	-76033	0.60701	0.44428	0.0392	0.2316	0.02036	0.12029
JUNB-13	-0.067	242748	0.47531	0.18715	0.0093	0.0377	0.00277	0.01125
NFE2-4	-0.067	73484	0.49767	0.19352	0.0390	0.4248	0.0121	0.13182
HBE1-6	-0.067	98095	0.35967	0.24149	0.0427	0.4791	0.01258	0.14121
HBE1+11	-0.067	-99907	0.26138	0.09093	0.0501	0.5310	0.00772	0.08186
HNRNPA1-3	-0.068	13680	1.39090	2.59115	0.3389	0.9620	0.64338	1.82635
RAB7A-30	-0.069	519787	0.59421	0.19910	0.2101	0.0340	0.07227	0.01168
NFE2+17	-0.069	-189042	0.19188	0.01449	0.0129	0.0240	0.00068	0.00127
HDAC6+2	-0.069	-12276	0.73199	1.50783	0.7329	0.9891	0.76997	1.03909
CALR-9	-0.069	122962	0.66756	0.30894	0.2696	0.3021	0.12243	0.13721
RAB7A-20	-0.069	375802	0.26525	0.29445	0.1971	0.1173	0.05508	0.03277
JUNB-14	-0.070	260344	0.89935	0.11107	0.0086	0.0373	0.00272	0.01179
PLP2+38	-0.070	-674959	0.33477	0.17389	0.0082	0.0122	0.00198	0.00294
HBE1-16	-0.071	611102	0.83031	2.39770	0.0086	0.1163	0.01213	0.16405
CALR+5	-0.071	-105900	0.96819	0.11339	0.4275	0.4130	0.14165	0.13684
CALR+20	-0.072	-526592	0.39720	0.24446	0.0373	0.0405	0.01162	0.01263
HBE1+9	-0.073	-93749	0.35233	0.87256	0.0280	0.5404	0.01552	0.29961
HBE1+10	-0.073	-94212	0.36006	0.86517	0.0280	0.5404	0.01563	0.3016
FTL+13	-0.073	-145640	0.28128	0.05854	0.0633	0.5155	0.00812	0.06615
CNBP+34	-0.073	-503196	0.19264	0.04920	0.0289	0.0415	0.00281	0.00404
JUNB+14	-0.073	-379488	0.39720	0.24446	0.0072	0.0257	0.00224	0.00801
HNRNPA1+14	-0.073	-121331	0.58965	0.20859	0.0173	0.1102	0.00607	0.03865
HDAC6+13	-0.074	-254442	0.60009	0.13462	0.0679	0.1091	0.0193	0.03101
RAD23A-39	-0.075	455780	0.68945	0.68099	0.0500	0.0369	0.03426	0.02528
FUT1+28	-0.075	-353060	0.52055	0.18367	0.0518	0.0649	0.01602	0.02008
PPP1R15A-18	-0.076	260859	0.80074	0.24431	0.0824	0.1277	0.03645	0.0565
PPP1R15A-19	-0.076	261318	0.86882	0.22779	0.0824	0.1266	0.03666	0.05631
HDAC6-17	-0.076	337977	0.40534	0.21591	0.0972	0.1743	0.02875	0.05157
C19orf43+6	-0.076	-80555	0.37844	0.18113	0.2369	0.3383	0.06202	0.08857
H1FX+34	-0.078	-515874	0.19653	0.05767	0.0420	0.2403	0.00447	0.02558
HBE1-3	-0.078	26981	1.35564	3.14976	0.1284	0.9644	0.26532	1.99289
CALR-8	-0.078	113240	0.89935	0.11107	0.2605	0.3105	0.08233	0.09812
PLP2+18	-0.079	-307457	0.30903	0.08245	0.0153	0.2830	0.00244	0.04518
FUT1+16	-0.079	-138419	1.08052	1.76018	0.1172	0.2209	0.16163	0.30464
RAD23A-25	-0.080	248897	0.36439	0.06376	0.1795	0.1432	0.02736	0.02183
PPP1R15A-37	-0.080	519671	0.78564	0.32995	0.0421	0.0305	0.02143	0.01555
CALR-37	-0.081	458217	0.73862	0.42907	0.0529	0.0336	0.02978	0.01893
WDR83OS-7	-0.081	257644	0.39720	0.24446	0.2608	0.4689	0.08127	0.14612

PQBP1+24	-0.082	-401034	0.33477	0.17389	0.0170	0.0220	0.0041	0.00531
CALR-36	-0.083	443551	0.94017	0.10774	0.0515	0.0336	0.01639	0.0107
COPZ1+2	-0.083	-20614	2.04421	3.83242	0.7984	0.9906	2.2347	2.77257
RNASEH2A-50	-0.084	731082	0.60170	0.25069	0.0305	0.0020	0.01185	0.00078
CALR+11	-0.084	-180868	0.84767	0.13244	0.1903	0.1458	0.06376	0.04884
NFE2+10	-0.085	-82315	0.65085	0.82416	0.0388	0.2240	0.02842	0.16408
HDAC6-35	-0.086	952410	0.21738	0.07006	0.0357	0.0000	0.00441	0
PPP1R15A+1	-0.086	-18103	0.79073	0.12027	0.7783	1.0000	0.24002	0.30839
HBE1-5	-0.088	73831	0.68451	0.68208	0.0558	0.5155	0.03813	0.35224
DHPS+53	-0.089	-746651	0.34986	0.07919	0.0659	0.0000	0.01097	0
WDR83OS+3	-0.090	-88080	0.84767	0.13244	0.4374	0.6884	0.14656	0.23066
NFE2+23	-0.091	-357802	0.33027	0.06187	0.0018	0.0059	0.00026	0.00085
NFE2+27	-0.093	-448341	0.18359	0.01761	0.0024	0.0022	0.00014	0.00012
HNRNPA1+1	-0.094	-53136	0.49767	0.19352	0.0873	0.6429	0.02709	0.19952
SEC61A1-37	-0.095	480813	0.57481	0.38487	0.1073	0.0807	0.05047	0.03797
RAB7A+44	-0.095	-555062	0.41950	0.12962	0.2856	0.0960	0.0666	0.02239
RPN1+30	-0.095	-579993	0.49403	0.30640	0.1229	0.0337	0.04782	0.01311
RAB7A+35	-0.096	-371911	0.29986	0.29010	0.2131	0.2430	0.06285	0.07167
CALR-24	-0.096	252783	0.34326	0.07245	0.1090	0.1307	0.01719	0.02061
FUT1+36	-0.097	-454355	0.72662	0.22555	0.0930	0.0263	0.03765	0.01066
FUT1+37	-0.097	-454827	0.63712	0.04753	0.0930	0.0263	0.01618	0.00458
CALR-4	-0.099	46842	1.06616	0.83749	0.3149	0.3915	0.29756	0.36997
PQBP1+8	-0.101	-103370	1.43163	2.90212	0.0725	0.5899	0.14778	1.20247
JUNB-7	-0.103	182983	0.31007	0.13274	0.0135	0.0416	0.00274	0.00844
FUT1-21	-0.104	199671	0.78293	0.11593	0.0694	0.1347	0.02091	0.04059
HBE1+32	-0.105	-981154	0.37787	0.16135	0.0044	0.0000	0.00109	0
PPP1R15A-29	-0.107	352695	0.44413	0.06687	0.0381	0.0720	0.00657	0.01241
HDAC6+30	-0.107	-865305	1.15321	0.19613	0.0313	0.0000	0.01489	0
PLP2+23	-0.107	-382097	0.73199	1.50783	0.0126	0.1258	0.01324	0.1322
CALR+16	-0.112	-393996	1.54310	6.53275	0.0634	0.0619	0.2013	0.19653
BCAT2+13	-0.113	-140226	0.55352	0.68700	0.0405	0.2797	0.02497	0.17246
PPP1R15A+42	-0.113	-456794	0.97125	0.03456	0.0320	0.0497	0.00586	0.00911
JUNB-9	-0.114	192276	0.56166	0.19686	0.0086	0.0416	0.00286	0.01383
CALR+10	-0.115	-177865	0.44079	0.07245	0.2092	0.1508	0.03739	0.02695
CALR+15	-0.116	-374352	0.44863	0.08694	0.0784	0.0681	0.01548	0.01346
JUNB+9	-0.117	-227248	0.44863	0.08694	0.0165	0.0345	0.00326	0.00681
FUT1+22	-0.118	-230003	0.33213	0.13027	0.1292	0.1250	0.02687	0.026
JUNB-37	-0.119	469757	0.42462	0.45928	0.0033	0.0133	0.00146	0.00586
JUNB-45	-0.120	610098	0.68945	0.68099	0.0045	0.0014	0.00308	0.00096
PLP2+24	-0.122	-388768	1.26353	2.66940	0.0107	0.1258	0.01965	0.2311
RPN1-12	-0.126	117695	0.57481	0.38487	0.6248	0.3642	0.29387	0.17128
RAD23A-44	-0.126	591882	0.60170	0.25069	0.0612	0.0336	0.02377	0.01304
CALR-27	-0.132	274422	0.41749	0.12498	0.0764	0.1073	0.01745	0.0245
CALR-44	-0.133	599096	0.60170	0.25069	0.0278	0.0306	0.0108	0.0119
PPP1R15A-11	-0.144	111272	0.33213	0.13027	0.3203	0.3002	0.06662	0.06244
WDR83OS-3	-0.151	125048	1.54310	6.53275	0.5983	0.5948	1.89961	1.8885
WDR83OS+57	-0.159	-868044	0.60170	0.25069	0.0218	0.0000	0.00847	0
GATA1-29	-0.159	457814	0.85965	0.49442	0.0142	0.0593	0.00926	0.03866
H1FX+26	-0.170	-374283	0.25861	0.12889	0.0474	0.2653	0.00865	0.04844
PQBP1-7	-0.180	185721	0.32571	0.08694	0.0252	0.3264	0.00424	0.05492

GATA1-3	-0.213	55321	0.18938	0.12208	0.0545	0.8822	0.00829	0.13414
JUNB+7	-0.245	-74399	0.48445	0.17635	0.0686	0.1581	0.02005	0.04621
HBE1+15	-0.255	-234335	0.75545	2.36111	0.0170	0.1823	0.0227	0.24352

Supplementary Table 10. Peripheral enhancer perturbation screen gRNA list.

The teble is too large to be included here. Please refer to the future publication of peripheral enhancer screen.

Supplementary Table 11. EOMES, GATA6 and SOX17 ChIP-MS data.

Accession	Gene name	DE-24h EOMES/IgG		DE-48h SOX17/IgG		DE-48h GATA6/IgG	
		log2FC	-log10 (p-value)	log2FC	-log10 (p-value)	log2FC	-log10 (p-value)
A0A075B6H9	IGLV4-69	-8.90	3.89	-9.76	3.49	-9.61	3.48
A0A075B6I1	IGLV4-60	-10.53	4.48	-13.68	8.22	-10.96	2.88
A0A075B6S5	IGKV1-27	-11.94	3.09	-12.19	2.76	-5.55	3.79
A0A087WW87	IGKV2-40	6.66	2.95	1.06	1.20	4.71	1.07
A0A0A0MRZ8	IGKV3D-11	-1.83	5.48	-2.57	1.27	1.33	0.65
A0A0B4J1V0	IGHV3-15	1.33	0.91	-2.25	1.03	1.56	0.64
A0A0B4J2D9	IGKV1D-13	-9.95	7.68	-7.62	4.92	-8.81	2.62
A0A0C4DH25	IGKV3D-20	-1.46	2.97	-1.53	2.72	0.00	0.00
A0A0C4DH72	IGKV1-6	-5.12	2.05	-8.66	2.86	-5.68	3.28
A0AV96	RBM47	2.52	0.99	-3.04	1.44	-5.00	9.25
A0M8Q6	IGLC7	5.29	4.94	3.65	2.15	7.90	8.54
A1L020	MEX3A	1.88	0.94	1.22	0.97	3.70	8.50
A2NJV5	IGKV2-29	2.61	6.07	-0.45	0.19	-0.37	0.14
A3KN83	SBNO1	1.35	2.29	-0.08	0.01	3.25	0.64
A6NDU8	C5orf51	4.60	3.79	-2.89	1.04	-0.47	0.15
A6NHR9	SMCHD1	2.07	0.93	2.52	2.83	1.68	1.59
B5ME19	EIF3CL	-1.24	0.65	0.77	0.45	-1.13	0.67
E9PRG8	C11orf98	2.60	2.06	5.92	4.95	4.97	5.05
O00139	KIF2A	2.78	3.59	0.08	0.10	-1.50	3.08
O00148	DDX39A	-1.12	1.30	4.11	1.66	2.59	1.13
O00151	PDLIM1	3.49	1.26	5.39	5.68	6.37	5.05
O00154	ACOT7	4.54	12.25	1.10	1.05	2.14	1.13
O00178	GTPBP1	2.35	0.95	2.30	0.99	0.35	1.82
O00193	SMAP	3.73	2.75	6.70	4.30	6.84	4.47
O00203	AP3B1	2.68	1.04	-3.32	0.94	-1.57	0.43
O00231	PSMD11	4.30	1.68	-2.18	1.46	-2.31	1.62
O00233	PSMD9	0.04	1.02	2.24	1.10	5.23	3.38
O00255	MEN1	-0.12	0.91	2.45	1.16	5.16	4.62
O00267	SUPT5H	-2.53	1.37	-0.54	0.31	1.29	0.72
O00268	TAF4	-0.14	1.52	1.92	0.99	1.46	1.60
O00273	DFFA	2.89	1.48	-0.83	1.05	-0.42	0.35
O00299	CLIC1	8.26	6.40	-1.54	5.57	-0.99	1.40
O00303	EIF3F	-1.64	1.54	-2.40	3.52	-2.50	6.24

O00311	CDC7	3.13	1.93	2.31	2.10	1.95	2.74
O00410	IPO5	0.97	1.57	-0.12	0.37	-3.24	2.00
O00422	SAP18	4.54	3.37	3.18	3.12	4.94	3.38
O00425	IGF2BP3	-1.20	0.39	-0.39	0.84	-2.87	1.21
O00442	RTCA	-3.48	1.09	0.52	0.16	3.69	1.63
O00479	HMGN4	2.68	2.50	2.78	1.00	0.68	2.19
O00482	NR5A2	-2.04	1.06	-4.83	6.27	0.80	2.28
O00487	PSMD14	6.35	8.41	1.56	1.16	1.68	1.20
O00488	ZNF593	0.00	0.03	1.77	1.11	1.72	1.19
O00512	BCL9	-5.15	7.02	2.32	1.06	3.19	1.19
O00541	PES1	3.97	8.97	5.64	11.42	5.47	9.69
O00560	SDCBP	-0.07	0.52	3.25	1.04	4.26	9.30
O00566	MPHOSPH10	4.56	2.70	2.66	0.98	4.31	2.90
O00567	NOP56	4.31	5.55	4.00	2.33	4.11	4.15
O00571	DDX3X	5.69	2.14	-0.13	0.09	1.48	0.88
O00762	UBE2C	0.14	0.09	3.51	6.20	3.10	3.68
O14497	ARID1A	6.62	7.49	7.06	9.18	7.49	9.67
O14503	BHLHE40	3.46	2.48	-1.51	1.84	0.69	2.00
O14519	CDK2AP1	1.13	0.96	-0.16	0.15	-2.65	1.69
O14530	TXNDC9	-3.23	1.66	-0.06	0.61	1.60	1.17
O14545	TRAFD1	-0.07	0.59	1.47	1.07	2.01	1.29
O14562	UBFD1	-1.20	0.31	-5.50	2.88	-4.33	2.21
O14578	CIT	2.04	3.49	1.05	4.52	2.50	8.98
O14607	UTY	-0.54	0.25	-4.37	4.18	-3.22	2.82
O14646	CHD1	-2.33	0.96	4.36	4.18	4.63	4.96
O14686	KMT2D	2.58	1.96	4.66	2.25	3.61	2.27
O14715	RGPD8	7.29	4.77	3.44	1.06	2.26	3.93
O14733	MAP2K7	1.85	1.42	-0.17	0.12	1.25	0.95
O14737	PDCD5	0.51	0.19	4.37	3.26	5.42	5.90
O14745	SLC9A3R1	0.56	0.78	0.44	0.63	-0.11	0.17
O14757	CHEK1	1.10	1.02	2.28	6.47	1.52	1.39
O14776	TCERG1	4.86	6.51	4.90	8.54	5.62	8.42
O14818	PSMA7	0.76	2.72	-4.36	4.15	-5.09	5.85
O14907	TAX1BP3	1.48	0.73	1.34	0.96	1.34	1.13
O14908	GIPC1	1.27	1.55	1.39	1.66	1.72	1.80
O14910	LIN7A	-0.11	1.16	2.03	1.10	2.26	1.17
O14929	HAT1	5.29	7.36	4.09	1.53	3.44	1.24
O14950	MYL12B	2.74	1.59	3.01	6.35	4.05	6.32
O14965	AURKA	-0.30	1.98	2.49	2.18	4.56	3.92
O14979	HNRNPDL	8.63	4.63	-0.18	0.68	-0.27	1.06
O14980	XPO1	7.49	5.92	1.22	0.45	3.52	1.82
O14981	BTAF1	0.96	4.68	1.35	1.96	2.99	1.62
O15014	ZNF609	-1.68	2.58	-2.21	3.55	-2.30	1.93
O15042	U2SURP	0.38	1.04	4.19	2.27	3.98	2.20
O15047	SETD1A	0.07	1.89	1.13	0.94	1.31	1.82
O15054	KDM6B	1.85	0.96	1.65	1.08	2.31	1.26
O15067	PFAS	2.69	8.36	2.74	2.67	2.73	3.44
O15119	TBX3	-0.10	0.84	1.02	0.42	2.66	1.83
O15160	POLR1C	3.02	2.00	-0.75	0.29	0.15	0.06
O15164	TRIM24	6.79	7.53	6.08	6.07	6.88	9.36

O15213	WDR46	2.36	3.81	4.63	4.07	4.53	3.52
O15226	NKRF	2.32	0.96	2.47	1.20	2.30	1.13
O15294	OGT	3.24	1.34	-0.18	0.68	-0.36	1.21
O15318	POLR3G	-0.01	0.13	-0.94	0.89	0.72	0.42
O15347	HMGB3	6.35	2.36	4.58	3.92	4.52	3.82
O15355	PPM1G	6.97	3.10	2.14	0.54	3.03	0.76
O15371	EIF3D	3.23	9.43	4.25	2.75	3.82	3.89
O15372	EIF3H	3.71	2.16	1.20	0.99	2.32	1.63
O15381	NVL	-1.11	1.67	0.40	0.50	-4.69	1.43
O15397	IPO8	0.65	0.95	0.86	1.15	1.19	1.22
O15417	TNRC18	0.78	7.69	-2.17	3.24	-2.25	2.65
O15446	CD3EAP	-1.45	0.53	0.35	0.18	0.54	0.28
O43143	DHX15	5.30	1.93	5.33	1.87	5.56	1.93
O43148	RNMT	2.68	0.96	-0.49	0.41	0.83	0.67
O43159	RRP8	-0.10	0.62	0.53	0.23	0.76	0.33
O43172	PRPF4	0.71	0.50	0.14	0.87	0.47	1.30
O43175	PHGDH	5.56	3.02	-0.53	0.17	-0.82	0.26
O43242	PSMD3	2.16	2.47	-3.03	2.72	-0.76	1.35
O43251	RBFOX2	5.58	7.01	2.30	0.66	3.45	0.98
O43252	PAPSS1	-0.11	1.85	-0.02	0.26	0.63	1.39
O43290	SART1	3.71	5.82	6.07	5.01	6.29	5.47
O43347	MSI1	-0.21	0.09	0.66	0.32	0.34	0.12
O43390	HNRNPR	7.70	6.39	4.57	5.93	5.43	4.76
O43395	PRPF3	-0.07	0.06	-2.51	1.89	-2.08	4.57
O43396	TXNL1	3.16	1.83	-0.39	0.76	-0.36	0.40
O43439	CBFA2T2	1.62	1.03	-1.20	0.68	1.66	2.70
O43447	PPIH	3.49	2.14	2.93	1.08	4.30	3.23
O43488	AKR7A2	3.13	5.00	1.05	0.60	0.36	0.19
O43491	EPB41L2	0.01	0.11	2.05	1.00	1.41	1.51
O43592	XPOT	-3.97	4.44	-4.52	6.01	-5.32	2.32
O43633	CHMP2A	4.78	5.05	5.26	4.39	2.80	1.09
O43660	PLRG1	4.94	5.59	5.79	6.60	6.18	4.81
O43665	RGS10	3.87	3.70	2.19	1.03	4.96	5.34
O43670	ZNF207	5.96	8.87	6.62	5.88	6.58	10.76
O43679	LDB2	3.03	1.93	1.58	2.25	0.46	0.19
O43684	BUB3	6.98	6.51	2.14	1.28	3.47	3.28
O43707	ACTN4	4.08	3.10	4.08	5.42	4.98	3.98
O43709	BUD23	3.10	5.45	1.35	0.79	0.15	0.07
O43719	HTATSF1	0.92	0.89	3.83	6.96	4.19	2.16
O43776	NARS	4.10	4.19	1.16	0.35	0.38	0.11
O43805	SSNA1	-0.02	0.25	0.20	1.23	2.41	4.62
O43809	NUDT21	6.16	1.68	-2.59	0.80	1.19	0.36
O43818	RRP9	2.15	1.42	0.19	0.13	-0.65	0.49
O43823	AKAP8	0.64	0.24	4.47	2.23	4.73	2.83
O43913	ORC5	1.98	2.68	1.07	2.29	2.01	1.93
O43929	ORC4	1.82	0.98	1.29	1.10	3.81	4.89
O60216	RAD21	1.05	0.83	1.29	1.21	-0.13	0.11
O60231	DHX16	0.41	0.62	3.81	1.46	3.32	5.12
O60244	MED14	5.25	10.13	1.63	1.05	1.57	1.10
O60264	SMARCA5	5.15	1.76	0.89	1.02	1.83	3.21

O60281	ZNF292	-0.12	2.85	1.92	0.96	3.84	5.88
O60287	URB1	-0.05	0.34	0.13	1.08	1.41	1.38
O60293	ZFC3H1	3.39	1.69	-2.85	1.89	-4.04	2.79
O60306	AQR	0.94	0.86	1.75	1.64	1.39	1.16
O60307	MAST3	-0.19	2.20	3.20	1.02	2.95	1.17
O60341	KDM1A	5.69	4.82	4.41	4.51	6.00	3.63
O60481	ZIC3	6.33	3.60	3.88	3.90	5.42	3.58
O60506	SYNCRIP	3.01	3.23	6.73	2.36	6.63	2.14
O60508	CDC40	-0.39	0.11	-4.93	4.39	-4.18	3.25
O60563	CCNT1	0.53	0.29	-0.08	0.04	2.83	1.32
O60583	CCNT2	0.39	0.45	-2.14	1.44	0.65	6.86
O60684	KPNA6	1.02	6.36	-2.44	2.79	-2.37	2.62
O60701	UGDH	5.57	4.49	2.77	2.24	3.93	3.32
O60716	CTNND1	2.06	1.53	-5.52	3.03	-3.21	1.37
O60763	USO1	1.55	0.96	0.17	1.47	1.30	1.44
O60812	HNRNPCL1	4.77	6.20	6.45	16.26	6.33	5.39
O60814	HIST1H2BK	1.70	1.87	3.62	1.34	2.07	0.79
O60828	PQBP1	5.64	1.81	0.33	0.50	0.93	1.53
O60832	DKC1	3.19	2.38	1.75	0.73	2.07	0.88
O60869	EDF1	4.40	5.12	3.49	1.46	3.91	1.54
O60870	KIN	1.43	1.06	2.65	4.62	4.10	4.45
O60884	DNAJA2	3.12	2.27	0.28	0.16	0.69	2.78
O60885	BRD4	0.35	0.54	3.26	1.34	3.48	1.42
O60934	NBN	2.20	4.77	3.57	3.82	3.12	2.42
O60942	RNGTT	6.17	3.76	2.15	2.54	0.82	2.42
O75083	WDR1	3.40	2.23	4.53	3.72	2.27	1.12
O75131	CPNE3	6.54	7.01	6.36	3.45	7.38	10.90
O75132	ZBED4	-1.08	0.35	2.71	1.10	2.55	1.06
O75150	RNF40	4.81	2.04	0.10	1.19	-0.36	0.89
O75152	ZC3H11A	-5.13	2.47	0.32	0.17	2.25	1.28
O75155	CAND2	2.92	0.95	0.11	0.72	0.33	3.48
O75190	DNAJB6	0.54	2.26	-0.27	0.80	-0.53	1.49
O75312	ZPR1	-0.06	0.03	-0.17	0.07	0.44	0.19
O75340	PDCD6	4.67	4.41	4.13	4.59	4.08	3.28
O75347	TBCA	-0.15	0.28	-0.24	0.70	0.11	0.14
O75362	ZNF217	4.83	2.91	5.09	2.52	5.71	2.42
O75367	H2AFY	1.23	1.40	5.56	4.01	4.45	2.95
O75369	FLNB	4.23	3.34	3.20	2.84	4.00	4.50
O75376	NCOR1	0.69	0.27	5.68	3.05	5.08	2.33
O75391	SPAG7	1.86	1.17	2.94	4.21	3.64	6.36
O75400	PRPF40A	2.55	1.05	3.35	3.73	3.59	3.50
O75448	MED24	-0.18	1.75	0.12	0.67	1.40	1.22
O75475	PSIP1	5.87	3.11	8.45	5.49	8.27	12.56
O75494	SRSF10	2.99	1.25	1.05	0.60	0.91	0.51
O75496	GMNN	0.88	1.03	-2.91	1.60	-4.40	3.99
O75525	KHDRBS3	1.25	6.62	-0.25	0.11	-0.70	0.51
O75530	EED	3.60	3.40	-2.38	0.93	-1.00	0.38
O75531	BANF1	4.82	5.35	3.51	1.26	4.04	1.41
O75533	SF3B1	4.03	2.67	3.28	3.50	3.01	4.22
O75534	CSDE1	0.70	0.38	0.18	1.17	2.35	3.54

O75554	WBP4	-2.70	1.69	2.16	0.90	1.94	0.82
O75593	FOXH1	5.26	8.87	-3.86	3.43	0.58	0.62
O75607	NPM3	8.89	5.60	5.59	1.75	5.57	1.61
O75626	PRDM1	5.30	6.70	0.36	0.43	0.94	1.99
O75643	SNRNP200	3.88	1.59	-0.65	0.43	-0.39	0.25
O75691	UTP20	0.29	0.16	1.63	1.31	-0.42	0.32
O75694	NUP155	-1.34	0.61	0.13	2.94	1.03	4.09
O75717	WDHD1	3.51	2.44	6.11	4.46	5.34	1.91
O75820	ZNF189	1.26	1.01	1.22	1.03	2.77	3.05
O75821	EIF3G	-0.16	1.24	0.21	2.26	3.97	3.14
O75874	IDH1	-0.32	0.35	0.56	2.01	0.48	1.53
O75909	CCNK	2.10	1.02	2.64	5.62	2.12	2.07
O75925	PIAS1	6.28	5.79	3.73	6.88	4.87	3.03
O75928	PIAS2	-0.13	1.43	2.08	1.07	4.57	7.23
O75934	BCAS2	4.21	7.15	4.09	3.15	4.97	6.52
O75937	DNAJC8	5.19	4.76	0.16	0.24	-0.07	0.15
O75940	SMNDC1	4.72	4.95	4.02	1.17	4.01	1.15
O76003	GLRX3	4.68	2.84	4.57	3.27	5.66	3.34
O76021	RSL1D1	1.78	0.92	6.55	4.23	4.93	3.62
O94761	RECQL4	-0.05	0.65	0.11	0.88	0.34	1.85
O94776	MTA2	-1.91	2.73	-0.30	0.22	0.09	0.07
O94842	TOX4	1.85	0.95	-0.27	0.11	1.43	0.74
O94880	PHF14	1.15	2.81	2.60	2.99	4.53	5.11
O94888	UBXN7	-5.43	2.15	-0.12	0.17	0.24	0.64
O94906	PRPF6	-3.23	3.81	1.85	2.25	-0.70	0.26
O94913	PCF11	2.32	3.77	4.29	5.54	4.73	6.60
O94953	KDM4B	-0.12	0.91	3.78	6.04	4.51	7.73
O94979	SEC31A	2.54	2.44	-1.18	0.61	0.32	0.15
O94992	HEXIM1	0.58	0.22	2.23	1.10	1.22	0.60
O95071	UBR5	1.18	0.86	-0.74	0.28	-0.56	0.23
O95081	AGFG2	-2.41	1.01	-2.33	0.96	0.43	0.13
O95104	SCAF4	2.98	3.81	2.88	1.32	0.03	0.01
O95125	ZNF202	1.49	0.87	-0.38	0.14	1.45	0.66
O95218	ZRANB2	2.88	11.91	3.59	2.42	5.08	9.85
O95232	LUC7L3	6.90	5.43	1.93	2.93	4.14	2.48
O95235	KIF20A	1.57	0.83	0.65	0.65	0.50	0.54
O95239	KIF4A	4.97	7.17	5.19	10.81	5.95	7.36
O95251	KAT7	1.63	0.93	1.65	0.70	1.58	0.67
O95319	CELF2	-0.07	0.69	3.99	2.93	5.35	4.38
O95347	SMC2	3.68	2.80	-1.69	0.78	-0.18	0.13
O95372	LYPLA2	5.83	9.84	4.52	3.53	6.30	5.09
O95373	IPO7	3.93	5.75	2.40	0.99	4.35	3.68
O95376	ARIH2	3.28	6.89	4.51	3.18	1.61	1.11
O95396	MOCS3	3.03	8.07	0.51	0.18	1.04	0.40
O95400	CD2BP2	3.88	2.78	2.99	1.49	2.91	1.38
O95409	ZIC2	5.53	1.99	0.93	1.20	2.90	3.43
O95429	BAG4	0.37	1.73	0.52	0.22	2.70	1.22
O95433	AHSA1	-0.03	0.38	0.06	0.46	3.68	2.65
O95453	PARN	2.42	1.95	2.95	1.60	1.85	1.04
O95478	NSA2	5.36	2.49	-2.35	1.80	-8.78	7.30

O95551	TDP2	2.87	2.32	2.36	2.44	3.24	3.23
O95619	YEATS4	2.49	2.52	1.68	1.93	2.90	3.60
O95639	CPSF4	-0.13	3.31	3.28	4.20	3.83	3.51
O95678	KRT75	-0.04	0.49	3.72	7.29	3.98	3.25
O95707	POP4	-0.09	0.61	0.05	0.59	0.43	4.95
O95747	OXSR1	-0.03	0.30	-0.04	0.27	0.30	9.32
O95758	PTBP3	-0.97	1.95	-1.88	2.82	-1.51	3.13
O95777	LSM8	4.50	4.01	-0.29	0.36	0.90	1.48
O95785	WIZ	2.43	1.30	1.42	2.16	1.87	2.52
O95789	ZMYM6	-0.22	0.13	-1.69	0.94	-0.05	0.02
O95793	STAU1	0.52	0.92	3.07	2.66	3.49	6.77
O95813	CER1	-0.01	0.14	3.37	3.63	3.84	6.74
O95926	SYF2	0.23	0.10	2.49	1.03	4.69	4.33
O95936	EOMES	8.02	4.13	5.19	4.11	6.73	3.57
O95983	MBD3	-0.82	0.98	-1.66	1.95	0.55	1.68
O95997	PTTG1	-0.15	3.11	-3.50	4.94	-2.00	1.69
O96006	ZBED1	1.29	1.09	2.03	1.07	4.34	5.10
O96017	CHEK2	3.79	3.60	2.24	0.75	1.24	0.41
O96019	ACTL6A	4.28	1.52	6.79	5.94	6.71	12.60
P00338	LDHA	2.61	0.78	2.39	3.39	1.33	4.34
P00390	GSR	2.38	0.95	0.09	4.09	3.96	1.04
P00403	MT-CO2	-0.05	0.52	0.13	1.07	2.60	1.11
P00441	SOD1	-2.40	1.54	1.02	0.89	0.17	1.34
P00450	CP	0.82	2.20	-0.22	0.67	-0.56	1.36
P00488	F13A1	-1.12	2.46	-0.93	0.43	-1.86	1.37
P00558	PGK1	5.18	5.84	0.46	1.70	0.59	2.03
P01008	SERPINC1	-0.17	0.59	-2.68	2.41	-2.98	5.34
P01009	SERPINA1	-0.10	0.24	1.26	0.42	2.71	1.14
P01023	A2M	-0.25	0.56	-2.66	2.34	-3.24	2.85
P01024	C3	-0.91	1.74	-2.09	1.02	-2.22	2.58
P01040	CSTA	-2.40	0.95	2.15	0.91	-0.32	0.11
P01593	IGKV1D-33	-7.23	9.59	-8.89	8.03	-5.76	1.71
P01599	IGKV1-17	-3.93	8.06	-5.78	6.22	-6.22	5.17
P01619	IGKV3-20	0.16	0.06	-2.74	6.65	-3.12	2.89
P01624	IGKV3-15	-2.09	7.42	-1.66	2.98	-1.03	1.63
P01700	IGLV1-47	-1.89	0.99	-1.15	0.49	1.74	0.45
P01743	IGHV1-46	1.15	0.34	4.19	8.72	1.99	1.28
P01780	IGHV3-7	2.63	4.96	-0.71	0.25	1.49	0.36
P01834	IGKC	2.38	0.62	-0.80	1.55	1.94	0.39
P01857	IGHG1	-1.70	3.65	-1.01	0.96	1.28	0.24
P01859	IGHG2	0.62	2.30	-2.64	1.69	-2.74	1.99
P01860	IGHG3	2.58	0.95	2.77	1.08	3.46	1.10
P01861	IGHG4	-0.76	1.45	-2.62	1.82	-1.96	1.96
P01876	IGHA1	1.51	0.90	-2.63	0.71	0.93	0.22
P02533	KRT14	1.73	0.96	0.55	0.15	0.60	0.17
P02538	KRT6A	-1.76	3.03	-0.59	0.50	-1.20	2.39
P02545	LMNA	1.49	1.37	4.28	3.96	4.36	3.47
P02647	APOA1	-1.41	0.95	-3.07	2.34	0.35	0.16
P02649	APOE	1.93	0.93	-0.40	0.12	-0.67	0.22
P02656	APOC3	0.24	0.93	-1.86	2.15	-2.75	4.97

P02748	C9	-6.85	2.26	-6.84	2.03	-4.42	4.28
P02753	RBP4	-0.34	1.21	-2.68	2.43	-3.17	2.53
P02768	ALB	0.19	0.88	-2.22	4.50	-2.40	3.53
P02787	TF	-2.97	1.93	1.57	0.81	3.52	1.65
P02792	FTL	-0.07	1.88	-2.18	1.00	-0.84	0.37
P04004	VTN	2.22	1.45	-2.38	0.84	-3.57	1.68
P04040	CAT	-1.55	1.05	1.20	0.43	1.87	1.22
P04075	ALDOA	5.26	2.46	5.16	2.52	4.39	2.52
P04080	CSTB	2.57	1.65	4.43	5.68	5.72	6.69
P04259	KRT6B	-5.91	3.23	1.61	1.40	-1.17	0.42
P04264	KRT1	-1.94	2.40	1.40	0.58	-0.06	0.05
P04406	GAPDH	2.03	4.85	1.42	1.57	1.91	1.99
P04792	HSPB1	5.92	4.13	5.32	2.42	4.91	2.10
P04843	RPN1	2.23	2.04	0.77	0.30	1.00	0.39
P04899	GNAI2	2.00	0.94	1.81	1.02	1.91	1.13
P05023	ATP1A1	1.35	0.96	1.15	0.57	1.30	0.68
P05089	ARG1	-0.12	2.28	2.43	1.00	2.19	1.27
P05109	S100A8	-3.05	2.29	-0.58	0.24	1.48	0.70
P05114	HMGN1	2.95	1.81	5.97	3.11	5.33	2.39
P05204	HMGN2	3.62	3.21	6.43	1.85	5.47	1.64
P05388	RPLP0	4.96	5.87	4.23	2.71	5.09	5.95
P05412	JUN	3.72	2.24	-1.87	1.54	-3.26	2.86
P05452	CLEC3B	-2.92	1.12	-1.16	0.35	-0.17	0.04
P05455	SSB	6.63	5.07	-0.05	0.06	-1.74	1.94
P05543	SERPINA7	-0.78	4.44	-2.65	2.28	-3.20	5.37
P05783	KRT18	1.84	4.33	0.41	0.51	0.48	0.61
P05787	KRT8	2.18	2.62	3.33	0.72	-0.65	1.34
P05937	CALB1	1.78	1.01	1.40	1.14	2.01	1.09
P06312	IGKV4-1	-6.69	7.73	0.73	0.43	0.19	0.15
P06396	GSN	-0.13	0.46	-0.07	0.09	-0.10	0.14
P06454	PTMA	0.00	0.00	1.64	0.94	0.34	2.03
P06493	CDK1	1.58	1.80	1.19	0.85	1.94	1.32
P06702	S100A9	-2.79	1.06	0.33	0.18	0.94	0.85
P06727	APOA4	-2.13	3.54	2.56	1.00	-0.41	0.13
P06730	EIF4E	4.17	4.74	4.97	4.99	4.74	5.12
P06733	ENO1	4.08	5.17	7.10	2.91	7.26	2.94
P06744	GPI	2.20	0.97	5.40	3.38	2.29	1.76
P06746	POLB	1.13	0.36	3.20	1.92	2.97	1.89
P06748	NPM1	2.81	3.14	4.52	2.15	3.71	1.89
P06753	TPM3	2.41	2.13	0.93	0.85	1.56	2.26
P07195	LDHB	7.73	6.57	2.48	1.87	3.18	3.66
P07237	P4HB	1.70	0.91	-1.57	0.54	-1.28	0.44
P07305	H1F0	2.31	1.52	5.33	2.16	3.85	1.72
P07355	ANXA2	3.30	3.20	0.61	1.38	-1.38	2.37
P07437	TUBB	3.16	2.86	1.97	2.90	2.03	2.56
P07477	PRSS1	-0.59	0.62	-0.75	0.50	-1.69	2.56
P07737	PFN1	4.54	8.23	2.38	1.03	2.49	1.06
P07814	EPRS	0.15	0.07	-1.42	1.02	-1.22	0.89
P07900	HSP90AA1	4.24	5.33	4.56	1.42	4.21	1.33
P07910	HNRNPC	3.23	3.21	4.49	5.59	4.64	4.67

P08047	SP1	0.94	0.82	1.97	1.02	2.95	4.22
P08238	HSP90AB1	1.35	3.56	-2.16	2.22	-2.33	3.82
P08243	ASNS	3.59	4.24	0.04	0.02	1.00	0.64
P08397	HMBS	1.73	1.87	3.29	4.06	3.61	8.52
P08579	SNRPB2	-0.11	0.57	-0.29	0.17	-0.26	0.52
P08621	SNRNP70	4.31	4.80	1.84	3.91	1.64	4.33
P08670	VIM	-0.11	1.96	-0.50	0.26	0.54	0.28
P08708	RPS17	1.51	1.50	1.17	1.67	0.80	2.28
P08727	KRT19	-0.96	1.27	-0.90	2.81	0.08	2.91
P08779	KRT16	-0.67	1.53	6.13	1.93	6.14	1.96
P08865	RPSA	4.28	2.06	0.41	0.31	0.45	0.60
P09012	SNRPA	2.65	5.03	3.76	2.63	6.54	3.47
P09211	GSTP1	8.93	2.87	6.33	1.57	7.44	1.77
P09234	SNRPC	4.08	1.85	1.33	3.07	-1.03	0.30
P09429	HMGB1	3.75	8.08	4.70	3.18	5.05	3.14
P09455	RBP1	4.49	9.03	3.22	2.42	1.85	1.57
P09651	HNRNPA1	4.74	8.73	5.75	6.81	6.03	4.62
P09661	SNRPA1	5.54	9.48	6.27	8.43	5.72	5.09
P09874	PARP1	2.41	4.95	5.34	3.66	5.75	3.49
P09884	POLA1	0.08	1.04	2.48	1.07	3.67	7.91
P09936	UCHL1	3.01	1.85	3.41	1.46	3.79	1.55
P09960	LTA4H	3.51	3.12	-1.04	2.48	-0.74	3.31
P0C0L4	C4A	-0.80	2.00	-1.31	1.82	-2.45	3.08
P0CG12	DERPC	1.44	1.10	3.17	1.08	5.92	4.59
P0DI83	RAB34	0.09	1.21	-7.81	4.12	-8.93	4.28
P0DMV9	HSPA1B	7.55	2.76	1.01	1.77	2.20	2.87
P0DOX6	Immunoglobulin	-0.40	4.25	-1.80	1.66	-1.21	1.42
P0DOX7	Immunoglobulin	2.30	1.38	1.84	1.44	5.12	1.03
P0DOX8	Immunoglobulin	-0.49	0.74	-0.99	0.57	0.49	0.19
P0DOY2	IGLC2	-0.01	0.00	-0.17	0.08	3.42	1.50
P0DP25	CALM3	1.33	0.85	1.08	0.93	0.61	0.75
P0DPK5	Putative	1.25	1.03	3.65	2.58	1.91	1.39
P10244	MYBL2	2.54	0.97	2.06	0.98	4.76	2.89
P10253	GAA	2.60	2.35	-0.48	0.18	0.28	0.10
P10412	HIST1H1E	0.07	0.06	6.77	1.36	4.81	1.01
P10588	NR2F6	3.58	3.62	-0.90	0.30	4.10	1.44
P10599	TXN	-0.05	1.33	2.11	1.94	1.81	1.88
P10768	ESD	3.64	2.45	2.87	2.37	2.87	2.26
P10809	HSPD1	2.88	2.21	0.22	0.14	-6.05	4.29
P11021	HSPA5	4.43	2.00	0.46	0.52	-0.16	0.16
P11142	HSPA8	3.10	2.57	3.59	3.08	3.92	3.59
P11169	SLC2A3	5.38	2.14	0.13	0.16	0.75	1.02
P11387	TOP1	2.96	0.99	6.22	5.04	5.34	3.59
P11388	TOP2A	3.23	3.03	2.39	1.97	2.16	1.94
P11586	MTHFD1	4.67	7.52	0.76	0.25	1.05	0.36
P11766	ADH5	3.10	1.01	-2.46	3.97	-4.23	1.61
P11940	PABPC1	1.24	1.85	1.97	1.97	1.91	1.85
P12004	PCNA	-1.82	2.68	4.15	5.36	2.98	1.06
P12035	KRT3	3.51	3.14	1.59	0.74	0.47	0.20
P12268	IMPDH2	2.12	0.96	1.03	1.03	2.08	1.06

P12270	TPR	2.57	0.91	3.80	1.28	3.99	1.33
P12277	CKB	8.35	6.35	1.09	2.93	1.48	2.93
P12814	ACTN1	-1.96	1.10	-4.16	3.15	-1.45	1.41
P12956	XRCC6	4.54	6.45	5.38	3.80	5.63	4.08
P13010	XRCC5	4.71	5.66	7.10	2.64	7.47	2.70
P13051	UNG	-0.06	0.56	1.47	0.96	5.54	2.18
P13056	NR2C1	3.34	5.73	-0.37	0.38	-0.15	0.90
P13489	RNH1	3.71	3.88	4.48	6.37	3.38	2.57
P13639	EEF2	4.24	3.00	1.44	1.05	1.38	0.89
P13645	KRT10	0.13	0.04	0.03	0.01	-0.44	0.13
P13646	KRT13	0.23	0.11	0.14	0.05	1.59	0.63
P13647	KRT5	-3.80	3.79	0.50	0.27	-0.56	0.33
P13667	PDIA4	1.69	0.99	1.02	0.52	-1.04	0.53
P13693	TPT1	6.16	7.39	4.63	4.12	3.60	2.81
P13797	PLS3	-0.16	1.78	0.85	0.84	0.23	1.36
P13929	ENO3	7.62	9.96	4.46	1.36	5.24	1.54
P13984	GTF2F2	4.18	2.27	6.81	7.85	6.36	3.62
P14324	FDPS	3.28	3.27	3.59	3.59	3.83	2.97
P14550	AKR1A1	4.61	3.74	4.66	3.87	4.26	5.27
P14618	PKM	-0.61	0.50	-3.26	4.95	-3.18	8.46
P14625	HSP90B1	2.22	2.47	1.41	1.42	1.32	1.49
P14678	SNRPB	6.02	2.99	8.56	5.53	8.48	10.00
P14859	POU2F1	2.16	7.47	-0.72	0.17	0.17	0.04
P14866	HNRNPL	1.55	1.76	1.52	1.66	1.44	1.52
P14868	DARS	3.08	2.51	3.51	5.16	3.29	4.30
P14923	JUP	-1.33	0.58	3.03	1.06	3.08	2.42
P15121	AKR1B1	3.01	0.97	5.27	2.49	6.30	5.73
P15311	EZR	11.27	6.17	4.32	3.57	4.20	5.97
P15374	UCHL3	0.87	0.59	1.23	0.71	0.85	0.48
P15531	NME1	4.86	2.87	4.03	2.04	4.36	2.03
P15880	RPS2	4.40	1.89	1.41	0.84	1.26	0.82
P15884	TCF4	2.69	1.32	0.88	0.23	1.33	0.35
P15923	TCF3	-0.44	0.67	0.62	0.24	2.71	1.56
P15924	DSP	2.09	1.50	3.81	2.13	2.70	1.94
P15927	RPA2	-0.32	0.31	-3.44	2.10	-2.31	2.07
P16104	H2AFX	-0.84	1.06	0.65	0.33	-1.67	0.87
P16152	CBR1	5.96	5.29	2.32	0.83	2.93	1.04
P16220	CREB1	4.91	2.79	1.01	0.27	0.62	0.17
P16401	HIST1H1B	1.57	1.53	7.12	1.46	5.32	1.13
P16402	HIST1H1D	-0.37	0.51	4.57	2.05	3.45	1.72
P16403	HIST1H1C	-0.15	0.18	5.46	1.56	4.02	1.22
P16615	ATP2A2	-3.40	0.98	0.15	0.85	2.65	1.06
P16949	STMN1	6.45	8.59	5.79	2.55	6.82	9.94
P17026	ZNF22	0.04	1.63	3.01	3.30	3.45	8.50
P17028	ZNF24	3.12	2.59	3.20	1.48	4.97	2.03
P17031	ZNF26	-0.11	0.82	1.29	1.08	0.40	2.19
P17036	ZNF3	0.91	0.80	0.17	2.61	0.46	4.07
P17096	HMGA1	5.10	3.12	0.26	0.74	-0.65	2.40
P17098	ZNF8	0.09	1.35	-3.33	2.62	-3.02	2.46
P17480	UBTF	8.99	7.45	5.62	4.25	5.66	12.39

P17535	JUND	2.67	6.56	1.90	1.08	3.78	4.85
P17544	ATF7	-3.29	2.49	-0.85	1.35	-0.42	0.65
P17676	CEBPB	4.41	5.62	-1.64	0.91	-1.39	0.78
P17844	DDX5	5.23	5.97	5.06	5.92	5.36	5.32
P17980	PSMC3	6.86	4.13	-0.73	0.39	2.96	1.53
P17987	TCP1	2.26	1.52	3.59	4.29	2.89	2.07
P18077	RPL35A	3.76	2.64	2.54	3.22	2.94	3.55
P18085	ARF4	3.33	2.13	3.26	5.10	2.20	1.85
P18124	RPL7	2.82	1.69	6.30	2.31	4.90	1.87
P18206	VCL	1.55	0.54	2.37	1.81	0.45	0.22
P18583	SON	1.95	0.94	0.57	0.78	0.89	1.27
P18615	NELFE	0.58	0.56	0.22	0.08	2.86	1.46
P18621	RPL17	6.85	3.81	4.86	2.19	3.92	1.72
P18669	PGAM1	2.62	1.79	0.87	0.31	-0.21	0.07
P18754	RCC1	6.55	4.86	7.57	3.24	7.51	2.90
P18887	XRCC1	3.43	2.64	1.79	2.31	4.63	3.73
P19013	KRT4	2.41	1.02	2.95	1.04	2.56	1.06
P19174	PLCG1	-2.66	1.05	-1.36	0.46	-1.18	0.39
P19338	NCL	0.75	1.61	7.14	2.12	6.69	1.99
P19387	POLR2C	-6.06	5.61	-3.72	2.36	-4.83	4.75
P19784	CSNK2A2	-0.11	1.11	-0.07	0.40	4.26	3.01
P19793	RXRA	2.87	2.65	-1.77	2.28	-1.57	2.16
P19823	ITIH2	0.19	0.23	-3.97	1.56	-2.71	4.03
P19827	ITIH1	-0.46	0.76	-1.15	0.69	-0.68	0.70
P20042	EIF2S2	0.91	0.91	0.33	2.18	1.81	1.42
P20073	ANXA7	4.23	10.78	-1.16	0.59	-1.04	0.53
P20248	CCNA2	-0.01	0.15	1.97	1.01	4.78	5.37
P20290	BTF3	0.15	0.26	2.07	0.64	0.79	0.23
P20585	MSH3	-0.26	4.60	-0.02	0.25	1.66	1.24
P20671	HIST1H2AD	0.59	0.61	5.88	1.73	4.01	1.27
P20700	LMNB1	2.75	7.03	2.13	4.84	2.49	7.42
P20930	FLG	-5.76	4.27	1.65	2.05	-0.41	0.72
P21333	FLNA	10.74	4.06	5.62	3.59	4.87	3.11
P21796	VDAC1	7.14	4.07	6.61	4.77	6.54	5.77
P22061	PCMT1	3.45	7.82	4.08	2.09	4.98	2.39
P22087	FBL	3.12	2.88	5.38	2.76	5.35	2.47
P22090	RPS4Y1	1.77	0.91	3.84	4.10	3.10	3.29
P22102	GART	1.95	1.54	1.52	3.39	1.17	1.53
P22234	PAICS	2.74	2.98	1.42	2.17	1.81	2.21
P22314	UBA1	5.41	4.29	3.40	1.53	3.32	1.50
P22626	HNRNPA2B1	2.93	3.56	5.36	4.49	5.86	4.79
P23193	TCEA1	6.06	4.68	6.51	5.39	7.23	11.51
P23246	SFPQ	6.33	6.70	6.11	4.98	6.71	4.73
P23284	PPIB	5.89	4.56	3.42	1.08	3.52	1.11
P23381	WARS	1.70	0.95	-0.98	0.34	-0.32	0.10
P23396	RPS3	2.88	1.80	2.13	1.43	1.48	1.15
P23497	SP100	-1.41	1.24	0.62	0.42	0.78	0.52
P23526	AHCY	3.27	3.38	-1.53	3.01	-1.76	4.06
P23528	CFL1	6.47	2.43	5.83	1.84	6.24	1.82
P23588	EIF4B	5.33	5.94	4.64	2.69	4.22	9.30

P23921	RRM1	5.18	6.23	5.50	2.36	3.81	1.67
P24534	EEF1B2	5.15	3.76	1.61	0.60	1.74	0.66
P24666	ACP1	6.23	8.96	4.54	4.13	5.90	4.18
P24928	POLR2A	2.07	2.24	4.05	4.36	4.54	10.09
P25205	MCM3	4.55	3.50	5.15	3.44	5.47	3.99
P25398	RPS12	5.32	2.82	6.44	3.29	5.85	4.62
P25440	BRD2	3.32	1.84	0.81	3.12	1.08	2.99
P25490	YY1	2.13	1.61	1.87	2.16	3.12	2.87
P25685	DNAJB1	1.35	0.92	3.70	7.44	4.25	7.59
P25705	ATP5F1A	5.24	7.38	-0.24	0.30	-0.01	0.01
P25786	PSMA1	3.72	4.15	3.84	2.51	4.17	2.10
P25787	PSMA2	0.04	0.06	-1.03	0.97	-0.87	1.78
P25788	PSMA3	0.72	0.98	0.16	2.44	1.50	1.28
P25789	PSMA4	6.66	4.89	1.88	1.68	4.05	3.38
P26038	MSN	5.30	5.09	2.95	7.60	2.59	2.25
P26196	DDX6	5.11	4.06	2.50	2.23	2.58	4.06
P26358	DNMT1	1.03	1.45	2.45	0.96	2.05	0.81
P26368	U2AF2	6.05	2.21	1.57	2.06	2.59	2.73
P26373	RPL13	1.36	1.73	3.70	3.10	3.01	3.23
P26583	HMGB2	7.18	3.35	8.34	3.29	8.85	3.36
P26599	PTBP1	4.18	5.12	3.84	5.35	4.42	5.44
P26639	TARS	4.15	7.85	2.42	3.39	0.50	1.19
P26641	EEF1G	2.24	2.85	3.52	3.26	3.68	3.30
P27169	PON1	1.02	1.04	-3.07	1.05	-2.79	0.97
P27348	YWHAQ	3.57	2.05	1.06	3.61	1.63	11.51
P27540	ARNT	-2.50	1.21	-4.89	4.26	-2.85	1.71
P27635	RPL10	5.03	2.38	4.15	2.54	2.82	1.88
P27694	RPA1	6.27	5.88	5.27	2.71	5.97	3.04
P27695	APEX1	6.32	7.34	-0.90	1.50	-2.07	1.86
P27708	CAD	0.68	0.43	0.61	0.97	1.14	5.89
P27816	MAP4	1.02	0.33	4.70	3.35	4.28	7.40
P28066	PSMA5	4.87	9.01	0.71	0.36	1.44	0.83
P28074	PSMB5	3.04	3.16	1.35	0.95	0.77	0.54
P28340	POLD1	3.84	10.40	2.11	1.97	6.01	3.95
P28347	TEAD1	9.31	4.57	-1.53	0.93	1.26	0.76
P28370	SMARCA1	1.61	0.95	2.56	1.82	2.92	1.14
P29083	GTF2E1	1.61	0.91	2.68	0.99	5.11	4.20
P29084	GTF2E2	3.27	3.87	-0.02	0.01	1.71	1.98
P29373	CRABP2	5.47	10.16	0.35	0.12	1.57	0.73
P29401	TKT	4.83	9.26	6.89	2.66	6.92	2.68
P29508	SERPINB3	1.27	0.92	0.88	0.32	-0.17	0.05
P29590	PML	2.91	2.93	2.31	1.37	1.76	1.11
P29692	EEF1D	3.34	2.33	-0.18	0.11	-0.73	0.44
P29762	CRABP1	7.55	11.20	2.49	1.64	2.05	1.38
P30041	PRDX6	4.90	5.39	3.22	3.18	3.53	2.81
P30043	BLVRB	3.73	2.23	1.70	0.63	0.97	0.35
P30048	PRDX3	1.79	1.23	2.43	1.08	1.77	0.78
P30050	RPL12	3.11	2.64	2.91	4.15	3.29	5.43
P30085	CMPK1	1.40	4.46	2.51	5.44	1.20	3.32
P30086	PEBP1	7.27	4.97	0.46	0.33	-0.53	0.51

P30101	PDIA3	1.90	0.98	2.51	4.40	1.61	1.28
P30153	PPP2R1A	3.15	1.75	2.58	1.20	3.68	1.60
P30414	NKTR	-2.56	1.06	0.14	0.85	2.02	1.15
P30520	ADSS	3.44	1.75	4.42	4.52	4.45	7.92
P30566	ADSL	3.14	3.76	2.13	4.72	1.82	2.24
P30626	SRI	6.22	8.74	2.57	1.28	3.79	1.87
P30876	POLR2B	2.58	0.94	1.78	1.15	2.29	1.11
P31025	LCN1	-1.90	0.65	0.48	0.15	1.34	0.44
P31151	S100A7	0.15	0.03	4.29	1.06	3.51	1.13
P31153	MAT2A	1.32	1.83	3.33	1.90	3.68	2.09
P31350	RRM2	10.55	4.17	0.07	0.85	2.13	1.18
P31483	TIA1	1.29	2.48	4.18	3.13	3.79	3.03
P31689	DNAJA1	5.39	3.30	5.57	7.54	6.11	6.40
P31939	ATIC	3.70	6.60	-0.85	0.68	-0.45	0.36
P31942	HNRNPH3	-0.37	3.04	-0.13	0.31	0.47	1.46
P31943	HNRNPH1	3.86	4.93	3.99	3.56	4.71	9.43
P31946	YWHAB	4.60	10.54	4.47	11.09	5.09	10.43
P31948	STIP1	4.72	8.22	4.48	1.90	4.59	1.99
P31949	S100A11	4.46	5.19	2.95	1.09	5.95	4.16
P32019	INPP5B	-1.83	0.57	3.48	6.09	1.78	1.13
P32119	PRDX2	0.68	0.92	3.36	1.40	3.29	1.38
P32243	OTX2	2.02	2.92	2.70	3.11	2.31	2.57
P32519	ELF1	0.02	0.16	-0.08	0.54	0.24	1.70
P32969	RPL9	1.02	1.07	7.18	3.60	6.51	5.01
P33176	KIF5B	0.87	3.09	2.73	0.99	4.79	7.44
P33316	DUT	4.49	8.44	5.69	3.21	5.69	4.96
P33981	TTK	2.72	7.40	-2.32	0.88	-0.73	0.25
P33991	MCM4	5.31	3.40	3.49	1.44	3.18	1.36
P33992	MCM5	-0.71	2.14	-3.16	1.80	-2.77	7.54
P33993	MCM7	-0.60	2.31	-1.08	1.57	-0.81	2.96
P34897	SHMT2	-0.32	1.80	-1.22	0.69	-1.80	1.54
P34932	HSPA4	3.03	1.28	2.47	5.77	1.65	3.45
P35030	PRSS3	2.73	1.06	0.55	0.50	-1.83	0.88
P35080	PFN2	-1.44	4.67	-5.04	4.35	-1.02	0.26
P35221	CTNNA1	3.06	2.94	1.39	1.19	2.11	5.81
P35222	CTNNB1	3.11	3.49	-2.24	1.17	-1.34	1.44
P35232	PHB	2.04	0.70	0.59	0.40	1.27	1.87
P35241	RDX	0.59	1.59	-0.19	0.11	-0.63	0.52
P35249	RFC4	-1.24	3.46	-3.07	3.21	0.14	0.18
P35250	RFC2	0.01	0.04	-0.82	0.30	-0.83	0.93
P35251	RFC1	2.23	1.51	0.29	1.22	0.67	1.83
P35268	RPL22	3.87	2.77	1.60	1.20	0.56	0.44
P35269	GTF2F1	-0.18	2.01	3.34	3.33	4.42	6.60
P35453	HOXD13	-2.45	1.05	-0.25	0.09	0.46	0.32
P35527	KRT9	-3.09	3.17	1.43	0.57	0.42	0.21
P35579	MYH9	-1.21	1.26	4.10	1.28	3.27	1.01
P35580	MYH10	3.69	9.80	4.24	2.83	3.53	2.45
P35606	COPB2	3.05	1.02	3.44	2.28	6.68	4.73
P35612	ADD2	-2.55	1.05	-1.16	0.39	-1.42	0.50
P35637	FUS	3.52	5.11	3.69	7.66	3.99	5.68

P35659	DEK	5.86	9.66	-1.22	0.31	0.09	0.02
P35716	SOX11	-0.01	0.06	0.03	0.32	2.36	2.63
P35789	ZNF93	-0.43	0.19	1.16	0.75	1.93	3.13
P35813	PPM1A	-0.13	3.27	0.04	0.33	0.43	2.47
P35900	KRT20	-0.11	0.98	2.29	1.00	0.34	1.67
P35908	KRT2	-0.80	0.55	0.05	0.04	-1.44	1.92
P35998	PSMC2	8.66	9.47	2.72	3.07	2.36	1.96
P36578	RPL4	3.11	4.05	5.14	4.08	3.75	2.89
P36955	SERPINF1	5.27	3.89	-1.00	0.48	-1.00	2.76
P36969	GPX4	0.42	0.20	-2.25	1.49	-2.56	2.42
P37108	SRP14	6.46	2.82	0.47	0.53	0.39	0.44
P37802	TAGLN2	1.09	0.94	4.57	4.36	6.08	4.94
P37837	TALDO1	-1.74	5.67	-2.92	3.19	-4.15	3.34
P38159	RBMX	3.65	6.05	5.82	5.19	5.45	8.16
P38432	COIL	1.98	2.06	1.01	3.55	3.39	7.00
P38646	HSPA9	2.33	1.44	-2.06	3.61	-1.88	3.46
P38919	EIF4A3	2.85	1.78	1.45	2.14	1.41	2.57
P39023	RPL3	3.62	2.63	3.86	3.74	2.77	2.82
P39656	DDOST	3.16	2.44	0.08	0.12	0.34	1.00
P39687	ANP32A	4.35	4.26	4.22	2.10	4.45	2.13
P39748	FEN1	6.20	3.00	7.29	5.59	7.59	5.15
P39880	CUX1	-0.69	0.69	-3.30	1.97	-0.78	0.56
P40121	CAPG	4.82	2.80	5.63	4.61	2.17	1.13
P40227	CCT6A	5.04	4.85	0.99	1.06	0.33	0.34
P40425	PBX2	1.20	2.08	3.11	3.52	4.15	9.22
P40429	RPL13A	3.96	2.61	5.96	2.51	5.11	1.93
P40692	MLH1	1.51	6.88	0.64	0.26	-0.57	0.28
P40763	STAT3	3.73	2.30	1.22	1.00	3.67	1.29
P40925	MDH1	4.79	6.94	0.06	0.54	2.40	1.08
P40926	MDH2	1.77	0.95	0.78	0.40	1.69	0.88
P40937	RFC5	2.46	1.64	1.53	0.76	0.87	0.39
P40938	RFC3	-2.04	1.88	-3.63	2.48	-1.39	1.49
P41091	EIF2S3	8.61	13.14	-3.09	4.13	-3.01	3.77
P41162	ETV3	0.01	0.05	1.39	1.03	2.00	1.10
P41208	CETN2	2.95	3.61	-2.27	1.46	-0.45	3.84
P41212	ETV6	3.86	4.49	2.39	1.62	4.15	3.37
P41223	BUD31	-1.96	3.41	2.84	0.75	1.83	0.48
P41229	KDM5C	0.05	0.53	-0.14	0.04	2.29	0.91
P41240	CSK	2.22	0.94	2.88	1.00	3.62	1.09
P41250	GARS	1.71	1.05	0.35	0.16	0.92	0.41
P41252	IARS	0.56	0.17	1.94	0.96	2.52	1.00
P41567	EIF1	0.03	0.04	-0.33	1.17	-0.33	1.28
P42166	TMPO	7.98	6.10	5.78	3.26	6.11	3.15
P42167	TMPO	3.10	2.98	4.72	3.06	5.85	4.29
P42224	STAT1	3.55	5.18	-0.04	0.46	3.17	6.01
P42285	MTREX	4.40	5.53	-0.86	0.65	-0.90	1.19
P42574	CASP3	4.41	12.50	0.39	0.46	1.53	0.93
P42677	RPS27	2.34	3.58	3.08	5.07	2.96	4.47
P42696	RBM34	0.46	3.60	3.75	4.19	0.90	3.48
P42704	LRPPRC	0.90	0.57	0.71	0.39	-0.48	0.39

P42766	RPL35	1.97	2.18	2.71	2.22	2.05	1.95
P43243	MATR3	9.38	3.72	6.87	5.66	8.00	7.28
P43246	MSH2	2.81	1.00	6.01	3.62	6.24	5.78
P43268	ETV4	-0.48	0.46	-0.03	0.01	-0.07	0.03
P43487	RANBP1	-1.21	1.27	-1.12	1.65	-1.29	1.87
P43490	NAMPT	-0.03	0.16	-4.27	2.07	-3.43	1.52
P43686	PSMC4	9.39	13.59	4.64	3.36	2.58	3.62
P43694	GATA4	3.51	1.58	7.99	3.68	9.32	8.11
P45880	VDAC2	5.50	6.62	4.34	2.52	4.63	3.04
P45973	CBX5	1.33	3.04	0.12	0.12	0.57	0.66
P45974	USP5	2.78	2.46	2.72	1.45	2.21	1.25
P46013	MKI67	2.38	1.01	6.08	3.75	5.11	4.24
P46060	RANGAP1	4.07	2.87	-2.84	2.29	-2.64	2.30
P46063	RECQL	4.22	2.23	6.20	3.69	5.12	2.91
P46087	NOP2	-6.65	3.44	-3.10	2.81	-3.53	2.98
P46100	ATRX	1.40	0.96	-0.20	0.05	1.11	0.35
P46108	CRK	-2.74	1.07	3.35	3.06	0.28	5.61
P46109	CRKL	3.80	3.25	1.97	0.89	2.23	0.99
P46776	RPL27A	3.82	4.56	2.64	3.16	1.84	2.29
P46777	RPL5	2.56	2.05	3.99	3.71	3.34	4.22
P46778	RPL21	7.70	4.22	5.00	1.16	4.40	1.03
P46779	RPL28	1.82	2.71	3.92	2.97	2.96	4.70
P46781	RPS9	1.41	1.07	1.67	1.16	1.63	1.23
P46782	RPS5	4.78	6.91	3.67	2.65	2.61	2.01
P46783	RPS10	4.35	2.35	0.86	0.37	0.32	0.13
P46937	YAP1	3.95	9.84	0.05	0.06	0.97	1.62
P46940	IQGAP1	-0.03	0.31	1.69	1.02	2.02	1.08
P47755	CAPZA2	3.70	1.92	4.95	3.39	3.20	2.85
P47756	CAPZB	2.83	1.75	0.92	0.46	2.28	1.15
P47813	EIF1AX	4.50	3.29	4.46	3.77	5.48	3.99
P47914	RPL29	-1.20	4.53	7.85	2.37	7.68	2.29
P48147	PREP	2.16	0.94	3.75	1.07	0.39	2.97
P48431	SOX2	2.94	5.77	2.33	1.00	1.83	1.94
P48556	PSMD8	1.81	1.14	-2.11	1.61	-2.19	1.85
P48634	PRRC2A	0.03	0.89	-0.59	0.22	0.23	0.08
P48643	CCT5	2.32	1.50	-0.71	0.77	0.77	0.46
P48729	CSNK1A1	2.23	1.02	-0.86	0.21	-1.53	0.42
P48730	CSNK1D	1.47	0.88	4.09	3.24	4.38	8.52
P48739	PITPNB	2.03	2.96	1.29	0.98	1.96	1.47
P48742	LHX1	3.67	2.55	6.07	10.67	7.06	5.96
P49005	POLD2	4.90	5.71	4.22	3.40	2.43	1.27
P49207	RPL34	2.01	2.96	3.55	4.57	3.33	3.63
P49321	NASP	5.49	4.43	4.70	5.71	4.57	5.26
P49327	FASN	-1.45	1.22	-2.01	1.25	-0.65	1.22
P49368	CCT3	-0.06	0.03	3.34	3.08	4.44	7.51
P49411	TUFM	3.43	2.58	2.61	3.55	3.30	3.48
P49454	CENPF	0.75	0.60	1.27	0.91	3.91	6.90
P49458	SRP9	1.11	1.09	4.98	3.39	2.56	1.13
P49585	PCYT1A	1.37	0.85	1.22	1.20	1.50	1.10
P49591	SARS	2.23	0.91	2.47	3.20	2.31	5.79

P49640	EVX1	4.15	1.86	-2.47	1.93	-1.53	6.32
P49643	PRIM2	-1.24	1.05	3.05	4.00	0.43	0.72
P49674	CSNK1E	0.21	0.07	1.06	0.52	1.82	0.89
P49711	CTCF	1.86	1.01	2.98	2.33	3.68	8.71
P49720	PSMB3	5.80	4.14	-2.32	0.90	-2.16	0.85
P49721	PSMB2	4.25	8.96	-3.53	0.97	-1.73	0.46
P49736	MCM2	4.56	2.05	2.99	1.55	2.85	1.11
P49750	YLPM1	0.74	1.23	0.05	0.19	0.53	0.63
P49755	TMED10	1.39	4.16	0.89	3.96	1.42	1.20
P49756	RBM25	3.76	5.12	2.63	1.01	5.59	11.11
P49773	HINT1	1.24	0.94	-3.17	2.88	-3.47	2.77
P49790	NUP153	4.11	1.71	2.99	4.53	4.70	5.10
P49792	RANBP2	9.92	7.37	2.73	1.33	3.35	1.57
P49848	TAF6	0.49	0.83	2.21	0.73	5.20	2.54
P49903	SEPHS1	2.38	1.73	-1.90	3.15	-1.49	2.27
P49915	GMPS	3.62	1.51	6.38	7.06	5.93	9.40
P49916	LIG3	-3.58	1.08	-4.52	1.29	-2.72	2.46
P49959	MRE11	-0.14	1.44	4.93	2.91	6.01	6.54
P50395	GDI2	4.52	2.79	1.88	0.77	1.39	0.59
P50453	SERPINB9	-3.29	0.73	3.06	3.40	2.49	5.55
P50454	SERPINH1	2.54	3.67	2.31	6.69	1.71	3.21
P50502	ST13	3.39	5.85	3.19	1.34	2.66	1.13
P50750	CDK9	-0.09	0.83	2.23	1.13	2.18	1.17
P50914	RPL14	7.07	4.70	6.01	4.38	5.17	4.94
P50990	CCT8	4.68	6.53	-0.69	0.50	0.40	0.18
P50991	CCT4	3.64	3.25	-2.99	1.86	-1.70	1.14
P50995	ANXA11	4.29	4.30	3.87	2.42	4.91	2.96
P51003	PAPOLA	2.36	2.06	2.95	1.63	2.64	1.50
P51114	FXR1	3.77	4.67	1.59	1.22	1.30	1.00
P51116	FXR2	3.24	6.01	0.11	1.65	0.29	1.80
P51149	RAB7A	4.67	12.95	-1.34	0.36	1.01	0.27
P51452	DUSP3	1.57	1.01	1.54	1.00	-0.93	0.61
P51530	DNA2	3.43	4.92	-2.15	0.94	-1.88	0.83
P51532	SMARCA4	0.99	1.77	-1.08	1.20	-0.91	2.44
P51570	GALK1	0.99	0.87	-0.65	0.18	-1.47	0.47
P51587	BRCA2	-0.28	0.78	-0.14	1.54	3.29	1.09
P51610	HCFC1	4.24	2.08	-1.67	1.73	-2.17	1.98
P51659	HSD17B4	1.61	1.28	2.22	2.07	2.35	2.03
P51665	PSMD7	5.12	3.73	-4.47	3.09	-5.09	4.71
P51692	STAT5B	-0.05	0.68	0.04	0.51	1.68	1.16
P51784	USP11	0.98	0.44	-1.43	1.99	-0.88	1.43
P51826	AFF3	1.71	0.96	-1.87	0.75	-2.92	1.73
P51858	HDGF	3.15	4.96	5.82	2.25	5.19	2.03
P51948	MNAT1	0.00	0.02	-0.66	0.23	-0.44	0.15
P51991	HNRNPA3	4.65	9.83	4.07	1.98	4.19	2.06
P52209	PGD	5.70	4.20	1.56	0.58	3.46	2.52
P52272	HNRNPM	4.41	7.27	6.05	4.43	6.84	6.94
P52292	KPNA2	2.22	2.60	-0.88	7.57	-0.77	5.87
P52294	KPNA1	0.12	2.32	2.78	3.13	3.17	3.28
P52298	NCBP2	1.20	1.07	2.76	2.01	2.62	2.05

P52434	POLR2H	1.26	1.00	-1.67	0.99	0.57	0.34
P52565	ARHGDIA	5.60	5.57	3.23	1.68	2.26	1.19
P52594	AGFG1	-0.03	0.36	3.91	8.01	0.37	2.61
P52597	HNRNPF	3.03	4.87	3.84	5.14	3.86	9.83
P52701	MSH6	0.83	1.44	-4.76	4.78	-5.25	4.11
P52747	ZNF143	3.90	3.92	2.64	2.40	4.85	5.40
P52756	RBM5	-3.26	1.38	3.64	1.51	2.69	1.16
P52788	SMS	3.18	5.92	0.83	0.36	1.68	1.30
P52907	CAPZA1	4.46	8.41	2.85	1.04	4.77	8.73
P52926	HMGA2	3.49	3.19	4.13	1.88	3.89	1.65
P52951	GBX2	-0.09	2.38	0.19	3.90	0.81	1.77
P53350	PLK1	4.47	3.37	-0.70	0.27	-0.38	0.16
P53396	ACLY	5.03	2.96	3.70	2.68	4.07	3.05
P53602	MVD	2.71	3.42	1.27	1.24	0.38	2.57
P53611	RABGGTB	1.43	0.94	-3.17	1.36	-0.27	0.46
P53621	COPA	3.18	3.70	4.02	3.71	2.77	5.51
P53999	SUB1	3.61	1.43	2.34	1.91	1.66	1.36
P54105	CLNS1A	4.00	3.98	0.48	0.20	1.65	0.98
P54132	BLM	0.60	1.45	-1.14	3.30	-1.56	3.44
P54136	RARS	3.74	3.17	1.90	0.99	1.78	1.11
P54198	HIRA	-2.27	3.88	0.57	0.61	1.18	0.85
P54252	ATXN3	2.20	4.77	0.71	0.22	0.59	0.18
P54259	ATN1	5.13	6.38	-1.72	0.48	2.54	0.73
P54277	PMS1	5.75	4.41	-0.68	0.64	-1.43	4.75
P54577	YARS	-2.35	1.00	-1.14	0.32	-2.82	0.87
P54578	USP14	1.63	0.74	0.81	0.27	1.75	0.68
P54652	HSPA2	3.58	6.02	2.24	1.00	2.13	1.33
P54727	RAD23B	0.97	0.87	2.77	1.02	2.62	1.51
P54920	NAPA	2.04	1.32	-4.44	2.71	-1.80	1.57
P55036	PSMD4	2.30	1.29	2.49	1.27	2.89	1.43
P55060	CSE1L	-0.40	0.33	2.01	1.66	1.11	1.20
P55072	VCP	-1.44	0.87	-4.03	3.00	-0.12	0.13
P55081	MFAP1	-0.05	0.72	4.96	3.96	3.99	2.67
P55196	AFDN	3.34	4.65	1.28	0.96	3.33	1.52
P55199	ELL	0.66	0.84	0.07	0.93	0.27	5.57
P55209	NAP1L1	6.43	4.90	5.19	4.67	5.11	6.35
P55265	ADAR	0.61	0.47	5.45	6.69	6.40	4.88
P55347	PKNOX1	-0.10	0.90	-0.03	0.26	4.19	4.02
P55769	SNU13	5.46	3.47	5.90	2.58	5.89	4.51
P55795	HNRNPH2	-0.05	0.09	3.22	4.67	2.54	2.47
P55809	OXCT1	-0.33	0.85	1.23	1.03	1.65	1.45
P55854	SUMO3	4.88	7.31	4.56	3.75	6.13	10.56
P55884	EIF3B	4.12	8.67	3.19	5.84	2.58	2.34
P56182	RRP1	2.46	2.17	0.25	1.28	-0.55	2.66
P56192	MARS	3.23	1.86	-0.48	0.13	-2.60	0.88
P56270	MAZ	6.13	9.13	6.25	7.81	6.80	6.93
P56537	EIF6	2.77	3.97	3.49	3.10	2.27	1.25
P56545	CTBP2	7.52	6.39	5.89	2.80	7.53	4.40
P56915	GSC	4.49	6.90	-1.43	2.33	-1.71	2.64
P57081	WDR4	-0.01	0.26	1.11	0.96	1.86	1.08

P57723	PCBP4	5.44	4.48	0.16	1.29	3.16	1.07
P57740	NUP107	4.09	2.66	1.76	1.16	3.34	2.11
P58317	ZNF121	-1.51	0.54	1.15	0.34	0.73	0.21
P58546	MTPN	4.39	4.44	5.79	9.06	6.53	4.39
P59190	RAB15	5.33	10.44	3.47	1.43	4.18	2.13
P60174	TPI1	0.84	1.53	1.89	1.07	2.39	1.30
P60228	EIF3E	3.91	2.30	2.79	2.25	3.06	2.18
P60660	MYL6	3.32	3.70	5.52	3.86	6.11	5.77
P60709	ACTB	3.48	7.49	1.18	2.55	1.57	2.97
P60842	EIF4A1	3.90	2.91	2.22	2.10	2.30	2.68
P60866	RPS20	5.51	2.69	5.18	1.75	4.31	1.50
P60900	PSMA6	-0.28	0.87	-1.13	2.47	-1.59	2.69
P60983	GMFB	0.65	0.16	-2.43	2.17	-1.64	1.55
P61024	CKS1B	0.95	0.47	4.02	2.95	5.49	2.44
P61077	UBE2D3	3.72	10.09	1.26	0.97	3.55	9.42
P61081	UBE2M	4.90	3.25	5.28	4.64	6.09	7.99
P61086	UBE2K	3.83	6.25	2.16	1.02	0.24	2.84
P61160	ACTR2	-0.13	1.07	0.20	1.52	1.56	1.20
P61201	COPS2	1.68	2.24	-3.06	3.32	-2.26	1.59
P61204	ARF3	5.73	4.17	0.22	0.19	0.56	0.38
P61221	ABCE1	3.34	4.61	0.08	2.70	0.46	1.58
P61244	MAX	1.56	7.78	0.37	0.16	1.81	1.06
P61247	RPS3A	7.09	4.52	7.35	6.66	6.64	4.67
P61254	RPL26	2.74	4.28	3.45	2.23	2.93	2.26
P61289	PSME3	4.15	2.72	5.29	4.76	6.19	4.46
P61313	RPL15	3.51	4.75	3.57	3.21	3.34	4.26
P61326	MAGOH	5.85	3.62	4.91	2.13	4.56	2.01
P61353	RPL27	2.20	1.74	3.17	3.67	2.54	2.67
P61513	RPL37A	2.30	1.67	3.47	1.96	3.31	1.78
P61604	HSPE1	4.05	1.36	-2.73	0.66	0.64	0.14
P61626	LYZ	2.53	0.95	1.81	0.46	1.26	0.41
P61923	COPZ1	2.06	0.97	0.23	1.16	4.54	6.80
P61956	SUMO2	7.38	3.18	3.90	2.26	5.12	2.58
P61962	DCAF7	0.60	4.48	-1.87	1.69	0.75	2.30
P61964	WDR5	1.39	3.68	0.12	0.17	0.34	0.50
P61978	HNRNPK	4.27	5.36	5.58	4.78	5.83	5.78
P61981	YWHAG	2.84	3.82	7.54	5.67	7.30	4.30
P62070	RRAS2	3.52	2.19	5.48	9.90	4.67	4.45
P62081	RPS7	5.37	2.22	1.81	1.70	1.18	1.31
P62136	PPP1CA	5.44	4.20	-0.17	0.08	1.04	0.82
P62191	PSMC1	7.70	2.29	1.65	1.14	1.87	1.25
P62195	PSMC5	9.96	6.21	0.97	5.81	0.85	1.58
P62241	RPS8	4.53	1.41	1.91	2.50	0.77	1.37
P62244	RPS15A	3.30	4.38	2.68	2.29	2.63	3.88
P62249	RPS16	2.44	3.83	2.67	6.50	2.37	5.88
P62258	YWHAE	4.75	4.02	5.16	4.93	4.84	10.39
P62263	RPS14	1.98	2.99	3.78	1.94	3.94	1.90
P62266	RPS23	2.64	3.63	2.03	4.02	1.71	4.32
P62269	RPS18	5.06	2.23	3.07	0.88	2.58	0.74
P62277	RPS13	6.22	2.89	4.33	1.84	3.52	1.45

P62280	RPS11	4.65	1.77	3.69	3.25	2.86	3.41
P62306	SNRPF	-0.03	0.19	-0.21	0.06	3.20	1.18
P62308	SNRPG	5.55	3.24	2.16	1.04	1.43	1.17
P62310	LSM3	-0.08	1.14	5.63	3.42	2.73	1.11
P62314	SNRPD1	5.28	3.19	5.59	2.45	4.66	2.26
P62316	SNRPD2	6.55	3.57	7.85	5.20	7.33	6.47
P62318	SNRPD3	7.10	9.22	7.12	5.91	7.07	6.03
P62333	PSMC6	4.37	1.86	0.44	0.15	0.14	0.05
P62424	RPL7A	2.79	2.75	3.42	2.33	2.01	1.49
P62487	POLR2G	-0.01	0.14	4.95	1.89	3.83	1.57
P62495	ETF1	4.15	2.68	4.58	3.60	2.64	4.33
P62701	RPS4X	3.62	3.14	4.07	2.30	3.30	5.35
P62714	PPP2CB	2.76	2.45	3.39	3.14	5.00	9.61
P62750	RPL23A	3.63	1.14	3.56	2.11	1.40	1.03
P62753	RPS6	7.36	7.99	2.66	0.98	1.07	0.39
P62760	VSNL1	1.41	4.20	1.33	1.11	2.37	8.85
P62805	HIST1H4A	0.54	0.78	3.29	2.09	1.36	0.91
P62826	RAN	3.24	4.25	3.46	6.86	3.57	5.91
P62829	RPL23	6.39	2.97	3.63	2.54	3.99	2.29
P62841	RPS15	1.10	2.63	2.07	0.99	0.78	0.36
P62847	RPS24	3.06	4.49	1.37	1.59	0.48	0.59
P62851	RPS25	1.45	1.48	0.97	0.70	-0.09	0.07
P62854	RPS26	-4.91	2.95	3.93	1.39	3.72	1.28
P62857	RPS28	5.84	7.74	7.58	3.71	6.03	5.33
P62861	FAU	0.26	0.15	2.38	3.51	1.62	2.71
P62888	RPL30	3.84	2.88	2.10	1.08	1.19	0.61
P62899	RPL31	2.04	1.66	3.28	2.25	2.17	1.78
P62906	RPL10A	5.73	2.81	4.81	2.43	3.42	1.75
P62910	RPL32	4.90	5.29	4.09	2.15	2.40	1.34
P62913	RPL11	5.10	2.49	5.45	2.09	4.23	1.67
P62917	RPL8	5.95	3.00	6.95	3.42	6.14	3.55
P62937	PPIA	4.98	4.64	5.02	3.10	5.69	3.29
P62942	FKBP1A	4.74	5.85	5.11	4.29	5.40	12.62
P62979	RPS27A	1.17	2.50	4.14	3.07	3.26	2.85
P62993	GRB2	-2.87	7.25	-3.07	6.09	-3.31	6.08
P62995	TRA2B	2.97	3.20	2.98	7.27	2.96	6.82
P63104	YWHAZ	6.06	4.60	4.64	1.69	4.82	1.76
P63165	SUMO1	7.82	7.33	3.22	0.82	3.64	0.91
P63167	DYNLL1	2.78	1.01	0.60	0.18	2.55	0.87
P63173	RPL38	0.03	0.88	7.38	2.19	8.54	5.37
P63208	SKP1	3.71	11.40	3.27	5.86	3.51	2.07
P63220	RPS21	1.56	0.48	3.27	1.74	3.89	1.90
P63241	EIF5A	7.78	8.38	5.34	3.09	5.25	2.48
P63244	RACK1	4.74	3.09	4.25	1.36	4.07	1.30
P63279	UBE2I	5.06	5.97	4.33	1.87	5.69	3.99
P67809	YBX1	6.81	4.28	4.71	2.20	3.72	2.14
P67870	CSNK2B	2.91	5.62	3.28	3.70	0.37	2.83
P67936	TPM4	-0.11	1.83	1.55	0.94	2.62	5.55
P68032	ACTC1	5.04	2.04	5.00	1.77	3.98	1.59
P68036	UBE2L3	3.94	1.58	1.44	1.58	-0.04	0.02

P68104	EEF1A1	2.81	3.41	2.13	2.31	1.47	1.85
P68363	TUBA1B	3.48	4.97	1.22	1.82	1.96	3.01
P68371	TUBB4B	2.02	3.68	2.07	1.92	1.90	1.77
P68400	CSNK2A1	4.33	3.54	2.80	1.69	2.92	1.87
P68402	PAFAH1B2	1.08	0.97	4.32	5.55	1.94	1.10
P68431	HIST1H3A	0.88	1.09	3.74	1.81	2.58	1.25
P68871	HBB	-0.91	4.12	-0.53	0.70	-0.92	1.21
P69905	HBA1	-0.82	4.98	-1.76	2.25	-1.79	3.19
P78316	NOP14	2.58	1.54	-3.23	2.19	-0.30	0.29
P78332	RBM6	1.15	0.87	-1.69	1.95	1.08	1.29
P78344	EIF4G2	2.98	1.03	2.78	1.01	3.09	2.25
P78346	RPP30	-0.15	3.00	0.06	0.52	0.89	1.12
P78347	GTF2I	-1.98	4.37	-3.09	2.89	-2.13	3.89
P78364	PHC1	1.11	0.95	1.96	0.98	1.98	1.70
P78371	CCT2	4.07	2.29	-0.70	0.38	2.06	2.05
P78406	RAE1	-2.83	0.96	0.42	0.12	-0.30	0.11
P78413	IRX4	3.25	10.97	0.42	0.22	2.99	1.71
P78527	PRKDC	1.08	1.11	2.01	2.53	2.21	4.47
P81605	DCD	-2.34	1.69	-0.63	0.53	-0.23	0.18
P82979	SARNP	5.61	9.03	-0.59	0.91	-0.34	1.60
P83731	RPL24	5.09	2.03	6.28	2.02	5.57	1.95
P83876	TXNL4A	2.10	1.00	0.85	1.00	0.22	2.23
P83881	RPL36A	3.66	5.89	0.32	0.34	-0.63	0.92
P83916	CBX1	5.39	6.21	6.74	3.17	6.88	3.37
P84022	SMAD3	-0.78	0.99	-4.32	1.51	-3.49	1.74
P84090	ERH	5.90	5.55	2.56	2.92	3.01	4.26
P84098	RPL19	2.42	3.60	0.61	0.88	0.82	1.01
P84103	SRSF3	5.42	7.57	5.39	2.39	5.26	2.24
P85037	FOXK1	-0.64	0.23	-2.03	1.36	0.38	1.80
P98170	XIAP	-4.65	2.42	-2.49	3.09	-1.68	2.34
P98175	RBM10	1.01	0.96	2.05	0.80	3.26	1.41
P98179	RBM3	6.10	8.54	4.38	5.09	4.69	3.27
P99999	CYCS	3.15	7.18	-0.21	0.27	-0.47	0.67
Q00341	HDLBP	4.73	4.27	-1.90	1.15	-0.40	0.59
Q00403	GTF2B	-1.72	0.76	1.75	0.71	2.09	0.85
Q00534	CDK6	1.52	0.57	1.60	0.50	-2.86	0.89
Q00610	CLTC	5.36	2.33	0.11	0.07	-1.13	0.85
Q00613	HSF1	-0.06	0.55	0.20	2.25	0.57	4.50
Q00688	FKBP3	3.07	5.46	1.34	0.63	1.09	0.51
Q00796	SORD	2.08	1.55	0.23	0.59	0.01	0.07
Q00839	HNRNPU	3.71	3.90	5.62	12.01	5.06	4.69
Q01081	U2AF1	2.48	0.68	6.31	2.24	7.26	5.24
Q01082	SPTBN1	3.01	1.70	0.67	0.28	-0.02	0.01
Q01085	TIAL1	1.20	1.66	3.94	1.47	4.60	1.65
Q01105	SET	2.88	1.83	3.12	1.04	2.38	0.80
Q01130	SRSF2	4.97	4.54	7.31	2.08	7.59	2.13
Q01469	FABP5	2.31	3.51	5.88	5.16	5.20	3.27
Q01518	CAP1	3.41	11.96	1.31	1.25	2.15	1.19
Q01546	KRT76	-1.39	1.52	0.90	0.38	1.43	0.62
Q01581	HMGCS1	-0.10	1.48	2.76	0.99	2.59	1.06

Q01650	SLC7A5	1.43	1.04	0.06	1.30	2.83	5.82
Q01664	TFAP4	3.58	6.44	1.47	1.14	3.84	6.94
Q01780	EXOSC10	-3.07	2.22	5.32	2.76	5.29	8.90
Q01826	SATB1	3.54	5.68	-6.66	3.55	-4.77	4.04
Q01831	XPC	-0.05	0.45	0.01	0.01	-4.02	5.51
Q01844	EWSR1	4.16	4.62	5.22	3.23	5.56	3.77
Q01860	POU5F1	1.64	1.66	0.17	0.23	0.31	0.44
Q01995	TAGLN	3.11	4.85	5.35	8.28	5.55	9.11
Q02241	KIF23	2.97	2.30	-4.59	4.87	-3.87	4.40
Q02413	DSG1	3.06	1.32	-1.52	1.96	-5.04	3.05
Q02447	SP3	1.16	0.92	1.99	1.19	3.96	6.71
Q02539	HIST1H1A	1.77	0.97	3.53	3.27	2.00	1.21
Q02543	RPL18A	6.77	2.32	5.30	3.88	5.47	3.03
Q02790	FKBP4	4.68	4.65	1.60	3.40	1.35	4.27
Q02878	RPL6	-0.85	1.28	1.67	2.57	0.45	1.16
Q02880	TOP2B	4.12	2.17	6.60	8.69	6.08	10.26
Q03001	DST	-0.11	0.70	3.38	1.02	7.45	9.28
Q03014	HHEX	1.64	1.54	3.37	4.29	4.88	3.87
Q03060	CREM	2.66	0.94	-0.05	0.33	4.94	7.42
Q03112	MECOM	-1.55	2.49	-2.29	2.10	-2.56	2.78
Q03252	LMNB2	-0.77	2.54	-0.07	0.11	-0.64	1.13
Q03701	CEBPZ	1.83	2.09	0.34	0.16	1.44	0.59
Q03938	ZNF90	-0.22	3.82	1.16	1.21	1.19	2.75
Q04323	UBXN1	3.46	8.02	-1.67	1.98	-2.18	2.24
Q04637	EIF4G1	4.48	3.82	3.94	3.24	2.87	2.87
Q04695	KRT17	-2.47	1.60	1.77	0.62	1.10	0.38
Q04724	TLE1	8.29	3.62	5.73	3.24	7.12	3.64
Q04726	TLE3	5.23	2.28	4.53	2.43	6.61	2.70
Q04727	TLE4	4.71	6.13	2.23	1.37	6.31	4.24
Q04837	SSBP1	4.65	3.38	1.08	0.35	0.92	0.30
Q04917	YWHAH	5.24	4.22	2.67	1.88	4.61	2.28
Q05048	CSTF1	-1.20	1.71	-0.06	0.06	0.28	0.35
Q05086	UBE3A	2.24	1.65	2.65	2.12	2.02	1.46
Q05519	SRSF11	6.39	10.94	0.43	1.28	0.15	0.44
Q05682	CALD1	0.70	0.64	3.44	4.84	2.85	4.30
Q06265	EXOSC9	2.45	1.00	2.45	1.05	0.38	2.46
Q06330	RBPJ	4.40	10.18	2.33	1.05	3.75	3.12
Q06416	POU5F1B	6.36	6.44	-1.53	0.52	-0.42	0.12
Q06455	RUNX1T1	1.98	2.45	-0.10	0.16	1.06	1.81
Q06587	RING1	-3.42	3.46	-3.74	1.70	-1.11	1.32
Q06830	PRDX1	3.02	7.01	2.83	2.21	2.77	2.47
Q07020	RPL18	4.69	4.77	4.10	4.02	3.65	4.06
Q07021	C1QBP	0.03	1.04	3.39	8.48	1.68	1.12
Q07065	CKAP4	1.90	0.98	3.04	6.64	0.43	5.07
Q07666	KHDRBS1	1.75	1.44	0.93	3.67	1.08	3.10
Q07864	POLE	3.32	2.48	-0.01	0.06	1.49	4.44
Q07955	SRSF1	5.15	3.25	3.30	5.32	3.26	4.26
Q08117	TLE5	5.42	4.42	5.33	3.44	6.70	3.34
Q08170	SRSF4	8.11	4.66	6.85	3.61	6.96	2.97
Q08188	TGM3	-2.02	0.73	5.61	4.68	2.17	2.37

Q08211	DHX9	4.11	4.57	3.23	2.68	3.20	2.70
Q08554	DSC1	-0.12	0.67	3.35	0.99	2.43	1.18
Q08752	PPID	2.21	0.99	-0.77	0.21	-0.63	0.17
Q08945	SSRP1	6.21	8.55	5.95	4.72	6.55	4.12
Q08AN1	ZNF616	2.05	0.99	2.12	0.67	1.97	0.62
Q08J23	NSUN2	3.03	2.80	3.58	2.73	3.16	2.56
Q09028	RBBP4	1.77	1.92	1.51	1.31	1.32	1.19
Q09161	NCBP1	4.01	1.77	0.82	0.91	0.50	0.80
Q09472	EP300	5.10	3.44	4.29	3.32	5.36	3.53
Q10570	CPSF1	2.58	1.36	3.51	2.30	4.03	2.89
Q12778	FOXO1	-0.12	1.18	2.28	1.01	5.17	6.00
Q12788	TBL3	3.96	1.93	-1.38	0.91	-1.53	1.00
Q12789	GTF3C1	4.93	5.13	5.15	4.90	5.04	7.26
Q12824	SMARCB1	4.49	2.21	1.05	2.70	0.99	1.27
Q12830	BPTF	2.89	4.17	0.07	0.03	0.31	0.12
Q12834	CDC20	7.76	5.24	-2.61	4.34	-4.94	4.02
Q12874	SF3A3	1.31	2.79	2.67	2.79	2.65	4.87
Q12905	ILF2	5.44	7.43	6.97	3.44	7.16	3.19
Q12906	ILF3	6.19	2.09	7.79	2.30	7.81	2.25
Q12931	TRAP1	3.70	3.30	1.94	0.98	3.01	8.07
Q12972	PPP1R8	3.68	3.72	4.05	2.44	3.76	2.02
Q12996	CSTF3	4.63	3.73	3.40	1.75	4.00	1.52
Q13042	CDC16	-0.74	0.35	0.03	0.58	2.97	7.38
Q13111	CHAF1A	1.81	1.83	1.26	1.17	2.75	6.34
Q13112	CHAF1B	2.59	1.32	4.63	6.70	4.87	2.87
Q13123	IK	-2.40	4.89	-1.03	1.32	-0.95	1.22
Q13126	MTAP	-0.08	0.55	3.86	2.87	2.51	1.30
Q13148	TARDBP	8.22	7.04	2.71	1.81	3.00	2.03
Q13151	HNRNPA0	6.00	2.83	1.15	4.04	1.81	5.48
Q13158	FADD	2.11	1.39	0.35	0.20	0.80	0.42
Q13162	PRDX4	1.66	0.86	0.38	0.12	-0.71	0.20
Q13185	CBX3	8.56	3.39	-0.59	1.20	-0.18	0.38
Q13200	PSMD2	7.24	5.78	2.12	4.22	2.78	4.82
Q13206	DDX10	1.11	1.13	4.59	3.65	4.08	3.72
Q13227	GPS2	-4.06	1.32	3.10	0.86	2.12	0.59
Q13242	SRSF9	4.92	2.47	1.93	1.91	1.76	1.74
Q13243	SRSF5	7.11	3.22	5.47	4.43	5.82	4.85
Q13247	SRSF6	4.39	4.67	6.46	7.73	5.88	5.11
Q13263	TRIM28	3.73	4.73	7.48	4.09	7.19	7.07
Q13283	G3BP1	2.07	0.96	-0.60	0.44	-1.51	1.11
Q13309	SKP2	1.40	1.03	-0.04	0.37	1.46	1.19
Q13310	PABPC4	3.56	2.27	2.70	7.76	3.09	3.10
Q13330	MTA1	1.30	1.60	6.04	4.27	7.49	6.18
Q13347	EIF3I	2.19	4.96	3.98	4.11	4.18	3.44
Q13356	PPIL2	4.04	2.64	-0.16	0.31	-1.41	0.75
Q13363	CTBP1	3.50	9.08	3.14	2.31	5.40	5.48
Q13409	DYNC1I2	1.39	0.83	1.14	1.03	0.44	4.57
Q13416	ORC2	1.89	4.33	2.72	2.20	3.15	2.42
Q13426	XRCC4	0.76	0.97	-0.75	0.40	-0.78	0.43
Q13427	PPIG	-0.66	0.79	1.33	4.11	3.42	4.47

Q13428	TCOF1	1.95	1.29	1.38	1.07	-0.15	0.21
Q13435	SF3B2	6.34	2.91	5.48	4.76	5.37	6.15
Q13442	PDAP1	-1.00	0.36	0.37	0.32	-0.53	0.51
Q13451	FKBP5	-2.26	1.10	0.63	0.19	0.70	0.21
Q13464	ROCK1	6.40	7.83	0.34	0.11	2.50	0.87
Q13472	TOP3A	3.18	2.85	1.42	0.50	1.57	0.56
Q13485	SMAD4	3.74	3.18	2.74	3.64	3.71	3.01
Q13506	NAB1	3.36	7.26	3.74	5.36	4.10	9.98
Q13509	TUBB3	4.55	3.71	0.76	0.35	2.29	1.63
Q13523	PRPF4B	5.94	3.48	-1.07	2.97	-1.52	1.28
Q13526	PIN1	4.02	1.53	5.42	2.65	5.77	2.45
Q13547	HDAC1	6.37	5.78	4.85	3.48	5.19	3.78
Q13573	SNW1	4.56	8.91	4.48	2.11	5.29	2.32
Q13595	TRA2A	1.26	3.23	1.03	1.53	0.50	6.56
Q13601	KRR1	-0.23	3.16	3.95	3.34	0.31	1.85
Q13616	CUL1	4.30	2.70	-4.43	3.97	-2.02	4.76
Q13617	CUL2	-2.15	1.10	-1.69	0.92	0.40	0.17
Q13618	CUL3	1.01	0.27	3.53	4.26	2.22	0.98
Q13619	CUL4A	0.75	0.54	0.84	0.80	-0.16	0.13
Q13620	CUL4B	0.88	1.89	-0.62	0.33	0.56	0.29
Q13642	FHL1	0.06	1.64	0.02	0.09	0.32	1.59
Q13765	NACA	2.11	2.31	1.01	1.27	-0.28	0.61
Q13813	SPTAN1	2.44	0.92	2.05	1.03	3.78	10.04
Q13823	GNL2	3.61	5.91	3.82	10.22	3.73	4.80
Q13838	DDX39B	6.31	1.89	2.68	1.62	2.28	1.39
Q13868	EXOSC2	2.30	1.00	3.09	5.20	3.52	2.54
Q13885	TUBB2A	3.63	3.60	2.02	1.07	2.46	1.12
Q13895	BYSL	-1.19	0.65	1.35	0.49	1.37	0.54
Q13907	IDI1	-0.11	1.85	1.65	1.06	3.61	2.84
Q13951	CBFB	3.41	2.87	2.45	5.10	3.95	2.95
Q14004	CDK13	-0.10	1.50	0.08	0.52	1.38	1.26
Q14008	CKAP5	1.55	6.24	0.48	1.47	2.25	1.12
Q14011	CIRBP	1.80	3.52	7.31	3.44	6.94	7.26
Q14103	HNRNPD	3.96	3.50	4.60	3.64	4.46	3.54
Q14119	VEZF1	5.61	10.07	3.30	6.35	5.40	5.64
Q14135	VGLL4	3.39	9.94	1.52	0.90	4.07	3.70
Q14137	BOP1	3.59	3.09	3.24	1.48	2.64	1.25
Q14147	DHX34	0.06	1.43	0.22	1.58	1.82	1.32
Q14149	MORC3	1.09	0.85	0.24	1.86	0.44	2.55
Q14151	SAFB2	3.34	2.14	1.58	1.43	1.58	1.46
Q14152	EIF3A	3.62	2.87	0.13	3.77	1.31	1.16
Q14157	UBAP2L	-0.36	0.19	1.97	3.04	0.20	0.38
Q14165	MLEC	-0.05	0.88	0.03	0.35	0.30	3.66
Q14166	TTLL12	5.52	3.95	3.53	1.52	2.08	0.96
Q14186	TFDP1	-2.99	0.98	1.99	0.98	1.92	1.08
Q14191	WRN	0.31	0.60	2.02	2.11	2.51	6.19
Q14194	CRMP1	3.28	3.54	-0.24	0.10	-0.09	0.04
Q14195	DPYSL3	2.53	2.30	0.00	0.00	1.78	0.97
Q14202	ZMYM3	3.88	5.91	3.51	2.00	4.31	2.78
Q14204	DYNC1H1	-1.17	1.32	-2.69	0.97	0.13	0.04

Q14240	EIF4A2	2.02	0.97	-4.57	5.37	-3.24	2.22
Q14241	ELOA	-1.73	1.07	0.01	0.01	1.13	1.61
Q14247	CTTN	2.23	1.75	0.63	0.21	0.30	0.10
Q14258	TRIM25	-0.09	1.31	2.22	1.24	1.51	1.24
Q14320	FAM50A	5.42	5.62	-1.01	2.01	-2.31	4.11
Q14469	HES1	4.31	2.35	0.06	0.22	3.21	6.83
Q14498	RBM39	7.33	5.94	7.46	4.87	7.48	5.59
Q14527	HLTF	1.29	1.54	0.96	1.10	4.29	7.30
Q14566	MCM6	3.00	3.19	2.40	3.80	2.49	4.01
Q14587	ZNF268	-0.08	0.57	2.16	1.10	0.29	3.50
Q14592	ZNF460	3.76	4.56	0.07	1.24	2.35	2.37
Q14593	ZNF273	2.71	0.95	1.13	1.03	1.63	1.07
Q14669	TRIP12	-0.45	0.44	3.28	3.63	2.92	2.83
Q14671	PUM1	0.23	0.10	-2.91	1.54	-2.31	1.10
Q14676	MDC1	1.13	1.08	0.76	1.02	0.72	0.82
Q14683	SMC1A	7.64	5.11	-0.46	1.31	-0.30	0.78
Q14684	RRP1B	2.04	1.79	3.79	2.20	2.52	1.67
Q14687	GSE1	2.35	2.75	-1.60	2.17	-0.34	0.52
Q14690	PDCD11	4.99	6.45	-0.10	0.12	-1.85	2.42
Q14691	GINS1	3.61	4.37	2.58	1.09	4.04	3.04
Q14692	BMS1	1.63	0.93	4.19	7.35	2.24	3.29
Q14694	USP10	1.85	1.00	-3.08	0.93	1.88	0.57
Q14697	GANAB	3.24	1.65	2.05	0.43	0.37	0.07
Q14739	LBR	2.22	0.94	4.26	2.79	4.54	2.84
Q14781	CBX2	4.10	3.56	-1.56	2.93	-1.36	2.69
Q14807	KIF22	4.06	9.51	2.68	6.65	3.78	8.06
Q14839	CHD4	-1.07	2.66	-2.19	1.24	-2.44	3.32
Q14847	LASP1	1.53	1.79	-0.26	0.26	0.37	0.38
Q14966	ZNF638	5.10	3.94	0.74	0.62	0.77	0.65
Q14974	KPNB1	4.52	2.48	1.94	1.02	3.47	1.81
Q14978	NOLC1	0.93	1.24	3.59	3.07	3.34	2.43
Q14980	NUMA1	6.27	4.44	5.30	5.05	4.92	4.93
Q14997	PSME4	4.83	5.59	-1.51	1.78	1.12	2.53
Q15007	WTAP	0.45	0.24	1.66	1.06	1.89	1.16
Q15008	PSMD6	3.28	3.16	0.74	0.87	0.64	1.29
Q15019	SEPTIN2	5.17	5.32	4.09	7.91	4.39	5.12
Q15020	SART3	4.28	10.90	5.86	5.34	5.65	5.23
Q15021	NCAPD2	3.01	1.65	2.86	7.64	2.90	4.31
Q15022	SUZ12	-0.04	0.39	1.74	1.03	4.04	2.65
Q15024	EXOSC7	1.50	0.94	0.26	0.21	-1.08	0.97
Q15029	EFTUD2	3.34	2.64	2.49	2.14	3.28	4.60
Q15046	KARS	4.27	2.62	0.12	0.04	0.77	0.29
Q15047	SETDB1	2.55	0.94	-1.74	2.96	-2.08	4.19
Q15050	RRS1	0.44	0.11	2.77	1.34	-2.41	1.21
Q15056	EIF4H	6.40	7.45	5.65	2.43	6.32	2.58
Q15059	BRD3	7.40	5.39	4.85	2.23	5.02	2.05
Q15061	WDR43	1.59	0.92	5.07	4.79	4.76	10.67
Q15084	PDIA6	5.68	4.06	2.80	1.10	5.42	6.69
Q15102	PAFAH1B3	2.14	0.96	3.69	2.67	3.19	6.35
Q15149	PLEC	-0.94	0.43	2.34	1.87	1.37	1.15

Q15181	PPA1	2.56	0.91	0.21	2.24	0.42	3.85
Q15185	PTGES3	4.77	4.28	4.78	3.24	5.14	3.17
Q15233	NONO	4.51	4.68	5.43	5.00	5.83	7.43
Q15269	PWP2	1.16	0.82	1.89	1.11	3.18	3.17
Q15287	RNPS1	4.05	3.51	3.03	3.82	3.31	3.95
Q15291	RBBP5	3.56	1.89	-0.19	0.08	-1.43	0.67
Q15345	LRRC41	3.74	0.97	3.76	2.61	4.40	5.00
Q15365	PCBP1	7.04	3.94	4.74	3.17	5.67	3.31
Q15366	PCBP2	8.83	5.36	4.52	3.50	5.15	3.34
Q15369	ELOC	2.68	2.15	2.87	6.30	4.34	4.53
Q15393	SF3B3	1.47	2.35	-2.94	2.61	-1.91	2.94
Q15397	PUM3	-1.08	1.77	-0.94	1.12	-1.10	1.41
Q15398	DLGAP5	-0.19	4.94	-0.63	0.21	0.07	0.02
Q15406	NR6A1	1.54	0.98	0.15	0.06	3.08	1.66
Q15417	CNN3	4.76	5.09	1.53	1.23	1.45	1.17
Q15418	RPS6KA1	-5.13	5.75	0.37	0.11	3.47	1.41
Q15424	SAFB	6.55	3.65	7.62	6.58	7.55	4.96
Q15427	SF3B4	3.83	3.22	6.13	7.90	5.43	4.18
Q15428	SF3A2	4.27	2.42	6.46	4.91	5.59	3.94
Q15459	SF3A1	-1.91	1.77	-1.06	0.67	0.53	0.50
Q15527	SURF2	-0.06	0.53	1.73	1.16	0.39	2.71
Q15532	SS18	4.59	7.11	1.64	1.05	4.28	4.62
Q15545	TAF7	0.61	1.04	-4.33	5.56	-6.27	5.06
Q15561	TEAD4	-2.13	4.11	-2.82	0.65	-1.61	0.36
Q15583	TGIF1	1.21	2.35	1.71	2.03	1.80	2.07
Q15596	NCOA2	5.68	6.27	3.21	1.91	4.40	7.51
Q15599	SLC9A3R2	-0.80	0.82	-1.07	0.50	0.65	0.31
Q15637	SF1	6.47	2.84	5.86	3.70	6.54	3.05
Q15648	MED1	1.29	4.54	1.86	2.29	1.48	1.17
Q15651	HMGN3	2.06	1.73	6.01	3.97	3.54	4.92
Q15652	JMJD1C	1.40	4.04	0.58	0.47	0.28	0.22
Q15654	TRIP6	4.21	3.76	1.09	1.05	3.52	6.00
Q15691	MAPRE1	3.72	4.16	1.38	0.46	2.39	1.21
Q15717	ELAVL1	9.14	4.46	2.94	4.38	3.86	8.06
Q15773	MLF2	3.53	6.46	4.25	5.26	4.56	5.07
Q15785	TOMM34	4.21	5.08	-3.81	1.91	-2.40	3.84
Q15796	SMAD2	5.03	1.92	2.91	1.04	3.52	1.21
Q15800	MSMO1	-1.56	0.62	0.15	0.76	1.63	1.16
Q15813	TBCE	-0.18	1.88	0.13	0.95	1.10	1.50
Q15819	UBE2V2	1.72	0.95	0.03	0.18	3.08	7.40
Q15833	STXBP2	1.29	0.90	0.12	1.05	3.36	1.11
Q15843	NEDD8	4.32	2.15	6.00	2.83	6.88	5.84
Q15906	VPS72	0.08	2.19	0.96	0.97	0.00	0.00
Q15928	ZNF141	0.03	0.26	3.75	3.54	6.01	4.07
Q15942	ZYX	3.55	4.80	1.73	0.49	-3.41	0.96
Q16181	SEPTIN7	1.65	0.73	-0.39	0.15	-0.29	0.11
Q16186	ADRM1	3.42	3.60	3.89	3.43	4.40	9.11
Q16204	CCDC6	-1.67	2.54	-5.53	1.56	-1.91	3.16
Q16401	PSMD5	3.94	1.38	0.96	0.40	1.44	0.60
Q16527	CSRP2	5.53	3.71	4.23	3.22	5.43	4.81

Q16531	DDB1	-1.88	2.79	1.14	1.13	1.66	2.27
Q16539	MAPK14	0.96	1.94	1.18	0.91	2.55	4.86
Q16543	CDC37	3.03	1.98	3.90	3.71	3.16	3.29
Q16555	DPYSL2	-1.02	1.66	-2.07	7.71	-1.17	4.76
Q16576	RBBP7	6.00	3.25	4.23	4.79	4.66	6.52
Q16629	SRSF7	5.18	4.16	4.06	4.19	4.07	3.14
Q16630	CPSF6	7.05	3.55	6.33	4.02	6.31	3.53
Q16643	DBN1	2.24	1.27	-0.56	0.42	-0.56	0.28
Q16644	MAPKAPK3	0.04	0.28	0.15	2.73	3.88	2.89
Q16649	NFIL3	1.71	1.06	1.90	1.15	2.28	1.32
Q16658	FSCN1	4.27	3.56	2.53	1.94	2.33	5.08
Q16763	UBE2S	0.38	0.15	1.91	0.93	1.69	0.82
Q16787	LAMA3	-1.17	0.22	-6.94	3.26	2.47	2.00
Q16831	UPP1	2.17	0.94	2.51	1.00	2.38	1.13
Q16851	UGP2	4.39	2.39	3.70	2.28	1.85	1.42
Q16853	AOC3	-1.49	3.15	-1.82	2.17	-2.28	3.18
Q1ED39	KNOP1	1.17	0.40	2.49	3.06	0.37	0.55
Q1KMD3	HNRNPUL2	2.81	0.86	2.26	1.25	2.48	1.30
Q29RF7	PDS5A	4.19	2.97	-3.47	1.33	-3.85	1.49
Q2KHR3	QSER1	4.72	8.64	0.99	0.30	2.53	0.81
Q2M1K9	ZNF423	2.71	0.96	0.61	3.33	4.41	6.82
Q2NL82	TSR1	1.78	0.92	3.23	2.47	3.70	6.22
Q2Q1W2	TRIM71	-0.18	0.32	-2.28	2.14	-0.37	0.38
Q2TAL8	QRICH1	2.95	3.78	0.36	0.13	1.85	0.71
Q2TAY7	SMU1	1.57	4.07	4.42	1.94	4.85	2.04
Q2TBE0	CWF19L2	2.90	1.74	4.71	5.39	4.71	3.76
Q32P41	TRMT5	-2.79	1.08	-4.55	2.52	-3.27	5.05
Q3MHD2	LSM12	1.05	0.54	1.60	1.13	3.12	2.26
Q3T8J9	GON4L	0.43	0.12	-2.96	2.24	-2.64	1.75
Q3ZCX4	ZNF568	1.63	0.97	3.22	3.36	3.20	7.04
Q49A26	GLYR1	0.13	1.22	2.03	1.08	4.84	4.70
Q49AG3	ZBED5	-1.90	1.70	-0.49	0.10	-1.63	0.39
Q4G0J3	LARP7	-1.19	0.81	2.96	1.92	1.79	1.39
Q52LJ0	FAM98B	0.52	1.77	-0.24	0.48	-0.27	0.52
Q53GS9	USP39	4.33	6.13	1.22	2.61	1.89	2.59
Q53HL2	CDCA8	0.99	0.99	0.74	1.13	0.86	1.26
Q562F6	SGO2	5.04	4.69	0.03	0.01	-6.53	5.70
Q562R1	ACTBL2	2.35	5.58	0.85	2.13	1.05	1.54
Q58FF8	HSP90AB2P	-0.10	1.37	3.88	3.96	2.34	1.19
Q5BKZ1	ZNF326	-1.65	2.21	-0.19	0.49	-0.19	0.39
Q5C9Z4	NOM1	0.26	0.28	3.92	8.83	3.72	2.87
Q5D862	FLG2	-4.51	2.05	1.72	0.67	-0.27	0.09
Q5F1R6	DNAJC21	-0.25	3.49	0.04	0.40	0.26	2.36
Q5JSZ5	PRRC2B	1.32	4.10	0.73	0.93	3.47	8.49
Q5JTH9	RRP12	3.20	1.87	3.89	1.25	1.69	0.54
Q5JVF3	PCID2	-1.01	0.89	0.35	0.13	-0.24	0.09
Q5JXB2	UBE2NL	7.35	3.82	1.35	0.43	2.51	0.92
Q5QJE6	DNTTIP2	-1.11	0.51	-1.66	1.76	1.46	1.51
Q5SXM2	SNAPC4	-0.08	0.55	-3.65	1.79	-4.20	3.11
Q5SY16	NOL9	0.89	1.29	1.51	1.00	2.27	6.96

Q5T200	ZC3H13	5.75	4.89	2.32	2.29	2.71	2.68
Q5T230	UTF1	6.29	4.48	-2.41	2.12	-1.53	1.32
Q5T3I0	GPATCH4	1.32	1.86	1.46	1.43	2.81	1.92
Q5T3J3	LRIF1	0.75	0.87	3.11	2.74	3.28	5.07
Q5T5X7	BEND3	6.57	5.04	-1.41	2.28	-0.92	1.90
Q5T653	MRPL2	4.09	8.40	0.00	0.00	4.75	3.79
Q5T6F2	UBAP2	-1.74	1.12	2.62	3.48	2.29	1.99
Q5T7N2	L1TD1	5.10	3.72	2.08	0.88	2.58	1.08
Q5T8P6	RBM26	4.48	5.79	4.00	2.64	3.25	2.09
Q5TBB1	RNASEH2B	-1.76	2.46	-0.93	1.23	-1.45	1.80
Q5TDH0	DDI2	-0.63	0.51	0.10	0.64	2.15	4.49
Q5TFE4	NT5DC1	1.49	2.02	2.10	1.08	3.76	5.60
Q5TGY3	AHDC1	1.06	0.63	0.33	0.16	5.75	3.41
Q5UIP0	RIF1	4.10	4.70	2.24	4.62	2.80	3.86
Q5VT52	RPRD2	5.37	8.12	2.21	1.14	3.06	1.55
Q5VTB9	RNF220	-0.04	0.23	3.83	3.48	3.28	1.97
Q5VTL8	PRPF38B	1.64	0.43	0.41	0.18	-0.52	0.23
Q5VTR2	RNF20	5.00	5.91	3.21	1.11	3.23	1.11
Q5VUA4	ZNF318	3.00	5.74	3.59	1.86	5.51	2.43
Q5VV52	ZNF691	1.65	7.91	0.30	2.36	0.56	2.08
Q5VVJ2	MYSM1	-0.06	0.84	2.01	1.04	2.18	1.03
Q5VWN6	TASOR2	-0.07	0.43	-1.36	0.58	-0.80	0.32
Q5VYK3	ECPAS	1.21	0.97	0.27	1.18	1.00	1.29
Q5VZL5	ZMYM4	6.08	8.39	5.76	3.91	6.14	6.48
Q5W0B1	RNF219	0.07	1.46	3.54	3.49	3.41	4.41
Q5XKE5	KRT79	3.36	1.16	-0.37	0.76	-0.81	2.19
Q63HK5	TSHZ3	-2.61	2.60	1.19	2.00	1.26	1.56
Q66PJ3	ARL6IP4	4.85	1.71	4.64	2.86	4.86	3.33
Q68CP9	ARID2	3.30	4.63	5.40	2.59	4.38	4.45
Q68CQ4	DIEXF	-0.14	1.45	-0.04	0.25	2.59	1.04
Q68E01	INTS3	0.03	0.37	1.64	1.05	0.36	2.26
Q69YH5	CDCA2	1.70	5.34	-0.50	0.63	1.51	1.74
Q69YN2	CWF19L1	2.80	1.80	1.02	1.76	0.08	0.12
Q69YN4	VIRMA	3.55	1.00	-1.39	0.49	2.04	0.74
Q6DD87	ZNF787	3.68	9.13	0.91	0.55	-7.29	6.76
Q6DKI1	RPL7L1	0.28	1.19	1.93	3.01	0.81	1.40
Q6DKJ4	NXN	0.38	1.05	2.63	1.55	1.19	0.47
Q6DN03	HIST2H2BC	2.07	2.33	1.64	1.26	0.32	0.24
Q6EEV6	SUMO4	9.76	9.28	4.53	2.25	5.81	2.47
Q6FI13	HIST2H2AA3	-0.60	0.51	4.30	1.10	2.83	0.73
Q6FI81	CIAPIN1	1.44	7.32	1.13	0.78	-0.62	0.68
Q6IE81	JADE1	-0.03	0.34	-3.45	1.02	-2.97	0.88
Q6IN85	PPP4R3A	-7.15	3.20	-3.78	5.32	-3.78	3.49
Q6IQ21	ZNF770	1.58	2.16	0.84	1.17	2.21	5.31
Q6IQ32	ADNP2	2.98	6.21	3.10	2.10	3.43	2.56
Q6IQ49	SDE2	2.43	3.62	2.49	1.87	3.04	2.26
Q6ISB3	GRHL2	3.71	5.21	0.83	3.12	3.79	6.30
Q6KB66	KRT80	-1.19	0.64	1.98	1.06	2.31	2.02
Q6KC79	NIPBL	-0.90	1.10	-1.23	1.98	-0.37	0.71
Q6L8Q7	PDE12	-0.05	0.28	1.73	1.15	2.26	3.26

Q6MZP7	LIN54	-2.04	3.27	-5.00	4.08	-4.13	2.57
Q6NSW7	NANOGP8	5.25	3.28	2.91	0.99	3.99	3.60
Q6NW34	NEPRO	8.23	2.60	-6.28	1.55	-7.24	1.86
Q6NWY9	PRPF40B	1.52	1.08	-1.41	0.88	-1.18	0.74
Q6NX49	ZNF544	-0.12	1.97	1.77	1.04	1.80	1.13
Q6NXE6	ARMC6	-1.70	1.72	0.71	0.32	2.63	1.68
Q6NXG1	ESRP1	5.06	4.43	2.59	1.36	5.01	2.19
Q6NZI2	CAVIN1	5.24	8.14	-0.03	0.46	0.24	2.11
Q6NZY4	ZCCHC8	-4.12	4.37	0.44	0.50	0.23	0.41
Q6P0N0	MIS18BP1	-0.01	0.05	1.75	2.39	2.51	2.35
Q6P1J9	CDC73	5.20	2.39	-0.15	0.06	0.98	0.48
Q6P1L8	MRPL14	-4.43	1.05	-6.72	8.59	-6.23	6.37
Q6P2Q9	PRPF8	0.14	0.24	-3.73	1.08	-0.98	0.30
Q6P3X3	TTC27	1.46	0.95	-0.02	0.23	1.31	1.13
Q6P4R8	NFRKB	2.15	3.52	-2.17	1.00	-0.40	0.16
Q6P6C2	ALKBH5	-0.18	2.89	0.05	0.02	1.87	0.67
Q6PCT2	FBXL19	-0.08	0.54	0.23	2.15	3.87	2.97
Q6PD62	CTR9	1.41	3.60	0.90	0.92	1.93	1.84
Q6PI98	INO80C	2.31	3.05	2.04	8.83	3.12	2.82
Q6PIW4	FIGNL1	-0.11	1.55	1.80	0.98	3.87	9.02
Q6PJ69	TRIM65	2.64	3.15	-0.01	0.10	0.27	2.01
Q6PJG2	ELMSAN1	3.15	3.62	3.25	4.54	4.72	4.02
Q6PJG6	BRAT1	0.46	0.17	-2.00	4.10	-2.06	1.54
Q6PJT7	ZC3H14	-0.92	3.07	-0.46	1.85	-0.23	0.85
Q6PKG0	LARP1	2.79	2.78	0.68	0.67	-0.04	0.11
Q6RFH5	WDR74	-0.38	0.35	-1.88	2.12	-2.63	6.43
Q6SPF0	SAMD1	3.89	3.67	1.57	0.80	3.05	2.35
Q6UB35	MTHFD1L	-4.65	4.21	-2.59	1.33	-2.00	1.05
Q6UN15	FIP1L1	2.89	1.69	2.32	1.61	1.52	1.11
Q6UWP8	SBSN	-0.15	1.02	1.73	1.12	1.30	1.19
Q6UX04	CWC27	4.82	4.57	3.39	1.34	2.84	1.12
Q6UXN9	WDR82	2.33	1.49	3.40	2.61	3.69	2.59
Q6VMQ6	ATF7IP	2.04	1.09	1.25	0.81	2.23	2.38
Q6ZN08	ZNF66	8.36	7.06	2.95	0.64	3.80	0.83
Q6ZN17	LIN28B	1.10	0.87	-0.68	1.02	3.36	3.47
Q6ZN55	ZNF574	3.80	4.72	1.22	1.08	2.96	4.00
Q6ZNA1	ZNF836	5.57	4.13	-0.70	1.18	-3.45	0.95
Q6ZRI6	C15orf39	-0.11	0.81	-7.10	4.43	-5.40	2.66
Q6ZRY4	RBPMS2	2.31	3.00	2.14	2.39	3.31	4.46
Q6ZU65	UBN2	-1.75	1.19	1.08	0.66	3.92	2.21
Q6ZUJ8	PIK3AP1	3.89	3.62	-1.73	0.88	-1.49	0.76
Q6ZW49	PAXIP1	4.54	3.97	-2.25	0.93	-0.20	0.07
Q71F23	CENPU	-0.13	1.17	0.16	1.51	0.51	3.99
Q71UI9	H2AFV	1.30	0.90	2.68	8.74	1.47	7.61
Q75N03	CBLL1	1.81	0.91	5.06	3.19	4.99	4.06
Q75QN2	INTS8	2.93	1.01	-2.23	0.92	-1.97	0.82
Q7KZ85	SUPT6H	1.19	0.76	-2.02	1.49	-0.48	3.18
Q7KZF4	SND1	4.45	4.29	4.59	2.66	3.90	4.66
Q7L014	DDX46	3.66	2.78	6.34	8.23	6.16	10.35
Q7L190	DPPA4	6.84	4.30	7.26	4.00	6.64	7.74

Q7L1Q6	BZW1	2.28	1.86	0.82	0.98	1.63	1.20
Q7L2H7	EIF3M	1.02	0.89	0.29	0.32	0.11	0.09
Q7L2J0	MEPCE	1.80	1.91	-0.59	0.24	0.12	0.05
Q7L2R6	ZNF765	6.90	8.58	7.17	5.76	7.54	8.43
Q7L4I2	RSRC2	-2.40	2.73	-0.24	0.07	2.28	0.72
Q7L9L4	MOB1B	4.21	4.34	2.73	1.21	3.48	1.48
Q7LBC6	KDM3B	5.41	2.04	6.72	3.24	4.91	4.71
Q7RTV0	PHF5A	1.91	1.02	-0.70	0.34	0.71	0.32
Q7Z2T5	TRMT1L	1.55	0.90	2.39	1.03	0.69	0.30
Q7Z2W4	ZC3HAV1	4.21	3.52	2.50	3.77	3.63	6.58
Q7Z333	SETX	-3.60	1.27	1.03	0.44	-0.26	0.11
Q7Z3K3	POGZ	4.04	1.41	0.71	0.73	2.02	1.84
Q7Z417	NUFIP2	1.56	0.87	-0.03	0.01	-0.39	0.18
Q7Z478	DHX29	0.48	0.60	3.49	1.60	2.22	1.04
Q7Z4Q2	HEATR3	3.69	9.36	3.02	1.81	2.71	1.68
Q7Z4V5	HDGFL2	2.66	2.30	5.65	12.57	5.08	7.34
Q7Z589	EMSY	1.77	3.72	-2.77	2.06	-2.72	2.45
Q7Z5J4	RAI1	2.35	7.09	-1.69	2.24	0.88	2.74
Q7Z5K2	WAPL	-1.93	1.18	-1.18	1.24	-0.96	4.03
Q7Z5L9	IRF2BP2	-0.19	0.12	0.59	0.21	1.60	0.91
Q7Z628	NET1	1.46	1.02	0.09	0.52	0.25	1.38
Q7Z6E9	RBBP6	-0.30	0.36	-0.61	0.42	1.49	1.49
Q7Z6Z7	HUWE1	1.00	0.86	0.09	0.05	0.22	0.11
Q7Z794	KRT77	0.21	0.07	-0.06	0.04	-1.37	1.78
Q7Z7F0	KHDC4	0.83	0.73	1.56	2.06	3.62	4.64
Q7Z7J5	DPPA2	2.31	8.56	0.21	3.13	0.36	2.71
Q7Z7K6	CENPV	2.79	2.25	3.14	4.63	3.13	4.34
Q86SE5	RALYL	4.84	3.03	4.39	1.43	5.27	1.81
Q86U38	NOP9	1.60	2.28	-0.44	0.16	1.04	0.43
Q86U42	PABPN1	6.44	4.04	5.78	2.57	6.34	2.97
Q86U44	METTL3	2.45	5.75	3.76	3.53	3.17	5.47
Q86U70	LDB1	3.83	3.70	2.41	0.84	4.39	1.44
Q86U86	PBRM1	2.53	1.15	6.40	3.25	5.60	6.41
Q86UA1	PRPF39	-0.04	0.33	1.42	0.65	-1.85	0.90
Q86UE8	TLK2	1.49	0.44	-0.80	1.14	-0.41	0.58
Q86UQ0	ZNF589	1.08	1.07	1.83	1.02	1.72	1.11
Q86UU1	PHLDB1	0.45	0.30	2.30	10.18	1.62	4.47
Q86UV5	USP48	3.36	9.65	2.26	1.06	4.21	5.51
Q86UW9	DTX2	3.54	4.78	-3.13	4.23	-1.40	0.87
Q86UZ6	ZBTB46	-2.95	1.05	-3.97	2.08	-2.59	3.76
Q86V15	CASZ1	-0.04	0.39	1.62	0.89	1.65	1.03
Q86V21	AACS	-0.01	0.10	2.31	1.06	4.37	5.75
Q86V81	ALYREF	3.72	5.05	2.24	3.49	2.33	3.15
Q86VF7	NRAP	-1.06	0.28	-6.38	3.51	-1.64	1.74
Q86VM9	ZC3H18	2.92	2.26	1.28	5.26	1.94	2.17
Q86VP6	CAND1	-3.66	3.08	-1.34	0.54	-1.66	0.68
Q86W50	METTL16	1.26	0.86	3.11	2.88	2.47	2.08
Q86WB0	ZC3HC1	-1.28	0.39	6.87	11.25	5.91	4.13
Q86WJ1	CHD1L	-0.18	1.97	1.26	1.01	0.26	2.07
Q86WR0	CCDC25	3.42	2.51	4.08	4.74	4.06	5.36

Q86WX3	RPS19BP1	4.47	4.24	2.11	1.37	4.14	2.34
Q86X53	ERICH1	1.38	0.94	-0.62	1.60	-4.16	2.74
Q86X55	CARM1	5.10	8.15	3.19	2.07	4.86	7.70
Q86X76	NIT1	1.17	0.91	1.58	1.05	1.43	1.05
Q86XP3	DDX42	-0.03	0.05	-1.80	3.28	-1.54	3.36
Q86Y13	DZIP3	1.47	1.29	-1.95	2.11	1.56	1.78
Q86Y37	CACUL1	-0.87	0.48	-4.82	6.36	-5.07	4.76
Q86Y46	KRT73	-2.37	2.98	0.77	0.20	1.52	0.60
Q86Y56	DNAAF5	0.97	0.46	0.52	1.75	2.75	3.31
Q86YL5	TDRP	-0.14	1.79	0.58	1.47	2.00	5.34
Q86YP4	GATAD2A	5.89	2.53	5.56	1.93	6.73	2.25
Q86YZ3	HRNR	-5.19	3.39	0.20	0.07	-0.81	0.37
Q8IU81	IRF2BP1	4.00	2.34	2.92	1.05	5.01	8.81
Q8IUE6	HIST2H2AB	-3.15	1.73	4.41	3.93	2.96	1.91
Q8IUH3	RBM45	0.07	0.55	1.78	1.04	3.05	2.17
Q8IVH2	FOXP4	2.28	2.85	1.34	0.51	2.79	1.04
Q8IVW6	ARID3B	8.31	13.68	6.76	2.87	8.42	2.88
Q8IWA0	WDR75	1.90	0.95	1.87	1.61	1.86	0.75
Q8IWI9	MGA	1.71	1.19	0.18	0.18	0.16	0.08
Q8IWS0	PHF6	1.68	1.21	3.52	2.58	3.37	2.59
Q8IWX8	CHERP	3.88	1.72	3.11	1.28	3.02	1.24
Q8IWZ8	SUGP1	2.06	1.59	-0.68	0.63	-0.12	0.19
Q8IX01	SUGP2	-3.20	2.63	0.71	0.31	1.72	0.79
Q8IX12	CCAR1	-2.40	1.47	-0.60	0.38	0.08	0.04
Q8IX90	SKA3	-0.03	0.44	0.17	2.91	0.43	2.65
Q8IXH7	NELFCD	1.83	0.97	3.24	2.87	4.46	2.82
Q8IXM2	BAP18	-1.71	1.05	3.12	2.28	2.72	1.87
Q8IXQ5	KLHL7	-0.10	0.77	-0.09	0.06	0.54	0.37
Q8IXT5	RBM12B	4.84	4.05	5.09	4.57	5.34	8.71
Q8IXZ3	SP8	4.50	4.16	3.65	1.81	4.22	1.90
Q8IY37	DHX37	2.31	4.67	1.46	1.61	-1.04	0.87
Q8IY67	RAVER1	5.20	4.85	3.69	1.32	4.57	1.60
Q8IY81	FTSJ3	0.80	0.76	3.53	3.45	1.98	1.99
Q8IYB3	SRRM1	3.87	3.06	4.01	3.45	3.90	5.48
Q8IYL3	C1orf174	1.54	1.00	4.81	4.72	0.41	2.47
Q8IZ40	RCOR2	0.17	0.78	3.03	1.11	3.57	1.28
Q8IZ73	RPUSD2	1.80	1.07	4.37	8.82	1.76	1.30
Q8IZ83	ALDH16A1	2.76	2.61	-0.05	0.02	0.51	0.20
Q8IZL8	PELP1	-0.07	1.30	0.03	0.15	1.73	1.12
Q8IZQ5	SELENOH	3.75	3.17	5.23	13.29	5.47	14.22
Q8N0T1	RBIS	1.01	0.92	2.91	1.82	2.52	1.58
Q8N0X7	SPART	2.16	0.97	0.07	1.12	2.85	1.10
Q8N163	CCAR2	5.90	2.69	5.05	4.03	5.06	3.36
Q8N1F7	NUP93	3.18	3.55	1.47	1.00	3.85	6.23
Q8N1G0	ZNF687	3.47	9.41	4.93	2.45	4.95	8.22
Q8N1G2	CMTR1	2.01	4.19	2.50	2.55	3.27	3.99
Q8N1G4	LRRC47	3.11	2.45	1.57	6.13	2.18	3.02
Q8N1N4	KRT78	-0.57	0.19	1.24	0.46	3.61	2.32
Q8N1W2	ZNF710	-0.09	1.53	2.96	2.25	3.90	4.52
Q8N201	INTS1	1.31	0.89	2.02	0.95	3.11	5.28

Q8N2M8	CLASRP	2.86	0.95	1.61	1.13	4.68	2.29
Q8N2W9	PIAS4	4.59	2.88	1.76	0.82	1.82	0.84
Q8N3U4	STAG2	5.15	13.78	2.60	1.13	2.77	5.33
Q8N488	RYBP	2.94	3.46	4.77	6.55	4.97	8.10
Q8N5A5	ZGPAT	1.75	1.55	3.83	7.87	4.61	8.02
Q8N5C6	SRBD1	2.34	1.36	0.70	1.61	1.49	1.24
Q8N684	CPSF7	1.53	1.47	1.92	1.81	2.59	2.47
Q8N6M0	OTUD6B	2.18	0.97	3.73	2.88	0.35	1.53
Q8N6T7	SIRT6	2.15	1.84	1.74	1.03	2.77	5.45
Q8N7C3	TRIML2	1.58	0.92	1.51	5.93	0.90	2.21
Q8N7H5	PAF1	0.02	0.28	3.90	3.53	2.08	1.20
Q8N8K9	KIAA1958	0.02	0.12	2.14	0.87	2.17	0.87
Q8N8S7	ENAH	1.77	1.08	0.11	0.62	5.04	3.96
Q8NAV1	PRPF38A	5.21	3.77	0.21	0.06	3.06	1.21
Q8NC51	SERBP1	5.82	3.29	3.31	1.78	3.00	1.65
Q8NCA5	FAM98A	5.41	3.75	5.22	2.95	4.62	4.96
Q8NCD3	HJURP	1.16	1.05	2.98	1.05	3.63	3.17
Q8NCF5	NFATC2IP	-0.23	3.57	3.89	2.50	6.24	5.65
Q8NCM8	DYNC2H1	2.09	1.06	2.47	1.08	3.60	4.10
Q8NCN4	RNF169	1.20	0.43	-2.04	0.98	0.02	0.02
Q8ND82	ZNF280C	-0.26	4.67	1.72	1.00	0.24	3.12
Q8NDF8	TENT4B	1.99	0.95	1.57	0.99	3.23	5.52
Q8NDT2	RBM15B	0.17	2.19	0.11	0.58	3.29	4.72
Q8NE71	ABCF1	2.65	1.89	0.83	0.25	-0.79	0.24
Q8NEJ9	NGDN	2.39	2.07	0.24	1.70	2.17	1.20
Q8NEY8	PPHLN1	-2.49	1.15	-3.03	2.83	-3.39	5.38
Q8NEZ4	KMT2C	2.84	3.76	2.23	1.71	3.15	2.10
Q8NFD5	ARID1B	4.94	7.37	4.45	2.87	4.80	4.64
Q8NFH3	NUP43	3.48	3.64	-0.93	0.38	1.68	0.73
Q8NFU7	TET1	0.02	0.20	-1.92	0.52	-1.22	0.33
Q8NFW8	CMAS	2.94	2.90	3.76	2.97	4.41	9.40
Q8NHU6	TDRD7	6.88	10.97	8.50	6.34	8.58	3.65
Q8NI36	WDR36	0.95	0.42	1.33	1.11	3.32	4.68
Q8TAF3	WDR48	0.03	0.57	1.20	1.04	0.40	3.27
Q8TAP9	MPLKIP	0.02	2.56	4.81	5.32	4.73	3.80
Q8TAQ2	SMARCC2	0.30	0.21	-0.43	0.41	-1.32	1.28
Q8TBK6	ZCCHC10	-0.14	2.16	1.90	1.14	4.20	8.33
Q8TD26	CHD6	3.34	0.98	-0.04	0.65	3.15	1.08
Q8TDD1	DDX54	0.66	0.35	1.46	3.05	-1.23	0.79
Q8TDI0	CHD5	1.79	0.92	5.25	6.25	5.40	5.19
Q8TDN6	BRIX1	3.29	4.84	4.82	4.53	4.81	4.56
Q8TEA8	DTD1	0.89	0.92	3.63	6.68	3.27	6.56
Q8TER5	ARHGEF40	-0.35	0.10	-1.05	0.36	-0.68	0.22
Q8TEX9	IPO4	2.39	3.46	1.08	1.13	2.64	4.71
Q8TF01	PNISR	2.17	3.72	-2.10	1.27	-1.19	0.76
Q8TF39	ZNF483	8.37	2.94	1.68	0.45	2.65	0.71
Q8TF47	ZFP90	-2.40	0.99	0.05	0.25	1.71	1.31
Q8TF68	ZNF384	5.11	5.93	1.14	1.52	1.21	1.91
Q8WTS6	SETD7	0.70	1.81	0.96	0.68	3.15	3.57
Q8WTT2	NOC3L	-0.15	1.78	2.43	1.28	0.74	0.40

Q8WU58	FAM222B	1.89	1.05	0.02	0.01	2.30	1.55
Q8WUA2	PPIL4	5.28	4.58	1.49	0.87	2.98	1.60
Q8WUA4	GTF3C2	0.38	0.67	1.36	1.25	4.06	9.18
Q8WUD4	CCDC12	2.35	0.95	2.85	1.02	5.91	8.71
Q8WUM0	NUP133	0.02	0.30	0.14	1.44	2.13	1.20
Q8WUM4	PDCD6IP	1.81	0.96	-3.43	1.67	-3.67	2.19
Q8WUQ7	CACTIN	0.00	0.02	2.80	0.99	2.92	1.14
Q8WVB6	CHTF18	-0.03	0.92	2.24	1.03	1.16	1.30
Q8WVC0	LEO1	0.10	1.24	2.90	1.05	0.39	3.85
Q8WVD3	RNF138	-0.10	0.87	1.70	5.72	3.65	4.33
Q8WVJ2	NUDCD2	1.49	0.88	-0.25	0.08	-0.31	0.11
Q8WVV9	HNRNPLL	2.26	1.65	-0.46	0.33	-0.38	0.26
Q8WVY7	UBLCP1	3.73	1.74	-1.57	0.38	-0.46	0.11
Q8WW12	PCNP	10.15	4.13	3.94	0.71	1.36	0.23
Q8WWQ0	PHIP	3.40	3.46	2.45	1.01	2.96	2.68
Q8WWY3	PRPF31	3.33	5.15	4.46	3.52	4.88	4.06
Q8WX92	NELFB	1.49	4.43	0.78	0.30	1.62	0.96
Q8WXA9	SREK1	2.47	3.47	1.26	0.71	3.89	1.86
Q8WXF1	PSPC1	3.55	4.03	3.44	3.20	4.09	3.84
Q8WXI9	GATAD2B	5.82	4.41	5.72	6.46	7.12	6.46
Q8WXX5	DNAJC9	4.04	4.39	5.69	10.42	5.06	4.43
Q8WXX7	AUTS2	3.05	1.75	3.06	1.04	6.92	10.86
Q8WY36	BBX	-1.80	0.90	2.86	7.40	3.53	4.93
Q8WYA6	CTNNBL1	2.78	6.84	0.63	0.73	1.49	1.58
Q8WYJ6	SEPTIN1	-0.24	0.61	-2.50	1.79	-2.81	6.16
Q8WYP5	AHCTF1	0.05	0.50	2.07	0.99	0.61	2.12
Q92499	DDX1	1.62	0.71	5.45	6.94	5.80	4.84
Q92522	H1FX	3.03	1.43	1.79	3.37	0.68	2.30
Q92526	CCT6B	2.88	1.00	2.30	1.07	2.98	4.47
Q92541	RTF1	0.58	0.79	3.85	3.06	4.27	5.91
Q92576	PHF3	4.60	1.96	0.94	0.32	2.74	0.96
Q92585	MAML1	3.96	6.07	4.01	2.52	5.28	8.70
Q92598	HSPH1	4.24	1.89	2.99	1.92	3.99	5.43
Q92610	ZNF592	3.71	1.01	-4.56	1.67	-5.07	2.28
Q92616	GCN1	3.14	2.83	-0.05	0.46	1.40	1.01
Q92618	ZNF516	3.62	2.78	0.36	0.25	1.92	1.81
Q92620	DHX38	0.52	1.35	-0.72	1.29	-1.35	2.08
Q92621	NUP205	4.26	7.96	0.04	0.19	1.80	1.07
Q92688	ANP32B	-0.56	0.86	2.17	0.96	1.95	0.87
Q92733	PRCC	-0.37	0.15	4.79	2.54	5.99	6.80
Q92754	TFAP2C	-0.01	0.10	0.01	0.07	4.27	4.55
Q92766	RREB1	-1.50	0.30	0.87	0.26	4.02	1.22
Q92769	HDAC2	8.19	5.60	0.57	2.03	1.45	3.26
Q92785	DPF2	1.17	2.04	-0.06	0.06	-0.35	0.41
Q92793	CREBBP	3.35	4.32	-0.19	0.38	1.46	3.30
Q92797	SYMPK	2.30	2.15	2.25	1.42	1.65	1.05
Q92804	TAF15	4.32	4.49	4.86	3.25	5.00	3.14
Q92833	JARID2	-0.18	0.11	1.24	0.48	3.57	1.27
Q92841	DDX17	6.83	2.98	8.83	3.59	8.97	3.90
Q92878	RAD50	5.45	3.05	6.23	5.98	7.75	3.58

Q92879	CELF1	-0.84	0.55	0.47	0.52	1.15	1.30
Q92890	UFD1	2.97	7.34	2.81	3.76	3.16	5.59
Q92905	COPS5	2.64	5.25	1.34	0.98	0.26	1.90
Q92908	GATA6	5.01	3.84	7.60	4.22	12.42	5.43
Q92917	GPKOW	-1.44	0.67	3.16	1.66	1.32	0.71
Q92922	SMARCC1	7.34	6.64	8.77	4.38	7.85	4.25
Q92925	SMARCD2	6.00	14.47	4.94	4.29	5.41	5.20
Q92945	KHSRP	5.45	8.97	6.47	3.93	6.97	4.10
Q92973	TNPO1	5.94	6.87	4.39	3.60	5.23	4.42
Q92979	EMG1	2.50	5.75	2.36	1.05	0.97	1.64
Q92995	USP13	1.39	0.63	-3.99	3.26	-1.11	1.56
Q93009	USP7	-2.11	0.92	1.53	2.22	0.93	0.49
Q93062	RBPMS	4.22	3.11	2.96	5.19	4.62	6.35
Q93074	MED12	0.80	0.85	-4.17	3.28	-2.59	2.06
Q93077	HIST1H2AC	0.47	0.92	3.39	1.72	1.25	0.72
Q969F1	GTF3C6	-0.09	0.77	1.89	0.98	0.25	2.33
Q969G3	SMARCE1	3.27	2.34	2.29	1.93	2.10	1.85
Q969Q0	RPL36AL	2.50	4.09	7.03	9.51	6.55	6.81
Q969R5	L3MBTL2	-0.10	1.28	1.70	2.09	1.85	5.06
Q969X6	UTP4	0.87	0.80	-1.14	0.66	0.26	0.13
Q96AE4	FUBP1	5.13	5.37	6.44	4.30	6.70	4.56
Q96AG4	LRRC59	-2.92	4.48	-2.80	3.01	-0.82	3.14
Q96AT1	KIAA1143	-1.28	0.40	-1.00	2.17	-1.55	2.89
Q96B26	EXOSC8	-0.18	1.25	2.60	1.06	2.20	1.04
Q96BD5	PHF21A	1.64	0.98	1.78	6.13	3.03	3.65
Q96BK5	PINX1	-1.26	0.99	1.73	0.98	1.73	0.97
Q96BR9	ZBTB8A	-0.33	0.11	0.83	0.17	1.30	0.27
Q96C00	ZBTB9	-0.02	0.29	0.23	1.16	4.11	6.36
Q96C57	CUSTOS	1.79	0.94	3.59	4.47	3.49	5.14
Q96CN5	LRRC45	5.73	6.72	1.95	1.49	1.08	0.88
Q96CT7	CCDC124	1.64	0.93	3.67	4.11	2.90	3.74
Q96DF8	ESS2	-0.67	0.25	-1.40	0.45	2.07	0.69
Q96DG6	CMBL	2.69	4.93	0.07	1.19	1.68	1.09
Q96DI7	SNRNP40	2.07	1.02	-3.70	3.95	-3.00	3.04
Q96DT7	ZBTB10	2.17	1.51	0.96	1.06	1.61	1.61
Q96E39	RBMXL1	3.55	4.11	0.31	0.43	0.89	1.24
Q96EA4	SPDL1	1.54	0.87	-2.87	2.44	-2.35	2.08
Q96EB6	SIRT1	3.15	1.81	-1.15	0.33	2.28	1.21
Q96EE3	SEH1L	3.63	1.00	-4.14	1.22	-1.73	1.18
Q96EI5	TCEAL4	1.27	1.04	2.84	2.57	3.12	2.89
Q96EP1	CHFR	-0.08	0.57	2.67	0.96	3.64	6.07
Q96EP5	DAZAP1	7.33	5.07	5.84	1.88	6.09	1.85
Q96ER3	SAAL1	-0.21	7.24	2.78	2.65	2.86	2.15
Q96EU6	RRP36	0.04	0.44	0.17	2.03	1.25	1.13
Q96EV2	RBM33	1.66	0.85	5.47	3.12	5.59	7.79
Q96EZ8	MCRS1	-0.21	4.20	1.84	6.40	3.04	3.97
Q96F44	TRIM11	2.52	0.94	4.19	4.01	5.46	5.07
Q96FJ2	DYNLL2	-0.19	2.24	1.09	0.96	1.94	1.09
Q96FW1	OTUB1	1.82	5.55	-0.28	0.29	-1.24	1.41
Q96FZ2	HMCES	1.65	1.20	3.80	3.49	4.45	5.44

Q96G21	IMP4	-5.67	4.80	-1.88	1.62	-2.84	2.26
Q96G46	DUS3L	1.01	0.97	2.02	1.05	3.78	3.46
Q96GD3	SCMH1	-0.20	2.32	-1.53	0.35	2.62	0.65
Q96GD4	AURKB	1.31	0.72	-2.17	4.01	-0.81	0.59
Q96GM5	SMARCD1	4.88	2.98	2.10	1.16	3.67	1.82
Q96GM8	TOE1	2.33	1.02	0.04	0.01	-0.42	0.16
Q96GQ7	DDX27	4.34	4.60	-2.14	1.56	-3.99	2.35
Q96GX5	MASTL	0.90	0.79	2.91	5.40	3.35	5.77
Q96HA7	TONSL	2.06	1.73	2.10	4.00	4.04	4.91
Q96HC4	PDLIM5	2.54	11.01	0.09	1.84	0.52	2.24
Q96HQ2	CDKN2AIPNL	2.93	4.03	-3.86	2.16	-1.89	2.18
Q96HR8	NAF1	5.52	5.11	-0.59	0.26	2.66	1.22
Q96I24	FUBP3	5.67	2.95	3.34	3.22	3.94	4.27
Q96I25	RBM17	4.41	5.37	3.18	1.44	4.12	1.87
Q96IR2	ZNF845	4.28	4.31	4.39	5.02	4.80	11.59
Q96IZ0	PAWR	3.59	4.46	1.02	0.65	0.30	0.19
Q96J01	THOC3	3.09	4.00	1.77	1.04	0.41	2.40
Q96JB3	HIC2	3.74	8.71	2.27	1.03	5.37	3.92
Q96JC9	EAF1	-0.07	0.48	0.06	0.78	0.20	1.76
Q96JM2	ZNF462	4.64	2.13	5.42	3.72	6.40	6.04
Q96JM3	CHAMP1	3.13	2.98	4.61	2.33	4.88	5.25
Q96JM7	L3MBTL3	-0.02	0.23	1.43	1.11	1.09	2.24
Q96JP5	ZFP91	-0.10	1.11	1.79	0.95	2.90	4.26
Q96K83	ZNF521	2.36	5.62	2.77	2.66	5.08	10.01
Q96KP4	CNDP2	1.96	2.59	3.30	5.29	1.13	2.15
Q96KQ7	EHMT2	2.07	1.55	3.54	5.77	4.12	3.70
Q96KR1	ZFR	4.52	4.90	4.94	2.04	5.58	2.23
Q96L73	NSD1	3.40	4.10	0.61	0.44	1.84	1.38
Q96L91	EP400	1.12	0.50	1.68	1.75	0.14	0.15
Q96L92	SNX27	2.92	0.95	2.30	1.00	2.93	1.23
Q96LT9	RNPC3	-0.10	2.30	1.13	0.95	2.70	3.17
Q96ME1	FBXL18	1.22	0.96	-0.07	0.51	4.29	2.07
Q96ME7	ZNF512	4.09	1.19	-3.67	1.54	-5.61	1.80
Q96MF7	NSMCE2	0.00	0.01	1.41	1.17	1.99	1.22
Q96MU7	YTHDC1	4.08	4.75	2.61	2.34	2.65	4.42
Q96MX3	ZNF48	2.57	4.08	1.10	3.47	1.62	1.82
Q96MY1	NOL4L	-0.04	0.66	1.84	0.94	4.39	6.13
Q96N58	ZNF578	0.99	1.02	0.10	0.70	1.37	1.25
Q96NB3	ZNF830	-1.92	1.02	-2.72	1.56	-2.04	4.52
Q96NC0	ZMAT2	3.80	4.62	5.75	5.97	5.41	4.85
Q96NL6	SCLT1	4.92	9.68	-0.06	0.48	0.11	0.95
Q96P11	NSUN5	-2.14	1.53	-0.57	0.55	-0.53	0.51
Q96P16	RPRD1A	11.74	7.03	-2.61	0.58	-2.80	0.62
Q96P63	SERPINB12	-0.87	0.34	1.75	1.10	3.18	3.97
Q96P70	IPO9	0.55	0.25	3.74	1.04	0.72	2.02
Q96PK6	RBM14	4.68	3.97	5.08	8.41	5.62	7.34
Q96PN7	TRERF1	3.10	1.97	-3.26	4.65	-4.53	5.71
Q96PU4	UHRF2	3.74	2.23	3.24	1.59	3.93	1.80
Q96PU8	QKI	7.02	6.04	4.87	1.54	5.93	1.76
Q96PV6	LENG8	1.73	0.90	3.49	2.75	3.89	2.51

Q96PZ0	PUS7	4.17	2.78	5.11	2.67	6.25	9.53
Q96Q11	TRNT1	3.07	2.98	-3.50	2.71	-2.72	3.78
Q96Q89	KIF20B	-1.22	1.13	-4.49	1.62	-2.91	1.17
Q96QC0	PPP1R10	0.94	2.90	5.54	2.66	3.62	2.66
Q96QD9	FYTTD1	0.15	1.67	-2.77	2.42	-0.86	0.67
Q96QE3	ATAD5	1.10	0.97	-0.33	0.13	0.19	0.09
Q96RE7	NACC1	2.43	1.30	-1.53	2.10	-0.18	0.60
Q96RN5	MED15	1.74	1.06	3.14	0.76	1.51	0.65
Q96RS6	NUDCD1	1.44	0.96	-0.56	0.35	-0.18	0.10
Q96RU2	USP28	2.16	0.96	1.93	2.42	3.12	2.33
Q96S94	CCNL2	-0.18	3.32	-2.24	0.95	1.03	0.44
Q96SB8	SMC6	2.38	2.28	1.43	0.63	1.04	0.45
Q96SI1	KCTD15	0.17	2.29	0.16	1.40	3.30	2.83
Q96SI9	STRBP	3.17	8.08	2.63	1.93	2.24	1.66
Q96SR6	ZNF382	-1.13	0.55	-1.40	1.00	-0.38	0.25
Q96ST2	IWS1	2.40	2.36	3.83	2.43	3.08	1.77
Q96ST3	SIN3A	-0.59	0.49	-0.24	0.37	-1.70	2.45
Q96SZ4	ZSCAN10	4.21	6.28	2.14	5.53	3.34	5.20
Q96T23	RSF1	0.01	0.16	1.81	1.08	1.55	1.26
Q96T37	RBM15	-4.51	4.56	-2.03	1.93	-1.06	1.61
Q96T58	SPEN	0.87	0.46	1.58	0.87	0.68	0.37
Q96T60	PNKP	-0.37	0.80	-0.96	0.76	-0.33	0.23
Q96T88	UHRF1	-0.49	0.12	2.60	2.72	3.09	2.40
Q99081	TCF12	0.73	0.84	0.06	0.06	1.93	1.80
Q99426	TBCB	4.08	10.10	5.12	8.79	5.46	3.81
Q99439	CNN2	3.69	2.52	-1.22	0.70	1.61	2.99
Q99456	KRT12	-2.54	1.42	-2.77	0.48	0.11	0.10
Q99459	CDC5L	2.36	1.19	0.36	0.45	-1.26	0.78
Q99460	PSMD1	2.88	1.27	1.12	1.26	1.09	1.28
Q99471	PFDN5	3.40	4.38	2.08	1.11	3.80	3.25
Q99496	RNF2	0.67	2.31	2.30	1.37	3.93	2.08
Q99497	PARK7	2.27	1.16	-0.33	0.11	2.18	0.95
Q99504	EYA3	2.43	3.36	3.54	3.46	4.63	11.46
Q99549	MPHOSPH8	3.26	3.31	-1.03	0.70	-2.25	1.51
Q99575	POP1	-0.21	2.60	0.11	0.91	1.03	1.06
Q99590	SCAF11	2.54	1.28	0.41	0.45	-0.21	0.21
Q99615	DNAJC7	0.96	1.50	0.37	0.20	0.06	0.04
Q99623	PHB2	4.40	4.81	4.46	3.11	3.60	2.22
Q99661	KIF2C	5.32	3.54	1.79	2.38	2.50	2.65
Q99697	PITX2	5.91	13.09	0.22	1.77	0.38	2.59
Q99708	RBBP8	2.45	1.01	-4.14	2.60	-3.94	2.43
Q99728	BARD1	-1.07	0.62	-1.84	0.93	-0.45	0.22
Q99729	HNRNPAB	3.84	4.14	5.84	6.12	5.97	4.21
Q99816	TSG101	-0.05	0.30	-2.29	2.56	-1.01	1.49
Q99829	CPNE1	3.89	7.10	2.79	3.42	4.24	8.90
Q99832	CCT7	-1.13	1.36	-2.22	2.45	-3.23	1.79
Q99836	MYD88	1.14	0.96	-0.02	0.43	2.05	1.07
Q99848	EBNA1BP2	1.85	0.73	6.64	6.19	5.60	7.09
Q99856	ARID3A	5.41	3.00	6.77	3.84	7.43	3.86
Q99873	PRMT1	5.08	5.56	2.99	1.45	3.48	3.31

Q99880	HIST1H2BL	0.43	0.38	3.27	2.15	1.55	1.08
Q99967	CITED2	2.03	11.36	2.25	1.02	4.03	3.99
Q99986	VRK1	-0.17	0.20	-4.95	3.75	-5.59	2.96
Q9BPY3	FAM118B	-7.18	4.18	4.51	1.98	1.90	1.19
Q9BQ04	RBM4B	1.77	0.92	4.26	3.03	5.28	5.46
Q9BQ15	NABP2	-0.17	1.96	1.76	1.02	0.31	3.08
Q9BQ39	DDX50	-0.09	2.10	1.07	0.63	0.90	0.52
Q9BQ52	ELAC2	1.28	1.60	-0.89	0.93	1.57	1.32
Q9BQ61	TRIR	-0.25	0.60	0.65	0.62	1.22	2.58
Q9BQ67	GRWD1	1.39	1.04	-2.45	1.03	0.49	0.20
Q9BQ75	CMSS1	0.73	1.10	2.21	0.86	-0.40	0.13
Q9BQG0	MYBBP1A	8.53	9.69	1.30	0.41	-0.65	0.20
Q9BRA2	TXNDC17	1.86	0.90	-2.30	3.84	-1.62	2.93
Q9BRJ6	C7orf50	-0.47	3.02	-1.27	1.31	-1.46	1.16
Q9BRJ7	NUDT16L1	0.11	1.30	4.43	2.73	4.61	4.44
Q9BRL6	SRSF8	7.85	7.05	8.82	9.54	8.77	8.47
Q9BRP8	PYM1	1.26	0.84	3.75	5.70	3.01	6.20
Q9BRT9	GINS4	0.45	0.34	-1.19	0.88	-0.46	0.61
Q9BRX5	GINS3	1.13	0.63	3.09	4.02	4.15	3.94
Q9BSC4	NOL10	-0.05	0.56	1.53	1.11	1.59	1.19
Q9BSD7	NTPCR	-3.25	1.00	-2.07	1.14	-1.70	1.22
Q9BT23	LIMD2	3.44	3.41	4.99	8.14	5.55	8.65
Q9BTA9	WAC	1.19	0.91	0.57	0.26	2.67	1.23
Q9BTC0	DIDO1	1.79	0.75	-2.47	3.34	-3.24	5.86
Q9BTC8	MTA3	-2.30	5.24	-1.31	0.25	3.32	0.67
Q9BTD8	RBM42	4.05	4.31	3.94	7.15	4.74	6.82
Q9BTE3	MCMBP	0.89	0.34	1.58	0.60	1.54	0.59
Q9BTE7	DCUN1D5	5.21	2.76	-1.27	0.32	-3.39	0.93
Q9BTL3	RAMAC	0.58	0.92	4.37	2.69	4.20	3.24
Q9BTT0	ANP32E	6.43	3.97	7.56	6.09	7.66	4.23
Q9BTW9	TBCD	2.03	1.06	0.92	0.31	-1.23	0.67
Q9BU76	MMTAG2	-1.13	0.63	4.09	1.84	6.48	3.12
Q9BUF5	TUBB6	1.57	1.02	-0.01	0.01	2.47	1.76
Q9BUI4	POLR3C	3.30	3.73	3.63	2.44	2.72	2.10
Q9BUJ2	HNRNPUL1	-2.92	4.37	1.92	1.45	1.16	1.65
Q9BUL5	PHF23	1.66	1.00	3.27	2.56	3.99	2.99
Q9BUQ8	DDX23	2.95	3.29	3.41	3.56	4.42	5.20
Q9BV38	WDR18	0.01	0.17	2.38	1.06	3.00	1.10
Q9BVA1	TUBB2B	5.38	5.29	2.62	3.03	2.61	6.20
Q9BVC3	DSCC1	-0.02	0.41	4.35	2.35	0.64	1.14
Q9BVC5	C2orf49	1.40	2.01	1.64	1.06	1.54	1.89
Q9BVI4	NOC4L	1.53	0.90	2.97	1.49	0.36	0.15
Q9BVJ6	UTP14A	0.28	0.88	4.90	3.85	3.14	4.77
Q9BVJ7	DUSP23	1.50	1.01	0.10	0.61	2.79	2.20
Q9BVP2	GNL3	2.57	0.98	1.14	2.15	0.83	1.39
Q9BW19	KIFC1	1.57	1.71	2.99	4.84	3.42	4.42
Q9BW71	HIRIP3	0.47	0.19	-2.27	2.48	-1.70	2.44
Q9BW85	YJU2	1.63	1.09	-2.43	2.16	-2.25	3.99
Q9BW91	NUDT9	3.91	4.07	2.64	1.09	2.55	1.05
Q9BWD1	ACAT2	1.37	3.68	0.22	0.28	-0.78	1.01

Q9BWE0	REPIN1	1.96	0.90	-1.93	0.64	-2.09	0.69
Q9BWF3	RBM4	7.61	6.78	8.55	5.65	8.97	5.66
Q9BWG6	SCNM1	0.92	1.09	1.50	1.03	0.42	2.50
Q9BWT3	PAPOLG	2.93	2.02	-1.79	0.97	0.05	0.03
Q9BWU0	SLC4A1AP	0.64	1.94	0.82	1.77	0.82	1.76
Q9BWW4	SSBP3	-2.88	2.69	0.33	0.15	2.57	1.52
Q9BXA9	SALL3	0.01	0.03	1.91	0.57	2.03	0.60
Q9BXF3	CECR2	1.42	2.76	0.28	0.24	1.94	1.84
Q9BXK1	KLF16	1.36	0.87	1.73	0.96	0.16	1.22
Q9BXP5	SRRT	5.87	11.72	6.80	3.91	6.63	7.44
Q9BXS6	NUSAP1	-0.19	2.26	0.11	0.85	1.52	1.35
Q9BXW9	FANCD2	1.13	1.06	1.58	1.23	1.92	1.19
Q9BXY0	MAK16	-0.08	0.89	3.98	3.04	3.30	4.79
Q9BY42	RTF2	2.54	2.73	4.91	5.34	5.37	7.60
Q9BY44	EIF2A	5.41	7.03	0.10	0.81	3.15	1.10
Q9BY77	POLDIP3	3.15	2.18	5.39	3.94	5.02	3.50
Q9BYD3	MRPL4	0.06	0.39	-2.38	1.48	0.59	1.59
Q9BYG3	NIFK	2.09	0.93	-0.38	0.15	0.37	0.38
Q9BYW2	SETD2	-0.11	1.92	1.81	1.22	-1.38	0.92
Q9BZ95	NSD3	-2.39	4.46	-2.03	1.31	-0.47	4.23
Q9BZE4	GTPBP4	0.38	0.72	4.82	2.80	4.34	7.49
Q9BZH6	WDR11	-0.24	0.14	-3.99	3.02	-5.90	2.62
Q9BZI1	IRX2	2.50	4.04	1.16	1.00	2.69	4.79
Q9BZJ0	CRNKL1	3.99	4.30	4.19	3.71	4.44	8.78
Q9BZK3	NACA4P	5.30	5.96	-0.35	0.10	1.41	0.49
Q9BZK7	TBL1XR1	6.86	6.13	1.04	0.51	2.43	1.22
Q9BZZ5	API5	5.51	6.39	6.63	11.54	5.88	3.32
Q9C0E2	XPO4	-0.10	0.03	-2.51	0.93	-1.08	0.39
Q9C0J8	WDR33	0.65	1.12	0.43	0.65	1.16	1.77
Q9GZL7	WDR12	3.22	6.08	2.41	2.20	3.44	2.82
Q9GZN2	TGIF2	0.11	2.04	0.12	0.67	1.63	1.26
Q9GZR1	SENP6	3.23	1.02	-3.19	1.99	-2.86	2.01
Q9GZR7	DDX24	2.15	1.05	-0.50	0.92	-2.01	2.06
Q9GZS1	POLR1E	-0.08	0.77	3.15	6.50	2.85	6.49
Q9GZS3	WDR61	0.66	0.68	-1.78	1.01	-2.07	1.29
Q9GZU8	FAM192A	0.09	2.49	3.11	0.98	5.30	4.30
Q9GZV8	PRDM14	5.02	5.84	0.69	0.33	1.16	0.57
Q9H009	NACA2	3.76	1.57	4.38	1.52	3.17	1.14
Q9H0A0	NAT10	2.79	2.43	3.59	3.37	4.30	3.31
Q9H0C8	ILKAP	4.60	6.50	3.86	3.63	4.56	4.94
Q9H0D6	XRN2	6.56	10.67	7.26	5.62	7.97	5.22
Q9H0E3	SAP130	2.55	2.49	3.50	5.58	4.35	5.71
Q9H0E7	USP44	2.36	3.02	-0.25	0.09	-0.28	0.10
Q9H0E9	BRD8	-0.09	0.78	0.07	0.44	4.63	3.84
Q9H0H5	RACGAP1	-0.45	0.23	2.00	1.66	3.75	8.03
Q9H0K6	PUS7L	4.42	4.23	0.83	0.38	-1.98	0.92
Q9H0L4	CSTF2T	2.29	2.33	5.36	3.13	5.56	2.84
Q9H0S4	DDX47	4.32	5.30	4.09	2.53	3.74	2.29
Q9H0Z9	RBM38	0.03	1.46	1.68	0.92	1.91	1.16
Q9H147	DNTTIP1	1.80	0.88	2.54	1.49	2.04	1.24

Q9H1B7	IRF2BPL	2.36	0.92	-0.43	0.43	-0.42	1.17
Q9H1E3	NUCKS1	-0.76	0.60	4.65	2.98	4.69	3.06
Q9H223	EHD4	3.29	2.73	4.87	4.07	2.29	6.34
Q9H2H8	PPIL3	2.87	1.72	3.15	1.79	4.68	2.33
Q9H2P0	ADNP	3.08	3.39	2.10	1.62	2.61	2.94
Q9H2U1	DHX36	3.62	0.93	0.35	0.33	3.26	3.30
Q9H2W2	MIXL1	8.18	5.19	2.67	3.29	4.23	3.74
Q9H2Y7	ZNF106	-4.19	2.68	-1.93	1.24	-3.14	1.63
Q9H307	PNN	6.23	3.41	6.07	6.38	5.25	7.92
Q9H334	FOXP1	-2.80	0.96	-3.52	2.06	-0.65	2.29
Q9H3K6	BOLA2	0.05	2.98	2.27	1.01	2.94	1.28
Q9H3P2	NELFA	3.63	2.29	5.86	5.81	6.73	5.02
Q9H3R5	CENPH	-0.20	3.69	-0.11	0.04	1.97	1.15
Q9H444	CHMP4B	4.27	4.90	3.68	1.59	4.02	1.74
Q9H4L4	SENP3	-0.04	0.01	4.66	2.14	6.05	3.60
Q9H4L7	SMARCAD1	5.41	3.39	1.23	2.39	0.48	1.03
Q9H4M9	EHD1	-0.15	1.51	4.23	3.24	2.69	1.40
Q9H4Z3	PCIF1	-0.07	0.80	3.86	4.87	2.95	6.73
Q9H501	ESF1	1.09	0.89	2.87	3.17	2.70	2.58
Q9H582	ZNF644	2.30	1.84	-1.20	2.06	0.79	1.48
Q9H583	HEATR1	-1.03	0.60	-0.29	0.29	-0.52	0.53
Q9H5H4	ZNF768	2.71	0.95	2.87	1.04	4.28	1.86
Q9H5V9	CXorf56	-0.03	0.33	0.08	0.58	0.35	2.43
Q9H6F5	CCDC86	0.03	0.13	5.13	10.44	4.15	6.13
Q9H6I2	SOX17	0.05	0.87	12.53	3.03	6.83	2.18
Q9H6R4	NOL6	5.08	5.10	2.53	1.04	2.88	1.28
Q9H6Y2	WDR55	-2.37	1.01	-1.33	0.32	-0.60	0.13
Q9H7B2	RPF2	0.95	1.15	3.85	3.12	1.27	1.66
Q9H7L9	SUDS3	0.98	0.88	4.12	3.18	4.74	5.67
Q9H7N4	SCAF1	1.89	0.95	2.25	1.00	3.28	6.50
Q9H7Z6	KAT8	3.65	2.41	-1.89	0.41	-1.62	0.35
Q9H814	PHAX	1.17	0.86	2.65	1.13	2.44	1.08
Q9H8G2	CAAP1	5.93	5.22	0.15	1.25	1.92	1.14
Q9H8H0	NOL11	-0.02	0.64	4.75	2.48	0.04	0.02
Q9H8M2	BRD9	-2.75	3.86	-2.95	4.61	-2.60	6.92
Q9H8V3	ECT2	2.26	0.94	-2.04	0.92	-0.17	0.06
Q9H8Y1	VRTN	7.54	7.31	7.17	8.25	7.96	5.16
Q9H910	JPT2	4.33	4.48	5.95	3.53	5.70	8.29
Q9H981	ACTR8	2.04	3.27	4.03	3.08	4.04	4.65
Q9H992	7-Mar	6.33	4.11	-3.12	1.92	-4.32	4.13
Q9H993	ARMT1	4.14	8.52	3.81	6.48	3.83	3.53
Q9H9A6	LRRC40	-1.92	1.03	-1.59	2.60	-0.65	0.65
Q9H9A7	RMI1	0.01	0.11	0.18	1.40	0.33	2.16
Q9H9B1	EHMT1	-1.10	3.06	-0.92	0.91	1.37	2.22
Q9H9F9	ACTR5	-0.17	1.87	3.01	4.66	1.57	1.05
Q9H9Z2	LIN28A	7.99	12.98	5.63	2.13	4.98	1.94
Q9HAF1	MEAF6	-5.53	3.91	0.91	0.27	2.29	0.71
Q9HAH7	FBRS	3.35	11.10	1.76	0.97	5.62	7.20
Q9HAV0	GNB4	1.01	0.43	1.29	0.98	3.57	4.59
Q9HAV4	XPO5	2.26	1.36	-5.05	5.57	-7.89	2.60

Q9HB07	C12orf10	-0.14	2.10	-0.94	0.25	0.09	0.02
Q9HB71	CACYBP	4.63	6.63	2.44	1.27	1.79	0.83
Q9HBE1	PATZ1	7.15	12.29	-1.96	5.45	-1.89	5.16
Q9HBL8	NMRAL1	2.82	1.80	2.78	4.92	3.89	1.91
Q9HBM6	TAF9B	-0.08	1.11	1.60	0.93	4.23	5.01
Q9HCD5	NCOA5	5.04	11.52	3.64	1.83	4.50	2.19
Q9HCE3	ZNF532	7.25	15.39	1.77	1.11	1.47	1.35
Q9HCE5	METTL14	1.58	0.82	0.35	0.16	-0.13	0.06
Q9HCG8	CWC22	0.46	0.34	1.44	0.71	2.81	2.50
Q9HCK8	CHD8	0.07	0.82	2.32	0.99	5.21	4.31
Q9HCM1	RESF1	-2.76	3.90	-3.84	1.14	-1.08	1.42
Q9HCM7	FBRSL1	1.58	1.00	-0.03	0.18	3.32	6.55
Q9HCS4	TCF7L1	3.30	3.36	3.41	3.47	5.08	5.43
Q9HCS7	XAB2	4.81	3.76	-3.23	1.36	-2.94	7.03
Q9HCU9	BRMS1	-6.37	5.23	-6.03	4.36	-6.52	2.54
Q9NP50	SINHCAF	2.57	1.01	1.63	0.68	2.92	1.23
Q9NP66	HMG20A	4.83	4.45	-0.44	0.62	1.06	4.30
Q9NP77	SSU72	-0.42	0.81	3.51	1.59	3.65	1.70
Q9NPA3	MID1IP1	-2.23	6.42	-5.81	6.10	-4.12	7.13
Q9NPA8	ENY2	-0.14	0.05	-2.08	0.94	3.66	1.54
Q9NPD3	EXOSC4	3.26	3.45	1.52	1.07	2.44	2.94
Q9NPF5	DMAP1	3.97	3.78	-0.03	0.04	0.24	0.31
Q9NPG3	UBN1	-0.01	0.32	2.32	1.06	2.63	1.20
Q9NPI1	BRD7	-0.10	0.69	2.94	3.69	4.58	3.49
Q9NQ29	LUC7L	2.63	4.74	2.38	2.73	2.42	4.80
Q9NQ55	PPAN	1.90	1.32	3.79	4.45	3.46	3.10
Q9NQ88	TIGAR	3.61	4.85	4.33	5.55	3.94	4.59
Q9NQB0	TCF7L2	0.54	0.77	-0.01	0.10	4.57	2.96
Q9NQG5	RPRD1B	4.82	5.03	-2.83	1.83	-1.47	3.42
Q9NQS7	INCENP	-0.07	3.48	-0.18	0.07	-1.69	0.86
Q9NQW6	ANLN	2.22	0.95	2.23	1.84	1.55	0.80
Q9NQZ2	UTP3	2.83	0.97	2.58	1.03	2.05	1.18
Q9NR30	DDX21	5.30	3.31	7.15	5.56	6.67	6.44
Q9NR31	SAR1A	3.03	2.92	0.24	0.11	0.29	0.20
Q9NR45	NANS	3.40	6.09	4.30	9.22	4.87	4.50
Q9NRL2	BAZ1A	-0.62	0.38	3.20	3.26	3.86	5.49
Q9NRN7	AASDHPPT	4.14	4.10	3.23	7.03	4.37	6.21
Q9NRX1	PNO1	2.66	2.11	0.07	0.33	-0.10	0.73
Q9NRX4	PHPT1	-0.04	1.28	1.49	1.02	3.39	5.02
Q9NRZ9	HELLS	5.04	3.18	3.59	1.52	5.81	2.44
Q9NS91	RAD18	0.14	0.47	0.33	0.15	1.52	1.11
Q9NSB4	KRT82	-1.45	2.36	-0.37	0.33	-0.68	0.62
Q9NSC2	SALL1	6.79	6.34	3.37	5.37	4.34	4.21
Q9NSI2	FAM207A	1.31	1.65	1.33	2.07	2.93	3.60
Q9NTI5	PDS5B	3.98	3.11	1.61	2.86	2.30	3.95
Q9NTJ3	SMC4	2.96	1.98	4.10	3.18	4.26	3.46
Q9NTZ6	RBM12	4.64	5.98	4.47	2.51	4.94	3.04
Q9NU22	MDN1	-0.17	0.38	-0.82	1.06	0.43	0.42
Q9NUL3	STAU2	-0.17	1.35	0.13	2.69	0.23	3.17
Q9NV06	DCAF13	2.35	1.00	2.52	1.08	0.70	1.98

Q9NVI1	FANCI	4.24	3.38	1.18	0.97	3.27	2.34
Q9NVN8	GNL3L	2.43	2.80	3.36	2.47	4.42	5.14
Q9NVP1	DDX18	3.17	2.63	1.99	1.45	1.83	1.91
Q9NVU7	SDAD1	-0.50	1.57	3.56	4.64	2.68	3.85
Q9NVX2	NLE1	2.74	0.71	1.76	0.99	2.46	1.74
Q9NW07	ZNF358	1.12	1.10	3.33	5.99	3.65	5.34
Q9NW13	RBM28	-1.34	1.47	1.08	0.42	1.31	0.51
Q9NW64	RBM22	2.69	3.51	2.24	1.39	2.76	1.70
Q9NW82	WDR70	2.18	1.43	3.52	2.15	3.55	2.16
Q9NWH9	SLTM	5.77	8.82	7.26	6.95	6.96	4.25
Q9NWY4	HPF1	2.26	1.78	2.05	1.09	2.15	1.33
Q9NX58	LYAR	0.13	0.07	2.38	1.50	0.72	0.47
Q9NXA8	SIRT5	0.18	2.66	0.20	2.86	2.52	1.05
Q9NXF1	TEX10	-0.12	0.81	0.42	0.76	-0.47	0.53
Q9NXF7	DCAF16	1.44	1.30	1.63	3.07	1.90	1.15
Q9NXG2	THUMPD1	2.56	1.92	5.45	6.67	4.90	3.13
Q9NXH9	TRMT1	2.70	1.75	2.55	1.12	0.78	0.34
Q9NXV6	CDKN2AIP	5.39	3.91	4.47	3.19	5.63	5.62
Q9NYF8	BCLAF1	3.45	4.89	3.19	5.99	3.60	5.25
Q9NYH9	UTP6	3.98	2.64	0.21	0.30	0.32	0.36
Q9NYP9	MIS18A	0.73	0.39	-3.33	2.19	-2.01	1.55
Q9NYV4	CDK12	-0.14	0.04	1.60	0.55	1.20	0.41
Q9NYZ3	GTSE1	1.43	1.06	3.40	6.09	2.16	1.13
Q9NZ63	C9orf78	1.17	0.89	0.17	0.91	1.18	1.32
Q9NZ71	RTEL1	-0.09	0.54	0.18	1.26	1.43	1.33
Q9NZC9	SMARCAL1	-1.09	0.57	0.90	2.81	0.29	0.43
Q9NZI8	IGF2BP1	3.93	1.80	2.93	2.47	1.62	4.77
Q9NZL4	HSPBP1	4.59	5.10	2.43	6.30	1.70	1.13
Q9NZL9	MAT2B	1.94	1.01	4.49	3.47	4.48	6.17
Q9NZT2	OGFR	-0.12	1.03	-0.62	0.38	-1.16	0.74
Q9P013	CWC15	4.87	4.26	0.69	0.37	0.58	0.31
Q9P031	CCDC59	0.10	1.84	5.23	3.38	5.78	5.37
Q9P0K7	RAI14	5.44	5.79	-2.99	2.11	-1.91	2.72
Q9P0M6	H2AFY2	3.54	4.25	5.16	5.13	3.83	3.50
Q9P0U4	CXXC1	-1.78	0.35	1.55	0.35	0.22	0.05
Q9P0W2	HMG20B	0.41	0.79	4.69	3.85	6.16	7.99
Q9P1Y6	PHRF1	-0.11	1.53	2.08	1.03	3.00	12.33
Q9P258	RCC2	7.65	5.65	5.11	2.77	5.81	2.52
Q9P273	TENM3	2.06	0.67	2.90	0.96	-0.55	0.15
Q9P2D1	CHD7	2.91	1.16	-2.86	2.59	-1.73	1.60
Q9P2E9	RRBP1	3.29	4.13	4.20	3.36	1.48	1.46
Q9P2I0	CPSF2	1.38	1.28	1.80	1.54	2.04	1.39
Q9P2J5	LARS	-1.23	2.37	-1.16	1.78	-2.92	3.07
Q9P2K5	MYEF2	-0.55	0.30	4.35	1.95	3.48	1.79
Q9P2M7	CGN	0.71	2.32	0.04	0.18	0.34	1.65
Q9P2N5	RBM27	4.33	2.77	5.74	3.45	7.63	3.43
Q9P2N6	KANSL3	0.11	3.00	-0.64	0.25	-1.96	0.88
Q9P2R6	RERE	4.70	3.93	-0.83	0.25	3.72	1.25
Q9P2W1	PSMC3IP	0.81	1.02	-1.49	0.99	0.83	0.54
Q9P2Y4	ZNF219	-0.59	0.46	-3.60	1.77	0.11	0.06

Q9UBB4	ATXN10	1.62	1.00	1.83	1.13	1.76	1.18
Q9UBB9	TFIP11	0.00	0.00	2.06	1.11	2.17	1.16
Q9UBC3	DNMT3B	3.93	3.46	1.95	0.67	1.22	0.42
Q9UBD5	ORC3	2.17	0.90	3.05	3.39	4.16	2.96
Q9UBE0	SAE1	3.67	3.01	2.81	1.08	2.76	1.06
Q9UBL3	ASH2L	3.15	1.00	5.14	5.00	4.34	3.13
Q9UBQ5	EIF3K	2.17	1.06	2.46	2.50	3.60	3.49
Q9UBQ7	GRHPR	-1.27	1.09	-3.76	2.17	-2.10	1.50
Q9UBT2	UBA2	2.41	3.83	2.86	3.47	3.44	5.90
Q9UBU8	MORF4L1	-1.08	0.57	3.14	1.68	3.10	1.65
Q9UBU9	NXF1	4.97	3.75	5.52	5.12	5.58	9.18
Q9UBW7	ZMYM2	0.11	0.08	-0.86	1.11	-0.55	0.70
Q9UDY2	TJP2	-2.61	4.32	-3.12	3.74	-1.79	1.68
Q9UEE9	CFDP1	3.17	6.48	4.69	3.08	4.45	3.04
Q9UER7	DAXX	-0.16	1.57	1.10	1.06	3.97	6.00
Q9UFC0	LRWD1	4.08	3.64	1.96	0.86	2.59	1.13
Q9UFW8	CGGBP1	4.19	2.20	4.37	3.34	5.31	9.75
Q9UGI8	TES	0.76	0.28	3.56	2.79	4.93	7.25
Q9UGU0	TCF20	-0.67	0.67	-3.67	2.92	-2.19	1.93
Q9UGU5	HMGXB4	0.67	0.77	1.44	1.45	-0.86	0.87
Q9UHB6	LIMA1	5.11	6.14	0.52	0.96	-0.79	4.90
Q9UHB7	AFF4	-1.50	0.96	-0.95	0.55	0.17	0.08
Q9UHD1	CHORDC1	2.39	2.21	2.25	1.36	0.37	0.22
Q9UHD8	SEPTIN9	3.13	1.86	-2.25	1.69	-2.16	1.59
Q9UHD9	UBQLN2	2.02	1.05	0.10	0.68	3.53	5.60
Q9UHI6	DDX20	2.83	3.46	0.73	1.59	1.95	7.41
Q9UHL9	GTF2IRD1	1.53	1.11	1.35	1.18	4.21	7.05
Q9UHR5	SAP30BP	0.81	0.63	2.01	2.08	2.47	2.92
Q9UHV9	PFDN2	6.05	3.45	-0.73	6.40	-0.50	1.90
Q9UHX1	PUF60	2.82	0.58	3.60	0.71	3.47	0.68
Q9UI30	TRMT112	4.36	6.95	0.50	0.59	1.16	1.63
Q9UI95	MAD2L2	1.03	0.41	0.39	0.94	1.79	4.45
Q9UIA9	XPO7	-0.20	3.67	1.45	0.96	0.25	3.81
Q9UIF9	BAZ2A	1.84	8.54	2.05	1.83	3.38	2.60
Q9UIG0	BAZ1B	6.16	4.09	3.09	1.26	4.61	1.68
Q9UIU6	SIX4	5.38	4.20	1.86	0.97	5.12	3.72
Q9UJA5	TRMT6	2.06	3.91	1.43	0.95	1.00	1.31
Q9UJQ4	SALL4	8.19	4.12	8.62	3.64	8.90	3.22
Q9UJU3	ZNF112	3.92	5.44	4.88	4.33	6.01	4.84
Q9UJV9	DDX41	0.66	0.48	-0.66	0.63	-0.31	0.33
Q9UJX3	ANAPC7	2.08	1.04	0.20	1.56	2.96	3.26
Q9UK53	ING1	-0.05	2.68	4.18	3.77	0.39	2.53
Q9UK59	DBR1	2.03	4.64	3.26	2.97	3.24	6.09
Q9UK61	TASOR	-0.11	1.73	-0.03	0.21	1.23	1.17
Q9UK76	JPT1	4.56	8.41	2.73	0.93	4.30	4.95
Q9UKA9	PTBP2	2.96	3.13	2.78	3.69	3.60	3.71
Q9UKD2	MRTO4	1.74	2.79	4.22	8.62	4.25	4.11
Q9UKF6	CPSF3	3.57	3.37	-4.49	3.13	-3.75	2.03
Q9UKJ3	GPATCH8	-0.01	0.16	1.42	1.00	0.37	2.40
Q9UKL0	RCOR1	3.54	3.98	3.21	9.77	3.53	2.65

Q9UKM9	RALY	7.72	4.36	7.72	2.83	7.86	3.16
Q9UKN8	GTF3C4	1.85	0.83	0.93	0.39	0.70	0.29
Q9UKV3	ACIN1	3.84	10.76	3.91	9.18	4.42	5.87
Q9UKX7	NUP50	1.07	1.86	-1.16	3.30	-0.47	1.48
Q9UL15	BAG5	0.07	0.94	0.06	0.61	3.65	7.97
Q9UL40	ZNF346	3.34	1.87	2.06	1.01	2.44	1.24
Q9ULD9	ZNF608	2.72	7.53	1.84	0.85	3.80	1.66
Q9ULJ3	ZBTB21	3.60	6.65	0.18	0.07	0.65	0.27
Q9ULK4	MED23	1.50	2.30	6.66	3.72	4.37	3.77
Q9ULL5	PRR12	5.19	3.81	4.54	3.29	4.94	7.88
Q9ULM3	YEATS2	-0.10	1.35	3.47	5.44	1.81	1.11
Q9ULR0	ISY1	1.28	1.08	0.94	0.70	2.94	2.15
Q9ULU4	ZMYND8	3.10	2.30	5.43	4.10	4.58	2.92
Q9ULW0	TPX2	4.11	4.55	0.88	3.52	1.06	2.84
Q9ULX6	AKAP8L	3.81	2.61	5.23	6.13	6.62	11.23
Q9UM19	HPCAL4	-2.24	0.93	-0.03	0.01	-0.53	0.17
Q9UMN6	KMT2B	2.46	1.23	0.36	1.90	3.00	5.80
Q9UMR2	DDX19B	2.50	1.00	2.46	0.98	5.67	5.07
Q9UMS4	PRPF19	3.76	3.47	2.74	0.86	3.31	1.04
Q9UMS5	PHTF1	2.46	1.00	0.08	0.63	0.17	1.29
Q9UMX0	UBQLN1	-2.67	1.56	-4.57	6.78	-2.89	2.80
Q9UMY1	NOL7	2.73	0.99	4.30	9.73	4.43	8.42
Q9UN79	SOX13	0.44	3.09	1.04	0.42	2.45	0.99
Q9UN86	G3BP2	2.07	0.94	0.47	0.15	1.17	0.40
Q9UNA4	POLI	-1.93	4.49	1.99	1.17	2.19	1.18
Q9UNE7	STUB1	-0.12	1.28	0.08	0.53	1.45	1.30
Q9UNF1	MAGED2	3.23	2.88	4.87	5.97	3.45	1.68
Q9UNP9	PPIE	0.62	0.70	2.97	2.82	3.44	5.15
Q9UNQ2	DIMT1	1.57	0.61	2.67	1.67	3.35	2.65
Q9UNS1	TIMELESS	2.46	1.75	0.50	1.35	-0.05	0.20
Q9UNS2	COPS3	-0.43	0.21	0.64	0.35	-0.12	0.06
Q9UNW9	NOVA2	1.16	0.97	0.00	0.02	0.34	2.84
Q9UNX4	WDR3	-0.13	1.32	0.54	3.53	1.45	3.13
Q9UNZ2	NSFL1C	-6.31	2.99	3.17	4.80	0.27	9.60
Q9UPN6	SCAF8	4.37	4.18	2.38	0.97	0.33	0.12
Q9UPN9	TRIM33	7.83	6.89	6.65	4.29	7.04	5.80
Q9UPP1	PHF8	0.76	0.95	2.47	0.94	4.80	3.13
Q9UPS8	ANKRD26	1.38	1.81	0.85	0.48	0.02	0.01
Q9UPT8	ZC3H4	6.29	3.32	2.94	1.00	2.95	0.98
Q9UPV0	CEP164	3.68	3.02	-2.48	3.37	-2.05	2.51
Q9UPW0	FOXJ3	3.47	3.71	0.17	1.88	3.39	3.31
Q9UPW6	SATB2	2.70	1.50	-2.31	3.28	-0.92	1.64
Q9UQ35	SRRM2	6.01	2.61	4.00	1.44	5.10	1.72
Q9UQ80	PA2G4	4.79	2.36	0.31	0.19	-0.66	0.74
Q9UQ84	EXO1	1.73	0.91	0.11	1.96	0.18	1.66
Q9UQ88	CDK11A	2.61	2.30	3.95	5.35	4.65	9.41
Q9UQ90	SPG7	-0.04	0.68	5.25	3.89	0.33	2.98
Q9UQE7	SMC3	2.38	1.70	2.26	2.17	2.25	1.94
Q9UQR0	SCML2	-0.08	3.28	-1.83	0.88	-1.71	0.82
Q9Y221	NIP7	6.81	2.27	2.52	0.50	1.89	0.36

Q9Y224	RTRAF	3.98	3.34	2.39	2.87	4.70	3.17
Q9Y230	RUVBL2	6.95	3.67	-1.69	2.41	-1.17	2.14
Q9Y232	CDYL	-0.05	1.45	0.01	0.01	0.51	0.22
Q9Y237	PIN4	2.01	1.00	-1.39	4.72	-0.58	0.78
Q9Y250	LZTS1	7.48	5.53	7.49	4.00	8.43	10.44
Q9Y261	FOXA2	3.00	0.92	0.22	0.11	1.68	3.55
Q9Y262	EIF3L	4.31	4.01	1.52	0.95	3.28	7.31
Q9Y263	PLAA	3.65	2.47	-2.77	1.24	-2.02	0.83
Q9Y265	RUVBL1	4.34	4.00	4.31	6.67	4.73	6.38
Q9Y266	NUDC	4.85	9.93	3.06	3.47	1.74	1.29
Q9Y277	VDAC3	-0.06	2.02	2.20	1.06	3.96	2.10
Q9Y2F5	ICE1	-0.06	0.87	0.04	0.45	0.45	3.95
Q9Y2K1	ZBTB1	1.58	0.93	3.00	2.34	3.88	9.55
Q9Y2K7	KDM2A	1.80	0.88	0.17	0.91	4.29	11.08
Q9Y2L1	DIS3	4.22	3.86	1.44	0.65	2.51	1.15
Q9Y2P8	RCL1	2.25	2.50	2.62	1.81	2.25	2.14
Q9Y2R4	DDX52	-0.11	0.04	3.34	2.53	2.78	2.39
Q9Y2S6	TMA7	2.27	3.34	2.61	1.73	2.31	1.59
Q9Y2U8	LEMD3	1.54	0.92	3.88	3.24	3.31	3.37
Q9Y2V2	CARHSP1	5.88	3.66	2.74	0.81	1.38	0.40
Q9Y2W1	THRAP3	-0.42	0.16	-2.42	2.41	-2.65	2.78
Q9Y2W2	WBP11	5.29	5.27	2.92	1.40	3.11	1.48
Q9Y2X3	NOP58	1.14	1.38	4.59	3.40	3.48	2.53
Q9Y2X9	ZNF281	-0.28	0.63	-0.25	0.17	0.66	0.52
Q9Y2Z0	SUGT1	-2.12	1.49	-2.03	1.60	-2.09	2.44
Q9Y314	NOSIP	1.97	2.56	0.45	1.66	1.53	3.28
Q9Y316	MEMO1	2.03	3.42	1.78	1.68	2.99	2.81
Q9Y324	FCF1	0.52	0.99	2.12	1.02	1.00	2.78
Q9Y330	ZBTB12	-1.54	3.24	4.41	3.59	3.38	2.31
Q9Y333	LSM2	5.17	5.07	4.98	2.72	6.23	6.99
Q9Y383	LUC7L2	6.38	8.15	5.57	2.25	5.22	2.11
Q9Y3A2	UTP11	2.94	2.55	4.56	6.56	3.69	4.82
Q9Y3A4	RRP7A	-0.85	0.34	-2.82	2.85	-2.97	3.97
Q9Y3B2	EXOSC1	-0.99	0.36	1.44	1.04	3.59	4.81
Q9Y3B4	SF3B6	3.41	8.16	5.06	6.61	5.00	3.50
Q9Y3B9	RRP15	-1.06	0.50	2.96	1.45	0.71	0.36
Q9Y3C1	NOP16	3.86	4.81	1.55	1.21	-0.18	0.14
Q9Y3C6	PPIL1	4.50	5.41	2.76	1.51	3.47	1.80
Q9Y3C8	UFC1	-0.07	2.43	4.10	2.01	2.50	9.89
Q9Y3F4	STRAP	1.42	1.50	-2.07	1.33	-1.06	1.22
Q9Y3I0	RTCB	1.04	1.48	-1.32	1.10	-1.09	1.43
Q9Y3I1	FBXO7	-0.12	2.32	-1.40	0.58	-0.84	0.34
Q9Y3T9	NOC2L	0.94	0.85	2.29	2.24	3.41	4.87
Q9Y3U8	RPL36	6.52	8.34	6.50	2.53	5.49	2.35
Q9Y3Y2	CHTOP	3.08	0.97	1.64	2.60	1.59	4.93
Q9Y3Z3	SAMHD1	2.08	0.97	-3.60	3.66	-0.78	0.97
Q9Y467	SALL2	5.01	2.10	3.84	1.30	4.93	1.60
Q9Y490	TLN1	3.31	10.27	-0.25	0.86	0.06	0.14
Q9Y4A5	TRRAP	0.57	0.97	2.00	1.26	1.48	0.98
Q9Y4B4	RAD54L2	2.15	2.50	1.65	1.70	1.75	2.02

Q9Y4C1	KDM3A	0.00	0.00	2.38	8.72	4.86	6.69
Q9Y4C8	RBM19	0.65	0.97	2.17	2.49	1.64	1.23
Q9Y4W2	LAS1L	1.77	2.31	3.13	3.25	3.02	2.31
Q9Y4W6	AFG3L2	2.18	0.61	3.27	1.68	-2.63	1.21
Q9Y4Z0	LSM4	-0.01	0.07	0.07	0.54	5.27	4.97
Q9Y530	OARD1	0.04	1.04	2.11	1.09	2.61	1.16
Q9Y570	PPME1	-0.15	1.95	0.10	1.01	1.87	1.25
Q9Y580	RBM7	2.84	1.42	4.36	1.98	4.27	1.99
Q9Y592	CEP83	2.79	2.39	3.13	3.21	2.92	2.64
Q9Y5A9	YTHDF2	-0.56	0.29	-1.72	1.22	-3.17	2.05
Q9Y5B0	CTDP1	0.07	1.83	0.71	2.03	-1.30	2.52
Q9Y5B6	PAXBP1	1.41	0.99	1.46	1.12	3.09	2.87
Q9Y5B9	SUPT16H	1.00	5.05	-0.31	0.11	-0.23	0.08
Q9Y5J1	UTP18	-3.79	2.77	4.16	4.70	3.57	2.37
Q9Y5K5	UCHL5	0.76	0.90	1.60	1.10	0.95	1.51
Q9Y5L0	TNPO3	3.46	3.28	-1.05	0.97	-0.46	0.50
Q9Y5N6	ORC6	-1.82	1.76	-0.09	0.07	-0.29	1.69
Q9Y5Q8	GTF3C5	0.78	1.90	0.55	0.65	0.71	6.41
Q9Y5Q9	GTF3C3	-0.74	0.35	2.79	0.58	3.12	0.73
Q9Y5S2	CDC42BPB	1.05	0.87	6.16	3.82	3.47	4.83
Q9Y5S9	RBM8A	3.11	4.27	4.28	2.97	4.08	2.78
Q9Y606	PUS1	1.15	0.85	0.08	0.04	-0.31	0.14
Q9Y617	PSAT1	4.11	2.92	0.75	0.23	-0.36	0.10
Q9Y618	NCOR2	2.44	0.56	1.00	0.60	-0.16	0.08
Q9Y646	CPQ	-0.08	2.62	0.10	0.47	0.35	2.29
Q9Y657	SPIN1	-0.43	0.38	1.17	2.67	2.02	3.07
Q9Y696	CLIC4	-2.28	2.64	-3.83	5.67	-2.59	5.03
Q9Y6A4	CFAP20	3.23	10.88	2.34	1.80	2.04	1.03
Q9Y6D9	MAD1L1	0.38	1.10	0.86	0.40	2.39	1.76
Q9Y6K1	DNMT3A	2.81	3.34	3.31	5.28	3.24	6.10
Q9Y6M1	IGF2BP2	-1.71	0.53	0.13	0.11	-1.35	1.18
Q9Y6Q9	NCOA3	2.14	1.51	2.61	3.21	4.55	5.02
Q9Y6X2	PIAS3	3.78	4.33	-2.46	2.26	-3.24	1.46
Q9Y6X8	ZHX2	5.50	4.85	4.98	3.61	6.68	9.05
Q9Y6X9	MORC2	2.17	2.71	1.56	0.83	2.96	1.74

BIBLIOGRAPHY

1 Signor, S. A. & Nuzhdin, S. V. The Evolution of Gene Expression in cis and trans. *Trends Genet* **34**, 532-544, doi:10.1016/j.tig.2018.03.007 (2018).

2 Mack, K. L. & Nachman, M. W. Gene Regulation and Speciation. *Trends Genet* **33**, 68-80, doi:10.1016/j.tig.2016.11.003 (2017).

3 Struhl, K. Fundamentally different logic of gene regulation in eukaryotes and prokaryotes. *Cell* **98**, 1-4, doi:10.1016/S0092-8674(00)80599-1 (1999).

4 Casamassimi, A. & Ciccodicola, A. Transcriptional Regulation: Molecules, Involved Mechanisms, and Misregulation. *Int J Mol Sci* **20**, doi:10.3390/ijms20061281 (2019).

5 Corbett, A. H. Post-transcriptional regulation of gene expression and human disease. *Curr Opin Cell Biol* **52**, 96-104, doi:10.1016/j.ceb.2018.02.011 (2018).

6 Lee, T. I. & Young, R. A. Transcriptional regulation and its misregulation in disease. *Cell* **152**, 1237-1251, doi:10.1016/j.cell.2013.02.014 (2013).

7 Walhout, A. J. Unraveling transcription regulatory networks by protein-DNA and protein-protein interaction mapping. *Genome Res* **16**, 1445-1454, doi:10.1101/gr.5321506 (2006).

8 Juven-Gershon, T. & Kadonaga, J. T. Regulation of gene expression via the core promoter and the basal transcriptional machinery. *Dev Biol* **339**, 225-229, doi:10.1016/j.ydbio.2009.08.009 (2010).

9 Taatjes, D. J. The human Mediator complex: a versatile, genome-wide regulator of transcription. *Trends Biochem Sci* **35**, 315-322, doi:10.1016/j.tibs.2010.02.004 (2010).

10 Sikorski, T. W. & Buratowski, S. The basal initiation machinery: beyond the general transcription factors. *Curr Opin Cell Biol* **21**, 344-351, doi:10.1016/j.ceb.2009.03.006 (2009).

11 Malik, S. & Roeder, R. G. The metazoan Mediator co-activator complex as an integrative hub for transcriptional regulation. *Nat Rev Genet* **11**, 761-772, doi:10.1038/nrg2901 (2010).

12 Yi, M., Tong, G. X., Murry, B. & Mendelson, C. R. Role of CBP/p300 and SRC-1 in transcriptional regulation of the pulmonary surfactant protein-A (SP-A) gene by thyroid transcription factor-1 (TTF-1). *J Biol Chem* **277**, 2997-3005, doi:10.1074/jbc.M109793200 (2002).

13 Kleinjan, D. A. & van Heyningen, V. Long-range control of gene expression: emerging mechanisms and disruption in disease. *Am J Hum Genet* **76**, 8-32, doi:10.1086/426833 (2005).

14 Wittkopp, P. J. & Kalay, G. Cis-regulatory elements: molecular mechanisms and evolutionary processes underlying divergence. *Nat Rev Genet* **13**, 59-69, doi:10.1038/nrg3095 (2011).

15 Bulger, M. & Groudine, M. Looping versus linking: toward a model for long-distance gene activation. *Genes Dev* **13**, 2465-2477, doi:10.1101/gad.13.19.2465 (1999).

16 Keller, S. H., Jena, S. G., Yamazaki, Y. & Lim, B. Regulation of spatiotemporal limits of developmental gene expression via enhancer grammar. *Proc Natl Acad Sci U S A* **117**, 15096-15103, doi:10.1073/pnas.1917040117 (2020).

17 Jiang, J. & Levine, M. Binding affinities and cooperative interactions with bHLH activators delimit threshold responses to the dorsal gradient morphogen. *Cell* **72**, 741-752, doi:10.1016/0092-8674(93)90402-c (1993).
18 Ramos, A. I. & Barolo, S. Low-affinity transcription factor binding sites shape morphogen responses and enhancer evolution. *Philos Trans R Soc Lond B Biol Sci* **368**, 20130018, doi:10.1098/rstb.2013.0018 (2013).
19 Hargreaves, D. C. & Crabtree, G. R. ATP-dependent chromatin remodeling: genetics, genomics and mechanisms. *Cell Res* **21**, 396-420, doi:10.1038/cr.2011.32 (2011).
20 Clapier, C. R. & Cairns, B. R. The biology of chromatin remodeling complexes. *Annu Rev Biochem* **78**, 273-304, doi:10.1146/annurev.biochem.77.062706.153223 (2009).
21 Kagey, M. H. *et al.* Mediator and cohesin connect gene expression and chromatin architecture. *Nature* **467**, 430-435, doi:10.1038/nature09380 (2010).
22 Vilar, J. M. & Saiz, L. DNA looping in gene regulation: from the assembly of macromolecular complexes to the control of transcriptional noise. *Curr Opin Genet Dev* **15**, 136-144, doi:10.1016/j.gde.2005.02.005 (2005).
23 Grubert, F. *et al.* Landscape of cohesin-mediated chromatin loops in the human genome. *Nature* **583**, 737-743, doi:10.1038/s41586-020-2151-x (2020).
24 Rao, S. S. *et al.* A 3D map of the human genome at kilobase resolution reveals principles of chromatin looping. *Cell* **159**, 1665-1680, doi:10.1016/j.cell.2014.11.021 (2014).
25 Sanborn, A. L. *et al.* Chromatin extrusion explains key features of loop and domain formation in wild-type and engineered genomes. *Proc Natl Acad Sci U S A* **112**, E6456-6465, doi:10.1073/pnas.1518552112 (2015).
26 Fudenberg, G. *et al.* Formation of Chromosomal Domains by Loop Extrusion. *Cell Rep* **15**, 2038-2049, doi:10.1016/j.celrep.2016.04.085 (2016).
27 Nora, E. P. *et al.* Targeted Degradation of CTCF Decouples Local Insulation of Chromosome Domains from Genomic Compartmentalization. *Cell* **169**, 930-944 e922, doi:10.1016/j.cell.2017.05.004 (2017).
28 Rao, S. S. P. *et al.* Cohesin Loss Eliminates All Loop Domains. *Cell* **171**, 305-320 e324, doi:10.1016/j.cell.2017.09.026 (2017).
29 Campos, E. I. & Reinberg, D. Histones: annotating chromatin. *Annu Rev Genet* **43**, 559-599, doi:10.1146/annurev.genet.032608.103928 (2009).
30 Gardner, K. E., Allis, C. D. & Strahl, B. D. Operating on chromatin, a colorful language where context matters. *J Mol Biol* **409**, 36-46, doi:10.1016/j.jmb.2011.01.040 (2011).
31 Rando, O. J. Combinatorial complexity in chromatin structure and function: revisiting the histone code. *Curr Opin Genet Dev* **22**, 148-155, doi:10.1016/j.gde.2012.02.013 (2012).
32 Bannister, A. J. & Kouzarides, T. Regulation of chromatin by histone modifications. *Cell Res* **21**, 381-395, doi:10.1038/cr.2011.22 (2011).
33 Cedar, H. & Bergman, Y. Programming of DNA methylation patterns. *Annu Rev Biochem* **81**, 97-117, doi:10.1146/annurev-biochem-052610-091920 (2012).
34 Jones, P. A. Functions of DNA methylation: islands, start sites, gene bodies and beyond. *Nat Rev Genet* **13**, 484-492, doi:10.1038/nrg3230 (2012).

35 Orkin, S. H. & Hochedlinger, K. Chromatin connections to pluripotency and cellular reprogramming. *Cell* **145**, 835-850, doi:10.1016/j.cell.2011.05.019 (2011).
36 Young, R. A. Control of the embryonic stem cell state. *Cell* **144**, 940-954, doi:10.1016/j.cell.2011.01.032 (2011).
37 Beisel, C. & Paro, R. Silencing chromatin: comparing modes and mechanisms. *Nat Rev Genet* **12**, 123-135, doi:10.1038/nrg2932 (2011).
38 Schmucker, D. *et al.* Drosophila Dscam is an axon guidance receptor exhibiting extraordinary molecular diversity. *Cell* **101**, 671-684, doi:10.1016/s0092-8674(00)80878-8 (2000).
39 Wojtowicz, W. M., Flanagan, J. J., Millard, S. S., Zipursky, S. L. & Clemens, J. C. Alternative splicing of Drosophila Dscam generates axon guidance receptors that exhibit isoform-specific homophilic binding. *Cell* **118**, 619-633, doi:10.1016/j.cell.2004.08.021 (2004).
40 Moazed, D. Small RNAs in transcriptional gene silencing and genome defence. *Nature* **457**, 413-420, doi:10.1038/nature07756 (2009).
41 Filipowicz, W., Jaskiewicz, L., Kolb, F. A. & Pillai, R. S. Post-transcriptional gene silencing by siRNAs and miRNAs. *Curr Opin Struct Biol* **15**, 331-341, doi:10.1016/j.sbi.2005.05.006 (2005).
42 Reyes-Turcu, F. E. & Grewal, S. I. Different means, same end-heterochromatin formation by RNAi and RNAi-independent RNA processing factors in fission yeast. *Curr Opin Genet Dev* **22**, 156-163, doi:10.1016/j.gde.2011.12.004 (2012).
43 Hagan, J. P., Piskounova, E. & Gregory, R. I. Lin28 recruits the TUTase Zcchc11 to inhibit let-7 maturation in mouse embryonic stem cells. *Nat Struct Mol Biol* **16**, 1021-1025, doi:10.1038/nsmb.1676 (2009).
44 Maller Schulman, B. R. *et al.* The let-7 microRNA target gene, Mlin41/Trim71 is required for mouse embryonic survival and neural tube closure. *Cell Cycle* **7**, 3935-3942, doi:10.4161/cc.7.24.7397 (2008).
45 Newman, M. A. & Hammond, S. M. Lin-28: an early embryonic sentinel that blocks Let-7 biogenesis. *Int J Biochem Cell Biol* **42**, 1330-1333, doi:10.1016/j.biocel.2009.02.023 (2010).
46 Levine, M. & Davidson, E. H. Gene regulatory networks for development. *Proc Natl Acad Sci U S A* **102**, 4936-4942, doi:10.1073/pnas.0408031102 (2005).
47 Macneil, L. T. & Walhout, A. J. Gene regulatory networks and the role of robustness and stochasticity in the control of gene expression. *Genome Res* **21**, 645-657, doi:10.1101/gr.097378.109 (2011).
48 Thompson, D., Regev, A. & Roy, S. Comparative analysis of gene regulatory networks: from network reconstruction to evolution. *Annu Rev Cell Dev Biol* **31**, 399-428, doi:10.1146/annurev-cellbio-100913-012908 (2015).
49 Beer, M. A., Shigaki, D. & Huangfu, D. Enhancer Predictions and Genome-Wide Regulatory Circuits. *Annu Rev Genomics Hum Genet* **21**, 37-54, doi:10.1146/annurev-genom-121719-010946 (2020).
50 Barski, A. *et al.* High-resolution profiling of histone methylations in the human genome. *Cell* **129**, 823-837, doi:10.1016/j.cell.2007.05.009 (2007).
51 Wang, Z. *et al.* Combinatorial patterns of histone acetylations and methylations in the human genome. *Nat Genet* **40**, 897-903, doi:10.1038/ng.154 (2008).

52 Creyghton, M. P. *et al.* Histone H3K27ac separates active from poised enhancers and predicts developmental state. *Proc Natl Acad Sci U S A* **107**, 21931-21936, doi:10.1073/pnas.1016071107 (2010).
53 Rada-Iglesias, A. *et al.* A unique chromatin signature uncovers early developmental enhancers in humans. *Nature* **470**, 279-283, doi:10.1038/nature09692 (2011).
54 Zentner, G. E., Tesar, P. J. & Scacheri, P. C. Epigenetic signatures distinguish multiple classes of enhancers with distinct cellular functions. *Genome Res* **21**, 1273-1283, doi:10.1101/gr.122382.111 (2011).
55 Marsman, J. & Horsfield, J. A. Long distance relationships: enhancer-promoter communication and dynamic gene transcription. *Biochim Biophys Acta* **1819**, 1217-1227, doi:10.1016/j.bbagrm.2012.10.008 (2012).
56 Anderson, E., Devenney, P. S., Hill, R. E. & Lettice, L. A. Mapping the Shh long-range regulatory domain. *Development* **141**, 3934-3943, doi:10.1242/dev.108480 (2014).
57 Symmons, O. *et al.* The Shh Topological Domain Facilitates the Action of Remote Enhancers by Reducing the Effects of Genomic Distances. *Dev Cell* **39**, 529-543, doi:10.1016/j.devcel.2016.10.015 (2016).
58 Zuin, J. *et al.* Nonlinear control of transcription through enhancer-promoter interactions. *Nature* **604**, 571-+, doi:10.1038/s41586-022-04570-y (2022).
59 Stees, J. S., Varn, F., Huang, S., Strouboulis, J. & Bungert, J. Recruitment of transcription complexes to enhancers and the role of enhancer transcription. *Biology (Basel)* **1**, 778-793, doi:10.3390/biology1030778 (2012).
60 Banerji, J., Rusconi, S. & Schaffner, W. Expression of a beta-globin gene is enhanced by remote SV40 DNA sequences. *Cell* **27**, 299-308, doi:10.1016/0092-8674(81)90413-x (1981).
61 Pennacchio, L. A., Bickmore, W., Dean, A., Nobrega, M. A. & Bejerano, G. Enhancers: five essential questions. *Nat Rev Genet* **14**, 288-295, doi:10.1038/nrg3458 (2013).
62 Arnosti, D. N. & Kulkarni, M. M. Transcriptional enhancers: Intelligent enhanceosomes or flexible billboards? *J Cell Biochem* **94**, 890-898, doi:10.1002/jcb.20352 (2005).
63 Panigrahi, A. & O'Malley, B. W. Mechanisms of enhancer action: the known and the unknown. *Genome Biol* **22**, 108, doi:10.1186/s13059-021-02322-1 (2021).
64 Sakabe, N. J., Savic, D. & Nobrega, M. A. Transcriptional enhancers in development and disease. *Genome Biol* **13**, 238, doi:10.1186/gb-2012-13-1-238 (2012).
65 Pachano, T., Haro, E. & Rada-Iglesias, A. Enhancer-gene specificity in development and disease. *Development* **149**, doi:10.1242/dev.186536 (2022).
66 Heinz, S., Romanoski, C. E., Benner, C. & Glass, C. K. The selection and function of cell type-specific enhancers. *Nat Rev Mol Cell Biol* **16**, 144-154, doi:10.1038/nrm3949 (2015).
67 Yanez-Cuna, J. O. *et al.* Dissection of thousands of cell type-specific enhancers identifies dinucleotide repeat motifs as general enhancer features. *Genome Res* **24**, 1147-1156, doi:10.1101/gr.169243.113 (2014).

68 Ahn, Y., Mullan, H. E. & Krumlauf, R. Long-range regulation by shared retinoic acid response elements modulates dynamic expression of posterior Hoxb genes in CNS development. *Dev Biol* **388**, 134-144, doi:10.1016/j.ydbio.2014.01.027 (2014).
69 Qian, P. *et al.* Retinoid-Sensitive Epigenetic Regulation of the Hoxb Cluster Maintains Normal Hematopoiesis and Inhibits Leukemogenesis. *Cell Stem Cell* **22**, 740-754 e747, doi:10.1016/j.stem.2018.04.012 (2018).
70 Nolte, C., Jinks, T., Wang, X., Martinez Pastor, M. T. & Krumlauf, R. Shadow enhancers flanking the HoxB cluster direct dynamic Hox expression in early heart and endoderm development. *Dev Biol* **383**, 158-173, doi:10.1016/j.ydbio.2013.09.016 (2013).
71 Oosterveen, T. *et al.* Retinoids regulate the anterior expression boundaries of 5' Hoxb genes in posterior hindbrain. *EMBO J* **22**, 262-269, doi:10.1093/emboj/cdg029 (2003).
72 Sharpe, J., Nonchev, S., Gould, A., Whiting, J. & Krumlauf, R. Selectivity, sharing and competitive interactions in the regulation of Hoxb genes. *EMBO J* **17**, 1788-1798, doi:10.1093/emboj/17.6.1788 (1998).
73 Gould, A., Morrison, A., Sproat, G., White, R. A. & Krumlauf, R. Positive cross-regulation and enhancer sharing: two mechanisms for specifying overlapping Hox expression patterns. *Genes Dev* **11**, 900-913, doi:10.1101/gad.11.7.900 (1997).
74 Ali, S. *et al.* Genomic features of human limb specific enhancers. *Genomics* **108**, 143-150, doi:10.1016/j.ygeno.2016.08.003 (2016).
75 Lettice, L. A. *et al.* A long-range Shh enhancer regulates expression in the developing limb and fin and is associated with preaxial polydactyly. *Hum Mol Genet* **12**, 1725-1735, doi:10.1093/hmg/ddg180 (2003).
76 Monti, R. *et al.* Limb-Enhancer Genie: An accessible resource of accurate enhancer predictions in the developing limb. *PLoS Comput Biol* **13**, e1005720, doi:10.1371/journal.pcbi.1005720 (2017).
77 VanderMeer, J. E., Smith, R. P., Jones, S. L. & Ahituv, N. Genome-wide identification of signaling center enhancers in the developing limb. *Development* **141**, 4194-4198, doi:10.1242/dev.110965 (2014).
78 Chiang, C. *et al.* Manifestation of the limb prepattern: limb development in the absence of sonic hedgehog function. *Dev Biol* **236**, 421-435, doi:10.1006/dbio.2001.0346 (2001).
79 Andersson, R. *et al.* An atlas of active enhancers across human cell types and tissues. *Nature* **507**, 455-461, doi:10.1038/nature12787 (2014).
80 Sabari, B. R. *et al.* Coactivator condensation at super-enhancers links phase separation and gene control. *Science* **361**, doi:10.1126/science.aar3958 (2018).
81 Zheng, J. B., Zhou, Y. H., Maity, T., Liao, W. S. & Saunders, G. F. Activation of the human PAX6 gene through the exon 1 enhancer by transcription factors SEF and Sp1. *Nucleic Acids Res* **29**, 4070-4078, doi:10.1093/nar/29.19.4070 (2001).
82 Kleinjan, D. A. *et al.* Long-range downstream enhancers are essential for Pax6 expression. *Dev Biol* **299**, 563-581, doi:10.1016/j.ydbio.2006.08.060 (2006).
83 Baizabal, J. M. *et al.* The Epigenetic State of PRDM16-Regulated Enhancers in Radial Glia Controls Cortical Neuron Position. *Neuron* **99**, 239-241, doi:10.1016/j.neuron.2018.06.031 (2018).

84 Sur, I. & Taipale, J. The role of enhancers in cancer. *Nat Rev Cancer* **16**, 483-493, doi:10.1038/nrc.2016.62 (2016).
85 Lidschreiber, K. *et al.* Transcriptionally active enhancers in human cancer cells. *Mol Syst Biol* **17**, e9873, doi:10.15252/msb.20209873 (2021).
86 Dalla-Favera, R. *et al.* Human c-myc onc gene is located on the region of chromosome 8 that is translocated in Burkitt lymphoma cells. *Proc Natl Acad Sci U S A* **79**, 7824-7827, doi:10.1073/pnas.79.24.7824 (1982).
87 Taub, R. *et al.* Translocation of the c-myc gene into the immunoglobulin heavy chain locus in human Burkitt lymphoma and murine plasmacytoma cells. *Proc Natl Acad Sci U S A* **79**, 7837-7841, doi:10.1073/pnas.79.24.7837 (1982).
88 ar-Rushdi, A. *et al.* Differential expression of the translocated and the untranslocated c-myc oncogene in Burkitt lymphoma. *Science* **222**, 390-393, doi:10.1126/science.6414084 (1983).
89 Erikson, J., ar-Rushdi, A., Drwinga, H. L., Nowell, P. C. & Croce, C. M. Transcriptional activation of the translocated c-myc oncogene in burkitt lymphoma. *Proc Natl Acad Sci U S A* **80**, 820-824, doi:10.1073/pnas.80.3.820 (1983).
90 Deng, R. *et al.* Disruption of super-enhancer-driven tumor suppressor gene RCAN1.4 expression promotes the malignancy of breast carcinoma. *Mol Cancer* **19**, 122, doi:10.1186/s12943-020-01236-z (2020).
91 Jeong, Y. *et al.* Regulation of a remote Shh forebrain enhancer by the Six3 homeoprotein. *Nat Genet* **40**, 1348-1353, doi:10.1038/ng.230 (2008).
92 Nelson, C. P. *et al.* Association analyses based on false discovery rate implicate new loci for coronary artery disease. *Nat Genet* **49**, 1385-1391, doi:10.1038/ng.3913 (2017).
93 Eppinga, R. N. *et al.* Identification of genomic loci associated with resting heart rate and shared genetic predictors with all-cause mortality. *Nat Genet* **48**, 1557-1563, doi:10.1038/ng.3708 (2016).
94 Nikpay, M. *et al.* A comprehensive 1,000 Genomes-based genome-wide association meta-analysis of coronary artery disease. *Nat Genet* **47**, 1121-1130, doi:10.1038/ng.3396 (2015).
95 Arking, D. E. *et al.* Genetic association study of QT interval highlights role for calcium signaling pathways in myocardial repolarization. *Nat Genet* **46**, 826-836, doi:10.1038/ng.3014 (2014).
96 Miller, C. L. *et al.* Disease-related growth factor and embryonic signaling pathways modulate an enhancer of TCF21 expression at the 6q23.2 coronary heart disease locus. *PLoS Genet* **9**, e1003652, doi:10.1371/journal.pgen.1003652 (2013).
97 van den Boogaard, M. *et al.* A common genetic variant within SCN10A modulates cardiac SCN5A expression. *J Clin Invest* **124**, 1844-1852, doi:10.1172/JCI73140 (2014).
98 van den Boogaard, M. *et al.* Genetic variation in T-box binding element functionally affects SCN5A/SCN10A enhancer. *J Clin Invest* **122**, 2519-2530, doi:10.1172/JCI62613 (2012).
99 Vahedi, G. *et al.* Super-enhancers delineate disease-associated regulatory nodes in T cells. *Nature* **520**, 558-562, doi:10.1038/nature14154 (2015).

100 Jostins, L. *et al.* Host-microbe interactions have shaped the genetic architecture of inflammatory bowel disease. *Nature* **491**, 119-124, doi:10.1038/nature11582 (2012).
101 Okada, Y. *et al.* Genetics of rheumatoid arthritis contributes to biology and drug discovery. *Nature* **506**, 376-381, doi:10.1038/nature12873 (2014).
102 Han, J. W. *et al.* Genome-wide association study in a Chinese Han population identifies nine new susceptibility loci for systemic lupus erythematosus. *Nat Genet* **41**, 1234-1237, doi:10.1038/ng.472 (2009).
103 Teruel, M. & Alarcon-Riquelme, M. E. The genetic basis of systemic lupus erythematosus: What are the risk factors and what have we learned. *J Autoimmun* **74**, 161-175, doi:10.1016/j.jaut.2016.08.001 (2016).
104 Shi, L. *et al.* Enhancer RNA and NFkappaB-dependent P300 regulation of ADAMDEC1. *Mol Immunol* **103**, 312-321, doi:10.1016/j.molimm.2018.09.019 (2018).
105 Jung, Y. H. *et al.* Recruitment of CTCF to an Fto enhancer is responsible for transgenerational inheritance of BPA-induced obesity. *Proc Natl Acad Sci U S A* **119**, e2214988119, doi:10.1073/pnas.2214988119 (2022).
106 Pasquali, L. *et al.* Pancreatic islet enhancer clusters enriched in type 2 diabetes risk-associated variants. *Nat Genet* **46**, 136-143, doi:10.1038/ng.2870 (2014).
107 Gaj, T., Sirk, S. J., Shui, S. L. & Liu, J. Genome-Editing Technologies: Principles and Applications. *Cold Spring Harb Perspect Biol* **8**, doi:10.1101/cshperspect.a023754 (2016).
108 Shlyueva, D., Stampfel, G. & Stark, A. Transcriptional enhancers: from properties to genome-wide predictions. *Nat Rev Genet* **15**, 272-286, doi:10.1038/nrg3682 (2014).
109 Li, S. *et al.* Overview of the reporter genes and reporter mouse models. *Animal Model Exp Med* **1**, 29-35, doi:10.1002/ame2.12008 (2018).
110 O'Kane, C. J. & Gehring, W. J. Detection in situ of genomic regulatory elements in Drosophila. *Proc Natl Acad Sci U S A* **84**, 9123-9127, doi:10.1073/pnas.84.24.9123 (1987).
111 Bellen, H. J. *et al.* P-element-mediated enhancer detection: a versatile method to study development in Drosophila. *Genes Dev* **3**, 1288-1300, doi:10.1101/gad.3.9.1288 (1989).
112 Bier, E. *et al.* Searching for pattern and mutation in the Drosophila genome with a P-lacZ vector. *Genes Dev* **3**, 1273-1287, doi:10.1101/gad.3.9.1273 (1989).
113 Siegal, M. L. & Hartl, D. L. Transgene Coplacement and high efficiency site-specific recombination with the Cre/loxP system in Drosophila. *Genetics* **144**, 715-726, doi:10.1093/genetics/144.2.715 (1996).
114 Butler, J. E. & Kadonaga, J. T. Enhancer-promoter specificity mediated by DPE or TATA core promoter motifs. *Genes Dev* **15**, 2515-2519, doi:10.1101/gad.924301 (2001).
115 Nagy, A. Cre recombinase: the universal reagent for genome tailoring. *Genesis* **26**, 99-109 (2000).
116 Meinke, G., Bohm, A., Hauber, J., Pisabarro, M. T. & Buchholz, F. Cre Recombinase and Other Tyrosine Recombinases. *Chem Rev* **116**, 12785-12820, doi:10.1021/acs.chemrev.6b00077 (2016).

117 Sternberg, N., Austin, S., Hamilton, D. & Yarmolinsky, M. Analysis of bacteriophage P1 immunity by using lambda-P1 recombinants constructed in vitro. *Proc Natl Acad Sci U S A* **75**, 5594-5598, doi:10.1073/pnas.75.11.5594 (1978).
118 Sternberg, N. & Hamilton, D. Bacteriophage P1 site-specific recombination. I. Recombination between loxP sites. *J Mol Biol* **150**, 467-486, doi:10.1016/0022-2836(81)90375-2 (1981).
119 Sternberg, N., Sauer, B., Hoess, R. & Abremski, K. Bacteriophage P1 cre gene and its regulatory region. Evidence for multiple promoters and for regulation by DNA methylation. *J Mol Biol* **187**, 197-212, doi:10.1016/0022-2836(86)90228-7 (1986).
120 Sauer, B. Inducible gene targeting in mice using the Cre/lox system. *Methods* **14**, 381-392, doi:10.1006/meth.1998.0593 (1998).
121 Sauer, B. & Henderson, N. Site-specific DNA recombination in mammalian cells by the Cre recombinase of bacteriophage P1. *Proc Natl Acad Sci U S A* **85**, 5166-5170, doi:10.1073/pnas.85.14.5166 (1988).
122 McLellan, M. A., Rosenthal, N. A. & Pinto, A. R. Cre-loxP-Mediated Recombination: General Principles and Experimental Considerations. *Curr Protoc Mouse Biol* **7**, 1-12, doi:10.1002/cpmo.22 (2017).
123 Metzger, D. & Chambon, P. Site- and time-specific gene targeting in the mouse. *Methods* **24**, 71-80, doi:10.1006/meth.2001.1159 (2001).
124 Brocard, J. *et al.* Spatio-temporally controlled site-specific somatic mutagenesis in the mouse. *Proc Natl Acad Sci U S A* **94**, 14559-14563, doi:10.1073/pnas.94.26.14559 (1997).
125 Kuhn, R., Schwenk, F., Aguet, M. & Rajewsky, K. Inducible gene targeting in mice. *Science* **269**, 1427-1429, doi:10.1126/science.7660125 (1995).
126 Gossen, M. & Bujard, H. Tight control of gene expression in mammalian cells by tetracycline-responsive promoters. *Proc Natl Acad Sci U S A* **89**, 5547-5551, doi:10.1073/pnas.89.12.5547 (1992).
127 Kim, H., Kim, M., Im, S. K. & Fang, S. Mouse Cre-LoxP system: general principles to determine tissue-specific roles of target genes. *Lab Anim Res* **34**, 147-159, doi:10.5625/lar.2018.34.4.147 (2018).
128 Klemm, S. L., Shipony, Z. & Greenleaf, W. J. Chromatin accessibility and the regulatory epigenome. *Nat Rev Genet* **20**, 207-220, doi:10.1038/s41576-018-0089-8 (2019).
129 Lee, C. K., Shibata, Y., Rao, B., Strahl, B. D. & Lieb, J. D. Evidence for nucleosome depletion at active regulatory regions genome-wide. *Nat Genet* **36**, 900-905, doi:10.1038/ng1400 (2004).
130 Thurman, R. E. *et al.* The accessible chromatin landscape of the human genome. *Nature* **489**, 75-82, doi:10.1038/nature11232 (2012).
131 Henikoff, S., Henikoff, J. G., Kaya-Okur, H. S. & Ahmad, K. Efficient chromatin accessibility mapping in situ by nucleosome-tethered tagmentation. *Elife* **9**, doi:10.7554/eLife.63274 (2020).
132 Boyle, A. P. *et al.* High-resolution mapping and characterization of open chromatin across the genome. *Cell* **132**, 311-322, doi:10.1016/j.cell.2007.12.014 (2008).

133 Hesselberth, J. R. *et al.* Global mapping of protein-DNA interactions in vivo by digital genomic footprinting. *Nat Methods* **6**, 283-289, doi:10.1038/nmeth.1313 (2009).
134 Buenrostro, J. D., Giresi, P. G., Zaba, L. C., Chang, H. Y. & Greenleaf, W. J. Transposition of native chromatin for fast and sensitive epigenomic profiling of open chromatin, DNA-binding proteins and nucleosome position. *Nat Methods* **10**, 1213-1218, doi:10.1038/nmeth.2688 (2013).
135 Mieczkowski, J. *et al.* MNase titration reveals differences between nucleosome occupancy and chromatin accessibility. *Nat Commun* **7**, 11485, doi:10.1038/ncomms11485 (2016).
136 Kelly, T. K. *et al.* Genome-wide mapping of nucleosome positioning and DNA methylation within individual DNA molecules. *Genome Res* **22**, 2497-2506, doi:10.1101/gr.143008.112 (2012).
137 Crawford, G. E. *et al.* DNase-chip: a high-resolution method to identify DNase I hypersensitive sites using tiled microarrays. *Nat Methods* **3**, 503-509, doi:10.1038/nmeth888 (2006).
138 Corces, M. R. *et al.* An improved ATAC-seq protocol reduces background and enables interrogation of frozen tissues. *Nat Methods* **14**, 959-962, doi:10.1038/nmeth.4396 (2017).
139 Buenrostro, J. D., Wu, B., Chang, H. Y. & Greenleaf, W. J. ATAC-seq: A Method for Assaying Chromatin Accessibility Genome-Wide. *Curr Protoc Mol Biol* **109**, 21 29 21-21 29 29, doi:10.1002/0471142727.mb2129s109 (2015).
140 Allan, J., Fraser, R. M., Owen-Hughes, T. & Keszenman-Pereyra, D. Micrococcal nuclease does not substantially bias nucleosome mapping. *J Mol Biol* **417**, 152-164, doi:10.1016/j.jmb.2012.01.043 (2012).
141 Lorzadeh, A. *et al.* Nucleosome Density ChIP-Seq Identifies Distinct Chromatin Modification Signatures Associated with MNase Accessibility. *Cell Rep* **17**, 2112-2124, doi:10.1016/j.celrep.2016.10.055 (2016).
142 Chung, H. R. *et al.* The effect of micrococcal nuclease digestion on nucleosome positioning data. *PLoS One* **5**, e15754, doi:10.1371/journal.pone.0015754 (2010).
143 Schmidt, F., Kern, F. & Schulz, M. H. Integrative prediction of gene expression with chromatin accessibility and conformation data. *Epigenetics Chromatin* **13**, 4, doi:10.1186/s13072-020-0327-0 (2020).
144 Park, P. J. ChIP-seq: advantages and challenges of a maturing technology. *Nat Rev Genet* **10**, 669-680, doi:10.1038/nrg2641 (2009).
145 Farnham, P. J. Insights from genomic profiling of transcription factors. *Nat Rev Genet* **10**, 605-616, doi:10.1038/nrg2636 (2009).
146 Brind'Amour, J. *et al.* An ultra-low-input native ChIP-seq protocol for genome-wide profiling of rare cell populations. *Nat Commun* **6**, 6033, doi:10.1038/ncomms7033 (2015).
147 Peng, S., Alekseyenko, A. A., Larschan, E., Kuroda, M. I. & Park, P. J. Normalization and experimental design for ChIP-chip data. *BMC Bioinformatics* **8**, 219, doi:10.1186/1471-2105-8-219 (2007).
148 Calhoun, V. C., Stathopoulos, A. & Levine, M. Promoter-proximal tethering elements regulate enhancer-promoter specificity in the Drosophila Antennapedia

complex. *Proc Natl Acad Sci U S A* **99**, 9243-9247, doi:10.1073/pnas.142291299 (2002).
149 Agelopoulos, M., Foutadakis, S. & Thanos, D. The Causes and Consequences of Spatial Organization of the Genome in Regulation of Gene Expression. *Front Immunol* **12**, 682397, doi:10.3389/fimmu.2021.682397 (2021).
150 Fulco, C. P. *et al.* Activity-by-contact model of enhancer-promoter regulation from thousands of CRISPR perturbations. *Nat Genet* **51**, 1664-1669, doi:10.1038/s41588-019-0538-0 (2019).
151 Xu, H., Zhang, S., Yi, X., Plewczynski, D. & Li, M. J. Exploring 3D chromatin contacts in gene regulation: The evolution of approaches for the identification of functional enhancer-promoter interaction. *Comput Struct Biotechnol J* **18**, 558-570, doi:10.1016/j.csbj.2020.02.013 (2020).
152 Dsouza, K. B. *et al.* Learning representations of chromatin contacts using a recurrent neural network identifies genomic drivers of conformation. *Nat Commun* **13**, 3704, doi:10.1038/s41467-022-31337-w (2022).
153 Dekker, J., Rippe, K., Dekker, M. & Kleckner, N. Capturing chromosome conformation. *Science* **295**, 1306-1311, doi:10.1126/science.1067799 (2002).
154 Denker, A. & de Laat, W. The second decade of 3C technologies: detailed insights into nuclear organization. *Genes Dev* **30**, 1357-1382, doi:10.1101/gad.281964.116 (2016).
155 Lafontaine, D. L., Yang, L., Dekker, J. & Gibcus, J. H. Hi-C 3.0: Improved Protocol for Genome-Wide Chromosome Conformation Capture. *Curr Protoc* **1**, e198, doi:10.1002/cpz1.198 (2021).
156 Lajoie, B. R., Dekker, J. & Kaplan, N. The Hitchhiker's guide to Hi-C analysis: practical guidelines. *Methods* **72**, 65-75, doi:10.1016/j.ymeth.2014.10.031 (2015).
157 Akgol Oksuz, B. *et al.* Systematic evaluation of chromosome conformation capture assays. *Nat Methods* **18**, 1046-1055, doi:10.1038/s41592-021-01248-7 (2021).
158 Lieberman-Aiden, E. *et al.* Comprehensive mapping of long-range interactions reveals folding principles of the human genome. *Science* **326**, 289-293, doi:10.1126/science.1181369 (2009).
159 Dixon, J. R. *et al.* Topological domains in mammalian genomes identified by analysis of chromatin interactions. *Nature* **485**, 376-380, doi:10.1038/nature11082 (2012).
160 Nora, E. P. *et al.* Spatial partitioning of the regulatory landscape of the X-inactivation centre. *Nature* **485**, 381-385, doi:10.1038/nature11049 (2012).
161 Sexton, T. *et al.* Three-dimensional folding and functional organization principles of the Drosophila genome. *Cell* **148**, 458-472, doi:10.1016/j.cell.2012.01.010 (2012).
162 Zufferey, M., Tavernari, D., Oricchio, E. & Ciriello, G. Comparison of computational methods for the identification of topologically associating domains. *Genome Biol* **19**, 217, doi:10.1186/s13059-018-1596-9 (2018).
163 Nanni, L., Ceri, S. & Logie, C. Spatial patterns of CTCF sites define the anatomy of TADs and their boundaries. *Genome Biol* **21**, 197, doi:10.1186/s13059-020-02108-x (2020).

164 Fullwood, M. J. & Ruan, Y. ChIP-based methods for the identification of long-range chromatin interactions. *J Cell Biochem* **107**, 30-39, doi:10.1002/jcb.22116 (2009).
165 Xi, W. & Beer, M. A. Loop competition and extrusion model predicts CTCF interaction specificity. *Nat Commun* **12**, 1046, doi:10.1038/s41467-021-21368-0 (2021).
166 Hsieh, T. S., Fudenberg, G., Goloborodko, A. & Rando, O. J. Micro-C XL: assaying chromosome conformation from the nucleosome to the entire genome. *Nat Methods* **13**, 1009-1011, doi:10.1038/nmeth.4025 (2016).
167 Krietenstein, N. *et al.* Ultrastructural Details of Mammalian Chromosome Architecture. *Mol Cell* **78**, 554-565 e557, doi:10.1016/j.molcel.2020.03.003 (2020).
168 Hsieh, T. S. *et al.* Resolving the 3D Landscape of Transcription-Linked Mammalian Chromatin Folding. *Mol Cell* **78**, 539-553 e538, doi:10.1016/j.molcel.2020.03.002 (2020).
169 Bonev, B. *et al.* Multiscale 3D Genome Rewiring during Mouse Neural Development. *Cell* **171**, 557-572 e524, doi:10.1016/j.cell.2017.09.043 (2017).
170 Wei, X. *et al.* HiCAR is a robust and sensitive method to analyze open-chromatin-associated genome organization. *Mol Cell* **82**, 1225-1238 e1226, doi:10.1016/j.molcel.2022.01.023 (2022).
171 Arnold, C. D. *et al.* Genome-wide quantitative enhancer activity maps identified by STARR-seq. *Science* **339**, 1074-1077, doi:10.1126/science.1232542 (2013).
172 Muerdter, F., Boryn, L. M. & Arnold, C. D. STARR-seq - principles and applications. *Genomics* **106**, 145-150, doi:10.1016/j.ygeno.2015.06.001 (2015).
173 Maurya, S. S. Role of Enhancers in Development and Diseases. *Epigenomes* **5**, doi:10.3390/epigenomes5040021 (2021).
174 Cong, L. *et al.* Multiplex genome engineering using CRISPR/Cas systems. *Science* **339**, 819-823, doi:10.1126/science.1231143 (2013).
175 Mali, P. *et al.* RNA-guided human genome engineering via Cas9. *Science* **339**, 823-826, doi:10.1126/science.1232033 (2013).
176 Ishino, Y., Shinagawa, H., Makino, K., Amemura, M. & Nakata, A. Nucleotide sequence of the iap gene, responsible for alkaline phosphatase isozyme conversion in Escherichia coli, and identification of the gene product. *J Bacteriol* **169**, 5429-5433, doi:10.1128/jb.169.12.5429-5433.1987 (1987).
177 Mojica, F. J., Diez-Villasenor, C., Soria, E. & Juez, G. Biological significance of a family of regularly spaced repeats in the genomes of Archaea, Bacteria and mitochondria. *Mol Microbiol* **36**, 244-246, doi:10.1046/j.1365-2958.2000.01838.x (2000).
178 Barrangou, R. *et al.* CRISPR provides acquired resistance against viruses in prokaryotes. *Science* **315**, 1709-1712, doi:10.1126/science.1138140 (2007).
179 Mojica, F. J., Diez-Villasenor, C., Garcia-Martinez, J. & Soria, E. Intervening sequences of regularly spaced prokaryotic repeats derive from foreign genetic elements. *J Mol Evol* **60**, 174-182, doi:10.1007/s00239-004-0046-3 (2005).
180 Bolotin, A., Quinquis, B., Sorokin, A. & Ehrlich, S. D. Clustered regularly interspaced short palindrome repeats (CRISPRs) have spacers of

extrachromosomal origin. *Microbiology (Reading)* **151**, 2551-2561, doi:10.1099/mic.0.28048-0 (2005).
181 Pourcel, C., Salvignol, G. & Vergnaud, G. CRISPR elements in Yersinia pestis acquire new repeats by preferential uptake of bacteriophage DNA, and provide additional tools for evolutionary studies. *Microbiology (Reading)* **151**, 653-663, doi:10.1099/mic.0.27437-0 (2005).
182 Brouns, S. J. *et al.* Small CRISPR RNAs guide antiviral defense in prokaryotes. *Science* **321**, 960-964, doi:10.1126/science.1159689 (2008).
183 Marraffini, L. A. & Sontheimer, E. J. CRISPR interference limits horizontal gene transfer in staphylococci by targeting DNA. *Science* **322**, 1843-1845, doi:10.1126/science.1165771 (2008).
184 Deveau, H. *et al.* Phage response to CRISPR-encoded resistance in Streptococcus thermophilus. *J Bacteriol* **190**, 1390-1400, doi:10.1128/JB.01412-07 (2008).
185 Jinek, M. *et al.* A programmable dual-RNA-guided DNA endonuclease in adaptive bacterial immunity. *Science* **337**, 816-821, doi:10.1126/science.1225829 (2012).
186 Jinek, M. *et al.* RNA-programmed genome editing in human cells. *Elife* **2**, e00471, doi:10.7554/eLife.00471 (2013).
187 Garneau, J. E. *et al.* The CRISPR/Cas bacterial immune system cleaves bacteriophage and plasmid DNA. *Nature* **468**, 67-71, doi:10.1038/nature09523 (2010).
188 Deltcheva, E. *et al.* CRISPR RNA maturation by trans-encoded small RNA and host factor RNase III. *Nature* **471**, 602-607, doi:10.1038/nature09886 (2011).
189 Urnov, F. D. *et al.* Highly efficient endogenous human gene correction using designed zinc-finger nucleases. *Nature* **435**, 646-651, doi:10.1038/nature03556 (2005).
190 Miller, J. C. *et al.* An improved zinc-finger nuclease architecture for highly specific genome editing. *Nat Biotechnol* **25**, 778-785, doi:10.1038/nbt1319 (2007).
191 Christian, M. *et al.* Targeting DNA double-strand breaks with TAL effector nucleases. *Genetics* **186**, 757-761, doi:10.1534/genetics.110.120717 (2010).
192 Zhang, F. *et al.* Efficient construction of sequence-specific TAL effectors for modulating mammalian transcription. *Nat Biotechnol* **29**, 149-153, doi:10.1038/nbt.1775 (2011).
193 Miller, J. C. *et al.* A TALE nuclease architecture for efficient genome editing. *Nat Biotechnol* **29**, 143-148, doi:10.1038/nbt.1755 (2011).
194 Li, T. *et al.* Modularly assembled designer TAL effector nucleases for targeted gene knockout and gene replacement in eukaryotes. *Nucleic Acids Res* **39**, 6315-6325, doi:10.1093/nar/gkr188 (2011).
195 Adli, M. The CRISPR tool kit for genome editing and beyond. *Nat Commun* **9**, 1911, doi:10.1038/s41467-018-04252-2 (2018).
196 Gasiunas, G., Barrangou, R., Horvath, P. & Siksnys, V. Cas9-crRNA ribonucleoprotein complex mediates specific DNA cleavage for adaptive immunity in bacteria. *Proc Natl Acad Sci U S A* **109**, E2579-2586, doi:10.1073/pnas.1208507109 (2012).

197 Hirano, H. *et al.* Structure and Engineering of Francisella novicida Cas9. *Cell* **164**, 950-961, doi:10.1016/j.cell.2016.01.039 (2016).
198 Mojica, F. J. M., Diez-Villasenor, C., Garcia-Martinez, J. & Almendros, C. Short motif sequences determine the targets of the prokaryotic CRISPR defence system. *Microbiology (Reading)* **155**, 733-740, doi:10.1099/mic.0.023960-0 (2009).
199 Hou, Z. *et al.* Efficient genome engineering in human pluripotent stem cells using Cas9 from Neisseria meningitidis. *Proc Natl Acad Sci U S A* **110**, 15644-15649, doi:10.1073/pnas.1313587110 (2013).
200 Kim, E. *et al.* In vivo genome editing with a small Cas9 orthologue derived from Campylobacter jejuni. *Nat Commun* **8**, 14500, doi:10.1038/ncomms14500 (2017).
201 Yamano, T. *et al.* Crystal Structure of Cpf1 in Complex with Guide RNA and Target DNA. *Cell* **165**, 949-962, doi:10.1016/j.cell.2016.04.003 (2016).
202 Kim, D. *et al.* Genome-wide analysis reveals specificities of Cpf1 endonucleases in human cells. *Nat Biotechnol* **34**, 863-868, doi:10.1038/nbt.3609 (2016).
203 Zetsche, B. *et al.* Cpf1 is a single RNA-guided endonuclease of a class 2 CRISPR-Cas system. *Cell* **163**, 759-771, doi:10.1016/j.cell.2015.09.038 (2015).
204 Abudayyeh, O. O. *et al.* RNA targeting with CRISPR-Cas13. *Nature* **550**, 280-284, doi:10.1038/nature24049 (2017).
205 Nishimasu, H. *et al.* Crystal structure of Cas9 in complex with guide RNA and target DNA. *Cell* **156**, 935-949, doi:10.1016/j.cell.2014.02.001 (2014).
206 Qi, L. S. *et al.* Repurposing CRISPR as an RNA-guided platform for sequence-specific control of gene expression. *Cell* **152**, 1173-1183, doi:10.1016/j.cell.2013.02.022 (2013).
207 Brezgin, S., Kostyusheva, A., Kostyushev, D. & Chulanov, V. Dead Cas Systems: Types, Principles, and Applications. *Int J Mol Sci* **20**, doi:10.3390/ijms20236041 (2019).
208 Komor, A. C., Kim, Y. B., Packer, M. S., Zuris, J. A. & Liu, D. R. Programmable editing of a target base in genomic DNA without double-stranded DNA cleavage. *Nature* **533**, 420-424, doi:10.1038/nature17946 (2016).
209 Gilbert, L. A. *et al.* CRISPR-mediated modular RNA-guided regulation of transcription in eukaryotes. *Cell* **154**, 442-451, doi:10.1016/j.cell.2013.06.044 (2013).
210 Friedman, J. R. *et al.* KAP-1, a novel corepressor for the highly conserved KRAB repression domain. *Genes Dev* **10**, 2067-2078, doi:10.1101/gad.10.16.2067 (1996).
211 Cheng, A. W. *et al.* Multiplexed activation of endogenous genes by CRISPR-on, an RNA-guided transcriptional activator system. *Cell Res* **23**, 1163-1171, doi:10.1038/cr.2013.122 (2013).
212 Wysocka, J. & Herr, W. The herpes simplex virus VP16-induced complex: the makings of a regulatory switch. *Trends Biochem Sci* **28**, 294-304, doi:10.1016/S0968-0004(03)00088-4 (2003).
213 Galonska, C. *et al.* Genome-wide tracking of dCas9-methyltransferase footprints. *Nat Commun* **9**, 597, doi:10.1038/s41467-017-02708-5 (2018).
214 Okano, M., Bell, D. W., Haber, D. A. & Li, E. DNA methyltransferases Dnmt3a and Dnmt3b are essential for de novo methylation and mammalian development. *Cell* **99**, 247-257, doi:10.1016/s0092-8674(00)81656-6 (1999).

215 Kearns, N. A. *et al.* Functional annotation of native enhancers with a Cas9-histone demethylase fusion. *Nat Methods* **12**, 401-403, doi:10.1038/nmeth.3325 (2015).
216 Shi, Y. *et al.* Histone demethylation mediated by the nuclear amine oxidase homolog LSD1. *Cell* **119**, 941-953, doi:10.1016/j.cell.2004.12.012 (2004).
217 Morgan, S. L. *et al.* Manipulation of nuclear architecture through CRISPR-mediated chromosomal looping. *Nat Commun* **8**, 15993, doi:10.1038/ncomms15993 (2017).
218 Liang, F. S., Ho, W. Q. & Crabtree, G. R. Engineering the ABA plant stress pathway for regulation of induced proximity. *Sci Signal* **4**, rs2, doi:10.1126/scisignal.2001449 (2011).
219 Shao, S. *et al.* Long-term dual-color tracking of genomic loci by modified sgRNAs of the CRISPR/Cas9 system. *Nucleic Acids Res* **44**, e86, doi:10.1093/nar/gkw066 (2016).
220 Kampmann, M. CRISPRi and CRISPRa Screens in Mammalian Cells for Precision Biology and Medicine. *ACS Chem Biol* **13**, 406-416, doi:10.1021/acschembio.7b00657 (2018).
221 Mali, P. *et al.* CAS9 transcriptional activators for target specificity screening and paired nickases for cooperative genome engineering. *Nat Biotechnol* **31**, 833-838, doi:10.1038/nbt.2675 (2013).
222 Maeder, M. L. *et al.* CRISPR RNA-guided activation of endogenous human genes. *Nat Methods* **10**, 977-979, doi:10.1038/nmeth.2598 (2013).
223 Perez-Pinera, P. *et al.* RNA-guided gene activation by CRISPR-Cas9-based transcription factors. *Nat Methods* **10**, 973-976, doi:10.1038/nmeth.2600 (2013).
224 Hilton, I. B. *et al.* Epigenome editing by a CRISPR-Cas9-based acetyltransferase activates genes from promoters and enhancers. *Nat Biotechnol* **33**, 510-517, doi:10.1038/nbt.3199 (2015).
225 Konermann, S. *et al.* Genome-scale transcriptional activation by an engineered CRISPR-Cas9 complex. *Nature* **517**, 583-588, doi:10.1038/nature14136 (2015).
226 Chavez, A. *et al.* Highly efficient Cas9-mediated transcriptional programming. *Nat Methods* **12**, 326-328, doi:10.1038/nmeth.3312 (2015).
227 Fang, L. *et al.* A Simple Cloning-free Method to Efficiently Induce Gene Expression Using CRISPR/Cas9. *Mol Ther Nucleic Acids* **14**, 184-191, doi:10.1016/j.omtn.2018.11.008 (2019).
228 Chavez, A. *et al.* Comparison of Cas9 activators in multiple species. *Nat Methods* **13**, 563-567, doi:10.1038/nmeth.3871 (2016).
229 Zhou, H. *et al.* In vivo simultaneous transcriptional activation of multiple genes in the brain using CRISPR-dCas9-activator transgenic mice. *Nat Neurosci* **21**, 440-446, doi:10.1038/s41593-017-0060-6 (2018).
230 Tanenbaum, M. E., Gilbert, L. A., Qi, L. S., Weissman, J. S. & Vale, R. D. A protein-tagging system for signal amplification in gene expression and fluorescence imaging. *Cell* **159**, 635-646, doi:10.1016/j.cell.2014.09.039 (2014).
231 Zalatan, J. G. *et al.* Engineering complex synthetic transcriptional programs with CRISPR RNA scaffolds. *Cell* **160**, 339-350, doi:10.1016/j.cell.2014.11.052 (2015).

232 Kunii, A. *et al.* Three-Component Repurposed Technology for Enhanced Expression: Highly Accumulable Transcriptional Activators via Branched Tag Arrays. *CRISPR J* **1**, 337-347, doi:10.1089/crispr.2018.0009 (2018).
233 Klann, T. S. *et al.* CRISPR-Cas9 epigenome editing enables high-throughput screening for functional regulatory elements in the human genome. *Nat Biotechnol* **35**, 561-568, doi:10.1038/nbt.3853 (2017).
234 Zhang, Y. *et al.* CRISPR-mediated activation of endogenous BST-2/tetherin expression inhibits wild-type HIV-1 production. *Sci Rep* **9**, 3134, doi:10.1038/s41598-019-40003-z (2019).
235 Saayman, S. M. *et al.* Potent and Targeted Activation of Latent HIV-1 Using the CRISPR/dCas9 Activator Complex. *Mol Ther* **24**, 488-498, doi:10.1038/mt.2015.202 (2016).
236 Xiong, K. *et al.* RNA-Guided Activation of Pluripotency Genes in Human Fibroblasts. *Cell Reprogram* **19**, 189-198, doi:10.1089/cell.2017.0006 (2017).
237 O'Geen, H. *et al.* Ezh2-dCas9 and KRAB-dCas9 enable engineering of epigenetic memory in a context-dependent manner. *Epigenetics Chromatin* **12**, 26, doi:10.1186/s13072-019-0275-8 (2019).
238 Schultz, D. C., Friedman, J. R. & Rauscher, F. J., 3rd. Targeting histone deacetylase complexes via KRAB-zinc finger proteins: the PHD and bromodomains of KAP-1 form a cooperative unit that recruits a novel isoform of the Mi-2alpha subunit of NuRD. *Genes Dev* **15**, 428-443, doi:10.1101/gad.869501 (2001).
239 Yeo, N. C. *et al.* An enhanced CRISPR repressor for targeted mammalian gene regulation. *Nat Methods* **15**, 611-616, doi:10.1038/s41592-018-0048-5 (2018).
240 Fulco, C. P. *et al.* Systematic mapping of functional enhancer-promoter connections with CRISPR interference. *Science* **354**, 769-773, doi:10.1126/science.aag2445 (2016).
241 Reilly, S. K. *et al.* Direct characterization of cis-regulatory elements and functional dissection of complex genetic associations using HCR-FlowFISH. *Nat Genet* **53**, 1166-1176, doi:10.1038/s41588-021-00900-4 (2021).
242 Thakore, P. I. *et al.* Highly specific epigenome editing by CRISPR-Cas9 repressors for silencing of distal regulatory elements. *Nat Methods* **12**, 1143-1149, doi:10.1038/nmeth.3630 (2015).
243 Luo, Y. *et al.* New developments on the Encyclopedia of DNA Elements (ENCODE) data portal. *Nucleic Acids Res* **48**, D882-D889, doi:10.1093/nar/gkz1062 (2020).
244 Korkmaz, G. *et al.* Functional genetic screens for enhancer elements in the human genome using CRISPR-Cas9. *Nat Biotechnol* **34**, 192-198, doi:10.1038/nbt.3450 (2016).
245 Sanjana, N. E. *et al.* High-resolution interrogation of functional elements in the noncoding genome. *Science* **353**, 1545-1549, doi:10.1126/science.aaf7613 (2016).
246 Diao, Y. *et al.* A new class of temporarily phenotypic enhancers identified by CRISPR/Cas9-mediated genetic screening. *Genome Res* **26**, 397-405, doi:10.1101/gr.197152.115 (2016).

247 Diao, Y. *et al.* A tiling-deletion-based genetic screen for cis-regulatory element identification in mammalian cells. *Nat Methods* **14**, 629-635, doi:10.1038/nmeth.4264 (2017).
248 Gasperini, M. *et al.* CRISPR/Cas9-Mediated Scanning for Regulatory Elements Required for HPRT1 Expression via Thousands of Large, Programmed Genomic Deletions. *Am J Hum Genet* **101**, 192-205, doi:10.1016/j.ajhg.2017.06.010 (2017).
249 Huang, J. *et al.* Dissecting super-enhancer hierarchy based on chromatin interactions. *Nat Commun* **9**, 943, doi:10.1038/s41467-018-03279-9 (2018).
250 Ulirsch, J. C. *et al.* Systematic Functional Dissection of Common Genetic Variation Affecting Red Blood Cell Traits. *Cell* **165**, 1530-1545, doi:10.1016/j.cell.2016.04.048 (2016).
251 Wakabayashi, A. *et al.* Insight into GATA1 transcriptional activity through interrogation of cis elements disrupted in human erythroid disorders. *Proc Natl Acad Sci U S A* **113**, 4434-4439, doi:10.1073/pnas.1521754113 (2016).
252 Xie, S., Duan, J., Li, B., Zhou, P. & Hon, G. C. Multiplexed Engineering and Analysis of Combinatorial Enhancer Activity in Single Cells. *Mol Cell* **66**, 285-299 e285, doi:10.1016/j.molcel.2017.03.007 (2017).
253 Hong, J. W., Hendrix, D. A. & Levine, M. S. Shadow enhancers as a source of evolutionary novelty. *Science* **321**, 1314, doi:10.1126/science.1160631 (2008).
254 Barolo, S. Shadow enhancers: frequently asked questions about distributed cis-regulatory information and enhancer redundancy. *Bioessays* **34**, 135-141, doi:10.1002/bies.201100121 (2012).
255 Cannavò, E. *et al.* Shadow Enhancers Are Pervasive Features of Developmental Regulatory Networks. *Curr Biol* **26**, 38-51, doi:10.1016/j.cub.2015.11.034 (2016).
256 Perry, M. W., Boettiger, A. N., Bothma, J. P. & Levine, M. Shadow enhancers foster robustness of Drosophila gastrulation. *Curr Biol* **20**, 1562-1567, doi:10.1016/j.cub.2010.07.043 (2010).
257 Frankel, N. *et al.* Phenotypic robustness conferred by apparently redundant transcriptional enhancers. *Nature* **466**, 490-493, doi:10.1038/nature09158 (2010).
258 Osterwalder, M. *et al.* Enhancer redundancy provides phenotypic robustness in mammalian development. *Nature* **554**, 239-243, doi:10.1038/nature25461 (2018).
259 Dailey, L. High throughput technologies for the functional discovery of mammalian enhancers: new approaches for understanding transcriptional regulatory network dynamics. *Genomics* **106**, 151-158, doi:10.1016/j.ygeno.2015.06.004 (2015).
260 White, M. A. Understanding how cis-regulatory function is encoded in DNA sequence using massively parallel reporter assays and designed sequences. *Genomics* **106**, 165-170, doi:10.1016/j.ygeno.2015.06.003 (2015).
261 Li, Q. V. *et al.* Genome-scale screens identify JNK-JUN signaling as a barrier for pluripotency exit and endoderm differentiation. *Nature Genetics* **51**, 999-+, doi:10.1038/s41588-019-0408-9 (2019).
262 Whalen, S., Truty, R. M. & Pollard, K. S. Enhancer-promoter interactions are encoded by complex genomic signatures on looping chromatin. *Nat Genet* **48**, 488-496, doi:10.1038/ng.3539 (2016).

263 Cao, Q. *et al.* Reconstruction of enhancer-target networks in 935 samples of human primary cells, tissues and cell lines. *Nat Genet* **49**, 1428-1436, doi:10.1038/ng.3950 (2017).
264 Xi, W. & Beer, M. A. Local epigenomic state cannot discriminate interacting and non-interacting enhancer-promoter pairs with high accuracy. *PLoS Comput Biol* **14**, e1006625, doi:10.1371/journal.pcbi.1006625 (2018).
265 Rezania, A. *et al.* Reversal of diabetes with insulin-producing cells derived in vitro from human pluripotent stem cells. *Nat Biotechnol* **32**, 1121-1133, doi:10.1038/nbt.3033 (2014).
266 Yang, D. *et al.* CRISPR screening uncovers a central requirement for HHEX in pancreatic lineage commitment and plasticity restriction. *Nat Cell Biol* **24**, 1064-1076, doi:10.1038/s41556-022-00946-4 (2022).
267 Hao, Y. *et al.* Integrated analysis of multimodal single-cell data. *Cell* **184**, 3573-3587 e3529, doi:10.1016/j.cell.2021.04.048 (2021).
268 Xiong, W. & Ferrell, J. E. A positive-feedback-based bistable 'memory module' that governs a cell fate decision. *Nature* **426**, 460-465, doi:10.1038/nature02089 (2003).
269 Wang, L. *et al.* Bistable switches control memory and plasticity in cellular differentiation. *Proc Natl Acad Sci U S A* **106**, 6638-6643, doi:10.1073/pnas.0806137106 (2009).
270 Cai, X. Exact stochastic simulation of coupled chemical reactions with delays. *J Chem Phys* **126**, 124108, doi:10.1063/1.2710253 (2007).
271 Walczak, A. M., Mugler, A. & Wiggins, C. H. Analytic methods for modeling stochastic regulatory networks. *Methods Mol Biol* **880**, 273-322, doi:10.1007/978-1-61779-833-7_13 (2012).
272 Zhu, Z. *et al.* Genome Editing of Lineage Determinants in Human Pluripotent Stem Cells Reveals Mechanisms of Pancreatic Development and Diabetes. *Cell Stem Cell* **18**, 755-768, doi:10.1016/j.stem.2016.03.015 (2016).
273 Dixon, G. *et al.* QSER1 protects DNA methylation valleys from de novo methylation. *Science* **372**, 146-+, doi:ARTN eabd0875 10.1126/science.abd0875 (2021).
274 Buenrostro, J. D., Giresi, P. G., Zaba, L. C., Chang, H. Y. & Greenleaf, W. J. Transposition of native chromatin for fast and sensitive epigenomic profiling of open chromatin, DNA-binding proteins and nucleosome position. *Nat Methods* **10**, 1213-+, doi:10.1038/Nmeth.2688 (2013).
275 Ghandi, M., Lee, D., Mohammad-Noori, M. & Beer, M. A. Enhanced regulatory sequence prediction using gapped k-mer features. *PLoS Comput Biol* **10**, e1003711, doi:10.1371/journal.pcbi.1003711 (2014).
276 Lee, D. *et al.* A method to predict the impact of regulatory variants from DNA sequence. *Nat Genet* **47**, 955-961, doi:10.1038/ng.3331 (2015).
277 Morgens, D. W. *et al.* Genome-scale measurement of off-target activity using Cas9 toxicity in high-throughput screens. *Nat Commun* **8**, 15178, doi:10.1038/ncomms15178 (2017).
278 Concordet, J. P. & Haeussler, M. CRISPOR: intuitive guide selection for CRISPR/Cas9 genome editing experiments and screens. *Nucleic Acids Res* **46**, W242-W245, doi:10.1093/nar/gky354 (2018).

279 Tang, Z. *et al.* CTCF-Mediated Human 3D Genome Architecture Reveals Chromatin Topology for Transcription. *Cell* **163**, 1611-1627, doi:10.1016/j.cell.2015.11.024 (2015).
280 Consortium, E. P. An integrated encyclopedia of DNA elements in the human genome. *Nature* **489**, 57-74, doi:10.1038/nature11247 (2012).
281 Wu, H. J. *et al.* Topological isolation of developmental regulators in mammalian genomes. *Nat Commun* **12**, 4897, doi:10.1038/s41467-021-24951-7 (2021).
282 Nasser, J. *et al.* Genome-wide enhancer maps link risk variants to disease genes. *Nature* **593**, 238-243, doi:10.1038/s41586-021-03446-x (2021).
283 Perez, A. R. *et al.* GuideScan software for improved single and paired CRISPR guide RNA design. *Nat Biotechnol* **35**, 347-349, doi:10.1038/nbt.3804 (2017).
284 Maston, G. A., Landt, S. G., Snyder, M. & Green, M. R. Characterization of enhancer function from genome-wide analyses. *Annu Rev Genomics Hum Genet* **13**, 29-57, doi:10.1146/annurev-genom-090711-163723 (2012).
285 Davidson, E. H. *The regulatory genome : gene regulatory networks in development and evolution*. (Academic, 2006).
286 Moris, N., Pina, C. & Arias, A. M. Transition states and cell fate decisions in epigenetic landscapes. *Nat Rev Genet* **17**, 693-703, doi:10.1038/nrg.2016.98 (2016).
287 Loh, K. M. *et al.* Efficient endoderm induction from human pluripotent stem cells by logically directing signals controlling lineage bifurcations. *Cell Stem Cell* **14**, 237-252, doi:10.1016/j.stem.2013.12.007 (2014).
288 Boyer, L. A. *et al.* Core transcriptional regulatory circuitry in human embryonic stem cells. *Cell* **122**, 947-956, doi:10.1016/j.cell.2005.08.020 (2005).
289 Uyehara, C. M. & Apostolou, E. 3D enhancer-promoter interactions and multi-connected hubs: Organizational principles and functional roles. *Cell Rep*, 112068, doi:10.1016/j.celrep.2023.112068 (2023).
290 Gasperini, M., Tome, J. M. & Shendure, J. Towards a comprehensive catalogue of validated and target-linked human enhancers. *Nat Rev Genet* **21**, 292-310, doi:10.1038/s41576-019-0209-0 (2020).
291 Tiyaboonchai, A. *et al.* GATA6 Plays an Important Role in the Induction of Human Definitive Endoderm, Development of the Pancreas, and Functionality of Pancreatic beta Cells. *Stem Cell Reports* **8**, 589-604, doi:10.1016/j.stemcr.2016.12.026 (2017).
292 Morrisey, E. E., Ip, H. S., Lu, M. M. & Parmacek, M. S. GATA-6: a zinc finger transcription factor that is expressed in multiple cell lineages derived from lateral mesoderm. *Dev Biol* **177**, 309-322, doi:10.1006/dbio.1996.0165 (1996).
293 Shi, Z. D. *et al.* Genome Editing in hPSCs Reveals GATA6 Haploinsufficiency and a Genetic Interaction with GATA4 in Human Pancreatic Development. *Cell Stem Cell* **20**, 675-688 e676, doi:10.1016/j.stem.2017.01.001 (2017).
294 Schrode, N., Saiz, N., Di Talia, S. & Hadjantonakis, A. K. GATA6 levels modulate primitive endoderm cell fate choice and timing in the mouse blastocyst. *Dev Cell* **29**, 454-467, doi:10.1016/j.devcel.2014.04.011 (2014).
295 Morrisey, E. E. *et al.* GATA6 regulates HNF4 and is required for differentiation of visceral endoderm in the mouse embryo. *Genes Dev* **12**, 3579-3590, doi:10.1101/gad.12.22.3579 (1998).

296 Replogle, J. M. *et al.* Combinatorial single-cell CRISPR screens by direct guide RNA capture and targeted sequencing. *Nat Biotechnol* **38**, 954-961, doi:10.1038/s41587-020-0470-y (2020).
297 Datlinger, P. *et al.* Pooled CRISPR screening with single-cell transcriptome readout. *Nat Methods* **14**, 297-301, doi:10.1038/nmeth.4177 (2017).
298 Adamson, B. *et al.* A Multiplexed Single-Cell CRISPR Screening Platform Enables Systematic Dissection of the Unfolded Protein Response. *Cell* **167**, 1867-1882 e1821, doi:10.1016/j.cell.2016.11.048 (2016).
299 Dixit, A. *et al.* Perturb-Seq: Dissecting Molecular Circuits with Scalable Single-Cell RNA Profiling of Pooled Genetic Screens. *Cell* **167**, 1853-1866 e1817, doi:10.1016/j.cell.2016.11.038 (2016).
300 Batut, P. J. *et al.* Genome organization controls transcriptional dynamics during development. *Science* **375**, 566-570, doi:10.1126/science.abi7178 (2022).
301 Juan, A. H. & Ruddle, F. H. Enhancer timing of Hox gene expression: deletion of the endogenous Hoxc8 early enhancer. *Development* **130**, 4823-4834, doi:10.1242/dev.00672 (2003).
302 Rodriguez-Carballo, E. *et al.* Chromatin topology and the timing of enhancer function at the HoxD locus. *Proc Natl Acad Sci U S A* **117**, 31231-31241, doi:10.1073/pnas.2015083117 (2020).
303 Xiao, J. Y., Hafner, A. & Boettiger, A. N. How subtle changes in 3D structure can create large changes in transcription. *Elife* **10**, doi:10.7554/eLife.64320 (2021).
304 Kim-Hellmuth, S. *et al.* Cell type-specific genetic regulation of gene expression across human tissues. *Science* **369**, doi:10.1126/science.aaz8528 (2020).
305 Marderstein, A. R. *et al.* Demographic and genetic factors influence the abundance of infiltrating immune cells in human tissues. *Nat Commun* **11**, 2213, doi:10.1038/s41467-020-16097-9 (2020).
306 Donovan, M. K. R., D'Antonio-Chronowska, A., D'Antonio, M. & Frazer, K. A. Cellular deconvolution of GTEx tissues powers discovery of disease and cell-type associated regulatory variants. *Nat Commun* **11**, 955, doi:10.1038/s41467-020-14561-0 (2020).
307 Karr, J. P., Ferrie, J. J., Tjian, R. & Darzacq, X. The transcription factor activity gradient (TAG) model: contemplating a contact-independent mechanism for enhancer-promoter communication. *Genes Dev* **36**, 7-16, doi:10.1101/gad.349160.121 (2022).
308 Dowen, J. M. *et al.* Control of cell identity genes occurs in insulated neighborhoods in mammalian chromosomes. *Cell* **159**, 374-387, doi:10.1016/j.cell.2014.09.030 (2014).
309 Wang, X. *et al.* Genome-wide detection of enhancer-hijacking events from chromatin interaction data in rearranged genomes. *Nat Methods* **18**, 661-668, doi:10.1038/s41592-021-01164-w (2021).
310 Yan, J. & Huangfu, D. Epigenome rewiring in human pluripotent stem cells. *Trends Cell Biol* **32**, 259-271, doi:10.1016/j.tcb.2021.12.001 (2022).
311 Islam, S. *et al.* Quantitative single-cell RNA-seq with unique molecular identifiers. *Nat Methods* **11**, 163-166, doi:10.1038/nmeth.2772 (2014).

312 Hwang, B., Lee, J. H. & Bang, D. Single-cell RNA sequencing technologies and bioinformatics pipelines. *Exp Mol Med* **50**, 1-14, doi:10.1038/s12276-018-0071-8 (2018).
313 Xu, Z., Sziraki, A., Lee, J., Zhou, W. & Cao, J. PerturbSci-Kinetics: Dissecting key regulators of transcriptome kinetics through scalable single-cell RNA profiling of pooled CRISPR screens. *bioRxiv*, 2023.2001.2029.526143, doi:10.1101/2023.01.29.526143 (2023).
314 Sziraki, A. *et al.* A global view of aging and Alzheimer's pathogenesis-associated cell population dynamics and molecular signatures in the human and mouse brains. *bioRxiv*, 2022.2009.2028.509825, doi:10.1101/2022.09.28.509825 (2022).
315 Luo, R. *et al.* Dynamic network-guided CRISPRi screen identifies CTCF-loop-constrained nonlinear enhancer gene regulatory activity during cell state transitions. *Nature Genetics*, doi:10.1038/s41588-023-01450-7 (2023).